



SATREPS



Landslide Risk Assessment Technology

*Proceedings of SATREPS Workshop on Landslides
- Mid-Term Activity Report -*

29-30 July 2014, Hanoi, Vietnam



Published by
International Consortium on Landslides (ICL)

Landslide Risk Assessment Technology

Edited by **Kyoji Sassa**
 Khang Dang

International Consortium on Landslides (ICL)
Kyoto – Japan

Preface for SATREPS 2014

Kyoji Sassa, Project leader

SATREPS Project: Development of landslide risk assessment technology
along transport arteries in Vietnam

Landslide risk reduction is societal pressing need in all mountainous countries. The necessity is especially strong in countries affected by heavy rainfalls, tropical monsoon and earthquakes. Global climate change is expected to increasingly affect the frequency and extent of heavy rainfall at local and regional level. Landslides are sometimes exacerbated by unregulated anthropogenic developments such as roads, railways, waterworks and mining. Vietnam is a country suffered by landslide disasters due to tropical monsoon, tropical weathering of rocks, earthquakes and rapid and extensive development of land in progress of economic growth. The establishment of effective landslide risk assessment technology is very much needed for nationwide safer geoenvironment and securing transport arteries.

Japan has much suffered by landslides triggered by typhoons, strong/long rainfall, snow melting as well as earthquakes. The necessity to reduce landslide disasters has promoted landslide science and technology in Japan. The Japan Landslide Society was established in 1965 which is the first and the unique national society on landslides at present in the world. The International Consortium on Landslides (ICL) launched at the UNESCO-Kyoto University Joint Symposium in January 2002 is an International non-governmental and non-profit scientific organization promoting landslide research and capacity building for the benefit of society and the environment. ICL has 59 members from 35 countries in 2014. It was registered in Kyoto Prefectural Government as NPO in 2002 and its headquarters is located in Kyoto, Japan. Major activities of the ICL are the publication of bimonthly full color journal “Landslides: Journal of the International Consortium on Landslides”, the International Programme on Landslides including IPL Projects in many countries/regions and the Triennial World Landslide Forum, and promotion of ICL regional and thematic networks and the World Centres of Excellence on Landslide Risk Reduction (WCoE). All activities are cooperated by ICL-supporting organizations (UNESCO, WMO, FAO, UNISDR, UNU, ICSU, WFEO and IUGS) and other various stakeholders (national and local governments, civil society, private sectors) contributing to landslide risk reduction.

Dr Doan Minh Tam, Director of the Institute for Transport Science and Technology of Ministry of Transport (ITST), Vietnam submitted the application form to join ICL on 1st April 2010, and ITST was approved on 18 May 2010 as the 49th member of ICL. Kyoji Sassa, Executive Director of ICL and Toyohiko Miyagi visited ITST in Hanoi and had lectures at the workshop to celebrate the registration to ICL on 16-22 August 2010. ICL and ITST visited and discussed with MOT, Mr. Ngo Thinh Duc, Deputy Minister and other staffs at MOT on the cooperation for landslide risk reduction in Vietnam.



*The first SATREPS planning meeting at MOT in Hanoi, Vietnam
Ngo Thinh Duc, Deputy Minister and other directors of MOT in the right side, and
Doan Minh Tam, ITST Director (standing), Kyoji Sassa and Toyohiko Miyagi and
others in the left side on 17 August 2010.*

Sassa and Miyagi visited landslides in the Son La area, further Sassa visited landslides along the Ho Chie Minh Route and the Haivan Pass area between Danang and Hue by the guide of Doan Minh Tam. Based on this joint discussion in Vietnam, ICL and ITST have applied for SATREPS project from Japan and Vietnam in October 2010. The greatest interest from ITST was to create human resources for landslide risk reduction in Vietnam through education and technology transfer from Japan to Vietnam. Apparently it is the most basic and important factor for sustainable development of landslide risk reduction in Vietnam.

The project application was accepted in June 2011, and the project has formally started in November 2011. The first two long-term trainees entered into the Doctor Course of Kyoto University and the Master Course of Shimane University on 1st October. Two long-term trainees entered into the Japanese universities in 1st April 2013 and three long-term trainees entered into the Japanese universities in 1st October 2013. Currently two doctor students and

five master students are studying in Japan. They have obtained research communication ability with Japanese researchers, technical knowledge and basic research skill on landslide risk reduction. They can help study of the short-term trainees in Japan and joined field investigation by the Japanese experts in Vietnam and translated necessary documents from Vietnamese to English and English to Vietnamese. Those are basic treasure and effective infrastructure for the implementation of this project, and guarantees the sustainability of the project and promoted capacity of Vietnam for landslide risk mitigation. More than ten long-term and short-term trainees are human resources for further cooperation between Vietnam and Japan.

[SATREPS 2014 Workshop on Landslides has three components.](#)

1. SATREPS Report Meeting from 9:00 - 17:00 on 29 July 2014.

4 working group leaders, 7 Vietnamese students, 11 Vietnamese and Japanese research members will report their activities. It aims to report SATREPS activities within the research group together with relevant people.

2. Landslide Technical Forum on Landslide Risk Assessment Technology from 9:20-12:00 on 30 July 2014. Invited speakers will introduce their research and experience related to this field. Participants are from relevant organizations as well as this project.

3. SATREPS Discussion Session "Past, present and forward" from 13:30-17:00 on 30 July 2014.

This is basically free discussion within all participants. Initially working group leaders will summarize “Past, Present and forward” of the project from their point of views, then perspectives for post-project cooperation between Vietnam and Japan will be presented from ICL and ITST. Then, commentators and participants are invited to talk or comment or advise on the past project activities, their values, future plan and possible contribution to this initiatives.

Acknowledgements

This project is a joint project between the Institute of Transport Science and Technology (ITST) and the Ministry of Transport (MOT) of the Social Republic of Viet Nam and three organizations in Japan: the International Consortium on Landslides (ICL), the Tohoku Gakuin University and the Forestry and Forest Product Research Institute (FFPRI). All research members are appreciated for their extensive contribution for the success of this project.

SATREPS (Science and Technology Research Partnership for Sustainable Development) is a joint programme funded by the Japan International Cooperation Agency (JICA) and the Japan Science and Technology Agency (JST). The SATREPS 2014 is also organized with the budget

and the supports from JICA and JST. The research group acknowledges both agencies for funding and their staffs and advisers for supporting efforts for the success of this project.



A handwritten signature in black ink that reads "Kyoji Sassa". The signature is written in a cursive, flowing style.

Kyoji Sassa
Executive Director
International Consortium on Landslides

Contents

Preface for SATREPS 2014	iii
Kyoji Sassa, Project leader	
Project Outline and Mid-Term Activity Report	1
Kyoji Sassa, Nguyen Xuan Khang	
Test results of a new high-stress ring shear apparatus (ICL-2) developed for Vietnam Project	32
Khang Dang, Kyoji Sassa, He Bin, Osamu Nagai	
Landslide mapping and detection of active landslide area from aerial photograph interpretation and field survey in central provinces of Vietnam	42
<i>Le Hong Luong, Toyohiko Miyagi, Shinro Abe, Eisaku Hamasaki, Dinh Van Tien</i>	
Mechanical characteristics of the August 6, 2012 Mihata landslide, Shimane Prefecture, Japan	50
Ngoc Ha Do, Fawu Wang, Yohei Kuwada	
Overview of Landslide Phenomena along Arterial Transport System in Vietnam	57
Tien Pham, Tam Doan, Luong Le	
Characteristic of landslides in Ho Chi Minh road, Vietnam	62
<i>Doan Huy Loi, Huynh Thanh Binh, Do Ngoc Ha</i>	
Preliminary investigation and research plan on Sorayama landslide, Shimane, Japan triggered by heavy rainfall	67
<i>Pham Thi Chien</i>	
Overview of extensive shallow landslides caused by typhoon Wipha (Oct.2013) in Izu-Oshima island and further research plan	72
<i>Vu The Truong, Satoshi Tsuchiya, Fumitoshi Imaizumi</i>	
Identification of slope deformation by the Particle Imaging Velocimetry (PIV) Analysis of air photos or laser scanning images in different periods	76
<i>Sakae Mukoyama, Kyoji Sassa, Doan Huy Loi, Hirotaka Ochiai, Toyohiko Miyagi</i>	
Development of integrated data and Web-based analysis software for Vietnam	82
<i>Keisuke Takimoto, Shiho Asano, Osamu Nagai, Hiroshi Fukuoka and Kyoji Sassa</i>	
Landslide mapping and the risk evaluation by aerial photo interpretation in Vietnam	87
<i>Toyohiko Miyagi</i>	
Landslide prevention and mitigation for road in humid tropical region	96
<i>DinhVanTien, Toyohiko Miyagi, Eisaku Hamasaki, Shinro Abe, Nguyen Xuan Khang</i>	
Topographic and geological factors of landslides along Ho Chi Minh Route in central Vietnam	107
<i>Shinro Abe, Dinh Van Tien, Hiroyuki Yoshimatsu, Tatsuya Shibasaki, Toyohiko Miyagi</i>	
Change the safety factors by the series of land deformation at a typical landslide along the National Road No.6, Vietnam	119
<i>Ngo Doan Dung Ngo Doan Dung, Eisaku Hamasaki, Tatsuya Shibasaki, Toyohiko Miyagi, Hiromu Daimaru, Dinh Van Tien, Le Hong Luong</i>	
Objective Function based AHP Risk Evaluation System in Humid Tropical Regions	123
<i>Eisaku Hamasaki, Toyohiko Miyagi, Dinh Van Tien, Ngo Doan Dung</i>	

Application of Digital Surface Model due to Structure from Motion	128
<i>Shoichiro Uchiyama , Toyohiko Miyagi</i>	
Progress in Landslide Dynamics	137
<i>Kyoji Sassa, He Bin, Khang Dang</i>	
Recent Development of the New High Stress Undrained Ring Shear Apparatus (ICL-2) and its Application	168
<i>Lam Huu Quang, Dang Quang Khang, Pham Van Tien, Doan Huy Loi, Nguyen Kim Thanh</i>	
Simulation of a rapid and long-travelling landslide using 2D-RAPID and LS-RAPID 3D Models	174
<i>Bin He, Kyoji Sassa, Osamu Nagai, Takara Kaoru</i>	
Landslide experiments on natural slopes and indoor landslide flume tests by artificial rainfall	179
<i>Hirotsuka Ochiai, Yasuhiko Okada, Mark E. Reid, Kyoji Sassa</i>	
Landslides on the road in Vietnam - Monitoring and solutions for landslide risk reduction	185
<i>Huynh Dang Vinh, Huynh Thanh Binh, Do Ngoc Ha</i>	
Development of landslide monitoring and data transfer system in the Hai van station landslide and the initial extensometer monitoring result behind the station	190
<i>Shiho Asano, Shinro Abe, Osamu Nagai</i>	
High-resolution rainfall simulations for disaster prevention using the Multi-Scale Simulator for the Geoenvironment (MSSG)	195
<i>Ryo Onishi, Keiko Takahashi, Wataru Sasaki , Tooru Sugiyama</i>	
Identification, monitoring and simulation of landslides in the Rječina River Valley, Croatia	200
<i>Željko Arbanas, Snježana Mihalić Arbanas, Martina Vivoda, Josip Peranić, Sanja Dugonjić Jovančević, Vedran Jagodnik</i>	
Landslide mapping and monitoring in the City of Zagreb (Croatia, Europe)	214
<i>Snježana Mihalić Arbanas, Martin Krkač, Sanja Bernat, Željko Arbanas</i>	
Analysis of a Deep-Seated Landslide in the Phan Me Coal Mining Dump Site, Thai Nguyen Province, Vietnam	227
<i>Do Minh Duc, Nguyen Manh Hieu, Kyoji Sassa, Eisaku Hamasaki, Khang Dang, and Toyohiko Miyagi</i>	
Hybrid Socio-Technical Approach for Community-based Landslide Risk Reduction in Indonesia	232
<i>Dwikorita Karnawati, Teuku Faisal Fathani, Wahyu Wilopo, Budi Andayani</i>	
Distributed hydrological Process through vegetation & surface soil layer using 30-minute current satellite-based rainfall intensity from NOAA-CPC	238
<i>Apip Arief, Kyoji Sassa</i>	

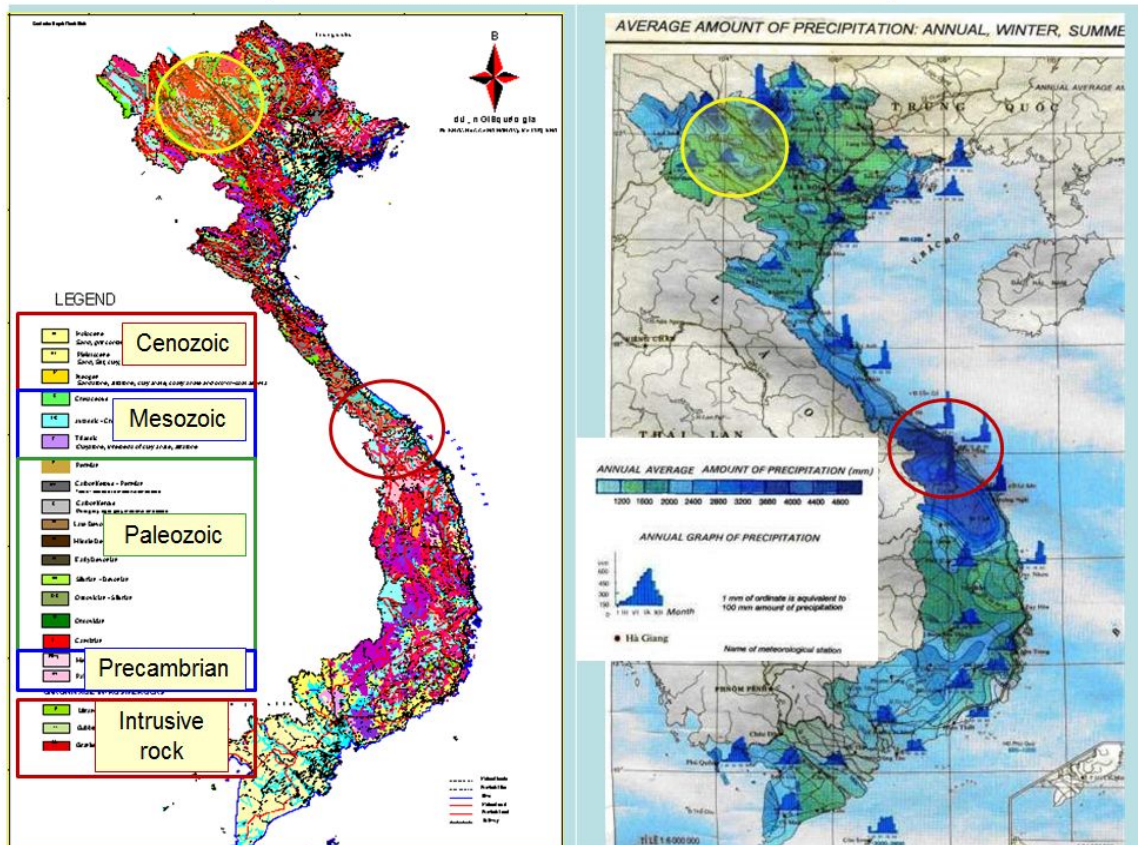
JICA-JST Joint Project in Vietnam

Development of Landslide Risk Assessment Technology along Transport Arteries in Viet Nam

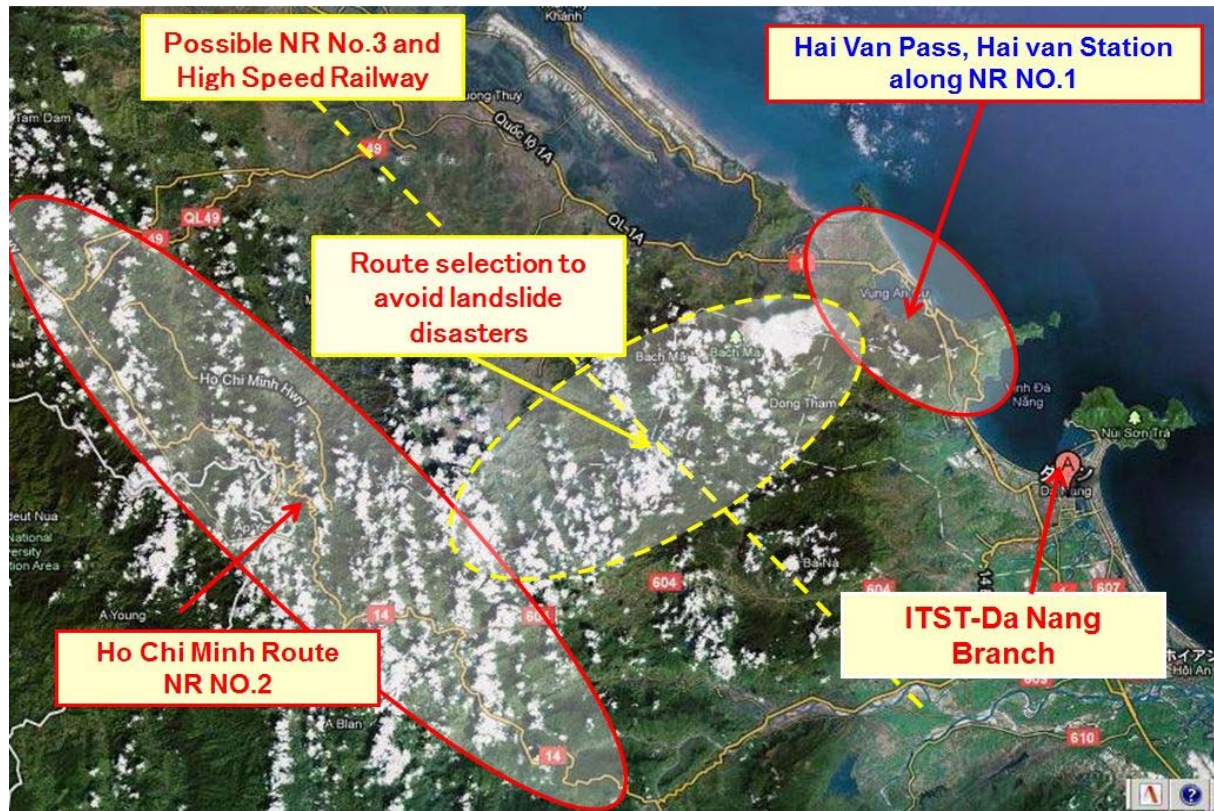
Project Outline and Mid-Term Activity Report

Kyoji Sassa, Project Leader
Executive Director of ICL
Nguyen Xuan Khang, Project Director
Director of ITST

Geology and Rain fall in Vietnam



The Investigation Sites in Da Nang (MM and RD in 2011)



Aim of SATREPS Joint research

- Mountainous areas of Greater Mekong Sub-region are subject to frequent slope disasters caused by a combination of weak ground, steep slopes, and tropical monsoon.
- Securing arterial roads connecting north and south Vietnam and people's lives in mountain area is the most important issue for national development.
- Establishment of an effective landslide risk assessment technology suitable for Vietnam is the key issue for disaster reduction.
- Technologies of landslide mapping, landslide risk identification, soil testing and computer simulation, landslide monitoring and early warning are jointly developed and transferred to Vietnam.
- An extensive human resources with an advanced landslide risk assessment technology are developed through capacity development in Japan and Vietnam.
- Network for landslide risk reduction is established in Vietnam, Japan and other mountainous countries.

Development of Landslide Risk Assessment Technology along Transport Arteries in Viet Nam

Overall Objective

Social implementation of the developed landslide risk assessment technology and early warning system will contribute to the safety ensuring of transportation arteries and residents in mountainous communities in Viet Nam.

Project Purpose

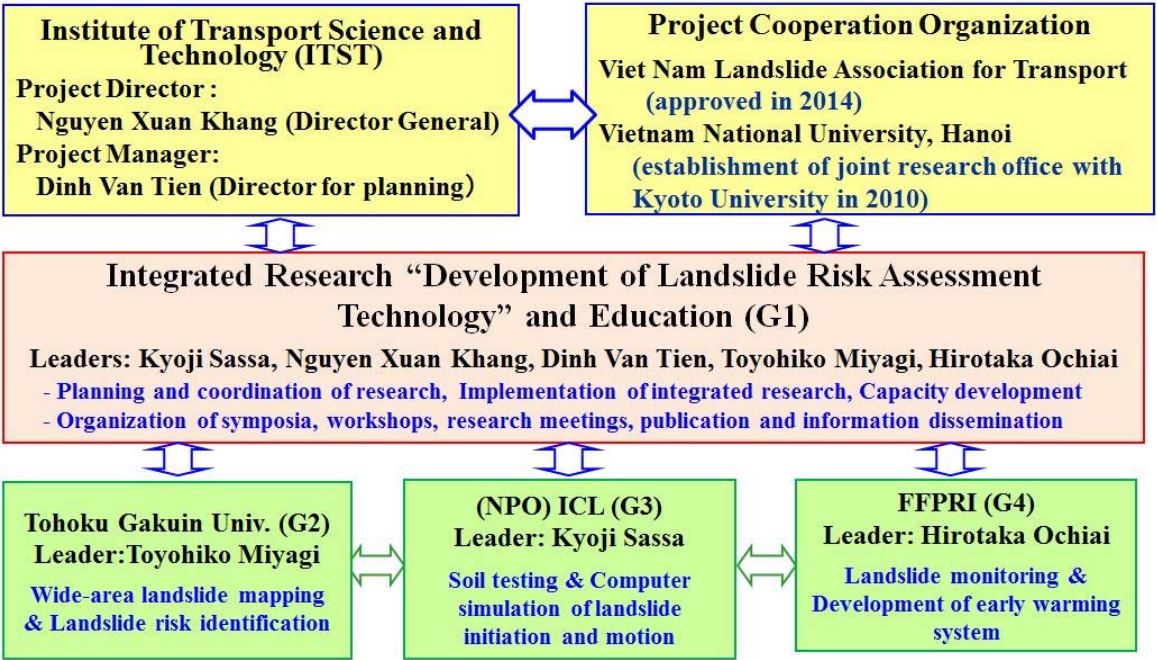
Landslide risk assessment technology to reduce landslide disasters along main transport arteries and on residential areas is developed, and education and capacity development for the effective use of this technology is implemented in Viet Nam.

Outputs

- 1. Landslide risk slopes will be identified by wide-area landslide mapping.
- 2. Landslide hazard assessment technology will be developed based on soil testing and landslide computer simulation.
- 3. Landslide risk evaluation by monitoring and early warning system will be developed.

As key issues to be overcome for National Development

Landslide risk assessment technology is established and human resources are developed for securing arterial roads crossing narrow country and securing safety of residents in mountainous area.



Expected Results

- Preparation of **integrated guidelines** for the application of developed landslide risk assessment technology and **capacity development** by **WG1 Joint Team of all groups**
- Wide-area landslide mapping and identification of landslide risk area by **WG2 Mapping Group**
- Development of landslide risk assessment technology based on soil testing and computer simulation by **WG3 Testing Group**
- Risk evaluation and development of early warning system based on landslide monitoring by **WG4 Monitoring Group**

Review of Activities (WG1)

Outline of Project Process (WG1)

1. After the adoption of SATREPS project in November 2011, using JICA and JST budgets, joint research in Vietnam were implemented in June, July and November, 2011, and in March, July, October and December in 2012, and February, April-May August, October in 2013, and March, May-June 2014. Three engineers were invited to Kyoto in January 2012, seven engineers invited to Kyoto, Sendai, Shizuoka and Matsue in May 2012, one engineer to UNESCO headquarter office in Paris in November 2012. The first JCC Meeting and the Kick-off meeting was held at ITST and MOT on 23 March, 2012. The second JCC meeting was organized at ITST on 8 May 2013, and the third and midterm evaluation meeting will be organized at ITST on 1st August 2014.
2. Project Document for activities and budget plan including the Vietnamese side budget was approved in the Government of Vietnam in December 2012 and A4 Form for equipment purchase and exemption of tax was approved by the Government of Vietnam in January 2014. Three directors/deputy directors from MOT and four Project director/Project manager/Directors of Danang Sub-institute and Road Labo from ITST were invited to Kyoto during ICL-IPL Kyoto Conference on 18-22 November 2013. ICL, ITST, MOT jointly discussed and agreed the further implementation plan including A4 form to purchase equipment in Kyoto.
3. Pilot study sites were once moved from Ho Chi Minh Route and National Highway No.1 near Danang to two landslides in Son La Province due to the proposal from Vietnam side in 2012. It was changed and moved to major transport arteries in Danang area in 2013. The current pilot study sites are the back slope of Hai Van station located the center of north and south Vietnam, Ho Chi Minh Route. Landslides along National highway No.6 are selected as additional testing sites because of close distance from ITST in Hanoi.

Review of Activities (WG1)

Capacity Development and Technological Transfer

1. Seven young researchers and engineers were invited from Vietnam to Japan to take Master's degree and Doctor's degree in the field of Landslide Risk Assessment Technology and they are studying in 4 universities; Kyoto University: one doctor and two master students, Shimane University: two master students, Tohokugakuin University: one doctor student, Shizuoka University: one master student. Three short term trainees are invited to Japan to study landslides and obtained Ph.D. as thesis doctors.

2. Vietnamese members (total 31 person x time) were invited by both JICA and JST budget for short term training, joint research, research presentation and discussion to Japan, UNESCO-Headquarters in Paris, WLF3 in Beijing from January 2012- June 2014.

3. Using MEXT budget and JST budget, ICL landslide teaching tools (TEXT, PDF and PPT) have been developed by Japanese members and cooperated international researchers from ICL. Each contributing organization has the copy right and the updating responsibility of each tool. Currently one tool was developed by VNU, Vietnam. New tools for country practices and case studies in Vietnam and a manual of ICL-2 (new ring shear apparatus for Vietnam) will be developed. All text tools will be translated into Vietnamese by long-term and short-term Vietnamese trainees. This tool is the guideline for the landslide risk assessment technology.

Review of Activities (WG2 and WG3)

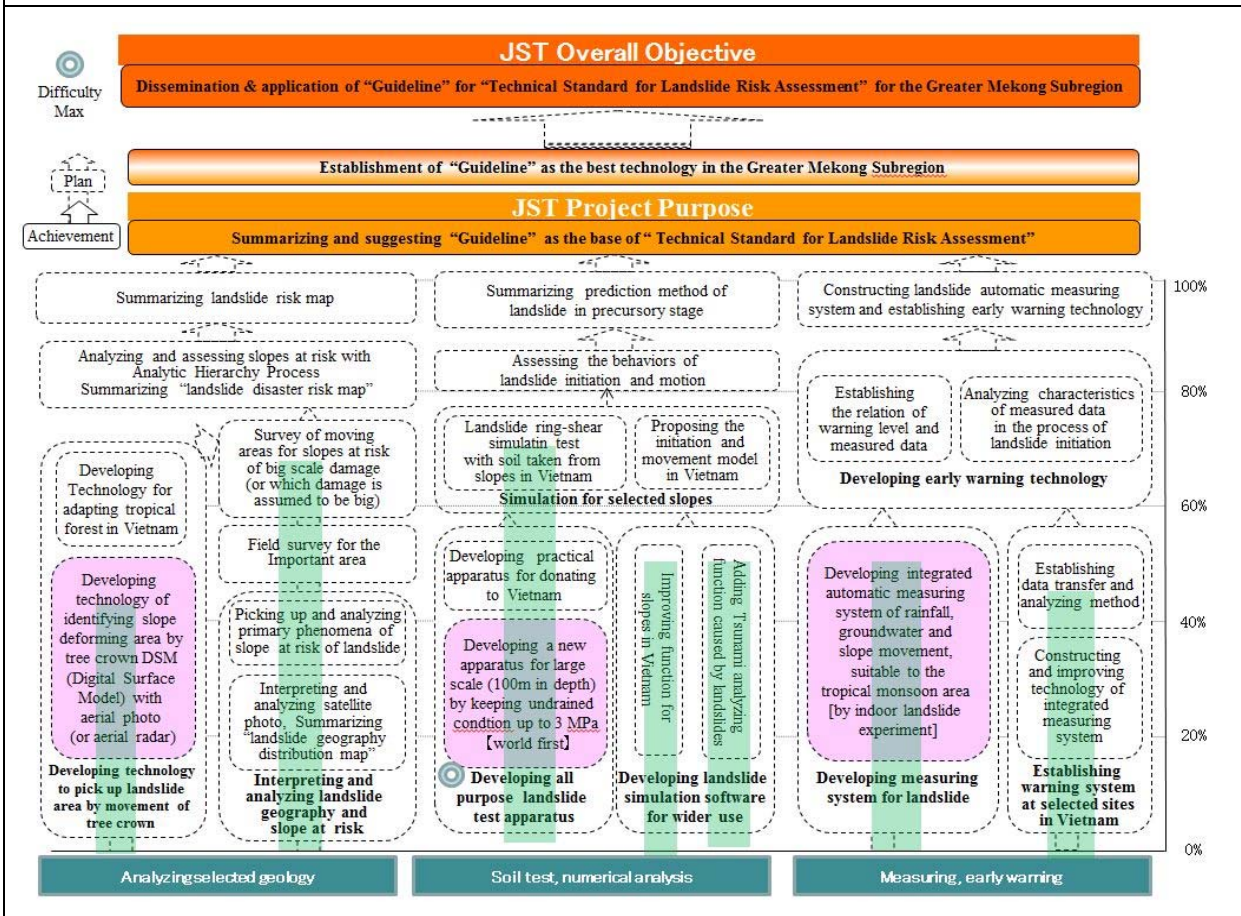
Research Progress of WG2 and WG3

WG2: Mapping group has investigated slopes along Ho Chie Minh Route (HCM) between Danang and Hue, the Haivan Station landslide area, and along National Road No.6 in Hoabinh Province near Hanoi. The group has established three sheets of landslide inventory map for HCM and one sheet for Haivan. The group identified and implemented detailed investigation on two moving slopes at risk causing big disasters from field investigation, one big landslide is No.18 landslide along HCM which might cause damages to a dam, another is Haivan Station landslide which may block the Vietnam Railway and damage passengers as well as the important mid-point station between North and South Vietnam.

WG3: Testing group has developed a new high stress ring shear apparatus using JST budget. It was applied for 1792 Unzen-Mayuyama landslide killed 15,000 persons. The results were published in the Proceedings of WLF3 2014 and accepted and published in *Landslides* in 2014. A new practical apparatus will be produced by the end of February 2015 and transported to ITST after enough training and testing in 2015. Three Vietnamese students in Kyoto University and two WG3 members invited from ITST have been trained to use it. WG3 has developed a computer simulation of landslide inducing tsunami wave and applied to the 1792 Unzen-Mayuyama.

Review of Activities (WG4)

WG4: Monitoring group developed an integrated monitoring system of extensometers, total station, and GPS in Japan. And preliminary implementation started in Hai Van Station landslide using extensometer purchased by JST budget. A slope deformation (18 mm) during rainfalls was monitored in October- December 2013. Most of monitoring equipment have already been transported to Danang, purchased or orders. Design and construction of the landslide experimental facilities has started including landslide flume and data logging system in ITST. And new multi-depth wireless tensiometer is developing.



JICA–JST Joint Project in Vietnam
Development of Landslide Risk
Assessment Technology along Transport
Arteries in Viet Nam

Progress Report
WG2 Mapping Group

Toyohiko Miyagi, WG2 Leader
Professor of Tohokugakuin University
Dinh Van Tien, Project Manager
WG2 Leader of ITST

WG2 Wide-area landslide mapping
and identification of landslide risk

Basic concept of the risk evaluation

Development the new methodology based by the mechanism
analysis and fact finding of actual landslide phenomena.

Target area 1: Quang Tri, Hue, Da Nang, Quang Nam, Quang Ngai,
Kontum province: Landslide feature have a very big diversity.

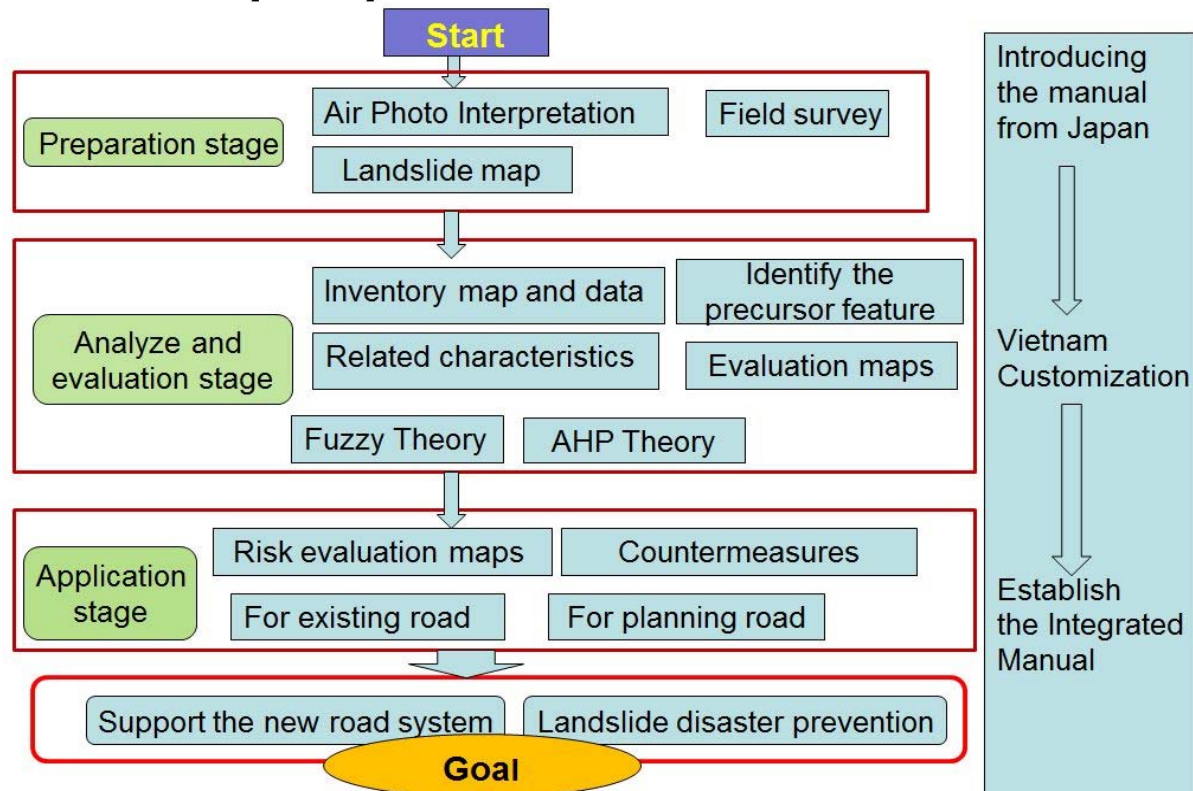
Target area 2: Haivan station landslide.

These two areas will concentrate all the project. It means the first
preferential.

Target area 3: NR.No.6 Hoa Binh province (Suburbs of Hanoi)

T. Miyagi, D.V.Tien
(ICL, Tohokugakuin University, Sendai Japan, ITST, Vietnam)

Over all perspective of V-J relations in WG2



Current Results of WG 2

• Mapping and risk evaluation in Vietnam

1. Establish the inventory map data of landslide area in Central Vietnam.
(Landslide mapping: 3 sheets 1/25000 HCM Route, 1 sheet Haivan area)
2. Identify the suspicious risky landslide area. (Risk related criteria identified)
3. Make the **inspection sheet** for reasonable field investigation. (Vietnam version is not yet producing)
4. Landslide Factor of Safety simulation carried at the KM95 landslide, Hoabinh.

• Technology development to pick up the precursor landslide in Japan and Vietnam

1. Field investigation data accumulated by two members

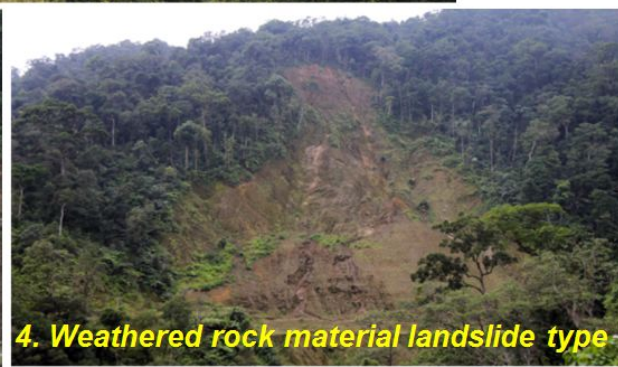
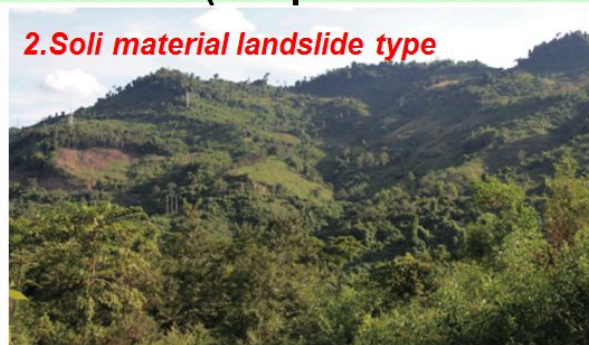
• Preparation and field visits for activities:

1. Purchase of Aerial photographs and topographic map (Aerial photograph: 1999, 1:33000, Monochrome, Direct print, 370 sheets. KhanDuc-Thanh My – A Luoi area along HCR and Haivan station area, Central Vietnam.)
2. Field visit for clarify the landslide phenomena at HCM route and Haivan station area in Central Vietnam, and KM95 landslide at Hoabinh Province along National Road No.6 near Hanoi.

The activities have been done from VN side

- Preparation materials for study
- Activities study plan: contents, progress , output products.
Study Location is in the center of Vietnam including Quang tri, Hue, Danang, Quang Nam, Kontum), along the National Highway No 1, Ho Chi Minh route (A Luoi – Prao- Thach My), National Railway line (Haivan Station).
- Survey: General about Nature of Study area (landform, geology and climate), history of landslide occurred , classification, characteristics of the element affect.
- Group workshop : introduce the Device for analysis interpretation air photo , software for Development of the technology to visualize the features of landslides, lecture about Relationship between number of Landslide's and geology feature
- Working with SACOM- Department of Defense to the support of the procedure of air photo, DEM and DSM and Map topology Map purchase.
- Discussion and submission (A4 form) Project equipment list for procedures for tax exemption
- Implementation of research content : survey sheet, detail survey trip and building up database for Mapping.
- Survey landslide site at Hải Vân railway station
to support for the group 3,4 : figure of landslide boundary direction of movement ,and support for monitoring equipment installation.

Some tentative results of field investigation Typology of landslide disasters along the HCM Road Fall type features (Slope failure type) Landslide type features(Deep seated landslide)



Typology and distribution features of Landslide along the Central HCM Route.

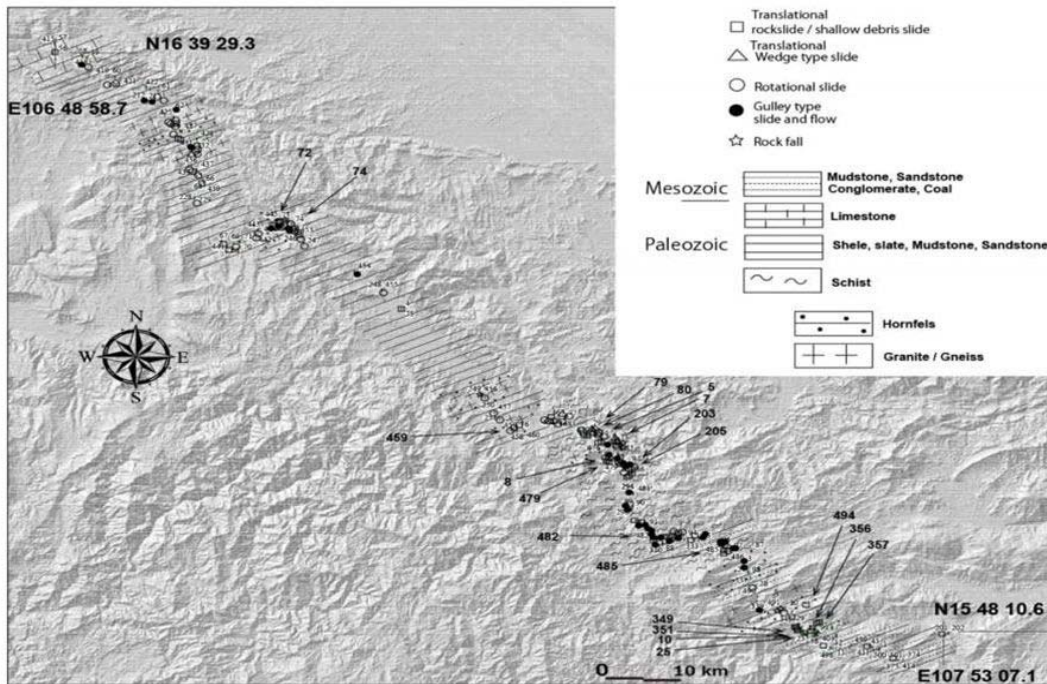
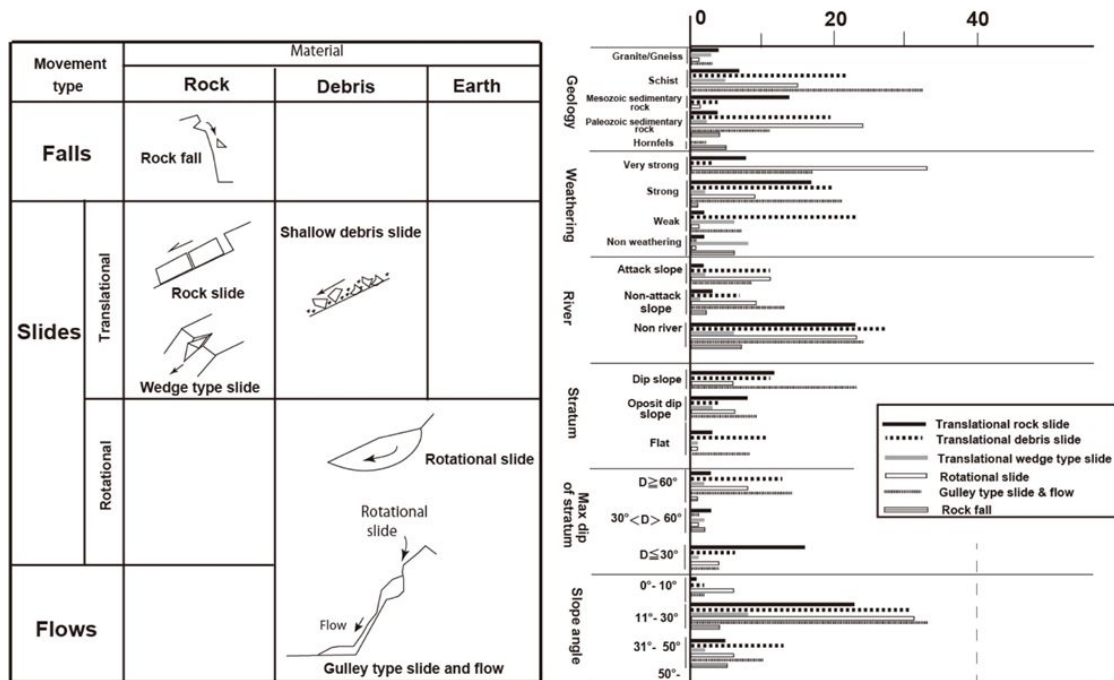


Figure 4 Landslide sites along HCMR (Numbers with an arrow are landslide sites of this paper)

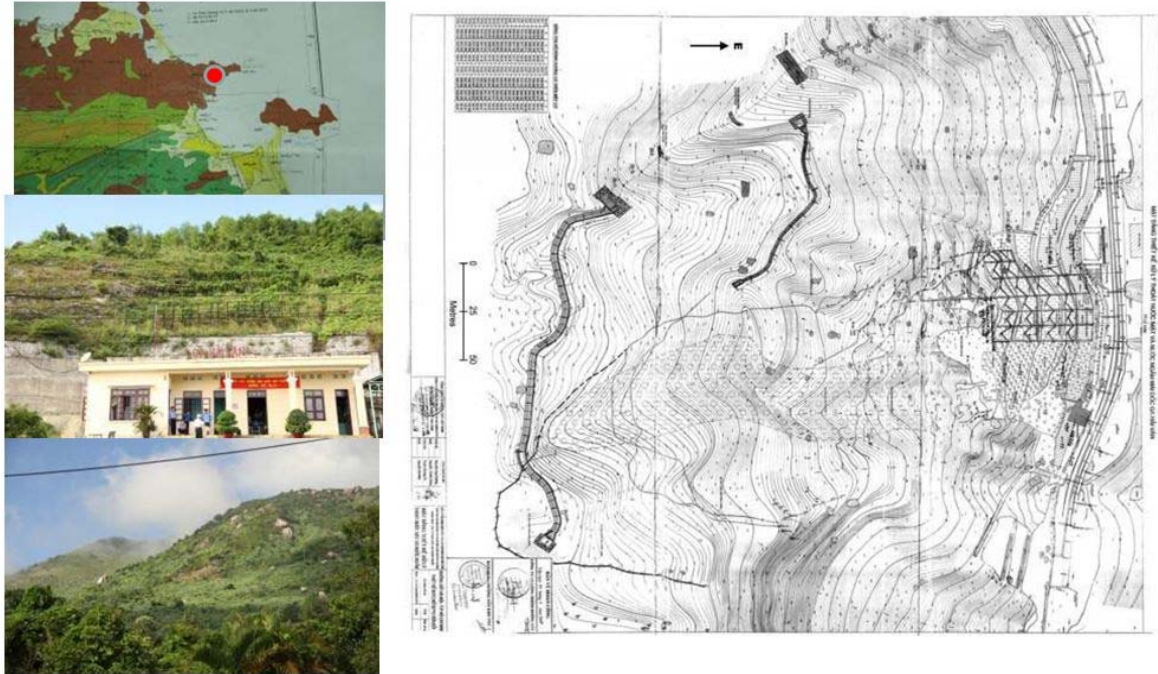
Types of landslide moving and the causative factors along the HCM route area



【Hai Van station landslide】

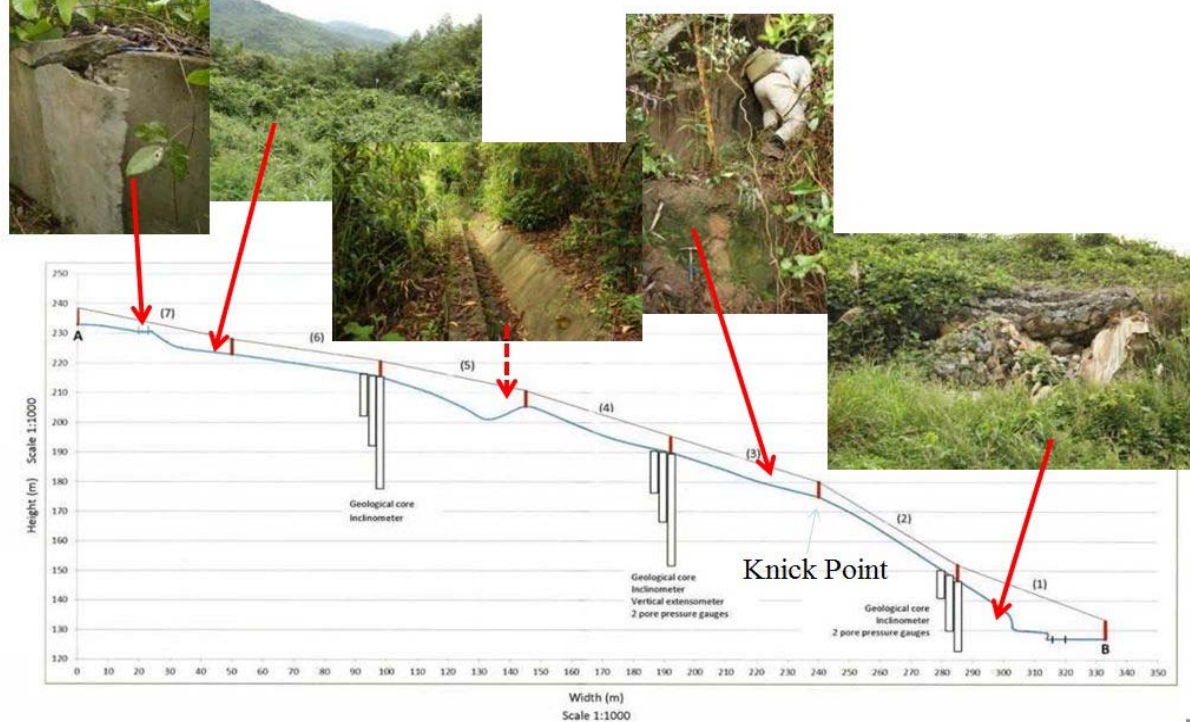
Geology of Hai Van Pass consists of Triassic granite.

In this area, hard boulders with several meters radius are left in the sand by deep weathering of granite, and they are scattered in the coastal slope like core stones. So, we can have a peculiar landscape. There are sites after collapse in the sand distribution of coastal slope.



Landform deformation relation to the landslide

Lowest part is moving strongly, Minor land deformation cracks, steppes distribute at the lower part of knick point in the cross section. The highest part also affected by mass movement.



Field Inspection Sheet (Small scale LS version)

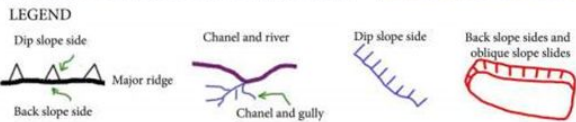
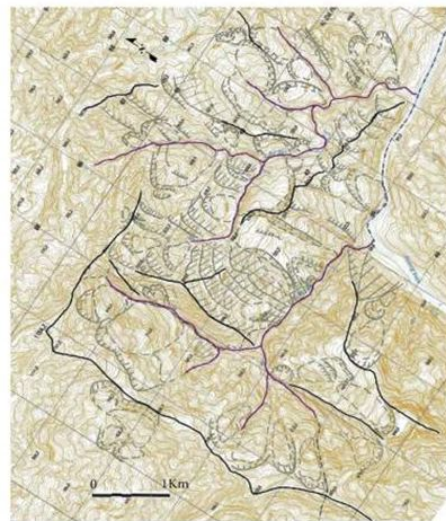
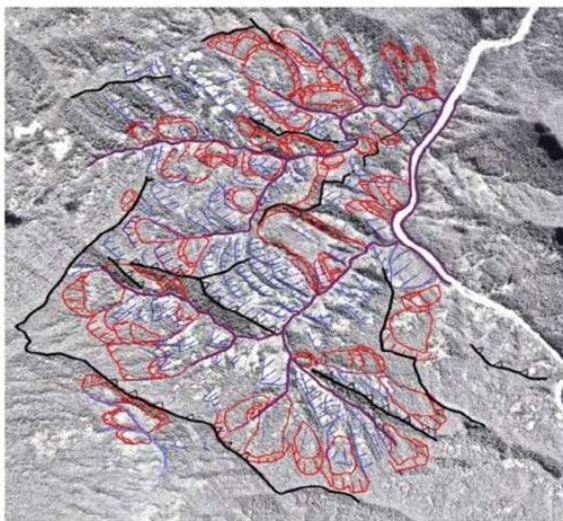
Landslide Field Inspection Sheet (Small scale LS version)				Write your risk evaluation level and the key contributing factors to the your thinking:							
Activities at the field				Check purpose for. (*)							
Location put on the map, Latitude and longitude, name of map, name of place, name of inspector, date		Illustrate the LS outline and mark the D-1		Back ground	Decide the LS area	Deduce the LS type, size, depth and the activities.	Deduce the mechanism, stage and the triggering force.	Relation to the Artificial land deformation	How contribute the risk evaluation such as AIFP and Fuzzy. (*)		
Identify factors	No	Check items	Records and descriptions								
A: Outline of LS and the geology	1	Geo-structure data from the map. (Dip Strike, Era, Key bed etc.)		5							
	2	Map and Air Photo data (Relation to the spatial arrangement of slopes)									
B: Outcrop features	1	Geomorphic setting at the slopes.									5
	2	Location of LS: Located at the attack side, slip side, terrace or hit the opposite bank.									2
	3	Type of land mass: Fresh Block, Weathered, Debris, Clayey									0
	4	Materials: Rock type, Hardness, Alternation, Metamorphics, etc.									1
	5	Spatial relation of Dip/Strike structure and the failure surface									3
	6	Distribution and the freshness of minor features such as the scarp, cracks, tiltings etc.									5
	7	Features of erosion such as Gully etc.									4
	8	Water features: Spring, oozing, percolation, surface water etc.									2
	9	Vegetation features: Tilting, Back off, Crepe dislocation etc.									3
	10	Any other remarkable features at ?									

Vertical axis: Field check items from wider to site scale view.

Horizontal axis: Evaluation view points for creation the risk evaluation method.

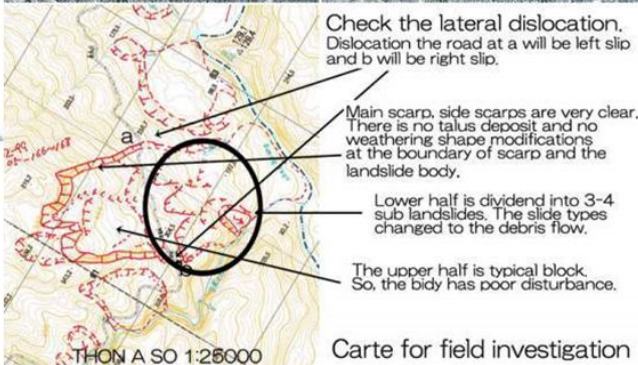
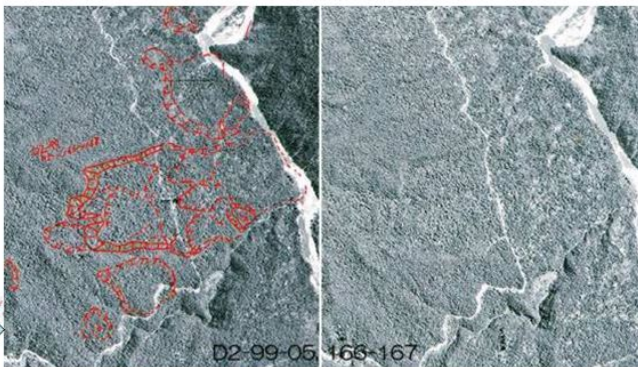
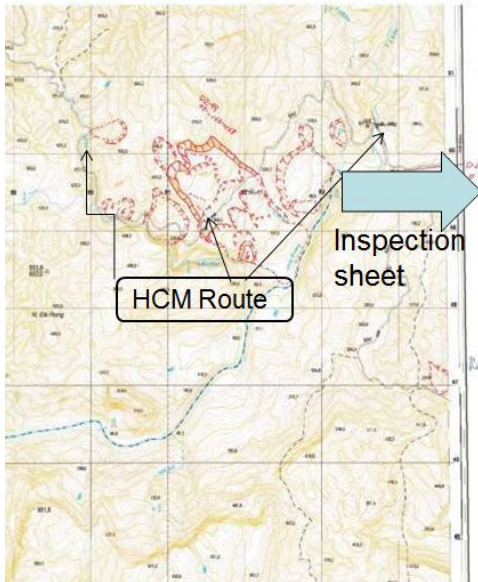
Put the value by your opinions

Large scale landslides distribute densely at a typical geo structure in Mesozoic sedimentary rock along the HCM route



Case study at LS 18 Le Hong Luong / Ngo Doan Dung

Sample of Landslide inspection sheet (API sheet)
Clear focusing for reasonable field investigation.



Facts of discussion and some photos at No. 18



Evidences of field observation

- Tilting retaining wall, Many cracks on the road
- Some dislocations appear at a part of LS body
- Some tilting trees
- Very big water come out from the middle part of the LS body
- Coal layer as the slip surface observed. The general trend of dip/strike is N40W, 15-20 S. Is this a Key bed?
- The evidences distributed at the western half of the LS area.
- LS No. 18 is very big (1km in width and 2km in length) but all part might be not active now.

Finally, the western half of the LS area must be active than eastern half.

Temporal results of the field study

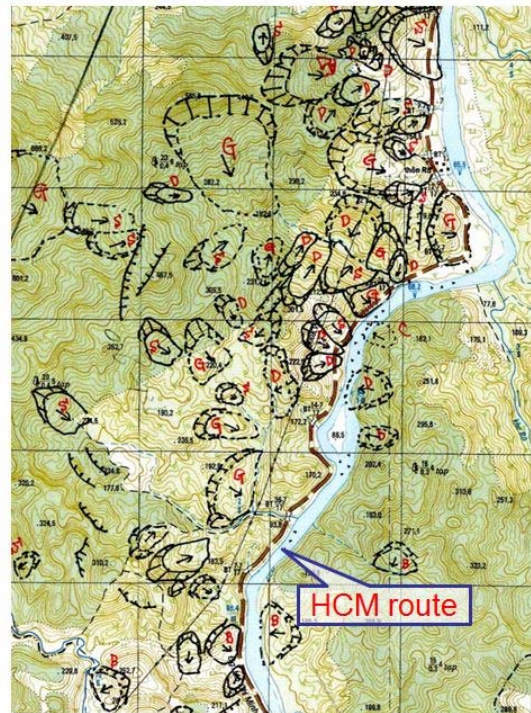
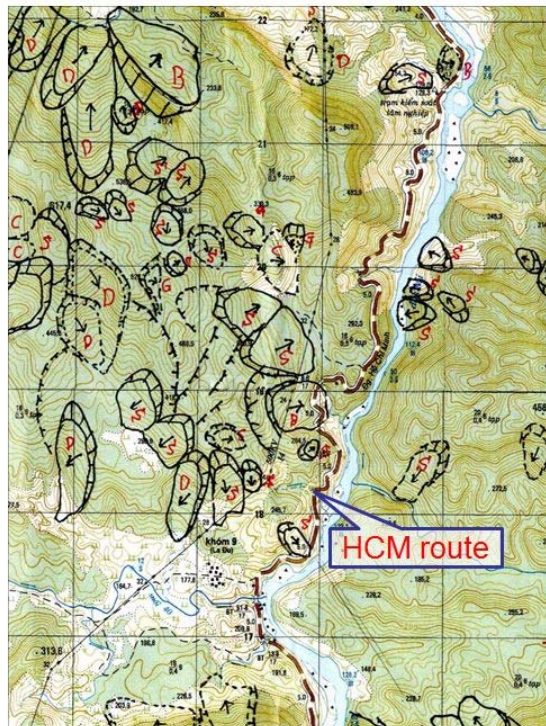
1. There are a number of Landslides distributed around No. 18 area. All of the slip surfaces is coal layer. This seems the coal layer might be control each landslide. The movement and sizes are also controlled by the structure.
2. I got the following output for my study.
 - Sometime we can recognize LS from aerial photo interpretation, but we don't know it is active or inactive, so field survey is very important
 - From field survey, we can recognize what is the most important factor which contributes to LS action.

Base on the series of study, I will make the paper this year

Modification the AHP inspection sheet based on the API

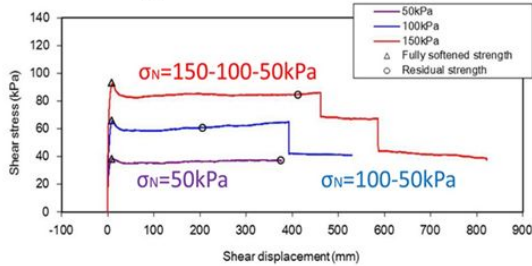
		Check list for risk evaluation of landslide				AHP score
Level II	Level III	Indicative signs of instability				sum
		High			Low	
A	a	20 Debris flow Mudflow, earth flow	13 Secondary scarps Secondary multi slump, mudflow	8 Head part depression Minor scarps	0 no sign	
	b	20 Clear and fresh surface ruptures Closely-spaced scarps & linear depression	13 almost clear and fresh surface ruptures a series of scarps & linear depression	8 not clear surface ruptures rounded scarps & buried depressions	5-0 hilly or bumpy, incision of slide mass	
B	c	10 sharp and clear crown	5 subrounded crown, talus deposition	2 rounded crown, gully erosion & talus deposition		
	d	20 collapse, Secondary slide	12 Partial collapse, Secondary slide	6 gullies small debris fan on foot	0 colluvial fan formation on foot	
C	e	20 undercut slope for mainstream or artificial excavation work	12 undercut slope for tributary or artificial work	6 slip off slope, orthogonal position to river	2 higher position of slip surface from river floor, or on terrace	0
	f	10 steep & high relief profile	5 rounded edge & convex profile	2 straight profile	0 concave profile	

Samples of Landslide distribution inventory map along the HCM route near Khan Duc town



Ring shear test data of KM95 landslide along the National road No. 6, Hoabin province

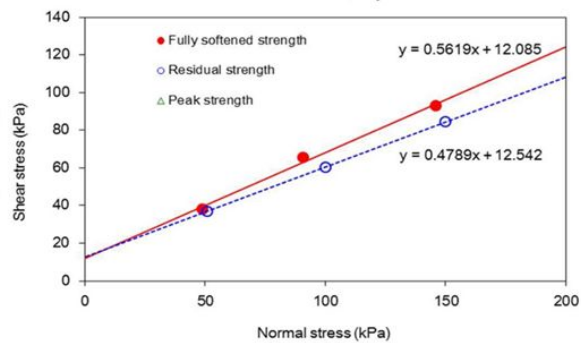
Ring shear test



$Cs' = 12.17\text{kPa}$, $\phi s' = 29.27^\circ$
 $Cr' = 12.54\text{kPa}$, $\phi r' = 25.59^\circ$



Shear surface

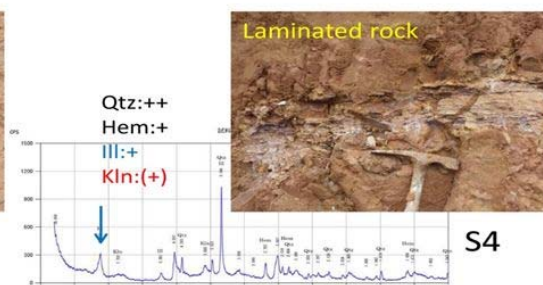
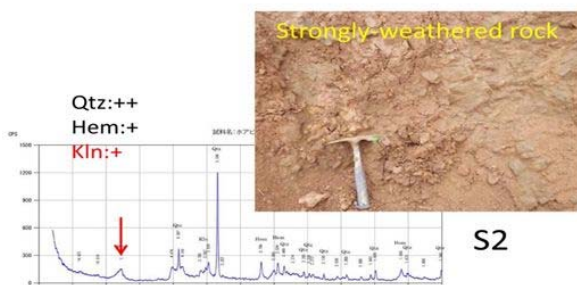
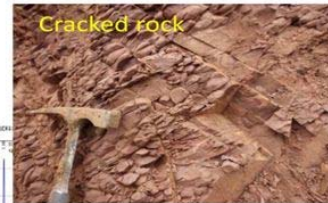
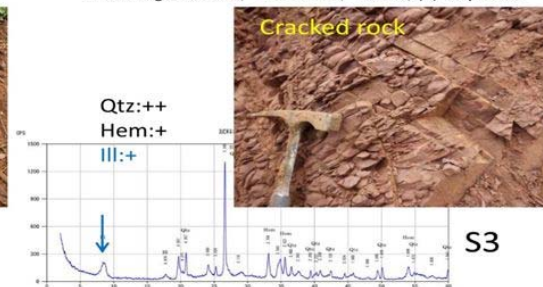
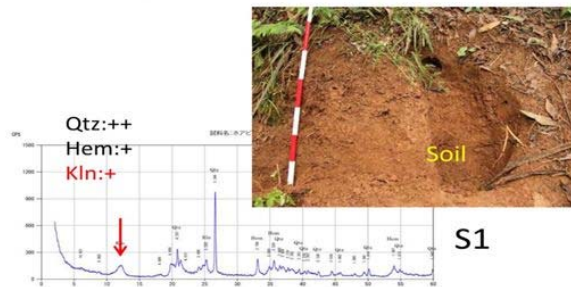


KM95 X-ray diffraction analysis

X-ray diffraction analysis

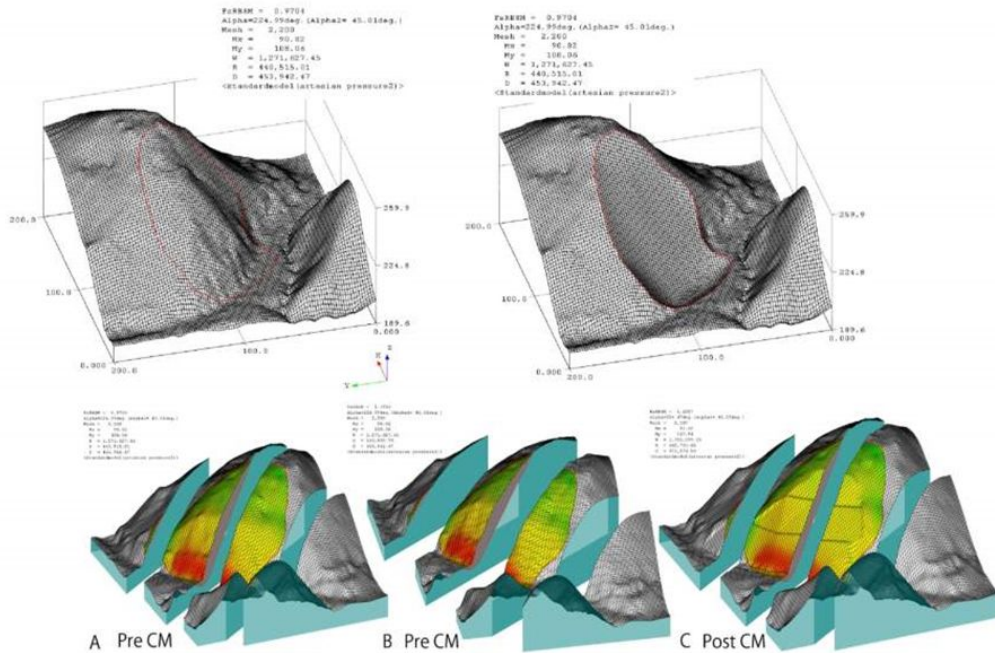
Mineral assemblages

Qtz:Quartz, Hem:Hematite, Ill:Illite, Kln:Kaolinite
 +++ strong reflection, ++ medium, + weak, (+) very weak

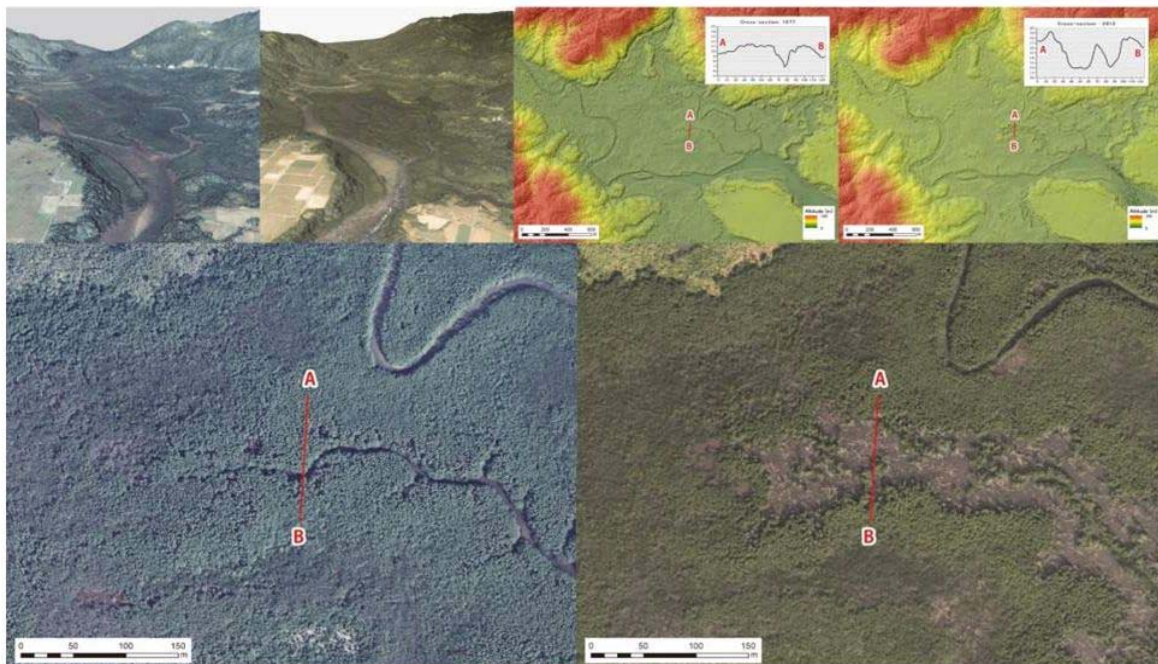


Focusing on clay minerals, fresh rock samples contain illite. On the other hand, weathered rock samples contain kaolinite.

Changes the SF by the urgent counter measure at KM95 landslide at NR No.6, Hoabinh



SfM base DSM establishing Mangrove forest crown destruction by typhoon

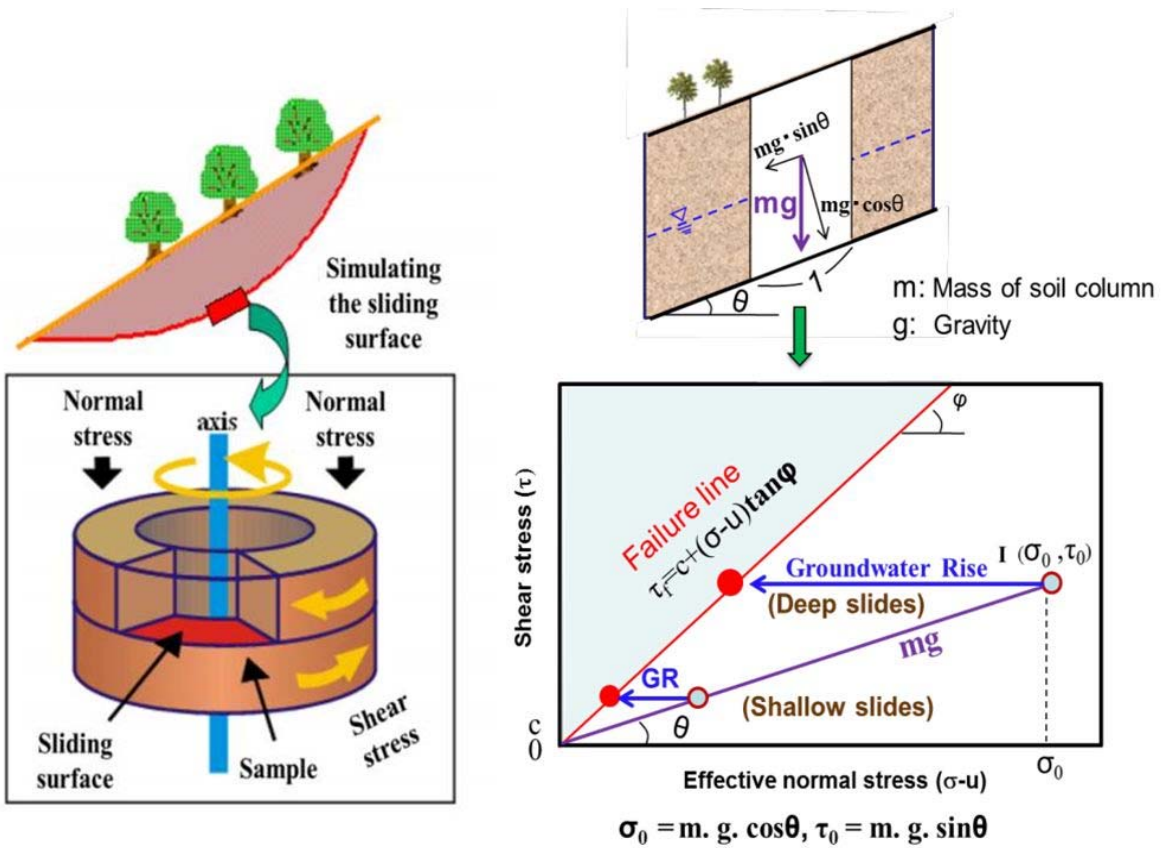


JICA–JST Joint Project in Vietnam
Development of Landslide Risk Assessment Technology along Transport Arteries in Viet Nam

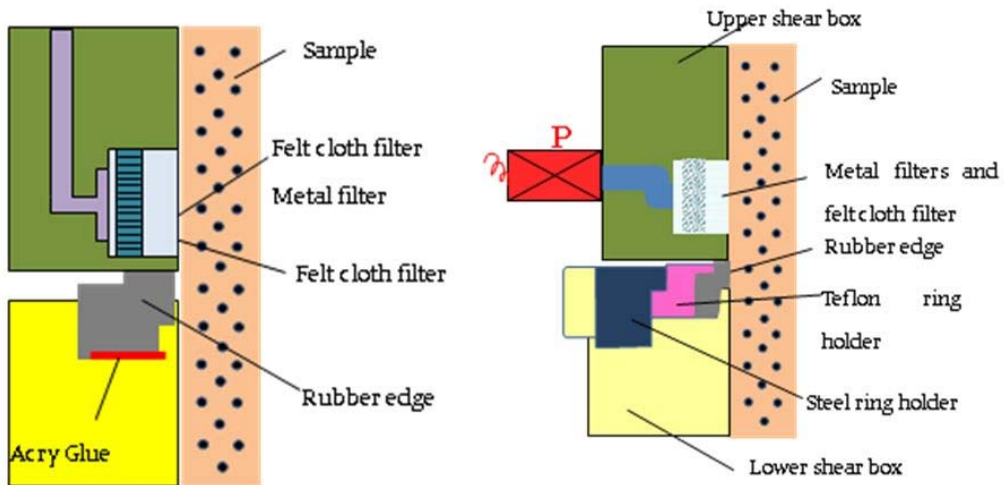
Progress Report
WG3 Testing Group

Kyoji Sassa
Lam Huu Quang

WG3 Leader
WG3 Leader of ITST



Undrained sealing of the gap in DPRI-6 (left) and ICL-2 (right)



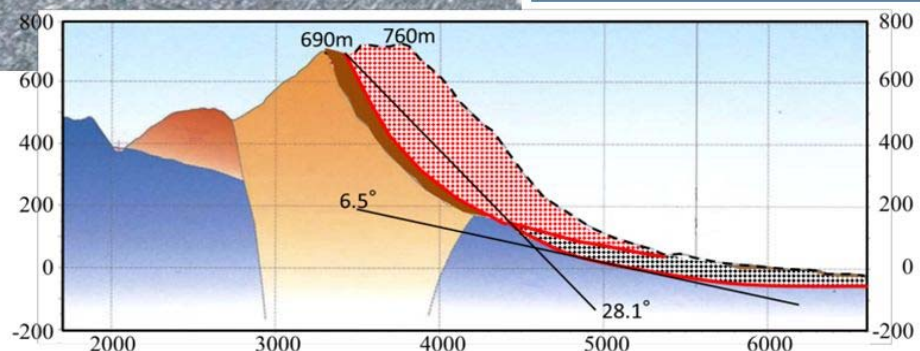
Rubber edge was pasted to the lower ring metal by glue in DPRI-6. Red color is glue.

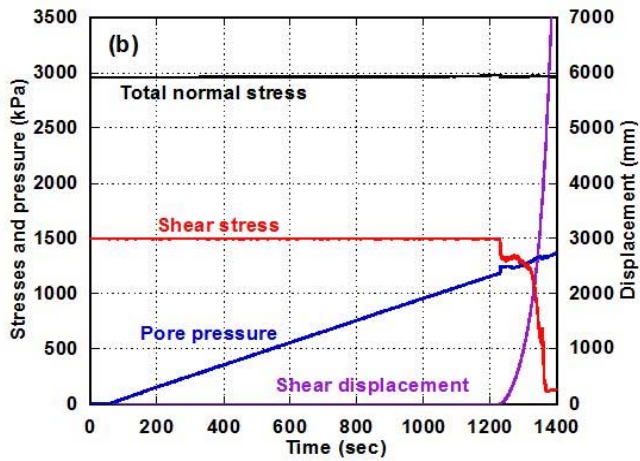
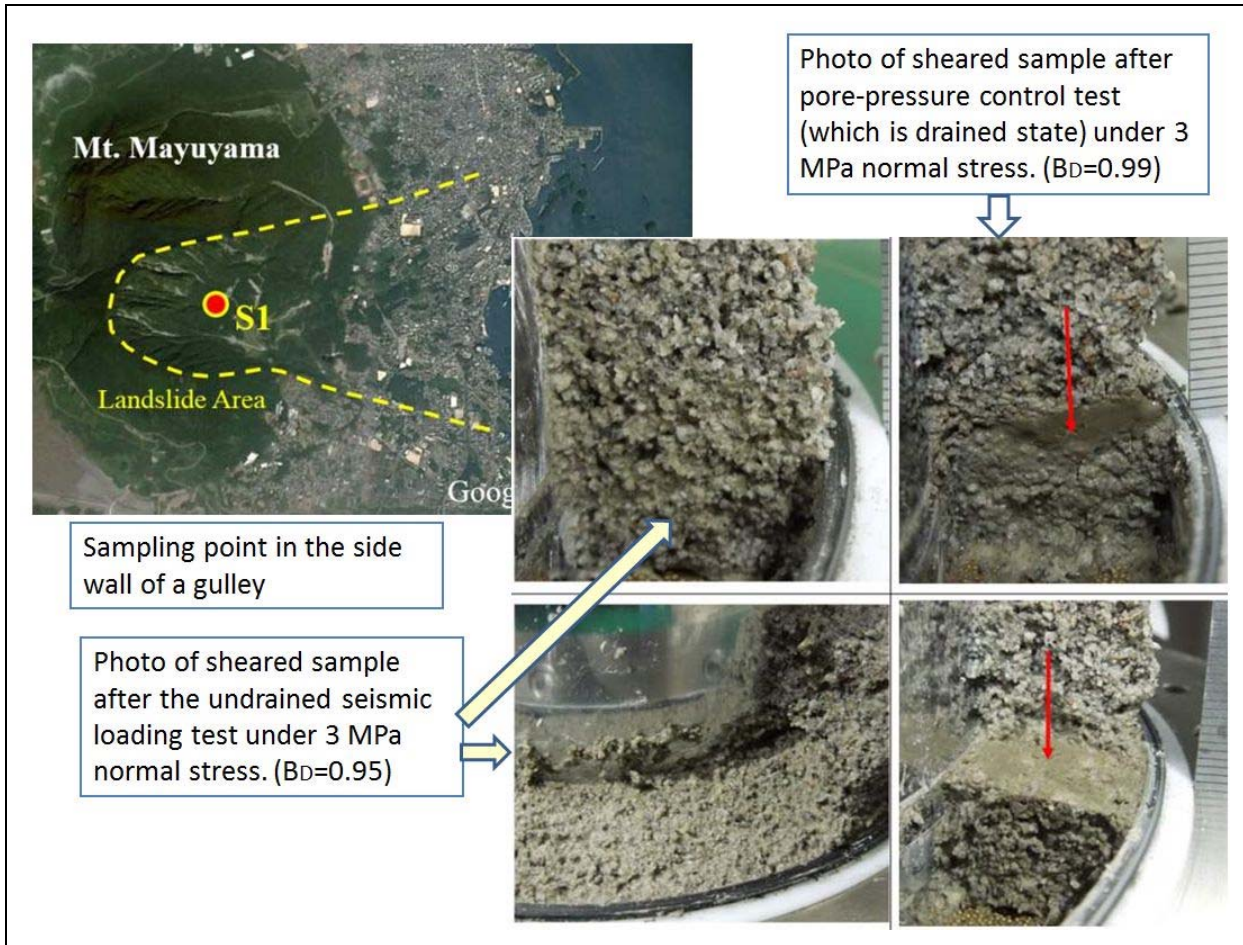
Rubber edge was pressed by Teflon ring which is pressed by metal ring in ICL-2. No glue is used. Glue can not be a completely equal thickness. It disturbs the necessary equal height of rubber edge for undrained condition under a high pressure.



Google photo of the 1792 Mayuyama landslide

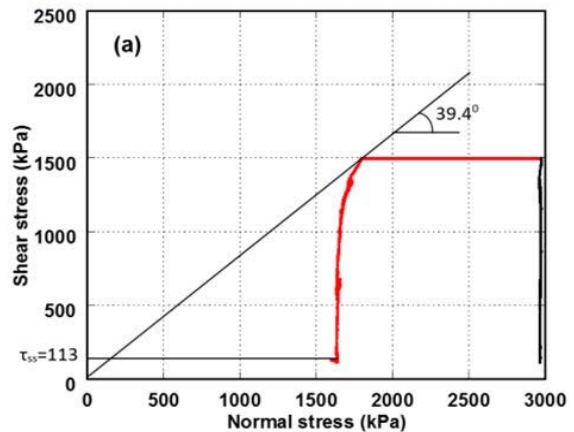
The section of the 1792 Mayuyama landslide (MLIT Unzen office, Japan 2002). The red and black dots in the landslide mass and two lines are interpretation by Sassa 2013

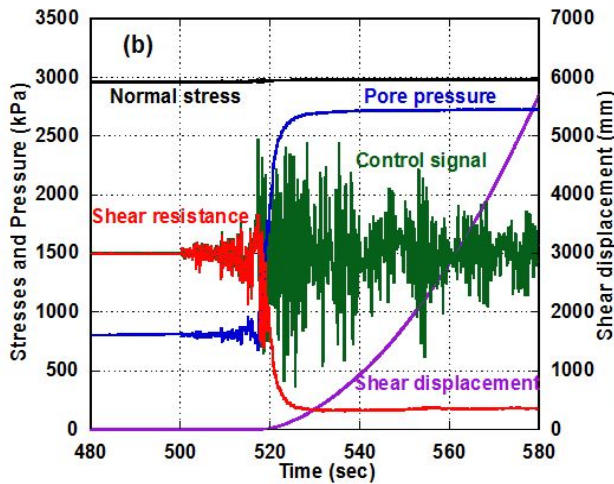




Landslide initiation test by increasing pore pressure. This test allows the volume change. Pore water pressure can move out/in the shear box. Namely drained test until failure.

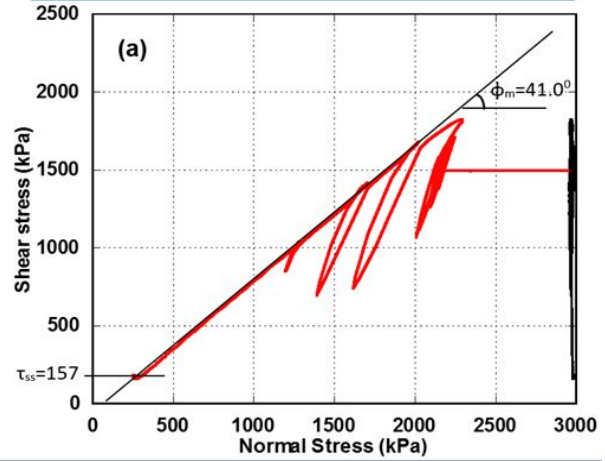
Failure occurred at the friction line of 39.4 degrees. Rapid shearing started after failure. The pore pressure generated inside the shear zone was well monitored.





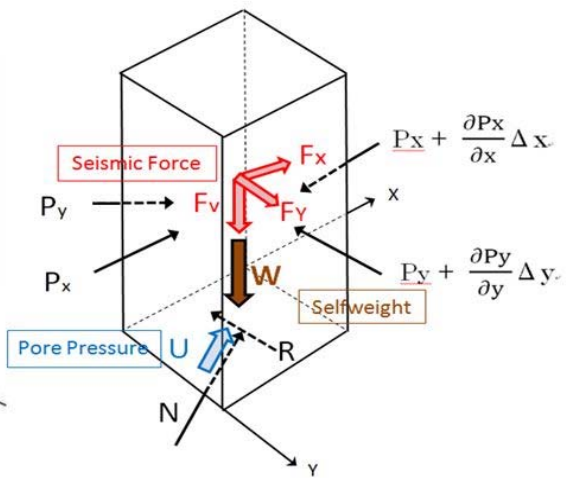
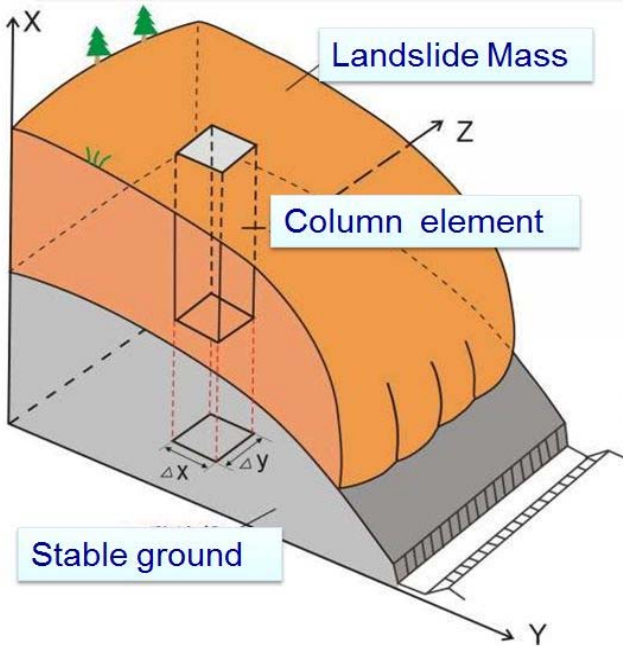
1. Initial normal stress (3 MPa) and shear stress (1.5 MPa) corresponding 26.6 degree were loaded.
2. Initial pore pressure (Pore pressure ratio : 0.27) was loaded.
3. The seismic wave of the 2008 Iwate-Miyagi earthquake triggered 67 million m³ landslide was loaded.

Failure occurred at the friction line of 41.0° (39.4°)
 Steady state shear resistance was 157 KPa (113 kPa)
 The necessary seismic acceleration was 216 cm/s².

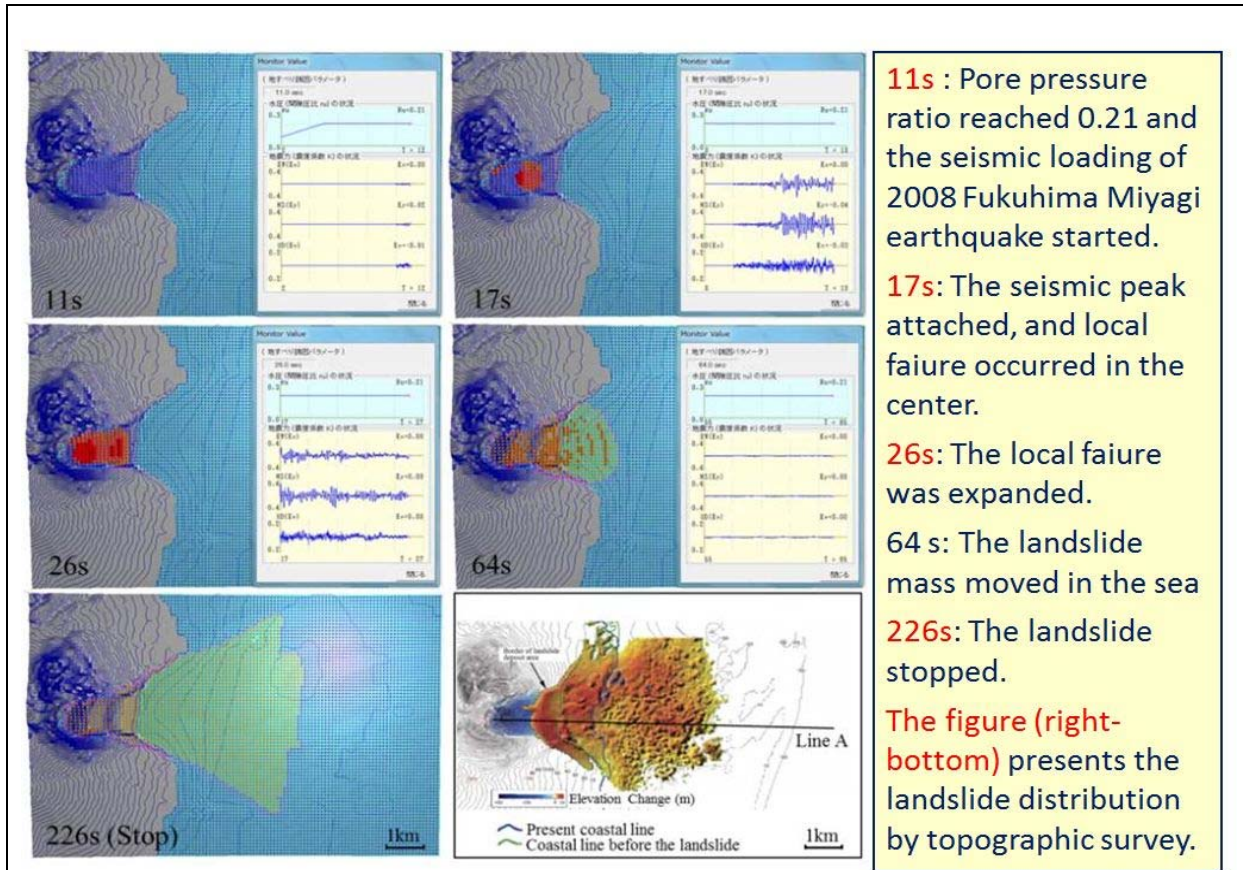


Integrated Landslide Simulation Model

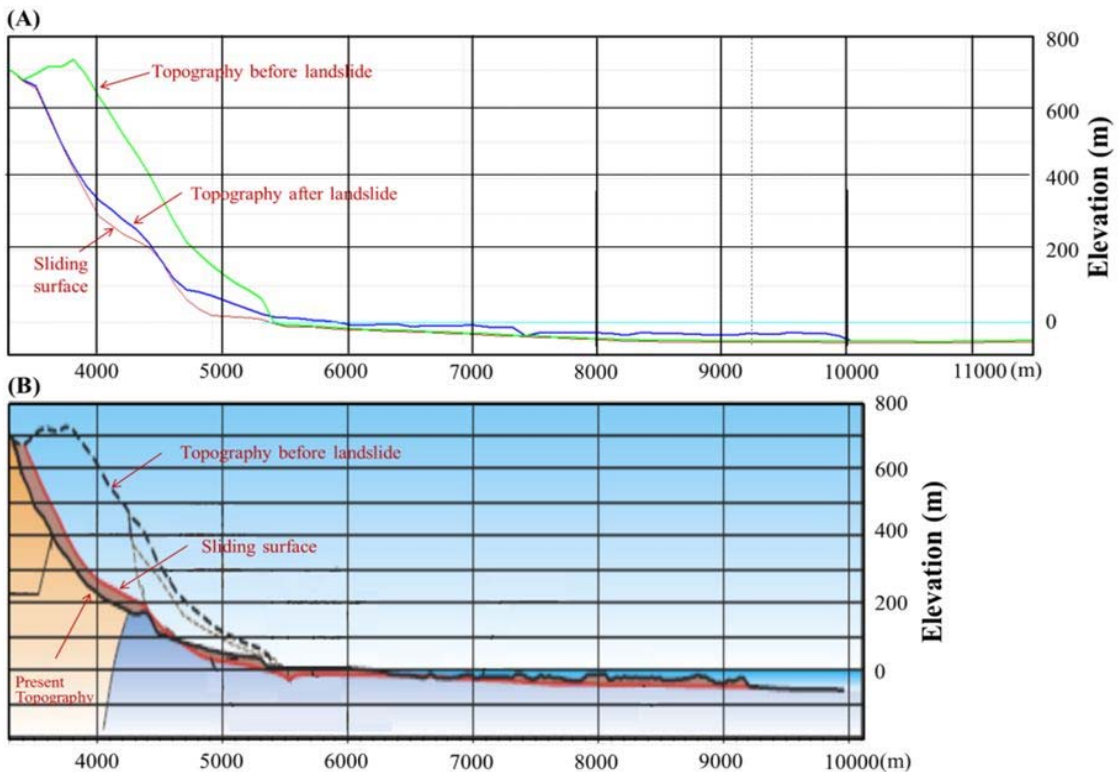
It can simulate the initiation and motion of landslides triggered by earthquakes and rains. It is calculated using the steady state shear resistance measured by the undrained ring shear apparatus.

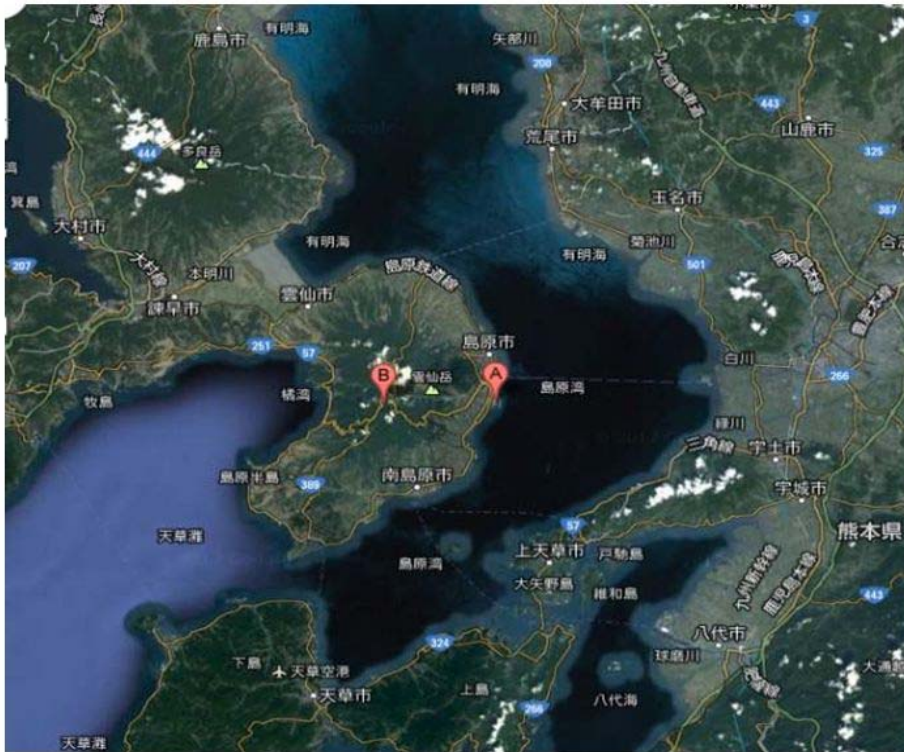


Forces acting on a column



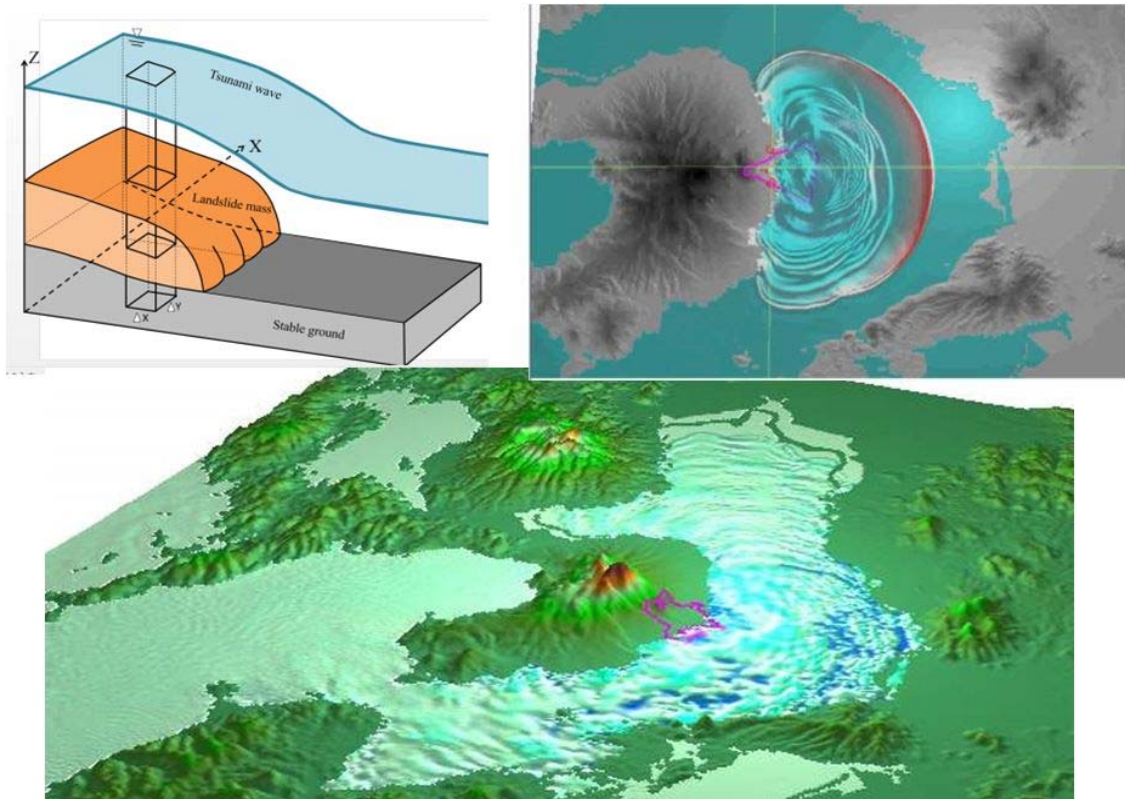
Comparison of the central section between the Ring-based LS-RAPID estimation and the topographic survey by MLIT 2002





A large landslide induced Tsunami wave and killed 15000 people in Japan. A Hai van station landslide may cause Tsunami if a rapid landslide occurs.

Modeling of landslide-triggered tsunami for the 1792 Unzen Mayuyama case



Sampling from a mountain ridge (No.1) and from the middle of slope (No.2)



Haivan- 2 (Less weathered white granitic sands) for deep landslides



Haivan- 1 (weathered brown granitic sands) for shallow landslides.

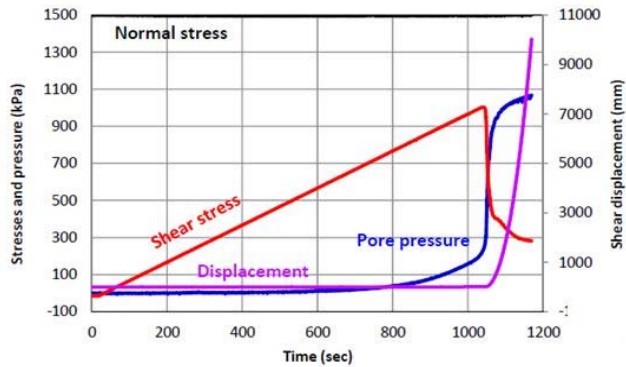


Fig. 1. Undrained stress control test on Haivan-2 with time series data

- 1 Date: 2014.6.25
- 2 Operator: Quang, Thanh, Loi
- 3 Sample: Haivan-2
- 4 Type of test: Undrained Stress Control
- 5 Drainage condition: Undrained
- 6 Specimen preparation: Saturated
- 7 $\alpha = 0.9$
- 8 Contact force: 1.5
- 9 BD value: 0.95
- 10 Consolidation $\sigma = 1500\text{kPa}$, $\Delta\sigma = 1\text{ kPa/sec}$
- 11 Shear stress control: $\tau = 1500\text{kPa}$, $\Delta\tau = 1\text{kPa/sec}$

The first successful test on the Haivan-2 sample using the developed ICL-2 undrained ring shear apparatus. Time series data (Left) and stress path (below) of a shear-stress monotonic-loading test.

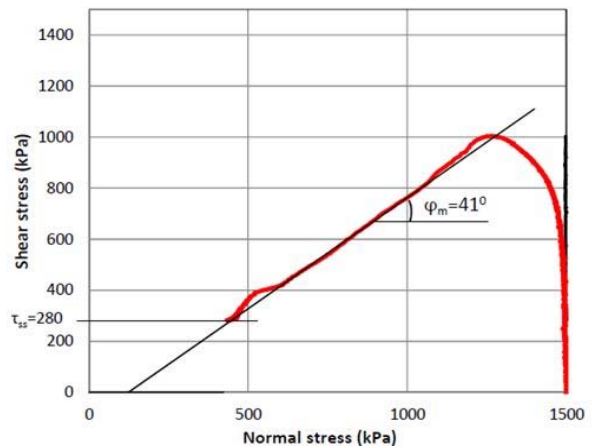


Fig. 2. Stress path of undrained stress control test on Haivan-2

JICA–JST Joint Project in Vietnam
**Development of Landslide Risk Assessment
Technology along Transport Arteries in Viet Nam**

Progress Report
WG4 Monitoring Group

Hirotaoka Ochiai **WG4 Leader**
**Director of Planning Dept., Forestry and
Forest Products Research Institute**
Huynh Dang Vinh **WG4 Leader of ITST**

**Group 4: Development of landslide monitoring
and early warning system**

Leader: Hirotaoka Ochiai

Research plan of this year

1. Test area for measuring is selected and observation system is established.

Hai Van station area near Da Nang city was selected as the first test site and observation items were selected. And their installation and measurement have started.

2. Observing wide movement of landslide

Items of the measurement such as total station and surface extensometer were selected and basic layout was planned. Access route to the total station base will be opened until summer.

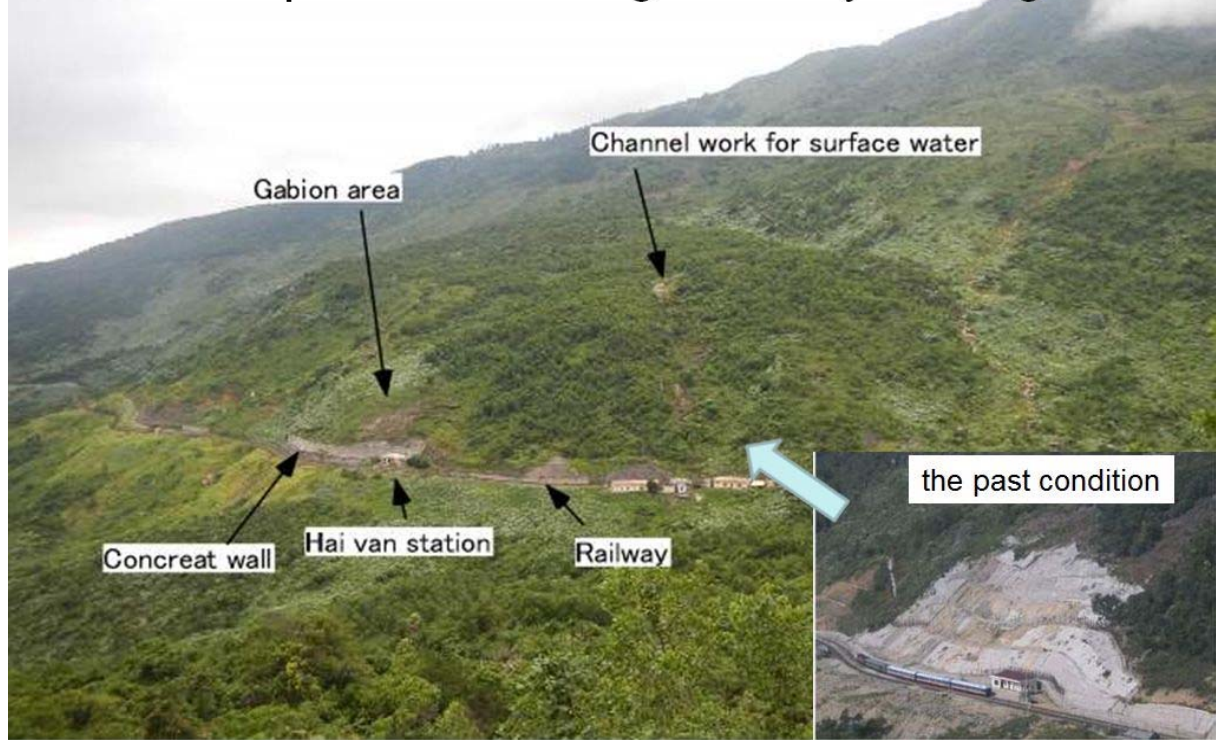
3. Development of automatic measuring system

Performance testing of surface extensometers in the active landslide area in Japan was started. Multi-depth wireless tensiometer was started to develop.

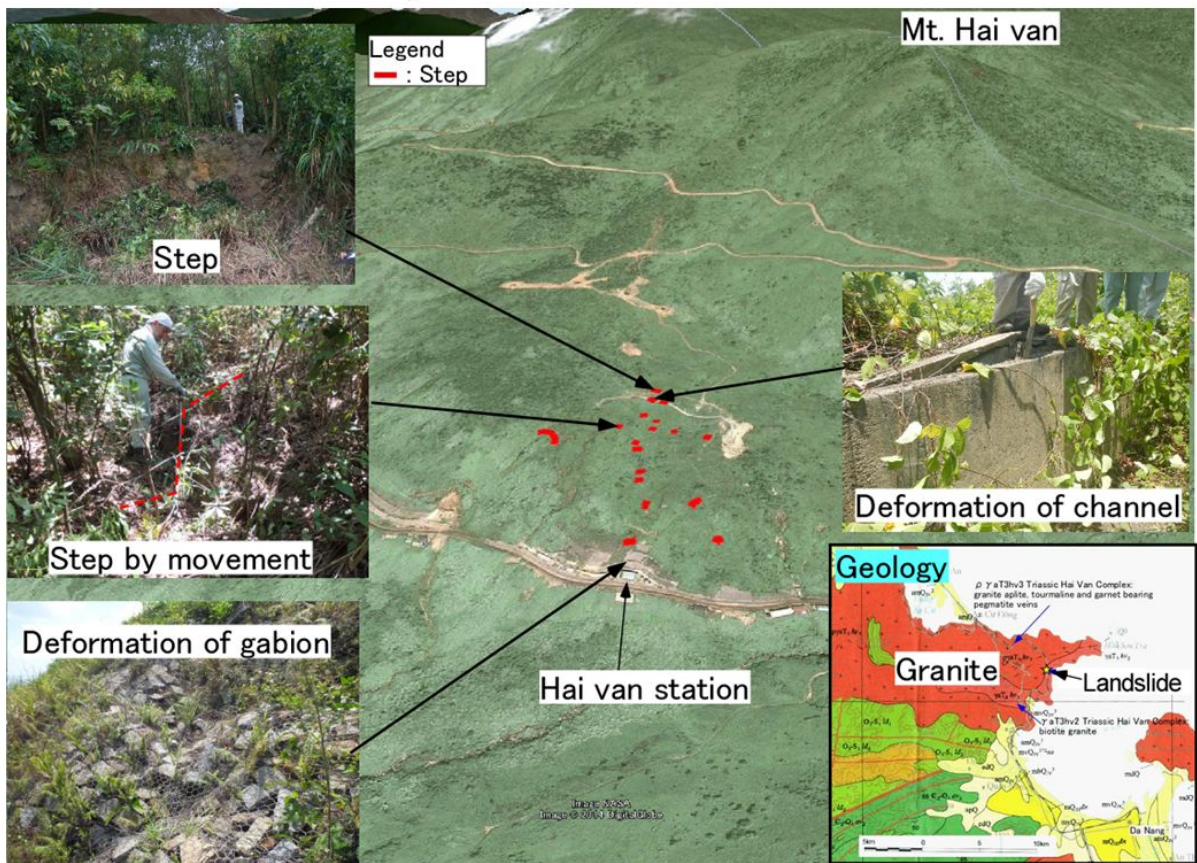
4. Preparation of landslide experiment facilities

Outline of the facilities for landslide experiment with rainfall simulator and their construction plan at ITST was discussed and will be designed. Their construction could be done in this fiscal year.

Field survey at Hai Van station landslide and total plan of monitoring and early warning



Field survey at Hai van station landslide area



Monitoring and early warning system

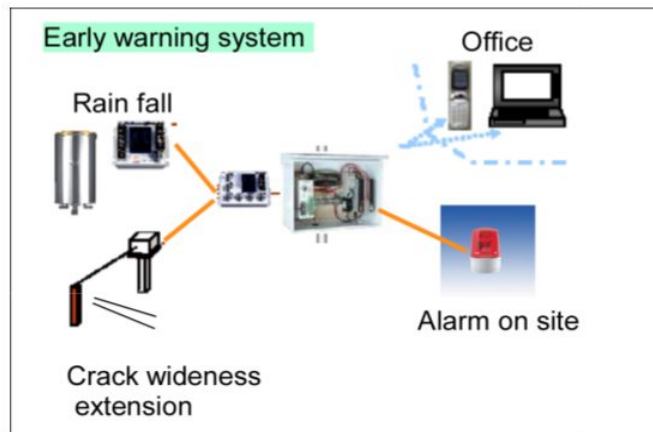
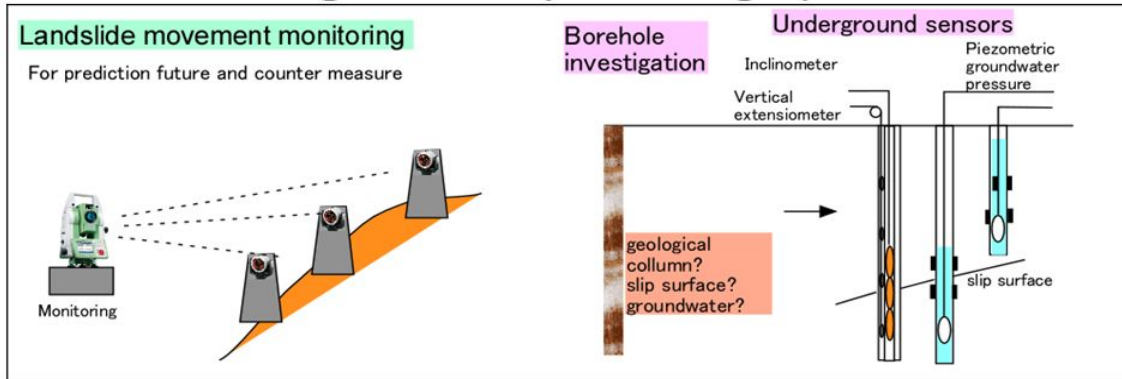
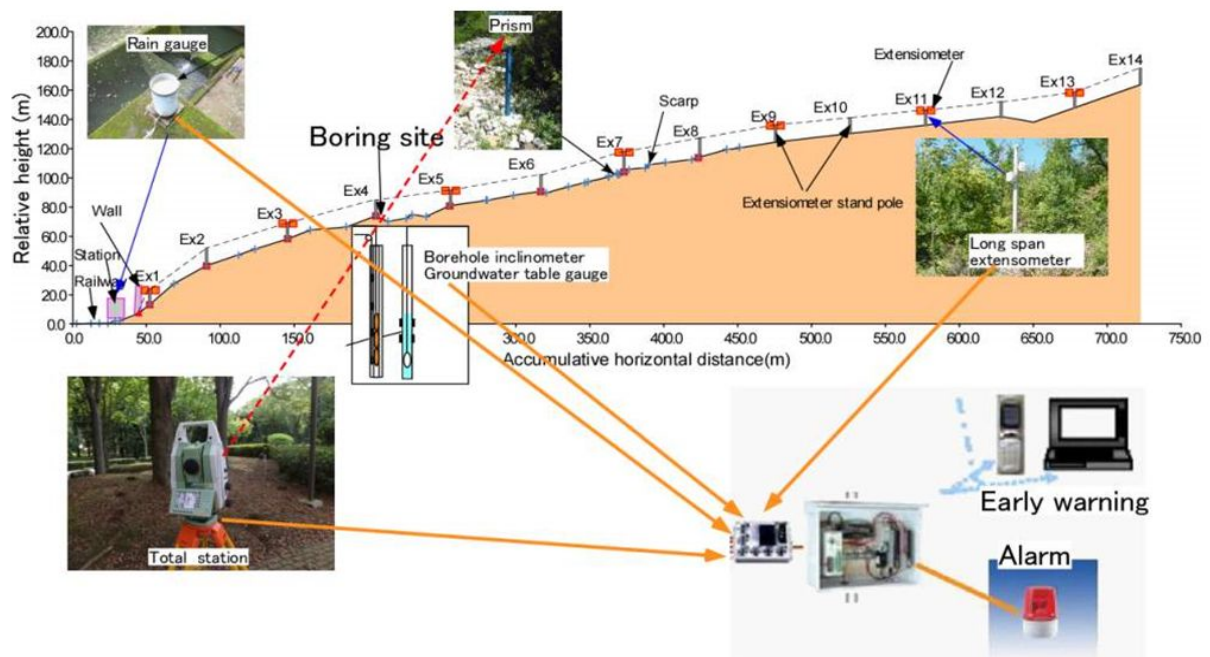
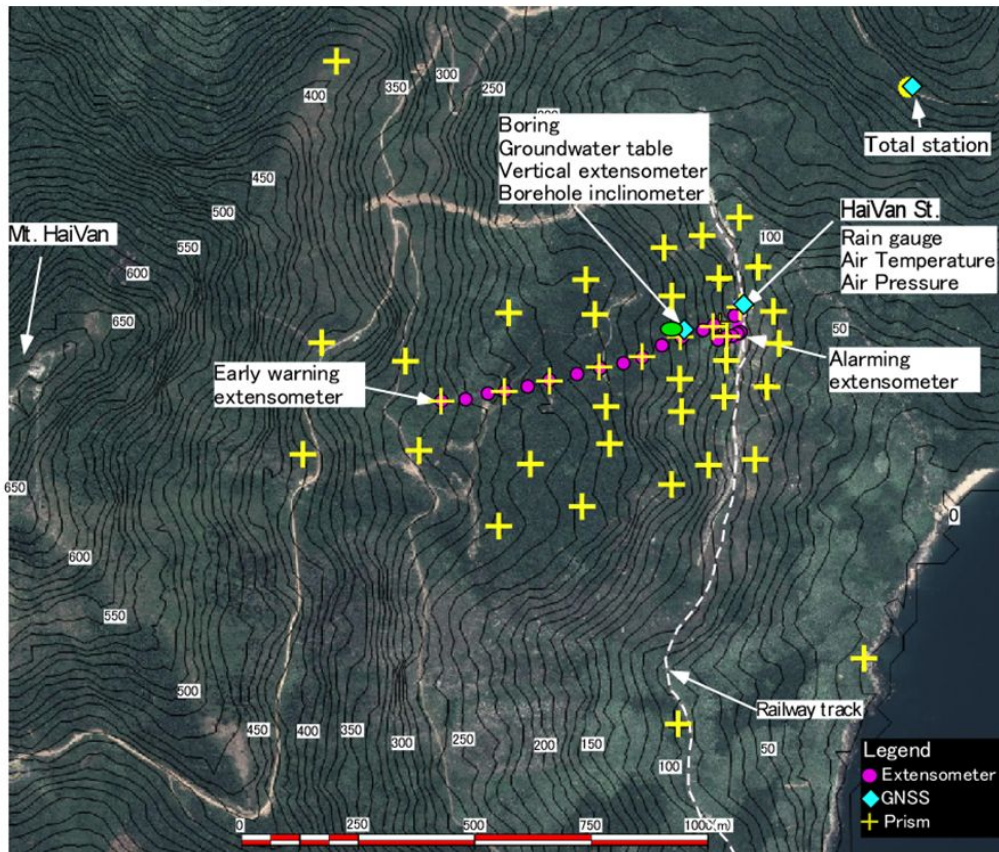


Image of observation and example of sensors

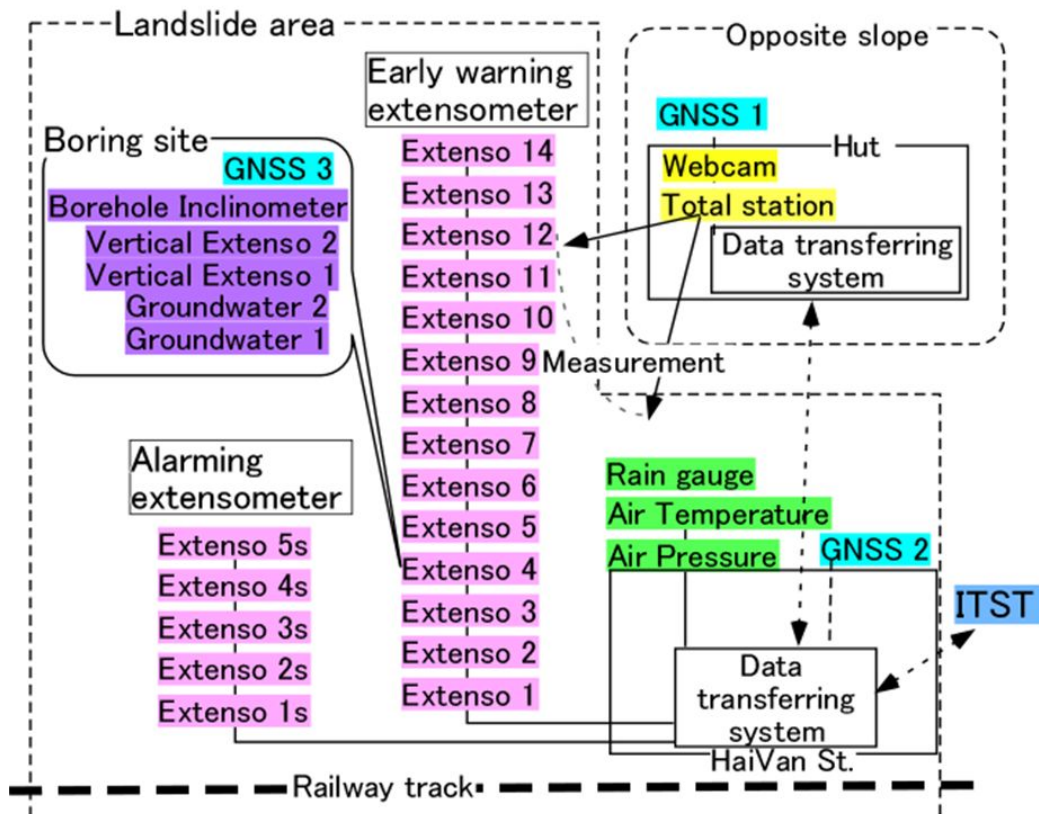


Observed data is transferred to main server and used for risk assessment.

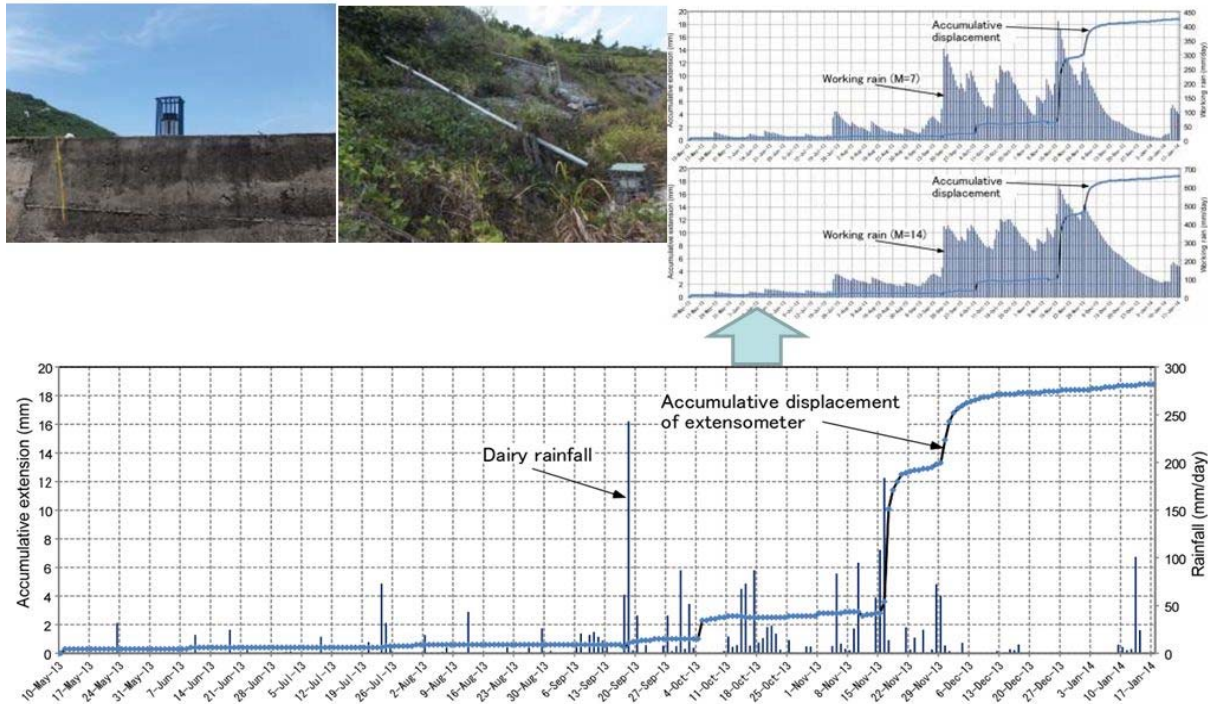
Monitoring sensor in Hai van station landslide



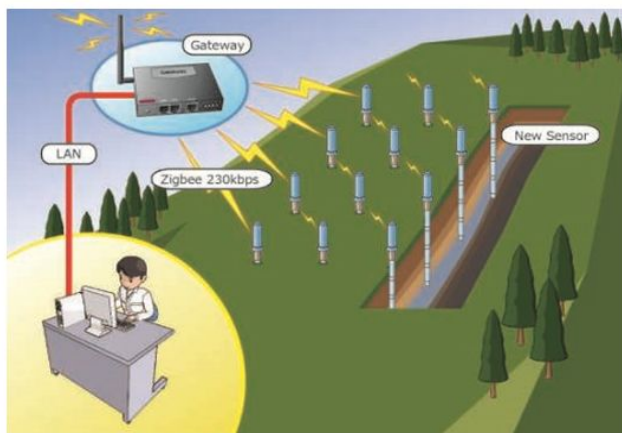
Monitoring data transferring in Hai van station landslide



Preliminary Observation of rain and displacement in Hai van



Development of Multi-depth Wireless Tensiometer



Development of new tensiometer using landslide flume

Based on the existing (mono-depth wired) tensiometer, wireless tensiometer is developed for measuring multi- depth and wide area. The performance tests have started by using landslide flume with artificial rainfall at FFPRI and DPRI(Disaster Prevention Research Institute) in Tsukuba from 2014.



Applicability will be tested at actual slopes of selected areas in Vietnam, then it becomes possible to monitor the occurrence of saturated groundwater widely, which could be the direct trigger of shallow landslide initiation in the extremely heavy rainfall under the climate change.



Performance test using landslide flume with artificial rainfall at FFPRI

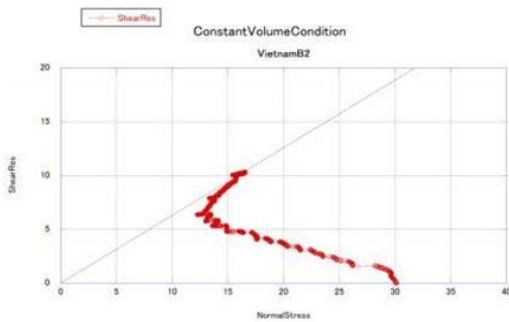
Preparation of landslide experimental facilities



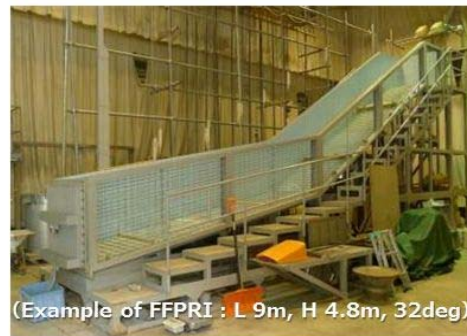
Landslide experiment facility with rainfall simulator

In fiscal year 2013, experiment facility was designed and the building was made. Data logging system and sensors are developing. Design of the testing flume has been started based on the soil properties of the weathered Granite taken from Hai Van area.

Participation of Vietnamese students in developing apparatus, observation and experiment are encouraged for human resources development. They are expected to be the key persons after they returned to Vietnam.



Soil properties of the weathered Granite taken from Hai Van area.



Design of the testing flume has been started.



Proceedings of the SATREPS Workshop on Landslides in Vietnam, 2014

Test results of a new high-stress ring shear apparatus (ICL-2) developed for Vietnam Project

Khang Dang^{1,2}, Kyoji Sassa¹, He Bin³, Osamu Nagai²

1) International Consortium on Landslides, Kyoto, Japan, e-mail: sassa@iclhq.org

2) Graduate School of Engineering, Kyoto University, Kyoto, Japan, e-mail: khangdq@gmail.com

3) State Key Laboratory of Lake Science and Environment, Nanjing Institute of Geography and Limnology, Chinese Academy of Sciences, Nanjing, China

Abstract Recently, a new high-stress ring shear apparatus is developing by Sassa and others in the International Consortium on Landslides (ICL) and named ICL-2. This apparatus is a part of Japan-Vietnam project on development of landslide risk assessment technology starting from 2011 and supported by the Science and Technology Research Partnership for Sustainable Development Program (SATREPS) of Japan. ICL-2 can simulate the initiation and motion of megaslides with more than 100 m depth. The undrained capacity succeeded of ICL-2 is 3 MPa, while maximum capacities in previous ring shear apparatus were only 1 MPa. This apparatus was applied to interpret the initiation and motion of 1792 Unzen Mayuyama megaslide which was triggered by an earthquake. This landslide directly killed 10,139 people in Shimabara area and the landslide mass entered into the Ariake sea and induced a large scale tsunami which killed 5,015 people in the opposite bank (Kumamoto Prefecture) and islands in Ariake sea. During a field investigation, two soil samples were taken from the source area and moving area for simulating initiation and motion of the landslide respectively. After that, parameters obtained by the tests were inputed to the integrated computer simulation model to estimate hazard area. This paper presents test results of ICL-2 which was rewritten based on the research of Sassa, Dang et al (2014) published in Landslides as “Development of a new high-stress undrained ring shear apparatus and its application to the 1972 Unzen-Mayuyama megaslide in Japan”.

Keywords Ring shear apparatus, ICL-2, Megaslide

Basic tests of the ICL-2 high-stress dynamic-loading undrained ring-shear apparatus

To examine the rubber-edge friction and the performance of the newly developed high-stress dynamic-loading ring-shear apparatus during drained speed-control and undrained monotonic stress-control tests, a series of basic tests were conducted using a sample taken from a megaslide, the Unzen-Mayuyama landslide.

Rubber-edge friction

The shear stress mobilized on the sliding surface is equal to the measured value of the shear load cell minus the rubber-edge friction. When a normal stress is loaded on the sample in the shear box, a lateral pressure acts on the rubber edge. The rubber edge is compressed by the lateral pressure, but due to an arch action of the rigid stainless steel shear box, less pressure will act on the soft rubber edge. The lateral pressure ratio (k : ratio of lateral pressure to vertical pressure) is approximately expressed by the Jaky's equation (Sassa 1988) as $k=1-\sin\phi$.

When $\phi=30^\circ$, $k=0.5$. We initially believed that the lateral pressure would be approximately $1/2$ to $1/3$ of the normal stress.

We therefore chose to fill the shear box with water and consecutively loaded normal stresses of 0.5, 1.0 and 1.5 MPa and sheared water in a speed-controlled test. Fig. 1 presents the measured shear resistance of the rubber edge at 0.5, 1.0, and 1.5 MPa.

The 1.5 MPa test result was unstable, however, 1.0 MPa and 0.5 MPa tests were stable. Both the 1.0 and 0.5 MPa tests indicated a rubber-edge friction of 20–25 kPa, however the value varied with shear displacement. The most important value is the steady-state resistance after

a large shear displacement. It was found to be 20 kPa at 0.5 MPa, and 25 kPa at 1.0 MPa.

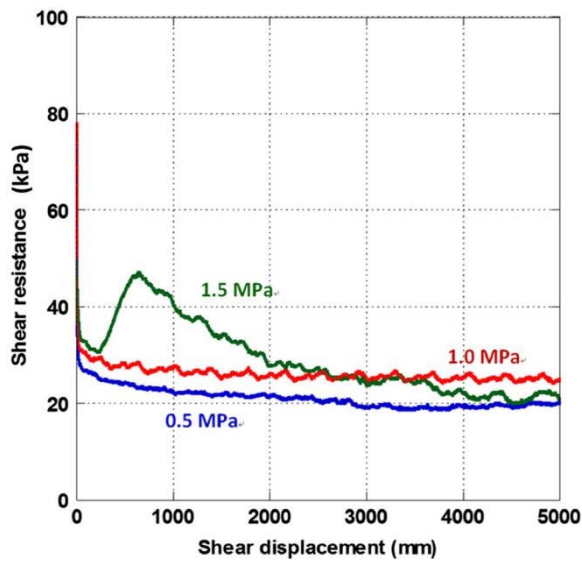


Fig 1 Relationship between rubber-edge friction and shear displacement. Shear box is filled with water. Shear speed: 10 mm/s. Loaded normal stress on water: 0.5, 1.0 and 1.5 MPa.

stresses, the load cells can be replaced by those of lower capacities.

Sample from the 1792 Unzen-Mayuyama landslide

For initial tests of ICL-2, we chose samples from the 1792 Unzen-Mayuyama landslide in Shimabara city, Kyushu Island, Japan. Mayuyama is a dome of the Unzen Volcano. The location of sampling is shown in Fig. 2. Sample S₁ was taken from a sand layer exposed along a torrent gully in the source area of the landslide. Sample S₂ was taken from the coastal area outside the landslide area to represent the soil overridden by the landslide. The mountain consists of volcanic lava rock and unconsolidated eruption products (debris and sands). The sliding surface of the landslide probably formed within a sandy layer rather than in the strong intact lava rocks and boulders. We took samples from a sandy zone exposed along a torrent gully side slope in the source area. The sample site is shown in Fig. 3 and the grain-size distribution of the sample is shown in Fig. 4.

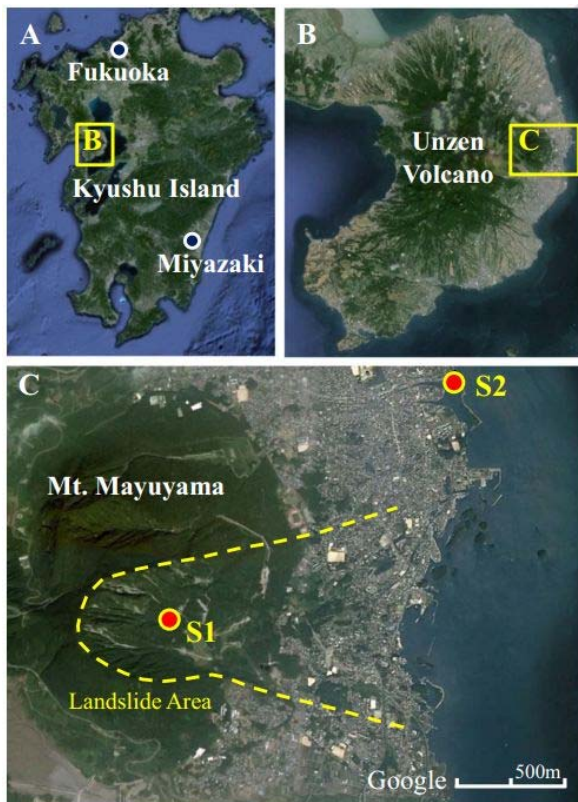


Fig 2 The sampling locations in the Unzen Mayuyama area (image from Google Earth)



Fig 3 Photo of the sand layer behind hammer from which sample (S₁) was taken. It is exposed in the bank of a torrent gully in the source area of the Unzen-Mayuyama landslide

The precision of the shear load cell and normal stress load cell are 0.01%–0.03% of full scale. The precision of the pore-pressure sensors is 0.14–0.15%. The precision of the rubber-edge frictional resistance (± 2.5) will be 0.08% of full scale (3 MPa) of the load cell for normal and shear stresses. When conducting tests at lower normal

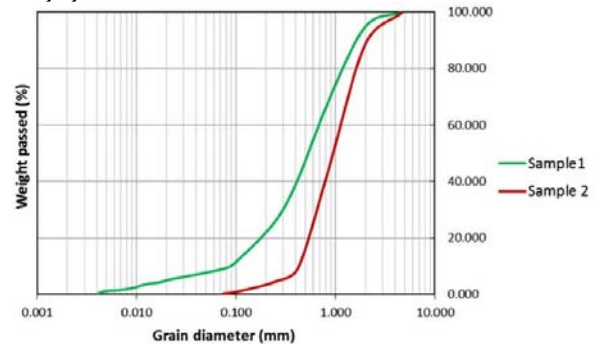


Fig 4 Grain-size distributions of sample 1 (S₁) and sample 2 (S₂)

A series of tests to examine the capability and performance of the ICL-2 apparatus were conducted on sample S1 from this megaslide.

Drained speed-control test

A drained test is the best way to measure the friction angle of a sample and also to check the apparatus without any effect of pore-water pressure. A drained speed-controlled test was conducted as a basic test. First, the sample was fully saturated to $BD=0.97$, consolidated to close to 3 MPa and then sheared at 0.2 cm/sec in the drained condition. After the shear surface had reached peak shear resistance, the drained normal stress was reduced to zero at a rate of $\Delta\sigma=5$ kPa/sec to obtain the drained stress path and friction angle of the sample (Fig. 5). The peak friction angle for S1 was 39.1° , and the friction angle during motion was 35.9° . The stress path and the friction angles appeared to be reasonable for the nature of the sample. The lower graph in Fig. 5 is the time-series data for total normal stress, shear resistance and pore pressure. Pore pressure remained zero throughout the test, since the test was under a drained condition.

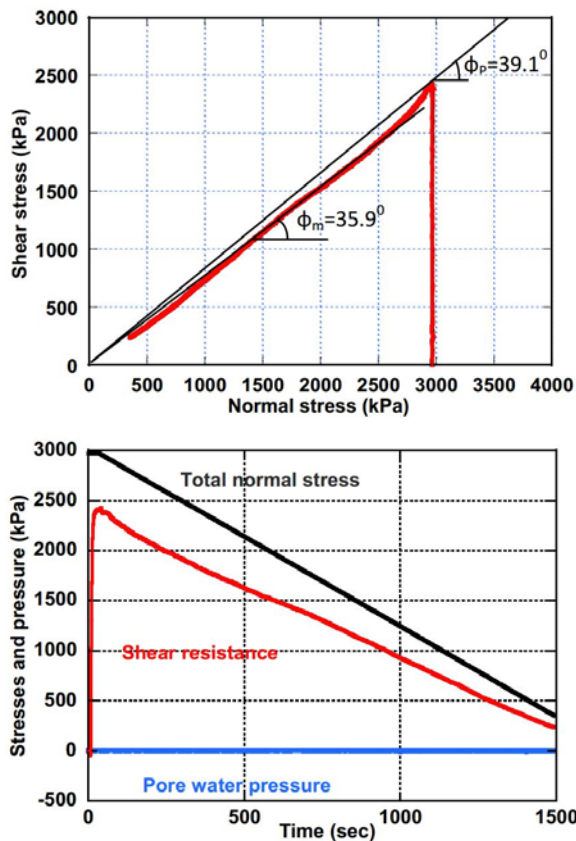


Fig 5 Drained speed-control normal-stress-reducing test on Sample S1. $BD=0.97$, velocity=0.2 cm/s. After reaching the peak, the normal stress was reduced at a rate of $\Delta\sigma=5$ kPa/s

This drained, speed-controlled test result indicated that each of the ICL-2 servo-control system for normal-stress loading and unloading,

the monitoring system, and the undrained capability of the apparatus could successfully function even under the very high normal stress of 3 MPa.

Undrained monotonic stress-control tests

The ring-shear test able to simulate the landslide phenomena is a stress-controlled test which can provide appropriate shear stresses under rainfall, earthquake or undrained loading in the moving landslide mass. Undrained monotonic shear-stress-control tests were conducted under four different normal stresses as tests of undrained capability, stress-control capability and precision of stress and pore-pressure monitoring.

For each test, normal stress was first loaded in the drained condition to close to the planned normal stress (0.3 MPa to 3.0 MPa). The shear box was then changed to the undrained condition, and shear stress was loaded gradually at a rate of $\Delta\tau=1-5$ kPa/sec. When the effective stress path reached the failure line, it began to decrease due to pore-pressure generation (the mechanism for this is sliding-surface liquefaction) along the failure line until the steady-state shear resistance was reached. Shearing was continued in each test until there was 3 m or more of shear displacement.

The stress paths and time-series data for each test are shown in Fig. 6 A to D. The stress path at a normal stress of 375 kPa (A) reached the failure line (39.8°) showing dilative behavior and then decreased along the failure line until it reached a steady-state shear resistance of 37 kPa. Negative pore-pressure was measured just before failure. After failure, the pore pressure increased during shear displacement. This is a typical sliding-surface liquefaction behaviour for a dense material: dilation of the sample near failure caused negative pore pressure, and grain crushing occurred in the shear zone. The resulting volume reduction, together with the accumulating post-failure shear displacement, generated positive pore pressure, even in the dense material.

Shear behavior at 1,030 kPa (B) normal stress was similar, but there was no negative pore pressure, although a zero pore pressure was measured just before failure. The steady-state shear resistance was 45 kPa, slightly higher than in the test at 375 kPa. The friction angle of the peak failure line was 41.2° , which also was slightly higher than at 375 kPa.

Shear behavior at 1,970 kPa (C) normal stress was contractive. Pore-water pressure was generated during shearing before failure. The steady-state shear resistance was 80 kPa.

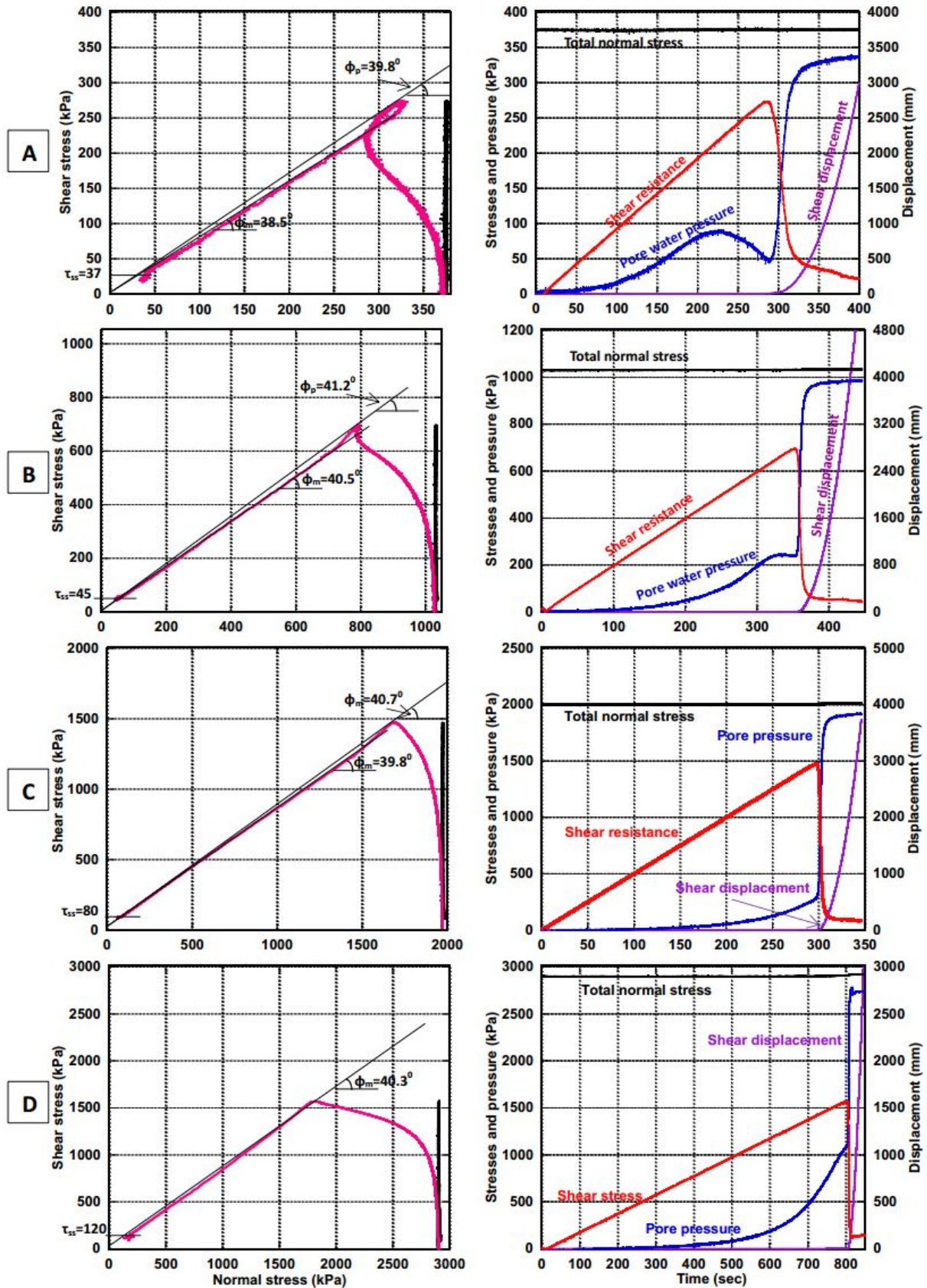


Fig 6 Undrained monotonic stress control tests at different normal stresses. Sample: S₁ from Unzen–Mayuyama. A Normal stress =375 kPa, $B_D=0.93$, $\Delta\tau/s=1$ kPa/s. b Normal stress =1,030 kPa, $B_D=0.95$, $\Delta\tau/s=2$ kPa/s. c Normal stress =1,970 kPa, $B_D=0.95$, $\Delta\tau/s=5$ kPa/s. d Normal stress =2,900 kPa, $B_D=0.96$, $\Delta\tau/s=2$ kPa/s

Shear behavior at a normal stress of 2,900 kPa, close to 3 MPa (D) presented a more contractive stress path and reached a failure line of 40.3° , then went down the line to a steady-state shear resistance of 120 kPa. The stress paths and time-series data of these four undrained monotonic stress-controlled tests showed no aberrations, and did not conflict with previous ring-shear tests such as Sassa et al. (2004, 2010) and others. All stress paths are plotted in the same figure in Fig. 7. As seen, the four tests overlapped along the failure line during motion at 39.8° .

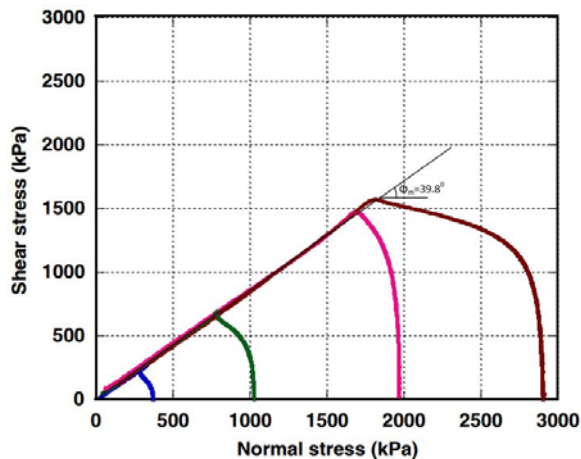


Fig 7 Combined undrained monotonic control test on Sample S1 ($B_D=0.93-0.96$)

Sliding-surface liquefaction

The concept of sliding-surface liquefaction was proposed by Sassa in 1996 and elaborated in later papers (Sassa et al. 2004, 2010, 2014). It is a key concept for pore-pressure generation in a shear zone and post-failure rapid landslide motion. Fig. 8 illustrates sliding-surface liquefaction in an undrained seismic-loading ring-shear test for volcanic sand taken from the 2006 Leyte landslide (Sassa et al. 2010). Grains in the shear zone were crushed during shearing under a normal stress greater than a critical normal stress at steady state (σ_{ss}). The soil structure failed and the soil reduced in volume. In a fully saturated undrained state, a high pore pressure is generated by a minimal reduction of volume. Then both the effective stress and the mobilized shear resistance are reduced. T1 in graph B in Fig. 8 is the onset of seismic loading. Pore pressure immediately started to decrease. This was interpreted as dilatancy occurring, which is a characteristic of dense materials. T2 in graph B (Fig. 8) is the start of post-failure shear displacement. The pore pressure was progressively increased to close to the normal stress and then kept constant. The difference between normal stress and pore-water pressure corresponds to the normal stress at steady state (σ_{ss}). T3 in graph B (Fig. 8) is the

start of steady-state high-speed motion, namely rapid landslide motion. The mobilized shear resistance at this stage is the steady-state shear resistance (τ_{ss}). Values of the steady-state shear resistance (τ_{ss}) from each test are given in Fig. 6.

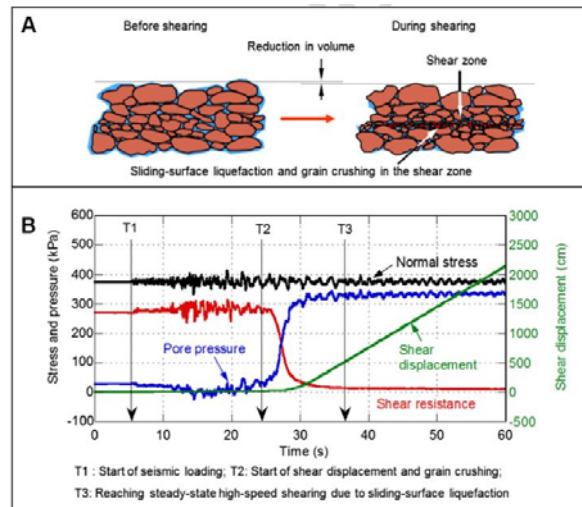


Fig 8 Illustration of the sliding surface liquefaction and a typical test result. Example for volcanic debris from the 2006 Leyte landslide (Sassa et al.2010)

The undrained test results for four different normal stresses, ranging from 375 kPa to 2900 kPa, are plotted in Fig. 7. All stress paths had the same friction angle (39.8°) during motion. All tests showed sliding-surface liquefaction, that is, high pore-water pressure generated during the post-failure shear displacement. The values of steady-state shear resistance range from 37–120 kPa. The test at higher normal stress shows the higher steady-state shear resistance, although the difference is smaller than the difference in loaded normal stresses.

Application of the ICL-2 apparatus to the 1792 Unzen-Mayuyama megaslide

The 1792 Unzen Mayuyama megaslide is both the largest landslide disaster and the largest volcanic disaster in Japan. This landslide killed 15,139 people including 10,139 in the Shimabara area. The other people were killed on the opposite coast by a landslide-induced tsunami wave: 4,653 in Kumamoto Prefecture, 343 on Amakusa Island and 18 people in other areas (Usami 1996). The landslide is illustrated on the cover of a leaflet published by the Unzen Restoration Office of the Ministry of Land, Infrastructure and Transport of Japan (2003), based on a topographic survey. This illustration is reproduced here (Fig. 9).

Fig. 10 is a cross-section of the Unzen-Mayuyama megaslide. The estimated ground surface before the landslide is based on the paintings of Unzen-Mayuyama from the top of Shimabara castle and other locations from the

Unzen Restoration Office of the Ministry of Land, Infrastructure and Transport of Japan (2002) referring to Inoue K (1999, 2000). The bedrock surface in the source area on the upper slope is drawn from the current topography and the bedrock surface in the lower area is estimated from drilling (Fig. 10). The authors of this paper suggest that there were two original landslide blocks (shown in Fig. 10 as blocks with red dots and black dots) and two possible sliding surfaces in the section. The lower block was assumed to have moved because of the undrained loading of the displaced landslide mass (red dots). The average slope angle of the sliding surface in the upper slope was 28.1° , and the average slope angle of the lower slope was around 6.5° .

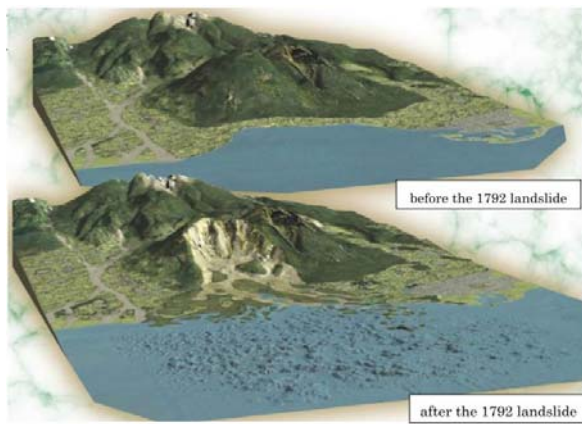


Fig 9 The 1792 Unzen Mayuyama landslide (estimation before and after the landslide) (Unzen Restoration Office of the Ministry of Land, Infrastructure and Transport of Japan 2003)

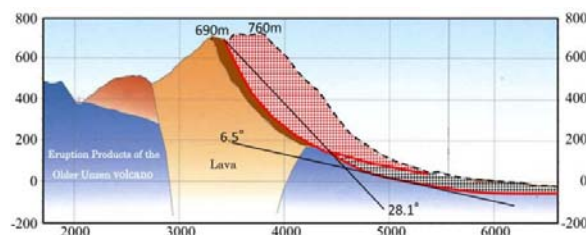


Fig 10 Section of Mayuyama landslide and its interpretation. Modified from the Unzen Restoration Office of the Ministry of Land, Infrastructure and Transport of Japan 2002

Ring-shear tests to simulate initiation of the Unzen-Mayuyama landslide

A series of earthquakes struck the Shimabara area in April, 1792. The largest earthquake hit the area on 21 May 1792.

The magnitude of this nearby earthquake is estimated to have been $M=6.4\pm 0.2$ (Usami 1996). Usami estimated that the seismic intensity at Shimabara was at least V and possibly VI. The Unzen Restoration Office, however, estimates that the seismic intensity which triggered the Unzen-Mayuyama landslide was VII, because

more than 30% of the houses were destroyed in the Shimabara area. Exact seismic accelerations may never be known, but probably were around 400 cm/sec^2 or greater.

The Japanese seismic intensities (Usami 1996) are:

V: $80\text{--}250 \text{ cm/sec}^2$ (where walls and fences are cracked, and Japanese gravestones fall down)

VI: $250\text{--}400 \text{ cm/sec}^2$ (where less than 30% of Japanese wooden houses are destroyed)

VII: More than 400 cm/sec^2 (where more than 30% of the houses are destroyed, landslides are triggered and surface fault rupture is seen).

The estimate of an acceleration of more than 400 cm/sec^2 by the Restoration Office is probably correct, as it is based on a detailed study of house damage.

There are no seismic records of the 1792 earthquake so we chose to use a record from a recent earthquake. The 2008 Iwate-Miyagi Nairiku Earthquake ($M=7.2$) triggered the Aratozawa landslide (67 million cubic meters) in Miyagi Prefecture.

The maximum recorded acceleration was 739.9 cm/sec^2 at MYG004 (National Research Institute for Earth Science and Disaster, Prevention (NIED)). We have used the Iwate-Miyagi earthquake wave form recorded in Miyagi Prefecture (MYG004) for the ring-shear simulation test and also in the computer simulation for 1792 Unzen-Mayuyama landslide.

We performed three tests on the sample (S1) taken from the source area of Unzen-Mayuyama (Fig. 2) to investigate the initiation of the landslide block in the upper slope (block with red dots in Fig. 10) using the ICL-2 apparatus.

Pore-water pressure control test

The first basic test for this landslide (Fig. 11) was to trigger landslide failure by increasing only the pore-water pressure.

Firstly, the sample was saturated (BD value, 0.98), then consolidated to 3.0 MPa normal stress and 1.5 MPa shear stress in a drained condition. This preparatory stage was to reproduce the initial stress in the slope, and is shown as a black line in Fig. 11.

This initial stress corresponded to a slope of $\arctan(1.5/3.0)=26.5^\circ$. This is a similar slope to the landslide block in Fig. 10.

Then, in order to simulate the pore-pressure-induced landslide process, the pore-water pressure was gradually increased at a rate of $\Delta\sigma = 5 \text{ kPa/sec}$. Failure occurred at a pore-water pressure of 1.2 MPa (a pore-water pressure ratio $ru=1.2/3.0=0.4$). The friction angle at failure was 39.4° .

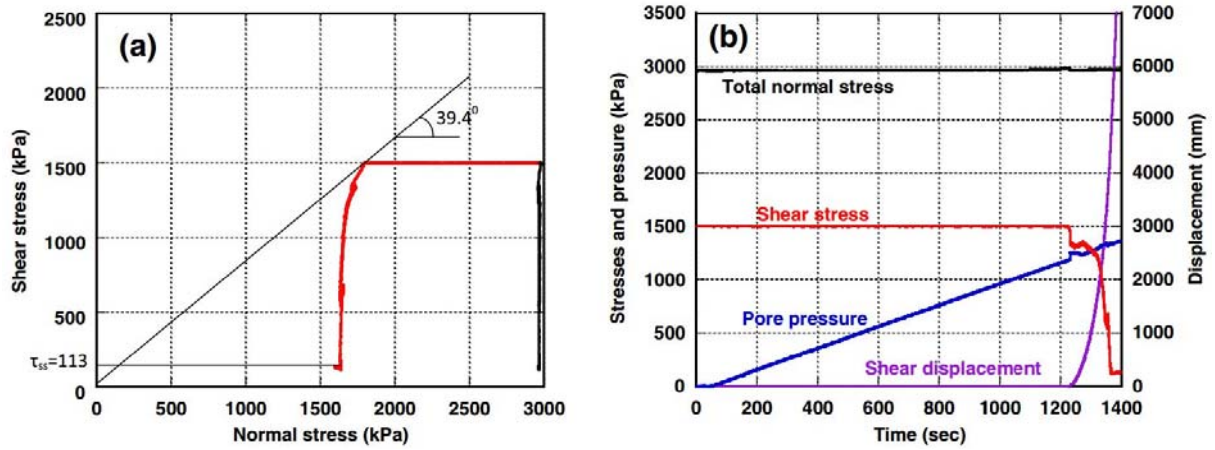


Fig 11 Pore pressure control test on sample 1. Sample: S₁ from Mayuyama source area. B_D=0.98

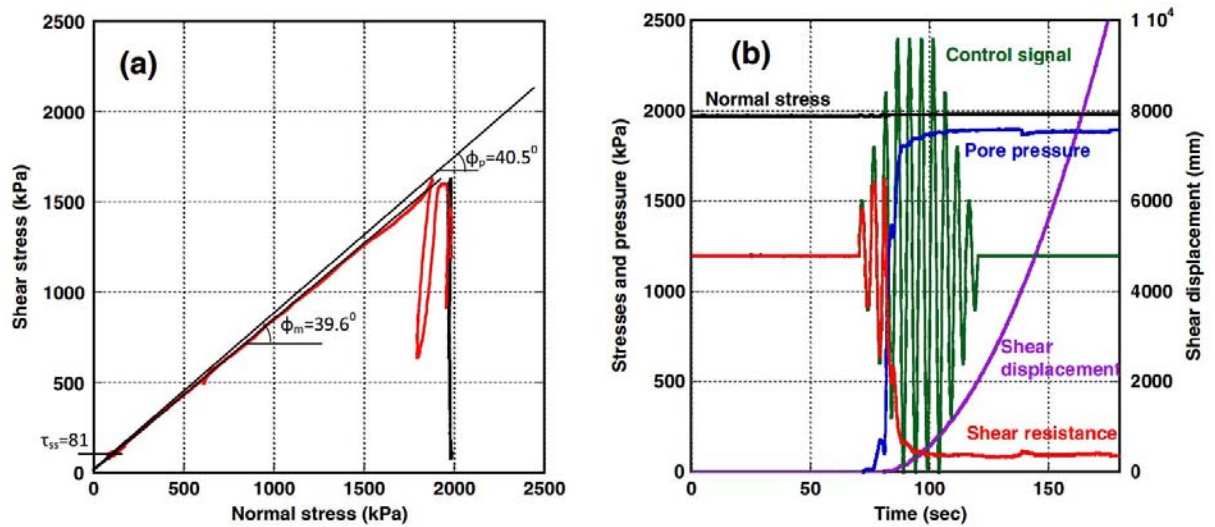


Fig 12 Undrained cyclic loading test on Sample 1. B_D=0.98, cycle rate: 0.2 cycle/s, shear stress step: 300kPa

Undrained cyclic loading test

The second basic test (Fig. 12) was an undrained cyclic loading test on the saturated Sample S₁. Initially, the saturated sample was consolidated at 2.0 MPa normal stress, then a 1.2 MPa shear stress was loaded in the drained state to create the initial stress state. The slope angle for this combination of normal and shear stresses corresponded to $\arctan(1.2/2.0)$, i.e. 31.0°. The shear box was then switched to the undrained state for the undrained cyclic loading test. We applied the control signal for the computer as follows: an initial cycle of shear stress increment of ±300 kPa was to be loaded as a sine curve, in which the second, third and fourth cycles of shear stress were to be loaded as increasing ±300 kPa in each step. (Normal stress was 2 MPa. It was expected that the soil would fail before the loading of the 4th cycle when the total shear stress would be 2.4 Mpa). Thereafter, three cycles would be kept constant before the cyclic shear

stress was reduced to zero. This computer signal was sent to the servo-amplifier for shear stress, while the control signal for normal stress was held constant.

The pore-water pressure generation during the test, mobilised shear resistance, and shear displacement were each monitored continuously during the test. The stress path and the time-series data for this test are shown in Fig.15. The shear stress reached the failure line during the second shear-stress cycle and shear stress decreased after the peak of the third cycle due to generation of high pore-water pressure. This phenomenon is what we have called sliding surface liquefaction. Then, the rate of shear displacement (the purple line in Fig. 12) accelerated and displacement reached to more than 10 meters. The peak friction angle was 40.5°, and the friction angle during motion was 39.6°. The steady state shear resistance was 81 kPa.

Seismic-loading test

The third test (Fig. 13) was a seismic-loading ring-shear test to simulate the landslide initiation of the Mayuyama landslide by the combined effect of pore-water pressure and earthquake shaking. Initially, the sample (S₁) was saturated (BD=0.94) and consolidated to 3MPa in normal stress and 1.5 MPa in shear stress (the corresponding slope angle was $\text{artanc}(1.5/3.0) = 26.6^\circ$). Then pore-water pressure was increased up to 800 kPa, (a pore water pressure ratio $ru=800/3000=0.27$) as the initial slope condition. An exact value remains unknown, but it must have been smaller than 0.4. A preparatory test (Fig. 11) showed that $ru=1.2/3.0=0.4$ was a critical pore-water pressure which could cause a landslide without an earthquake. The earthquake which triggered the 1792 Unzen-Mayuyama landslide was estimated to be Magnitude $M=6.4\pm 0.2$, with a seismic intensity of VII during the earthquake; in the Japanese standard this corresponds to a seismic acceleration of more than 400 cm/sec², as explained above.

The maximum recorded seismic acceleration in the 2008 Iwate-Miyagi earthquake was 739.9 cm/sec², which caused the Aratozawa landslide. We loaded the N-S component of the 2008 Iwate-Miyagi earthquake record (maximum acceleration is 739.9 cm/sec²) at MYG004 as the additional shear stress. For precise pore-pressure monitoring, as well as to maintain servo-stress control, a five-times slower rate was used in applying the recorded seismic acceleration. The test result is shown in Fig. 13.

The green line indicates the control signal. The maximum value is 2,469 kPa (1500+969 kPa) and the minimum value is 369 kPa (1500-1131). The loaded acceleration (a) is calculated from the ratio of seismic acceleration and gravitational acceleration: $a/g= 969/1500$ or $a/g=1131/1500$, because $ma=969$ kPa, and $mg=1500$ kPa, expressing the landslide mass at unit area as m. The acceleration corresponds to +633 cm/sec² and -739 cm/sec². Therefore, the control signal for shear stress sent to the ring-shear apparatus exactly corresponded to the monitored acceleration record.

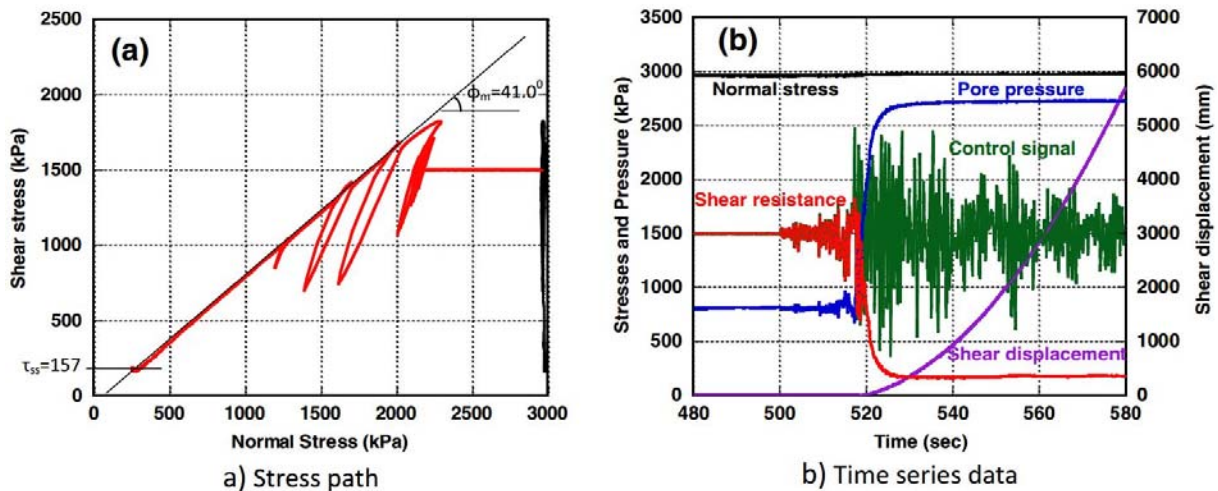


Fig 13 Undrained pore water pressure and seismic loading test. Sample: S₁ from Mayuyama source area. BD=0.94

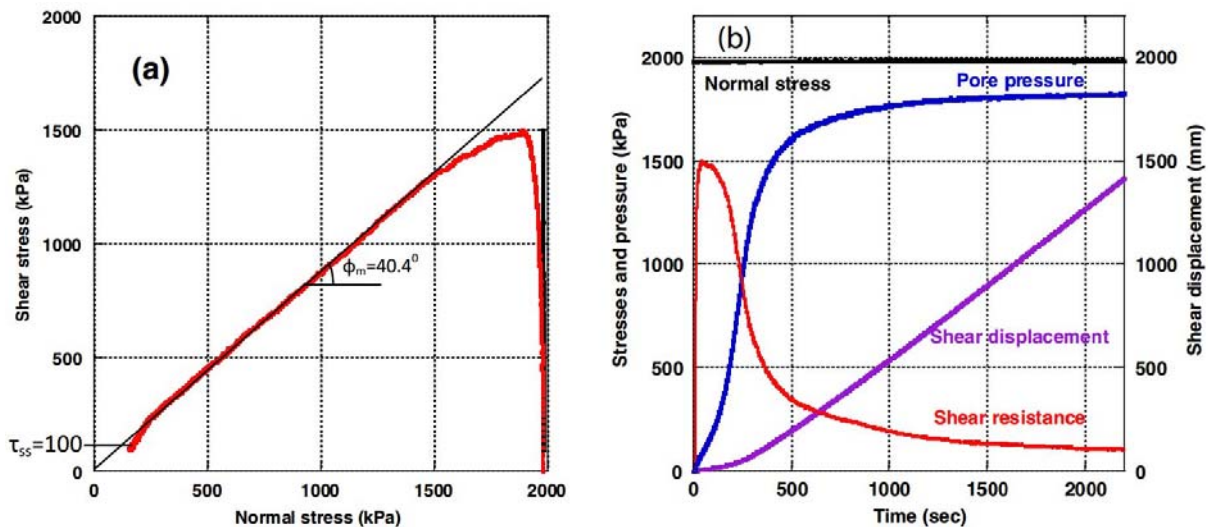


Fig 14 Undrained speed-control test on sample 2. BD=0.95, shear velocity=0.1 cm/s

As Fig. 13 shows, failure occurred around 1,825 kPa, namely $a/g=(1825-1500)/1500=0.22$; the necessary acceleration to failure was 216 cm/sec². This test result suggested that a lesser earthquake shaking (of around $216/633=0.34$) than occurred in the Iwate-Miyagi earthquake could have caused failure under a slope condition with a pore-pressure ratio of 0.27. The steady-state shear strength was 157 kPa.

Ring-shear tests to simulate the motion of the Unzen-Mayuyama landslide

We collected two samples during the Unzen-Mayuyama field investigation. One sample (S₁) was taken from the current ground in the source area (red dot zone of Fig. 10) of the Unzen-Mayuyama landslide to study the initiation of the landslide.

In order to investigate the motion of the landslide, we took another sample (S₂) from a location close to the landslide area, but not covered by the landslide source area mass, i.e. from exposed ground along the coast. We assumed that S₂ could represent soils in the lower slope and deposits along the coast (black dot zone of Fig. 10).

We first carried out a basic undrained monotonic speed-control test on S₂ (Fig. 14). The peak shear strength appeared below the failure line. The friction angle during motion was 40.4°, and steady-state shear resistance was 100 kPa. The friction angle and the steady-state shear resistance were similar to S₁ (40.3° and 120 kPa). Thus, both samples were very similar in their undrained shearing behaviour, even though they were sampled from different points.

When a landslide mass on the upper slope moves, it applies undrained loading to the soil mass on the lower slope and initiates motion of the lower slope in addition to the motion from the upper slope. A study of a landslide-induced debris flow, where the landslide mass in the slope moved onto and mobilized a torrent deposit, was reported in Sassa et al. (2004), although the stress level is much different.

ICL-2 was used to simulate undrained loading on the black-dot layer in the lower slope (Fig. 10) using the displaced mass from the upper slope (red-dot block). Fig. 15 presents the test result of an undrained dynamic loading test simulating this scenario.

Firstly, the initial normal stress and the initial shear stress ($\sigma_0 = 1,000$ kPa, $\tau_0 = 150$ kPa, corresponding to an 8.5° slope) were loaded in the drained condition to reproduce the initial stress state at the bottom of the black-dot layer. The normal stress was increased to 2,790 kPa (which is close to the 3 MPa capacity of the

apparatus) as the undrained load, although a 400-m-deep initial landslide will result in a greater normal stress. If the lower slope mass can resist the undrained load from the upper slope without raised pore-water pressure, it may resist around 2,374 kPa ($2,790 \times \tan(40.4^\circ)$) in this dynamic loading. However, as seen in Fig. 15, a high pore-water pressure was generated in the undrained loading. The sample failed at 720 kPa and its steady-state stress was 80 kPa. The landslide mass from the upper slope should scrape off a layer of the lower slope and move together as a combined greater mass toward the sea. This scenario was proven to be possible by this landslide simulation test using ICL-2.

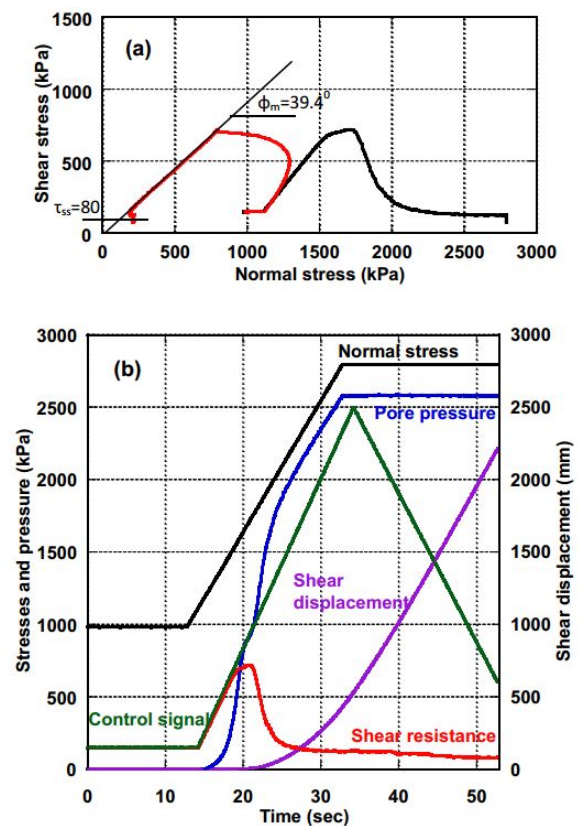


Fig 15 Undrained dynamic loading test on sample 2.BD=0.97, initial stresses ($\sigma_0=1,000$ kPa, $\tau_0=150$ kPa)

Acknowledgments

We thank the Unzen Restoration Office (Mr. Yasuyuki Satou), the Unzen Volcanic Area Global Geopark Office (Mr. Kunihisa Terai) and the Unzen Museum (Mr. Shinichi Sugimoto), as well as Dr. Hideaki Yanagisawa of Tohoku Gakuin University, Sendai and Mr. Hendy Setiawan of the Disaster Prevention Research Institute, Kyoto University for their cooperation during field investigation and sampling, and provision of various data on the Mayuyama landslide.

Development of ICL-2 is a part of the project “IPL-175: Development of landslide risk assessment technology and education in Vietnam and other areas in the Greater Mekong Sub-region”. This project was proposed by ICL and the Institute of Transport Science and Technology of the Ministry of Transport, Vietnam for the SATREPS programme, which is financed by the Japan Science and Technology Agency (JST) and the Japan International Cooperation Agency (JICA). The proposal including the development of ICL-2, and the donation of the developed apparatus to Vietnam was accepted. We acknowledge both agencies and their staffs for their support during this study

References

- Araiba K, Nagura H, Jeong B, Koarai M, Sato H, Osanai N, Itoh H, Sassa K (2008) Topography of failed and deposited areas of the large collapse in Southern Leyte, Philippines occurred on 17 February 2006. Proc. International Conference on Management of Landslide Hazard in the Asia-Pacific Region (Satellite Symposium on the First World Landslide Forum). pp. 434-443.
- Catane SG, Cabria HB, Tomarong CP, Saturay RM, Zarco MA, Pioquinto WC (2007) Catastrophic rockslide-debris avalanche at St. Bernard, Southern Leyte, Philippines. *Landslides* 4(1):85-90.
- Inoue K (1999) Shimabara-Shigatusaku Earthquake and topographic changes by Shimabara catastrophe. *Journal of Japan Society of Erosion Control Engineering* 52(4):45-54.
- Inoue K (2000) Shimabara-Shigatusaku earthquake and topographic change by Shimabara Catastrophe in 1792. *Geographical Reports of Tokyo Metropolitan University*, No. 35, pp.59-69.
- Konagai K, Johansson J, Tajima Y, Fujita T, Tomimasu Y, Nomura F, Date M, Katagiri T (2008) Provisional report of the damage caused by the June 14th 2008 Iwate/Miyagi Prefectures Earthquake. *Seisan Kenkyu* (Institute of Industrial Science, University of Tokyo), 60 (6): 531-535.
- Miyagi T, Yamashina S, Esaka F, Abe S (2011) Massive landslide triggered by 2008 Iwate–Miyagi inland earthquake in the Aratozawa Dam area, Tohoku, Japan. *Landslides*, 8 (3):99-108.
- Nakada S, Suzuki H, Furuya T (1992) Volcanic hazard at Unzen, Japan. *International Newsletter Landslide News*, No.6, pp.2-6.
- Nakada S, Suzuki H, Furuya T (1999) Volcanic hazard at Unzen, Japan. *Landslides of the World* (editor: Kyoji Sassa), Kyoto University Press, pp. 311-316.
- Sassa K (1988) Geotechnical model for the motion of landslides. In: Proc. 5th International Symposium on Landslides, “Landslides”, Balkema, Rotterdam, vol. 1. pp 37-56.
- Sassa K (1992) Access to the dynamics of landslides during earthquakes by a new cyclic loading high-speed ring-shear apparatus. 6th International Symposium on Landslides. “Landslides”, A.A. Balkema, Vol. 3, pp. 1919-1937.
- Sassa K (1996) Prediction of earthquake induced landslides. Proc. of 7th International Symposium on Landslides, A.A. Balkema, Trondheim, Vol.1, pp.115-132.
- Sassa K, Fukuoka H, Wang G, Ishikawa N (2004) Undrained dynamic-loading ring-shear apparatus and its application to landslide dynamics. *Landslides*, 1 (1):7-19.
- Sassa K, He B, Dang K, Nagai O, Takara K (2014) Plenary: Progress in Landslide Dynamics. *Landslide Science for a Safer Geoenvironment, Proceedings of the Third World Landslide Forum*, Springer, Vol.1, pp.37-67.
- Kyoji Sassa, Khang Dang, Bin He, Kaoru Takara, Kimio Inoue, Osamu Nagai (2014) A new high-stress undrained ring-shear apparatus and its application to the 1792 Unzen–Mayuyama megaslide in Japan. *Landslides*, published online (DOI 10.1007/s10346-014-0501-1).
- Sassa K, Nagai O, Solidum R, Yamazaki Y, Ohta H (2010) An integrated model simulating the initiation and motion of earthquake and rain induced rapid landslides and its application to the 2006 Leyte landslide. *Landslides*, 7 (3): 219-236.
- Schuster R, Alford D (2004) Usoi Landslide dam and Lake Sarez, Pamir Mountains, Tajikistan. *Environmental & Engineering Geoscience*, 10 (2): 151-168.
- Stone R (2009) Peril in the Pamir. *Science*, 326, pp.1614-1617.
- Unzen Restoration Office of the Ministry of Land, Infrastructure and Transport of Japan (2002) The Catastrophe in Shimabara -1791-92 eruption of Unzen-Fugendake and the sector collapse of Mayuyama. An English leaflet (23 pages).
- Unzen Restoration Office of the Ministry of Land, Infrastructure and Transport of Japan (2003) The Catastrophe in Shimabara-1791-92 eruption of Unzen-Fugendake and the sector collapse of Mayuyama. A Japanese leaflet (44 pages).
- Usami T (1996) Materials for comprehensive list of destructive earthquakes in Japan. University of Tokyo Press.



Proceedings of the SATREPS Workshop on Landslides in Vietnam, 2014

Landslide mapping and detection of active landslide area from aerial photograph interpretation and field survey in central provinces of Vietnam

Le Hong Luong⁽¹⁾, Toyohiko Miyagi⁽¹⁾, Shinro Abe⁽²⁾, Eisaku Hamasaki⁽³⁾, Dinh Van Tien⁽⁴⁾

1) Tohoku Gakuin University, Division of human informatics course of human information, Sendai, Japan, e-mail: lehongluong@gmail.com, miyagi@izcc.tohoku-gakuin.ac.jp

2) Okuyama-Boring Co., Ltd, Yokote, Japan, e-mail: abe@okuyama.co.jp

3) Advantech Co., Ltd, Sendai, Japan, e-mail: hamasaki@advantechtechnology.co.jp

4) Institute of Transport, Science and Technology, Hanoi, Vietnam, e-mail: dvtien.gbn@gmail.com

Abstract Landslides are destructive and an annually recurring phenomena which cause disruption of traffic and fatalities along transport arteries in Vietnam, especially in central provinces of Vietnam. These landslides are caused by deep weathering processes, high precipitation and cut slopes. This paper presents a summary of our findings such as landslide distribution map... in central provinces of Vietnam based on aerial photography interpretation and field surveys. It covers: (1) landslide distribution map, (2) landform deformation features in partially landslides, (3) types, sizes and dynamic characteristics of moving masses in relation to geologic structure and weathering process. Finally we try to evaluate the risk of landslide based on an AHP approach.

Keywords Central Vietnam, Landslide mapping, Risk evaluation, Deep weathering, Geologic structures

Introduction

Landslides in mountainous areas and along transport arteries are a serious hazard. They seriously affect living conditions, resulting in loss of human life, substantial property damage and possible disruption of vital transport and communication links.

In central provinces of Vietnam landslides occur frequently. According to the Ho Chi Minh project management unit's report, there are 1600 landslides & slope failures which account for a total length of 146Km out of the 2499Km-long Ho Chi Minh road. These are mostly concentrated along the 1200Km from Quang Binh to Dak Lak province (central provinces of Vietnam). Many landslides result from the reactivity of aged

landslides after slopes were cut for road construction. Most of them occur in the rainy season.

The area studied is located between Prao and Thach My towns in the central provinces of Vietnam (Figure 1). The area has a tropical monsoon climate with two seasons: a typhoon and high rainfall season lasting from September through March and a dry season lasting from April through August. The study area has an annual average temperature of 25.6°C and receives an average rainfall of 2,300- 2,800mm. Rainfall is typically highest between October and November and lowest between January and April.



Figure 1 Location map of study area.

Geologically, the study area is situated at the edge of a Paleozoic fold belt known as the Truong Son Orogenic Zone, where the main deformation occurred during the early Carboniferous period.

The geological structure has 1 main complex and 5 main formations: the Dai Loc complex, the A Vuong, Nong Son, Huu Chanh, Khe Ren, Ban Co formation. These consist of gneiss, granite, siltstone, sandstone, mudstone, conglomerate and thin beds or lenses of coaly shale.

The high precipitation and fractured, weathered sedimentary rocks in this area make it extremely prone to landslides.

Identify landslide by aerial photo interpretation

We established the map of topography distribution at Prao and Thach My area. Over 100 black and white aerial photographs were used for interpretation and analysis of the area. They are named D2-99 and were taken in 1999. With this approach, landslides can be easily recognized. Geomorphological features associated with mass movements such as scarps, landslide bodies, gullies, trenches, debris flows and rockfalls can also be mapped. All the landslides could be

distinguished as slides, flows or slope deformations. The state of activity of the landslides is classified as either active, inactive or dormant.

Along 35Km Ho Chi Minh road from Prao to Thach My town, 28 landslides were recognized as shown on Figure 2. These were assigned numbers from 1 to 28. Some landslides were easy to recognize; landslide No.18 for example has a very clear main scarp and side scarp. There is no talus deposit and no weathering shape modifications at the boundary scarp and the landslide body. The lower part is divided into 3-4 sub landslides and slide type changed into that of a debris flow. The upper half is a typical block, so the body has low levels of disturbance. In the case of landslide No.1, half of the scarp is very clear, and the remaining crown scarp is dissected. With others landslides, most crown scarps are dissected. Landslides No.2, 3, 5 to 17 and from No.19 to No.28 are examples of this. A detailed map of the landslides in the study are presented in Figure 2.

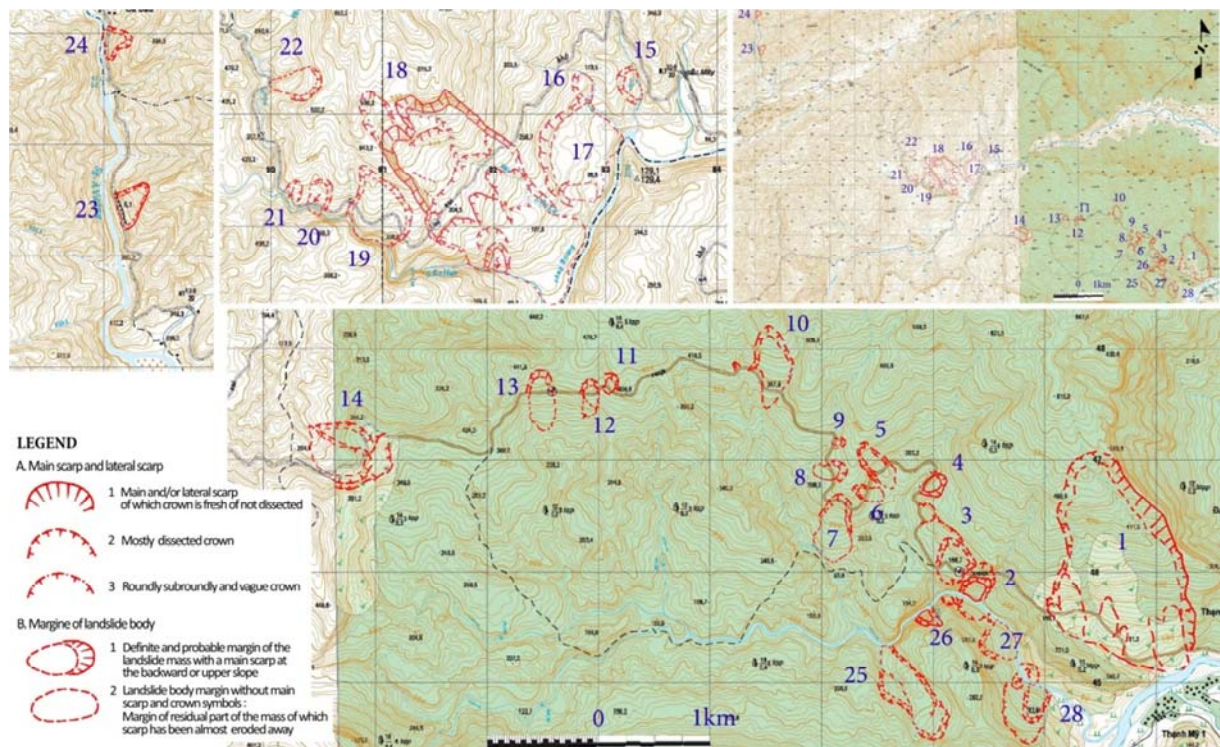


Figure 2 Landslide distribution map along the Ho Chi Minh road between Prao and Thach My town.

On Thon A So area, the example of the typical landslide topographic area is also shown in Figure 3. The area located at the part of northward homo-clinal slope at a southern part of major Mesozoic sink line (Figure 10). In Figure 3 there are a big number of landslides and scarps are distributed, and there are very remarkable topographic features identified, the scarps are distributed at the northward dip slope, on the contrary many types of landslide topographies locate to other direction of slope the size of

landslides are relative of small but it easy to indentify in size, and such landslides and scarps distribution are strongly reflective the geology structure. It means in case of landslide distribution and the type in case of the Mesozoic sedimentary rock controls the characteristics (Figure 5).

On the other hand, the small or shallow landslides are not easy to recognise by aerial photo interpretation. I show one typical place in Figure 4. This area is located on the south west of

Prao town area, from aerial photo interpretation we recognise the present of a number of small ravines, gullies bare land (no vegetation area) are also distribute. Very unfortunately, these bare lands are not easy to identify with real scars. These suggest that many small landslides had taken place. They are able to be soil or rock flow

and occurred on upper weathered soil layer and tend to follow existing stream channels or ravines. Moving material can travel from tens of meters to thousands of meters flow downhill and wash out trees, homes ... that are in their path. These landslides are so small and were not sketched on topographic map.

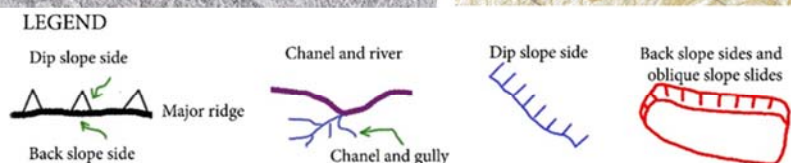
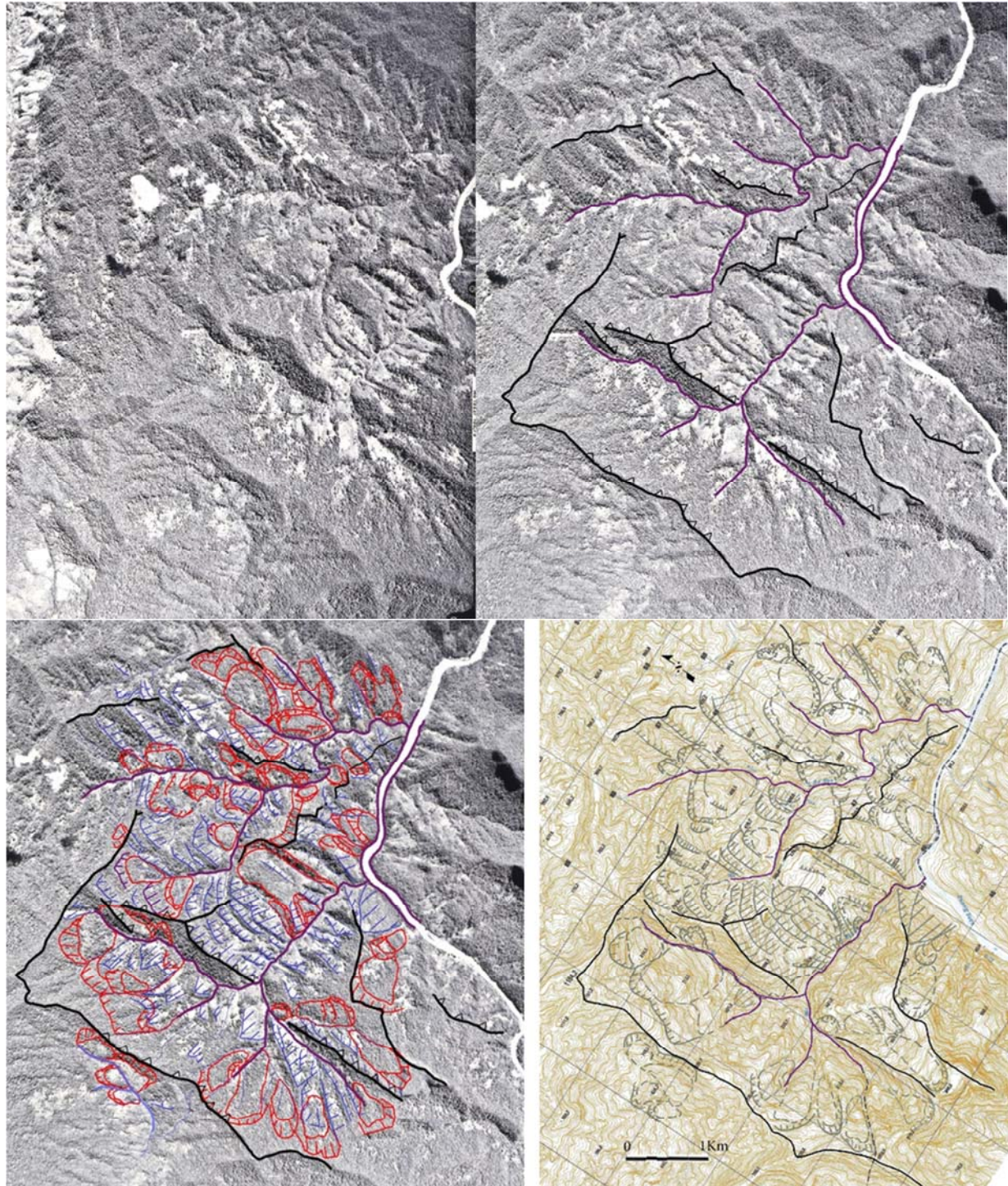


Figure 3 Stereo pair aerial photo (D2-99-06-415 & 416) show main joint plane and bedding plane having tendency to parallel to or dipping with slope.

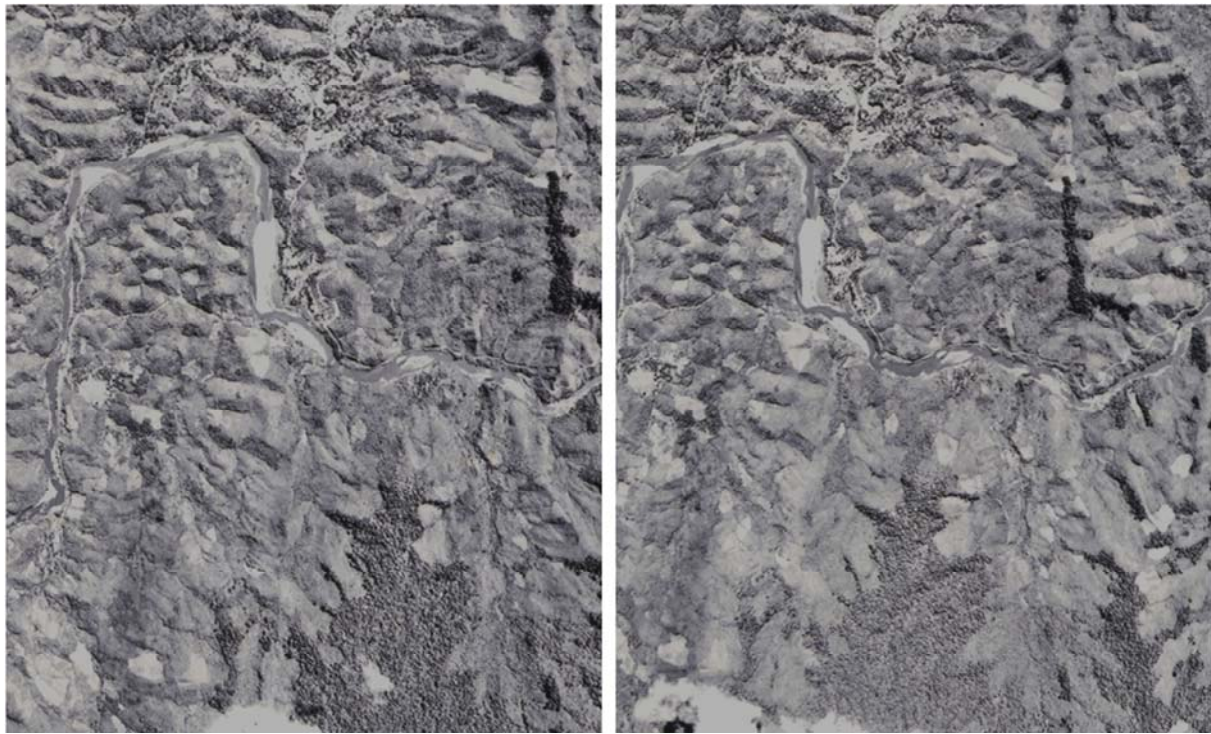


Figure 4 Stereo pair aerial photo (D2-99-05-434 & 435) at south west of Prao area (were taken in 1999).

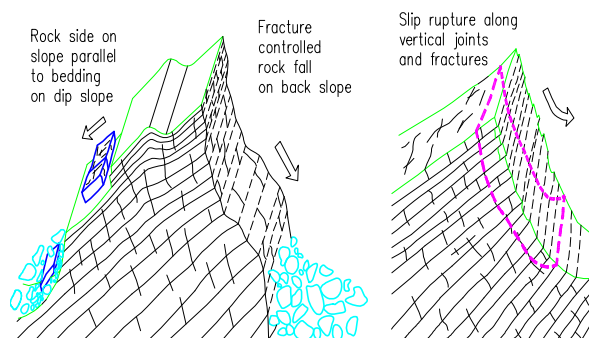


Figure 5 Parallel bedding in rock causing slides.

Inspection sheet for risk evaluation

An inspection sheet (Figure 6) was used for risk evaluation of potential reactivation based on an AHP approach, which involves the geomorphic factors within and outside of landslides. On the inspection sheet, some items, as key to the evaluation of the probability of landslide occurrence, were categorized as follows. The large categories of classification contains: (I) The micro landforms of the landslide body as an aspect of the characteristics of movement, (II) The boundary of major landslide landform components as an aspect of the time process, (III) The landslide topography and the adjoining environment as an index of geomorphic setting. They each have the medium classifications of 9

categories; A: manner of movement, B: degree of sharpness C: degree of instability of landslide body, D: probability of direct feature of landslide action E: between the top edge of main scarp and the upper slope F: between the main scarp and the body, G: between the landslide body and the frontal slope, H: the toe part of landslide body, I: the lower part of landslide body. The items of the medium classifications further divided into small categories, which were checked indexes in the inspection sheet. Each classification was compared as a pair of items based on AHP. For convenience, the categories as shown on the inspection sheet are arranged from the left to the right. The detailed description of this inspection sheet can be seen in *Landslide Risk Evaluation and Mapping - Manual of Aerial Photo Interpretation for Landslide Topography and Risk Management* (T.Miyagi; G.B.Prasad; C.Tanavud; A.Potichan and E.Hamasaki, 2004). The inspection sheet is basically used by highly-skilled engineers. In the case of landslide No.18 (as mentioned in Figure 6) the scores are a result of discussion by many engineers. The other landslides not yet discussed, so scores can not be put into Table 1. The results show that landslide No.18, has a high possibility of reactivation.

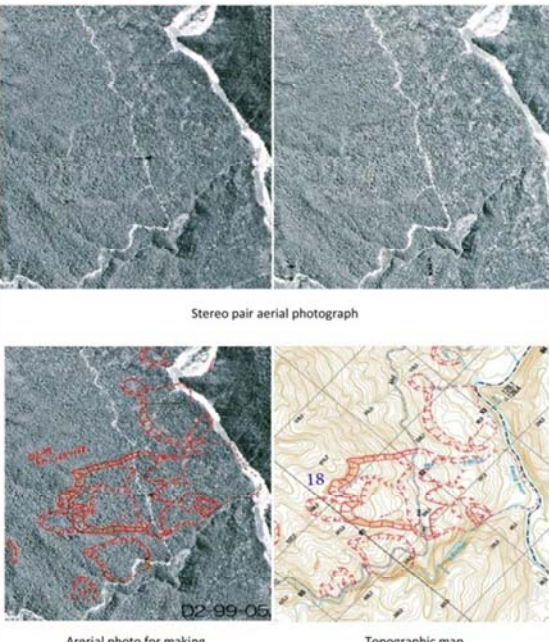
Inspection sheet		Inspection record sheet for landslide risk evaluation					LS No: 18		
LS No: 18 Aerial photo No: D2-99-05 (167-168) Date of aerial photo taken: 1999 Name of topographic map: Thon A So Topographic map scale: 1/25000		Major division	Main factor	Observation theme	Unstable factor		Remarks	AHP score	
 <p>Stereo pair aerial photograph</p> <p>Aerial photo for making</p> <p>Topographic map</p>		Micro landform features in landslide body	Characteristics of active landslide	A: Type of movement	Flow mound Pressure ridge 12,1	Minor scarp 4,9	Separation scarp Depression trench 2,0	8,5	
				B: Level of clearness and micro landform components within LS body	Huge no. of deformed blocks and clear micro topographic boundary 19,5	Clear micro-topography smooth boundary 12,5	Unlear blocks deformed block 6,0	Smooth boundary 5,5	15
				C: Level of stable	Head block separate from lower part 13,9	Gullies development 3,6	Linear erosion Development 1,5		10
				D: Direct features of movement	Cracks and scarlet 18,8	Tree crown deformation 6,3			16
				Other minor features	(Causes: Swamped land, Pond, Deformed, Crack, change?)				
Level of after moving deformation at major boundaries		Age distribution	E: Top edge main scarp	3,8 Echelon	3,2 Main scarp	1,8 Creeping slope	1,5 Gully extension	1,3 Modify to smooth slope	3,5
			F: Boundary of the main scarp and the body	3,1 Non deposition	1,8 Talus	1,1 Large-scale talus	0,6 Smooth deformed by creeping and Talus development		2,5
			G: Boundary of landslide body and the front slope	1,0 Non deformed landslide body	0,5 Gully	0,4 Debris cone	0,3 Smooth surface	0,3 Topography	0,3 Disappeared surface
Landslide and adjacent environment		Geomorphic setting	H: Landslide body toe	Face to the undercut slope of river 8,6	Face to the river 4,4	On the flat plain 1,6	Hit to opposite slope	0,9	4,4
			I: Change of the potential of instability at lower half of body	19,2 Increasing	9,2 Moderate the change of relief energy	2,7 Decreasing		6	
Particularily removable deformed block in landslide		Yes Non (Total No. small blocks)							
		(In accessible meters length of landslide)							
Risk of landslide occurrence base on your experience		Large → Middle → Small					Total points of AHP assessment	No. 66,4	
		Score by own inspector						No. 70,0	
Comment and view of each selection									

Figure 6 Inspection sheet of risk evaluation based on an AHP approach to landslides on the Ho Chi Minh road.

Table 1 Characteristics of landslide unit.

LS No	Size (m)	Landslide Type	Depth of slip (m)	Land Cover	AHP score
01	1,000x2,000	Rotational rock slide	70-100	Degraded Forest	
18	1,500x2,000	Rotational slide	70-150	Forest	70
19	260x 260	Rotational slide	20-35	Forest	
20	100x 250	Translational rock slide	3-15	Forest	
21	80x 125	Translational rock slide	3-15	Forest	
23	250x 350	Rotational rock slide	5-25	Shrubs and Grass	

Field work surveys

Field work activities were conducted along the Ho Chi Minh road, involved verifying the landslides that had been identified during preliminary aerial photo interpretation. Probability of landslide occurrence was evaluated, and geological structure was observed. The length, width, and depth of these landslides were inspected and recorded.

Only 6 landslides (No.1, 18, 19, 20, 21, 23) were observed in the field because of lack of time. We hope that next field survey, some landslide features in Prao and Thach My area that mentioned above will be verified in the field. Field observation show that landslide No.1, No.19, No.20, No.23 are likely to be a rockslide (rotational-translational slide) formed by

fractures and displacement of sedimentary rocks over a weaker layer (e.g. mudstone or coal layer). There is no other evidence of recent movement - trees on the landslide backwall are straight and not distorted, nor are there cracks in the ground. Thus, these landslides are classified as inactive.

In the case of landslide No.21, no deformation or subsidence is present on the road and foot slope (Figure 7) but there are some cracks (Figure 8) on the crest slope. These cracks broke the concrete U-ditch along the crest slope and water effused from the landslide body was observed. Thus, the authors have assumed that though a small part of the upper side slope may be classified as active, it is nonetheless a shallow landslide and the overall landslide is inactive.

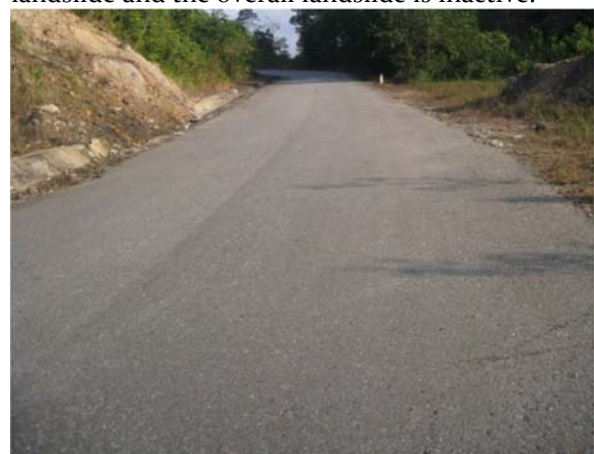


Figure 7 No deformation or cracks on the road at landslide No.21.



Figure 8 Cracks on top of slope and concrete ditch at landslide No.21.

In the case of landslide No.18, there is some evidence that can be observed on the western half of the field. These include, for example: the tilting retaining wall, some dislocations which appear at a certain part of the landslide body, some tilting trees and a considerable volume of water effusing from the middle part of the landslide body. The aerial photo shows that this landslide occurred once, a relatively long time ago, and was followed in 2007 by a reactivation landslide which damaged the road. After that, a retaining wall was put in place as a countermeasure, and concrete was used to strengthen the existing road. The countermeasures were, however, ineffective. The retaining wall was observed to be tilting, with a displacement of about 5-10cm, and there were many cracks on the road and concrete pavement. This evidence was observed to be distributed only upon the western half of the landslide area. This landslide is very large, about 1.5km in width and 2km in length. It may be the case, however, that all its parts may be inactive at present. Finally, the authors formed the conclusion that the western half of the landslide area must be more active than the eastern half (Figure 9)



Figure 9 Some evidence of landsliding was observed at a part of landslide No.18.

Based on field surveys, the authors agreed that the type of landslide in the study area is a translational-rotational slide. The size and type thereof were recorded and shown in Table 1.

Identifying geological structure and making observations on the slip surface

Geologically, (Figure 10) along Ho Chi Minh road between Prao and Thach My town is mostly composed of Jura and Trias sedimentary rocks. The strata exposed in this area are the Nong Son formation and Ban Co formation. The Nong Son upper formation consists mainly of sandstone and siltstone with interbeds of conglomerate, a thin bed of lenses of coaly shale, thick seams of anthracite; containing *Cladophlebis nebbensis*, *Dictyophyllum nathorstii* and *Podozamites lanceolatus*. The Ban Co formation consists of cherty quartz conglomerate, gravelstone, and sandstone, with interbeds of siltstone; containing *Classopollis*, *Neoraistrickia taylori*, *Coniopteris* (Geological and mineral resources map of Viet Nam, 1995). This formation is easily traced in the field as shown in Figure 11, Figure 12 and Figure 13. It is necessary to understand the bedding plane in order to understand the patterns and distribution of landslides within the study area.

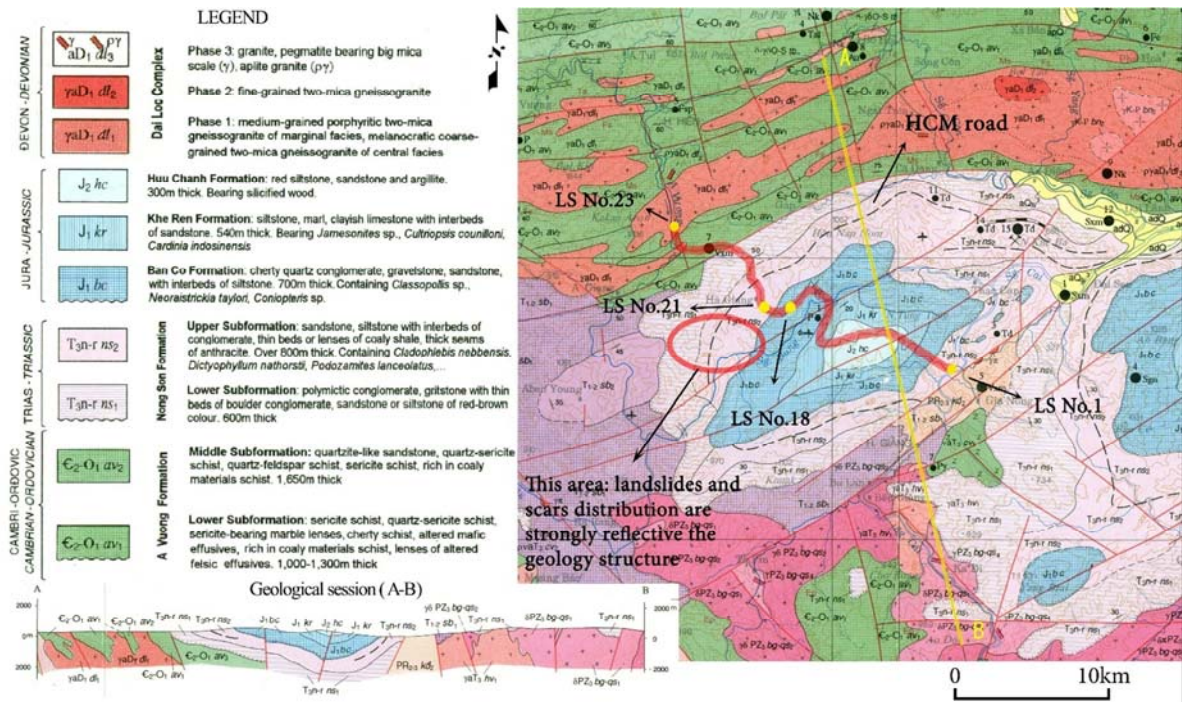


Figure 10 Geological map along HCM road between Prao and Thach My town (red colour line: Ho Chi Minh road, LS No.1, etc: landslide location).

Field observation shows that below the weathering crust about 1-5m thick, on the upper sedimentary rocks layer, there are lot of vertical joints (fractures). These fractures allow water and surface moisture to penetrate the rock and weaken mudstone, siltstone and the coal layer, causing an increase in weight, reducing the bonding strength between two layers and thus promoting failure. With regard to most of the landslides observed, the authors recognized that landslides extended into sedimentary rock and were a rotational or translational type of slide, formed by displacement of sedimentary rocks over a weaker layer (e.g. mudstone or coal layer). Of particular importance was the presence of coal layers, shale and mudstone within a slope/landslide between sedimentary rocks (sandstone, siltstone) as shown in Figure 11, Figure 12 and Figure 13. The authors all assume this is a controlling factor causing landslides in the study area.

In the cases of most of the landslides observed in this study, the slip surface had been covered by debris, but it was exposed in landslide No.20 & 21 (Figure 12). In these cases, the slip surface is smooth and parallel to the bedding plane, and the strike and dip are N45°E and 15°SE. If this bedding plane is a keybed and controls landslides No.15 to 21, we can calculate the depth of slip surfaces. For example: the depth of slip surface of landslide No.15 is 109m, landslide No.16 45m, landslide no.17 104m, and landslide No.18 has a slip surface of 162m. These results are not in accord with field observation and aerial photo interpretation, where the depth of slip surface

often ranges from 1/10 to 1/7 as large as the width of a landslide. Thus, there may be at least two coal layers in this study area. This problem will be investigated during the next survey.



Figure 11 Coal layer and fractured rock consisting of sandstone, mudstone and conglomerate on landslide No.18.

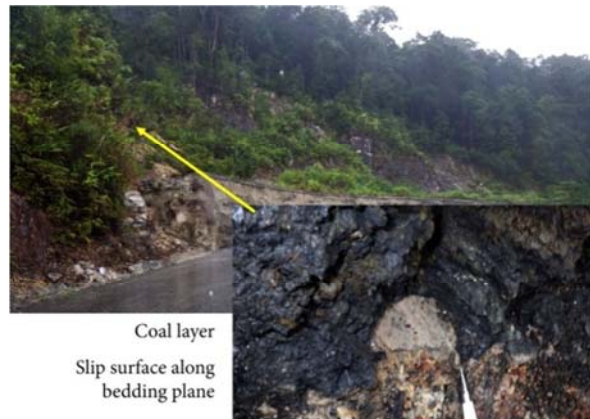


Figure 12 Coal layer, landslide No.20.



Figure 13 Coal layer, landslide No.21.

Conclusion and discussion

From aerial photographs, many landslides were recognized on area from Prao to Thach My town and have formed initial characteristics of landslides: landform deformation features, types, sizes and dynamic characteristics of movement.

Field survey activities are very important to verify the characteristics of the landslides. Through such activity we can evaluate probability of landslide occurrence, recognize active zones, and the type, size and main factors contributing to landslides. At the initial stage only 6 landslides location were observed and investigated in field, next stage authors will try to investigate all the features that had been identified during preliminary aerial photo interpretation.

All landslides along Ho Chi Minh road occur as translational-rotational slides of well-bedded sedimentary rocks such as mudstone, sandstone, siltstone and schist. The landslides reflect the controlling factors of bedding plane and weathering. This paper has attempted to explore the distribution of landslides in the study area and how the distribution relates to these controls.

With regard to most of the landslides in the study area, the authors recognized the presence of coal layers within a landslide left exposed on slopes after landslides occurred. The authors assumed that this coal layer is a main factor in controlling and causing landslides.

The strata in the studied area are mainly bedded sandstone and siltstone. The slip surface of the landslide has the tendency to parallel the bedding plane within beds or lenses of coal shale.

References

- Landslide Risk Evaluation and Mapping - Manual of Aerial Photo Interpretation for Landslide Topography and Risk Management, Toyohiko Miyagi, Gyawali B. Prasad, Charlchai Tanavud, Aniruth Potichanand Eisaku Hamasaki, (2004) Report of the National Research Institute for Earth Science and Disaster Prevention.
- Geological and mineral resources map of Viet Nam on 1:200,000, (1995) General department of geology and minerals of Viet Nam.



Proceedings of the SATREPS Workshop on Landslides in Vietnam, 2014

Mechanical characteristics of the August 6, 2012 Mihata landslide, Shimane Prefecture, Japan

Ngoc Ha Do^(1,2), Fawu Wang⁽¹⁾, Yohei Kuwada⁽¹⁾

1) Shimane University, Project Center on Natural Disaster Reduction, Shimane, Japan, e-mail: hangoc910@gmail.com

2) Institute of Transport Science and Technology, Center of Geotechnical Science and Technology, Hanoi, Vietnam (WG4)

Abstract Shimane Prefecture is one of the three areas in Japan strongly affected by landslides. In the early morning of 6 August 2012, the Mihata landslide occurred in Izumo city, Shimane Prefecture, Japan. The landslide was not triggered by obvious rainfall, nor by an earthquake. However, a high-precipitation event was recorded in the Sada district of Izumo city on 6 July 2012, one month before the landslide occurred. A field investigation was conducted to examine the mechanical characteristics of this landslide. Samples were collected from the sliding zone in the main scarp. A series of direct shear tests, triaxial tests, and ring shear tests were conducted to analysis the shear resistance behaviour of the Mihata landslide's samples. The results show that a high pore-water pressure developed because of the shearing effect, which may explain the sudden collapsed of the landslide. LS-RAPID software was used to simulate the initiation and movement of the landslide.

Keywords Mihata landslide, precipitation, pore water pressure, shear resistance

Introduction

Rainfall events and landslides in Shimane Prefecture, Japan

Shimane Prefecture is located along the western coast of SW Japan. Earthquakes are less common in this region than in other parts of Japan. However, Shimane has a high average annual rainfall between 2,000 and 2,200 mm, with especially heavy seasonal rainfall in July and August each year (Japan Meteorological Agency, 2012). Consequently, landslides triggered by heavy rainfall are frequent in this region. Recently, heavy rainfall events seem to be increasing in both frequency and intensity. According to Japan Meteorological Agency, very high-precipitation

events were recorded in 2012 and 2013. On August 24, 2013, heavy rainfall was recorded in Gotsu city, in the central part of Shimane Prefecture. The total daily precipitation recorded was 386.0 mm, with a 10-minute maximum precipitation of 20.5 mm, and 1-hour maximum of 92.5 mm. This was the heaviest precipitation recorded in Gotsu city in the preceding 38 years. The heavy rainfall caused flooding, and many landslides occurred over a large area. One person was killed, and many houses and the transportation system were damaged (Wang et al., 2013).

On July 28, 2013 heavy rainfall was recorded in Tsuwano city, in the southern part of Shimane Prefecture, near the border with Yamaguchi Prefecture. The hourly precipitation recorded in this event was 381.0 mm, with a 10-minute maximum of 25.0 mm, and a 1-hour maximum of 91.5 mm (Japan Meteorological Agency). As for the Gotsu event, this was the heaviest precipitation recorded in Tsuwano city in 38 years. This disaster caused extensive damage to houses and the transportation infrastructure. The railway connecting Shimane Prefecture and Yamaguchi Prefecture was cut in three places, and landslides along local roads also severed these routes in several sections (Wang et al., 2014).

Change in the global climate has the potential to affect people's lives greatly. Heavy rainfall events seem to be becoming more severe in Shimane Prefecture. Floods and landslides have been widespread, and these have caused serious damage, as shown by the above examples. Therefore, study about the mechanical characteristics of landslides are required to minimize loss of life and property in the region. The Mihata landslide is an individual landslide was investigated in this study (Fig. 1).

Mihata landslide

The Mihata landslide occurred in in the early morning of 6 August 2012. The landslide was not

triggered by obvious rainfall, or by an earthquake. However, a high-precipitation event was recorded in the Sada district of Izumo city on 6 July 2012, exactly one month before the landslide. The maximum hourly precipitation recorded was 74 mm, with a 10-minute maximum of 21.5 mm. Although smaller than the Tsuwano and Gotsu events described above, this was also a 37-year record rainfall for Izumo city. Light rain fell for a few days after the main event, and all rainfall ceased on 21 July. At that time the Mihata slope did not show any obvious signs of deformation. On 26 July 2012, a small collapse occurred at the right end of the slope, near the Mihata River. A main scarp with a height of 3 m was detected in the Mihata landslide on 2 August 2012. A large and sudden deformation then occurred on 6 August 2012, creating a main scarp 20 m in height (Fig. 2).



Figure 1 Side-view of the Mihata landslide (taken by Do N.H., 26 Nov. 2012)



Figure 2 Main scarp of 20 m in height (taken by Do N.H., 15 Oct. 2012)

Features of the Mihata landslide

The landslide had a length of 130 m, a height of 80 m, and a width of 200 m. Many large cracks were present on the main body of the landslide. The displaced material at the toe of the landslide

overran a local road on one side, but traffic around the landslide was not seriously affected. Other routes could be used to bypass the obstruction. There was no loss of life or damage to buildings around the landslide area.

Geology

Andesite-dacite pyroclastic deposits are the main host rock in the area. A rhyolite dike cuts across the top of the mountain from east to west. Porphyrites are also exposed in the valley, downstream of the junction of Mihata and Tanbe rivers. This porphyrite is bordered by a dacite dike at its northern edge, and by granite to the south. Smaller NE-SW trending rhyolite and andesite dikes occur on the southeastern side of the mountain. Talus deposits covering the slopes can be separated in younger and older talus deposits, possibly created by landslides many years ago (Fig. 3).

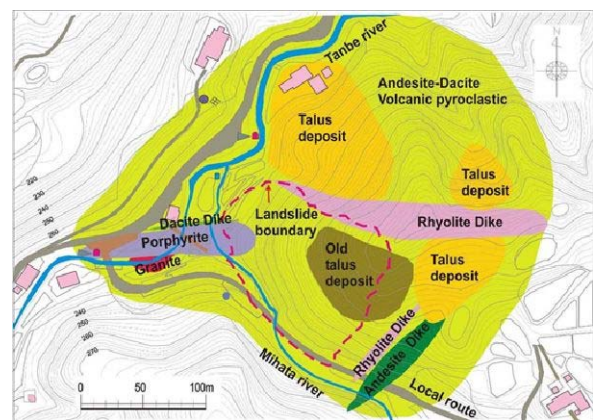


Figure 3 Topography and geology map of Mihata landslide (modified from Fujii et al. 2013)

Monitoring data

A monitoring and warning system was installed by Fujii company after the landslide occurred, to monitor any further movement and to ensure the safety of people and vehicles in the immediate area (Fujii et al., 2013). The monitoring equipments were including extensometers, rainfall gauge, and ground-water level measurements. Three boreholes BP1, BP3, BP6 were drilled along the longitudinal section to take samples and setup the ground-water level measurements (Fig. 4). The monitoring data show that ground-water changed in borehole BP6 around 5 m follows the rainy days from Nov. 2012 to Apr. 2013.

Mechanical characteristics of the landslide

Field investigation was conducted to examine the mechanical characteristics of this landslide. Samples were collected from the sliding zone in the main scarp. A series of soil mechanical tests

were conducted to study the mechanical characteristics of the Mihata landslide.

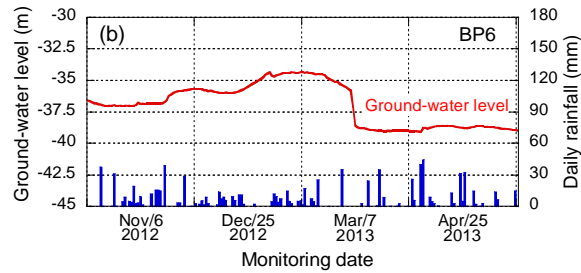
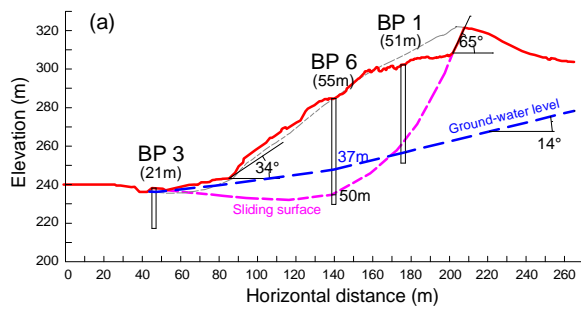


Figure 4 Ground-water level (a) arrangement along longitudinal section of the Mihata landslide; (b) with daily rainfall data in borehole BP6

Particle-size analysis and soil classification

This test was conducted to determine the distribution of particle sizes in soils. Soil samples collected from the field were kept in the drying oven for 24 hours in 60°C. Then the sample was divided into two portions. One portion contains only particles retained on the 2.00-mm sieve while the other portion contains only particles passing the 2.00-mm sieve. The portion retained on the 2.00-mm sieve was separated into a series of fractions using the 75.0-mm, 50.0-mm, 37.5-mm, 25.0-mm, 19.0-mm, 9.5-mm, 4.75-mm and 2.00-mm. The samples retained on each sieves were weighted and determined the total percentage passing for each sieve. The portion passed the 2.00-mm sieve was determined by hydrometer test. The percentage of particle sizes are gravel (35.5%), sand (37.5%), silt (20.9%), and clay (6.1%) (Fig. 5).

Samples also was conducted the test for liquid limit, plastic limit, and plasticity index of soils. The liquid limit (LL), the plastic limit (PL) and the plasticity index (PI) were estimated at 58, 39, and 18, respectively. Therefore, the soil sample was classified as MH (poorly graded sand with silt and gravel) (Fig. 6).

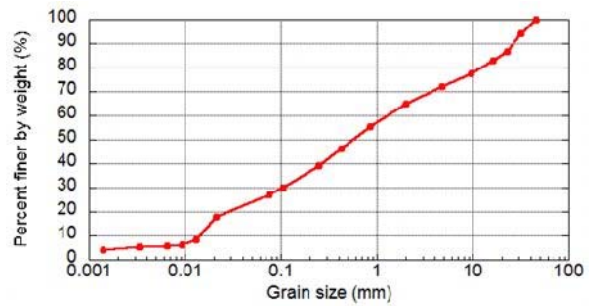


Figure 5 Grain size distribution of the Mihata landslide sample

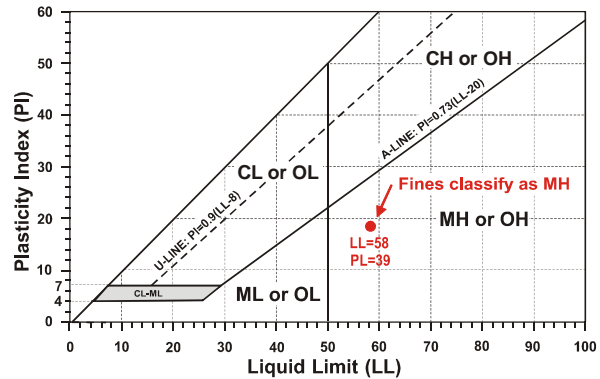


Figure 6 Soil classification in the PI-LL chart

Direct shear test results

The sample portion contains particles retained on the 0.85-mm was remolded to conduct the direct shear test. The samples shape were cylinders with the diameter of 60 mm and the height of 20 mm. According to standard JGS 0561:2000 (Method for consolidated constant pressure direct shear test on soils), 14 samples were conducted with both dry conditions and wet conditions. With dry condition, four samples were conducted in constant speed condition at 0.01 mm/min with different normal stress at 50 kPa, 100 kPa, 150 kPa, and 200 kPa, respectively, to estimate the internal friction angle and the cohesion of soil. Other three samples were conducted at the same normal stress at 100 kPa, but in different speeds condition at 0.01, 0.03, 0.1, and 1.0 mm/min. The same method was applied for other seven wet samples at saturated water content ($w=36\%$).

Figures 7 presents the direct shear test results with horizontal displacement series data. These results show that shear speeds affected the shear strength in the Mihata landslide, strongly affected in wet samples (Fig. 8).

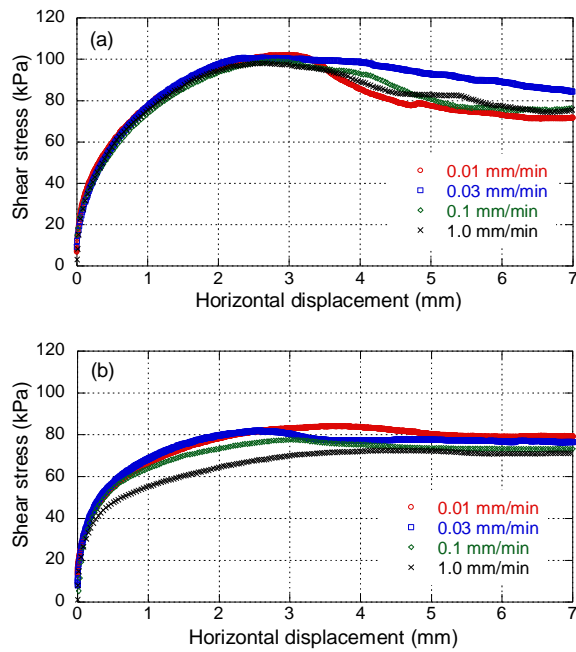


Figure 7 The relationship between shear stress and horizontal displacement at different shear speeds with (a) dry samples and (b) wet samples

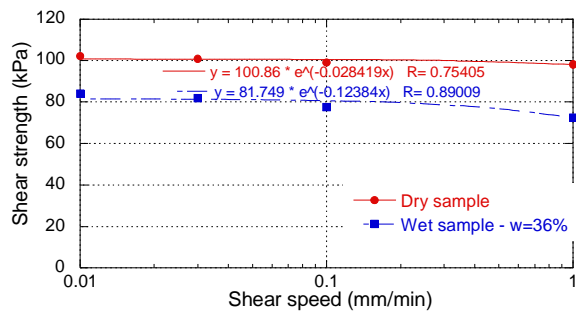


Figure 8 The relationship between shear strength and shear speed in direct shear tests

However, the direct shear test could not measure the pore water pressure in the initial state and during shearing, the important component affected to the shear strength. Therefore, triaxial tests were also conducted to measure the shear strength of soil.

Triaxial test results

The sample portion contains particles retained on the 2.00-mm was remolded to conduct the triaxial shear test. The samples shape were cylinders with the diameter of 50 mm and the height of 100 mm. According to standard JGS 0522:2000 (Method for consolidated-undrained (CU) triaxial compression test on soils), 4 samples were conducted with different vertical normal stress (σ_v) at 50 kPa, 100 kPa, 150 kPa, and 200 kPa (Fig. 9). The samples were first fully saturated and consolidated at specify vertical normal stress. Then, they were sheared in the shear-speed control mode at 1%/min until the the deformation reached to 20%.

The effective stress paths of all tests reached to the same failure line (Fig. 10).

From the stress paths graphic result in triaxial test results (Fig. 11), we considered the stress acting on the sliding surface at the depth of 50 m, point A (s_o, t_o). Assuming the unit weight of the sliding mass is 18 kN/m³. The initiation stress of soil element at the depth of 50 m was under the failure line, point A (700 kPa,300 kPa). It means the initiation state of soil element was stable.

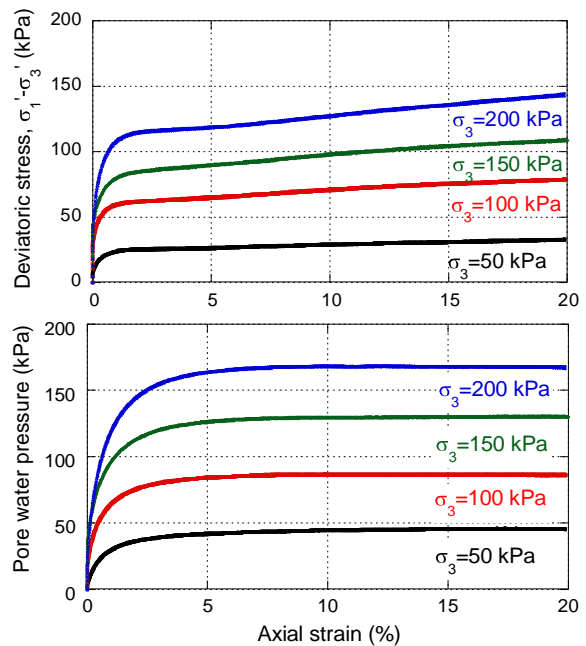


Figure 9 Results of triaxial shear tests with axial strain data

When ground-water level increases, pore-water pressure (u) increases. Then, the stress moves toward to the left. When the stress reaches the failure line, shear failure will occur. The pore water pressure needs to increase 280 kPa to reach the failure line. According to Sassa et al. (2013), the pore water pressure acting on a soil element is:

$$u = z_w \gamma_w \cos^2 \theta$$

[1]

Where z_w , γ_w , θ are, respectively, vertical depth of ground water level, unit weight of water, ground-water slope angle.

Therefore, vertical depth of ground-water level needs a height of 30 m to increase 280 kPa pore-water pressure. The average ground-water level is at the depth of 37 m. In this case, the ground-water level needs to increase 17 m higher than the average ground-water level. However, according to the monitoring data, the ground-water level changes only around 5 m within a year. It looks like that the ground-water level was difficult to increase 17 m higher to reach the failure. It may has other factors affect to the

mechanism of the landslide. Therefore, the ring shear tests were conducted to study about the shear strength and pore water pressure of landslide materials during a long shear deformation.

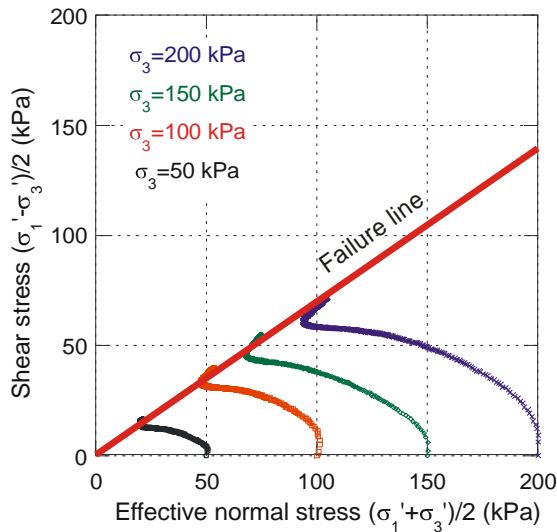


Figure 10 Stress path in triaxial test

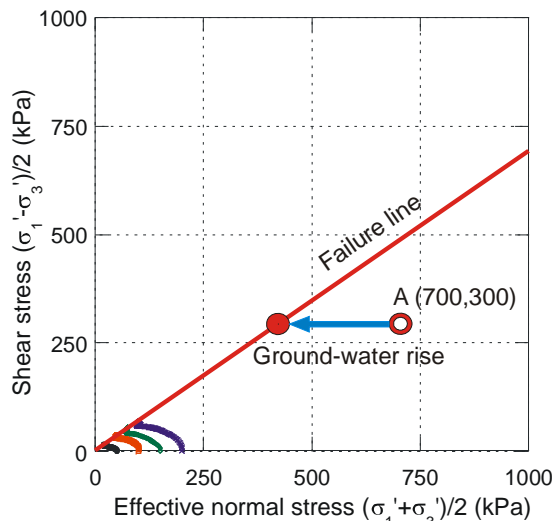


Figure 11 Landslide initiation mechanism due to ground-water rise – An assumption of a soil element stress A (700 kPa, 300 kPa) at the depth of 50 m

Ring shear test results

Using the same soil particles with triaxial test, the sample portion contains particles retained on the 2.00-mm was remolded to conduct the ring shear test. The ring shear test apparatus (ICL-2) was used to simulate the landslide dynamics. The apparatus is the latest model of undrained dynamic-loading ring shear apparatus developed by Sassa et al. (2013) in conjunction with SATREPS project in Vietnam. To examine the shear behaviour of the samples from the Mihata landslide, two tests were conducted: (a) undrained shear speed control and (b) pore water pressure control (Fig. 12).

In the undrained shear speed control test, the sample was first fully saturated and consolidated at 1,000 kPa normal stress. Then, it was sheared in the shear speed control mode at 2 kPa/sec. The effective stress path reached to the failure line, then the stress path went down until reaching a certain value. The final state was the steady state of the sample (Sassa et al., 2013). When shear stress was increased, pore-water pressure started to increase immediately. When the shear resistance reached to peak value, pore-water pressure was 250 kPa and still increasing as shear displacement increasing. This test result presents that the samples were high generated excess pore water pressure (more than 200 kPa) during shearing. It can be calculated as the ground-water level rising 21 m. Combining this result with the calculation in the triaxial test result, it may possibly explain the trigger and the process of the Mihata landslide.

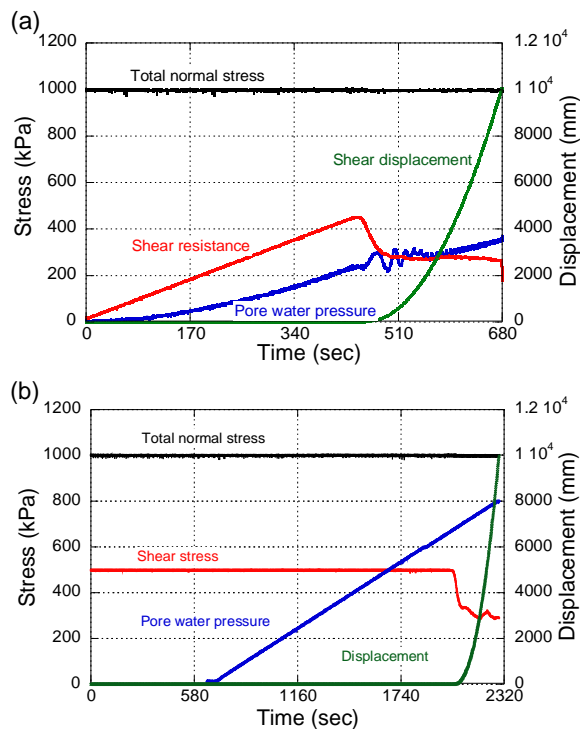


Figure 12 Results of ring shear tests with time series data: (a) undrained shear speed control ($B_D=0.98$); (b) pore water pressure control ($B_D=0.98$)

In the pore water pressure control test, the sample was also first fully saturated and consolidated at 1,000 kPa normal stress. Then, the pore water pressure was gradually increased at the speed of 1 kPa/sec. The failure occurred at pore water pressure of 700 kPa. This test result shows that Mihata landslide mass can move rapidly even if it was triggered by a slow rate of pore water rise during rainfall.



Figure 13 Sliding surface liquefaction and grain crushing in the shear zone in ring shear test

In both two tests, the grains in the shear zone were crushed and the volume of the soil is reduced after 10 m shearing (Fig. 13). The shear resistance (τ_{ss}) in both two ring shear tests above reached the same residual strength, or steady state (Sassa et al., 2013) of the soil was very high (280 kPa). Therefore, the sliding mass did not move for a long distance after the failure in Mihata landslide. This data was used for a new integrated computer simulation model (LS-RAPID) simulating the initiation and the motion of the landslide.

Simulation the initiation and motion of the landslide by the integrated computer model

We used the LS-RAPID software to simulate the initiation and motion of the landslide. The soil parameters including internal friction angle, excess pore pressure, lateral earth pressure coefficient, shear resistance of sliding surface at steady state were measured in triaxial test and ring shear test as above. The values of $\tan\phi_p = 0.75$, $c_p = 20$ kPa, $\tau_{ss} = 280$ kPa, $k = 0.55$ were used as input data of the LS-RAPID software to simulate the initiation and motion of the landslide. Simulation stopped when the zero velocity for all meshes appeared. Time in the figure 14 (b) shows the time from the start to the end of motion. The air photo taken from a helicopter and the simulation results presented in the 3D view from a similar angle are presented (Fig. 14).

Discussion and conclusions

Through field investigation and direct shear tests, triaxial tests, ring shear tests on the motion mechanism of the Mihata landslide, a possible explanation for the Mihata landslide is concluded as follows:

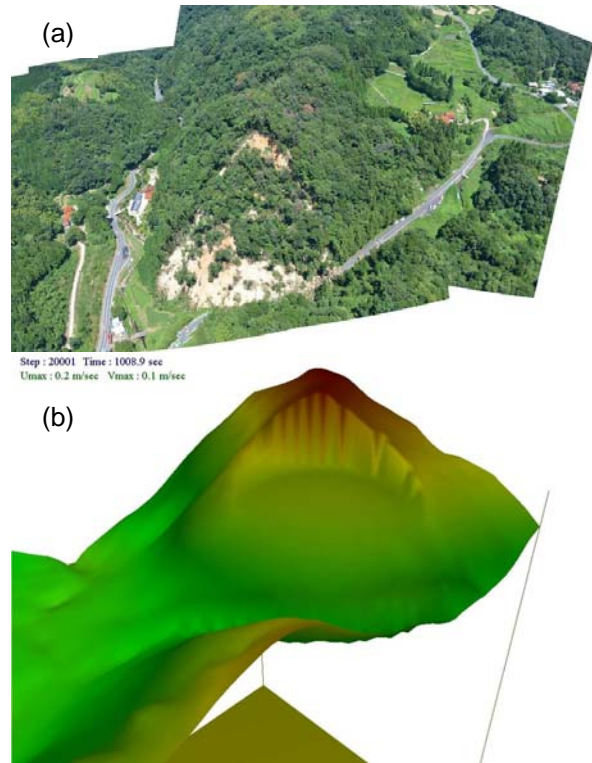


Figure 14 Air photo by Fujii et al., 2013 (a) and the result of computer simulation (b) of the Mihata landslide

1. Historical heavy precipitation within 37 years on 6 July 2012 (one month before Mihata landslide occurred on 6 August 2012) infiltrated into the soil which has low permeability, causing ground-water level to rise, leading to initial movement.
2. During the initial movement of some weak zones within the sliding mass, high excess pore water pressure was generated in shearing zone.
3. The sliding mass moving slowly, leading the excess pore water pressure to increase slowly until reaching the failure value. Then whole landslide mass rapidly collapsed.
4. The sliding mass did not move for a long distance after the failure because of a high residual strength, or high steady state of Mihata landslide soil.
5. Higher precipitation due to climate changing, global warming, more frequently the risk of landslides occur in Shimane Prefecture, Japan. Monitoring and early warning systems are necessary and important in the potential landslide areas, even in the day without rainfall or earthquake activities.

Acknowledgments

We are grateful to Dr. Fujii S. and Dr. Saito R. of Fujii Foundation Company, Prof. Kyoji Sassa of International Consortium on Landslides (ICL), and our colleagues at Shimane University for their support during this study.

References

- Fujii I, Fujii S, Shinguu A (2013) Management system of huge landslide and its mechanism, Landslide disaster in Sanin area, Japan Landslide Society, 133-143 (in Japanese language)
- Japan Meteorological Agency web site (2012) <http://www.jma.go.jp/jma/index.html>
- Sassa K, He B, McSaveney M, Nagai O (2013) TXT-tool 3.081-1.2 Landslide dynamics, ICL Landslide Teaching Tools, 215-237
- Wang FW, Shinmitsu R (2013) <http://www.geo.shimaneu.ac.jp/wangfw/database/homepage/about4.html>
- Wang FW, Kuwada Y, Shinmitsu R, Tasaka I, Araiba K, Endo M (2014) Landslides triggered by a heavy rainfall at the boundary of Yamaguchi and Shimane Prefectures in July 2013, Journal of the Japan Landslide Society, Vol.51, No.2 (218), 30-33 (in Japanese language)



Overview of Landslide Phenomena along Arterial Transport System in Vietnam

Tien Pham⁽¹⁾, Tam Doan⁽²⁾, Luong Le⁽³⁾

1) Kyoto University, Kyoto, Japan, e-mail: phamtiengtvt@gmail.com

2) Institute of Transport Science and Technology, Hanoi, Vietnam, e-mail: dmtam2006@yahoo.com

3) Tohoku Gakuin University, Sendai, Japan, e-mail: lehongluong@gmail.com

Abstract In Vietnam, the mountainous area accounts for three fourths of total mainland area and distributed along the length of the territory. Most of national highways pass the mountains where the geological structure is complex with grave cleavages of soil layers and effected by dangerous cleavage terrain due to earth crust's powerful tectonics. Moreover, Vietnam is located in the highest rainfall area in the world with the highest average annual rainfall from as much as 3,000-4,500mm/year. So landslides often occur along transport arteries in annual rainy season caused large loss of economic, serious traffic congestion on highway and threaten to the stability of local communities. In this study, the characteristics, extent, scale and triggering factors of landslides are characterized by reviewing collected data from the past events as well as analyzing effected condition of natural slopes. Besides, we also represent some landslide reduction methods applied in Vietnam, especially thorough measures with permanent structures to protect and enhance the stability of the slopes on arterial roads which are impacted by landslides.

Keywords Landslide reduction methods, Vietnam, triggering factors.

Introduction

In Vietnam, the main railway and road routes of transport network mainly run from the north to the south. According to statistics up to 2006 of Ministry of Transport (MOT), Vietnam has more than 90 national highways with 17,300 km of a total length and it accounts for 6.87% of total length of road network. In which, three quarters of length of highway goes through mountainous regions and about 30% of those pass through areas with complex geological structures, influenced by the tectonic destruction zones. Similarly, a percentage of 30% in length of its other routes are located on the plains where the geology is fluvial deposits, marine sediment or soft ground. Besides, Vietnam is geographically located in the highest rainfall area in the world and affected by monsoon climate. Typhoon and flood often occur with an annual density of 5 to 10 times/ year and they are usually from June to November, equally 99% of frequency of annual floods.

As a result, landslides frequently occur on transport arteries during rainy season, especially the new traffic routes have been building and reconstructing. The total annual volume of landslides reach to several hundred thousands of cubic meters. Landslides not only caused traffic congestion on roads and serious economic loss by destroying infrastructures, but it also taken around 30 people per year and threatened to the stability of local communities in mountainous regions. Annual State Funds for flood prevention, traffic guarantee and landslide treatment on road network often account for hundreds to thousands of billion VND.

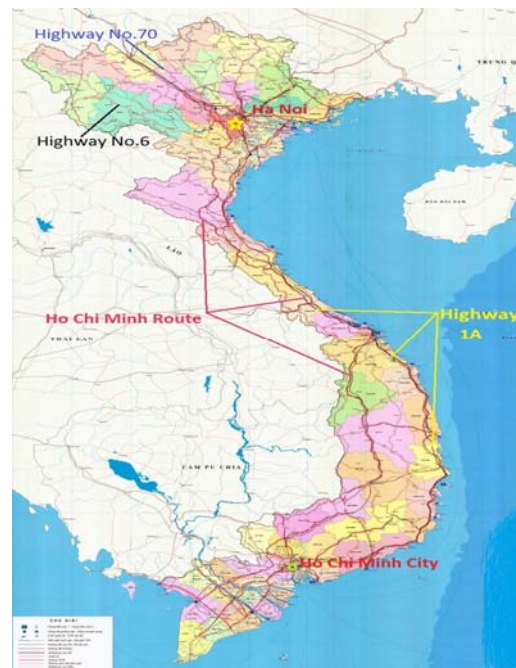


Figure 1 National Transport Network in Vietnam

Statistics on landslides along main transport arterial in Vietnam

In Vietnam, landslides occur frequently and mostly on roads such as Ho Chi Minh (HCM) route and Highway 1A in the central region and along Truong Son range, the north-west region roads like Highway No.6, No.2, No. 4D, No.37, No.70, No.279 and so on (Fig.1).

Landslides on Ho Chi Minh route

Ho Chi Minh route is a lifeline system which runs from the north to the south of Vietnam with the total length of 3,167 km being built completely in 2020. Because of passing through complex mountainous topography and severe climate conditions, this road has the most landslides with more than 1600 sliding points on some locations such as Huong Khe-Tan Ap, Pheo Bac-Bung Road, Hien-Thach My, Kham Duc-Dac Zon, Dac Zon-Dac Pet, Da Deo Pass, Phuoc Tuong Pass, Hai Van Pass and so on (according to statistical data of Institute of Transport Science and Technology-ITST). Typically, landslide point at Km516 + 713 to Km516 + 891 induced by prolonged and heavy rainfall with a cumulative precipitation of 428,1mm in October 2003. Sliding body was 100,000 m³ in volume with the length of 172m along foot slope and a depth between 2 to 5m. This event had damages to retaining wall partially and ditch system on the top of slope completely. In 2007 rainy season, a series of 187 sliding points happened on locations from Dakrong-Ngoc Hoi with a medium and large scale and concentrated in road sections such as A Dot-A Tep, A Tep- Hien, Hien-Thach My, Kham Duc-Lo Xo Pass (Fig.2). Similarly, due to storm No.5 in 2007, landslides occurred on Da Deo Pass and others point after a heavy rainfall. Consequently, a down movement of several thousand cubic meters of soils caused traffic congestion in a week and affected storm prevention works, rescue operation of 250,000 residents in flood areas as well.

According to Ministry of Natural Resources and Environment in 2008, the detailed survey results in 13 sections along Ho Chi Minh route shown that there were 8 fierce landslide prone locations in rainy season including:

- Da Deo - Khe Cat section located in Bo Trach-Quang Binh province with the length of 9km has 4 sliding points at scales from 1000 m³ to 100,000 m³ in volume.
- The Northern of U Bo section in Bo Trach-Quang Binh province (29km in length) has one landslide point with the volume of large-scale and 30 small and medium scale points.
- The length of 10km on Khu Dang Pass in Quang Binh province has 3 large-scale sliding points up to 350,000 m³ in ground volume.
- The length of 31km on Cong Troi Pass in Quang Binh province has 15 landslide points with medium and large-scale.
- The length of 22km on Sa Mu Pass in Quang Tri has 13 small and medium scale sliding points and 3 large-scale sliding points from 40,000 m³ to 80,000 m³.
- Hai Ham Pass (25km in length) in Thua Thien Hue has 4 medium scale sliding points and 24 large-scale sliding points.
- The length of 25km on Song Bung Pass in Quang Nam has 4 large-scale landslide points with a volume up to 200,000 m³.
- On Lo xo Pass in Kom Tum province (length of 20km) has 7 large-scale sliding points (Fig.3).

Landslides on National Highway 1A

Highway 1A is an important road throughout Vietnam passing through 31 provinces and cities. It starts at Friendship Pass between border Vietnam and China in North and ends at Km 2301 +340 in Ca Mau province in

south. According to MOT, landslides mainly occur on road sections in rainy season nearby rivers or through the Passes as follows:

- Ngang Pass: landslides occurred from Km 595 to Km 600 with a small or medium scale. The main reason is because of the rain water poured from a large basin on foot slope then led to erosion of slopes.
- Phu Gia and Phuoc Tuong Pass: having 10 sliding points with a medium and small scale.
- Hai Van Pass: 11 medium and large scale sliding points occurred in the northern branch from Km 984 to Km 994 +800 +00 in 1999. The landslides destroyed a road section of 33m in length and made a traffic jam in 5 days (Fig.4). At the southern branch, there were 9 medium and large scale landslides happened along the length of 9.2 km after the storm in 1999.
- Deo Ca Pass: From Km 1356+400 to Km 1360 in Phu Yen province, 3 landslides generated after a prolonged rainfall in 2005. Most seriously, a down movement of 30,000 m³ soils buried 150m of road in length.
- Co Ma Pass in Phu Yen, there were 17 landslides along 17km in length with medium and large scale.

Landslides on National Highway No.6

On the 504km in length of highway No.6 connecting Hanoi and the north-west region provinces, there are 10 high steep Passes with the length from 4 to 32km. Most of its length go through mountainous terrain, so there are more than 50 landslides most commonly to take place in rainy season. Typically, due to impact of the October 2007 storm in the period from 2nd to 6th, a 400-500mm heavy rainfall induced a deep flood on road and a serious sliding phenomenon. The total volume of soil mass was 250,000 m³ led to traffic jam in 7 days and destroyed 17,000 m² asphalt pavement (Directorate for Roads of Vietnam). Similarly, the 2012 landslide occurred at Km 138.5 by a movement of 30,000 m³ of soils which caused traffic congestion in several days (Fig.5).

Besides, landslide phenomena also happened regularly with medium and large scale in the north-west region roads (Highway No.2, No.3, No.4A, No.4D, No.37, No.79) and in the central region roads (Highway No.8A, No.12A, No.27, No.49A, No.24), etc.

Characteristics and classification of landslides

Landslide characteristics

According to studies of some authors like Doan Minh Tam, Nghiem Huu Hanh and Uong Dinh Khanh, landslide phenomena occur under certain rules as follows:

- First, sliding rarely took place when slope angles are less than 15° while landslides occurred sparsely from slopes between 15°-25°. For slopes between 25° and 30° landslides were most commonly, and landslides initiated very intensely with slopes steeper than 35°.
- Second, landslides are often generated on the high pass road and the locations which have fault fractures with cleaved topography, complex geological structure or high level of erosion. Especially, landslides occurred in the strongly weathered region with a thick weathering crust and bedding of materials are downward on the road.



Figure 2 Landslide on HCM Route



Figure 3 Landslide at Lo Xo Pass on HCM Route



Figure 4 Landslide on Road No.1



Figure 5 Landslide on Highway No.6, 2012

- Next, landslides were very common to occur in the weathered layers of large debris soil. In contrast, these phenomena occurred very little with weathered clay, red soil weathered crust of lateritic soil or a lower thickness of weathered layers.

- Final, landslides occurred on the routes which have high slopes and slopes are not treated appropriately. There were many failures induced by losing the foot of slopes or changing of equilibrium conditions of slopes.

Highway No.6, Ho Chi Minh Route. Other landslides with transitional or segmental surface happen in some locations on Ho Chi Minh and National Highway 1A depending on the shape of bedrocks.

Landslide classification in Vietnam

According to scientists and International Consortium on Landslides (ICL), landslides can be divided into principal categories such as Falls, Topples, Slides, Spreads, Flows and Complex. In Vietnam, basing on characteristics of slope failures on roads, Assoc. Prof. Ho Chat and Doan Minh Tam classified landslides as Slides, Earth Falls, Flows and Topples/Rock falls. In which, slides account for only 15% on roads but it has the largest scale, most serious and most complex level treatment. Landslides as falls occur with a very high frequency and most common take 60% on road (Fig.6).

Slides: These phenomena are most popular in the steep hills or adjacent areas of material excavations. The volume of landslides are about several hundreds to millions of cubic meters such as North-West route, along Ho Chi Minh route and other national highways in Middle Central area and in some places, notably the provinces of Hue, Quang Tri, Ha Tinh, Quang Nam, Quang Ngai, etc. Rotational landslides often occurred on cutting slopes or fill slopes having homogeneous geological structure such as landslides on Da Deo Pass,



Figure 6 Landslide classification

Earth Falls: The landslides often occur in rainy season but damages are not large. It is distributed in some roads such as highway No.8, No.9, No.21, No.14, No.19, Ho Chi Minh route as well.

Flows: This type often occurs as a mixture of materials and the flow of water caused by heavy rain poured from the upper basin or a combination with the effects of groundwater flow. For the cutting bed, there is an appearance of soil erosion phenomenon at first, then mass of earth detach from the top of slopes and failure gradually develops downward along the flow and is in direct proportion to flow velocity. Flows are very dangerous with considerable and long-term consequences by causing the damage of infrastructures,

sweeping away properties or burring residential regions. Some places where have many flows including mountainous roads in the central region, Highway No.6, Ho Chi Minh route and so on.

Topples and Rock falls: This phenomenon commonly occurs after prolonged rains or in the rainy season on the north-west roads and Ho Chi Minh route in the central coast region. Rock volume is not large but they are very dangerous and likely to cause accidents or traffic jams.

Triggering factors and analysis

The occurrence of landslides is as the result caused by synthetic impacts of a series of factors including geology, geomorphology, meteorology, hydrology and human activities. In which, role of each element is also different at each time to induce sliding.

Causes of natural condition, climate and hydrology

As Vietnam's geographical location is bordered by Pacific Ocean, it is influenced by the monsoon climate with the average annual rainfall from as much as 3,000-4,500mm/year and located in the highest rainfall area in the world. Roads often pass through areas where climatic condition is the most unfavourable by intended rainy season with concentrated and heavy precipitation (Fig.7).

Rain not only erodes the slope, but it also saturates the soil layers and results in an increase of unit weight, then reduces shear resistance. Besides, rains create ground water which generate hydraulic pressure causing erosions. Finally, hot and humid tropical climate accelerates the weathering of rocks on the slope surface, thereby reducing the strength of the rock leading to a high risk of landslides.

Causes of topography and geomorphology

The topography where the routes are located on consists mainly of medium and high mountains with altitude from 1000 to 2500m. The largest cleavage of terrain of 1,200m - 1,400m in depth. The river systems originate from the slopes of high mountains, thereby the rivers are very steep with the shape of V. Slope angles of terrain are between 30° to 60°. These terrain create favorable conditions for the sliding process.

Moreover, the routes pass through tectonic faults areas leading to strong cleavage terrain including a lot of valleys, streams, steep slopes or erosion slots. Those are the reasons for formation of tectonic fault zones where ground is broken and easy to be friable, discrete as well. All factors affect the slope stability during construction and operation of roads.

Causes of complex geological condition

Due to heavily tectonic activities, the geological structure in the Northwest and the Central Region

where the routes go through are very complex and often largely variable with many fault system fracture zones (Fig.7). Depending on structural component of slopes and weathering degree of rocks that landslides are large-scale or small-scale. Sliding often happens due to heterogeneous materials including argillite; sedimentary rocks and sandstones mixed with clay, rock clays mixed with schist, argillaceous limestone or thin layers of limestone.

Another factor, slope failures are very easy to occur on bedding plane because primary bedding of ground on the slope have direction to roads.

Causes from human activities

In the construction stages, people have effects on natural slopes and its equilibrium such as detonation, material excavation, cutting or filling slopes, slope grade resulting in losing toe of slopes, making higher and steeper slopes, etc.

Some measures to prevent landslides applied in Vietnam

In order to handle landslides, three solutions were used largely including the temporary measures, semi-permanent measures and thorough permanent measures. These landslide prevention and treatment based on survey results, classification, analysis of conditions and causes.

Temporary measures use rock gabions, temporary structures. These measures do not treat and prevent slope failures completely but it limits the impacts of flows to toe of slopes directly by changing temporary flow direction partially.

Semi-permanent measures: Some solutions is used commonly such as building low retaining wall, gravity or stone masonry retaining walls, consolidating the slope surfaces by concrete structures, planting vegetation, and combining surface drainage (Fig.8).

However, the most optimal solution to handle landslides is solidification with permanent structures to protect and enhance the stability of the slopes on arterial roads such as reinforced concrete wall using concrete pile foundation, retaining wall combined with protective nets or anchors, anchor piles combined with cutting slopes to reduce load, surface consolidation and drainage, security corridors, etc. Besides, Vietnam has been applying the modern technologies and solutions in the world effectively to tackle landslides, including retaining walls using reinforced concrete piles for deep-seated landslides, arched wall, reinforced concrete frames using high strength steel anchors for large-scale landslides, underground water drainage gullies or water-lowering boreholes, anchored retaining walls (Fig.9).

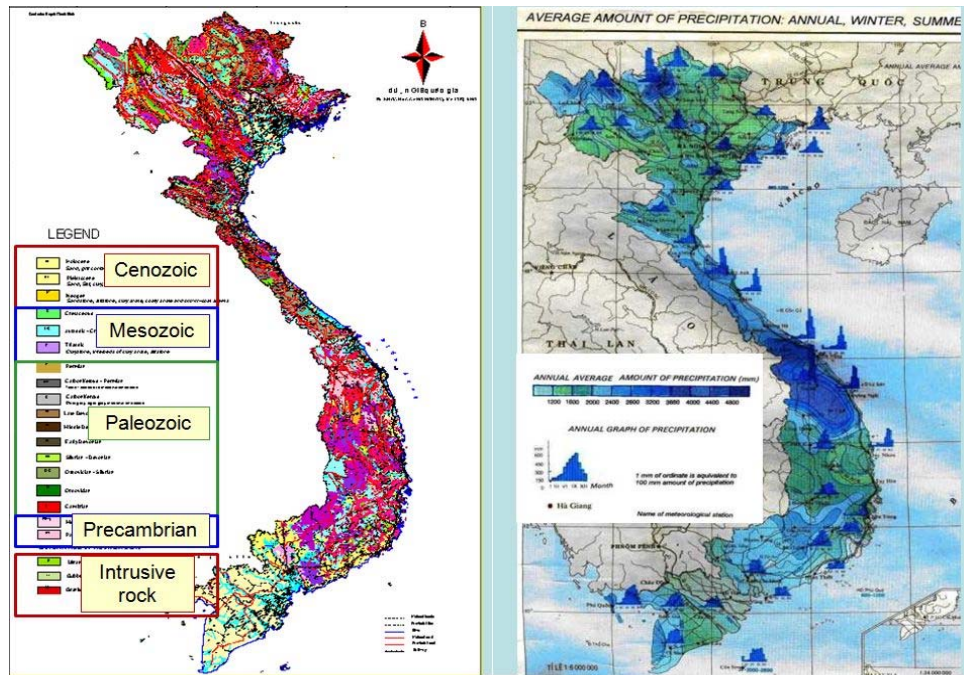


Figure 7 Topography, Geology and Rainfall in Vietnam



Figure 8 Concrete retaining wall and slope solidification combined with surface drainage for landslide in Da Nang city



Fig.9 Combination of reinforced concrete frames and OVM anchors to prevent landslide on Da Deo Pass

Conclusions

Vietnam is located in landslide prone areas highly in the world due to extreme monsoon climate and natural conditions. Statistical data and records noted that rainfall is the main triggering factors driven to landslide occurrences. Landslide distribution is along main transport arteries in the north-west region roads (Highway No.6, No.2, No. 4D, No.37, No. 70), in the central region and along Truong Son mountainous range (Ho Chi Minh route and Highway 1A) and so on. A fact shown that although Vietnam have been taking various solutions to landslide occurrence, such disasters still take place very frequently in monsoon rainy season. From this situation, research on landslides and its impacts to produce appropriate countermeasures has a significant role to cope with tremendous damages and losses, especially, development of landslide risk assessment based on state of art technologies become an urgent requirement. These advance technologies are considered as effective solutions to prevent and mitigate negative impacts bringing safety and security to sustainable society.

References

Research on selection and application conditions of the new technologies for landslide prevention in road routes, Doan Minh Tam, 2008.
 Some initial studies on landslides in the mountains areas of central coastal provinces and its methods of assessment, Nghiem Huu Hanh, 2010.
 Landslide phenomena on some transport routes in Cao Bang province and its vicinity, Uong Dinh Khanh, Le Duc An, Lai Huy Anh, Vo Thinh, Tong Phuc Tuan, Nguyen Ngoc Thanh, 2006.
 Construction Geology, Nguyen Uyen, Nguyen Van Phuong, Nguyen Dinh, Nguyen Xuan Dien, Construction Publishing House, Ha Noi, 2003.



Proceedings of the SATREPS Workshop on Landslides in Vietnam, 2014

Characteristic of landslides in Ho Chi Minh road, Vietnam

Doan Huy Loi⁽¹⁾, Huynh Thanh Binh⁽²⁾, Do Ngoc Ha⁽³⁾

1) Kyoto University, Kyoto, Japan, e-mail:doanhuyloidkt@gmail.com

2) Institute of Transport Science and Technology, Hanoi, Vietnam, e-mail:thanhbinh166@gmail.com

3) Shimane University, Shimane, Japan, e-mail:hangoc910@gmail.com

Abstract In Vietnam, Ho Chi Minh road (HCM road) is a second important national road constructed with a vast investment. It plays an important role in the economic development and social political stability of Vietnam. HCM road cuts through complicated topographic and geologic conditions. So, landslides phenomenon usually occurs in HCM road especially during rainy seasons. Landslides buried roads, threatening the lives of the residential areas along the route, causing damage to life and property every year hundreds of billions VND. Therefore, the promotion of research and actively disseminates propaganda and apply measures to prevent landslides efficiently on transport routes and in residential areas in the local mountains is a needed job. It is essential, meaningful in term of science and society. It is all for the purpose of social security, traffic safety and contributing in maintaining stability and economic development in mountainous areas in Vietnam. Institute of Science and Technology of Transport from 2000 to date has done field work, analysis of topographic maps, characteristic climate of the relevant documents, the paper highlighted the main features of the landslide rocks Branch West Road Ho Chi Minh City on geology, geomorphology, tectonic and human impact on the slope. This paper present result of studies on landslide phenomena on the west branch of the Ho Chi Minh road.

Keywords Ho Chi Minh road, landslide, Quang Nam Province, Truong Son mountain, rainy seasons

Introduction

Ho Chi Minh Road is a highway in Vietnam. It will connect Cao Bang province with Ca Mau province with the total length of 3.167 km. In the provinces of Quang Binh, Quang Tri, Thua Thien Hue and Quang Nam, the road divides into two separate roads: Ho Chi Minh Highway East and

Ho Chi Minh Highway West. Ho Chi Minh Highway East is a well-travelled road with many trucks, towns and restaurants along it. There are few steep hills on the Ho Chi Minh Highway East, with the exception of the portion of the highway in Quang Nam just before it merges with Ho Chi Minh highway West. Conversely, Ho Chi Minh highway West cuts through extremely mountainous areas with steep hills. Hence, in the rainy season, landslides phenomena occurs frequently. According to the general report of the Ho Chi Minh project management committee, along HCM road has 1539 points landslide, with a length of 130km equivalent. Nowadays, some points have been reinforced by several different measures, such as cutting slopes, stone walls, retaining walls, reinforced concrete combined with surface water and ground water drainage. The study area is Ho Chi Minh route, branch from Dakrong (Quang Tri province) to Thanh My (Quang Nam province). It is about 250 kilometres in the Middle of Vietnam. (Figure.1). In this study, the geological, geomorphologic settings, hydrogeological characteristic were investigated.

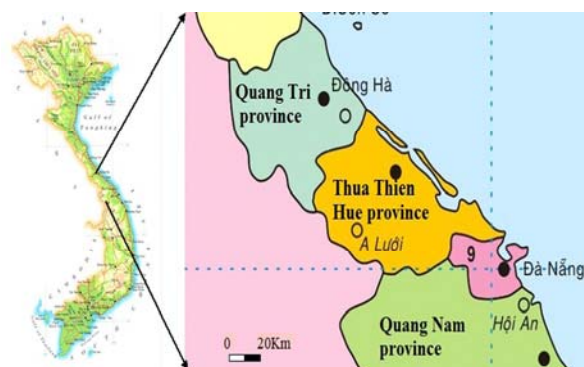


Figure. 1 Location of the study area

Natural characteristics along the route

Topography and geomorphology characteristics

In general, the route goes through the top of the Truong Son mountains, passing Quang Tri, Thua

Thien Hue and Quang Nam provinces. Topography entirely of rugged mountain ranges with peaks as high as Dong Ngai mountain (1.774m), Mang Mountain (1.702m). The topography in this area is intersected with the main direction northwest - southeast. Also the area is influenced by tectonic faults Dakrong - A Luoi with the northwest - southeast direction over 200km long. Along the tectonic is wide crushed zone 2 - 5km width.

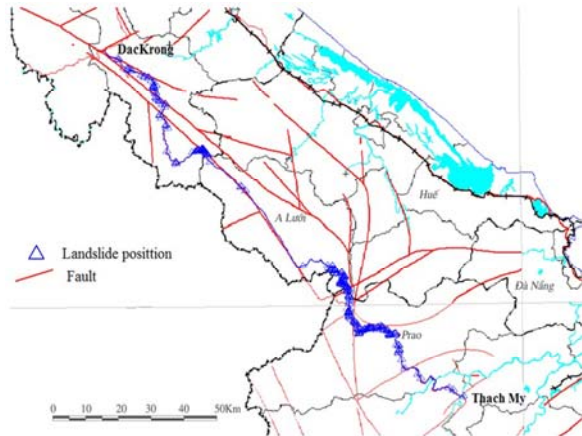


Figure. 2 Map of the tectonic faults and landslides distribution on the Dakrong - Thanh My

Meteorological characteristics

The route passing through the area is characterized by tropical monsoon climate with rainy regime and moisture in very extreme rainfall concentrated in a short time, large changes in space and time. Due to the mountainous terrain, so the higher slopes usually occur heavy rainfall. Average rainfall is distributed unevenly depending on terrain and geographical location.

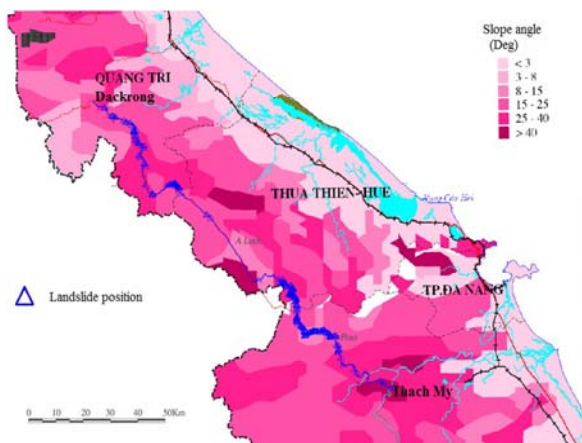


Figure. 3 Map of the slope angle distribution between Dakrong - Thanh My

Hydrogeological characteristics

In general, the mean annual rainfall about over 4000mm/year along this route, focusing on

October, November and September, accounted for 68-79% yearly rainfall, and average air humidity about 79 - 92%. The rainfall is often concentrated during the period of extrem climate events such as tropical cyclones. The time of heavy rain is commonly is 3-4 days.

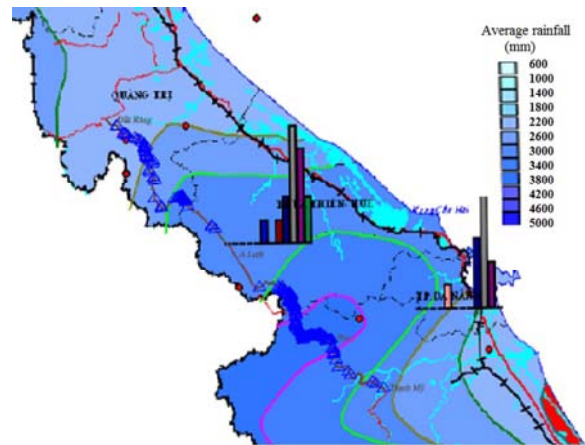


Figure. 4 Map of the average rainfall distribution between Dakrong - Thanh My

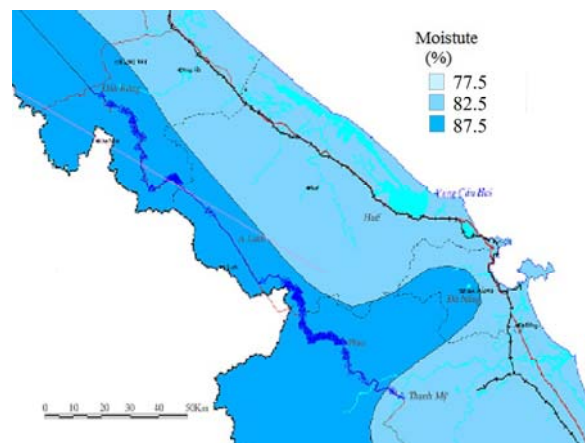


Figure. 5 Map of the moisture distribution between Dakrong - Thanh My

Geological settings along the route:

The geological setting of the study area are very complicated and are characterized six formations: the A Vuong, Dai Loc, Tan Lam, Dak Lin, Dong Trau and Tho Lam. According geolical data, the formations encountered in Ho Chi Minh route described respectively as follows:

A Vuong formation (€-O1av):

A Vuong formation is distributed into 3 bands: Tam Ky - Phuoc Son, Da Nang - A Vuong - Gold River and west of Pleiku range. Main ingredients include slate Serisit - layered thin quartz sandstone alternating Quaczit form.

Dai Loc formation (γ_3^{2dl})

Dai Loc formation is granite complex of Dai Loc type S is divided into 3 phases including:

Phase 1: two-mica granite porphyritic medium grain types, as Minister fringe gneiss, biotite granite with dark grained porphyritic muscovite forms, forms the central gneiss;

Phase 2: two-mica granite medium-grained gneiss forms;

Phase 3: granitic pegmatite with large mica flakes, granite aplite.

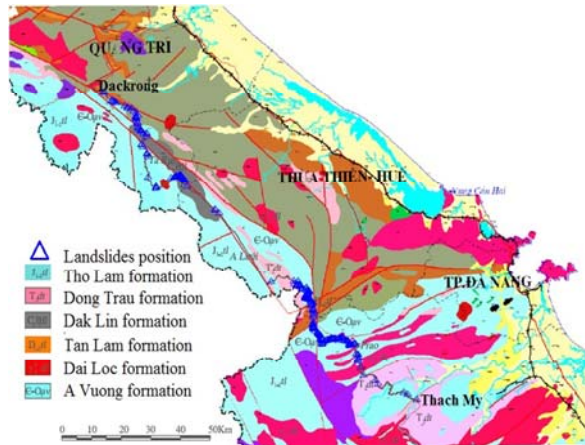


Figure. 6 Map of the geology between Dakrong - Thanh My

Tan Lam formation $D_{1-2}tl$

Tan Lam formation is composed mainly of medium grain sandstone to siltstone alternating particles and thick layered shale rock powder is transferred to the alternating red shale, thin layering, lenses.

Dak Lin formation C_2P_1dl

Dak Lin formation is composed mainly of silicon Slate, sandy siltstone, shale - silicon, tuff andesit, andesit - porphyrit and basalt andesit - porphyrit 200m thick; layer between the andesit - porphyrit and tuffaceous rocks of alternating clay - silica, clay powder 150m thick; layer under the alternating shale limestone lenses of limestone, tuff layer sandwiched andesit, andesit - porphyrit 250m thick.

Dong Trau formation T_2dt

Dong Trau formation is the volcanic origin and the terrigenous sediments is characterized by lithological changes in many local road. major component from bottom to top of sand powder is transferred to the extrusive rocks with little siltstone, then shale is a thick layer of silicon black rock schistosity.

Tho Lam formation $J_{1-2}tl$

Tho Lam formation consists of 3 layers: Ban Co, Khe Ren and Huu Chanh. Tho Lam formation is composed mainly siltstone, sand particles, clay, lime, thin layered shale, from 5 to 35m thick.

Features of landslides on the route

Nowadays, Landslides hazard on Ho Chi Minh National route, branch Dakrong- Thanh My has been very strong in intensity and volume. From the time they put into operation 2003 up to now, each year the Project Management of Ho Chi Minh route has to establish sustainable projects for construction of approximately 50 landslides at a cost of 200 billion VND. But in rainy season every year, about 150-250 landslides still occur. Based on survey data collected, landslides on the route is divided into some sections as follows

Section 1: From Dakrong to Ta Rut

The section 1, approximately 40Km (from Km257T to Km297T), has about 43 landslides (density about 1.1 landslides per 1km). The route goes along the main branch in Dakrong with slope angle on the left side $> 40^\circ$. The landslides are about 40m long and 30m high.



Figure. 7 Landslide at section 1

Section 2: The PeKe pass

The section 2, approximately 8km (from Km314T to Km322T), has about 33 landslides (density about 4 points per 1km). This section has a complex layers of Dai Loc formation and A Vuong formation with the form of high mountainous terrain, steep slopes, rocks are strongly folded, crumpled. The landslides are about 30-70m long and about 20-50m high.



Figure. 8 Landslide at section 2



Figure. 10 Landslide at section 4

Section 3: From A Dot to PRao

The section 3, approximately 80km (from Km372T to Km460T), has about 141 landslides (density about 1.8 points per 1km). We can see the line passing through the tropical regions of tectonic faults A Vuong - Se Kong take the form of high mountainous terrain, steep slopes, rocks are strongly folded, crumpled. The landslides occur mostly on the upper slope. The landslides are about 30-150m long and about 20-70m high.



Figure. 9 Landslide at section 3

Section 4: From Prao - Thanh My

The section 4, approximately 50km (from Km460T to Km510T), has 23 landslides (density about 0.46 points per 1km). Previous sections mainly for A Vuong hydro-electric power and a new refund after 2006, the number of landslides is not fully reflected. The landslides occur mostly on upper slope. The landslides are about 40-80m long and about 20-50m high.

The main reasons cause landslides

The main reasons cause landslides on the route can be divided into 4 main reasons: geology, geomorphology, meteorology and human activities. The reasons for this are reviewed in detail the study area.

Geological reason

Petrographic characteristics and weathering crust of the route through are the main geologic causes related to landslides in the study area and they are pretty close relationship with each other. The results of our survey show that the composition of Tho Lam, Dong Trau, Dak Lin, Tan Lin, A Vuong formations are weathering products from rocks composed of sandstone, siltstone, quartz, shale, limestone be able to cause of landslides very high. And the original stone Granite complex Dai Loc cracked and crushed up, facilitate the process of chemical development, often form thick weathering crust, averaging 4-5 m, moreover to several tens of meters, is the cause of landslides when heavy rainfall. In addition, modern tectonic movement and activities of the fault zone lead to many cracked blocks of bedrock which accelerates the weathering process that can make condition suitable for the landslides..

Geomorphology reason

High terrain, high slope angle are favorable for landslides. The statistical results of our field shows the number of landslides proportional to the high of terrain and the angle of slope. There are over 57% of the distribution of landslides in areas where the terrain elevation from 500 to 1000 m and angle slopes greater than 40°.

Meteorological reason

Landslides generally occur on occasion with prolonged heavy rainfall intensity. Due to topography, geography should be the route passing through the area with average annual rainfall usually > 4000 mm, the highest compared with the average rainfall in Vietnam. Precipitation

on October, November and December accounted for 68-79% annual rainfall, air humidity 79-92% average are able to cause landslides occurring more and more .

Human activities reason

The human activities such as cropping foot slope when making routes, construction of the heavy load on the slopes, the transport operation of motor vehicles and the use of mine breaking ground cause landslides on the routes.

The cutting and burning of forest vegetation cover loss was also caused significant cause rock landslides. For areas with good natural forest landslides phenomenon occur less.

Some solutions to minimize disaster

Depending on natural conditions of each region, the current state landslides on route and economic conditions of each stage can offer solutions to minimize disaster and prevent landslides suitable stone. There are two main groups of solutions as follows:

The group of non-structural solutions

Propagate widely to people to realize the importance of threats from natural hazards and specially landslides hazards caused in particular for preventive measures.

Application of GIS analysis systems and early warning for the area where the risk of landslides.

The prompt removal of people, public works are in the danger zone by the landslide hazard to the safety position.

The group of structural solutions

At small slopes, we can construct the drainage system and underground drainage to limit the harmful effects of the water, vetiver erosion control to stabilize the slopes.

At high slopes, we can apply the powerful combination of approaches such as cutting slopes, gabion embankments, stone walls, retaining walls,

reinforced concrete combined with surface water and ground water drainage, .

At huge slopes having deeper sliding, we can apply more new technologies such as ground prestressed anchors.



Figure. 11 The landslide prevention by using OVM anchor reinforce

Reference

Doan Minh Tam. Research technology choices and conditions apply new technologies to combat soil loss on the road, 2008. Study project

Ho Chat, Doan Minh Tam. Manual protection and reinforcement of the road, 1985 Publisher of Transport.

Lam Trinh . Overcoming consequences of flooding on the Ho Chi Minh, 2009 . Transport Journal.

Lee W. Abramson, Thomas S. Lee, Sunil Sharma, Glenn M. Boyce. Slope Stability and Stabilization Method, 2001 John Wiley & Sons, New York.

Profile of sustainable design survey of works from 2003 to present. Institute of Transport Science and Technology.

Txutovich, N.A. Soil Mechanics (Translated from Russian), 1969. Science Publishing House.

Uong Dinh Khanh et al. Current status of landslide hazards on some roads in the province and high in the vicinity, 2005. Publisher of Transport.

V.D. Lomtadze. Geological Engineering (Translation from Russian), 1982. Publisher College and Technical secondary schools in Hanoi.



Proceedings of the SATREPS Workshop on Landslides in Vietnam, 2014

Preliminary investigation and research plan on Sorayama landslide, Shimane, Japan triggered by heavy rainfall

Pham Thi Chien

- 1) Shimane University, Project Center on Natural Disaster Reduction, Shimane, Japan,
e-mail: chienpham1612@gmail.com
- 2) Institute of Transport Science and Technology, Hanoi, Vietnam

Abstract Landslides are natural hazards that are common worldwide. Landslides affect public utilities, transportation networks, and cause property damage worth several millions of dollars. A lot of factors can combine to induce landslides. These include geological factors (weathering, presence of discontinuities, permeability constraints), morphological factors (slope geometry, terrain condition, subterranean erosion), physical factors (high precipitation, volcanic eruptions, earthquakes), and anthropogenic factors (land use pattern, road construction, deforestation). Every year, several landslides are recorded on the mountainous areas of Japan and Vietnam, due to the topographic condition of these areas, coupled with high record of rainfalls, especially in summer period, when rainfall infiltration exceeds surface runoff.

The main aim of my present research is to analyze the effect of high precipitation on landslides considering the topic: "Evaluating the impact of heavy rainfall to initiation and motion of landslide on slopes". The study methodology will employ Midas GTS NX and LS-Rapid softwares to simulate the initiation and motion mechanism of select landslides. Midas GTS NX is a simulation program which utilizes the finite element method and involves soil-structure interaction. Midas GTS NX can analyze landslide problems by non-linear analysis method with seepage and slope safety analysis, coupled with seepage-slope analysis. On the other hand, LS-Rapid is a simulation program developed to analyze landslide initiation and motion based on natural condition of the material. This will be done by performing simultaneous simulations using the proposed softwares, and carrying out field monitoring and investigation on select landslides, so as to obtain the geotechnical properties of the material which will be used in carrying out the simulation. The research hopes to have detailed understanding of the initiation

process and dominant factors which control initiation and motion mechanism of landslides considering different factors such as geological condition of landslide materials and the relationship between rainfall infiltration and surface runoff.

Keywords: Landslide, rainfall, seepage, slope, landslide initiation, landslide motion.

Introduction and background

Landslide is among the many natural disasters that often occur during rainfall and snowmelt seasons in some countries in the world where rugged mountainous terrain exists. A landslide is defined as "the movement of a mass of rock, debris, or earth down a slope" (Cruden, 1991). Based on data collected by EM-DAT, a map of worldwide occurrence of avalanche/landslide disasters was developed, starting from 1974 to 2003.

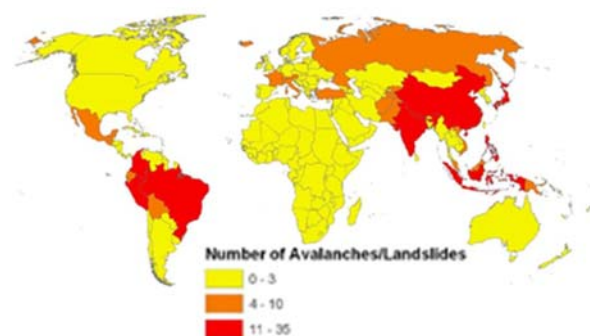


Figure 1 Number of occurrences of avalanche/landslide disasters from 1974 to 2003 (Source: EM-DAT – The OFDA/CRED International Disaster database)

Heavy rainfall is one of the major triggers of landslides. During the rainy season, rainfall penetrates into potential landslide zone, and increases the soil bulk density of the soil, as well as soften the soils, thus reducing the stabilizing

force. In addition, pore water pressure rises rapidly; this decreases the effective stress and shear strength in the potential sliding zone. After high excess pore water pressure is generated, the soil mass suddenly loses a large portion of its shear resistance and flows in a manner resembling a subaqueous flow, forming a landslide.

However, there are various possible mechanism of slope failure. Pore pressure generation in saturated slopes from heavy rainfall events effects multidirectional groundwater seepage into a soil profile and possible cause static liquefaction. Furthermore, some observed and analysed landslide trigger by rainfall without the formation of pore pressures in the soil, but slope failure is due to a loss in unsaturated shear strength when suction had dissipated.

The analysis of seepage forces, infiltration of water into the soil from unsaturated to saturated regimes, and soil shear strength in both cases are very important in analyzing landslide initiation. The most unfavourable case in infiltration scenario is often used when assuming that ground water level rises to coincide with the saturated slope surface. In this case, additional infiltration is not possible and rainfall infiltration effect cannot impact further.

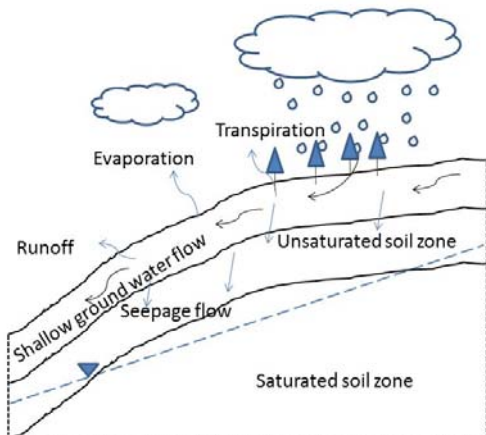


Figure 2 Physical seepage progress reduces rainy

At the initial stage, the slope was unsaturated, rainfall infiltration will have significant effect on the pore water pressure. The pore water pressure changes will occur as the movement progress which the infiltrating water goes downward into the soil layers. In addition, the development of seepage forces in the slope depends on the evolution of the pore water pressure.

Proposed study area

Sorayama landslide (coordinates: 35.418704, 133.081137) located in Shimane prefecture, Japan, is chosen for this study. The first time the

landslide occurred was on 4 September, 2013. The landslide occurred after few days after of heavy rainfall. A cumulative rainfall amount of 85 mm was recorded on the day the landslide occurred. The length of retaining concrete wall of broken road and the deformation of drainage was about 16 m (in Figure 4). The landslide travelled downslope and blocked a road (Figure 4), causing traffic to be diverted to another road. Furthermore, two extensometers S₁, S₂ (in Figure 7) were installed to monitor further movement of the landslide.

The second time Sorayama landslide occurred again on October 24th, 2013 after a typhoon went past the area. The typhoon (rainfall on that day was recorded at 103.5mm/day with strong intensity) caused the first landslide continued developing and strong active. Simultaneously, another landslide appeared in the body of the first landslide. The retaining concrete wall totally collapsed and extended to about 46m on the road and the extensometers S₁, S₂ were broken. The whole body of the landslide is 35 m wide and 80 m long, with slip surface angle varying from 4° to 13°.

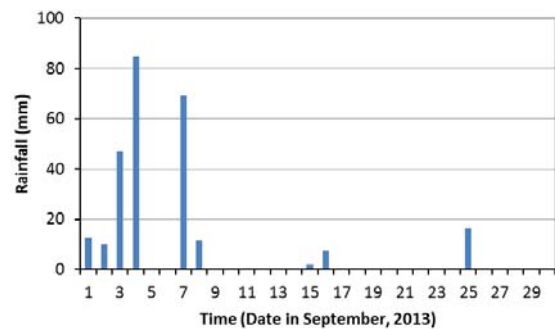


Figure 3 Rainfall data in September, 2013



Figure 4 Sand sacks on the road on the first time the landslide occurred (at position 7 in the Figure 7)

From bore hole data, the geological condition and soil type within the slope include: colluvial deposit (dt); tuff and clay (Tf-C); talus, scree deposit (tl); dacite – clay (Da-C); dacite – weathered (Da-WR); dacite – weathered – tuff – soft rock (Da-WR-Tf-SR); Cg-SR: conglomerate – soft rock. The thickness of the weathered crust ranges from 7 m to 12 m. Moreover, bouldery

material, including weak mudstone and hard volcanic rock were found at the maincarp of the landslide.

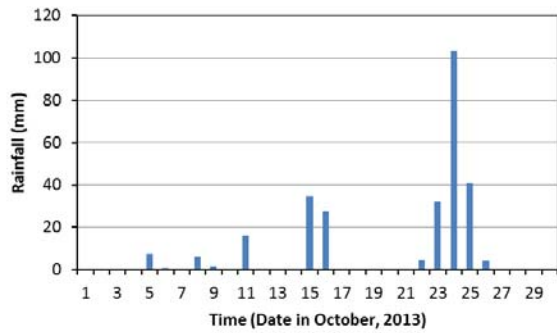


Figure 5 Rainfall data in October, 2013



Figure 6 The road on the 2nd time landslide happened (the position 4 in the Figure 7)

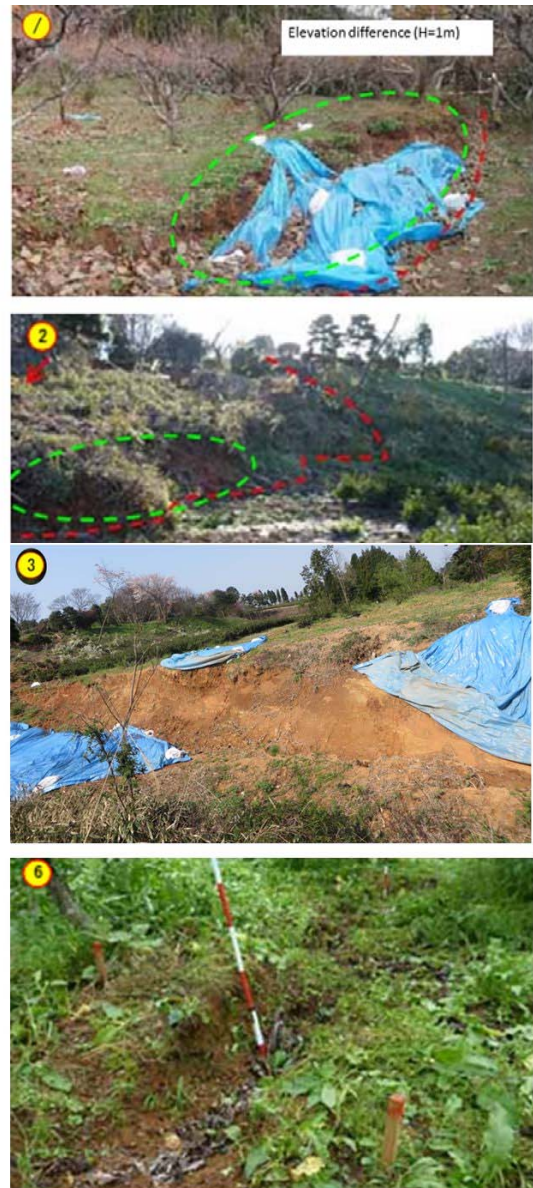
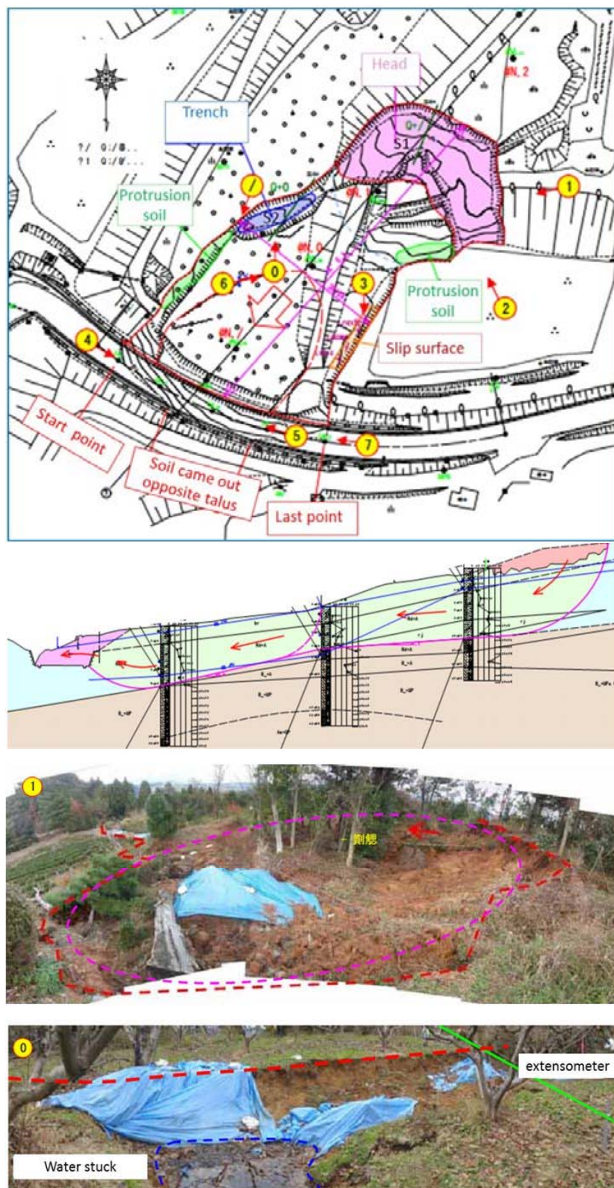


Figure 7 Pictures and sketch of Sorayama landslide (Source: Fujii consulting & associates, Matsue, Shimane, Japan)

It can be seen that Sorayama landslide was triggered by the effect of heavy rainfall and weathering of the bed-rock unit within the slip

zone. On 4 September, heavy rainfall caused saturated condition in the slope layers. Then, the soil bulk density and pore water pressure

increased, which reduced the cohesion between particles, and forming in saturated soil layers and creates hydraulic pressure that reduced the effect of friction between the crust and bedrock. These led to the triggering of a small landslide. On 24 October, a typhoon with high rainfall intensity increased the landslide activity to potential failure condition, as runoff water infiltrated inside cracks which were created by the initial movement of the landslide. Dynamic flows existed in the underground existing cracks widened and increased the rate of erosion and scouring of the slope material, as shear strength decreased rapidly. Self-weight of the soil layers combined with hydraulic pressure prompted the slope to collapse completely. Moreover, the landslide body appeared large crack as a small another future landslide (at position 8 in Figure 7). However, this landslide will occur be impossible in future due to slope angle is small.

Research methodology

A finite element method (FEM) is very effective analysis method for solving the geotechnical problems. In this method, the continuous domains are divided into subdomains (e.g. elements). These domains are linked together at the nodes. In the subdomains, equivalent problem is solved approximately on basic functions for each element, boundary value problems with stable solution and continuity between elements. There are many commerce computer programs using FEM code such as: MIDAS GTS, Geoslope, Plaxis, LS-Rapid, etc.

The study methodology is to combine the Midas GTS NX and the LS-Rapid software to monitor landslide. A landslide model 3D will be installed by Midas GTS NX and LS-Rapid from collected data from the landslide site. Simultaneous analysing by software, carrying out monitoring and investigation of landslide in the field to compare and modify with analysis in software to give a precise result that approach real in the field. Evaluations heavy rainfall's impact upon the initiation and motion of landslides can be inferred from the aforementioned model analysis and monitoring.

Seepage analysis

Midas GTS NX can analyze seepage condition including steady state analysis and transient analysis. In this study, transient analysis model will be used to analyze the landslide when rainfall changes according to time. Moreover, this model can compare slope between the fully dried initial state and saturated state. Hence, the transient analysis can be used to estimate the time it takes to saturate the interior part of the

slope and analyze the saturated condition of the slope.

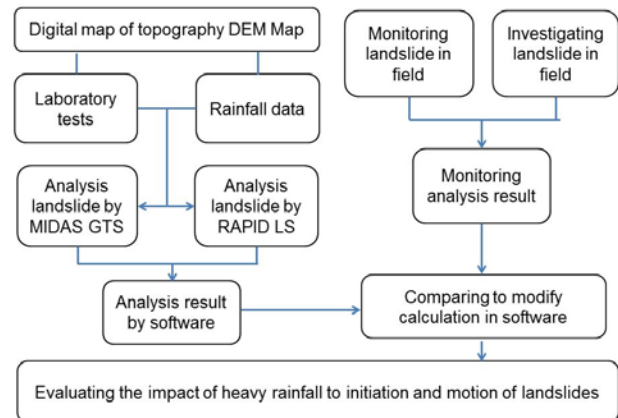


Figure 9 Diagram of studying method

Stability slope analysis

The slope always has a self-weight potential energy due to gravity and external forces such as pore water pressure, applied load, earthquake and wave force, which act on the slope and affect its stability.

A slope failure occurs because of heavy rainfall when the internal shear stress due to the self-weight and external forces is greater than the shear strength of the slope soil.

In this study, strength reduction method (SRM), a nonlinear FEM-coupled strength reduction analysis will be applied in Midas GTS NX. The SRM uses a numerical analysis method to analyze the minimum safety factor and failure behaviour using various slope geometry, load and boundary conditions.

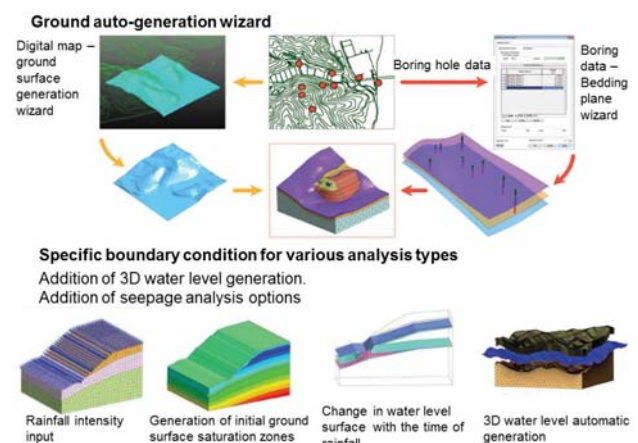


Figure 8 Input data in Midas GTS NX with 3D model (Source: Midas GTS NX tutorial papers)

Describe initiation and motion of landslide

LS-Rapid is a simulation model which was developed by Prof. Kyoji Sassa (International Consortium on Landslides) to analyze landslide initiation and motion based on natural condition data. It will be applied to describe movement

progress of Sorayama landslide that approach real in the field.

Monitoring

Carrying out landslide monitoring in the field such as measuring movement of landslide. Monitoring result will be used to compare and modify with analysis result by software.

Conclusion

Analyzing landslide trigger by heavy rainfall is very complex such as slope examining surface condition and pore-water pressure changing depend on many factors such as duration of the rain, rainfall intensity, permeability of soil, initial soil condition, the depth of ground water level.

My study will focus on changing pore water pressure and internal stress in soil during heavy rainfall to understand the initiation mechanism of landslides as well as its failure process.

References

- Collins DB, S.M.ASCE, Znidarcic D, M.ASCE (2004), Stability analyses of rainfall induced landslide, McIntyre Library, ILL University of Wisconsin Eau Claire, WI 54702-5010.
- Johari A, Sarah D, Daryono RM (2008), Hydrological condition leading to landslide initiation, 68/ MEDIA TEKNIK SIPIL/JULI 2008.
- Lanni C (2012), Doctoral thesis in environment engineering, XXIV cycle, Faculty of Engineering, University of Trento.
- Sassa K, He B, McSaveney M, Nagai O (2013), ICL Landslide Teaching Tools, International Consortium on Landslide, ISBN 978-4-9903380-2-0.
- Sassa K, Canuti P, Yin Y Editors (2014), Landslide Science for a Safer Geoenvironment, International Consortium on Landslide, ISBN 978-3-319-04995-3.



Proceedings of the SATREPS Workshop on Landslides in Vietnam, 2014

Overview of extensive shallow landslides caused by typhoon Wipha (Oct.2013) in Izu-Oshima island and further research plan

Vu The Truong⁽¹⁾, Satoshi Tsuchiya⁽²⁾, Fumitoshi Imaizumi⁽³⁾

1) Shizuoka University, Department of Environment and Forest Resources Science, Shizuoka, Japan, e-mail: thetruong01@yahoo.com⁽¹⁾, afstuti@ipc.shizuoka.ac.jp⁽²⁾, afimaiz@ipc.shizuoka.ac.jp⁽³⁾

Abstract: Heavy rainfall-induced landslides are mostly superficial and are initiated in soil slopes where a permanent groundwater table is often absent due to slope steepness and dry environmental conditions. Surficial in such slopes are mostly in a state of partial water saturation. Significant disasters are systematically recorded in Izu-Oshima islands, Japan where pyroclastic deposits overlie carbonate massifs. In October 2013, heavy rainfall of typhoon Wipha triggered flow-type shallow landslides along the slopes of the western side of Mihara Mountain. Landslides turned into debris flows and killed 35 people, 4 people were missing, more than 70 homes were destroyed. Unusual rainfall of more than 800 mm/day was an unusual phenomenon (return period > 500 years). Devastated area (0,67km²), in which landslides and debris flow caused severe erosion and deposition occupy 39% of entire basin area (1,7km²), collapse area (0,09km²) in which landslides occupy 5% of entire basin area, erosion area (0,22km²) occupy 12,9% of entire basin area. The results of the initial investigation carried out at the landslide site are described in this paper in order to pursue the landslide mechanism using a saturated-unsaturated flow analysis.

Keywords: Rainfall, Shallow landslide, Flow-type, Saturated-unsaturated.

Introduction

Heavy rainfall can lead to shallow slips in slopes that are initially in a state of partial water saturation. The failure surface of shallow slips is commonly situated between 0.5 and 3 meters in soil depth and runs subparallel to slope surface along an interface between soil cover and bedrock. The whole sliding mass is often several meters to tens of meters wide, several tens of meters long and sums up to a couple of hundred to thousand cubic meters in volume (Dai et al. 1999). Shallow slides in steep slopes (30 to 40°), composed of loose colluvial deposits mostly mobilize

completely to form debris flows. Actually, flow-type failures such as debris flows and flowslides are reported to result most often from shallow slips (Iverson et al. 1997). Although landslides under the action of variations of positive (compressive) pore pressures are well documented and probably most recurrent, they may also happen in unsaturated conditions. Such is the case for slopes where the substratum is not in particular less permeable than the soil cover and the contribution of capillary forces to slope stability is substantial (Godt et al. 2009).

Significant disasters are systematically recorded in Izu-Oshima island, Japan where pyroclastic deposits overlie carbonate massifs. Izu-Oshima is a volcano island, which has a 3-4 km across summit caldera and a central cone, in Izu Islands about 120km SW of Tokyo (Fig. 1). A major eruption from Izu-Oshima volcano in 1986 produced spectacular lava fountains up to 1600 m height and a 16-km-high subplinian eruption column. In October 2013, typhoon Wipha passed over the island of Izu-Oshima, bringing strong winds and heavy rainfall (more than 800 mm in 24 hours) that triggered shallow flow-type landslides along the slopes of the western side of Mihara Mountain. Thirtyfive people have been killed, 4 people missing, and more than 70 houses destroyed in the resulting extensive shallow landslides and following debris flow. The trees, surface soil and volcanic ash deposition becomes debris flow reached the sea.

The results of the initial investigation carried out at the landslide site are described in this paper in order to pursue the landslide mechanism using a saturated-unsaturated flow analysis.

Outline of Izu-Oshima disasters

Cumulative rainfall observed at 9:00 15th October in Oshima observatory was about 20 mm. Then rainfall intensity started to increase at around 0:00 of 16th, and it was observed at 3:00 of the

same day, the rainfall about 118 mm and at 4:00 the rainfall about 118.5 mm. After 24-hours, total rainfall was 824 mm (Fig. 2). At that time, it also was observed of rainfall about 61.5 mm and 412.5 mm respectively in Oshima Kitanoyama observatory (Fig. 2), a distance of approximately 4km to the North from Oshima observatory (Fig. 1). In addition, the interviews from the local residents were carried out and estimated the occurred time of shallow landslides at from 2:30 to 3:00 16th October.

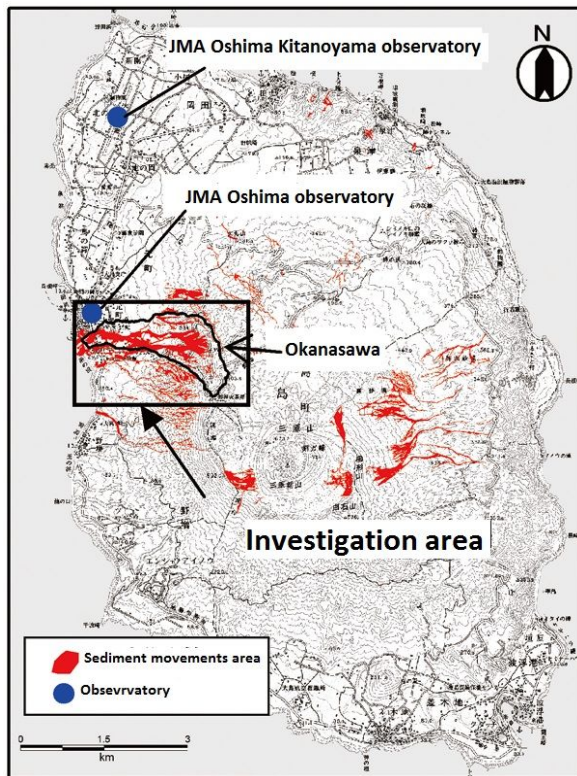


Fig. 1 The sediment movement area by the typhoon Wipha and position of observatory (Reference)

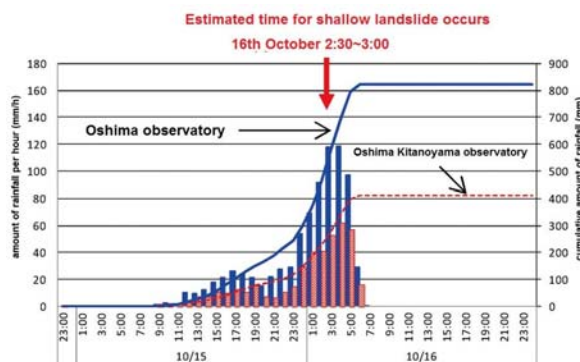


Fig. 2 Hourly and cumulative rainfall of typhoon Wipha (Observed by Japan Meteorological Agency)

Geological setting

The geology of Izu-Oshima Island was volcanic origin. Outline of overlie geology in investigation

area: Orthopyroxene-augite basalt lava and associated andesite lava, Orthopyroxene-augite basalt scoria and spatter, Orthopyroxene-augite basalt lava, Augite basalt lava, Olivine - augite basalt scoria, Basalt scoria, Pyroclastic fall deposits and lava flows.

Field investigation

An average depth of the surface slope collapse was evaluated 0.92 m by Cone Penetration Test. And 6 combinatorial soil samples were carried out in laboratory for determine physical properties of soil. The soil profile of the collapsed area is shown in Fig. 3



Fig. 3 View of shallow landslide site

The slip surface is plainly with hummocky (Fig. 3), and depth of shallow landslides is spatially variable. Also can be seen the ground surface is plainly with unevenness and high density of vegetation. Field investigations showed that two species of trees, *Ilex crenata* var. *hachijoensis* and *Eurya japonica*, are dominating this area. Two species of tree have different characteristics as follows: The first type is the tree with height of 5-6m, diameter of 5-12cm and density of 1600 trees / ha. And the second type of tree with height of 8-10m, diameter of 15-20cm and a density of 700 trees / ha. The plant roots of investigation area was grow up and concentrated in the near surface soils, stretched in the transverse direction and did not seen vertical root. The root system was observed diameters of from 1 - 3 cm, depth of 0.5 - 0.8m or more and about 1m of wide rise up. In general, root system contribute as an anchor in the slip surface. Poor root system in the investigation area did not work as anchors, in conjunction with rainfall, and was not sufficient to keep slope stability.

Figure 4 shows results of the cone penetration test. This test was a method used to determine the geotechnical engineering properties of soils and delineating soil stratigraphy. The blue coloured line shows the depth profile of the geotechnical engineering properties of soils outside of the collapse and the red coloured line shows that in side of the collapse.

The results show the delineating soil stratigraphy as follows: the soil layer with average depth of about 15 cm from ground surface, the Tephra layer with average depth of about 85 cm from soil layer, the Scoria layer with average depth of about 230 cm from Tephra layer and the Basalt layer with average depth of about 120 cm from Scoria layer (Fig. 4).

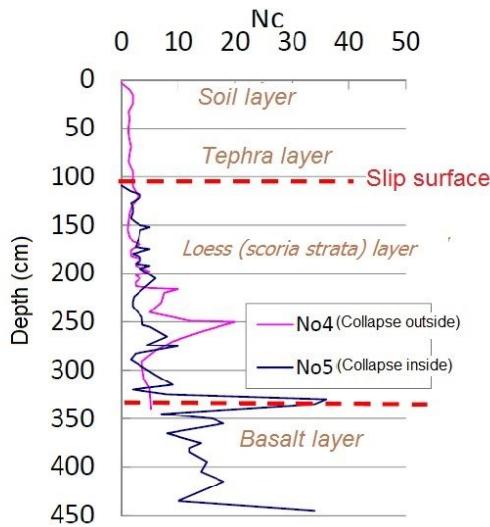


Fig. 4 Geotechnical engineering properties of soils and delineating soil stratigraphy

The result also showed the hardness and consolidation of soil layer from ground surface to slip surface is lowest.

Strength and hydraulic properties

The results of laboratory experiments with soil samples for determine the strength and the hydraulic properties of soil are shown in Fig. 5 and Fig. 6, respectively.

The safety of any geotechnical structure is dependent on the strength of the soil. If the soil fails, the structure founded on it can collapse. Understanding shear strength is the basis to analysis soil stability problems like: lateral pressure on earth retaining structures; slope stability and bearing capacity. Direct Shear Test was carried out in laboratory with soil samples and the results of them shows the shear strength of soil under saturated condition. Cohesion and friction angle (C and ϕ) of soil layer were determined from Direct Shear Test with 4.4 kPa and 12.7° , respectively.

In addition, the experiment with soil samples for the hydraulic properties of soil was also carried out in laboratory to determine the relationship between volumetric water content and pressure head and between volumetric water content and hydraulic conductivity. From the experimental results can be seen the hydraulic conductivity tends to increase when the soil in a

saturation state, and it tends to decrease when the soil in drying condition.

Understanding of that relationships is important in the analysis of rainwater infiltration into soil and its effect to slope stability. These relationships are known as the water retention curve and the hydraulic conductivity function, respectively.

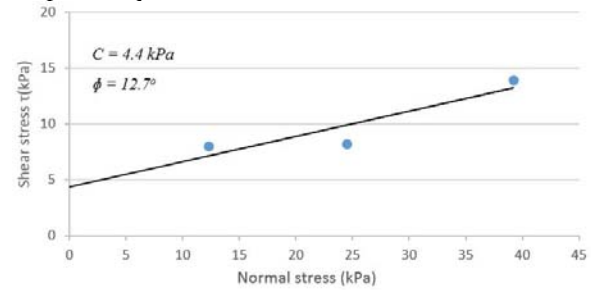


Fig. 5 Shear test result

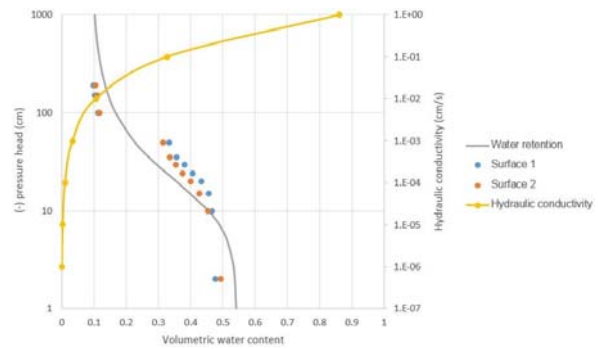


Fig. 6 Relationship between volumetric water content and pressure head and hydraulic conductivity

Plan study

The field investigations and laboratory experiments to obtain calculation conditions for the slope stability analysis. We will pick up soil samples at various points and investigate spatially distributed physical and hydraulic properties of soil.

Next step of study plan is the analysis combined saturated-unsaturated flow by FEM, to estimate the level of groundwater table, and then to obtain the pore water pressure. The safety factors and its variation during and after the rainfall will be evaluated by stability analysis.

Finally, we can reproduce the initiation of shallow landslides during heavy rainfall in Izu-Oshima Island and explain initiation mechanism of the landslide.

Acknowledgments

The work presented in this paper was made possible through the support of members of Laboratory of Forest Hydrology and Erosion Control Engineering – Department of Environment and Forest Resources Science – Shizuoka University.

References

- Ning Lu and Jonathan W. Godt, (2013) Hillslope Hydrology and Stability. Cambridge University Press. (ISBN 978-1-107-02106-8) 437p.
- Ishikawa Y, Ikeda A, Kashiwabara Y, Ushiyama M, Hayashi S, Morita K, Tobioka S, Onodera T, Miata N, Nishio Y, Ogawa H, Suzuki T, Iwasa N, Aoki T, Ikeda T , (2014) Debris Disasters caused by Typhoon Wipha (T 1326) in Izu Oshima on Oct. 16, 2013. Japan Society of Erosion Control Engineering, Vol.66, No5 January 2014.
- Eichenberger J, Nuth M, Laloui L, (2011) Hydromechanically coupled analysis of transient phenomena in a rainfall-induced landslide. 2nd International Symposium on Computational Geomechanics, Dubrovnic, Croatia, p. 547-556.
- Egeli I, Friat Pulat H, (2011) Mechanism and modelling of shallow soil slope stability during high intensity and short duration rainfall. Scientia Iranica, Transactions A: Civil Engineering 18 (2011), p.1179–1187.
- Nakamura H, Koyama T, Lee K, Yamada M, Ohnishi Y, (2013) Numerical simulations for rainfall induced slope failure – rainwater infiltration mechanism and evaluation of slope stability during torrential rainfall. Caspian journal of Applied Sciences Research, 2(AICCE'12 & GIZ'12), p.431-439, 2013.



Proceedings of the SATREPS Workshop on Landslides in Vietnam, 2014

Identification of slope deformation by the Particle Imaging Velocimetry (PIV) Analysis of air photos or laser scanning images in different periods

Sakae Mukoyama⁽¹⁾, Kyoji Sassa⁽²⁾, Doan Huy Loi⁽³⁾, Hiroataka Ochiai⁽⁴⁾, Toyohiko Miyagi⁽⁵⁾

1) Kokusai Kogyo Co. Ltd., Tokyo, Japan, sakae_mukoyama@kk-grp.jp

2) International Consortium on Landslides, Kyoto, Japan, kyoji.sassa@gmail.com

3) Kyoto University, Disaster Prevention Research Institute, Kyoto, Japan, doanhuyloidkt@gmail.com

4) Forestry and Forest Products Research Institute, Tsukuba, Japan, ochi@ffpri.affrc.go.jp/okada10@ffpri.affrc.go.jp

5) Tohoku Gakuin University, Izumi-ku, Sendai, Japan, e-mail: miyagi@izcc.tohoku-gakuin.ac.jp

Abstract It has been difficult to measure small ground deformation like slow landslide movement efficiently in wide area with high accuracy. We present a new method for measuring the movements of landslides in detail by using temporal high-resolution DEM. In this method, the technique of image matching analysis applied for the calculation of 3D-vector of ground displacement. This method is effective for landslide analysis with 3D-model from temporal LiDAR data, and also has possibility for analysis with temporal aero-photographs or satellite images.

Keywords Landslide, LiDAR, Image-matching, PIV

Introduction

Usual method for monitoring landslide such as in-situ measurement by equipment on the ground has been not able to measure two-dimensional movements spatially and accurately. In recent years, it has become possible to obtain high-resolution point cloud topographic data with airborne laser scanner (LiDAR survey), and to grasp deformations of ground surface clearly by high-definition geomorphic images.

Figure 1 shows existing techniques of spatial survey for ground displacements. There are various kinds of measuring methods including ground survey and satellite image survey. However there is a vacant gap around 1m order movement and 10 km² spatial area survey. The objective of this study is to fill this gap with efficient and high-performance method, using digital topographic data by aerial survey.

Methodology

There are two methods for estimation of ground displacements from point cloud data. First method is the analysis by point cloud to point cloud calculation. It is known as ICP (Iterative Closest Point) algorithm (*Teza et al., 2007*). Second one is the surface model to surface model analysis. It is based on the Raster Image Matching Correlation algorithm and additional calculation for vertical displacements by elevation value of DEM. Both of the method has similar approach which is to find best position of post-movement by minimizing differences between temporal topographic models. In this study we chose second approach and applied Geomorphic Image Matching Analysis named 3D-GIV (Geomorphic Image Velocimetry) (Mukoyama, 2011; and Japan Patent No. 4545219). Why velocimetry? Because the physical dimension of displacement per interval time can be recognized as an average velocity.

Figure 2 shows the conceptual scheme of the method. The general steps for analysis are followings.

- ① Prepare temporal DEM.
- ② Calculate geomorphic quantity.
- ③ Convert to orthographic digital Images.
- ④ Conduct Image Matching Analysis.
- ⑤ Estimate horizontal component of displacements.
- ⑥ Calculate vertical component from elevation values of DEM around vector's head and tail.
- ⑦ Complete 3D-Vectors plotting.

For image matching analysis, we applied existing PIV algorithm. PIV (Particle Image

Velocimetry) is originally developed for fluid analysis. That is essentially composed of 2-dimensional Image Matching to find the position to minimize the differences of brightness distribution in the small search windows. Instead of the particle images, we applied digital

geomorphic images for image matching. Orthographical, low noise and high-contrast image is best and we usually use slope angle or geomorphologic openness images in 8 bit grayscale.

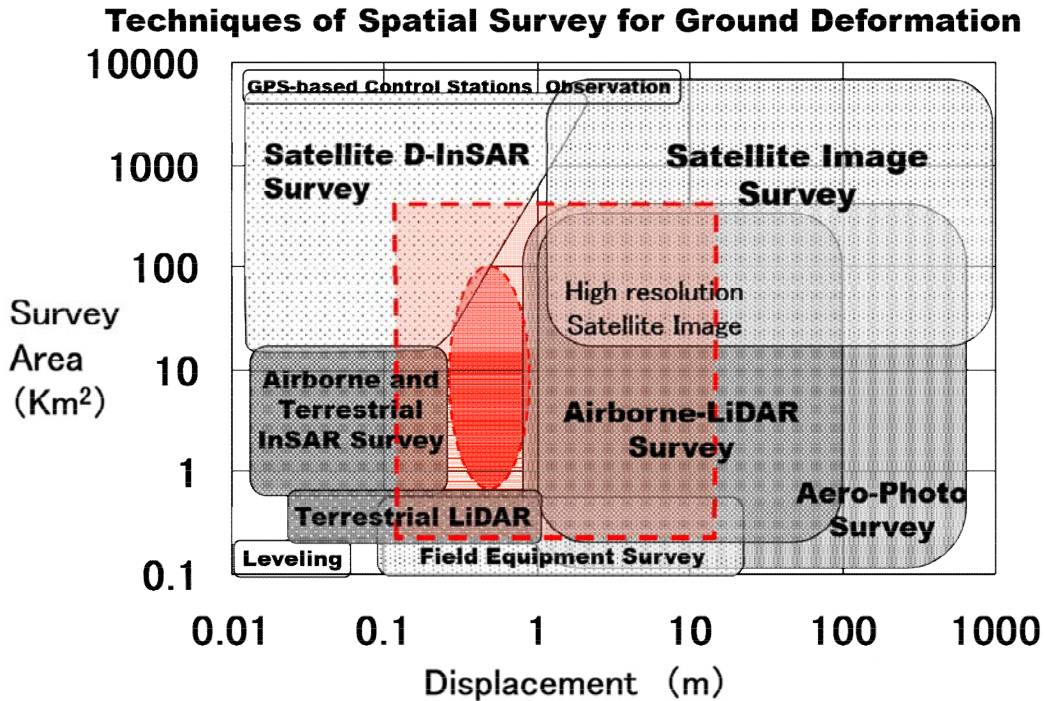


Figure 1 Existing techniques of spatial survey for ground displacements
Area with dashed line indicate suitable zone for 3D-GIV by LiDAR data

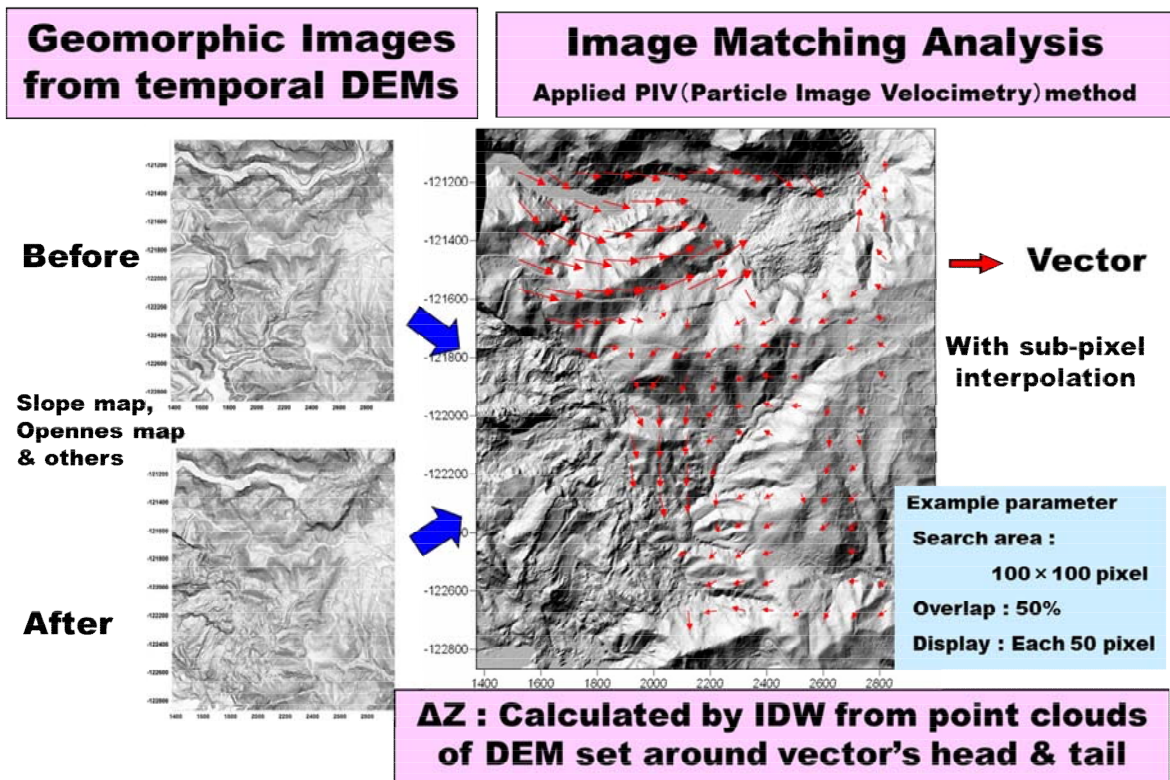


Figure 2 Conceptual scheme of the 3D-GIV method

The advantage of this approach is that it can grasp the momentum average obtained by removing the effect of the singularities, because it measures the displacement of the spatial region from huge random measuring points.

For the images used in this study, 1 pixel is the single grid size of 2 m×2 m DEM. And the size of the search window is 64 pixels × 64 pixels. In the image matching algorithm, sub-pixel interpolation was applied. It is normally possible to calculate displacement of about 1/10 pixel size. Since single grid size of topographic data was set to be 1 pixel, it is assumed that the reliable displacement is 0.2 m.

This method requires topographic surveys before the event. In Japan, over 60 % of national land has been covered with public-work LiDAR data before 2013. Additionally, some areas are covered with archived data by private companies for commercial use.

Case study

In Japan, there are many landslides in mountainous regions. Since olden days they had been used as good rice fields because their moderate slope and rich water supply prepare good locations for rice cultivation. However, in winter Northern Japan area is covered with snow. And sometimes, landslides move suddenly and quickly in snowmelt season.



Figure 3 Location of Shimekake landslide and Koshio landslide

Study area is located nearby Mt. Gassan volcano and named as Shimekake Landslide. Geology of the field is composed by Neogene sedimentary and pyroclastic strata in gentle

folding structure with dolerite seat intrusions. The remarkable movement of landslide occurred in the spring of 2009.

Field investigation of Shimekake landslide and PIV results

The Landslide research team found about 2m scarp at the top and about 1m scarp at the middle of landslide area. Some minor scarps divided the landslide area into some small blocks.



Figure 4 Main scarp at the top of slope (Taken by Landslide Research Team, 2009)



Figure 5 Minor scarp near the toe of slope



Figure 6 Sliding surface at the toe of landslide area

The movement area has the length in 1000 m, and a width of 800 m. From borehole data, the sliding surface has depth about 100m. We find small river crosses the toe of landslide.

The material of sliding layer is soft clay. The material of the upper layer is debris that consists of turf and weathering products of sandstone and clay stone. The lower layer almost is clay so this landslide is a reactivate type clayey landslide the movement is slow.

This area has several GPS points and GPS data showed the movement is estimated to continue in the future. So it is necessary to establish the reactivity of this landslide.

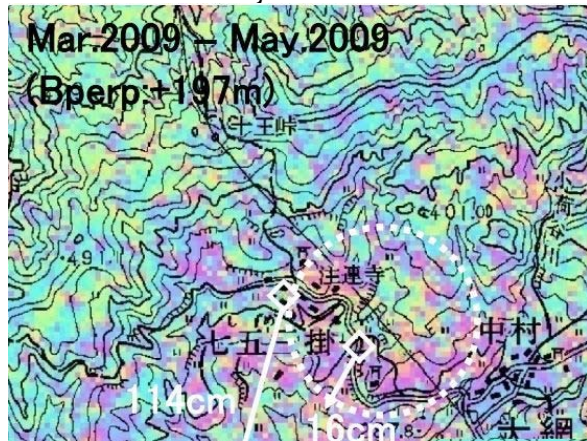


Figure 7 GPS monitoring after damage (After A.Suzuki and et al, 2009)

In this paper, we will present the result of PIV method and compare with GPS data.

Maximum total displacement of 4 months reached over 7 m and maximum daily movement measured by GPS survey was about 6 cm (Iwasaki *et al.*, 2011). With the ground surface displacements steep scarps, gabens and open cracks have been appeared on the crown of landslide brock.

In this study, the analysis conducted with topographic images made from multi-temporal DEMs created by LiDAR surveys in December 2004 and June 2009. Figure-6 and Figure-7 shows the temporal geomorphic images of landslide. These images are gray scale openness maps made from a pair of 2m grid-DEM. On the images areas in high-brightness are rice paddies and roads.

From the results of 3D-GIV analysis we calculated the amount of surface displacement and created motion vector map. Figure 8 shows the spatial distributions of the displacements. Vectors are calculated by image correlation between small search windows and plotted at the intervals of 32m, in this case. On this whole image we can get a full picture of landslide movement in easy-to-understand way.

Figure 8 shows the maximum of ground movement is about 7.6 m. It is conformable with GPS results (over 7m). On the other hand, the vector directions are the same with GPS points.

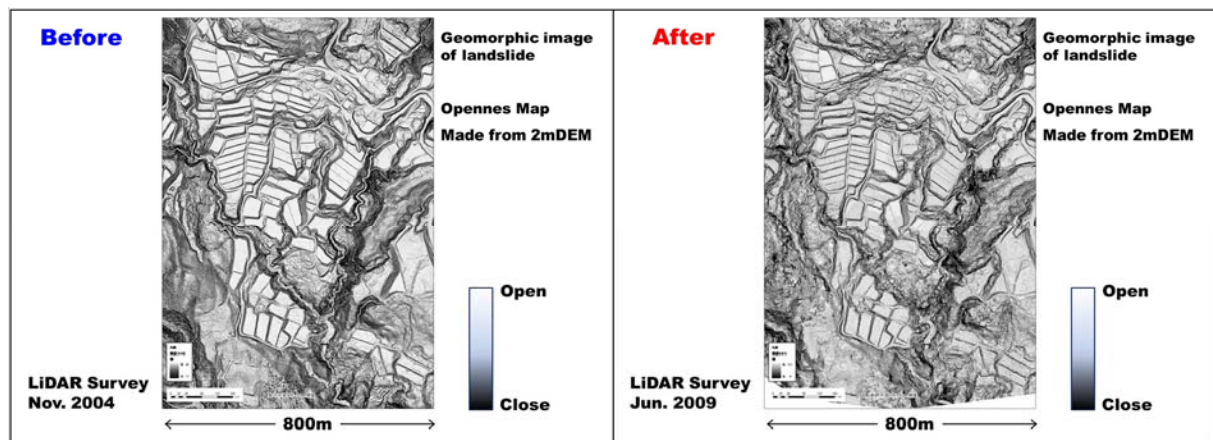


Figure 8 Geomorphhic Image of Shimekake landslide in 2004 and 2009

A planned study site in Japan

For future research we conduct three methods to study Koshio landslide in Nagano Prefecture. There has been landslides movement in past history. Accelerated movement occurred after torrential rains in June, 1992. Immediate damage included the destruction of a small check dam, deformation of 8 small check dams, and tension cracks that developed along the slope. Further movement of the slide mass damaged residential structures and the National Highways, and buried Kashio River. By 1994, the slide movement has slowed down due to the effective mitigation measures. However, the Upper Block shows an

annual movement of 300 mm, therefore We should continue to study this landslide by using PIV method and experiment method such as ring shear test. This research method is described in the following diagram.

The Koshio landslide is rapid landslide and active landslide. Therefore, it is good for apply PIV method.

Our future goal of this study is to establish Dynamic and Kinematic Geomorphology in Engineering Geology. We hope 3D-GIV method, as a Geoinformatic technology, will open the new field of Geoscience and Technology.

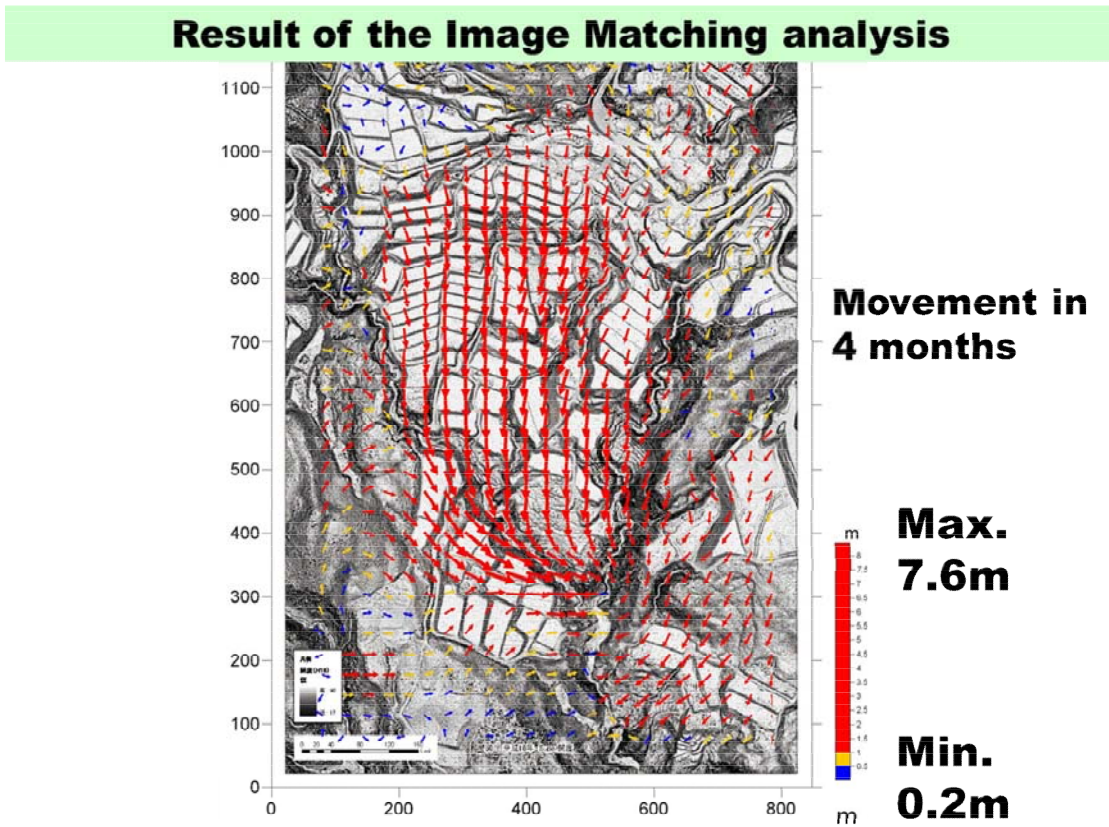


Figure 9 Horizontal moving vectors of ground displacements of landslide. Vectors are plotted at the intervals 32m in this case

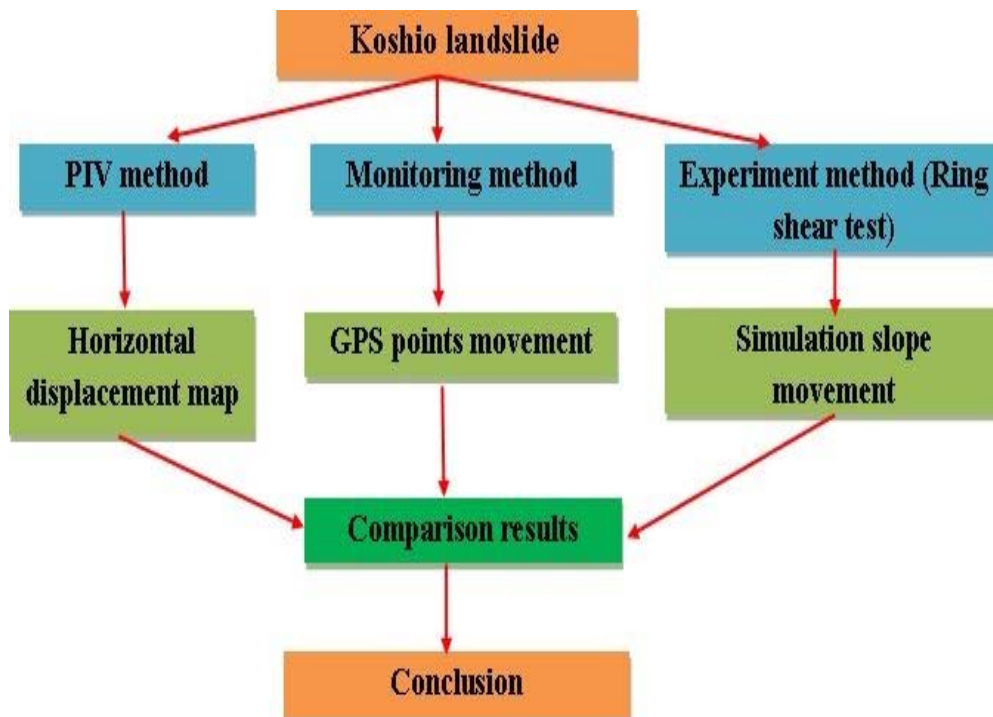


Figure 10 Three research methods for Koshio landslide in Nagano prefecture

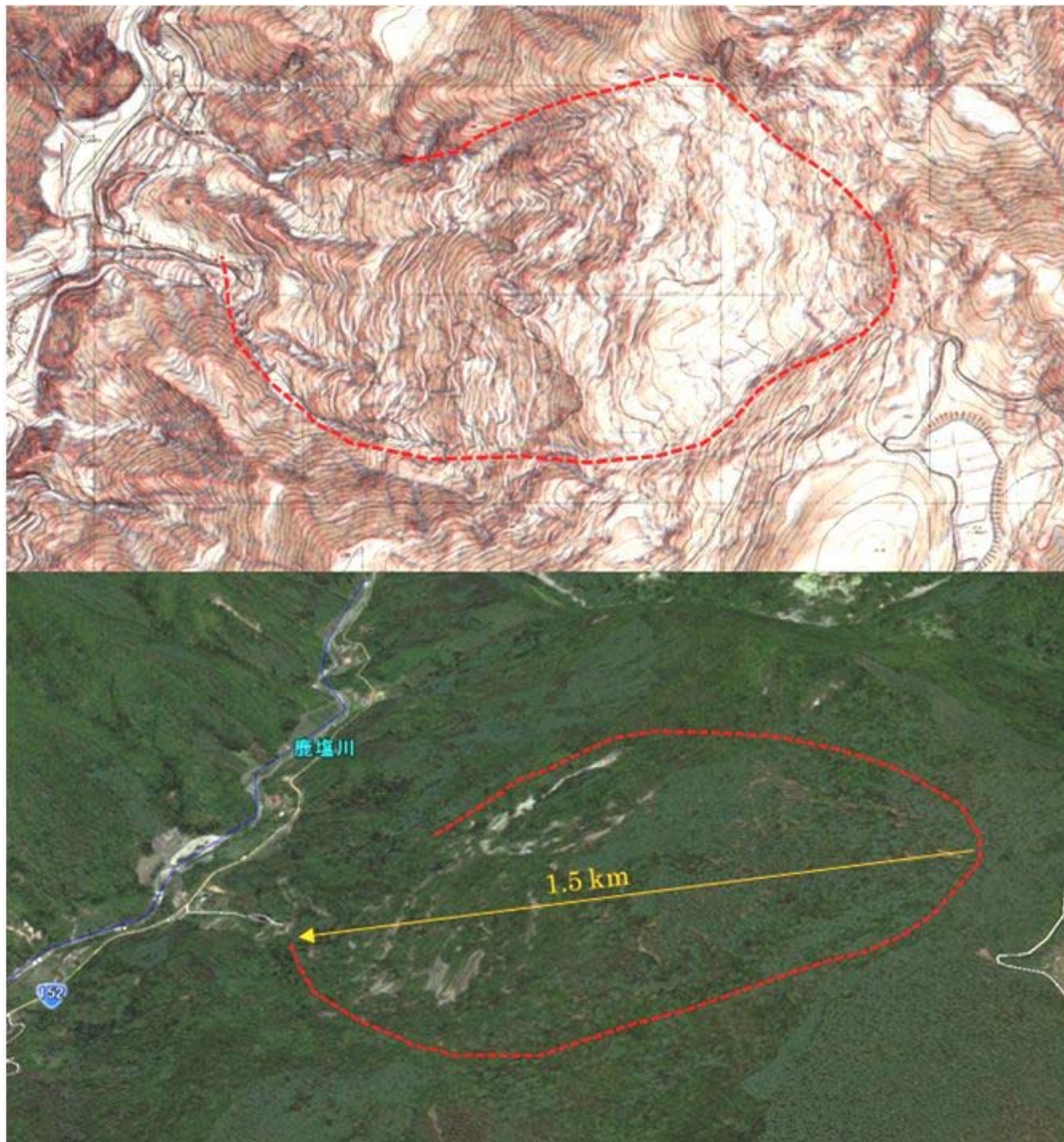


Figure 11 Google and topographic maps of the Koshio landslide in Nagano Prefecture

Conclusion

The initial result of PIV method has satisfactory result. This method can apply for larger scale. From this result, we can assess this area is unstable. Therefore, we can know the area is necessary to establish the warning and evacuation system.

Traditional photogrammetric analysis for landslide movement required manual orientation, photo-interpretation and measurements of particular points before only a few scattered vectors were calculated. On the other hand, dense cluster of motion vectors are available automatically by the 3d-GIV method. This new method is applicable to various surveys of post-event and monitoring of pre-event.

Additionally, this new method has a possibility to apply for analysis of DSM images. If the condition of the vegetation in study area is generally stable and constant, image matching

analysis work well and displacements area can be extracted as analysis with DEM images. So, high-resolution aerial photographs or satellite images will be also useful for making DSM data.

For further study, we expect to make the landslide risk map based on PIV method.

References (in the alphabetical order)

- Iwasaki, T., T. Arakawa, H. Nakazato, T. Masunari, N. Shimizu (2011), Development of a displacement monitoring system using GPS for installation immediately after a large-scale landslide. *Journal of the Japan Landslide Soc.*, Vol. 48, No. 2. (In Japanese)
- Mukoyama, S. (2011), Estimation of Ground Deformation Caused by the Earthquake (M7.2) in Japan 2008, from the geomorphic Image Analysis of High Resolution LiDAR DEMs. *J. Mt. Sci.* (2011) 8: 239-245
- Teza, G., A. Galgalo, N.Zaltoron, and R. Genevois (2007), Terrestrial laser scanner to detect landslide displacement fields: A new approach, *Int. J. Remote Sens.*, 28(16), 3425-3446.



Proceedings of the SATREPS Workshop on Landslides in Vietnam, 2014

Development of integrated data and Web-based analysis software for Vietnam

Keisuke Takimoto⁽¹⁾, Shiho Asano⁽²⁾, Osamu Nagai⁽³⁾, Hiroshi Fukuoka⁽⁴⁾, Kyoji Sassa⁽⁵⁾

1) GODAI Development Corp., Systems Engineering Department, Kanazawa City, Japan, takimoto@godai.co.jp:

2) Forest and Forest Products Research Institute, Department of Soil and Water Conservation, Erosion Control Laboratory, Tsukuba City, Japan, shiho03@ffpri.affrc.go.jp:

3) International Consortium on Landslides, Research Promotion Officer, Kyoto City, Japan, nagai@iclhq.org:

4) Kyoto University, Landslide Dynamics Section, Research Center on Landslides, Disaster Prevention Research Institute, Kyoto City, Japan, fukuoka.hiroshi.4v@kyoto-u.ac.jp:

5) International Consortium on Landslides, Kyoto, Japan, sassa@iclhq.org:

Abstract This software consists of two subsystems. Subsystem first is used to generate a common integrated database from the various different measuring instruments data format. The HaiVan station area near Da-Nang, various measuring instruments for land slide monitoring have been installed. Computer installed in the office of Hanoi, performs data collection and remote control via the Internet VPN, the instrumentation of them. There are three types of monitoring software to perform the collection and this control, data output method and format of the data is different in those monitoring software. In order to effectively utilize the data collected, it is necessary to be integrated in a same locale time series and to be classified in each instrument and instrument type. Thus, the data collected by 3 type monitoring software are picked up periodically, edited into a format that is integrated, and are registered into integrated database on this subsystem. Another subsystem is providing the user with a Web-based user interface for land slide situation analysis by using integrated database which generated on first subsystem. This subsystem show you measuring instruments group charts, measuring instruments location map, and will suggest a real time land slide collapse prediction when it's possibility could be high. It's also possible to download stored data. The Web-based applications of these, not only can be used at Hanoi office, but also can be accessed from all over the world through internet.

Keywords monitoring, integrated, Web-based, vpn, collapse prediction

Overall structure

In order to explain this software, is shown in Figure 1 an overall outline view. This Figure is made up of measuring equipment, data transmission equipment, transmission line, a computer that controls them, monitoring software, software development objects of this time.

Integration of the transmission path and the data transmission system

In the case of the HaiVan, the number and type of measurement equipment is large as Table 1, external interface is Ethernet and RS-232C. There was a need to integrate them. In addition, it was necessary to also take into account the expansion of IP camera on-site monitoring.

Table 1 measurement equipments list and interface

Measurement equipment	Number	interface
Extension meter	25	RS-232C
Groundwater pressure gauge	6	RS-232C
Borehole extension meter	6	RS-232C
Rain gauge	1	RS-232C
Air pressure and temperature gauge	1	RS-232C
Total Station(TM50) (30 mirror measurement points)	1	RS-232C
GNSS Surveying System	3	Ethernet
IP Camera (Expansion plan)	2	Ethernet

Therefore, we consider a method of first converted to TCP/IP packet over Ethernet and RS-232C signal of all, to telecommunications. This is because it is intended that the external interface to control via a network measurement equipment

of RS-232C. Of course, it is not necessary to convert the equipment with Ethernet interfaces, it is remotely controlled as it is. In order to achieve this conversion, the hardware device called SERIAL-ETHER converter, driver software for the PC is required.

Next, a method of transmitting up to ITST of Hanoi from Hai Van station measurement data has been considered. All devices of the Hai Van station nearby, there is a need to be controlled

from a computer in ITST(Hanoi). So we consider to be integrated on the same local network with VPN (Virtual Private Network) both sites. In previous surveys, the Hai Van station peripheral, mobile phone of VIETTEL is available has been reported. However, this mobile radio wave may or may not be used for data communication of up to Hanoi, it was necessary to test the communication by visiting the site actually.

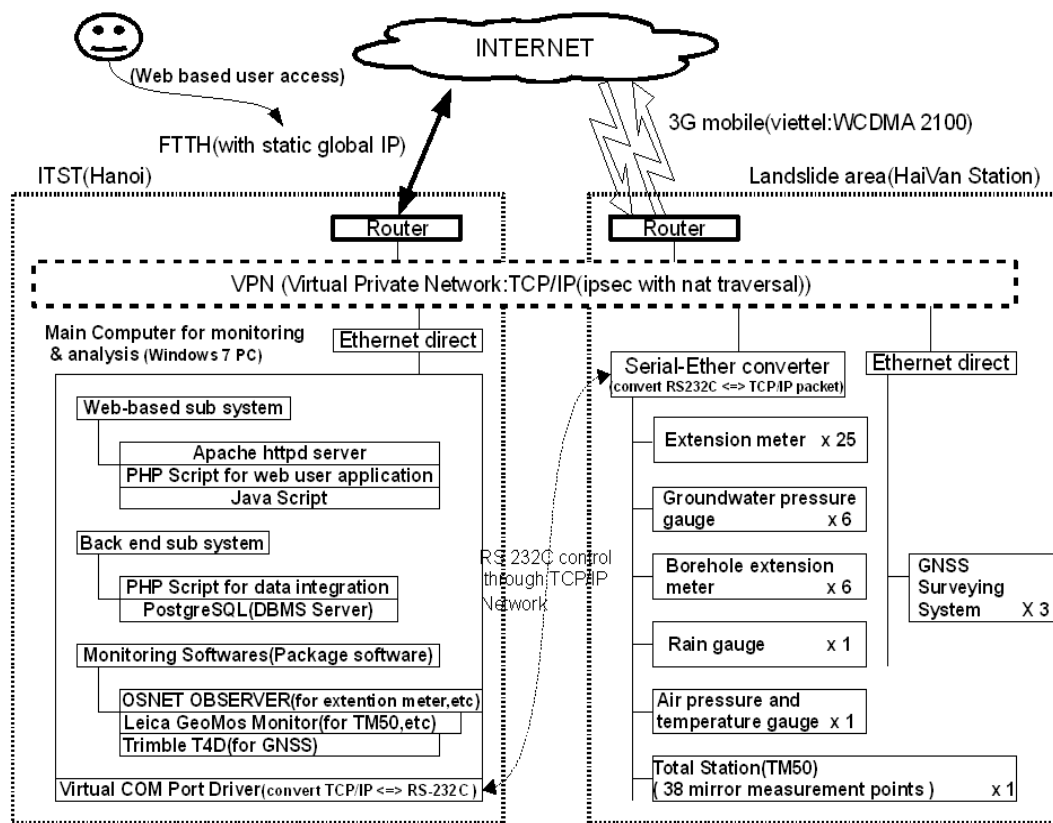


Figure 1 Overall structure(measuring equipment, data transmission equipment, transmission line, a computer that controls them, monitoring software, software development objects of this time)

HaiVan station communication environment survey

Advance preparation and survey items

Our team conducted a survey of communication environment in Hai Van Station between June 16 to 18. There are three items to survey. The first is, 3G mobile in the Hai Van Station: The effective speed of investigation (VIETTEL WCDMA-2100) communication. Second, 3G mobile: to identify the relay 3g stations (VIETTEL WCDMA-2100). Third. Test connection to the VPN host router that was installed in Japan on the assumption ITST(Hanoi). As preparation, we were prepared router and USB dongle available in Vietnam 3G mobile, was tested it by mounting the viettel SIM.

Table 2 Equipment list in survey of communication environment in HaiVan Station

Equipment or host	Number	Location
ROUTER(YAMAHA RTX-810)	1	HaiVan St
USB 3g dongle (ZTE MF190)	1	HaiVan St
Note PC	1	HaiVan St
Battery(8AH 12V)	1	HaiVan St
SMART phone	1	HaiVan St
Viettel SIM	2	HaiVan St
VPN Cloud (openvpn Server)	1	Japan
ROUTER(YAMAHA SRT-100) (Global static IP assigned) Assumed (Hanoi) ITST	1	Japan

The other equipment, notebook PC, battery, and smartphone which specify 3g station position were prepared. In addition, we have obtained in Vietnam the Viettel SIM. Equipment list at the time of testing is TABLE 2.

Survey results

It conducted a survey of the effective communication speed on the front of the HaiVan Station, indoor, the roof June 16 and 17. Was carried out in how to connect with OPENVPN to cloud server that was installed in Japan from HaiVan, repeated five times to download and upload files of 10M bytes in FTP, and recorded average speed(kbps). Result is Table 3.

Table 3 Effective communication speed test in HaiVan Station(5 times average unit:Kbps)

Test enviroment	Upload (Kbps)	Download (kbps)	result
Front of HaiVan St (train not stay)	964.5	843.2	good
Indoor of HaiVan St (train not stay)	93.1	65.1	bad
Roof height of HaiVan St (train not stay)	1154.1	932.1	good
Front of HaiVan St (train stay at station)	52.1	32.4	bad
Indoor of HaiVan St (train stay at station)	21.4	18.3	bad
Roof height of HaiVan St(train stay at station)	1132.2	1011.4	good

At the same time, the analysis by smart phone, the position of the source of the radio waves since been found, is shown in Figure 2.

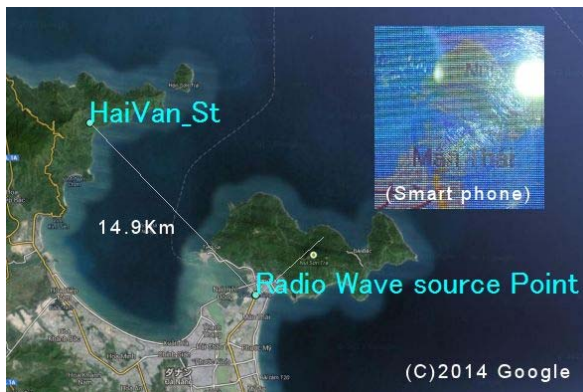


Figure 2 Viettel 3G mobile radio wave source point which indicated on smart phone and distance from HaiVan station. We measured distance with QGIS(Quantum GIS).

The June 18, and made the connection test with the VPN host router installed at the Japan assuming the ITST (Hanoi). Type of VPN was used after adding NAT traversal to IPSEC. The Internet connection by 3G mobile, that the global IP address is assigned to the terminal is rare, in many cases, the reason for using this VPN type, because assigned private address of the provider-

specific (Carrier Grade NAT). For PPTP type commonly used in the VPN, it is speculated because if a failure occurs in the VPN connection is often, if (IPSEC + NAT traversal), less failure most established. Connection test results with Japan is in good condition, and has established a VPN connection in about one minute after starting the router. The management screen of the VPN connection after the Vietnamese side of the router (YAMAHA RTX-810) in Figure 3, The management screen that you see through the VPN from the Vietnam side of the Japanese side (YAMAHA SRT-100) in Figure 4, Japanese side staff indicates a management screen that referenced Vietnamese router (YAMAHA RTX-810) through the VPN in Figure 5.



Figure 3 (Screen Shot)The management screen of the VPN connection after the Vietnamese side of the router (YAMAHA RTX-810(Japanese setting)).



Figure 4 (Screen Shot)The management screen that you see through the VPN from the Vietnam side of the Japanese side (YAMAHA SRT-100(Japanese setting)).

Make sure that the confirmation of this VPN connection test, we assume the status of a power failure, and pull out the power plug of the Vietnamese side router, and turn on the power to

refer to plug again, VPN connection was established again, We have finished all the tests.



Figure 5 (Screen Shot)Japanese side staff indicates a management screen that referenced Vietnamese router (YAMAHA RTX-810(Japanese setting)) through the VPN.

Summary of HaiVan station communication environment survey

Prior to this study, we had hoped that the upload speed of communication in the HaiVan station is 700Kbps or more. That after investigation of fact, it is well has been found. However, in order to always maintain its speed, it is necessary to an outdoor sensitive antenna height of the roof above the station building, is drawn to the router places the coaxial cable. Also, that the type of VPN is effective IPSEC + NAT traversal has been demonstrated. This study, plan to VPN connection over the Internet ITST (Hanoi) and HaiVan station, it has become possible to proceed as planned.

3 monitoring software and Back end sub system

3 monitoring software

Monitoring software of three is incorporated in the computer installed in ITST side. They control the measurement equipment of Hai Van Station, collect measurement data on a regular basis, and outputs in a reusable format the data. In the table 4 input/output and functions of the software.

Back end sub system

Back-end subsystem to monitor at regular intervals the output of the monitoring software of three. Acquires the data immediately when there is output data, formats the data format of a common format, and performs insert common database (PostgreSQL). At that time, it is

necessary to be integrated in a same locale time series and to be classified in each instrument and instrument type. it should be noted particularly is that the basis for the time stamp of the data output by the monitoring software is different. OSNET OBSERVER and Leica GeoMoS Monitor are local time(Vietnam Local Time). but Trimble T4D to output the data in the GPS time. Therefore, the back-end system, corrected to local time the time stamp on this GPS time.

Table 4 input/output and functions of 3 monitoring software

monitoring software (control equipment)	Control interface (sampling cycle)	Data output type	Data output Cycle
OSNET OBSERVER (Extention meter) (Groundwater pressure gauge) (Borehole extension meter) (Rain gauge)	COMport (5min)	File (CSV)	5min
Leica GeoMoS Momitor (Leica TM50) (Air pressure and temperature gauge)	COMport (1min)	DataBase (MSSQL)	1min
Trimble T4D (GNSS Surveying system)	Ethernet (1 sec)	File (CSV)	1hour

Another important role of the back end sub system, is that doing collapse prediction calculation in real time, to inform the risk to the user.

Web-based sub system

This subsystem provide instruments group charts(Ex Figure 6), measuring instruments location map(Ex Figure 7), and will suggest a real time land slide collapse prediction when it's possibility could be high. Because they are created in the web-based all, ITST not only (Hanoi), and is accessible from all over the world. Programming language are using javascript and PHP.



Figure 6 Example of instruments group charts

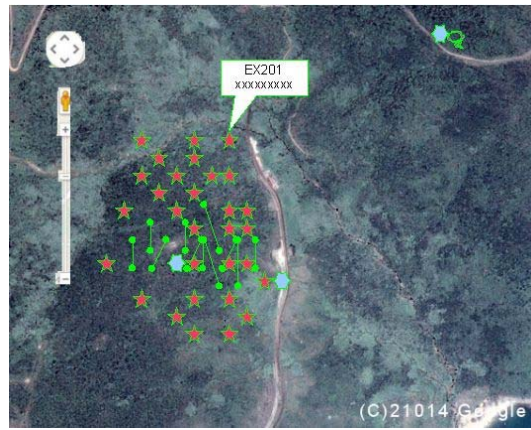


Figure 7 Example of measuring instruments location map

References (in the alphabetical order)

- Leica Geosystems C, (2014) GeoMos Monitor OSAS
- Technos Inc. C, (2009) OSNET OBSERVER
- Trimble Navigation Limited C, (2007)-(20013) TRIMBLE 4D CONTROL.
- YAMAHA Corporation,C,(2014). Manual of RT-Series, <http://www.rtpo.yamaha.co.jp/RT/manual.html>,18,jun, 2014.
- Wikipedia Corporation,C,(2014). Viettel Mobile, http://en.wikipedia.org/wiki/Viettel_Mobile,3,jun,2014.



Proceedings of the SATREPS Workshop on Landslides in Vietnam, 2014

Landslide mapping and the risk evaluation by aerial photo interpretation in Vietnam

Toyohiko Miyagi⁽¹⁾, Eisaku Hamasaki⁽²⁾, Dinh Van Tien⁽³⁾, Le Hong Luong⁽⁴⁾, Ngo Doan Dung⁽⁵⁾

1) Tohoku Gakuin University, Izumi Campus/2-1-1 Tenjinzawa, Izumi-ku, Sendai, Japan, e-mail: miyagi@izcc.tohoku-gakuin.ac.jp

2) Advantech Co., Ltd, Aoba, Sendai, Japan, e-mail: hamasaki@advantech.co.jp

3) Institute of Transport Science and Technology, Hanoi, Vietnam, Vietnamese leader of WG2. E-mail: dvtien.gbn@gmail.com

4) Graduate student of Tohoku-Gakuin University, Sendai, Japan/ ITST, Vietnam, e-mail: lehongluong@gmail.com

5) Institute of Transport Science and Technology, Hanoi, Vietnam, Vietnamese leader of WG2. E-mail: ngodoan@gmail.com

Abstract Landslide is a domain clearly distinguished from the surrounding slope. That is, it regards as a landslide topography is has an feature with very clear unit. Here, the landslide as the research object is a typical landslide phenomenon which has three the geomorphic and geological elements called the “Main Scarp”, “Landslide Body” and “Slip Surface (Surface of Rapture)”. As an important characteristic of a landslide, some part of destructed moving body which remains on a slope as a movable body, and it mentions the point that this movable body has the characteristic which works again. When this point is identify, it has the potential of reactivation repeatedly and it is necessary to note the point that it causes a disaster. That is, it is necessary for the land formed of the landslide to evaluate a possibility remove. This is the landslide risk evaluation.

On the other hand, it may also be called risk evaluation of landslide generating to give the aim also including the place which the landslide has not generated "whether a landslide occurs at what kind of place." This is called susceptibility evaluation in many cases. In order to evaluate Susceptibility, it is necessary to grasp where the actual landslides are distributed fundamentally. However, it performs now at Susceptibility evaluation tried in various places in many cases only by operation of the parameter considered to be concerned with landslide generating generally considered as the distribution actual condition of landslide geographical feature is not grasped.

Creation of landslide distribution map is a fundamental procedure which leads to slope disaster mitigation. The places which the

landslide occurring area are grasped correctly and are figure-ized. The possibility of the re-activation which this landslide place each that was figure-ized has is grasped. Techniques, such as AHP, are used for this works. In this project, the landslide topographic area distribution map was created in two areas of Central Vietnam. Based on these pieces of distribution maps, a field survey is performed rationally, and the movement characteristic of the landslide itself will be grasped, the mechanism of generating is also will considered.

Keywords Landslide mapping, Geomorphology, Risk evaluation, Susceptibility evaluation, Micro landform, Aerial photo interpretation

Landslide topography

Landslides, being natural disasters, are considered threats to life and financial capital. Research on landslides has been employed in the fields of science and technology development that relate to natural disaster prevention. That is to say, it has become applied science that is: ‘utilized when landslides unfold and natural disaster occur’. Recent projects on ‘understanding the host of risks linked to landslides’ or ‘risk evaluations of landslide topographies’ in Japan’s academic community focusing on landslides have made great advances; moving from past counter measures towards forecasting inference of landslide risks. We have promoted and contributed to these developments. Thus, this paper builds on these advances and reflects chronologically on how ‘technology aiming to

understand existing risks of landslides' has been constructed and linked to the risk evaluation, and discusses the significance of mapping landslide phenomena.

The Introduction of Aerial Photo Interpretation and Recognition of Landslide Terrain

Engineers and academics have broadly applied utilization of aerial photography since the 1960s. At Tohoku University's research laboratory for geography a 1/40000 monochrome aerial photography set taken by the US military was installed. This was done for the purpose of analysing aerial photography and land classification in national land surveys. In and around 1965, various scholars pointed out that 'landslide topography' formed through landslides can be recognized by aerial photography analysis (ex. Ichise, 1964). Furthermore, applying aerial photo interpretation in terrain surveys for dam constructions, cases of unexpected unstable ground 'resampling landslides' were pointed out.

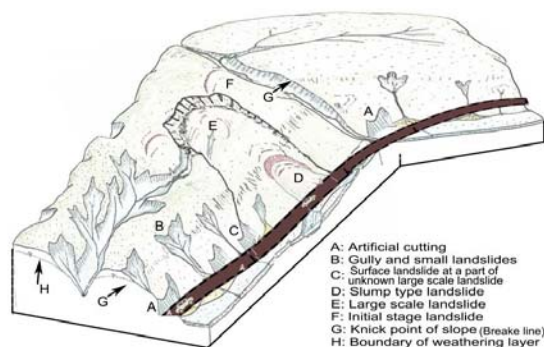


Figure 1 Relation between Landslide Topography and Slope Disasters

This is an example of a road showing a range of slope destructions and landslides occurring (B, C, D), while in the background of the landslide D we have large-scale landslide topography E which cannot be seen from the road. In this case, landslides C and D are the foremost parts of landslide E and occurred as a result of previous collapse.

Scientists of geomorphology and engineers who have applied the reading of aerial photographs of the foot of volcanoes in the Ōhu Mountains have discovered an expanding topography caused by massive landslides marked by rough undulations and unusual horse shoe shape cliffs. In an abstract of a conference presentation entitled 'A Landslide Topography of Funagata Rempō Hokuroku' (Chida et al., 1971) concluded that the results of a land survey show that this is a landform formed by landslides. At the same time, Hatano analyzed the 'Sendai' area using a 1/200000 topographical map and provided a map highlighting various slope terrains possibly

created through landslides (Hatano, 1972). Hatano was probably the first in Japan who illustrated the distribution conditions of large-terrain landslides. Since Hatano's revelations Terado, Miyagi, Shimizu, and Yamagishi have put forward distribution maps of landslide terrains for various areas in Japan.

In order to locate 'landslides' as significant factors forming slope terrain, time was required for the National Research Center for Disaster Prevention (today the National Research Institute for Earth Science and Disaster Prevention) to conduct research and publish 1/50000 Landslide topographic area distribution maps. Moreover, the analysis following the discovery over landslide topography was conducted with great scientific interest in important topographical questions of 'how slopes develop'. The introduction of aerial photo interpretation has advanced research on quaternary tectonic movements and the development of topography which has focused on the recognition of terraces and active faults. The recognition of landslides was advanced addressing the question of how to locate mass movement as a factor in explaining the topographical development of slopes.

The analysis of landslides through aerial photo interpretation allows us to distinguish topographical areas created through landslides from those which did not result from landslides. Landslide terrain is clearly demarcated from general slopes through slip precipices. The main part of a landslide is surrounded by slips and recognized as consisting moving objects as the landslide body. Landslide topography is constituted by slip surface so called surface of rapture and moving material called landslide body. Various types of shape and inclination of slip precipices exist. Moreover, the moving parts themselves undergo various changes in form and substance in the process of movement which appears in the form of micro-topographical features at the surface of the moving part.

From Recognizing and Mapping Landslides to Risk Evaluation of Landslides

As a vast range of landslide topographies has made clear, the meaning of these distributions became the object of inference. Looking at the distribution of a large quantity of landslide topographies in the southern Ohu back born mountains in the Tohoku region, criticism was expressed arguing that 'given the large quantity of landslides disaster prevention would be impossible', while others questioned the wisdom of referring to 'everything as a landslide'. It was here that the Japan Landslide Society's Tohoku

and Hokkaido regional branches have published their own reviews on knowledge and technology with regard to landslides and landslide prevention. The publication entitled ‘Landslides and Landslide Topography in the Tohoku Region’ published by the society’s Tohoku branch (Japan Landslide Society Tohoku Branch, 1992) has used employed both terms: ‘landslide’ and ‘landslide topography’, and thus clearly emphasized the differentiation between landslides as a phenomenon of material movement of slopes and landslide topography which is formed as a result of such a phenomenon.

Naturally, the topography caused by the effects of landslides creates particular landslide topographies. Furthermore, it has been pointed out that the micro-topography constituted through landslide topography corresponds to the material character and movement of landslides (Miyagi, 1979). Landslide topography consists of a host of basic units of topography. Each of the topography units is formed by peculiar processes; thus, it has been suggested that by understanding the formation of micro-topographies it is possible to investigate the form of movement and the location of the slide structure, as well as the formation processes of landslide topographies, and the mechanisms of landslides (Kimata and Miyagi, 1985). Later, this idea was linked to the

“Autonomic Destruction Process” of landslide topographies. Here it was argued that ‘through the occurrence of a destruction of an initial landslide action at the slope the conditions of the material and water system change in the damaged area. This can serve as a cause for the occurrence of secondary landslides. Here, deformed and transformed conditions of the material and water cause peculiar forms of landslide (surface change and formation of micro-topographies as reflections of scale, frequency, and movement form)’ (Miyagi, 1990) (see Figure 2, below). As a result, we can examine the characteristics of the instability and the movement of each specific landslide unit by setting an indicator axis and by investigating the conditions of change.

Time from Occurrence of Initial Landslides until Reduction and the Intermittent of Landslide Activity

A overwhelmingly large number of landslide topographies take a very long time before reduction. Some argue that in case of large-scale landslides of more than 1 km², a time frame of more than 100,000 years is required (Yanagida and Hasegawa, 1993). If this is the case, landslide disasters exist in extremely long time horizons which transcend human time

Initial situation (Stress field, solid-state of rock, Geology)		Geomorphic setting (Stages of geomorphic development)				Slope gradient			
Autonomous destruction process	Solid-state of rock	Destruction			Landform features			Triggar of action	
		Type	Scale	Frequency	Plan	Scarp	Micro landform	Outer	Inner
Stage I Release from residual stress	Elastic	Destruction dominant	Large	Seldom	Round	Crack Sugging Linear graben	Original shape Warp	Deepening Shape of mountain	
Stage II Glide at bedding plain Slump as describe an arc						Large Separation scarp Slide scarp	Block	Type and magnitude of rainfall	inner stress field distribution
Stage III Fracturral slip Folding slide Debris slide						Minor scarp	Pressure ridge		relocation of water by micro landform
Stage IV Flow type slide	Fluidic	Viscosity flow dominant	Small	Frequent	Long obal	Small scarp	Slightly hammocky wavey smooth		Trap

Figure 2 Hypothesis of Autonomic Destruction Processes Caused by the Occurrence of Initial Landslides

The 1992 published ‘Landslides and Landslide Topographies in the Tohoku Region (Japan Landslide Society Tohoku Branch)’ contains geological maps and allocation maps of landslide topographies, counter-measure examples for local authorities for landslide prevention, as well as information on how to analyze a landslide topography, geology, allocation, mechanisms and risk. As such, this has been a comprehensive and ambitious work relating to our current tasks.

perceptions but are fatal phenomena which can occasionally occur. Many of the existing landslide topographies are not dangerous, but a few have reached stages at which they frequently cause damage. Here, we can assume that depending on the location of the landslide (topographic location

conditions: e.g. foremost parts of a movement object which confront frontal slopes of rivers are in unstable conditions), landslides have become more unstable, and a small number of these landslides constitute under a number of specific conditions an unstable area of high risk. Through

understanding and evaluating these conditions, we may evaluate which landslide topographies will cause natural disasters in the near future. Experiencing trial and error, risk evaluation of landslide topographies has taken forward to its current form.

Substantial analysis of the risk evaluation methods of the landslide topography in the Tohoku region have been conducted for Iwate Prefecture's Sediment Control Division and Miyagi Prefecture's Natural Disaster Prevention and Sediment Control Division, and have served as the basis for the drafting of manuals (Miyagi et al., 2004).

Risk Assessment and Efforts of Technological Advancement

It goes without saying that risk assessment, (that is, assessment of the stability and instability of landslide areas which is predicated in the principle of disaster prevention and an understanding of the use of land) is conducted through evaluating the characteristics of the material and water, as well as the surface of slide. However, given the vast number of existing landslide topographies it is, from an economical and personnel standpoint, impossible to conduct sufficient on-site surveys or boring surveys. It would be a rational solution if the degree of risk could be assessed through some indirect method.

The idea of assessing the degree of risk of individual landslide topographies through aerial photograph interpretations, while being only a first step in the process of evaluation, represents a procedure in which critical areas (that is, areas which require careful on-site surveys) are selected and in which surveys are focused.

We were confronted with significant problems in conducting concrete risk assessments. Before we had to assess the risks of a given landslide topography, we did not discuss the basic problem of 'how unstable were landslide topographies, disregarding the way in which these micro-topographies have been recognized'. That is to say, firstly, we have to consider whether we can find a corresponding relationship between the appearance of a landslide topography (that is, the micro-topography), and internal structure, (that is, the movement form), the material characteristics, and the structure of the slide. Secondly, we have to consider to what extent indicators shown by the landslide topography directly relate to its risk assessment.

Here, we introduce an example which analyses the correspondence between the micro-topography of the moving part of the landslide, the internal part of the moving part which constitutes the topography and the characteristics of the slide surface.

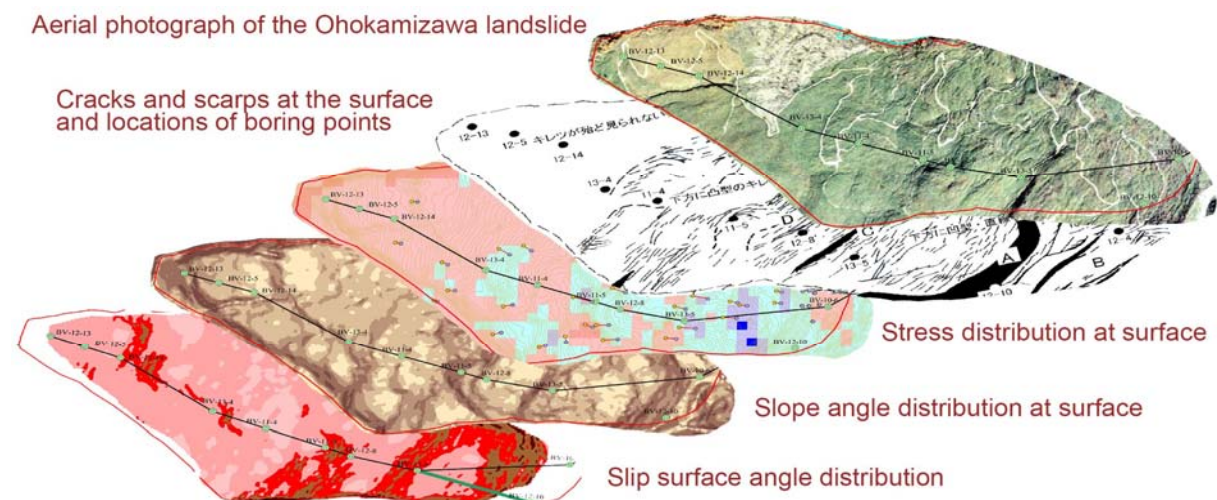


Figure 3 A series of data in case of Ohokamizawa landslide

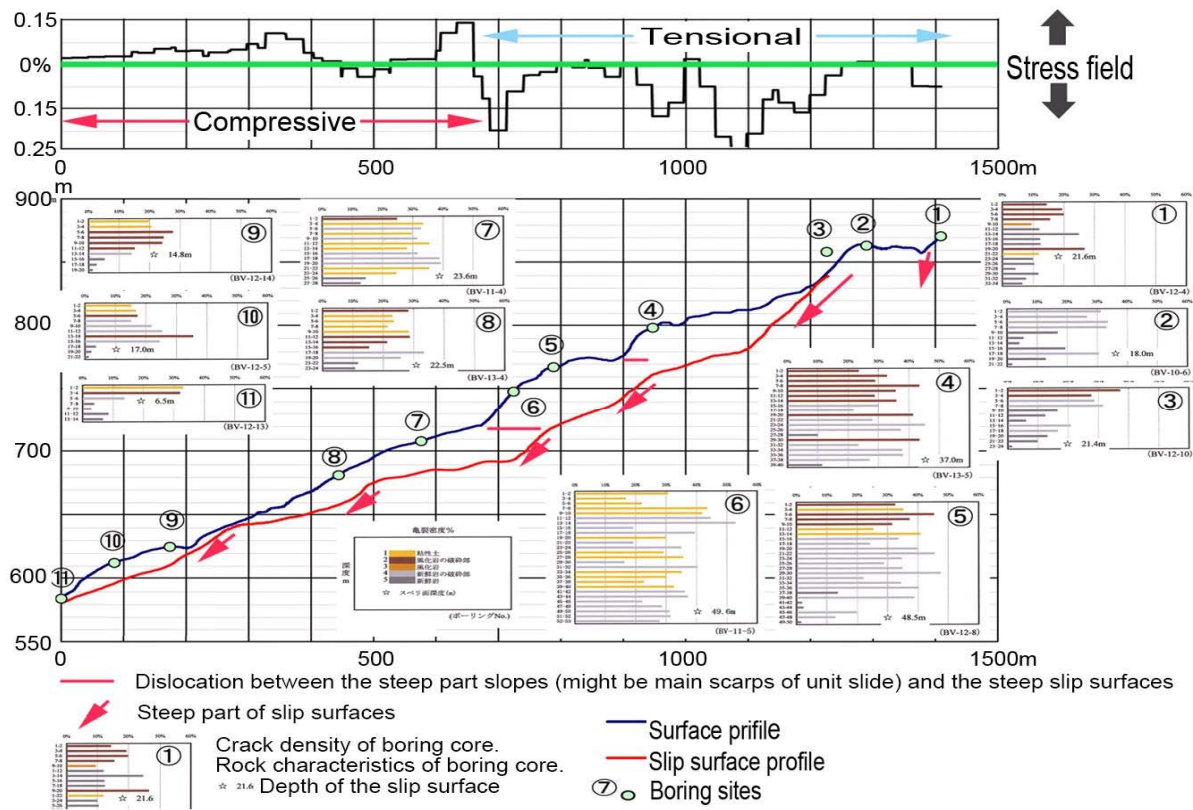


Figure 4 Landslide cross section of the Ohokmisawa landslide

The Ohokamisawa Landslide area is an active large-scale landslide which reaches a length of 1.3 km, and is one of the prominent landslides in Japan which has been subjected to detailed surveys (see Figure 3).

Figure 3 above follows this survey data. We explain the data very briefly below. The vertical sections of the slide surface (Surface of ruptures) are developing in several active steps, and the landslide topography's (vertical sections at the ground surface) slope surface and upper parts show a variety of staircase patterns. The material of the moving part consists of background and upper parts of the landslide area of new trenches created through new rocks while the middle part consists of rock debris and colluvium like deposit; the lower region of the moving part consists of cohesive soil (see the bar graph in Figure 4, below). Using data gathered by a large number of extensometers at the ground surface, we see that the upper-region of the moving part tends to be pulled, while the lower region tends to be placed under pressure. If we look at the micro-topography (minor cliffs, cracks and slope precipices) we see that a host of large-scale scarps is located in the rear of major slope precipices. Around the upper parts surrounding major slopes a vast number of convex cracks

develop. The form of the cracks and minor scarps changes to become convex in the lower part, demarcating a large-scale precipice. Furthermore, the 1/3 lower part of the landslide body, the crack and scarp disappears and changes into hummocky ground surface. The evidence alluded to above illustrates that in the process of a large-scale landslide topography, a forefront landslide lower-part of approx. 300m occurs, while landslides of similar scale repeatedly occur in this case about four times thus far. In the meantime, each landslide is active through entailing particular slide surfaces, due to the monoclinic structure of slopes in the layers of the given region. Moreover, in the background of the main landslide slope, we see expanding parallel cracks which indicate the occurrence of new landslides.

The evidence introduced here illustrates the moving mechanisms and material characteristics of landslides as expressed in a micro-topography.

That is to say, 'if can predict the particular movement and material characteristics of a landslide, we may be able to analogize the risk of a reoccurrence of a landslide'.

Establishment of an AHP-Based Risk Assessment Method for Landslides

Stereopair photos (Date of taken, Photo No., Scale 1: 10000) Topomap : Tsubakidai Akita prefecture Japan There are a series of research data including the well wall photos, slip surface datas and boring core datas etc.		Check list of landslide features for landslide risk evaluation						AHP Score
<p>Base of Base map: Sheet No. 3</p> <p>These are cracks around here</p> <p>A number of lands distribute and incline to forward of landslide body</p> <p>Major slope Sharp and straightly lying</p> <p>There are cracks around here</p> <p>The landslide is heavily large. Length: 50m, Width: 20m, Depth: 2-4m. There are many large cracks in the main scarp. There are several large scale minor scarps. There are many small scale scarps in the toe part. There are many small scale scarps in the gully crevices. Many slope accumulation modification by weathering are still poor.</p>	Major division	Main factor	Observation there	Unstable factor		Remarks		
	Characteristics of active landslide	A: Types of movement	Pressure ridges	Large and unstable	Minor scarp	Small and stable	Scale	Location
	Characteristics of active landslide	B: Level of clearness and micro landform components in the body	Clear micro-geography boundary	12.1	4.8	2.0	8.5	
	Characteristics of active landslide	C: Level of stable	Head block separates from lower end	12.5	5.5	6.5	19.5	
	Characteristics of active landslide	D: Direct features of movement	Cracks and scarps	12.5	5.5	6.5	13.9	
	Characteristics of active landslide	Other minor features	Gullies	12.5	5.5	6.5	18.8	
	Age distribution	E: Top edge main scarp	Chertion	1.0	1.0	1.0	3.8	
	Age distribution	F: Boundary of the main scarp and the body	Non-deposition	1.0	1.0	1.0	3.1	
	Age distribution	G: Boundary of landslide body and the front slope	Non-deformed landslide body	1.0	1.0	1.0	1.0	
	Age distribution	H: Landslide body middle	Non-deformed landslide body	1.0	1.0	1.0	4.4	
Age distribution	I: Landslide body lower face to the other near course	Increasing	18.2	8.2	2.7	6		
Particularity recognizable deformed block in landslide Yes - Non (Total No. small blocks)								
Risk of landslide based on your own experience: Large → Middle → Small							Total points of AHP assessment	79 No.
Score by own inspector: T. Miyagi							No	38
Reference No.								
Name of Man								

Figure 5 Example of an AHP evaluation sheet

The discussion on risk assessment of Iwate Prefecture began with the recognition of micro-topographies. The method applied at this time is the AHP approach introduced by Hamasaki. Japan experiences landslide disasters almost every year. It is for this reason that many surveys are conducted and countermeasures put in place. Engineers who have rich on-site experience and are familiar with the technology aerial photo interpretation have supported the basic academic knowledge and contributed to judgments on the risk of landslides in the area. However, in many cases this experience cannot be expressed plainly in words. While senior engineers evaluate someone's 'views as appropriate or as the masterly performance', it is difficult to communicate this

understanding to junior scientists and engineers. Risk assessment employing AHP has emerged from the discussions of these engineers who possess these views. Concretely, using practical sample pictures, seven engineers are summoned for the purpose of debating problems of defining a micro-topography constituting a landslide, its recognition, as well as which indicators are important in showing risks of a micro-landform. Through reiterating such debates unclear concepts are restructured into clear definitions. As such, ideas are created as to 'which micro-landforms are to extent indicators of instability'. **This process transforms tacit knowledge into explicit knowledge.** It is here that data sheets on landslide risk assessments are produced.

Level II		Level III	Indicative signs of instability				AHP score
			High			Low	sum
A	Micro topographic features on a surface of a landslide mass	a	20 Debris flow Mudflow, earth flow	13 Secondary scarps Secondary multi slump, mudflow	8 Head part depression Minor scarps crack, pressure ridge	0	
		b	20 Clear and fresh Closely-spaced scarps & linear depression	13 almost clear and fresh a series of scarps & linear depression	8 not clear rounded scarps & buried depressions	5-0	
B	Deformation of marginal zone	c	10 sharp and clear crown	5 subrounded crown, talus deposition	2 rounded crown, gully erosion & talus deposition		
		d	20 collapse, secondary slide	12 Partial collapse, secondary slide	6 gullies small debris fan on foot	0	
C	Locality of landslide	e	20 undercut slope for mainstream or artificial excavation work	12 undercut slope for tributary or artificial work	6 slip off slope, orthogonal position to river	2	
		f	10 steep & high relief profile	5 rounded edge & convex profile	2 straight profile	0	
						0	

Figure 6 An example of modification the AHP inspection sheet due to the discussion processes (Hamasaki et al, 2014)

Assessed indicators of micro-landforms are easier to comprehend, if few in number. Definitions of these indicators should be clear. Furthermore, one should not ignore the configurationality of the micro-landforms subjected to recognition. Based on these considerations, items shown in Figure 5 below have been determined and allocated. AHP assessments of each check-item are the outcome of reiterated paired comparisons conducted in discussions among the group of engineers mentioned above. The allocation of the check-items distinguishes between main slip precipices of landslides and their moving parts, while categorizing them into three assessment axes based on their topographic location as a micro-landform's border part, internal region of a moving part, or front-region of a moving part; here, a series of recognition axes are established for each micro-landform. It is not easy to recognize a micro-landform through aerial photo interpretation. Analysts with little experience may come to false assessments which may directly link to ambivalent risk assessment scores. Thus, at present it is necessary to establishment training programs for those analysts.

Application the landslide mapping to the Vietnam project area

The authors started the landslide topographic area mapping to the project area. The frame of the mapping strategy is as follows. Mapping will carry by the aerial photo interpretation by three dimensional stereo pair photos. The identification of landslide unit is recognize the morphometric sequences of slopes first. Then, we identify the break line in relation to the slope deformation by landslide. So, the identification is recognizeing the micro topography of landslide main scarp and recognize the area and the boundary of landslide body. There is a limit of identification because of the scale of aerial photos, sharpness of the print quality, forest cover etc.

In case of Vietnam, the preparation of aerial photos is also very difficult. The scale of using aerial photo was 1 by 33000. It means that the

possibility of landslide identification is larger than 200 in width.

We carried the mapping at Haiban pass area, several places along the HCM Route (National Road No.2) in Central Vietnam.

Tentative results of large scale landslide distribution and the characteristics.

Haivan pass area: The area mostly consists of one large land mass by granitic rocks. The slopes of the area are categorized in to three types.

The first one is, smoothly connecting with crest slope, side slope and foot slope. The crest slope is convex profile in cross and longitudinal direction, and thin weathering materials. Side slope is steep usually, and sheeting joints and cubic joint developing. Out crops of boulder are also common. The boundary of the foot slope and side slope is usually smooth. The foot slope is consists by boulder and small matrix. The boulder develops the boulder field. It called Block Meer in geomorphological. This is the one of the typical arrangement of slopes on granitic area. Secondary, that is Ridge and ravine topography. This is quite usual landforms by the normal process of erosion, transportation and sedimentation. The third is landslide topography. In case of Japan, the topography is not so common. Although, among the Haiban Area, especially the eastern part form the Haiban pass, there are a number of landslide topographies distribute. The deep slope failure type landslide is also abundant.

Ho Chi Minh Route area: We are carrying the landslide mapping from Khan Duc to A Luoi area. The distance is about 200km long of HCM route. Among there, the characteristics of the small scale and shallow landslides along the HCM route are mostly recognized by the series of data collection by ITST and current project (Abe et al, 2014). On the other side the, the characteristics of moving tendency and the distribution is studying now. The distribution tendency of large scale landslides might be categorize in to four zones. The zone is strongly related to the geology and weathering features. That is the zone of Pre-Cambrian, Cambrian to Ordovician, Mesozoic, Mesozoic to Paleozoic.

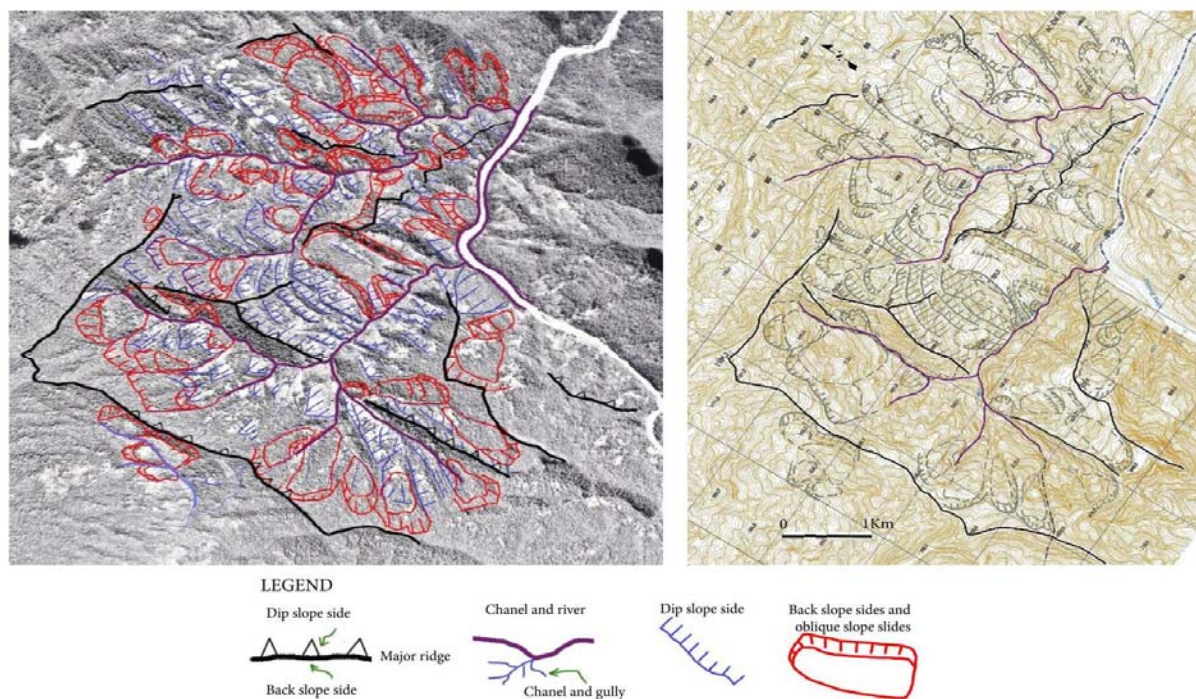


Figure 7 Example of the large scale landslide concentrating area north western part of Thach My (After Luong et al, 2014) town.

The Pre-Cambrian zone: Between Khan Duc town and Than My town, the geology is mainly consists of Pre-Cambrian schist and gneiss. And the rocks receive strong and deep weathering processes. Additionally, there is Quaternary terrace deposit also develops at Khan Duc area. The surface landslides and shallow landslides distribute widely. Earth flows are also very abundant. The large scale landslides are also very concentrate. The type of movement has large diversity. Large scale, slumping - mud flow type landslide concentrate near Khan Duc town. Multiple slump type landslides concentrate at 10 km north from Khan Duc. Huge landslide distribute at 20km Northwest from Khan Duc. This is 3km by 3km basically. The landslide moved by deep sheeted movement. After the movement, Debris flow and Rock avalanche type landslide occurred at the part of landslide body and side scarps. The serious large scale landslides in relation to the artery road are only few sites.

The Mesozoic zone: Between Than My Town to Prau Town, the geology mainly consist of the Triassic to the Jurassic. The rock consist with sedimentary rock such as reddish sandstone, mud stone, conglomerate. A number of thin coal or organic rich layers are also inter bedded among the sedimentary rocks. The weathering structure is not so big affection to mass movement. The zone is also characterized the twin syncline structure. So, the large scale landslides are very frequent in spite of the poor surface and shallow landslide. The slip surfaces are developing at the upper part of coal layers. Also, among the silicified sedimentary rock layers, a number of slip

surfaces might be developing. Fig. 7 is a sample of landslide concentrating area. We are easy to recognize the tendency of landslide movements are strongly controlled by the geological structure.

The Cambrian to Ordovician zone: Between the Prau town and About 20 km north of town, there are many sorts of landslide concentrate. The geology of the area is mainly consists of schist to shale mainly. The dip of layers, are highly steep and the rock changed to thinly foliage structure. The weathering tendencies are also characterized. Basically, the chemical weathering deeply developing and some of part has the wedge shape weathering is also developing. Such complicate and deep weathering structure might be affected the landslide. By this causes, there are shallow landslides and surface landslides very much concentrate. On the other side, large scale landslides are distributes at many places.

The Mesozoic to Paleozoic zone: Between the A Luoi to 50km south of the town, there are high altitude and steep slopes developing, and the area are covering by deep forest. The geological structure of the zone is relatively much complicate and strongly sheared. The strike structures are north to south mainly and the dips are vertical. Weathering affection is also deep. Although, the large scale landslides are seldom here. But shallow landslides and deep slope failures are concentrating along the HCM route.

Tasks of WG2 of the latter half of the project

The mapping group has two tasks basically. One is the mapping and risk evaluation for mitigate the landslide hazard. Till the first half, we carried the field investigation and mapping the large scale landslide identification. The activities were able to done by the basic data of ITST side studies. Some draft version result such as recognition of landslide phenomena, mapping and risk evaluation. Although, the data collection for evidence, mapping quality, set up the inventory data, inspection sheet establishment still are ongoing yet. The identification of the precursor feature is started this year. The technology will develop quickly. We would like to carry for final results.

Acknowledgments

First of all, we would like to express their appreciation to SATREPS. The scheme makes the great opportunity the advance the technology and the risk mitigation not only in Vietnam but also in the humid tropical region.

We also express to Professor Sassa leader of the project, Mr. Khang director general of ITST, Vietnam and all member of the WG2.

References

- Abe S. Tien DV. Yoshimatsu H. Shibasaki T. Miyagi T. (2014) Topographic and geologic factors of landslides along Ho Chi Minh route in central Vietnam. Proc. Of the SATREPS workshop on landslides in Vietnam.
- Chida N, Sugawara K, Miura O (1971) Landslide phenomenon in the Northern slope of Mt. Funagata. Q.J. Geogr. 23-3, 175., in Japanese.
- Hamasaki E. Miyagi T. (2014) Objective function based AHP risk evaluation system in humid tropical regions. Proc. Of the SATREPS workshop on landslides in Vietnam.
- Hatano S. (1974) Landforms of rapid mass movement origin process (Recent progress of geomorphology 8), Soil Mech. Found Eng. (Tsuchi to Kiso). 22-11, 85-93. In Japanese.
- Ichise Y. (1964) Landslide identification by the aerial photo interpretation. Bul. Nat. Resources Res. 62, 12-22. in Japanese.
- Japan Landslide Society Tohoku Branch (1992) The landslide and landslide topography in Tohoku, Japan. 141ps and 80 maps. In Japanese.
- Kimata R. and Miyagi T. (1985) Basic components of landslide topography. J. of Japan Landslide Soc. 21-4, 1-9, in Japanese.
- Luong LH. Miyagi T. Abe S. Hamasaki E. Tien DV. (2014) Landslide mapping and detection of active landslide area from aerial photograph interpretation and field survey in central provinces of Vietnam. Of the SATREPS workshop on landslides in Vietnam.
- Miyagi T. (1979) Landslide in Miyagi prefecture. Sci. Rep. Tohoku Univ. ser.7 (Geogr.), 29, 91-101.
- Miyagi T. (1990) The risk evaluation by the landform classification in landslides. Proc. Symposium by Japan Landslide Society. P.1-5. in Japanese.
- Miyagi T, Prasada GB, Tanavud C, Potichan A. Hamasaki E. (2004) Landslide risk evaluation and mapping: manual of aerial photo interpretation for landslide topography and risk management. Rep. Nat. Res. Inst. Earth Sci. and Disaster Prevention (NIED). 66, 75-136.
- Miyagi T. Hamasaki E. (2013) Risk evaluation of landslide topographic area by aerial photo interpretation. Sssa K. et al eds. Landslide Science for safer geoenvironment. 2. 491-497.
- Saarty TL. (1980) The analytic hierarchy process. McGraw-Hill Book Company, New york. P.235.
- Shimizu F. Oyagi N. Inokuchi T. (1982-1988) The map of landslide topography. Rep. Nat. Res. Inst. Earth Sci. and Disaster Prevention (NIED). 1-6. in Japanese.
- Terado T. (1978) Large scale mass movements in central part of Ohou Back Born range, Japan. QJ Geogr. 30-4, 189-198. in Japanese.
- Verns DJ. (1978) Slope movement types and processes. Landslides; analysis and control. T.R.B. Special report No. 176, 11-33.
- Yagi R. (2003) Micro topography in the landslide body and the developing processes. Geomorphol. Journal Japan. 24-3, 261-294. in Japanese.
- Yanagida M. Hasegawa S. (1993) Morphological dating and dissection process of landslide topography. In Novasad S, Wagner P. eds. Landslide. Proceedings of the 7th Int. Nat. Cofere. And field workshop on landslides. P.117-121.



Proceedings of the SATREPS Workshop on Landslides in Vietnam, 2014

Landslide prevention and mitigation for road in humid tropical region

Dinh Van Tien ⁽¹⁾, Toyohiko Miyagi ⁽²⁾, Eisaku Hamasaki ⁽³⁾, Shinro Abe ⁽⁴⁾, Nguyen Xuan Khang ⁽⁵⁾

1) Institute of Transport Science and Technology, Hanoi 84, Vietnam, dvien.gbn@gmail.com

2) Tohoku Gakuin University, Department of Regional Design, Sendai, Japan, miyagi@izcc.tohoku-gakuin.ac.jp

3) Advantechonology co.,Ltd., Department of Technology, Sendai, Japan, hamasaki@advantechonology.co.jp

4) Okuyama Boring Co.,LTD, Japan, abe@okuyama.co.jp

5) Institute of Transport Science and Technology, Hanoi 84, Vietnam, nxkhang@itst.gov.vn

Abstract The landslide phenomenon is considered as a natural disaster directly affected the development of mountainous areas in general to the traffic and transportation sector particularly. From the damages of typical landslides in Vietnam such as on Highway No. 37 (at Chen Pass), Son La Province, The Nam Non Bridge on the Western Route, Nghe An Province, at Hai Van Pass Station, on Highway No. 6 and along the Ho Chi Minh Route in the Central, it is able to be recognized that the responding in face to this dangerous phenomenon seems to be quite passive. This paper proposed a new plan proactively to prevent and mitigate the occurrence of this natural disaster for the new design and management of roads through mountainous terrain areas. The core of the new plan is to build up a landslide risk assessment map (LRAM) by the combination of the inventory map which based on methods of collect historical data, field surveys and interpretation of aerial photos and the landslide susceptibility map which is analysed from landslide manifestation in study area and landslide causative factors such as topography, geomorphology, geology, climate and human impact as a basis for predicting the future. For landslide susceptibility map, methods of analytical hierarchical process approach or fuzzy relation are applied. This proposed map indicates boundary, active status of each landslide as well as the susceptibility of each coordination to landslide that is fully effective for landslide prevention and mitigation of hilly and mountainous areas with humid tropical climate, including Vietnam.

Keywords: Landslide, map, inventory, susceptibility, Traffic, Vietnam

Vietnam's natural features relating to landslide

Vietnam is located on the Indochina Peninsula in Southeast Asia, with the population of about 90 million people and the terrain changes as natural Zones. The topography of Vietnam is varied depending on the natural areas. Overall, Vietnam is composed of three geographic domain extends from North to South. In which, the North has mountainous terrain concentrated in the Northwest and the Northeast, plus the Red River Delta; the Central has a strip of coastal plain and high mountains called Truong Son mountain range adjoins Laos; and the South's major terrain is the Mekong Delta. .

The average annual rainfall throughout the country is from 1,200 to 3,000 mm and can reach to 4,000-4500 mm/year in some particular areas in the Central. The average sunshine duration is 1,500 and 3,000 hours/year and the average temperature fluctuate from 5°C to 37°C. Particularly, sometimes the temperature drops to 0° C (at Sa-Pa) or increases to 40-45 ° C (for instant, in Hanoi, Ha Tinh, Quang Binh). Vietnam usually has to deal with typhoons and floods every year, with an average of 7 to 10 typhoons/ year.

In such natural conditions, landslide is one of the most popular natural phenomena occurring on road network in rainy season in Vietnam, while it is located in extreme climate areas where are impacted by heavy rain, high terrain, strong

cleavage and complex geological structure..

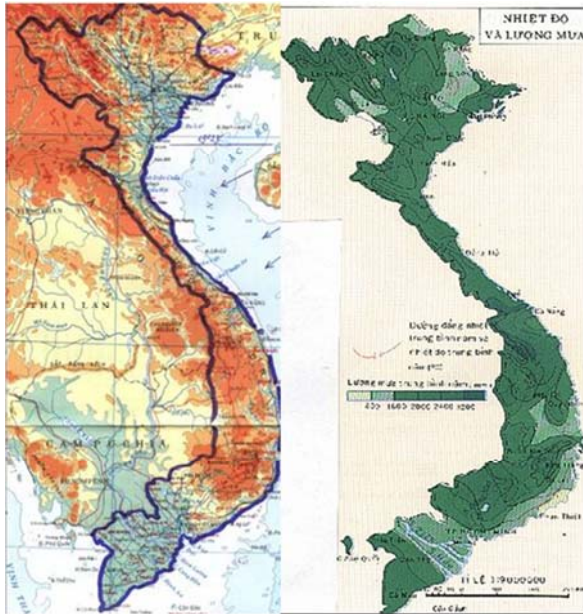


Figure 1: Terrain and rainfall distribution map of Vietnam

Landslides Damaged the Transport System in Vietnam.

To get an overview of landslide activities, we collected information and analysed data of some large typical landslides occurred on Highway No. 37 (at Chen Pass), Son La Province, The Nam Non Bridge on the Western Route, Nghe An Province, at Hai Van Pass Station, on Highway No. 6 and along the Ho Chi Minh Route in the Central.

Chen Pass Case



Figure 2: Overview of Chen Pass zone

National Highway No.37 connects Red Star Town, Hai Duong Province to Cu Nui intersection, Mun Village, Hua Nhan Commune, Bac Yen District, Son La Province in Vietnam. The landslide occurred at km 447 +500 - : - Km 448 +100 of National Highway No.37 is considered as shallow slide but large scale with of the width of 650

meters and the height of 950 meters in size, on the concave slope which bounded by two water lines converge. The average slope was 20 degrees with the strong cleavage surface.

This zone has a complex structural stratigraphy. Clay coating is golden brown chips with many debris, multi-mineral rolling rocks. The state changes from hard to soft. The cover is weathered, has strong ability to absorb water. That is the targets of cohesion and friction angle decreased when being hydrated. The original rock beneath is ultra-mafic rock in grey-green, dark grey and light grey colours, derived from magma eruption and shallow intrusion and beneath is the crystalline schist sandwiched with grey limestone particles.

The movement of the slope was triggered by the combination causes of the mechanical properties deterioration of soil and rock which was water permeable and saturated due to heavy rain and the cut slope when upgraded and renovated national Highway No.37 in 2003 at the foot of landslide block. The movement of mass destructed partial HighwayNo.37 at 2positions and formed 4 scraps on slopes with a height from 5-19m.



Figure 3: Description of scrap on the landslide body

The countermeasures using geotechnical technology or structure to terminate the movement of the landslide were too complicated and not financially feasibility. A bypass project nearby has been launched, however with the same conditions of topography, geology and hydrology the bypass are still capable to meet similar risk.

Landslides along National Highway No.6, Hoa Binh Province

National Highway No.6 is one of the arterial roads connecting Hanoi to Hoa Binh, Son La, Dien Bien and the other northern provinces of Vietnam with a total length of 504 kilometres. Along the particular section from Km 78 +300 to Km 158

through Hoa Binh City, Cao Phong, Tan Lac and Mai Chau Districts, the slope failure phenomena of artificial cut slope, falling down to the pavement often appears threaten traffic safety and cause traffic jam.



Figure 4 : The landslide distribution map of Hoa Binh Province area.

Only in the scale of Hoa Binh Province, there are about 30 observed landslide zones in which 12 locations have high frequently failures as partly rapid slope landslides. These locations were evaluated and assigned as very high sensitive points in the countermeasure plan. The sensitivity was assessed on the basic of comparison of some factors affect the stability of the cutting slope such as slope angle, digging height of roof, appear of cracks, natural geological formations and history of tectonic activities. These activities were considered as cause create new faults that disrupted the geology structure and changed characters of metamorphic and crumpled fractured sedimentary rock, improved water infiltration, reduced shear capacity of rocks in the region.

Most serious one was rapid slope failures of 150,000 m3 of debris from the artificial slope which was passive occurred on 2012 Jan 16 at Km 138 +750, located in Dong Bang commune, Mai Chau district, killing two people and causing congestion traffic for several days. Another most recent rapid slope failure of more than 20 thousand m3 of soil and rock on 2013 Feb 22 (in dry season) at Km 138 +800, causing traffic jams for hours. Thankfully, this landslide did not damage the lives and property of the people.

Sensitive assessment of moving slopes is a complex issue depending on many factors, which need to be analyzed on the basis of a combination of scientific analysis and expert opinion. The identification and assessment of risk positions in a number of cases can be recognized through signal of movement such as partly slides moving or cracks appearing on the slopes through site survey or by analysing of some particularly sensitive parameters such as geological structure,

slope characteristics, height of slope. However, it did not provide an accurately and qualitatively comparative evaluation. Some slopes belong to high-risk and very high-risk group of landslide even there are no signs of movement can not be found. In case of landslides along National Highway No.6, Hoa Binh Province. Most positions are selected on the basis of landslide occurred as partly rapid slope failures.



Figure 5: The rapid slope failure at Km 138 +750, Dong Bang Commune, Mai Chau District, Hoa Binh Province

Landslide at Nam Non Bridge.

The Nam Non Bridge is an importance technical key of road West Nghe An, My Ly commune, Ky Son district, Nghe An province. The bridge was designed as pretreated concrete structure crossing the lake of Ban Ve hydropower plant. In June of 2011, Ban Ve hydropower plant began content the water. The water level in the lake rose up from elevation from +185 to +200 m. The abutment which was located on the down slope of mountain beside and deep in resin up water elevation, was detected movement 30cm horizontally and 40cm vertically.



Figure 6: Landslide at Nam Non Bridge, West Nghe An road, My Ly commune, Ky Son district, Nghe An province

The survey for the cause of movement was conducted and exposed that this abutment located on form landslide, which was re-active under the influence of heavy rain, rising up the

water level of lake and the activity of cutting natural surface slope for temporary construction road. This landslide size was 950m in width and 1150m in height. A sliding block with size of 400m in width and 500m in height showed the significant sign of movement and made three deep cracks from 18-20m.

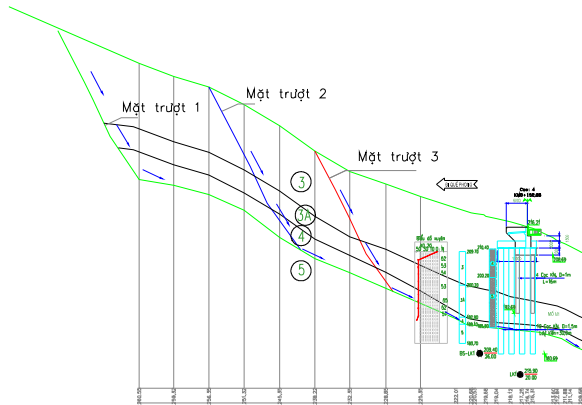


Figure 7: Longitudinal profile of moving mass

Geological investigation combined with geophysical survey results shows that geological profile including five layers.

Layer 1 is Pebble grit, which only distributed in the river area;

Layer 2 is yellow brown clay soil, hard plastic state with 1.2 to 2.2 m thickness.

Layer 3 is strong weathered siltstone with TCR = 20-30%, RQD = 0, 9.5 m thickness;

Layer 4 is strong to moderate weathered siltstone; TCR = 55-60%, RQD = 20-30%, 20.6 m - 34.2 m thickness, and

Layer 5 is Sandstone in blue gray, light gray, dark green color, slightly weathered, little cracks, greater than 5m thickness. The slip surface is predicted at the bottom of layer 4

Both provided plans for landslide countermeasure to meet the requirement of safety operation and long-term use of the road and the bridge that are handled to stop movement of the landslide and finding a new place for reconstruction of bridge are not economic and engineering feasibility. Exploiting temporary solution and non-continuous monitoring are employed to ensure traffic for the time being

Hai Van Station Pass Case

Hai Van Pass station is a particularly important position on the north-south railway line in the central region. Located on the lower position of the peak of Bach Ma Mountain, overlooking the beach where has special geological structure with unconsolidated soil mixed with block granite rocks, yearly this position accepted a very large rainfall (over 3000 mm / year). Every day over 30 trains pass through this station. This landslide phenomenon is the greatest threat to the lives of

passengers using trains when passing through this area in the rainy season.

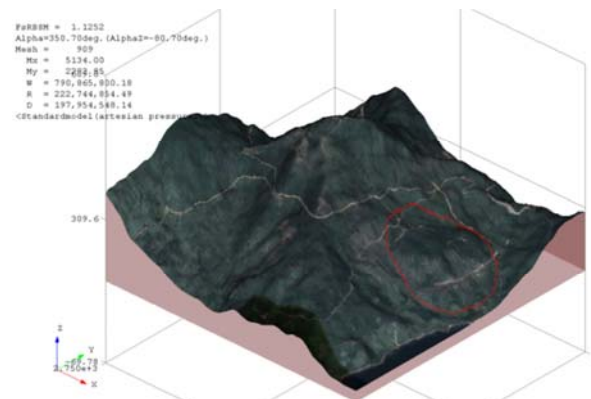


Figure 8: Model Acad 3D of Hai Van Pass Station

This landslide position was strengthened by concrete frame and retain wall and put in operation in 2004 Dec 31. Then Less than 4 months from operation and have not "facing" with the rainy season, this construction work was serious damage.

A 10 square meter block of soil in slope mountain collapsed. Construction materials, concrete patches, steel bars for landslide strengthening had broken and rushed. Many "orphaned" rocks loose leg or rolled down, located in the middle of slopes wondrously. Railway line and station located right at the foot of this mountain was a serious threat.



Figure 9: Location landslides at Hai Van Pass station

The cause of the damage seems related to unsuitable strengthening solution that was not yet fully appreciated the classification and scale of landslide.

Landslides along the Ho Chi Minh route via Vietnam Central

Ho Chi Minh route from Pac Bo to Dat Mui is nearly 3200 km long. The whole route is divided into 3 segments. (The Pac Bo - Hoa Lac; Hoa Lac-The Binh Phuoc intersection, Chon Thanh - Dat

Mui). Ho Chi Minh route section via Vietnam Central is one in segment 2 and considered as one of the best damage section influenced by of the landslide phenomenon.

After the traffic operation, since 2006, along the Ho Chi Minh route in the Central, many landslides have occurred. According to the statistical data before 2012, on the study zone 472 artificial slope failures appeared with different size. There were 8 particularly sections along the Ho Chi Minh Route with high landslide risks, potentially frequent in rainy seasons, including Da Deo - Khe Gat Pass, the Northern of U Pass, Khu Dang Pass, Cong Troi Pass, Sa Mu Pass, Hai Ham Pass, Song Bung Pass and Lo Xo Pass.

According to survey data, the most of artificial slope failures were cut-slope of road, which was collapsed under directly impact of rain. As to the type of movement they could be divided into three main categories, which are: Slide (32.1%), fall and toppler (55.9%) and flow (11.9%).



Figure 10: illustrates typical landslides often occur in HCM-Vietnam route

The studding record of survey could show that most landslide phenomenon had character of shallow landslide, largely related to raining fall, the surface of the terrain which was strong weathering and the direction of geological slope layer had the same direction with cutting slope of the road. Slip surface usually appeared at the position of interface geological or different weathering layers. In those cases, Slip surface usually had non-large radius and toe of surface of rupture usually ended up at middle or end of the cutting slope of the road embankment. Accumulation of landslide was soil or debris and greatly influenced by surface water and ground water, moved following stream over the road Surface

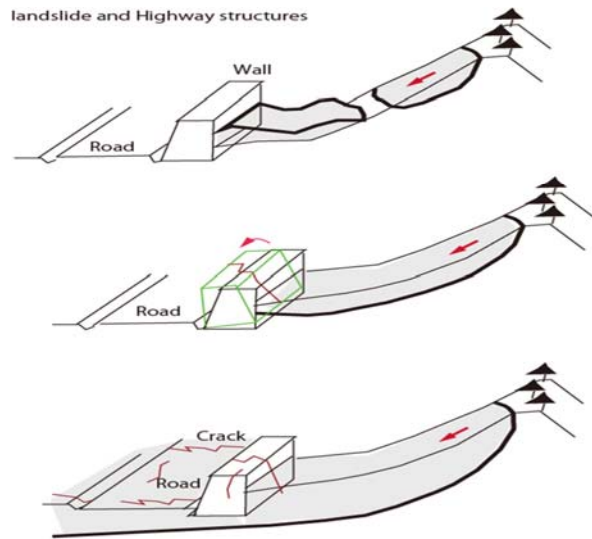


Fig. 11: Illustration of landslides on the Ho Chi Minh Route

However, a small member of Slip surface with a large radius, which was predicted as old landslides, located under the road embankment. The sliding movement of the deflection and accumulation zone of deep landslide created cracks and in some cases putted pavement or facilities of road over and they is continues to move with slow velocity depending on the water absorption of the sliding block.

The most of cut-slope failures on the HoChiMinh road had classification characteristics close with the fall and topple causing by unsuitable cutting slope design and non-protection slope from water penetration through cracking and strong weathering texture of the surface layers, which was removed vegetation, and surfacing cut off partly.

Generation mechanism of Wedge type slides

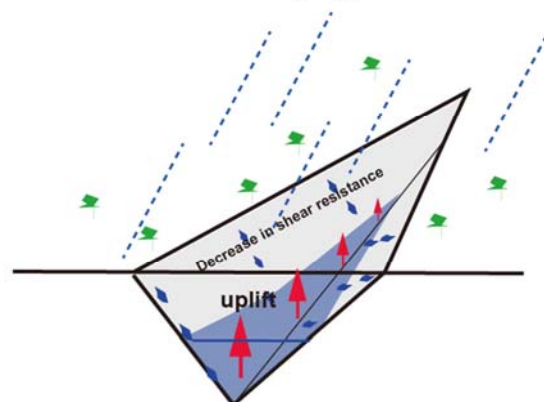


Fig. 12: mechanism of flow related to the geology character of surface

The movement could be recognized firstly from the upper step or middle steps of the cutting slopes, after that combined with other phenomena such as erosion,

(Rock falls was found in some cases but the number of this phenomenon is small.) Result of this phenomenon, the remain slope were more steep and some cases was nearly vertical created high potential energy for slope failure to continue development.

At Most those locations the direction of geological slope layer which was strong weathering was reverse with cutting slope surface of the road. Depending on the material of surface, movement here of all most slope failures were Earth fall/topple, debris fall/ topple. Material after slope failure occurred was unconsolidated soil, debris and water.

Flow was phenomenon, which observed pretty on the research area directly related to the geological characteristics of the surface and the phenomenon of surface water flow. The development of the small gullies is the initial manifestation of the phenomenon due to the movement of soil particles or fragments of withering surface which had special characters as Wedge type following surface water.

The small gullies developed larger and larger and created deep gullies on the surface of slopes, and in some cases they likened together and as the result the slopes failure by the cause of this phenomenon or others type of landslide such as slide or fall .

Current situation of survey, design and management of mountainous roads

Survey and design new mountainous roads

The objectives of the survey and design of traditional mountain roads are built up a reasonable and shortest route between the interested points are based on the original topographic maps with different scales. On the basis of road alignment from topographic maps, alternatives are carried out site topographical surveys, site geological, hydrological

investigation. Depending on the degree of importance of the road that the survey and design are divided into basic design, engineering design and construction drawing design. However selected alternatives largely bases on feasible road alignments of basis design step.

The feasible selected alignment is often determined on the basis of considerations of economic indicators and synthesis techniques such as appropriation to the terrain, meet requirement of traffic engineering and transportation, lowest construction costs and minimal fee for maintenance... to comply with the code 22 TCN 263-2000 for survey of motorways and standards TCVN 4054-2005 for road design.

For the effects of natural phenomena such as landslide, despite the standard 22 TCN 171-87 had been issued (Process Engineering geological survey and design for countermeasures to stabilize embankment of road in the landslide activity area), but the instructions for selection of the road alignment to prevent and mitigation of landslide phenomena are too general and mainly focused on countermeasure in case landslide occurred.

The important information that the designer need to decide the direction of alignment to prevent and mitigation landslide areas are: where is high landslide sensitivity, type, location, boundary and dimensions (including width, height and depth) as well as the moving of landslides.

By the conventional survey methods, especially in areas with mountainous terrain, which is covered with dense vegetation, the identifying information of landslide is very difficult. In addition, the movement of the slope is a complex issue with many affecting factors related to topography, geomorphology, geology, climate and hydrology as well as the impact of the people, so to evaluate the sensitivity of each position requires in-depth knowledge of experts.

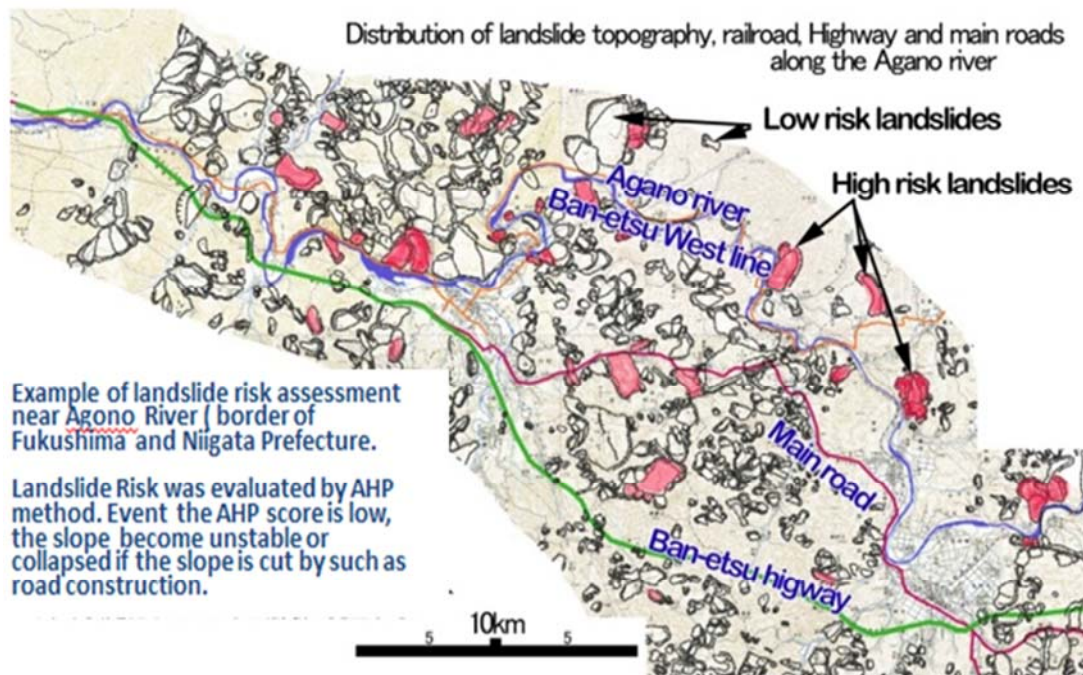


Figure13: Illustration of the design highways Ban-Etsu, Japan which was designed to avoid sensitive landslides

Failure to recognize the important information related to the landslide phenomenon as well as non-assess the sensitivity of the phenomenon leads to road alignment are selected going through high sensitive areas, even going through the body of blocks form large scale landslide to which only small effects of excavation of slope or may be other adverse factors the movement will continue to slide with different speeds. Rapid failure slope caused by heavy rain is one of typical landslide encountered along the mountain roads.

Many new roads, soon after operating, in adverse conditions of heavy and extended rains, landslides occurred in large numbers with different scales has stalled traffic, causing damage for the lives and property of the community. To Some roads which is during the construction process, this drawback has revealed when the technique key points of the project alignment was chosen at position which has form large-scale landslide that conventional survey process did not detect out. In such cases the change of this position will lead to huge costs for changing road alignment or for investment of countermeasure to stop movement of landslide.

Management and Exploitation of mountain roads

To exiting mountain roads are being exploited today, landslides during the rainy season are kicking phenomenon occurring frequently and were passive to management unit. The main difficulties of this problem beside budget for maintenance and giving out mitigation Countermeasure that's limited management tools.

Landslide susceptibility Map has been developed along some mountain roads, however, the scale of them is quite large and only suitable for general study. The unit manages of highway through mountainous areas will require detailed Landslide susceptibility maps and comprehensive information of landslide as mentioned than general information of large scale one.

Beside this Landslide Countermeasures to stop and minimize the impact of the phenomenon were applicated along the road but for each solution, the applications were based on experience that there are no standard specifically for this application. The forecast for creation of plan of the unit management to deal with the landslide phenomenon, especially during the rainy season every year should be based on a number of tools and support such as:

(1) Landslide susceptibility Map and inventory map with scale of 1/2000, 1/5000, 1/10000 and 1/250000;

(2) The guidance and support to predict the evolution of the specific landslide (landslide simulation) and post-result of the landslide phenomenon when it occurs (landslide hazard map),

(3) Tools for quantitative monitoring of sensitive factors of the specific landslide, especially in the importance position with high frequency extraction and having early warning facilities for such those positions.

With the tools, the unit management will transfer from the passive countermeasures which mainly based into experience through

conventional site survey previously to the new form of active one.

So to proactively deal with these landslide phenomena for designing new roads and road management which are being exploited, a new plan must be put in place. Apart from the current standard, a guideline/standard to prevent and mitigate from landslide for the design, construction and maintenance of transportation projects need to be studied and built base on identification and prediction of the sensitivity landslide phenomena.

Propose a new plan proactively to prevent and mitigate landslide

The core of the new plan is to build up a landslide risk assessment map (LRAM) by the combination of the inventory map which based on methods of collect historical data, field surveys and interpretation of aerial photos and the landslide susceptibility map which is analysed from landslide manifestation in study area and landslide causative factors such as topography, geomorphology, geology, climate and human impact as a basis for predicting the future.

Objectives and principles of LRAM

The fact is that if we depend on landslide inventory or susceptibility only, The landslide prevention and mitigation is not effective and insufficient because event with some zones, which was evaluated as low risk of landslide, the unstable slopes still occurred. The overall objective of this plan is to find a method to deal with the phenomenon of landslides proactively, based on create a tool to answer these basic questions as where is landslide occurred, What is the current moving status, which is the area with high landslide risk possibility comparing to other neighbouring regions and the impact them to the development.

For the transport sector, the construction standards to prevent and minimize damage from landslide for the design, construction and maintenance of transportation projects should be built base on the inventory and susceptibility map, which is defined here after as landslide risk assessment map (LRAM). This LRAM is a combination of (1) Inventory map where the landslide areas are identified in which all necessity in formation such as coordinates, size, boundary, movement status (in the past and present in) will be showed and (2) Landslide susceptibility map which is built on analysis landslide causative factors through their relationship rule of them to landslide before.

Although there are conflicting views among the experts, however, research on methods to LRAM are based on principles that are widely accepted theories or proven (Varnes, 1984; Carrara et al., 1991; Hutchinson and Chandler, 1991; Hutchinson, 1995; Turner and Schuster, 1996; Guzzetti et al., 1999 Guzzetti, 2005).

The principles can be described as follows:

(1) The main condition causing landslides can identify, and most can be shown on the map. In fact, the slopes which be destroyed remain clear characteristics which can be realized mostly through aerial photographs through stereoscopic projection, or on the basis of field surveys (Rib and Liang, 1978; Varnes, 1978; Hansen, 1984; Hutchinson, 1988; Cruden and Varnes, 1996; Dikau et al., 1996; Guzzetti, 2005).

2) For the landslides, "the past and the present are the key to the future" (Varnes, 1984; Carrara et al., 1991, Hutchinson, 1995). Under this hypothesis, landslides in the future may occur in the same geological conditions, geomorphology and hydrogeology as it happened before. Therefore, to understand clearly about the movement of landslide in the past is very importance to assess landslide causes (Varnes, 1984; Carrara et al., 1991, 1995, Hutchinson, 1995; Guzzetti et al., 1999 Guzzetti, 2005).

3) These conditions have led to landslides can be used to identify cases likely landslides occur in the future. These conditions may be varied and interrelated in many ways. However, if a related process can be understood, then, using extrapolation from the information point / area can be applied to the wider area.

Several authors (Crozier, 1986; Hutchinson, 1988; Dietrich et al., 1995; Guzzetti, 2005) admitted that the conditions causing landslides (the factor is not stable), or indirectly or directly in relation to the destruction of the slope, which can be collected and used to build the model predicts landslide, because the phenomenon of landslides are controlled by the laws of mechanics.

4) Landslide occur in a spatial and temporal can be deduced from the investigation on the basis of experience, or calculated through an analysis of the information or inferred from the physical model. Therefore, a region is at risk of taking classes sorted by different probabilities (Carrara et al., 1995; Soeters and Van Westen, 1996; Aleotti and Chowdhury, 1999; Guzzetti et al., 1999 Guzzetti, 2005).

General scheme for LRAM is shown in Figure 16.

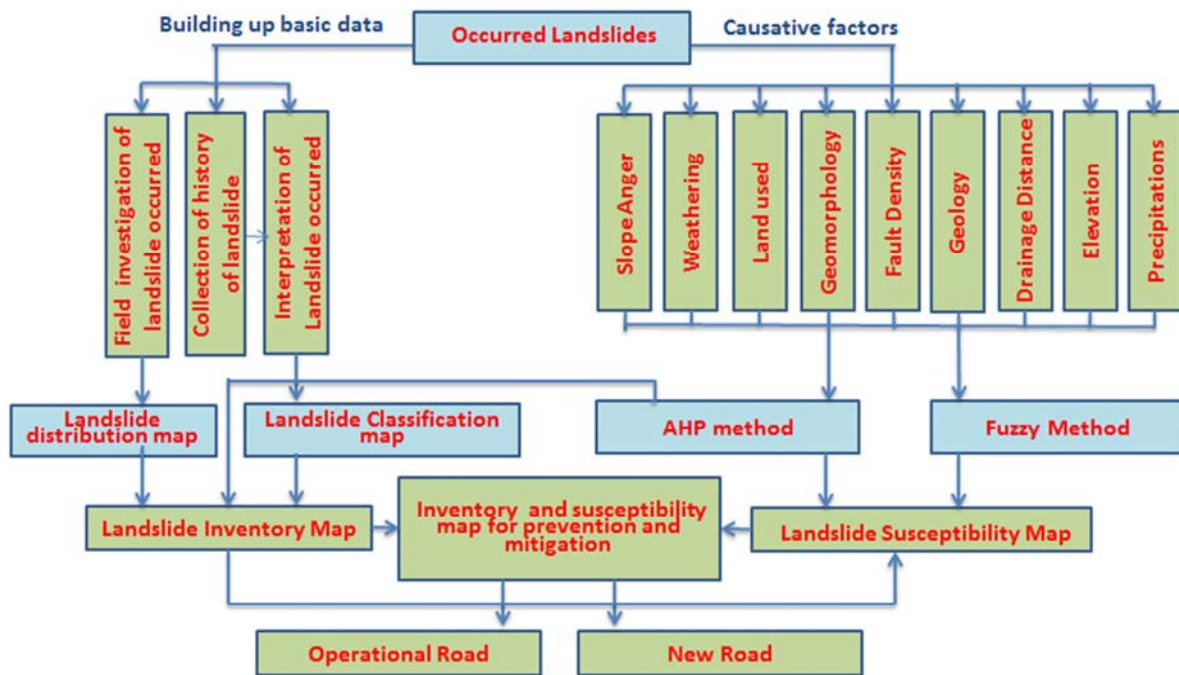


Figure 14: General scheme for LRAM

Landslide Inventory map

Landslide Inventory map is considered as the basic database which is built on the basis of distribution and classification maps. With objective of information providing such as type, location, boundary and size, including width, height and depth as well as the moving of landslide, this kind of maps with smaller ratio of 1: 25000 will be very useful for the design of new roads and management of the existing roads.

Three basic methods commonly used for inventory maps were employed: field recognizance to investigate landslide occurrences, collection of historic information of landslide and interpretation of landslide occurrences from aerial photographs.

With the development of theory Geomorphology and technology interpretation aerial photographs, most of the phenomena of surface movements can be identified and explanation, including the phenomenon of landslides. The interpretation of aerial photographs over time combined with topographic maps can

- (1) Provide an overall picture of the land including land use,
- (2) Landform classification and vegetation classification can be determined
- (3) The terrain deformation caused by landslides,
- (4) A landslide distribution map can be completed by transcribing the interpreted information into topography map,

- (5) The characteristics of the landslide displacement can be explained, which can provide a reasonable method for survey and design solutions to cope. (Pro. Toyohiko Miagi).

Besides identifying the locations, which had happened landslide phenomenon, to combine with the methods of analysis and evaluation by analytic hierarchy process (AHP) it can provide the level of sensitivity to landslide movement of positions, which are identified.

The detailed analysis of smaller scale aerial photographs can make more detailed map showing the internal characteristics of landslide, create the ability to predict the next movement of sliding block. This is significant for the study and offer solutions to stop or mitigate for the specific landslide case, especially large-scale one.

In case there is only a period of aerial photography is provided, the landslide movement can be determined through the moving signs during field survey. Through field surveys combined with the knowledge of the geology and geomorphology, landslide characteristics such as Main body, main scarp, head, crown, cracks, of landslide can be determined.

Signs of displacement of landslide can be realized through identification slip surface, cracks, altitude difference, the subsidence locations, change or destroy artificial works as well as signs of vegetation. The movement as well as its direction of land masses can be analysed from the appearance of stress on surface slope

(tension, compression and shear stress)
(Dr. Shinro Abe).

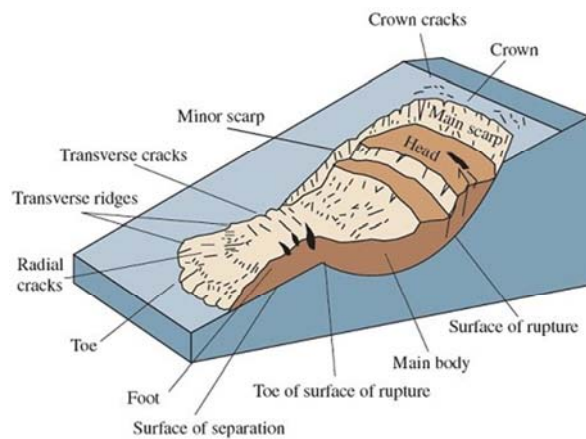


Fig. 15 Block diagram of idealized of landslide

Deformation of the slope surface concerns to its moving mechanism. Characteristics of deformation of the head, legs and boundaries of landslide related to appearance of tension, compression and shear stress respectively

Landslide susceptibility map

In general, the landslide susceptibility map usually consists of three main processes: (1) landslides Situation Analysis and associated factors cause, (2) Develop a database and (3) model selection, calculation methods and creating landslide susceptibility map

Basic contents of Landslides Situation Analysis and causative factors is creating inventory map. The basic parameters such as type, location, boundary and size, including width, height and depth as well as the moving status of the landslide are the basis for analysing the relationship between the landslide mechanism and the factors which influence to the process in study area. The preliminary assessment of relevance between the current state of the distribution of landslides and the factors that be related as terrain slope, rainfall, land cover, geology, geomorphology, crust, or fault lineament density ... can be based on the analysis, superposition of maps in GIS and field investigation.

The database design is based on accurately determining the factors affecting landslides process in the study area, shown by the creation the component map of causative factors. Theoretically, there are many factors affecting the movement of landslide, which contains the elements of direct and indirect factors. In general causative factor groups include: (1) topography, geomorphology, (2) geology, (3) climate, and (4) impact.

The element factors of causative factor groups will be assessed, classified and selected to provide sensitivity factors to the landslide phenomenon. Normally sensitivity factors influencing to the landslide usually are mentioned as the slope angle, weathering, geomorphology, fault density, Geology, Drainage distance, Elevation, Precipitation, Land use.

However, depending on specific conditions, on the basis of discussion and evaluation of the expert about the level of the importance of each factor as well as the availability of data sources that the creation of this map is different. Important requirement for component maps of causative factors that affect the landslide process in the study area is scale of map. Basically this map must have a scale the same with susceptibility map that we want have.

Two mathematic methods usually are employed for susceptibility map, that are methods of analytical hierarchical process approach (AHP) which is based on weighted influencing assessment factors of experts or fuzzy relation which is based on comparison affected parameters of the occurred landslides and parameters of position that we want to predicted.

On the basis of selected mathematic methods, GIS software is often used to create the susceptibility Map through the overlapping causative component maps in the same geographic coordinates. The landslide susceptibility zonation map with four landslide susceptibility classes, i.e low, moderate, high, and very high susceptibility for land sliding, is derived based on the correspondence with an inventory of observed landslides.

Creation of LRAM

The finally process of Creation of LRAM is showing information of inventory map and susceptibility map in the same geographic coordinates. The basic information parameters of LRAM include classification, location, boundary and size, moving status, and susceptibility to the occurred landslides as well as prediction of landslide susceptibility class for the zone that landslide has not happen yet.

Conclusion

Due to the unique natural conditions, as discussed above, the landslide is one of the natural phenomenon usually occurs seriously in severe arterial roads passing through mountainous regions of Vietnam in the rainy season. By analyzing the effect of landslide to specific locations and arterial road it can be recognized that strategy to deal with natural phenomena previously for the design and

management of construction in order to prevent mining the roads in mountainous areas and mitigation is passive and low efficiency.

The use of LRAM as presented above with the current survey methodology will be useful for the designer in choosing the optimal road alignment which satisfies the economic and technical requirements. Selected road alignment prefers to avoid active landslides, high susceptibility landslide zones. In case selected alignment cannot prevent mentioned zones, the designers have to actively provide proactive and minimize solutions response. For existing roads, LRAM will be useful in the landslide classification, sensitive assessment of each position and support for hazard map in case landslide occurred, giving early warning system to ensure the safety of lives and property and actively giving out countermeasures for high susceptibility positions before landslide takes place.

A new proposed plan as mentioned is giving out which bases on creation of LRAM to go with the current standard will be effective for both economic and technical aspects, contributes to reducing the damage of landslide phenomenon arising due to climate change to traffic systems particularly and the development of infrastructure in general.

References

1. Dinh Van Tien (2011); Application of an analytical hierarchical process approach for large-scale landslide susceptibility mapping in zone which locates along Ho Chi Minh road from Thanh My to Kham Duc, Quang Nam Province. Main joint research project between Ministry of Transport (MOT) and Ministry of Science and Technology (MST)
2. Dinh Van Tien, Doan Minh Tam (2010) Mapping method for landslide susceptibility along the Ho Chi Minh Road. A Paper on Road and Bridge Magazine which belongs to Vietnam Science and Technology Association, No1+2/2012.
3. Dinh Van Tien (2010). Application of analytical hierarchical process approach for landslide susceptibility mapping in zone which locates along Ho Chi Minh road from Nghe An Province to Kon Tum Province. Main joint research project between Ministry of Transport (MOT) and Ministry of Science and Technology (MST).
4. Dinh Van Tien, Doan Minh Tam (2011). Landslide situation in Vietnam and Cooperation with the International Consortium on Landslides in enhancement of research and treatment for landslides on road network. Proceedings of the 10th Anniversary of ICL – January 2012, Kyoto.
5. Tran Tan Van (2006) and the authors - Report the results of the project - Survey to assess the status, the risk of landslides some sections of the Ho Chi Minh Highway, National Highway 1A and caustic treatment measures ensure traffic safety, production and life of the residential area
6. Kyoji Sassa (2011) "Development of technology risk assessment of landslides along the main roads in Vietnam," Paper presented at the Scientific Conference Son La, 2011.
7. Toyohiko Miyagi - Landslide topography mapping through aerial photo interpretation
8. Eisaku Hamasaki, Toyohiko Miyagi - Risk Evaluation using the analytical hierarchical process (AHP) - introduction to the process concept, 9. Kyoji Sassa, Bin He, Mauri McSaveney, Osamu - ICL Landslide teaching tools
10. Application of an analytical hierarchical process approach for landslide susceptibility mapping in a Luoi district, Thua Thien Hue province, Vietnam
11. Shinro Abe (chapter 2 and 3) - Key points in field work for landslide Engineers



Topographic and geological factors of landslides along Ho Chi Minh Route in central Vietnam

Shinro Abe⁽¹⁾, Dinh Van Tien⁽²⁾, Hiroyuki Yoshimatsu⁽³⁾, Tatsuya Shibasaki⁽⁴⁾, Toyohiko Miyagi⁽⁵⁾

- 1) Okuyama Boring Co., Ltd, Yokote, Japan, e-mail: abe@okuyama.co.jp
- 2) Institute of Transport Science and Technology, Hanoi, Vietnam, e-mail: kqh@itst.gov
- 3) Kawasaki Geological Engineering Co., Ltd, Tokyo, Japan, e-mail: yoshimatsuh@kge.co.jp
- 4) Japan Conservation Engineering & Co., Ltd, Japan, e-mail: t-shibasaki@jce.co.jp
- 5) Tohoku Gakuin University, Sendai, Japan, e-mail: miyagi@izcc.tohoku-gakuin.ac.jp

Abstract In central Vietnam, Ho Chi Minh Route (HCMR) runs from south to north along the border with Laos. In this area, HCMR is often closed due to numerous landslides during the rainy season. Thus, there is an urgent need to determine the generation mechanism of landslides and to conduct risk assessment. For this purpose, this area was chosen as one of the study areas for this project. This study focuses on landslides occurring at approximately 180 locations along the 150 km distance (linear distance) from Thanh My (west of Da Nang City) and the intersection with National Route 9 (west of Quang tri). The landslides are classified based on the type of movement in order to determine the triggering mechanism. The survey was conducted from 2012 to 2014. The type of landslide movement in this area differs significantly depending on whether if the area is Paleozoic metamorphic zone or Mesozoic sedimentary zone. In metamorphic area, weak aspect such as schistosity, beddings, faults, and joints associated with geological structures become shear planes. Translational slides (wedge type) and rotational slide/flow (gully type) occurs often in this area, with the infiltration of surface water and breaking of rocks by weathering as the cause. On the other hand, in Mesozoic sedimentary area, translational rock slides are most common, where coal layers disrupted by fold structures function as the slip surface. It was shown that these landslides are not simply caused by heavy rain and weathering typical of the tropics, but are closely associated with geology, geological structure, development of rivers, and cuesta topography. This result shall be an important indicator in future landslide risk assessment.

Keywords Translational rock slide, gully, wedge slide, coal-bed

Study area

The subject of this study, Ho Chi Minh Route (HCMR), is located in the mountains of central Vietnam ranging in elevation from 60 to 1000 m (Fig.1). The study area, HCMR, runs north to south parallel to the border with Laos. Near Prao, HCMR is adjacent to the border. Between Prao and Aruoi, it passes several mountain passes, thus the road has many curves. However, along the rivers between the mountain passes, there is thin, flat terrain where settlements are scattered.

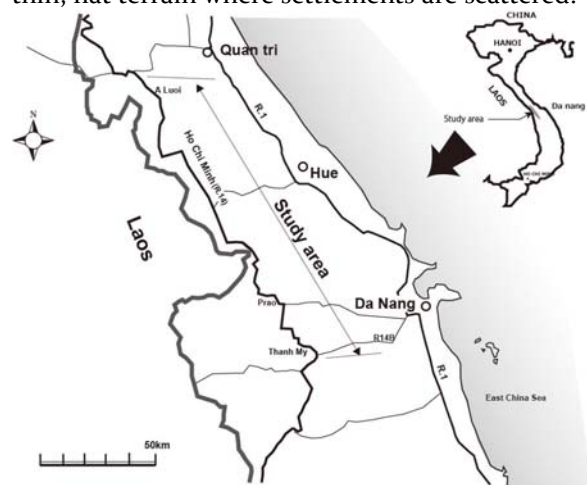


Figure 1 Study area

Outline of geological features

In terms of geological structure, the geological features of Vietnam are divided into six categories: NORTHEAST BLOCK, NORTHWEST BLOCK, TRUONGSON BLOCK, KONTUM BLOCK and NAMBO BLOCK (Fig.2). As the boundaries of TRUONGSON BLOCK and

KONTUM BLOCK in particular, the geological features and structures are largely different in the northern and southern parts. Palaeozoic and Mesozoic rock layers are much more widespread in the northern part of Vietnam than in the southern part. There are also a number of faults, as well as complex geological structures. In the south, there is Proterozoic rock enclosing Archeozoic rock known as Kontum massif, at around 14° north latitude. Hardly any Paleozoic rock is distributed south of this basement rock. In addition, basaltic plateaus which erupted between the Neogene and Quaternary era can be found around the western borders (Tran, 1995; JOGMEG,2000).

Of the geological categorizations of Vietnam mentioned above, it is the geological features of the southern part of the "Truongson Block" area which is the focus of this study(Fig.2). In the study area, the geological features of the northern part is mainly made up from sedimentary rocks such as mudstone, siltstone, sandstone, conglomerate, limestone, marl and shale from the Paleozoic era, metamorphic rock consisting largely of quartz schist and mica schist from the Paleozoic era, as well as granite. The distribution of these shows a tendency for arrangement in a northwest-southeasterly direction parallel to the national highway Route 14.

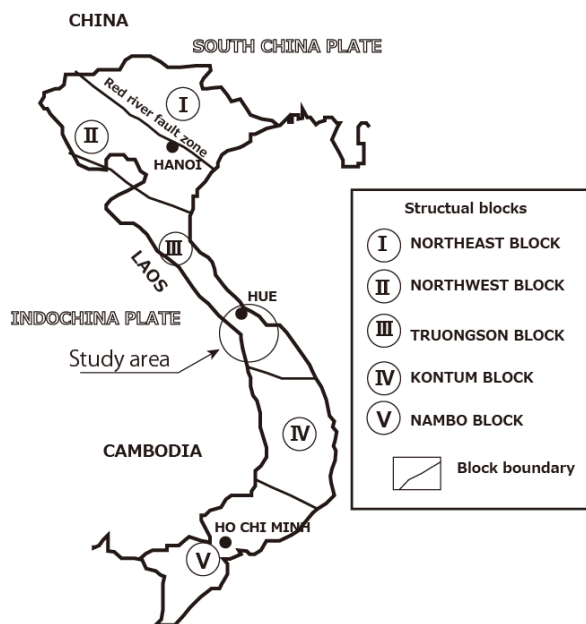


Figure 2 Geological tectonic divisions of Vietnam (from Tran, 1995)

From 16° north latitude to around 15° 30' north latitude in a southerly direction, the geological features at the center of the study area are mainly made up of sedimentary rock such as mudstone, sandstone, conglomerate, shale and limestone of the Mesozoic era. On the sloping surfaces of this area, cuesta land formations and gentle slopes which reflect the homoclinal structure of the stratum can be found in abundance. Further,

layers of coal of anywhere between 10cm and several meters in thickness are found in between these sedimentary rocks.

Paleozoic and Mesozoic granite is widespread across the study area as a whole, and metamorphic rock which becomes hard Hornfels can be found in this area(Fig.3).

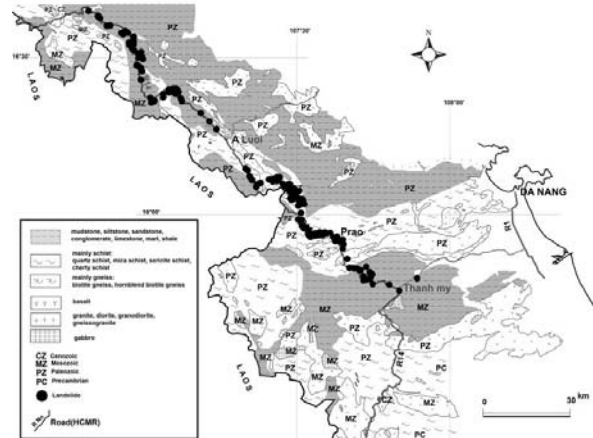


Figure 3 Geological map of study area Based on Tran (1995)

Movement type, landforms, and geology of landslides

Classifications and names of landslide movement types

Our site reconnaissance confirmed 182 landslides along HCMR (Fig.3, Fig.4). We followed the classification of Varnes (1978) for landslide movement types. But, most landslides that affect the road during landslide disasters in the past fall within three characteristic landslides. Thus, in addition to the classifications of translational rock slide, rotational slide, and rock fall, the following three landslide classifications were added: 1) translational wedge type slide where a moving mass slides in a triangular form, 2) translational shallow debris slide where debris of thickness under 1 m slide down the bedrock, and 3) gully type slide and flow where an arc-shaped sliding mass originating at the upper area of a slope slide down the slope surface, and the morphology resembles an erosional gully (Fig.4, Fig.5, Fig.6).

The geology along HCMR is dominated by Paleozoic sedimentary rocks such as limestone, shale, slate, and tuff in the northern areas including A luoi, with Paleozoic metamorphic rocks such as schist and gneissoid granite in the central areas including Prao, and Mesozoic sedimentary rocks consisting of sandstone with coal seams, mudstone, and conglomerate in the south. Also, in some parts, granite is exposed, exhibiting hornfels and gneissoid granite on the edges (granite/gneiss). Landslides often occur in the mountainous areas excluding the flat lands (Fig.4).

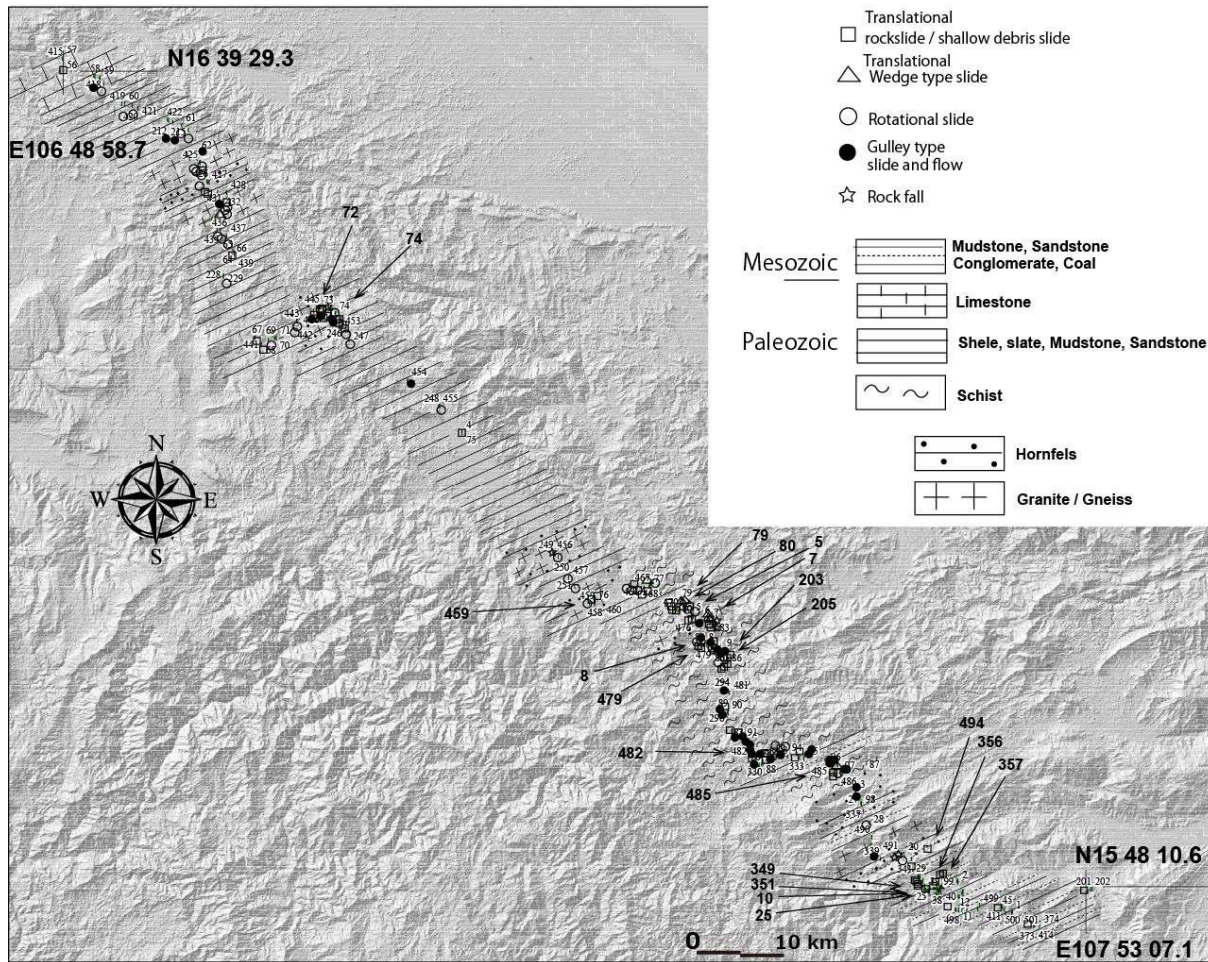


Figure 4 Landslide sites along HCMR (Numbers with an arrow are landslide sites of this paper)



Figure 5 Moving types of landslides along HCMR (No74: Translational shallow debris slide, No.10: Translational rock slide, No8: Rotational slide, No.7: Translational wedge type slide, No.72: Gully type slide and flow)

Movement type	Material		
	Rock	Debris	Earth
Falls	Rock fall		
Slides	Translational Rock slide Wedge type slide	Shallow debris slide	
	Rotational		Rotational slide
Flows			Gulley type slide and flow

Figure 6 Moving types of landslides along HCMR

The connection between landslide movement types and geology

Landslide movement types, geology, and the degree of erosion were classified (Table.1), and the relationships were investigated.

For the degree of weathering, brown to yellow-brown soil was considered very strong, soil containing gravel as strong, partially open cracks as weak, and fresh bedrock as unweathered.

Table 1 Landslide moving type, Geology and weathering

Type of movement	Translational rock slide	
	Rotational slide	
	Translational wedge type slide	
	Gulley type slide & flow	
	Rock fall	
	Translational shallow debris slide	
Geology	Granit/Gneiss	
	Schist	
	Mesozoic mudstone, sandstone, conglomerate	
	Paleozoic shale, mudstone, sandstone, limestone	
	Hornfels	
Weathering	Very strong	soil
	Strong	gravel
	Weak	with many cracks
	Unweathering	fresh

The number of landslides based on geology (Fig.7) and its percentage (Fig.8) show that gully type slide and flow is the most common type at 40% in the areas of schist. Translational shallow debris slide follows. Approximately 70% of landslides in the area of Mesozoic sedimentary rocks were translational rock slides. Rotational slide and translational shallow debris slide are common in the area of Paleozoic shale and sedimentary rocks. Gully type slide and flow are next common. Approximately 60% of landslides in the area of hornfels distribution are rock fall.

Granite/gneiss has a small distribution and has few examples of landslides, but various types of landslides do occur including translational wedge type slide.

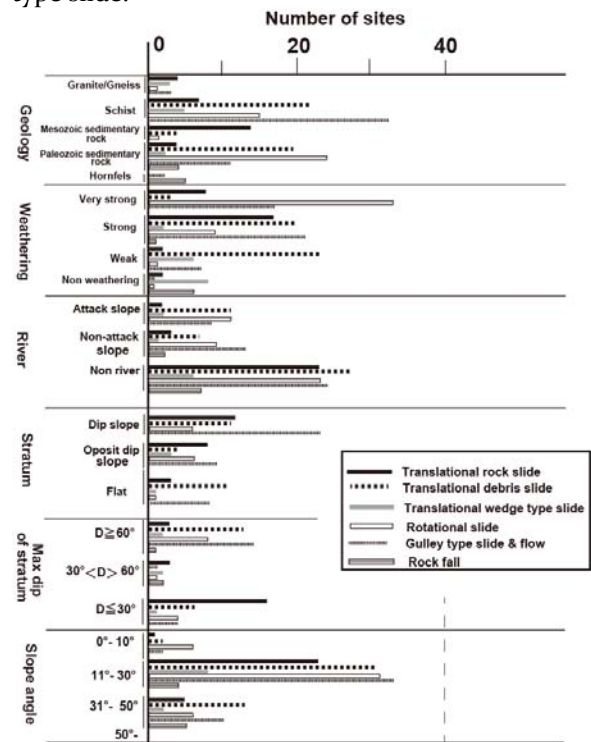


Figure 7 The number of landslide movement types based on the cause of occurrence

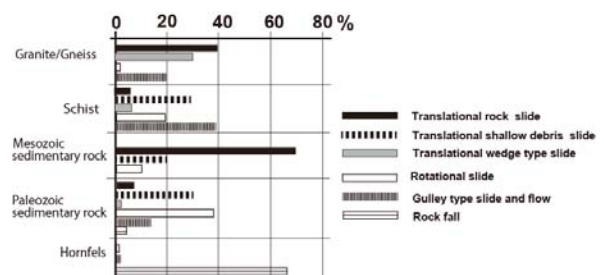


Figure 8 Ratio of landslide movement types based on geology

When the study area is divided into a northern Paleozoic sedimentary zone (zone A), central Paleozoic metamorphic zone (zone B), and southern Mesozoic sedimentary zone (zone C), the dominant landslide movement types are translational shallow debris slide and rotational slide in zone A, gully type slide and flow and translational shallow debris slide for zone B, and translational rock slide in zone C. This indicates that there is a strong relationship with the above-mentioned geology (Fig.9).

Many landslides occur in the area of strong weathering. Especially in Paleozoic metamorphic and sedimentary rocks, rotational slide, translational shallow debris slide, and gully type slide and flow have occurred in the weathered parts of the bedrock. In contrast, translational wedge type slide and rock fall occur without the effects of weathering. Translational rock slide dominates the area of Mesozoic sedimentary rocks,

and these are common in the area of weak weathering where rock composition still remains (Fig.10).
 weathering where rock composition still remains

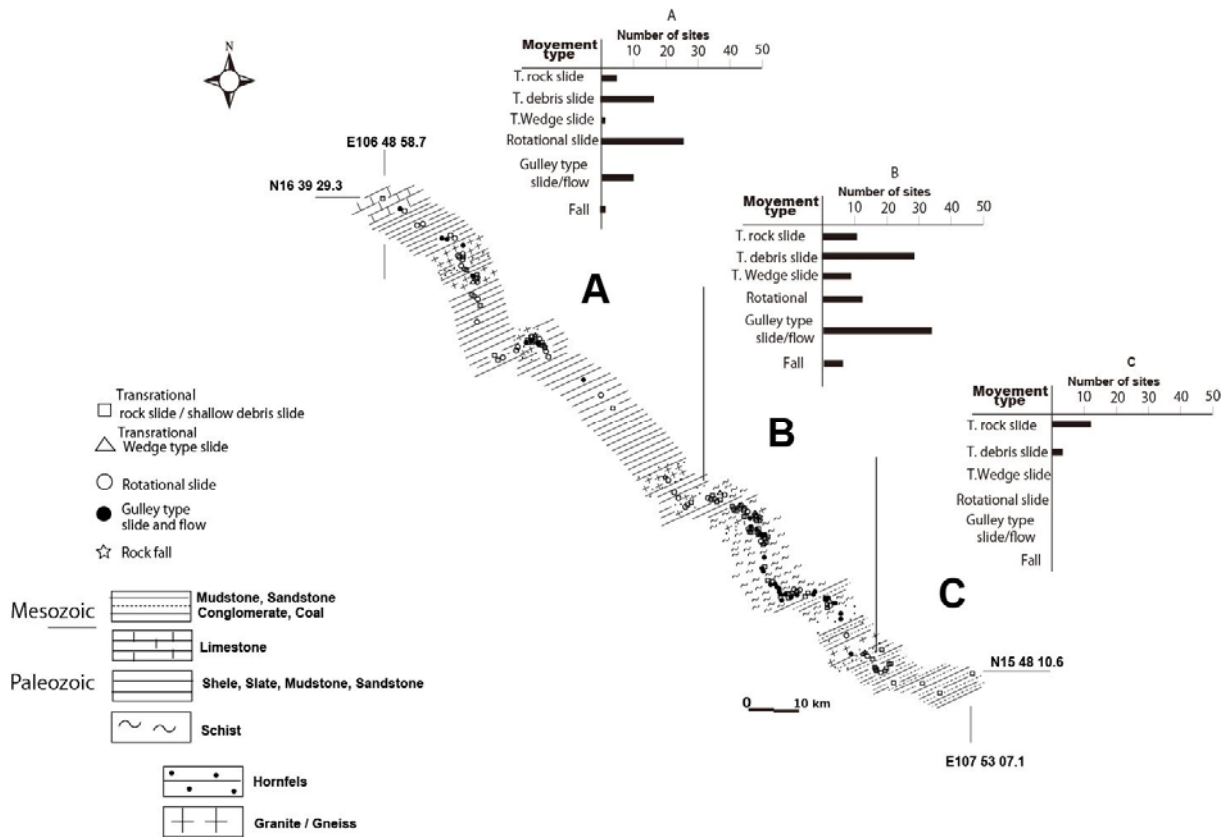


Figure 9 The number of landslide movement types based on the area

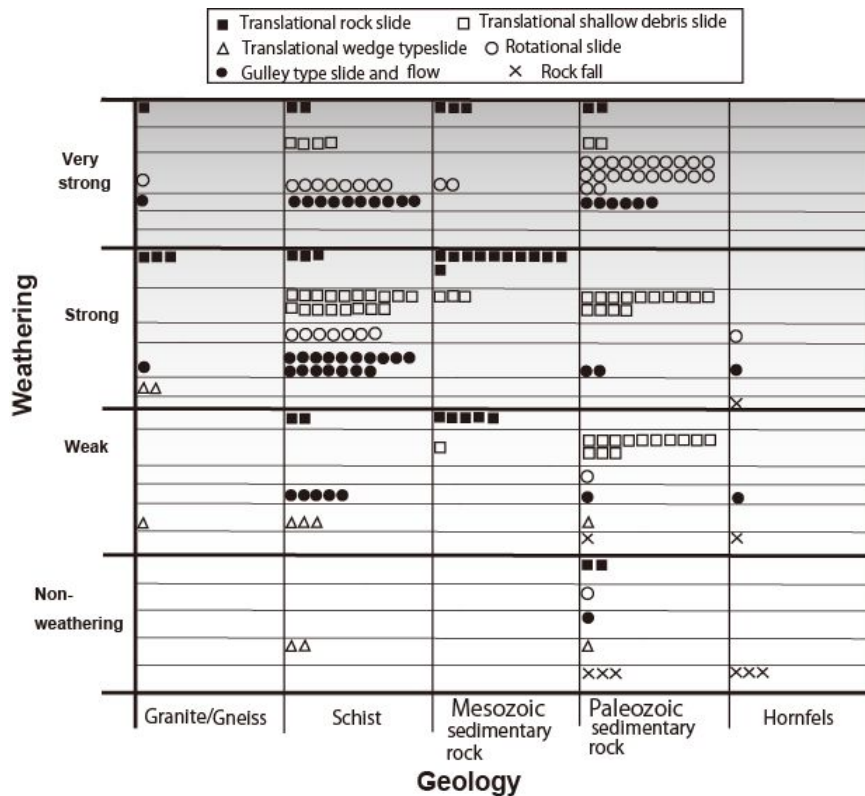


Figure 10 Geology, weathering, and landslide movements (the number of each mark indicates the number of landslides)

Also, in the Mesozoic sedimentary zone (C in Fig.9), cuesta landforms of the same width as the sloped structures and the length of over 10 km concatenate (Fig.11), and translational rock slide occur commonly within these structures.



Figure 11 Cuesta landforms developed in Mesozoic sedimentary rocks

Cracks and faults in the bedrock and landslides

Cracks in the bedrock

Landslides occurring in the study area often move along cracks in the bedrock such as bedding of the formation, schistosity, and joints. So, for this study, the cracks in the bedrock and fault directions were measured for the landslides in Paleozoic metamorphic rocks and Mesozoic sedimentary rocks (Fig.12).

Cracks and faults in gneiss/granite outcrop No. 7 and schist outcrop No. 485 of Paleozoic metamorphic rocks are concentrated on the first and the third quadrants in the Schmidt net, indicating NW-SE strikes and dips of a relatively high angle (over 60°) (Fig.12). The wedge type

slide that is characteristic of this study area moves along the schistosity and crack surfaces of the formation layers. Side scarps of the landslide at No. 79 correspond to a fresh schistosity surface (N 30° W, 60° E) and the direction of the cracks in the bedrock (N 40° E, 70° W). The trend and plunge of the line that intersects both side scarps are N 15° E and 50° based on the analysis on the Wulff net. Also, the side scarps intersect at 80° (Fig.13). The scarps of the wedge type slide that occurred in the outcrop of schist/granite at No. 7 correspond to cracks. The trend and plunge are N 12° E/40°, and the angle at which side scarps intersect is 55° (Fig.13). These landslides all use schistosity surfaces or cracks as the side scarp, and move perpendicular toward the road with the sliding surface angle of 40 to 50°.

Mesozoic sedimentary rocks consist of sandstone with coal seams and conglomerates. We observed cracks in sandstone and conglomerate separately from cracks in coal seams and in dark gray mudstone that contains a large amount of carbonates similar to coal seams. Both coal seams and mudstone are present within sandstone and conglomerate. The results show that the cracks in coal seams and dark gray mudstone all tend to concentrate in the second and the fourth quadrants in the Schmidt net. This means that these cracks have the strike of NE-SW with the dip of 50 to 60°. Also, cracks in sandstone and conglomerate that contain these coal seams concentrate in the first and the third quadrants in the Schmidt net, having the strike of NW-SE and a dip of over 60° (Fig.12).

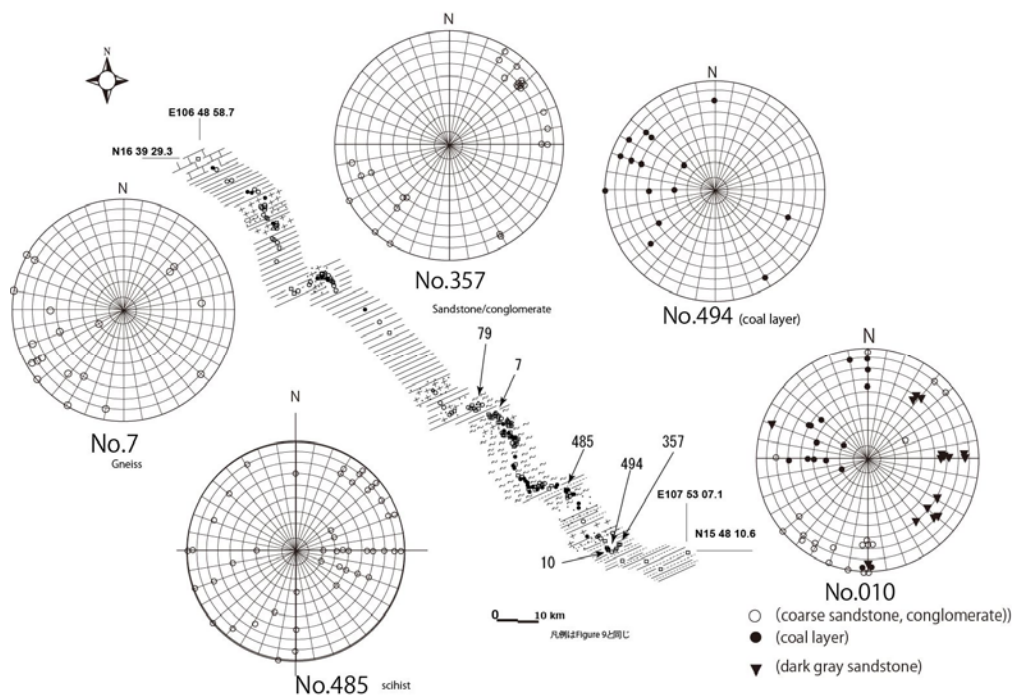


Figure.12 Cracks and faults in the Schmidt net (Lower hemisphere)

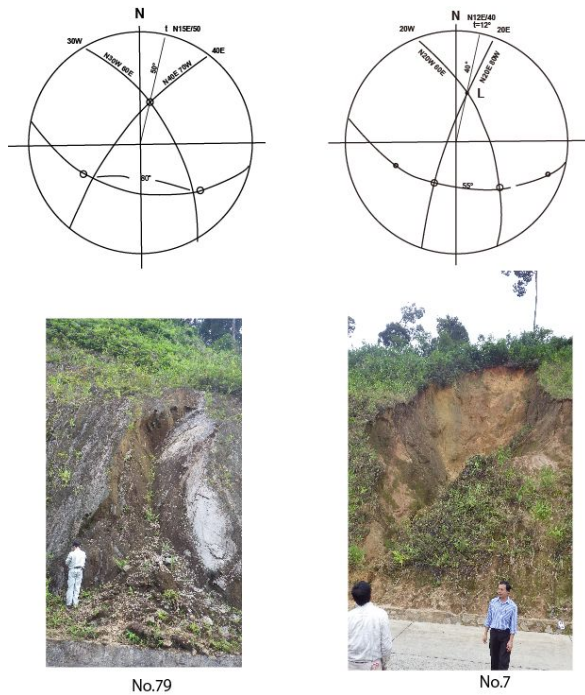


Figure13 Formation analysis of wedge type slides using the Wulff net

Faults

Sides of landslides occurring in gneiss/granite and schist correspond to black slickenside with scratches. Slickenside with scratches is often observed in fractured coal seams of Mesozoic sedimentary rocks as well. We observed the direction and the angle of faults including these small faults (Fig.14). On the other hand, small faults within coal seams have strikes scattering from E-W, N-S to NE-SE, with the dip of relatively low angles (30 to 80°) compared to the faults in other layers. The plunge of the scratches present on the surface of these faults is 60° for schist outcrop No. 203, 50° for No. 479, 30°, 30°, and 50° for No. 485, thus all are relatively low angles. The plunge of the scratches on the faults in Mesozoic sandstones and conglomerates is also low angle at 30°. In Paleozoic metamorphic rocks and Mesozoic sedimentary rocks, faults in mudstone, sandstone, conglomerate, schist, and gneiss/granite all concentrated in the east, or the first and the third quadrants in the Schmidt's net (Fig.14). These results excluded coal seams. This implies that these faults have the strike of N-S to NW-SE with a dip of 70 to 90°.

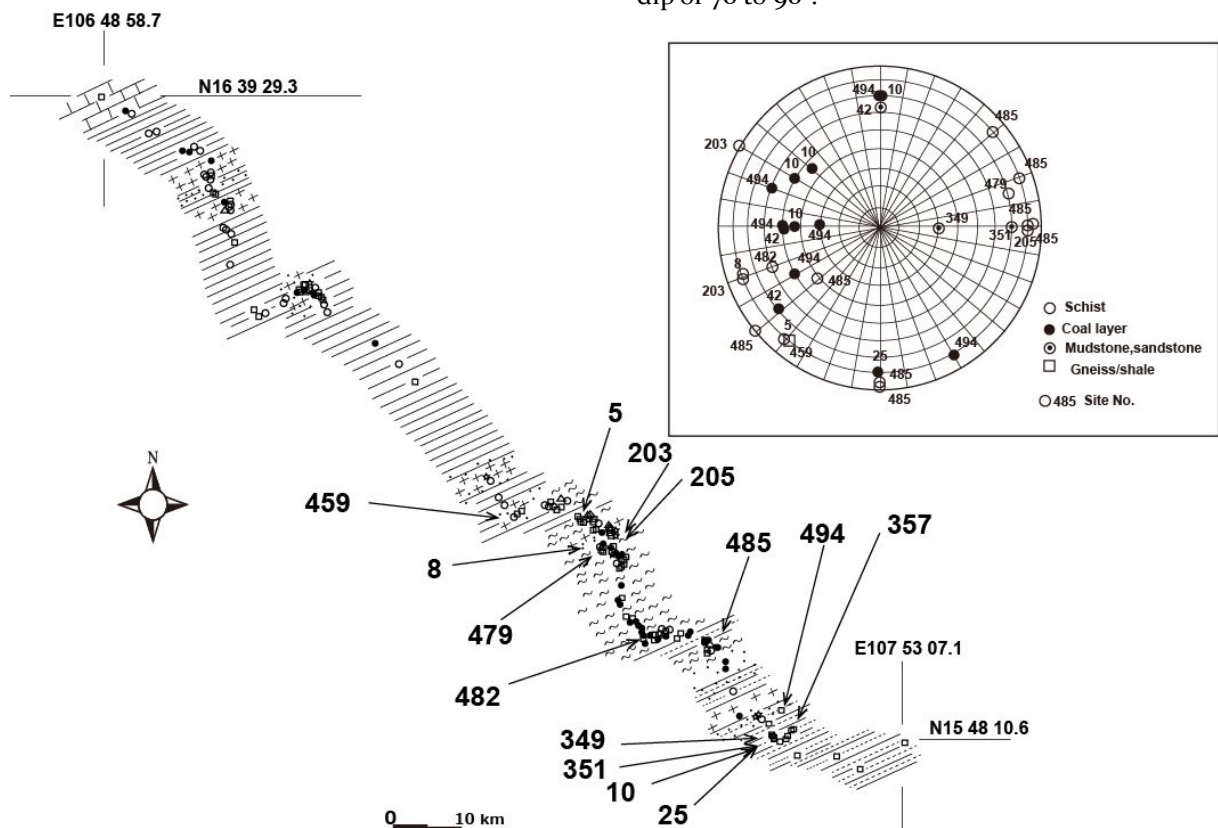


Figure 14 Strike, dip, and distribution of faults in the Schmidt net

Cracks, faults, and weathering of the bedrock

At No. 485, there is a rocky mass of width 60 m x height 15 m x depth 30 m (Fig.15). The rock type is weakly-metamorphosed muddy-sandy schist. It has the strike of N 70° E with a dip of 70° S. This

mass of rock is truncated by a nearly vertical fault trending NW-SE. But, the plunge of scratches on this fault has a relatively low range of 30 to 50° (Fig.15).

Also, there are fine joints developed in this rock in the same direction as the faults (Fig.16). Reddish-brown soil penetrates deep along these faults, schistosity, and joints (A, B in Fig.15). This

means that rainwater permeates underground along geologically weak surfaces such as faults, cracks, and schistosity, enhancing the weathering in the deeper parts of the bedrock.

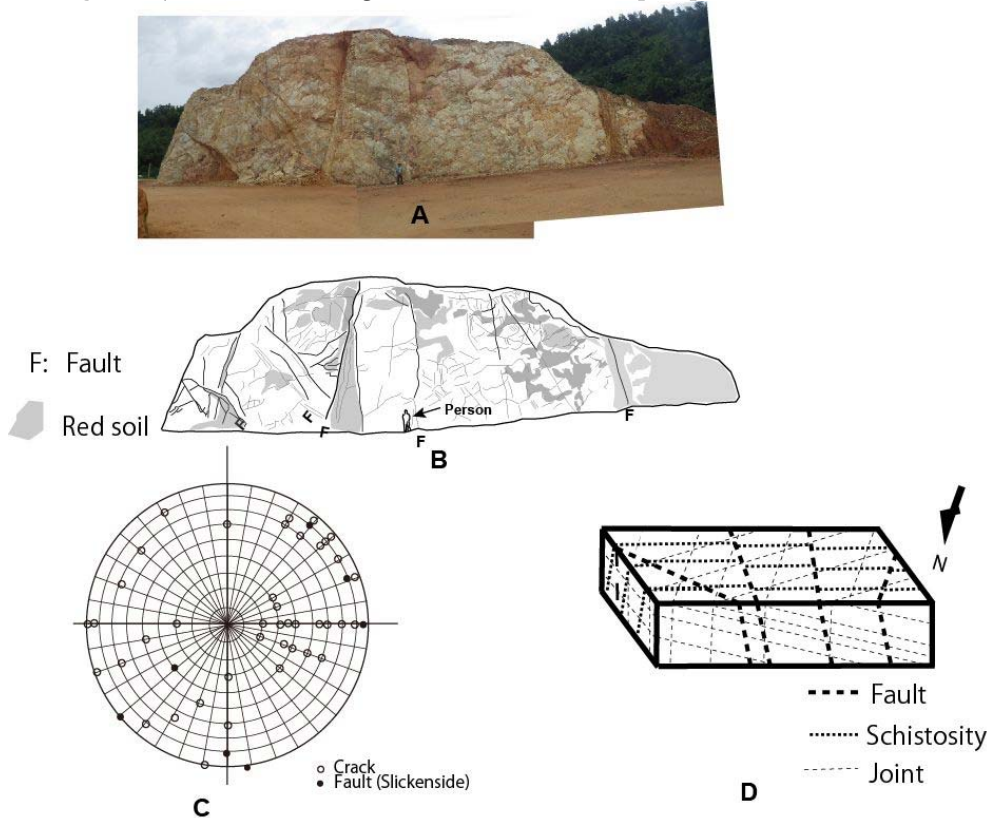


Figure 15 Photographs from the point No. 485 (A), sketches (B), the Schmidt net showing cracks (C), and the model of the whole rock mass (D)



Figure 16 Cracks (right) and faults (left) at No. 485

The X-ray diffraction results of this brown soil identified clay minerals that originate from the metamorphic rocks, such as quartz, illite, and kaolinite. The brown color of the soil is likely from a small amount of iron oxide.

Landslides in Mesozoic sedimentary rocks

Landslides in Mesozoic sedimentary rocks differ from the previously-mentioned Paleozoic sedimentary rocks and metamorphic rocks, and occur as translational rock slides. Granites are exposed at the border with Paleozoic metamorphic rocks, and contact metamorphic rocks are noted in the surrounding area (Fig.9).

Sandstone with coal seams and conglomerate are heavily folded in this area, but the folding decreases to the south. To the south of No. 20 in Fig. 17, cuesta landforms of over 5 km x 5 km with the same strike and dip have developed (Fig.11). HCMR passes through these cuesta cliffs from No. 20 to No. 341. To the south of that point, it truncates the west side of cuesta back slopes. And near No. 356, it truncates cuesta back slopes, then it heads south from the area of No. 42, arriving in Tanh my. Cracks have formed in sandstone, conglomerate, and coal seams between No. 345 to No.10 due to heavy folding. Especially, the coal seams are finely fractured (Fig.18). It forms a structure with a southward dip from the area near No.10. Prior to

arriving at No. 25, four translational landslides of 10 to 50 m wide have occurred (Fig.20). These landslides move independently of each other using coal seams in sandstone and conglomerate as the sliding surface (Fig.19).

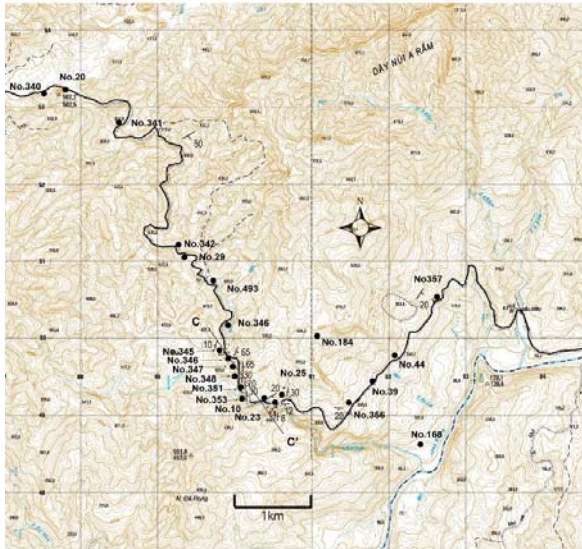


Figure 17 The map of Mesozoic sedimentary rocks survey points

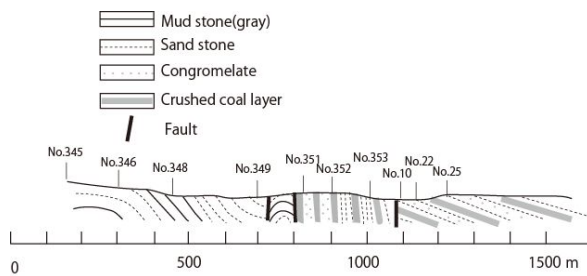


Figure 18 Schematic C-C' cross-section of Fig. 17



Figure 19 Landslides in coal seams (No.10 (left), No.25 (right))

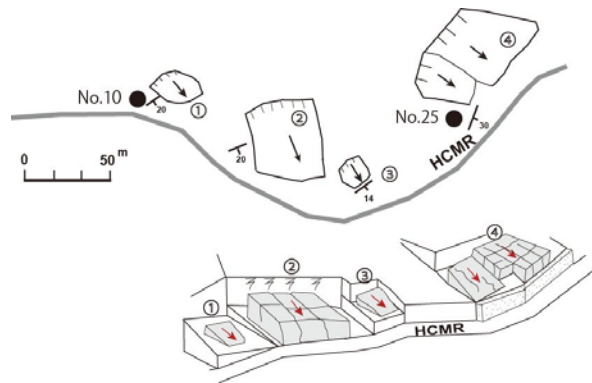


Figure 20 Translational rock slide around No.10-25

The effects of landslides are seen on the road and retaining walls between No. 356 and No. 44 in Fig.17. Especially since 2011, on the 400-m stretch from No. 356, new cracks of 5 to 10 cm have appeared after heavy rains each year (Fig.21). The surrounding area corresponds to cuesta landforms of the same strike and dip. Landslides of both length and width of over 1 km are confirmed on satellite photos. The side of an old landslide using a coal seam as the sliding surface can be seen in the outcrop at an old quarry about 1 km east of this point (Fig.22). Therefore, this large-scale landslide is identified as a translational landslide with a coal seam as the sliding surface, similar to 4 slides noted between No. 10 to No. 25.



Figure 21 Effects of landslides on a 400-m stretch of the road near No. 356



Figure 22 Ancient translational rock slide and slide surface of coal bed (right) -No.357-

Discussion

There is a common characteristic movement type in landslides in the study area. Thus, landslides are classified into translational rock slide, translational shallow debris slide, translational wedge type slide, rotational slide, gully type slide and flow, and rock fall. The changes in the movement types of these landslides depend on geology, geological structure, and weathering of bedrock characterized by bedding, schistosity, cracks, and faults in the geological structures. In Paleozoic sedimentary rocks in the northern part of the study area, common types of landslides are rotational slide in the weathered mudstone, sandstone, and shale, and translational shallow debris slide in the weathered surface areas with a thickness of bedrock under 1 m. In Paleozoic metamorphic rocks in the central region, gully type slide and flow in weathered red schist, and translational shallow debris slide in the less weathered area occur commonly. Most landslides in Mesozoic sedimentary rocks in the south are translational rock slides using coal seams in sandstone and conglomerate as the sliding surface. Occurrence of these landslides is associated with cuesta landforms of the same strike and dip, and fracturing of the geological layers due to folding.

Gully type slide and flow, and translational wedge type slide occurring in metamorphic rocks have basically the same occurrence mechanism. Translational wedge type slides have side scarp or a base that matches a weak surface such as schistosity, faults, and joints (Fig.23). Gully type slide and flow occurs in the areas of advanced weathering such as ridges and steep slopes. But, when the shape of the origin is investigated, many translational wedge type slide shapes can be confirmed (Fig.24). Bedrock around Plao is heavily weathered and brown in color, and many landslides have occurred. Since fresh bedrock surfaces can be observed in rivers at the bottom of the slope, the thickness of the weathered portion is considered to be 10 to 20 m. This brown soil has

high clay content and its permeability is considered low. Weathering can reach deep in areas like this as rainwater percolates along faults, joints, and schistosity as mentioned earlier. Therefore, in the areas with less weathering, translational wedge type slides are common, and in contrast, gully type slide and flow is common in the weathered areas. A large-scale landslide in schist noted at No. 80 can be considered a complex of multiple wedge type slide and flow (Fig.25). When these landslides occur in a row, or as a complex, the movement will resemble a large-scale rotational slide.

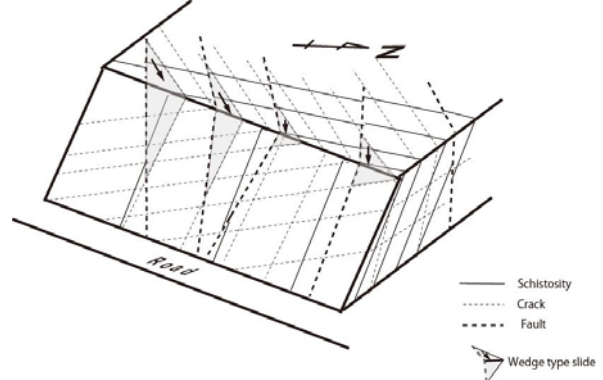


Figure 23 Schematic diagrams of cracks and faults with wedge type slides in metamorphic rocks

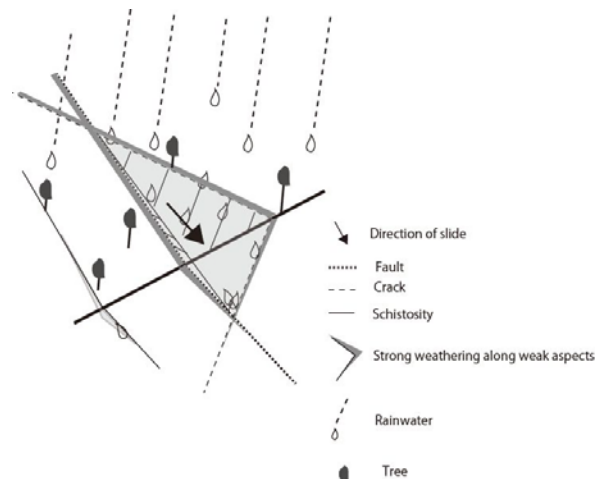
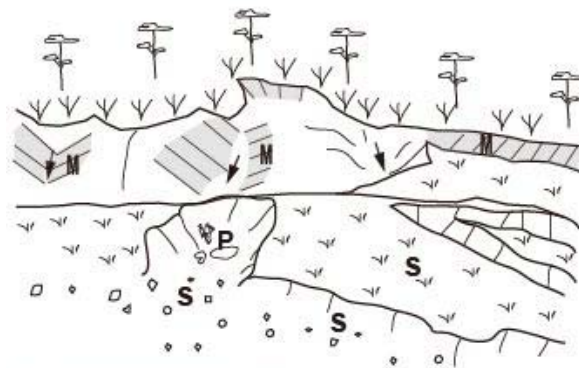


Figure 24 Formatemetics of cracks, faults, and weathering within sch wedge type slides



- M** schistosity plane
- S** landslide sedimentation soil
- P** person

Figure 25 A large-scale landslide occurring as a complex of wedge type slides (No.5)

Landslides in Mesozoic sedimentary rocks use the fractured coal seam within sandstone and conglomerate. Kaolinite and micas were identified in the X-ray diffraction results of clay in the sliding surface at No.25.

The residual strength $\Phi' r$ from ring shear tests was 11 degrees, resembling the value from Tertiary landslides in Japan (Fig.26).

The uniaxial compressive strengths of sandstone, conglomerate, and coal seams were converted from the Schmidt hammer test. The result shows a notably low value for the coal (Fig.27). Cracks occurring at regular intervals on sandstone and conglomerates (joints) and small faults in coal seams can be considered as deformation structures accompanying folding of sandstone and conglomerate with a brittle competent layer or muddy coal seam as the ductile incompetent layer. In other words, it can be said that periodic disturbances continue during heavy rainfalls due to crack development in sand and conglomerate from fold structures, fracturing and argillation of coal seams, and percolation of rainwater into these cracks.

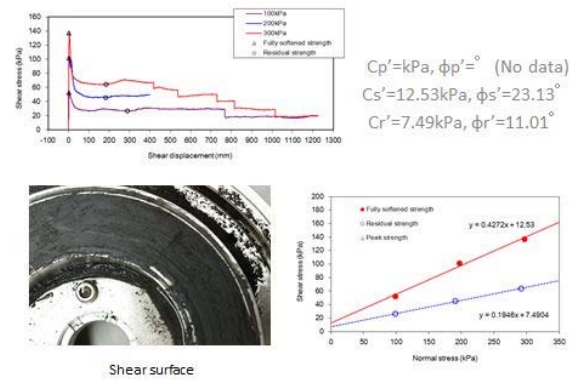


Figure 26 The results of ring shear test on sliding surfaces in the coal seam

site No	UniaXial compressive strength N/mm ²	
	No.42	No.10
Quartz conglomerate	373.9	
Quartz sandstone	227.9	84.7
Coal layer	68.5	—
Crushed coal layer	13.5	unmeasurable

Figure 27 Uniaxial compressive strength conversion by the Schmidt hammer

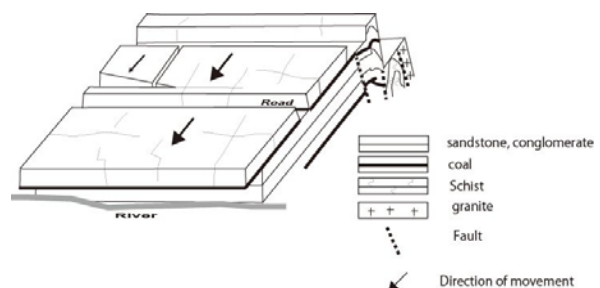


Figure 28 Large scale translational rock slide in Mesozoic sedimentary area

In addition, rock falls are noted in hard bedrocks such as Paleozoic shale and Mesozoic sedimentary rocks that are constrained by beddings and joints, and where creep is present within the area of hornfels distribution.



Figure 29 Rock fall in the hornfels distribution area (No.20)

Conclusions

Approximately 180 landslides confirmed along a 150-km stretch of HCMR were researched. The results are as follows.

In this study area, many landslides occur as a road hazard. These landslides have a movement

type characteristic of the geology and weathering of the area. Therefore, landslides in this study area were classified into translational rock slide, translational shallow debris slide, translational wedge type slide, rotational slide, gully type slide and flow, and rock fall.

The occurrence of these landslides is closely related to the geology of the area and weathering. In other words, in Paleozoic sedimentary rocks in the northern part of the study area, rotational slide is common in the weathered area and translational shallow debris slide is common in the less weathered area. Gully style slide and flow are most common in metamorphic rocks in the central part of the study area, concentrated in the highly weathered areas. In the areas with less weathering, translational shallow debris slide is more common. Most landslides in Mesozoic sedimentary rocks in the south are translational rock slide using coal seams as the sliding surface.

Weathering of metamorphic rocks in the central area is advanced deeper due to penetration of rainwater through weak surfaces such as schistosity and joints, and also due to the development of faults. In the study area, translational wedge type slides develop using the intersection of these weak surfaces as the sliding surface. With increased weathering, this develops to gully type slide and flow. Landslides in sedimentary rocks of the southern part of the study area are controlled by cracks in the bedrock. Coal seams in sandstone and conglomerate acting as the sliding surface are fractured and have many small faults. These small faults in the coal seams have different orientations from the fault direction and the dip

of the whole study area. Therefore, it is considered as deformation structures in sandstone and conglomerate as a brittle competent layer and muddy coal seams as a ductile incompetent layer associated with folding structures.

Mesozoic mud stone, sandstone, and conglomerate (excluding coal seams), and Paleozoic schist and gneiss/granite are truncated by faults with the strike of N-S to NW-SE and a high-angle dip of 70 to 90°. Thus, faults likely occurred post-Mesozoic due to uplifting of granite.

The above results showed that landslides in the study area have various movement types. There is a wide range of geology and geological structures leading to these various movement types, such as cracks forming in association with post-Mesozoic folds and faults, fracturing of coal seams associated with fold structures, weathering of bedrock due to percolation of rainwater along cracks, and development of cuesta landforms.

References

- Cruden DM and Varnes DJ, (1996). Landslide types and processes, Landslides investigation and mitigation, Special report 247(A. Keith Turner and Robert L.Schuster, eds.). TRB, National Academy Press, Washinton D.C. pp.36-75.
- Tran Ngoc Nam (1995). The geology of Vietnam , A brief summary and problems. Geosci. Repts. Shizuoka Univ., 22. pp.1-10.
- JOGMEG(Environmental research on resources development, Japan Oil, Gas and Metals National Corporation (2000). The Socialist Republic of Vietnam. 52p.



Proceedings of the SATREPS Workshop on Landslides in Vietnam, 2014

Change the safety factors by the series of land deformation at a typical landslide along the National Road No.6, Vietnam

Ngo Doan Dung⁽¹⁾, Eisaku Hamasaki⁽²⁾, Tatsuya Shibasaki⁽³⁾, Toyohiko Miyagi⁽⁴⁾, Hiromu Daimaru⁽⁵⁾, Dinh Van Tien⁽⁶⁾, Le Hong Luong⁽⁷⁾

1) Institute of Transport Science and Technology, Hanoi, Vietnam, Vietnamese member of WG2 and short term trainee in Japan, e-mail: ngodoandung@gmail.com

2) Advantech Co., Ltd, Aoba, Sendai, 0081, Japan, e-mail: hamasaki@advantech.co.jp

3) Japan Conservation Engineers Co.,Ltd, Japan, e-mail: shibasaki@scs.dpri.kyoto-u.ac.jp

4) Tohoku Gakuin University, Izumi Campus/2-1-1 Tenjinzawa, Izumi-ku, Sendai, 0081, Japan, e-mail: miyagi@izcc.tohoku-gakuin.ac.jp

5) Forestry & Forest Products Research Institute, Japan, email: daimaru@affrc.go.jp

6) Institute of Transport Science and Technology, Hanoi, Vietnam, Vietnamese leader of WG2 and short term trainee in Japan, e-mail: dvtien.gbn@gmail.com

7) Institute of Transport Science and Technology, Hanoi, Vietnam, Vietnamese member of WG2 and short term trainee in Japan, e-mail: lehongluong@gmail.com

Abstract According the economic development in recent years, the needs of expanding especially the traffic route which connects the Vietnam inside and neighboring countries by are greatly growing. Many slope disasters have occurred in various places with expansion of a major traffic routes. Now, landslide disasters are slope disaster phenomena main for Vietnam. From now on, also in the area of the neighbourhood expected, development will think that the same phenomenon is caused. I think that the research and experience which are cherished in the SATREPS project by ITST/JST/JICA can contribute to disaster prevention of whole Southeast Asia greatly. We are conducting to clarify the soil strength characteristic, mapping of landslide topographic feature, and how to set up the reasonable countermeasure for disaster control, mitigation and the potential evaluation, etc. in this project.

Here, the example of the landslide in the National Route 6 of the Hanoi suburbs, near Hoabinh province will be introduced. Although this landslide is not huge, the state immediately after disaster generating is indicated comparatively in detail. Moreover, an understanding is also advancing a series of field survey. The current field investigations are, make up the micro landform classification map for the realization the slope movement tendency, clarify the geological structure and soil strength, and landslide topography measurement by laser survey. Based on these, we will carry the 3

dimensional landslide stability analysis by ADCALC3D. By the series of study, the overall perspective will be realized. The series of the studies will have been documenting for teaching sample.

Keywords landslide, safety factor, land deformation, countermeasure, National Road No.6, Hoabinh province, Vietnam, ADCALC3D software, SATREPS

Introduction of the KM95 landslide

The target landslide is belong to Hoabinh province, located at 95 km far from the starting point of National road No.6 at Hanoi. The road is connecting Vietnam Capital City and North-western provinces of Vietnam. Route length of 504 km and the road that goes through 4 provinces and cities (Ha Noi, Hoa Binh, Son La and Dien Bien), which travel through Hoa Binh province is 119 km long (from Km 39 to Km 158). In 2001, this route was the renovation and upgrading of the section from Hoabinh to Son La (from Km 78+300 to Km 303+790) with grade - III standards on mountainous of road and completed on March 2005.

Since being put into operation, this sections has promote investment efficiency, service better for the travel and transportation of goods and people efficiently serve the construction of Son La and Lai Chau hydropower plant and the role of transnational routes. However, since then, on sections from Km 78 +300 to Km 158 landslide

occurs annual and rock from landslides are fall down the road.



Figure 1 Overview of the KM95 Landslide

Because this road is an important artery. The traffic is highly frequent and many people use for daily life. Although, along the road, there are big number of landslide hazardous area are distribute. Some of them are still moving. In case of Hoabinh province, there are around 30 landslides distribute along the National Road No. 6, in which 17 active landslides. Among them, the KM 95 landslide happened at December, 2009. The size of the landslide was about 100 meters in width, 80 meters in height and deduced the depth 10~20 meters. It located at a part of small peninsula like topography. The toe part expose to the road surface and up lifting is also occurred.

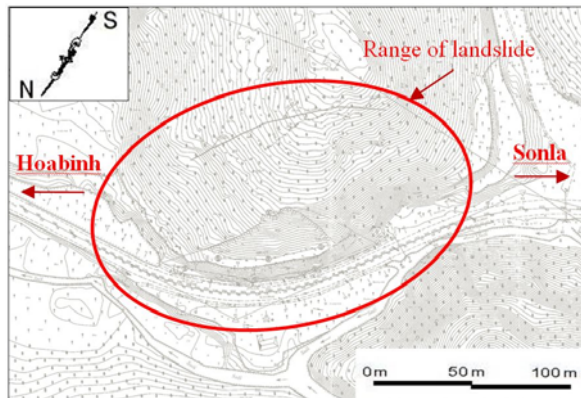


Figure 2 Contour map of the KM95 landslide

Ministry of Transport and People's Committee of Hoa Binh Province carried the urgent inspection and carried the urgent repair work. That is cut the deformed micro topography and cleaned the surface. Frame works for surface adjustment carried. And concrete steps sat not only for the walking but also for the water discharge. Although, during the job, the new scarp has been appeared at the behind higher part of the countermeasure area. The displacement of the scarp had getting larger and larger. The plan of it is typical horse shoe and the top part displacement is reach to 1.5 meters high vertically.

According to such new deformation, the temporal water discharge and shut the infiltration works had carried. It is just set the small spillway and outlet. The bottom of scarps part was filled by clay. The spillway by concrete was also sat. The scarp deformation was stopped. After the urgent countermeasure work, there are no secondary features of landslide phenomena.

Tendency of land and geologic features at surrounding area

The site of KM95 landslide is located at the part of peninsula shape area. There was no typical landslide topography. But the surface features have some distinctive shallow landslide characteristics (Figure 3).



Figure 3 Some distinctive shallow landslide characteristics around KM95 landslide

The geology is consist of Mesozoic sedimentary rocks such as reddish medium sandstone, mudstone. The structure has some inclination but the dominant dip and strike is developing slightly against the dip direction of the direction of KM95 landslide. The weathering tendency is deeply and strongly developed.



Figure 4 Relatively fresh rocks

Material characteristics

X-ray diffraction analysis

Clay mineral characteristics of the weathered materials are examined by X ray analyser. Soil faces are categorized to crack rock, laminated rock, strongly weather rock and soil. The result is very clear. That is, relatively fresh rocks include illite. But according to the weathering advance, kaolinite getting appears.

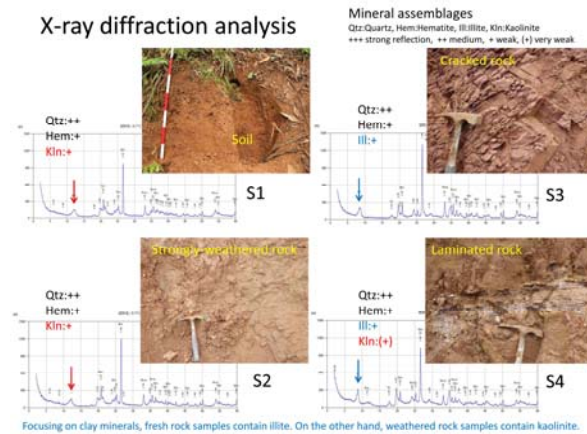


Figure 5 Data of the X-ray diffraction analysis

Soil strength of the area

The soil strength data is also evaluated. Soil samples had taken at nearby the landslide area. Because there are similar landslide features are occurred.

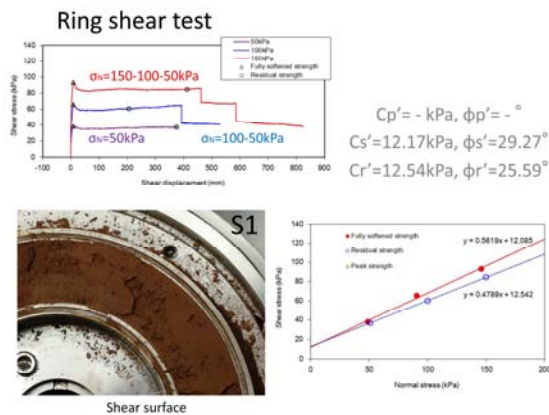


Figure 6 Data of the ring shear test at the KM95 landslide

Safety factor evaluation by ADCALC3D

The project introduced the relatively convenient three dimensional calculation software, ADCALC3D. ADCALC3D has three types of 3D landslide stability analysis: Hovland, Janbu3D and RBMS3D.

We tried the series of estimations. The initial data of the landslide topography had taken in 2011

at the occasion of set up the countermeasure. The other data by means of the topography of after the countermeasure carried that had taken at last March (2014). The topographic features are transferred to X.Y.Z digital data.

Figure 7 is the 3D image of the KM95 landslide area (left) and deduced slip surface structure (right). The methodology of deducing will discuss. Although, according to the actual field displacement by the developing cliff, this case seems the typical and simple slump type landslide. And the toe part was also appeared as the budging at road. We carried the series of safety factor evaluation. The calculation approach of slope stability analysis RBMS3D.

Table 1 The results of estimations carried by the 3 dimensional landslide stability analysis by ADCALC3D

Title	C	phi	γ	Fs	R	D
Unit	KPa	°	KN/m ³		KN	KN
Pre-cut	10	25	18	1.19	540,831	453,942
Pre-cut & C=0	0	25	18	0.97	440,515	453,942
Post-cut	10	25	18	1.24	463,721	375,276

Figure 8 is the results of estimations. The initial FS set as 0.9704 because of the actual landslide phenomena. And recalculate by the data of C and phi, the FS marked as 1.1914. The estimation after the urgent counter measure condition, the FS marks 1.2357. This shows the safety level improved 5%. But the 3D image shows the high stress concentration area at toe part (red colour zone).

Topographic features of surround the KM 95 Landslide

Figure 2 shows the topography of the before the disaster 2009. According the map, there is the typical landslide topography at the eastern side of the KM95 landslide. At year 2012, clear and large horses shoe shape cliff stretched at the upper slope of the area of counter measure. The cliff stretched to eastern side of the KM95. There is clear and small landslide topography. The similar scale of KM95 landslide might be located in many areas. These landslides are not so huge, but if it moving, the materials move to road. The amounts will much enough the take human's life. Then, we must pay attention to these landslides. And if there are a number of such landslide risks, we have to consider the way of the technique of evaluation of its instability and construct the way of decision making system for get the most reasonable way of monitoring, countermeasure, field inspection etc.

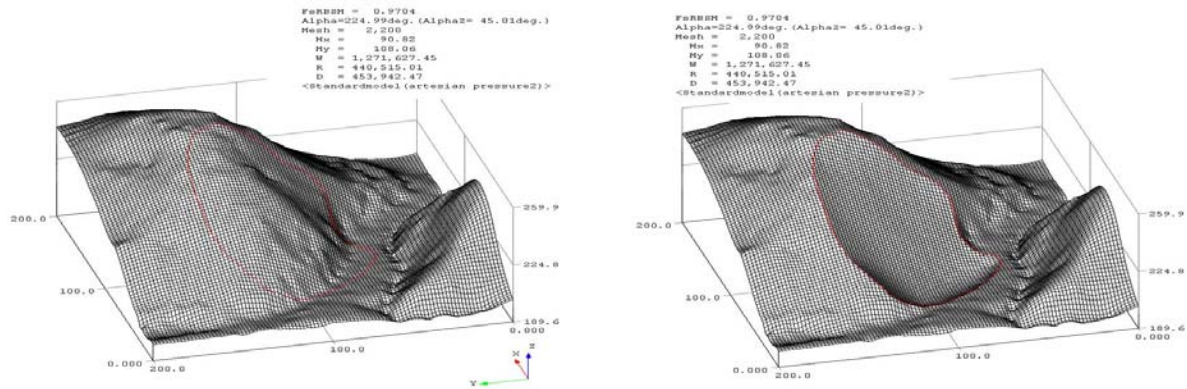


Figure 7 The 3D image of the KM95 landslide area (left) and deduced slip surface structure (right)

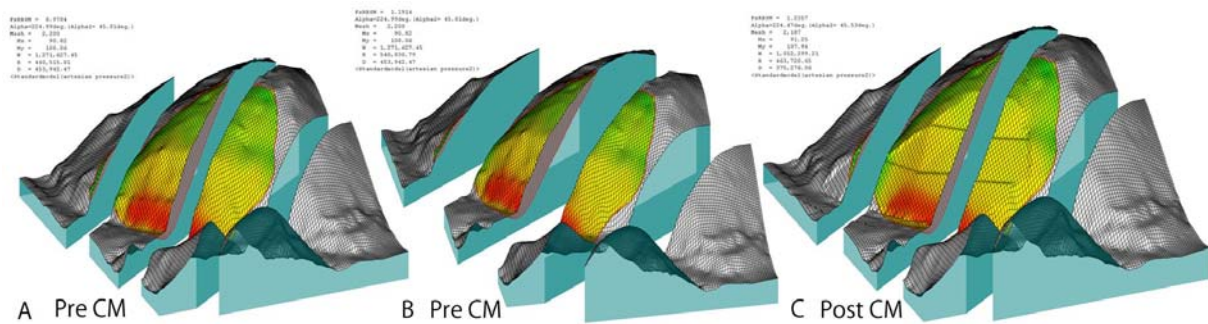


Figure 8 The results of estimations carried by the 3 dimensional landslide stability analysis by ADCALD3D

Acknowledgments

First of all, I pay my sincere gratitude to ITST leaders, Prof. Kyoji SASSA and the honourable every renowned Professors of different Universities in Japan many officers and engineers from Government and private sectors, field officers and Japanese coordinators, who give us some chances to study in Japan, many research experiences.

I would especially like to thank Prof. Noriyuki CHIBA, Dr. Hiroyuki YOSHIMATSU, Dr. Shinro ABE, Mr. Takeshi KATO and the other members of WG2 of Vietnam project, who have contributed their outstanding efforts through their presentations, lectures, site visits and

laboratory testing for the support to writing this article.

References

- HAMASAKI Eisaku, TAKEUCHI Norio, OHNISHI Yuzo, (2006) Development of simplified discrete limit analysis for three-dimensional slope stability problem. *Landslide – Journal of the Japan Landslide Society* Vol.42. No.5 (2006), January, pp.389-397
- HAMASAKI Eisaku, MIYAGI Toyohiko, TAKEUCHI Norio, OHNISHI Yuzo, (2007) Risk evaluation of the earthquake triggered landslide on the land reclamation slope by three dimensional instability analysis of simplified RBSM. *Landslide – Journal of the Japan Landslide Society* Vol.43. No.5 (2007), January, pp.251-258



Objective Function based AHP Risk Evaluation System in Humid Tropical Regions

Eisaku Hamasaki⁽¹⁾, Toyohiko Miyagi⁽²⁾, Dinh Van Tien⁽³⁾, Ngo Doan Dung⁽⁴⁾

1) Advantech technology co.,Ltd., Department of Technology, Sendai, Japan, hamasaki@advantechtechnology.co.jp

2) Tohoku Gakuin University, Department of Regional Design, Sendai, Japan, miyagi@izcc.tohoku-gakuin.ac.jp

3) Institute of Transport Science and Technology, Hanoi 84, Vietnam, dvtien.gbn@gmail.com

4) Institute of Transport Science and Technology, Hanoi 84, Vietnam, ngodoandung@gmail.com

Abstract AHP is the method of refining a plan like the risk assessment system for landslides, and the assessment system from analysis. This method is expected to apply to humid tropical region in the near future. AHP is a decision making tool and the structure is divided into hierarchy criteria and hierarchy alternatives. However, some other method, such as multiple regression analysis, is statistical inductive approach using many sample data.

In the nature or data collection at the field, we are not able to get the enough number of statistical data to fully explain the model. Particularly, number of landslide's data often is not enough to make statistical model. On the other hand, AHP method is easy way and more deductive using human experiences than other method. As well as, AHP can be converted to explicit knowledge from tacit knowledge we have as technology. However, these models using AHP are necessary to be verified using by some objective function, such as regression equation or probability of error. This occasion, we like to describe how to verify AHP application utility by some objective function.

Keywords Landslide, AHP, Objective function, Risk evaluation system, Explicit knowledge, Tacit knowledge

Review the AHP approach for the landslide risk evaluation

The AHP is one of the statistical approaches of the decision make processes. It has the characteristics for guide the making decision by a pair comparison or a pair parameters evaluation approach due to decision making. The structure is combined the factors such as the goal, criteria and alternatives. The calculation approaches will

categorize into two groups. That is an approach of "relative comparison" and "absolute comparison".

Relative approach for decision making

One of the most expected AHP approach for application for decision making about the identification of the most suitable countermeasure. In such case, the flow chart clearly mention the goal as the suitable particular countermeasure, criteria such as the view point of economical, execution, effectiveness, durability, maintenance etc. And as the alternatives such as pile, anchor, embankment, cut, drainage, and monitoring will necessary (Fig. 1). The relative approach is easy and is basically logical to use for such purpose. Although, in case of Japan, the approach never have been tried yet.

Mr. N.G.Dung will promote the study in the project of SATREPS.

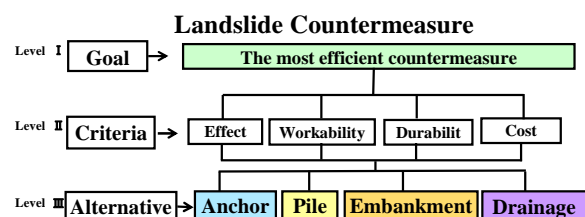


Figure 1 Example of AHP model

Absolute approach to risk evaluation for landslide unit

The AHP approach has been adopted to risk evaluation to the landslide topographic area. The methodology is already constructed. For example, many reports have been published. And it applied to the actual landslide risk evaluations.

In case of AHP application to the risk evaluation, the relative approach has some difficulties. The target landslide area distributes anywhere abundantly. So, the compare the alternatives in each criteria is impossible. In this

case, the absolute approach is might be useful. This approach is explains as follows. 1) The standard criteria establish by the evaluation and discussion to the data package of micro features of landslide topography and the spatial distribution. 2) The meanings or the value of the

indicators to the contribution of reactivation possibilities should be decided by items. The items distributed to the check sheet. The contribution values decided and put the score by the discussion by high level engineers (Fig. 2).

Check list for risk evaluation of landslide				AHP score	
Level II	Level III	Indicative signs of instability			sum
		High ←		→ Low	
A	Micro topographic features on a surface of a landslide mass	a	Grade of fracturing of landslide mass	20 Debris flow Mudflow, earth flow 13 Secondary scarps Secondary multi slump, mudflow 8 Head part depression Minor scarps crack, pressure ridge 0 no sign	
		b	Clearness of surface ruptures	20 Clear and fresh Closely-spaced scarps & linear depression 13 almost clear and fresh a series of scarps & linear depression 8 not clear rounded scarps & burried depressions 5 ••••• 0 hilly or bumpy, incision of slide mass	
B	Deformation of marginal zone	c	Grade of degradation of main scarp	10 sharp and clear crown 5 subrounded crown, talus deposition 2 rounded crown, gully erosion & talus deposition	
		d	Condition of toe part	20 collapse, Secondary slide 12 Partial collapse, Secondary slide 6 gullies small debris' fan on foot 0 colluvial fan formation on foot	
C	Locality of landslide	e	Erodibility of toe part of landslide mass	20 undercut slope for mainstream or artificial excavation work 12 undercut slope for tributary or artificial work 6 slipoff slope, orthogaonal position to river 2 higher position of slip surface from river floor, or on terrace 0 terrace	
		f	Potentiality of instabilization at toe part of landslide mass	10 steep & high relief profile 5 rounded edge & convex profile 2 straight profile 0 concave profile	

Figure 2 Example of a data sheet through AHP aerial photography

It is needless to say, in case of actual application to the risk evaluation, the verification is necessary (Fig. 3).

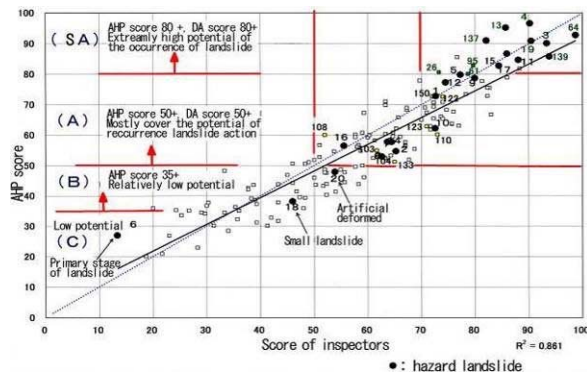


Figure 3 Relationship between AHPscore and Score of inspectors

Verification trial

Here we would like to introduce the two kinds of model for verification. One is the combined application model of buffer movement analysis

and the other is the error provability analysis as new GIS statistical analysis technique.

By the way, the development of the risk evaluation model to the landslide topographic area, that advance was with the technique of aerial photo interpretation. There is the necessity the skill acquirement such as the topography of the landslide identification and micro landform classification by aerial photo interpretation. The skill is strongly reliance to the study of geomorphology and geology. The skill will be able to application in case of the Humid Tropical and Deeply Weathered Environment such as Vietnam.

The current model of risk evaluation to the landslide unit is useful. But there are some difficulties. That is not able to evaluate the susceptibility to the area of outside of landslide unit. The approach of aerial photo interpretation is only useable to the landslide unit. The approach is standing the point of view that is “the unit”. If we think the risk evaluation to all the area of slopes, it will have some contradiction. The idea of application to all slopes is based on the view point of “the continuity”.

The difficulty of the size is also important. The model can use for relatively large scale landslide unit. Because of the possibility of identification the unit depend on the quality and scale. In case of Vietnam, the scale is 1 - 33000. This is too small for identify the surface landslide. In case of landslide mapping in Japan, 1 - 40000 photo use usually. And the size of identification decides larger than 150 meters in width one.

This means the approach of aerial photo interpretation is not able to use for the ideal design of route. Needless to say the small or surface landslide is also very dangerous. Such matter is discussing with Mr. D. V. Tien in ITST, Vietnam.

Combined application model of buffer movement analysis

The basic idea of the evaluation model of the susceptibility is as follows. The objective variable is the actual distribution of landslide sites or the area which is established by AHP, GIS etc. The explanatory variable is defined by AHP value that is caused by the series of parameters of morphometric features such as relief energy, above ground opening degree, inclination, catchment area etc. Here, the “combined application model of buffer movement analysis” will be trial use to the new GIS statistical analysis.

The model is not similar to the former one. In before, the causes were presumed from each physiographic characteristic of landslide. If we say presume in this approach, that is like a thinking the bird eye view. The characteristics of the model will say as follows. Firstly, the data of land features (topography, geology, landslide indicators, etc.) are collected from the area of buffering area. The data collection area means the buffering area which will shift to one direction step by step. Secondary the comparison of the actual landslide distribution and the score of buffering data is estimate as the level of harmonic proportion (Fig. 4).

Objective function for model verification evaluation

When we use the model for susceptibility evaluation, we have to carry the verification.

For example, in each buffer, we will get the correlation coefficient between the AHP score and the overlapping degree of landslide distributions. That is the numerical formula of the correlation coefficient as the objective function.

Furthermore, if we will be able to prepare the number of data, the specificity will be increase as the probability function.

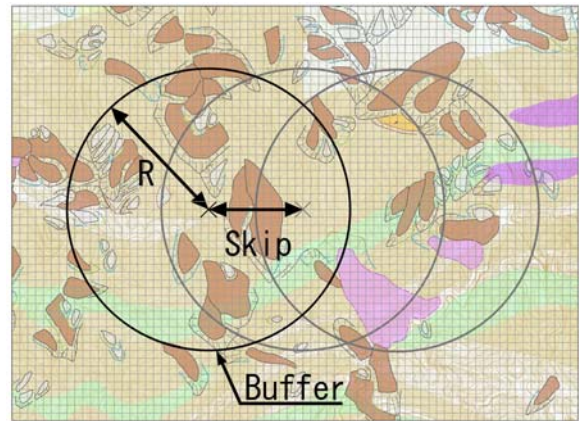


Figure 4 Buffer movement analysis conceptual diagram

Here, we have to think about the level of explanation of actual landslide distribution and the susceptibility assessment in all slopes. The buffer will divide in to the “existing” of “not existing”. The “existing” is means landslide including in the buffer.

While, if the distribution of data of AHP scores normal, the distribution of “probability density function” will divide clearly. The two normal distributions separate clearly, this means that the evaluation of the susceptibility is well explained. So, the each median Y among the mean AHP score will decide as the temporal standard. For example, in case of “no existing” buffer group, there is the part of larger than the normal distribution of the probability. The “no existing”, area means “probability of error” as the actually “no existing” but decide to “existing”. On the other side, the probability of smaller than Y of the normal distribution of the probability of “existing”, that also means “probability of error”. Thus, we would like to define as the “blender probability”. The model adaptability is explains as the distance or the overlapping of two AHP score distribution. (Fig. 5, Fig. 7,8)

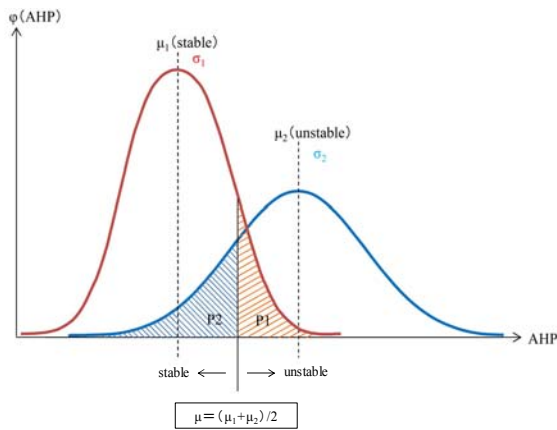


Figure 5 Distribution model of malpractice probability

Summary

This occasion, we discussed the importance of the setting the objective function and the verification if we try the susceptibility evaluation and AHP approach to the slopes instability analysis. And also, we introduced new statistical approaches. That is the approach of the causative factor selection and the statistical analysis with buffer movement analysis based on the samples of landslide actual distribution. And the “blender probability” was defined. This is useful for separation of the “existing” or “no existing” distribution and the related parameter identification.

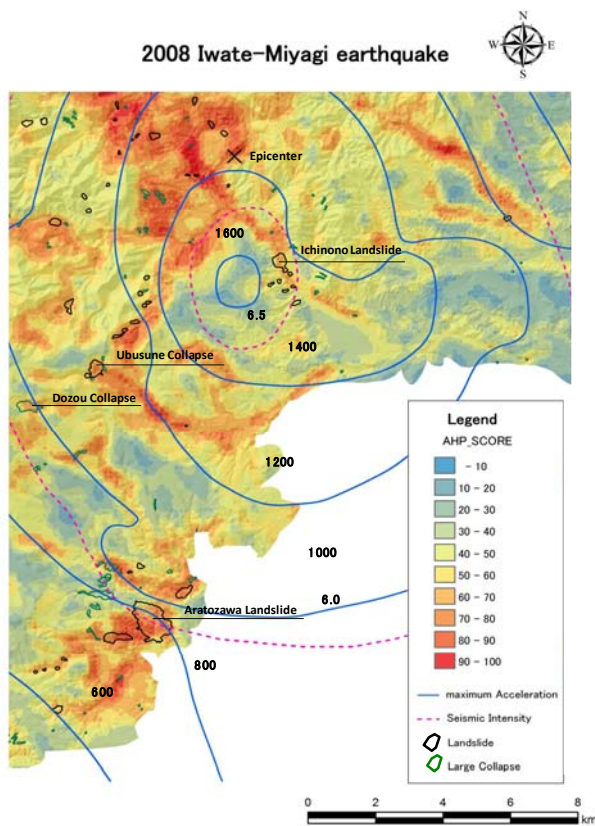


Figure 6 2008 Iwate Miyagi Sustainability Landslide model

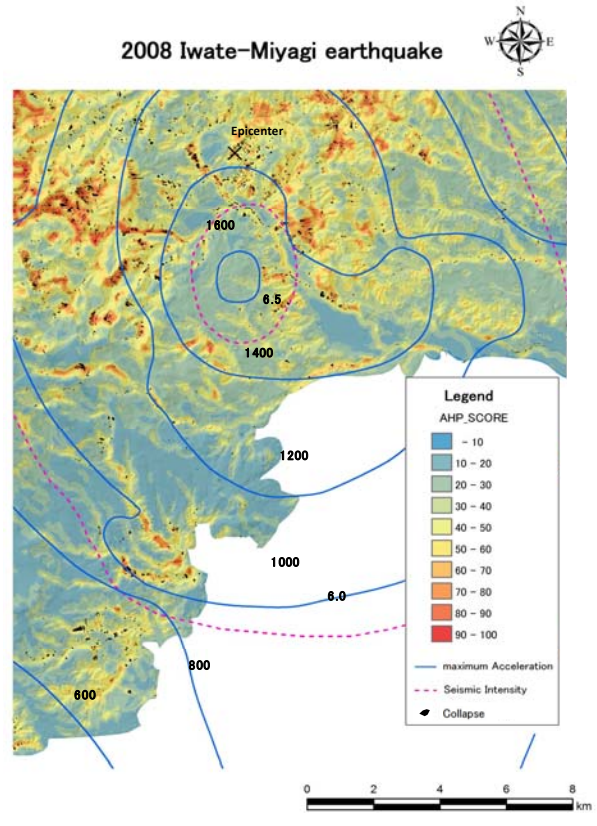


Figure 7 2008 Iwate Miyagi Sustainability collapse model

Acknowledgments

First of all, I would like to express Vietnam project Leader and our supervisor, Prof. Kyoji Sassa, who give us some chances to study Vietnam Area, many research experiences. And, I would like to thank the other members of WG2 of Vietnam project, Dr. Hiroyuki Yoshimatsu, and Dr. Shinro Abe, Dr. Hiromu Daimaru, Mr. Takeshi Kato, Mr. Tatsuya Shibasaki, and Ms. Akemi Yoda. They provided at all levels of the research project. Finally, I would like to thank Ms. Haruna Ishikawa from Advantech technology co.,ltd for the support to writing this article.

References

- HAMASAKI Eisaku, HIRAI Takesa, MIYAGI Toyohiko, (2003)Evaluation of the Probability of Landslide Occurrence by AHP based on the Results of Aerial-photo Interpretation. Conference Proceedings of the 42nd Annual Meeting of Japan Landslide Society, 19-22 August 2003., Japan. pp. 227-230
- HAMASAKI Eisaku, (2013)Structure of the AHP method, and Landslide Risk Evaluation System based on it, Daichi ga ugoku. Touhoku branch of Japan Association for Slope Disaster Management. Japan. 20-48p
- MIYAGI Toyohiko, PRASADA Gyawali B, TANAVUD Charlchai,POTICHAN Aniruth, HAMASAKI Eisaku, (2004)Landslide Risk Evaluation and Mapping - Manual

of Landslide Topography and Risk Management, Report of the National Research Institute for Earth Science and Disaster Prevention No.66. Report of the National Research Institute for Earth Science and Disaster Prevention. Japan. 75-137p

SAATY Thomas L., (1980)The Analytic Hierarchy Process. McGraw-Hill Book Company, NewYork. 265p.

YAGI Hiroshi, HAMASAKI Eisaku, MIYAGI Toyohiko, SASAKI Akihiko, (2012)Risk evaluation method of quake-induced landslides using AHP, Earthquake-induced Landslides.Journal of the Japan Landslide Society. Japan.182-183p



Proceedings of the SATREPS Workshop on Landslides in Vietnam, 2014

Application of Digital Surface Model due to Structure from Motion

Shoichiro Uchiyama⁽¹⁾, Toyohiko Miyagi⁽²⁾

1) National Research Institute for Earth Science and Disaster Prevention, Ibaraki, Tsukuba, Japan,
e-mail: uchiyama@bosai.go.jp

2) Tohoku Gakuin University, Izumi Campus / 2-1-1 Tenjinzawa, Izumi-ku, Sendai, 0081, Japan
e-mail: miyagi@izcc.tohoku-gakuin.ac.jp

Abstract Mega-typhoon, with wind velocities of more than 30 m/s, caused damage to the mangrove forest in the downstream basin of the Nakama River in the southeast part of Iriomote Island (Taketomi town, Yaeyama county, Okinawa Prefecture, Japan) in September 2006 and September and October 2007 (Saitoh et al., 2009.) To study the damage, digital surface models (DSMs) with a ground resolution of 0.3 m/pixel and orthophotos created from aerial photographs taken in 1978 and 2012 are compared. DSMs and orthophotos are obtained by creating three-dimensional models using structure from motion (SfM) and providing the models with three ground control points. Consequently, DSMs and orthophotos with a high degree of accuracy are created. The misregistration is 10 m. In addition, the area, distribution, and change in terrain of fallen trees damaged by the typhoons can be detected. High-accuracy DSMs of areas without digital elevation data can be created by the SfM processing of aerial photographs. Moreover, changes on the earth's surface can be captured quantitatively by using aerial photographs taken at different times.

Keywords Structure from Motion, Digital Surface Model, Aerial photograph, Change detection, Mega-typhoon, Iriomote Island

Introduction

This study aims to determine changes to the earth's surface between two different times. We create digital surface models (DSMs) and orthophoto using structure from motion (SfM) from photographs taken at different times. SfM is a technique that obtains three-dimensional information on a subject by estimating the photographing locations from several photographs (Uchiyama et al., 2014.). By

obtaining DSM difference to detect change in the height of earth's surface, it is possible to observe changes in the earth's surface state by comparing orthophotos. The reasons for undertaking the detection of changes between two different times using aerial photographs are as follows:

- Japan has an archive containing more than one million photographs covering a time span of 60 years and the entire country.
- Photographic interpretation of aerial photographs by experienced personnel allows the detection of changes to the earth's surface; however, this method is unsuitable for analyzing a large number of aerial photographs or for large areas.

SfM is a basic computer vision technology and has been studied since the 1990s. In recent years, an application with GUI has been released that combines some SfM technologies. With this application, researchers without the knowledge of computer technology are now able to use SfM. Users of the SfM application are easily able to generate three-dimensional models from more than one aerial photograph or from two photographs taken with a digital camera and ground control points (GCP). An application that can be used to generate DSMs and orthophotos, based on three-dimensional models, has also been released. Thus, researchers are able to create geospatial information of a given area with high accuracy; moreover, they are able to use geographic information system incorporating existing geospatial information as well as their own data. Creation of a three-dimensional model using SfM with aerial photographs involves two steps: one is to true up the principal point of the data of scanned aerial photograph from the original photographs, and the other is to provide accurate coordinates for three-dimensional models created with SfM, that is, GCPs. Using SfM on aerial photographs taken at two different

times, we create orthophotos and DSMs that are later used to create elevation tints and cross-profiles. We also study pitch movement on the

earth's surface, as well as changes between the two different times from the interpretation of the orthophoto of changes on the earth's surface.

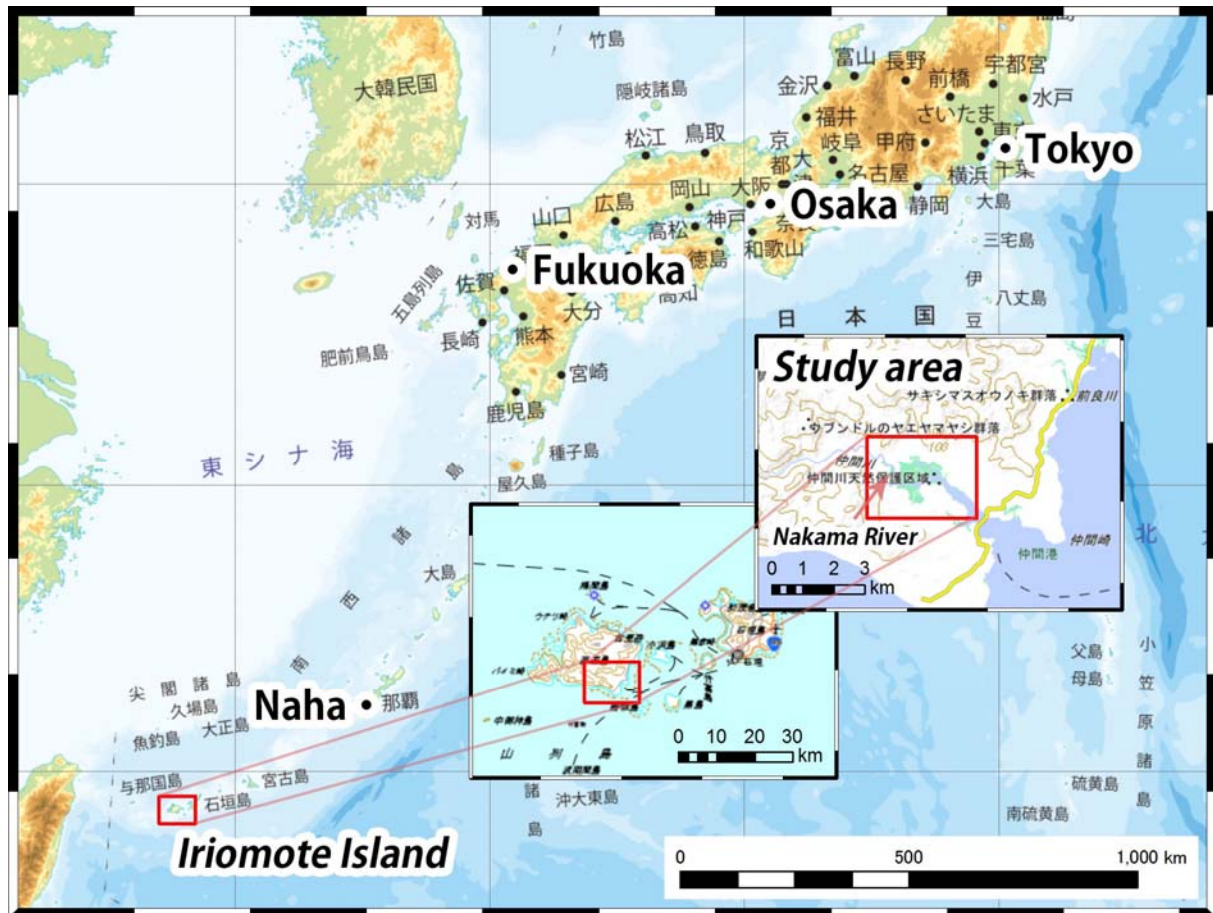


Figure 1 Study area

Method

Study area and aerial photographs

In this study, we concentrate on the downstream basin of the Nakana River in the southeast part of Iriomote Island (Taketomi town, Yaeyama county, Okinawa Prefecture, Japan, Figure 1.) There were several reasons for selecting this area. Megatyphoons, with wind speeds of more than 30 m/s, passed through the area in September 2006 and September and October 2007 (Saitoh et al., 2009.) Damage, such as soil loss and fallen trees in the mangrove forest, was because of these typhoons. Consequently, various changes in topography and vegetation occurred, such as exposure of the ground due to the loss of the mangrove forest and change in the river width. These changes are presumed to mean that it is possible to interpret pitch movement on the earth's surface; therefore, we decided to focus on this area. Particularly concentrating on the shape, area, and aspect of the earth's surface exposed by the fallen trees, we attempt to extract the aspect of the typhoon damage of the mangrove forest. Aerial

photographs taken in 1978 (1:10,000 scale) and 2012 (1:20,000 scale) are used as data.

Position adjustment of the principal point for aerial photographs

This section explains how to adjust the scanned aerial photographs so that the automatic corrections to the interior orientation parameters, such as lens principal point location and lens distortion, function properly during structure-from-motion processing. The procedures below describe how to align the principal point locations and adjust the pixel size in each photograph in the scanned aerial photograph data. This process is required only for aerial photographs scanned with an optical scanner; it is not necessary for aerial photographs taken with a digital aerial survey camera. In this study, we conducted this process for the aerial photographs taken in 1978. The workflow is as follows:

- Step 1) Alignment of aerial photograph orientation: adjust (rotate) the photograph such that the instruments are displayed on the right side of the screen.

- Step 2) Minor adjustment of the rotation: correct the rotation of the photograph using the fiducial marks shown on the aerial photograph.
- Step 3) Adjustment of pixel size: make the pixel sizes of all data identical along the vertical and horizontal axes.

In the following two sections, we describe the details of the most important steps in this process, i.e., Step 2 and Step 3.

Minor adjustment of rotation of the photograph in Step 2

Upload the data (photograph) into Adobe Photoshop. A fiducial mark (shown by the symbol “x”) is seen at each corner of the image. Connect the two fiducial marks at the bottom of the image using the Ruler Tool. Expand the image to its maximum magnification (3200%), and drag (move) the end of the line using the Ruler Tool to the pixel area at the exact center of the fiducial mark. Use Straighten in the options bar while keeping the Ruler Tool selected. With this correction, the inclination of the image is corrected, and the two lower fiducial marks are aligned along the same line (Figure 2.)

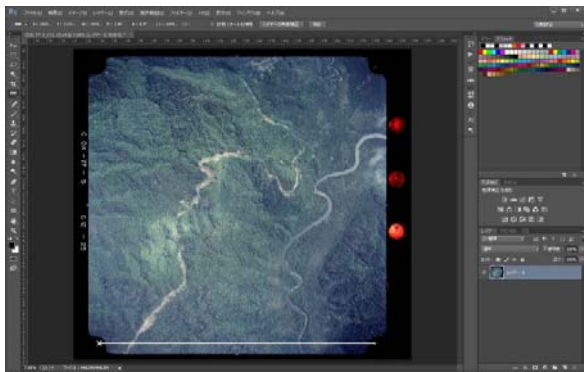


Figure 2 Minor adjustment of rotation of the photograph using the Ruler Tool

After completing the Step 2 procedure, the fiducial marks at the four corners of the aerial photograph image constitute a precise rectangle, if there was no distortion from the scanning equipment or on the film during scanning. However, for real images, it is rare for the fiducial marks at the corners to be located exactly on the vertices of the rectangle. There is always some degree of deviation from the vertex, and unfortunately, there is no way to correct this (or to identify precisely the cause(s) of this deviation). As any unnecessary correction of a superficial deviation only adds to the image distortion (i.e., worsens the accuracy), leave any remaining deviation untouched and proceed to the next step.

Pixel size adjustment in Step 3

In this step, the four sides of each image are adjusted to ensure that the vertical/horizontal axis of every image has pixels of equal size and to remove the black bands on the sides of the images. Locate the intersection of the two guidelines (i.e., horizontal and vertical light blue lines) in the center area of the fiducial marks in Photoshop. Figure 3 shows an image in which the four guidelines are running correctly through the four fiducial marks. The next step is to remove the black band on the four sides of the photograph. As the aerial photograph image is to be found outside of the guidelines, enlarge the selection to include the outside of the black band. The distance between guidelines (both horizontal and vertical lines) and the black band (in pixels) must be measured with the Ruler Tool. Select the zone enclosed by the guidelines with the Rectangular Marquee Tool. Expand the selected zone using the Expand Tool. After confirming that the boundary of the selected zone is not within the black band, cut out the image. Check the minimum horizontal and vertical pixel value of all the clipped images. Crop all images to the size with the minimum horizontal and vertical pixel values.

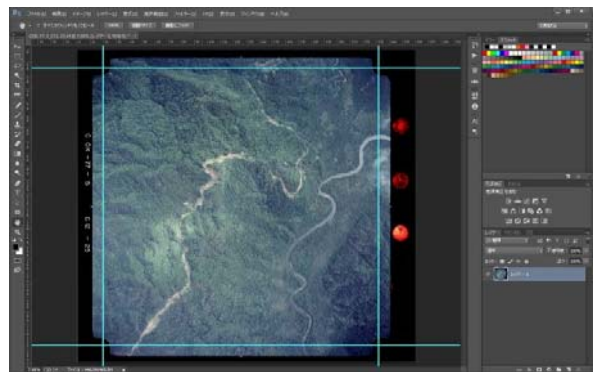


Figure 3 The image in which the four guidelines are running correctly through the four fiducial marks

Creating a three-dimensional model with SfM

We use sixteen and nine aerial photographs for 1978 and 2012, and create three-dimensional models with SfM in two different years. The SfM software used is Agisoft PhotoScan Pro 1.0.4. The parameters used to create the model are shown in Table 1. The projection error, i.e., the accuracy indicator for the model, was set at less than 1.0 during the three-dimensional model creation. Figure 4 and 5 show bird’s-eye view of three-dimensional models created with aerial photographs taken in 1978 and 2012. At this point in the process, the three-dimensional models are not yet given geospatial coordinates.

Table 1 The parameters used to create the model in SfM software

Property	Value
General	
Cameras	16
Aligned cameras	16
Markers	3
Point Cloud	
Points	179 175 of 288 016
Effective overlap	2.17458
Reprojection error	0.366353 (1.0014 max)
Alignment parameters	
Accuracy	High
Image pair preselection	Disabled
Maximum points per photo	0
Constrain features by mask	Yes
Matching time	21 minutes 16 seconds
Alignment time	14 seconds
Dense Point Cloud	
Points	140 169 332
Reconstruction parameters	
Quality	High
Depth filtering	Aggressive
Processing time	10 minutes 53 seconds
Model	
Faces	28 023 688
Vertices	14 017 849
Reconstruction parameters	
Surface type	Height field
Source data	Dense
Interpolation	Enabled
Quality	High
Depth filtering	Aggressive
Face count	28 129 841
Processing time	4 minutes 32 seconds

Property	Value
General	
Cameras	8
Aligned cameras	8
Markers	3
Point Cloud	
Points	573 101 of 623 835
Effective overlap	2.22619
Reprojection error	0.226091 (0.950411 max)
Alignment parameters	
Accuracy	High
Image pair preselection	Disabled
Maximum points per photo	0
Constrain features by mask	No
Matching time	5 minutes 58 seconds
Alignment time	54 seconds
Dense Point Cloud	
Points	75 095 109
Reconstruction parameters	
Quality	High
Depth filtering	Aggressive
Processing time	6 minutes 5 seconds
Model	
Faces	15 022 067
Vertices	7 514 449
Reconstruction parameters	
Surface type	Height field
Source data	Dense
Interpolation	Enabled
Quality	High
Depth filtering	Aggressive
Face count	15 075 858
Processing time	2 minutes 34 seconds



Figure 4 A Bird's-eye view of the three-dimensional models created with aerial photographs taken in 1978. The gully in the middle is a target of this study.



Figure 5 A Bird's-eye view of the three-dimensional models created with aerial photographs taken in 2012. The gully damaged by typhoons in the middle is a target of this study.

GCP configuration

The latitude, longitude, and the elevation of more than two points in a three-dimensional model constructed using SfM constitute geospatial coordinates and can be used as geospatial information. In this study, elevation and a latitude/longitude location interpreted from GSI maps are used as GCPs. Three points are set as GCPs for each year, and they are used in the output DSM and orthophotos. Figure 6 shows orthophoto overlain with the topographical map of 1978. Figure 7 shows shaded relief map (created from DSM) overlain with the topographical map of 1978.



Figure 6 The orthophoto overlain with the topographical maps of 1978

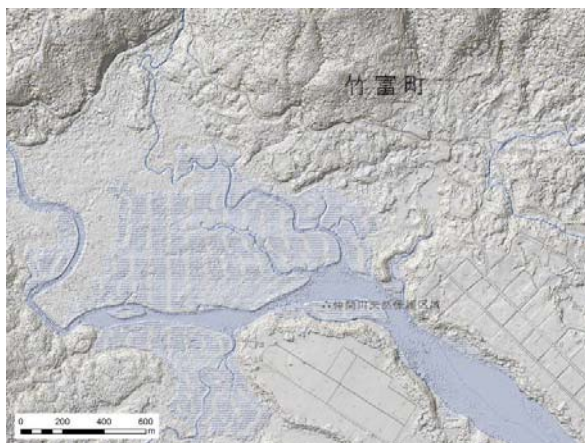


Figure 7 The shaded relief map (created from DSMs) overlain with the topographical maps of 1978

Analysis of changes on the earth's surface

We analyze the changes on the earth's surface using observation of large-scale orthophotos as well as the altitude-tint maps and DSM cross-sections. To interpret the changes in the height from the water surface in detail, we define each change of coloration on the altitude-tint maps as representing one meter. We set the direction of the measuring line to draw cross-sections across the gully. Figure 8 and 9 show altitude-tint maps of the analyzed areas of 1978 and 2012. Enlarging the scales of the orthophotos to approximately 1:1,500, we create four large-scale orthophoto maps from the upstream side to the downstream side. Figure 10 and 11 show two large-scale orthophotos of the same areas for 1978 and 2012.

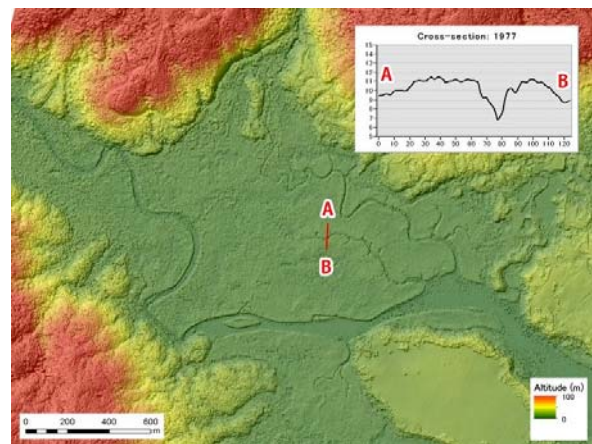


Figure 8 The altitude-tint map of the analyzed areas of 1978 and cross-section at A-B line

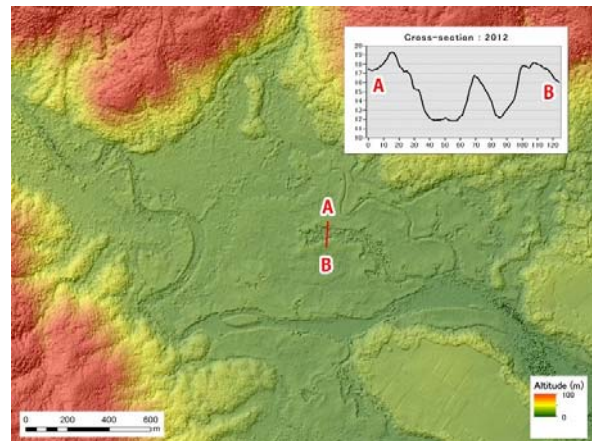


Figure 9 The altitude-tint map of the analyzed areas of 2012 and cross-section at A-B line

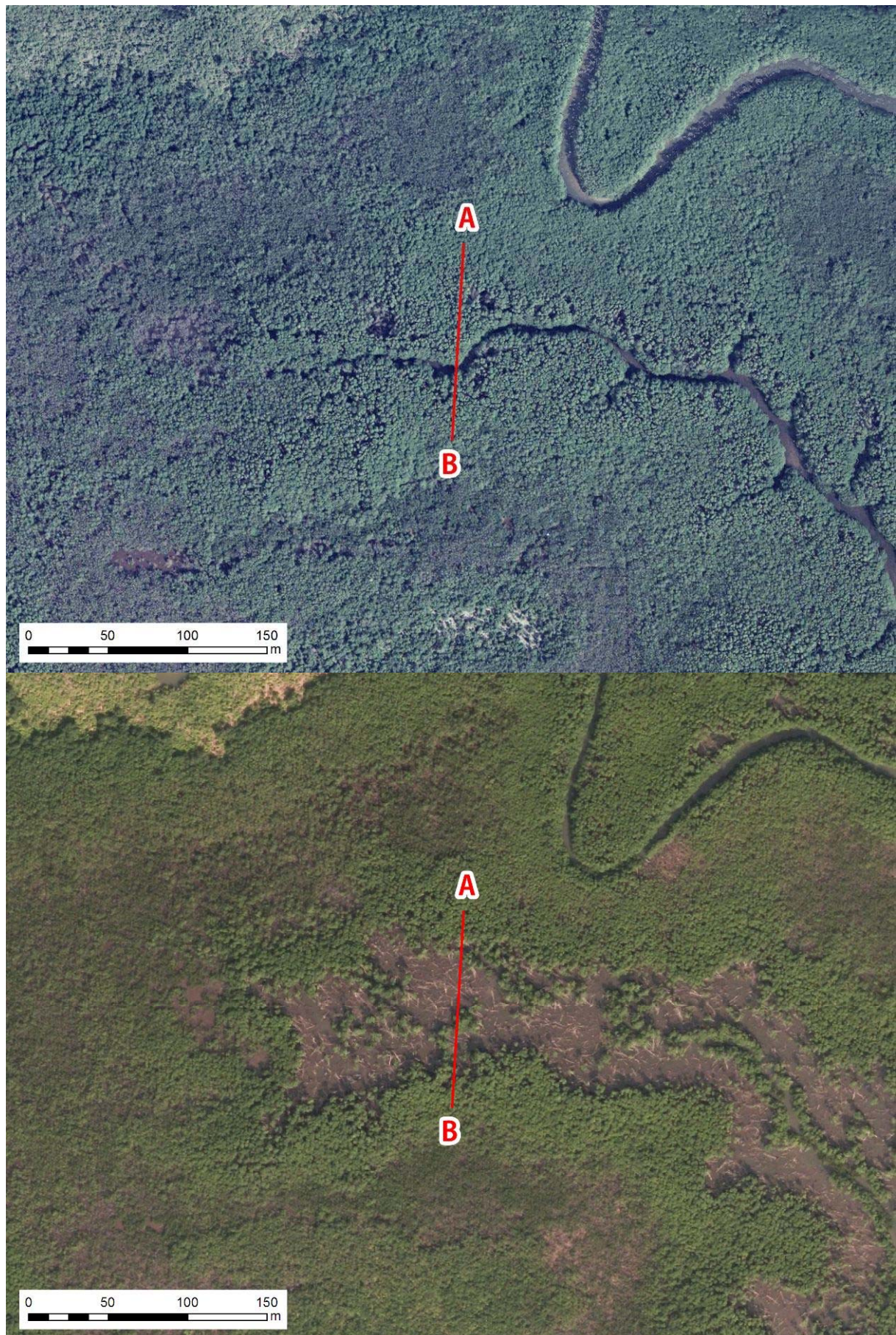


Figure 10 Large-scale orthophotos of the upstream for 1978 (upper) and 2012 (lower)



Figure 11 Large-scale orthophotos of the downstream for 1978 (upper) and 2012 (lower)

Results

DSM and orthophotos are obtained by the SfM processing of aerial photographs taken at two different times. Here we describe the positional accuracy and the result of the observation of DSM and orthophotos.

Accuracy of the three-dimensional model created with SfM

Three-dimensional models are created by the SfM processing of aerial photographs; three GCPs are provided for each model. DSMs and orthophotos, each with a resolution of 0.3 m/pixel, are obtained from aerial photographs taken in 1978 and 2012. The misregistration in the horizontal direction between the road on the topographical map and the road on the orthophoto is about 10 m on average, and at most 20 m. Figure 12 shows the example of the differences between the topographical map and orthophoto for 2012, respectively.

Observation of DSM and large-scale orthophotos

The results obtained from DSM and orthophotos, each with a ground resolution of 0.3 m/pixel, are as follows. Both the altitude-tint map (Figure 9) and the orthophoto (Figure 10 and 11) of DSM in 2012 show that fallen trees because of the typhoon are gathered around the gully. Trees have fallen in various directions because of the typhoon. Moreover, the forest floor elevation around the gully destroyed by the typhoon is raised. Although a portion of trees are still standing among the gully, many trees are fallen and spread peripherally. The river mouth region is less damaged. The same destructions of the forest are distributed in some other place in the study area.



Figure 12 The examples of the differences between the topographical maps and orthophotos for 2012. Red arrows indicate the differences between intersection of the topographical map and orthophoto's.

Conclusions

DSM with high accuracy can be obtained by creating three-dimensional models from the processing of aerial photographs using SfM; however, DSMs do not include elevations. High-resolution orthophotos were also obtained. In this case, DSMs and orthophotos had a ground resolution of 0.3 m/pixel. Such horizontal accuracy of position results in gaps of about 10 m on average, and it is precise enough to be used practically. In addition, aerial photos taken at different times can be used to ascertain changes on the earth's surface, such as damage on the forest floor due to a typhoon. In future studies, we will measure highly precise GCPs using a GPS survey, thus verifying the perpendicular accuracy. We will attempt to extract the differences between two aerial photographs. Thus, analysis of changes in the vertical direction, e.g., growth of a forest, will become possible, as well as horizontal changes such as the expansion of a forest floor. With continuing progress in technology for the detection of changes on the earth's surface between different times, we are able to contribute to the development of academic research and also a variety of other areas, including government and disaster prevention. In addition, SfM is applicable as a means for obtaining highly precise DSM in areas for which digital terrain data do not exist.

References

- Ayako Saitoh, Shigeyuki Baba, Toyohiko Miyagi (2009): Fundamental studies on the recovery process of Bruguiera gymnorrhiza forests damaged by typhoons in Funaura Bay, Iriomote Island, Japan, *Mangrove Science*, 6, pp. 41-52.
- Hinako Suzuki, Shoichiro Uchiyama, Hiroshi Inoue (2014): Utilization of SfM with low-quality aerial photographs: a case study of Niigata earthquake in 1964, *Proceedings of the General Meeting of the Association of Japanese Geographers*, 27-28 March 2014, 87, pp. 318.
- Hinako Suzuki, Shoichiro Uchiyama (2014): Generating an orthophoto from SfM calculation with the low-quality air photographs taken in the 1964 Niigata earthquake, *Japan Geoscience Union Meeting 2014*, 28 April-2nd May, 2014, HTT33-P02.
- Shoichiro Uchiyama, Hiroshi Inoue, Hinako Suzuki (2014): Approaches for Reconstructing a Three-dimensional Model by SfM to Utilize and Apply this Model for Research on Natural Disasters, *Report of the National Research Institute for Earth Science and Disaster Prevention*, 81, pp. 37-60.
- Shoichiro UCHIYAMA, Toyohiko Miyagi (2014): Change extraction from DSMs calculated multi-time aerial photographs - A case study at a mangrove forest in downstream area of Nakama River, Iriomote Island, Japan, *Proceedings of the General Meeting of the*

- Association of Japanese Geographers, 27-28 March 2014, 87, pp. 317.
- Shoichiro Uchiyama (2014): Generating three-dimensional models by a software that unifies structure from motion (SfM) and multiview stereo (MVS), Japan Geoscience Union Meeting 2014, 28 April–2nd May, 2014, HTT33-05.
- Shoichiro Uchiyama, Hiroshi Inoue, Hinako Suzuki (2014): Utilization of Structure from Motion and multi-view stereo (SfM-MVS) on geomorphometry, Japan Geoscience Union Meeting 2014, 28 April–2nd May, 2014, HTT08-P01.



Proceedings of the SATREPS Workshop on Landslides in Vietnam, 2014

Progress in Landslide Dynamics

Kyoji Sassa¹, Bin He², Khang Dang¹, Osamu Nagai¹, Kaoru Takara³

1) International Consortium on Landslides, Kyoto, Japan, e-mail: sassa@iclhq.org

2) Key Laboratory of Watershed Geographic Sciences, Nanjing Institute of Geography and Limnology, Chinese Academy of Sciences, Nanjing, China

3) Disaster Prevention Research Institute (DPRI), Kyoto University, Uji, Japan

Abstract Landslide Dynamics is a relatively new field in Landslide Science. Reliable scientific knowledge to assess the motion of landslides including hazard area, speed and depth is needed to reduce human loss from landslides. However, the initiation and motion of landslides is not easy to explain quantitatively because of pore-pressure generation during initiation and motion, and continuing changes in grain size, grain shape and water content of the involved soils in the shear zone. An apparatus has been developed to physically simulate the formation of sliding surfaces and the post-failure motion of the involved soils under realistic stresses. It can simulate pore-pressure increase due to rain water infiltration and dynamic loading due to earthquakes in the field, and can monitor pore-pressure generation, and mobilized shear resistance together with shear displacement. The apparatus has evolved from the model DPRI-1 in 1984 through DPRI-2, 3, 4, 5, 6, to the model ICL-1 in 2011 and ICL-2 in 2013. This apparatus which is called as the landslide ring-shear simulator is now in use in foreign countries. This paper presents the progress of the landslide ring-shear simulator and its application to earthquake-induced landslides, the 2006 Leyte landslide killing over 1000 people, the 1792 Unzen Mayuyama landslide killing 15,000 people, and a hypothetical Senoumi (Stone flower sea) submarine megaslide using a cored sample from 190 m below the sea floor. A new integrated computer model (LS-RAPID) simulating the initiation and motion using soil parameters obtained from the landslide ring-shear simulator has been developed (Sassa et al 2010) in parallel to the development of landslide ring-shear simulator. LS-RAPID was applied to the three earthquake-induced landslide cases mentioned above. The simulations included two triggering factors: pore-water pressure and three-component seismic waves. The combination of landslide ring-shear simulator and integrated

landslide simulation model provides a new tool for landslide hazard assessment.

Keywords Landslide, dynamics, progress, ring shear apparatus, landslide simulation, computer model

Introduction

This paper was reformatted for SATREPS 2014 from the Sassa et al (2014) Plenary Lecture in the Third World Landslide Forum held in Beijing on 2-6 June 2014.

Slope-stability analysis is to study whether a slope fails or not, and is the main tool for the study of landslide initiation. *Landslide dynamics* is to study landslide mobility after failure. The former study focuses on the design of engineered slopes including embankments and earth dams, and also the prevention of occurrence of landslides. The later study focuses on landslide hazard and risk assessment to identify the hazard level, area exposed to hazard and landslide velocity if the landslide were to occur. These data are necessary for early warning, evacuation and land-use planning to reduce human loss. The necessary geotechnical parameters and deformation in testing for each study are different. Slope-stability analyses need the peak shear resistance at failure and the mobilized shear deformation/displacement is usually of the order of a few mm or cm before the failure, although this depends on the sample size. On the other hand, landslide dynamics needs the steady-state shear resistance mobilized during post-failure motion. Results of basic geotechnical tests such as the triaxial test and direct shear tests are used in slope stability, while the results from physical simulation tests (i.e. undrained dynamic-loading ring-shear test) reproducing the sliding surface and post-failure motion are used in landslide dynamics. The comparison is shown in Table 1.

Table 1 Slope stability and landslide dynamics

Necessary items for both analysis	Slope stability	Landslide dynamics
Objectives of analysis	Design of engineered slopes and prevention of landslide occurrence	Landslide-risk assessment for early warning, evacuation or land-use planning
Necessary parameters	Shear strength parameters (Shear resistance at failure)	Steady-state shear resistance during post-failure motion
Necessary deformation in testing	Order of mm to cm until failure	Order of m in shear displacement
Difference from the initial state of grain size/shape/structure	The initial state is mostly kept	The initial state is completely lost
Testing methods	Element tests such as triaxial tests and direct shear tests	Physical simulation test to reproduce sliding surface and post-failure motion (i.e.: Landslide ring-shear simulator)
Application of measured data	Slope-stability analysis	Numerical simulation of landslide motion
Basic science/analysis	Soil mechanics—stability analysis	Soil dynamics—landslide dynamics

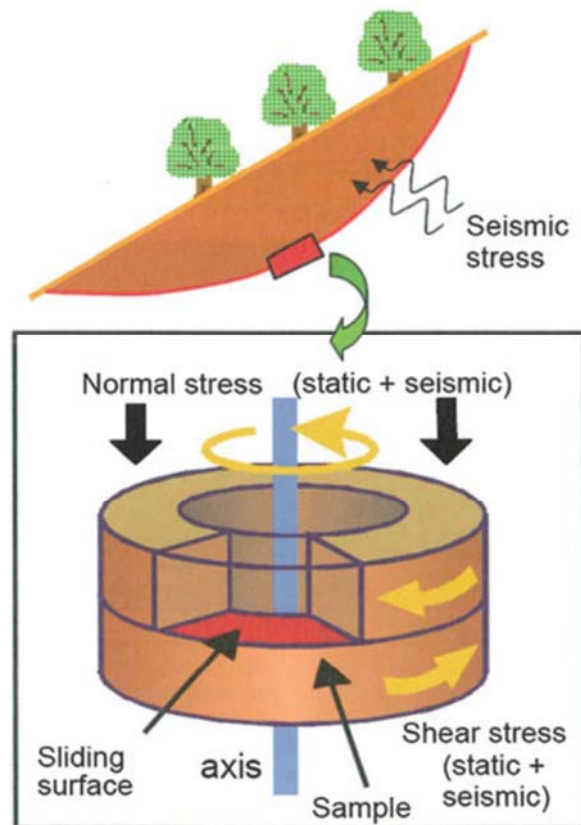


Fig. 1 Concept of landslide ring-shear simulator

The science of slope-stability analysis advanced much earlier than landslide dynamics. Many people are killed by landslides especially in the developing countries due to urbanization and extensive regional development. Expensive landslide prevention works are difficult in developed countries as well as in the developing countries within limited budgets. The most effective and economical way to reduce human loss from landslides is landslide-hazard assessment and disaster preparedness including early warning, evacuation and land-use planning. A limited displacement and/or a low speed of motion may cause failure of structures but not be dangerous for humans. A high-speed, long-runout and wide-spreading motion may cause a great disaster. The significance of landslide dynamics is becoming more important.

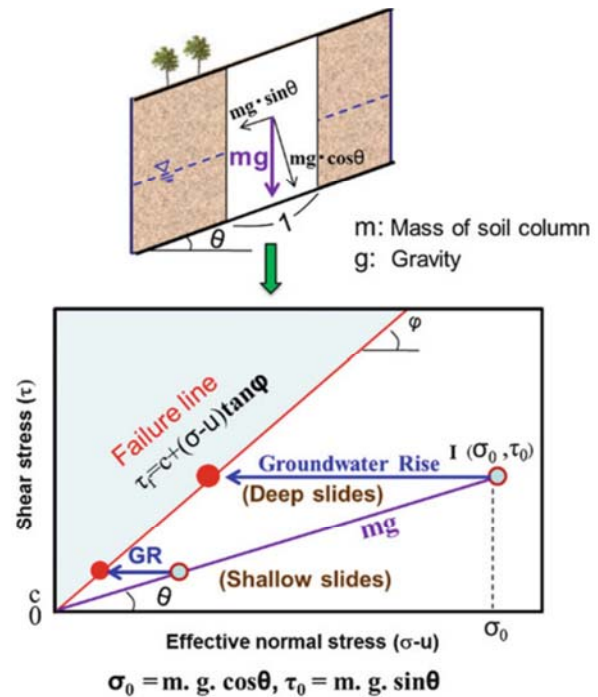


Fig. 2 Initiation by ground water rise (pore-pressure increase)

Development of Landslide dynamics needs a tool to measure the mobilized geotechnical parameters after the formation of a sliding surface - the post-failure strength reduction to its value at steady-state motion. It also needs an integrated computer model to simulate both the initiation and the motion of the landslide within the same programme using the geotechnical parameters mobilized in the landslide motion. This contribution summarises three decades of development of our tools for measuring dynamic geotechnical parameters (namely the landslide ring-shear simulator) and our development of a computer simulation from the initiation to the motion. It focuses on the research and technological developments which have been implemented in the Disaster Prevention Research Institute (DPRI), Kyoto University, Japan and the International Consortium on Landslides since 1984.

The landslide ring-shear simulator

Aim and concept of the landslide ring-shear simulator

The formation of a sliding surface is not a simple phenomenon. Strain is not defined in the shear zone. Grains of soil in the shear zone are crushed or broken. Size and shapes of grains in the shear zone are changed. Those changes necessarily affect pore-water pressure due to volume change in the shear zone. The extent of changes is different for different soils such as volcanic or sedimentary, angular or round, hard or soft minerals. The confining stress level much affects the behaviour of grain crushing in the shear zone. It is difficult to infer a reliable general principle for all the cases of concern.

The basic concept of the landslide ring-shear simulator (Fig.1) is to reproduce the stresses due to gravity, seismic force or pore pressure on soils taken from the field and to observe what happens; fail or not fail, excess pore-water pressure generated or not generated in the initiation, failure, and post-failure processes, and how much shear resistance is mobilized in the whole process.

Fig.2 illustrates the landslide initiation mechanism due to increase of pore-water pressure in deep and shallow slides. The upper figure shows the soil column with a unit length along the bottom of a soil (weathered rock) layer, or more precisely, a landslide-susceptible layer. The weight of the soil column is expressed as $m \times g$ in Fig.2. where, m is a mass of the soil column, and g is gravity.

If no ground-water table exists within the soil column, that is, zero pore-water pressure is acting, the initial stress at the bottom on this column is plotted as "I" in the stress-path figure of normal stress and shear stress.

Normal stress at I is $\sigma_o = mg \cdot \cos\theta$, Shear stress at I is $\tau_o = mg \cdot \sin\theta$

Note:

(1) The initial stress point is located on the line with an inclination of angle θ .

(2) The distance between the origin and the stress point I presents $m \times g$ (= the weight of soil column).

When ground-water level increases, pore-water pressure u increases. The stress moves toward to the left. When the stress reaches the failure line, shear failure will occur at the stress at failure (shown as red circle along the failure line. Deeper slides need a greater pore-pressure rise as seen in the figure 2.1.1.2.

$$\tau_f = c + \sigma \cdot \tan\phi \quad [1]$$

Fig.3 presents the loaded stress in the slope (a: left figure) and the stress path during earthquakes

(b: right figure). The initial stress acting on the bottom of the landslide-susceptible layer (mg) is plotted as A_o (if no pore pressure is acting, it is the same as I in Fig. 2.1.1.2). When an earthquake occurs and a cyclic seismic load is applied, the loaded stress is expressed by $k \cdot mg$, where k is seismic coefficient which is the ratio of seismic acceleration (a) and gravity (g), namely $k = a/g$.

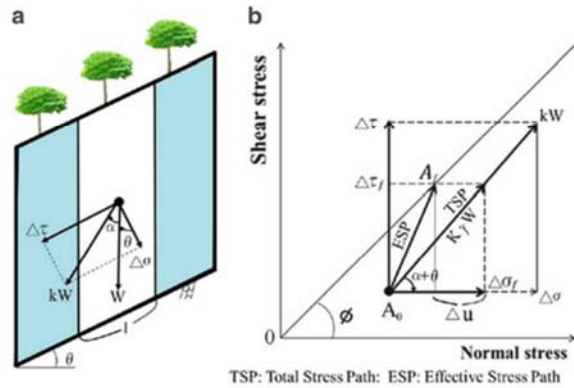


Fig. 3 Initiation by seismic loading during earthquakes. (a) Loading stresses in the slope, (b) Stress paths during earthquakes

When expressing the direction of seismic force as α from vertical direction, the direction of the seismic stress increment in the stress diagram (b) is expressed as $(\alpha + \theta)$.

The effective stress path during an earthquake is not in the same direction as the total stress path.

Fig.3 illustrates the case where the initial stress + the seismic stress reach the failure line.

When pore-water pressure is generated during seismic loading, the effective stress path shifts from A_o to A_f .

When the seismic stress reaches or even crosses the failure line, the difference between shear stress and shear resistance is used to accelerate the soil column. Each time period when stress crosses over the failure line is short. If post-failure shear-strength reduction does not occur, the shear displacement will be very limited and stabilized after termination of the earthquake. However, if shear resistance is much decreased after failure, rapid motion will occur due to the difference between applied shear stress and mobilized shear resistance on the sliding surface. The landslide ring-shear simulator (undrained dynamic-loading ring-shear apparatus) can reproduce the post-failure motion, measure the pore-water pressure generated in the shear zone and the resulting shear resistance during motion including that under steady state conditions.

Development of the dynamic-loading ring-shear apparatus series (from DPRI-1 to ICL-2)

Sassa and colleagues of the Disaster Prevention Research Institute (DPRI), Kyoto University and the International Consortium on Landslides (ICL)

have developed a series of dynamic-loading ring-shear apparatus from DPRI-1 (initial version, 1984), DPRI-2, DPRI-3, DPRI-4, DPRI-5, DPRI-6, DPRI-7, ICL-1 and ICL-2 (the latest version, 2013). To reproduce most earthquake-induced landslides it is necessary to maintain an undrained condition in the soil sample. Pore-water pressure is very important in the mechanism of the long runout landslides. Maintaining an undrained condition and measuring pore-water pressure accurately are difficult to achieve. Models DPRI-1 and DPRI-2 could not create the undrained condition although rapid shearing could be produced. Model DPRI-3 was an intermediate version from the initial model to the developed version of the apparatus. Model DPRI-4 was a trial version, and models DPRI-5 and DPRI-6 were produced at the same time after obtaining a special budget to mitigate earthquake disasters soon after the Hyogoken Nambu Earthquake in 1995. These two apparatus are developed versions of an undrained dynamic-loading ring-shear apparatus having the features of undrained condition, pore-water pressure monitoring near the sliding surface, and dynamic loading (regular cyclic or filtered real seismic record). These two apparatus succeeded reproducing sliding-surface formation and measuring post-failure motion in rain- and earthquake-induced landslides. Sassa planned to test large-scale landslides and aimed to test under 2 MPa (DPRI-5) and 3 MPa (DPRI-6). However, these devices failed to reach this intended high stress state in a stable manner and also failed to maintain an undrained condition under this high stress state. For these reasons sensors were changed to smaller capacities. They successfully tested up to 500 kPa (with one successful test to 630 kPa in Fig. 12 in DPRI-5). The latest models ICL-1 and ICL-2 use a different loading system, successfully allowing higher normal stress and maintaining an undrained condition up to 1 MPa (ICL-1) and 3 MPa (ICL-2).

The aim of models DPRI-1 to DPRI-7 was scientific research to achieve high-precision results for science. The aim of models ICL-1 and ICL-2 is for practical use, less expensive to manufacture, lower-cost maintenance, and the capability to be maintained abroad. Both apparatus were developed to donate to developing countries, one to Croatia and the other to Vietnam.

We introduce the initial apparatus DPRI-1, the intermediate DPRI-3, one of the developed stage (DPRI-6, the largest model), and the latest and most advanced model ICL-2 using three figures of the structures (Fig.4, Fig.5 and Fig.6) and two tables of characteristics (Table 2) and sealing structures for maintaining undrained condition

(Table 3). Fig.4 presents the structure of models DPRI-1 and DPRI-3.

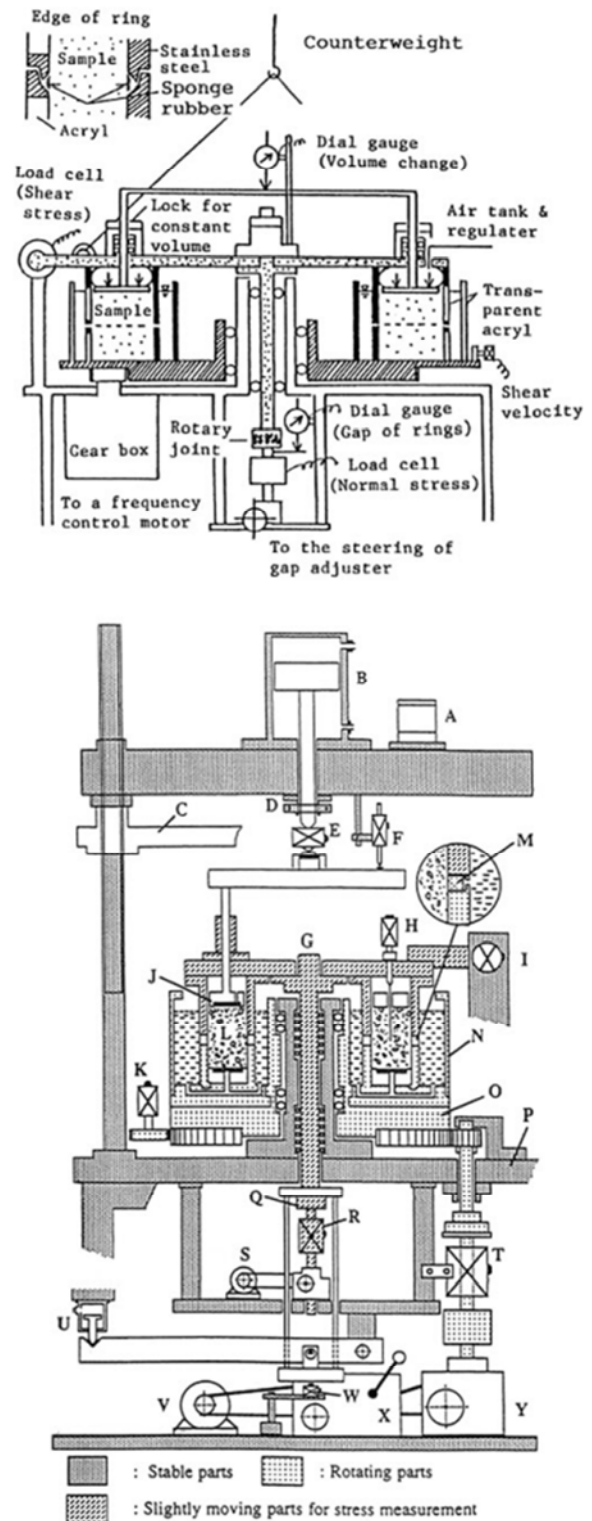


Fig. 4 The initial stage of apparatus of DPRI-1 and the intermediate apparatus of DPRI-3

The initial model (DPRI-1 in the upper figure of Fig.4) aimed to reproduce the shear zone of debris flows. The concept was to use a circular device to represent an endless flume. Loading stress is achieved with a motorcycle inner tube. This was not an undrained condition. A water container was attached outside the shear box. Sponge rubber was pasted in the gap between

upper and lower shear boxes as shown in Table 3. Water could move freely through the edge. The DPRI-3 structure is presented in the figure. 4.

In January 1995, the Kobe earthquake occurred and 36 persons were killed by a rapid landslide. The mobility of the landslide was one of a debris flow, however, there was no rain at all during this very dry season and no water present in a very small river at the toe of the slope. A landslide study was needed to investigate this mechanism and to mitigate future landslide disasters. Funding to develop an advanced undrained dynamic-loading ring-shear apparatus was obtained. Then, we developed two apparatus (a large shear box (25–35 cm) and a smaller one (12–18 cm)). We aimed to produce a high stress of 2–3 MPa. To create this capacity, DPRI-6 has two stress- and speed-control servo-motors (37 kW) and DPRI-5 has a 37 kW motor plus an oil piston to give additional shear load around peak failure strength. Both attempts failed to produce such a high shear force. We could not maintain the undrained state at such high stresses, and also we

could not control the normal stress at such a high level. This was caused by several reasons: at high load, the tall poles of the frame were extended, and the horizontal beam to load normal stress was deformed. The deformation was elastic, and when sudden stress change occurs, the servo-control system could not work properly due to the oscillation.

We had great difficulty reproducing stresses and shear failure with crushable sand grains at such high stress levels. The structure and the photo of DPRI-6 are shown in Fig.5. One advancement was a vertical positioning bar (shown in red in Fig.5 right) passing through the central axis. The bar was fixed to the loading plate and moved together with the upper shear box. The displacement of the bottom of the vertical positioning bar was measured by a gap sensor connected to the stable base, namely the lower shear box. The gap between the upper shear box and the lower shear box was measured by a gap sensor with a precision of 1/1000 mm.

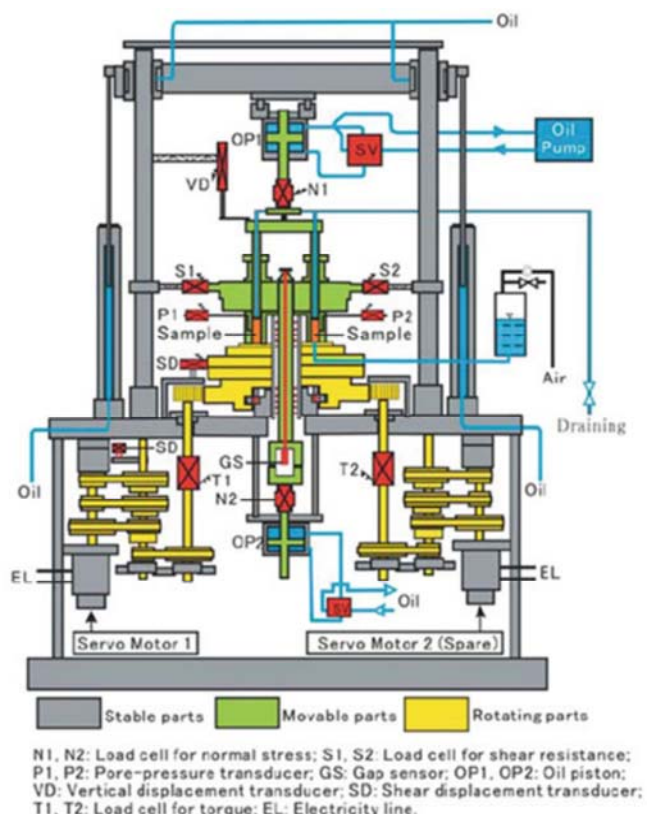
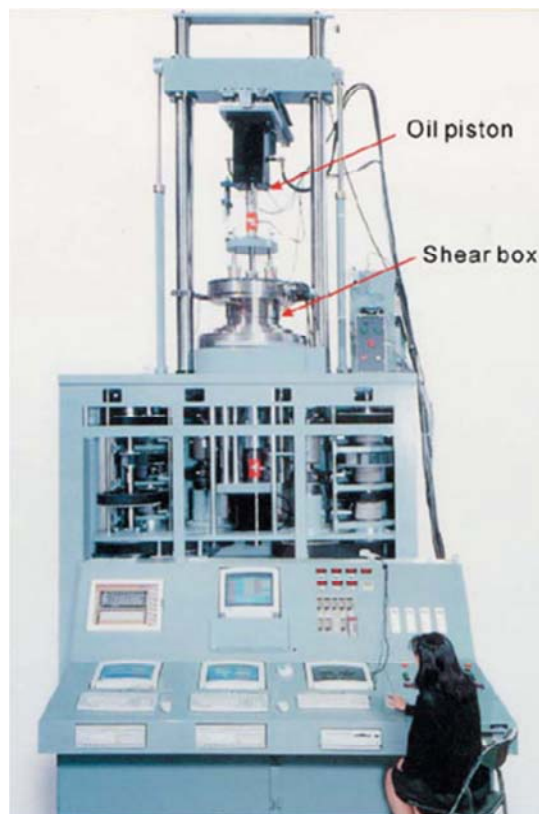


Fig. 5 The developed stage of apparatus of DPRI-6. Models DPRI-5 and DPRI-7 are the basically same system though the shear-box size, the maximum velocity and the loaded maximum stresses are different

However, it was unsuccessful in avoiding oscillation in the gap servo-control system at a level of MPa.

Fig.6 presents the latest model undrained dynamic-loading ring-shear apparatus which has been developed to simulate megaslides up to 3 MPa, and planned to be donated to Vietnam in 2014. The ease of maintenance in Vietnam was a

major consideration in the design. A photograph of the main apparatus is presented in the left top (A). Figure B presents the mechanical structure of model ICL-2. The greatest difference between (ICL-1 and ICL-2) and (DPRI-3 and DPRI-6) is the system for loading normal stress. Models DPRI-3 and DPRI-6 have a long loading frame consisting of two long vertical pillars and one horizontal

beam. The frame is extended and compressed in pillars and deformed in beam during changes in loaded stress due to cyclic and seismic loading and sudden stress changes when grains or soil structures fail due to high normal or shear stress. This sometimes disturbs the function of the servo-control system and an oscillation occurs. To minimize the effect of extension/compression and deformation, the loading frame is removed in the ICL series. The basic concept returns to the DPRI-1 loading system without the loading frame. In

DPRI-1, an air tube pressed to the sample and the loading cap which was restrained by the central axis. The loading normal stress is provided by a tensile stress along the central axis. Models ICL-1 and ICL-2 achieve this via a loading piston in place of a air tube. Fig.6 B and D shows the structure and the servo-control system of ICL-2. Oil pressure within the loading piston is controlled by servo-valve (SV) using the feedback signal from the load cell (N) measuring the normal stress.

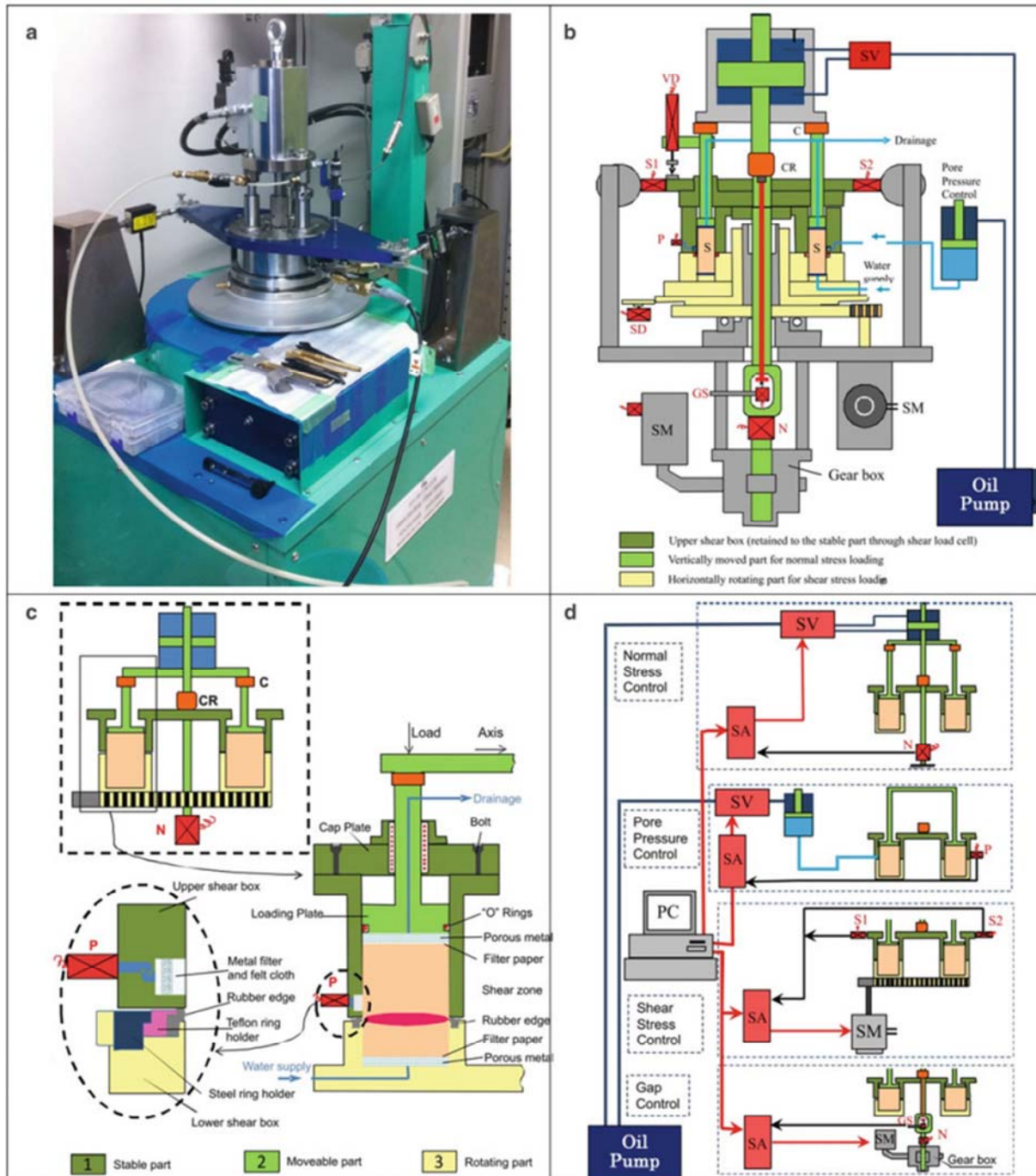


Fig. 6 The most updated and practical apparatus of ICL-2. ICL-1 and ICL-2 are developed for use and maintenance in foreign countries. (a) Photograph of the main apparatus, (b) Mechanical structure of the main apparatus, (c) Close-up view of the shear box and the undrained sealing and pore pressure monitoring, (d) Servo-control systems for normal stress and pore pressure through servo-valves (SV) and servo-control systems for shear stress and gap through servo-motors (SM)

Table 2 Characteristics of each stage of the ring shear apparatus (DPRI-1, 3, 6 and ICL-2)

Type	Characteristics
DPRI-1	<ul style="list-style-type: none"> • Aim: to reproduce debris-flow motion under a certain normal stress within a rotational channel • Target: Debris flows frequently occurred in Volcano Usu, Volcano Sakurajima and others in Japan • Normal stress Maximum normal stress: 40 kPa Loading system: Rubber tube by air compressor and regulator which was installed between the loading plate and the top cap of the upper shear box (no loading frame) Monitoring: one load cell by automatic side-friction canceling • Shear stress Shear box: 300–480 mm in diameter and transparent acrylic shear box Loading system: Speed-control motor Maximum shear speed in the center of shear box: 100 cm/s • Gap control, undrained condition, and pore pressure monitoring Gap control system: Manual gap control by measuring the position change of the upper loading plate Sealing of sample leakage: Silicon rubber Undrained condition: Not possible No pore pressure measurement • Major reports: Sassa (1984) in 4th ISL and Sassa 1988 in 5th ISL, Lausanne
DPRI-3	<ul style="list-style-type: none"> • Aim: to reproduce earthquake-induced landslides. • Target: Ontake landslide triggered by the 1984 Naganoken-Seibu earthquake in Japan. • Normal stress Maximum normal stress: 500 kPa Loading system: Loading piston with air servo-valve, compressor and loading frame to support piston Monitoring: two load cells, one for loading pressure, another for side friction within the shear box • Shear stress Shear box: 210–310 mm in size with a transparent acrylic outer ring Loading system: Stress-control and speed-control motor Maximum shear speed in the center of shear box: 37 cm/s • Gap control, undrained condition, and pore-pressure monitoring Sealing of water leakage: Polychloroprene (®Neoprene) rubber edge passed on the lower ring (Rubber hardness Index, 45°JIS) Gap control: Servo-gap control system by measuring the position change of the upper loading plate and adjusting by servo-motor (Extension of central axis was neglected) Undrained condition and pore-water pressure monitoring: It was improved from 6th ISL in Christchurch 1992–1994 Successful undrained condition: 400 kPa Pore pressure was monitored by a needle inserted close to the shear zone in 1992. It was monitored from the gutter (4 × 4 mm) along the whole circumference of the upper-outer shear box 2 mm above the gap in 1994 Major reports: Sassa (1992) in 6th ISL and 7th ICL in 1996
DPRI-6	<ul style="list-style-type: none"> • Aim: to develop landslide ring-shear simulator • Target: Nikawa landslide killing 34 persons. Triggered by the 1995 Hyogoken-Nambu earthquake • Normal stress Maximum normal stress: designed for 3,000 kPa. However, normal stress servo-control system does not function well. Tests were conducted to 750 kPa by changing the normal stress load cell Normal stress loading system: Loading piston by oil servo-valve and oil-pressure pump and loading frame to support piston Monitoring: two load cells: one for loading pressure, the other for side friction within the shear box • Shear stress Shear box: 250-350 mm in size with non-transparent outer and inner rings of stainless steel. Maximum shear speed in the center of shear box: 224 cm/s • Gap control, undrained condition, and pore-pressure monitoring Rubber edge in the gap: Polychloroprene rubber with Rubber hardness Index, 45° JIS Gap control: Piston with oil servo-valve and oil pressure pump by measuring the position change of the upper loading plate. To avoid the effect of extension of central axis, a displacement guide was installed within the central axis Successful undrained condition: 550 kPa Pore pressure is monitored along the entire circumference of the upper-outer shear box 2 mm above the gap (same with DPRI-3) • Major reports: Sassa et al. 2004 in Landslides, Vol.1, No.1
ICL-2	<ul style="list-style-type: none"> • Aim: to develop a landslide ring-shear simulator for mega-slides (3 MPa normal stress) and able to be maintained in a developing country • Targets: 1792 Unzen Mayuyama landslide killing 14,528 persons and submarine mega-landslides including a 30 km wide and 20 km long possible landslide trace in Senoumi, Suruga Bay in Japan • Normal stress Maximum normal stress: 3 MPa Normal-stress loading system: Loading piston by oil servo-valve and oil pressure pump which is retained by the central axis (no loading frame) Monitoring: One load cell with automatic side-friction canceling • Shear stress Shear box: 100–142 mm in diameter with non-transparent outer and inner rings of stainless steel Shear speed in the center of shear box: up to 50 cm/s • Gap control, undrained condition, and pore-pressure monitoring Rubber edge in the gap: Polychloroprene rubber with Rubber hardness Index, 90°JIS Gap control: Mechanical jack driven by a servo-control motor with feed-back signal of gap sensor for the position change of the upper loading plate. (to avoid the effect of extension of central axis, a displacement guide is installed within the central axis) Successful undrained condition: 3 MPa Pore pressure is monitored along the whole circumference of the upper-outer shear box 2 mm above the gap Major reports: Contributed to Landslides in 2013 and this paper

When a testing programme has been selected and a control signal given for monotonic stress, cyclic or seismic stress loading, oil is pumped into the loading piston, loading the normal stress by pulling on the central axis. The normal stress acting on the sliding surface

(upward) is retained by the central axis (downward), and this load is measured by the vertical load cell (N). In this system, the role of the two long pillars used in models DPRI-5, 6, and 7 was replaced by one short central axis column and the role of the long horizontal beam is replaced by the loading piston. Deformation of this system is much smaller than in the frame loading system. This structure enables stable servo-stress-control. The minimum deformation during cyclic and seismic loading and possible sudden stress change due to grain crushing on sands has enabled maintenance of an undrained state up to 3 MPa during tests.

Another difference between the DPRI series apparatus (DPRI-5, 6, 7) and the ICL series is the rubber edge which has a critical role for sealing. Rubber edges of all DPRI series apparatus were glued to the shear box. A constant thickness of glue is impossible to achieve and the height of the upper surfaces of the rubber edges of the inner ring and the outer ring must be the equal to maintain an undrained condition. Hence after a new rubber edge had been glued to the shear box, it had to be machined by a skilled technician. In the ICL series, the rubber edges are fixed without glue as is illustrated in Table 3 (ICL-2). This shape (grey color) of rubber edge is processed from a constant-thickness rubber plate. A number of rubber edges of this shape can be commercially purchased in reasonable cost. The rubber edge is simply placed on the lower ring. Then the rubber edge is pressed by a Teflon ring holder, and this holder is pressed in turn by a steel ring holder fixed by a set of screws. No glue or specialist machining are needed.

The Teflon ring holder was designed for the high stress of ICL-2 (3 MPa). Because the rubber edge type of DPRI-6 was deformed outwards due to a high lateral stress and could not maintain undrained state. To prevent such deformation in the ICL series, a Teflon ring horizontally supports the rubber edge. The height of the rubber edge is gradually reduced by wear during experiments. If the steel ring holder were to touch the upper ring, it would mobilize a large shear resistance and damage the upper ring. The Teflon ring is softer than steel and has low friction, and so it causes no damage. However, when wear allows the Teflon ring to touch the upper ring, it can be noticed that it is time to change rubber edge.

Models ICL-1 and ICL-2 have been developed for practical use for landslide risk assessment in other countries including developing countries. Model ICL-1 is small, light-weight and transportable, and capable of testing up to 1 MPa at low shearing speed (5.4 cm/sec). Model ICL-2 was designed for up to 3 MPa and up to 50 cm/sec. Both apparatuses are commercially available as

practical testing machines (although careful handling is needed). Apparatus ICL-1 was donated to Croatia and it is currently working in the laboratory of the Faculty of Civil Engineering, University of Rijeka. Apparatus ICL-2 is planned to be donated to the Institute of Transport Science and Technology (ITST) of the Ministry of Transport, Vietnam.

Application of the landslide ring-shear simulator

The undrained dynamic-loading ring-shear apparatus (landslide ring-shear simulator) of the developed stage of ring-shear apparatus (DPRI-5 and 6) were applied to many cases and reported in Sassa et al 2004, 2005, 2010 and others). Two test results using DPRI-5 are introduced here.

Initiation and motion of landslides triggered by earthquakes (Higashi-Takezawa landslide)

Fig. 7 presents the Higashi Takezawa landslide triggered by the 2004 Mid-Niigata Prefecture earthquake (M 6.8). The landslide occurred within a previous landslide mass as illustrated in the figure. The sliding surface was formed at the contact between a siltstone layer and a sand layer. We tested two samples taken from the siltstone and the sand layer. We performed a cyclic loading test and also a seismic loading test using the nearest seismic record. The test results were reported in Sassa et al (2005). Fig. 8 shows the time series data (a) and the stress path (b) of the seismic loading test on sands taken from the landslide. The green color line in Fig. 8 (a) is normal stress. The wave form of normal stress can reproduce the calculated normal stress from the monitored seismic record. The red color line in Fig. 8 (a) presents shear stress. The shear stress cannot exceed the failure line, so the shear stress over the shear strength is cut off. The blue color line shows the pore pressure generated in the sample. It was increased during seismic loading and also in the progress of shear displacement, reaching a level very close to the normal stress. Therefore, the steady-state shear resistance was very low as shown in the red effective stress path (ESP) in Fig. 8 (b). Accordingly, the apparent friction angle (calculated from the ratio between the mobilized shear resistance and the total normal stress) was only 2.5 degrees. The blue color line in Fig. 8 (b) is the total stress path (TSP). Cyclic loading tests were conducted on silts taken from the silt layer (Sassa et al 2005). No pore-water pressure was generated during cyclic loading tests for silts and limited motion occurred only while the loaded stress was over the failure line, but stopped immediately the loading stopped. We concluded that the sliding surface probably formed at the base of the sand layer, and not at the top of the siltstone layer.

Table 3 Progress of the sealing of the gap

Type	Section of Sealing	Notes
DPRI-1		<ul style="list-style-type: none"> Sponge rubber was pasted on the upper edge Samples were glass beads and coarse sands Drained condition
DPRI-3 (initial)		<ul style="list-style-type: none"> Square shape of the polychloroprene rubber edge (Rubber Hardness Index is 45° JIS) was pasted onto the lower ring Incomplete undrained condition Water bath is set outside of the shear box Unsuccessful pore-pressure measuring
DPRI-3 (final)		<ul style="list-style-type: none"> Stair shape of the polychloroprene rubber edge (Rubber Hardness Index is 45° JIS) was pasted onto the lower ring Successful undrained condition up to 400 kPa under 0.1 Hz cyclic test Successful pore-pressure measuring through the gutter along the whole circumference in the upper ring
DPRI-6		<p>Stair shape of the polychloroprene rubber edge (Rubber Hardness Index is 45°JIS) is pasted onto the lower ring After rubber edge is pasted, the upper surface of inner and outer rubber edges needs to be processed by a lathe or file to ensure that the rubber surface is everywhere the same height Successful undrained condition up to 550 kPa under realistic seismic wave loading Successful pore-pressure measuring through the gutter along the entire circumference in the upper ring</p>
ICL-2		<p>The polychloroprene rubber edge (grey) (Rubber Hardness Index is 90°JIS) was pressed by a polytetrafluoroethylene (teflon) ring holder (pink) which was pressed by a stainless steel ring No glue was used. The rubber edge was simply placed and pressed Successful undrained condition up to 3,000 kPa Successful pore-pressure measuring up to 3,000 kPa</p>

Application to landslide-induced debris flows.

Another example of the application of the landslide ring-shear simulator is for the 2003 Minamata debris-flow disaster. A landslide occurred on a mountain slope and the landslide mass moved onto a torrent deposit. A sliding surface was created within the torrent deposit and the enlarged mass including the initial landslide mass plus the scraped torrent deposit flowed along the torrent and killed 15 people in a village constructed on an alluvial fan.

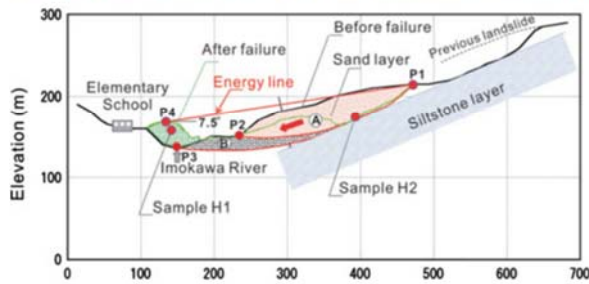


Fig. 7 The Higashi-Takezawa landslide induced by the 2004 Mid-Niigata Prefecture earthquake (M 6.8)

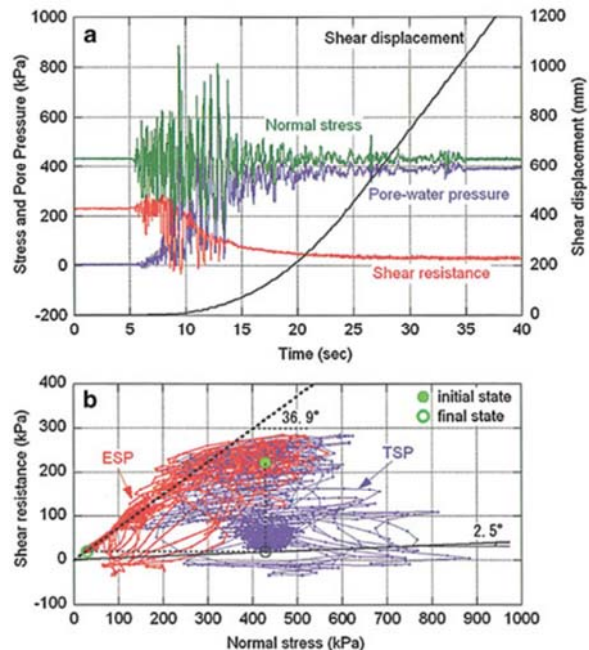


Fig. 8 The result of the seismic loading ring shear test by DPRI-6 for sands taken from the landslide

Fig. 9 explains the model of the landslide-triggered debris flow (Sassa et al. 1997). The stress on the base of the soil column is presented in Fig. 9-b. The initial stress at the base of the torrent deposit is expressed by the point “A”. If no excess pore pressure is generated during rapid loading by a moving landslide mass, the stress point moves to point C by adding the static stress (ΔW) to the initial stress. In addition, by adding the dynamic stress (F_d) to the static stress, the total stress moves to point B. Therefore, the stress path in the actual field case tends to move from point A to point B. However, when the stress path reaches the failure line, it moves along the failure line as seen in Fig. 9b, because the stress path cannot exceed the failure line. At the point where the dynamic stress reduces to zero, the total stress moves back to the stress point C, namely the sum of W_o and ΔW . Denoting the angle of thrust during the collision with the torrent deposit as α and the dynamic stress as F_d , using a dynamic coefficient $k_d = (F_d / \Delta W)$, the dynamic shear stress and normal stress are expressed as:

$$F_d \cos \alpha = \tau_d, \quad F_d \sin \alpha = \sigma_d \quad [2]$$

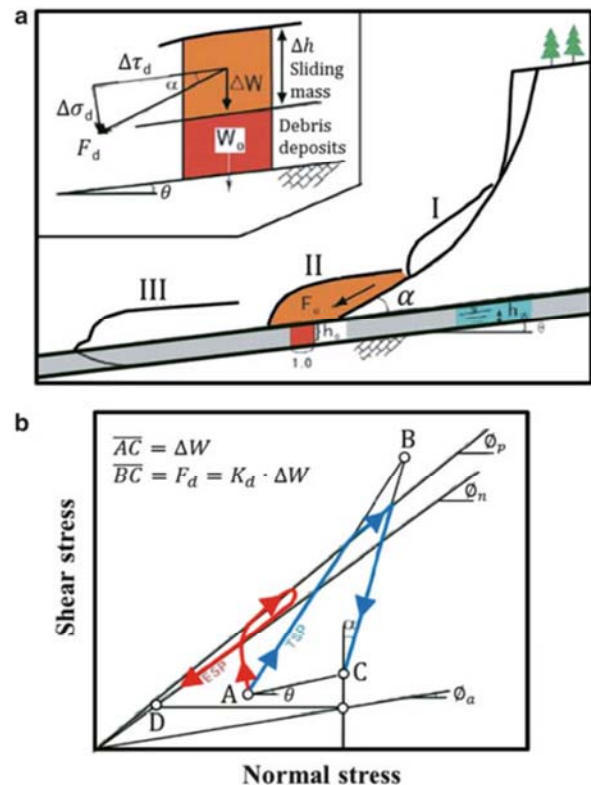


Fig. 9 Thematic figure of the landslide-induced debris flow (Sassa et al.1997). (a) Illustration of the model; (b) stress path of the torrent deposit during loading. α : angle of thrust between the slope and the torrent bed; F_d : dynamic stress; k_d : dynamic coefficient ($F_d/\Delta W$)

The stress path from A to B to C is the total-stress path (TSP) in the case where no pore pressure is generated. However, excess pore

pressure is likely to be generated during loading and also during shearing after failure. In this case, the effective-stress path (ESP) will deviate from the total-stress path(TSP) as a curved line from A to D.

When the landslide mass moves from a steep slope to a gentle slope, the angle α is great, but when the landslide mass (i.e., the debris flow) travels along the torrent, the angle α is zero. Fig. 10 presents the test result simulating the case of the landslide (debris) mass moving onto the torrent deposits. The gradient of the torrent bed was 15° , the depth of the torrent deposit was 2–4 m, and the dynamic coefficient was 0.9. Because of rapid loading by the fast-moving slide mass (more than 10 m/s), the test was carried out under undrained conditions similar to the seismic loading test. A sliding surface was formed inside the torrent deposits which were composed of reworked andesitic lava or tuff breccia. The test result of this landslide ring-shear simulator visualized that the torrent deposit must shear and move together with the original slide mass. Only 18.5 kPa was necessary as an additional shear stress to cause shear failure. The mobilized apparent friction angle was only 1.9° in this rapid and undrained loading condition as seen in the stress path (Sassa et al. 2004).

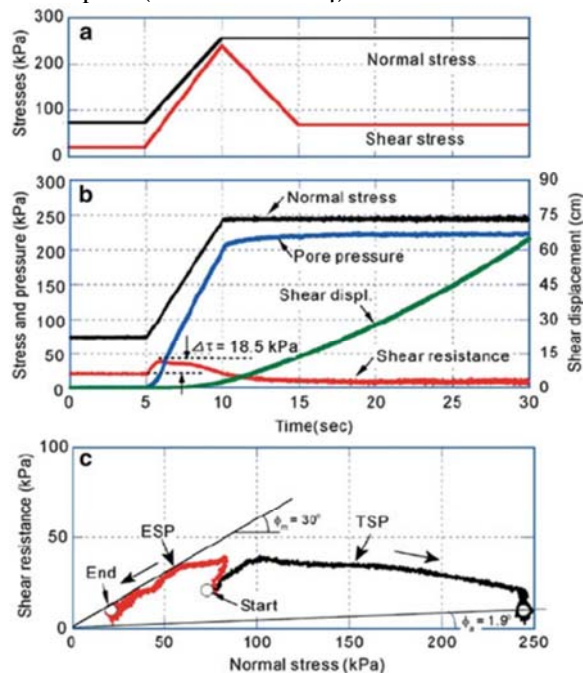


Fig. 10 Test result simulating the torrent deposit scraped by undrained loading of a moving landslide mass ($B_D=89$). (a) Control signal for normal stress and shear stress simulating the undrained loading on the torrent deposit, (b) Monitored loaded normal stress, generated pore pressure, mobilized shear resistance and shear displacement during undrained loading, (c) Monitored total stress path (black) and effective stress path (red) during undrained loading

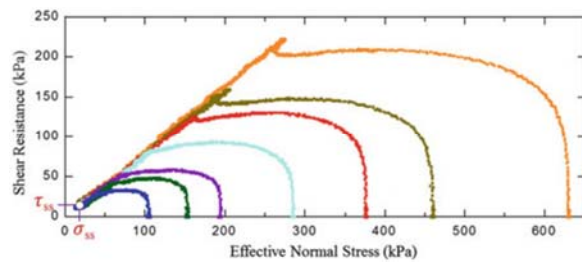


Fig. 12 Steady-state shear resistance under different normal stresses ($B_D=0.95-0.96$) from Okada et al. (2000)

Development of a numerical simulation using measured parameters

Theory of the integrated simulation model

The basic concept of this simulation is explained in Fig. 11. A vertical imaginary column is considered within a moving landslide mass. The forces acting on the column are (1) self-weight of the column (W), (2) seismic forces (vertical seismic force F_v , horizontal x-y direction seismic forces F_x and F_y), (3) lateral pressure acting on the side walls (P), (4) shear resistance acting at the base (R), (5) the normal stress acting at the base (N) given by the stable ground as a reaction against the normal component of the self-weight, (6) pore pressure acting at the base (U).

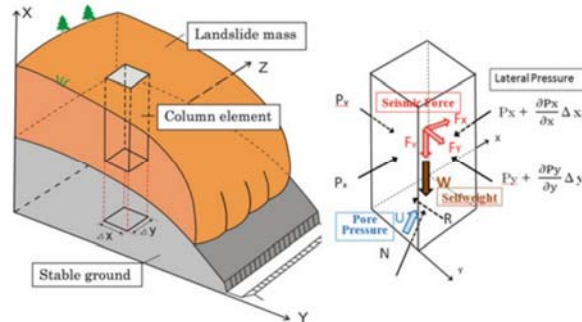


Fig. 11 Concept of landslide simulation model (Sassa et al.2010)

The landslide mass (m) will be accelerated by a force (a) given by the sum of these forces: driving force (self-weight + seismic forces) + lateral pressure + shear resistance

$$am = W_p + \left(\frac{\partial P_x}{\partial x} \cdot \Delta x + \frac{\partial P_y}{\partial x} \cdot \Delta y \right) + R \quad [3]$$

Here, R includes the effects of forces of N and U in Fig. 11 and works in the upward direction of the maximum slope line before motion and in the opposite direction of landslide movement during motion.

The slope angle varies depending on the position of the column within landslide mass. All stresses and displacements are projected to the horizontal plane and calculated on the plane (Sassa 1988).

Effect of soil depth in the landslide mass on the steady-state shear resistance

The most important factor in predicting the motion of landslides is the steady-state shear resistance. The term “Steady State” is defined as the stress state at the failure surface in which shear displacement will proceed without any change of stress. Steady-state shear resistance is affected by pore-pressure generation in the shear zone. The Nikawa landslide was triggered in the Osaka formation by the 1995 Hyogoken Nanbu earthquake. It killed 34 people in Nishinomiya city, Hyogo Prefecture, Japan. Fig. 12 presents test results for weathered granitic soils taken from the Osaka formation (Okada et al 2000). All soils with different normal stresses reached the same steady-state shear resistance (τ_{ss}) in the undrained ring-shear test. The steady state without any further stress change is interpreted as meaning that there is a certain critical normal stress for each soil below which no grain crushing and volume reduction will occur. The critical normal stress for steady state for this soil is σ_{ss} . Initial stresses varied from 110 to 630 KPa. All of the effective stress paths in these undrained monotonic ring-shear tests reached the same failure line and followed down the failure line due to the pore-pressure generation and were stopped upon reaching steady state (σ_{ss}, τ_{ss}). The depth of the landslide mass changes in the process of movement across different ground topography. The total normal stress acting on the sliding surface changes, but the mobilized steady state shear resistance is constant. This relationship was used in the new integrated computer simulation model (LS-RAPID) simulating the initiation and the motion of landslides.

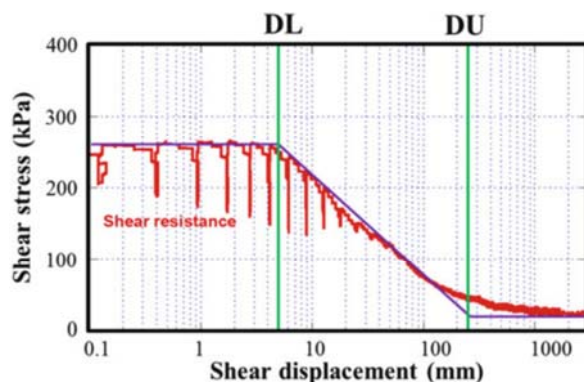


Fig. 13 Shear-resistance reduction after failure to steady state ($B_D=0.98$)

Shear resistance reduction after failure to the steady state

Fig. 13 is the result of a cyclic loading ring-shear test on Tertiary-age sand in which a rapid landslide (the Higashi Takezawa landslide shown in Fig. 7) is triggered by the 2004 Mid-Niigata

earthquake. The shear resistance started to decrease after a shear displacement (DL) of 5 mm at the peak shear strength. The landslide initiation process continues until the point DL. After DL, the shear resistance continued to decrease until it reached a steady state after some hundred millimetres of displacement. This relationship of reduction in shear resistance is approximated by a straight line (the purple line in the figure). In this case, the initiation of steady state appears to be at DU (240 mm).

Modelling of both process of landslide initiation and motion was difficult in a single model. Therefore, the slope-stability analysis dealt with the initiation of landsliding until failure, while landslide runout analysis dealt the landslide motion. There was no method able to model both the initiation and motion in a single integrated model. The undrained ring-shear test enables modeling of both the initiation and the motion in the following approximation (Sassa et al 2007).

Stage 1 (before failure)

$$\text{for } D < DL : \tan \phi_a = \tan \phi_p, c = c_p, \gamma_u = \gamma_u \quad [4]$$

Stage 2 (steady state)

$$\text{for } D > DL : \tan \phi_a = \tan \phi_{a(ss)}, c = 0, \gamma_u = 0 \quad [5]$$

Stage 3 (transient state)

for $DL \leq D \leq DU$:

$$\tan \phi_a = \tan \phi_p - \frac{\log D - \log DL}{\log DU - \log DL} \cdot (\tan \phi_p - \tan \phi_{a(ss)})$$

$$c = c_p \left(1 - \frac{\log D - \log DL}{\log DU - \log DL}\right)$$

$$\gamma_u = \gamma_u \frac{\log DU - \log D}{\log DU - \log DL} \quad [6]$$

Effect of saturation on steady-state shear resistance

Pore water pressure generation is affected by the degree of saturation. The relationship between pore-water pressure parameter $B = \Delta u / \Delta \sigma^3$ and the degree of saturation (Sr) can be measured in triaxial tests. Fig. 14 (A) is the relationship between the B-value and the degree of saturation and was obtained by isotropic triaxial compression tests on the torrent deposits in the 1984 Ontake debris avalanche at different degree of saturation (Sassa 1988). The sliding surfaces in the landslide and the ring-shear test are both direct shear state. However, the B value in the triaxial compression state and $B_D (= \Delta u / \Delta \sigma)$ in the direct shear state are the same in isotropic soils. This relationship is a reference for the effect of saturation on the steady-state shear resistance.

The steady-state shear resistance is changed by the degree of saturation of the soil. We measure the fully saturated steady-state shear resistance

from the undrained, fully saturated ring-shear test (namely the point of “full saturation” in Fig. 14 (B)).

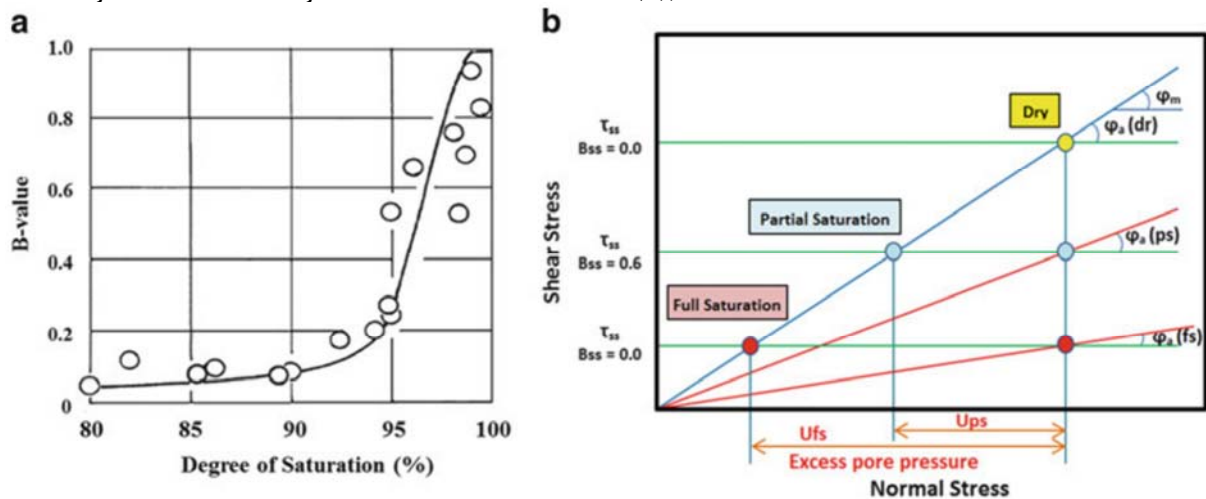


Fig. 14 Effect of saturation on the steady-state shear resistance. (a) Effect of degree of saturation on the pore-pressure parameter B-value (ratio of generated pore pressure for confining pressure increment by undrained triaxial test. Sassa 1988); (b) Conceptual figure of steady-state shear resistance at different soil saturation levels

If field conditions are dry, the steady-state shear resistance of the mobilized dry soil layer will be the point “Dry” just above the acting total normal stress shown in Fig. 14 (B). We use a parameter of pore-pressure generation rate B_{ss} which is very similar to pore-pressure parameter B, although B is defined in the undrained isotropic compression triaxial test while B_{ss} is defined in the undrained ring-shear test. In Fig. 14 (B), we denote the steady-state shear resistance at full saturation as τ_{ss} ($B_{ss} = 1.0$) and the dry steady state as τ_{ss} ($B_{ss} = 0.0$). If the proportion of pore-pressure generation is 60% of the full saturation, the steady state is denoted as τ_{ss} ($B_{ss} = 0.6$). As found in this figure, the apparent friction angle $\phi_a(dr) = \phi_m$ in the dry state. $\phi_a(fs)$ at full saturation is the lowest, $\phi_a(ps)$ at partial saturation has an intermediate value.

Application of LS-RAPID simulation to a simple slope condition and the 2006 Leyte landslide

Application of LS-RAPID to a simple slope

The performance of the initiation process of LS-RAPID was examined by applying it to a simple imaginary slope and comparing the results with safety factors obtained from some conventional limit equilibrium slope stability analyses: 1) Fellenius, 2) Bishop simplified, 3) Janbu simplified, 4) Spenser, and 5) Morgenstern-Price methods. The imaginary slope which is composed of three slope parts: flat ground at the top, a steep slope in the middle and a gentle slope at the bottom. The area of simulation is 350 m wide and 440 m long, the size of mesh is 10 m, the maximum vertical landslide depth is 40.53 m, the total landslide

volume is 231,300 m³. The imaginary landslide body was created in the form of an ellipsoid.

The initiation process due to pore pressure increase was examined by inputting three pore-pressure ratios; $r_u=0.4, 0.5, 0.6$. The characteristic of LS-RAPID is the expression of strength reduction during deformation and progressive failure, while the limit-equilibrium slope-stability analyses assume that the whole landslide sliding surface fails at once.

A relatively strong slope was considered which could be failed by a high pore-pressure ratio supplied from the bed rock. The values of $\tan\phi_p = 0.8, c_p = 50$ kPa, $\tau_{ss} = 50$ kPa, $k = 0.5, B_{ss} = 0.99, \tan\phi_m = 0.60$ were given to the entire simulation area. As the parameters of the shear-resistance reduction, the shear displacement at the start of reduction DL was given as 10 mm, and the shear displacement when steady-state shear resistance DU was reached was given as 1,000 mm. Local failure and shear-strength reduction starts first at a mesh (site) where the shear displacement first reaches DL = 10 mm, then it may develop to a progressive failure.

In order to compare this simulation result to the safety factors by the limit-equilibrium slope stability analysis such as Fellenius, Bishop, Janbu, Spencer, Morgenstern-Price, enough large shear displacement minimizing the effect of progressive failure was chosen to be 2 m instead of 10 mm for DL, and 5 m for DU, respectively. The large shear displacement DL is effective to restrain the effect of shear-resistance reduction and the progressive failure in the initiation process. The simulation results are shown in the form of 3D perspective views in Fig. 15. The contour line is 2.0 m pitch.

The red color line shows the area of the moving landslide mass. The red color appears when/where the velocity at a mesh exceeds 0.5 m/s.

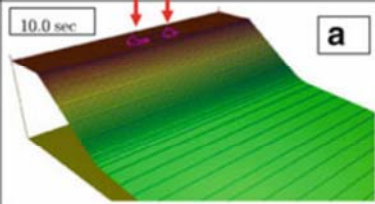
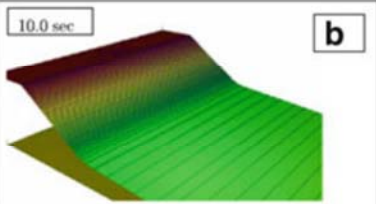
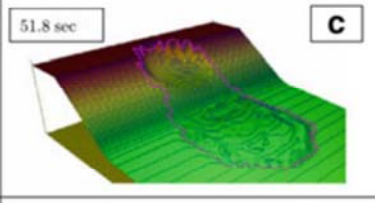
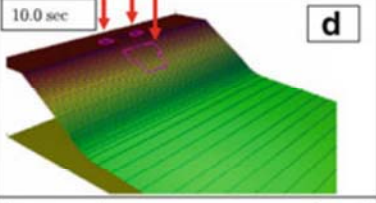
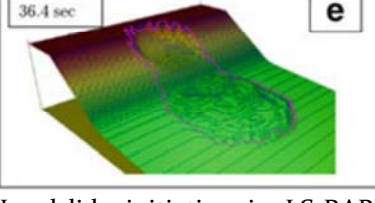
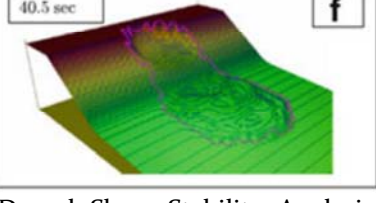
PP ratio r_u	Landslide simulation RAPID		Slope stability analysis				
	DL=10mm, DU=1000mm	DL=2000mm, DU=5000mm	Fel. (*1)	Bisp (*2)	Jan (*3)	Spn (*4)	M&P (*5)
0.4			1.545	1.443	1.381	1.433	1.431
0.5			1.351	1.207	1.151	1.200	1.199
0.6			1.155	0.973	0.923	0.970	0.970

Fig. 15 Landslide initiation in LS-RAPID and Slope Stability Analysis (Sassa et al.2010). Values of parameters: $\tan\phi_p=0.8$, $C_p=50$ kPa, $\tau_{ss}=50$ kPa, $k=0.5$, $B_{ss}=0.99$, $\tan\phi_m=0.60$, $\alpha=0$. Each mesh size =10 m, each contour interval=2m, simulated area=350x440 m. *1 Fellenius, *2 Bishop simplified, *3 Janbu simplified, *4 Spenser, *5 Morgenstern-Price

DL = 10 mm, DL = 1000 mm

In the case of $r_u=0.4$ in Fig. 15-A, only two small areas at the top of the slope showed slight movement and two red colored circles were observed, but no further progressive failure appeared.

For $r_u=0.5$ and 0.6 , rapid landslide motion appeared as shown in Fig. 15-C, E.

DL = 2,000 mm, DU = 5,000 mm

No motion appeared for $r_u=0.4$, limited deformation appeared for an instant in the case of $r_u=0.5$ as shown Fig. 15-B, D. A rapid landslide occurred for $r_u=0.6$ (Fig. 15-F). The border of landslide initiation is between $r_u=0.4$ and 0.5 for smaller DL-DU, and it is between 0.5 and 0.6 for larger DL-DU.

Time

Simulation stops when a zero velocity appears for all meshes. Time in the figure shows the time from the start to the end of motion. Ten seconds for A, B, D is a pre-determined minimum calculation time, because the initial velocity is zero, and some calculation is necessary to know if movement will start or not.

Safety Factors

For the central section of this landslide mass 2D slope stability analyses were implemented using the stability analysis software “Slide V5” by Rocscience Inc. The same peak shear strength parameters and the same pore pressure ratio ($\tan\phi_p=0.8$, $c_p=50$ kPa, $r_u=0.4, 0.5, 0.6$ were used in all stability analysis methods. The calculated safety factors for 1: Fellenius, 2: Bishop simplified, 3: Janbu simplified, 4: Spenser, 5: Morgenstern-Price are shown in the right column of Fig. 15. The onset of landslide motion, namely the unit safety factor ($FS=1.0$) appears when the value of r_u is between 0.5 and 0.6 for four models. For the Fellenius method, the factor of safety becomes unity ($FS=1.0$) when the value of r_u is between 0.6 and 0.7 . Therefore, the border of stability is same with the border by LS-RAPID in the case of long shear displacement (2 m) until the start of shear-strength reduction except in the Fellenius method. The difference between LS-RAPID and the limit equilibrium slope stability analysis comes mainly from LS-RAPID’s consideration of local shear and progressive failure vs the overall shear of the whole landslide body at once. The differences between the three dimensional analysis (LS-RAPID) and the two dimensional analysis can not be examined in this way.

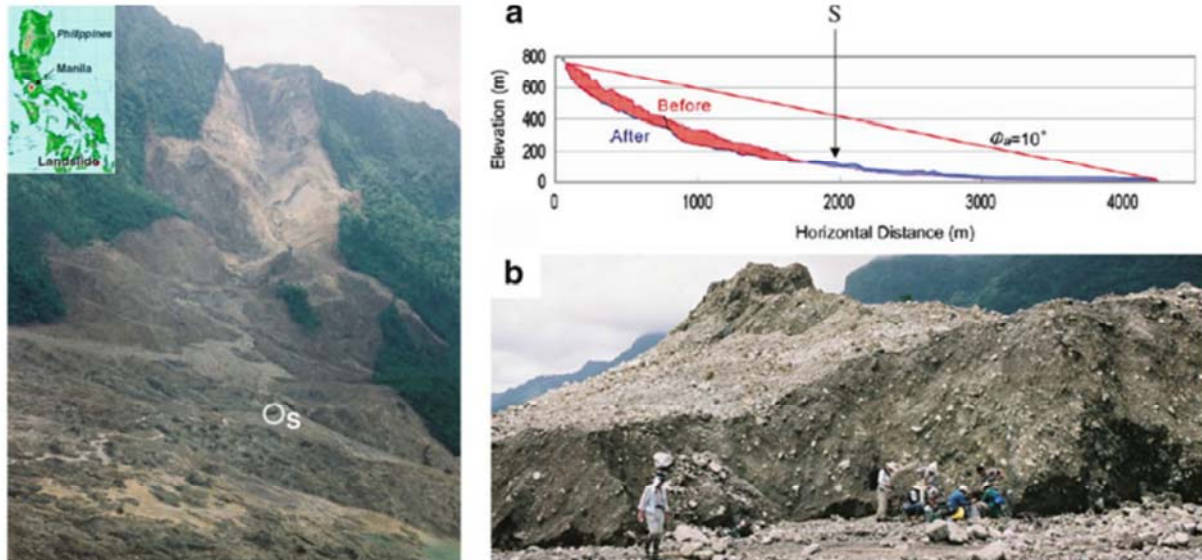


Fig. 16 Photo and section of the 2006 Leyte landslide. Left: The front view of the Leyte landslide on 17 February 2006 and sampling point S; Right: The central longitudinal section of landslide (a) and the sampling point S at the bottom of flow mound (b)

Application of LS-RAPID to the 2006 Leyte landslide

A rapid and long-traveling landslide occurred on 17 February 2006 in the southern part of Leyte Island, Philippines. The landslide caused 154 confirmed fatalities and 990 people missing in the debris. The International Consortium on Landslides (ICL) and the Philippine Institute of Volcanology and Seismology (PHIVOLCS) jointly investigated the landslide on the ground and from a helicopter. Fig. 16 is a frontal view of the landslide taken by K. Sassa from a helicopter. A planar surface of hard rock is seen at the left side of the head scarp. Other parts of the slope seem to be weathered volcanoclastic rocks or debris. The landslide mass moved from the slope and deposited on the flat area. Many flow-mounds or hummocky structures were found. The features of this landslide were reported by Catane et al. (2007).

The longitudinal section of the central line of the landslide (Fig 3.2.2 A) was surveyed by a non-mirror total station and a ground-based laser scanner in the field and compared with a SRTM (Shuttle Radar Topography Mission) map before the landslide which was implemented by H. Fukuoka, a member of the team and colleagues from Philippines. The red-color part shows the initial landslide mass while the blue-color part presents the displaced landslide debris after deposition. The length of landslide from the head scarp to the toe of the deposition was around 4 km. The inclination connecting the top of the initial landslide and the toe of the displaced landslide deposit is approximately 10° , which indicates the average apparent friction angle mobilized during the whole travel distance. The value is much smaller than the usual friction angle of debris

(sandy gravel) of $30\text{--}40^\circ$. Therefore, it suggests that high excess pore-water pressure was generated during motion. Fig. 16-B shows a flow mound that travelled from the initial slope to this flat area without much disturbance. Movement without much disturbance is possible when the shear resistance on the sliding surface became very low; thus, movement of the material is like that of a sled.

The material of the flow mound is volcanoclastic debris, including sand and gravel. We observed the material in the source area from the surface and by hand-scoop excavation in the valley-side slope after the landslide. It consisted of volcanoclastic debris or strongly weathered volcanoclastic rocks. It is regarded to be the same material (either disturbed or intact) as observed in the flow mound shown in Fig. 16-B. Therefore, we took a sample of about 100 kg from the base of the flow mound shown in the point “S” in the section of Fig. 16-A) and the photo of Fig. 16-B. The location is in the center of travel course and just below the source area. Then, we transported the material to Kyoto, Japan.

A dynamic-loading ring-shear test was conducted as follows. The sample was set in the shear box (250 mm inside diameter, 350 mm outside diameter) of apparatus DPRI-6, and fully saturated ($B_D = 0.98$). The stress acting on the sliding surface of the deepest part (around 120–200 m) is very high. However, because of the capacity of this apparatus DPRI-6 (ICL-2 was not yet developed in 2006): the sliding surface was assumed for the test to be 35 m deep and at an inclination of 25° . The unit weight of the soil was assumed to be 20 kN/m^3 . In the preliminary test to increase pore-water pressure until failure, the failure line of this material was obtained. It has a friction angle of $s 39.4^\circ$ and almost zero cohesion.

In the simulation test of a rain- and earthquake-induced landslide, the normal stress corresponding to that of 5 m lower than the critical ground-water level (i.e., further 5 m rise of ground-water level shall trigger the landslide) was first loaded on the sample. Then, the shear stress due to the self-weight of the soil layer was loaded. It is the stress point shown by the white circle in Fig. 17-a. Using the three components of seismic record observed at Massin (PHIVOLCS, Code number: MSLP, Latitude: 10.1340, Longitude: 124.8590, Elevation: 50.0), normal stress and shear stress acting on the shear surface of 35 m deep with 25° inclination on the direction of the Leyte landslide were calculated so that the peak seismic stress may correspond to the range of seismic acceleration of 60–200 gal which was estimated from the seismic record, attenuation by the hypocentral distance, amplification by the contract between the base rock and the volcanoclastic debris and the focusing effect of the mountain ridge (Sassa et al. 2010).

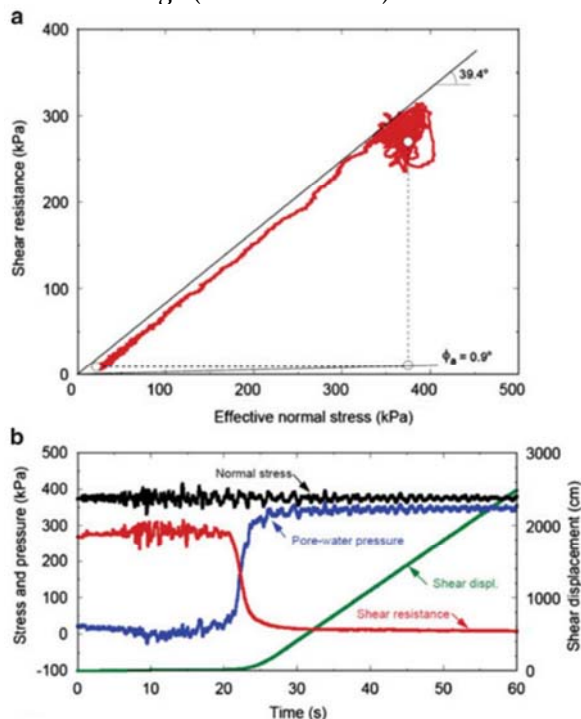


Fig. 17 Test result of the ring shear test of the sample taken from flow mound ($B_D=0.98$). (a): Stress path. (b): time series data of stresses, pore pressure, shear resistance and shear displacement

Fig. 17-a presents the stress path of the test. The effective stress path showed a complicate stress path like a cloud. The stress path reached the failure line repeatedly. Therefore, this small seismic stress failed the soil structure and grains during the period of stress reaching the failure line. It generated a pore-water pressure (blue color line) due to grain crushing and volume reduction, and it was accelerated in progress of shear displacement (green color line). Namely sliding-surface liquefaction occurred. The value

reached a very small steady-state stress (red color line). This process is presented in the time series data around the failure in Fig. 17-b. The mobilized apparent friction coefficient defined by steady-state shear resistance divided by the total normal stress was 0.016 (0.9°).

Explanation of Sliding-Surface Liquefaction in this test result.

The sliding-surface liquefaction is a key finding in the progress of landslide dynamics. It was reported in Sassa, 1996, Sassa et al 1996, Sassa 2000. The test result of Fig. 17 presents one of the best examples of “Sliding Surface Liquefaction”. It is here explained in Fig. 18 A and B.

Grains in the shear zone are crushed during shearing under a normal stress greater than a critical normal stress at steady state (σ_{ss}). The soil structure failed and was subjected to volume reduction. In the fully saturated undrained state, a high pore pressure was generated by a minimum reduction of volume. Then, both of the effective stress and the mobilized shear resistance were reduced. T1 in B figure is the onset of seismic loading. Immediately pore pressure started to decrease. It is interpreted that a dilatancy occurred which is a characteristic of dense materials. T2 in B figure is the start of post-failure shear displacement. The pore pressure was progressively increased to close to the normal stress and then kept constant. The difference between normal stress and pore-water pressure corresponds to the normal stress at steady state (σ_{ss}). T3 in B is the start of steady-state high-speed motion, namely rapid landslide motion. The mobilized shear resistance at this stage is the steady-state shear resistance (τ_{ss}). A rapid motion was reproduced in this simulation test.

The most important parameter for landslide motion was the steady-state shear resistance (τ_{ss}). The steady-state shear strength was very low (less than 10 kPa in Fig. 17). The testing condition was full saturation ($B_D = 0.98$) and the loading stress corresponded to 35 m deep (much shallower) and the sample used may be more weathered than that in the deep landslide body. So we selected $\tau_{ss} = 40$ kPa as a practical value for this landslide. Various combinations of values of factors can be considered. It was not easy, but we assumed the following: The landslide was deep and the material seemed to be intact in the source area as seen in Fig. 16. Then, we estimated that the peak friction and peak cohesion before motion in the source area should be high ($\tan\phi_p = 0.9$, $c_p = 100$ – 300 kPa); the part of the head scarp shown in Fig. 16 would be not saturated because it was close to the ridge, probably there was less ground water to generate excess pore-water pressure. A value of $B_{ss} = 0.1$ – 0.2 was assigned in this area; the middle

part was probably more saturated ($B_{ss} = 0.4-0.6$) and the lower part in the paddy fields on the flat area was probably well saturated ($B_{ss} = 0.9-0.97$); The landslide body was stiff in the top, and moderate in the middle and much disturbed in

the lower part and on the flat area (lateral pressure ratio $k = 0.2-0.7$); The shear displacement of shear strength reduction was estimated as $DL = 100$ mm, $DU = 1,000$ mm referring to the test of Fig. 17.

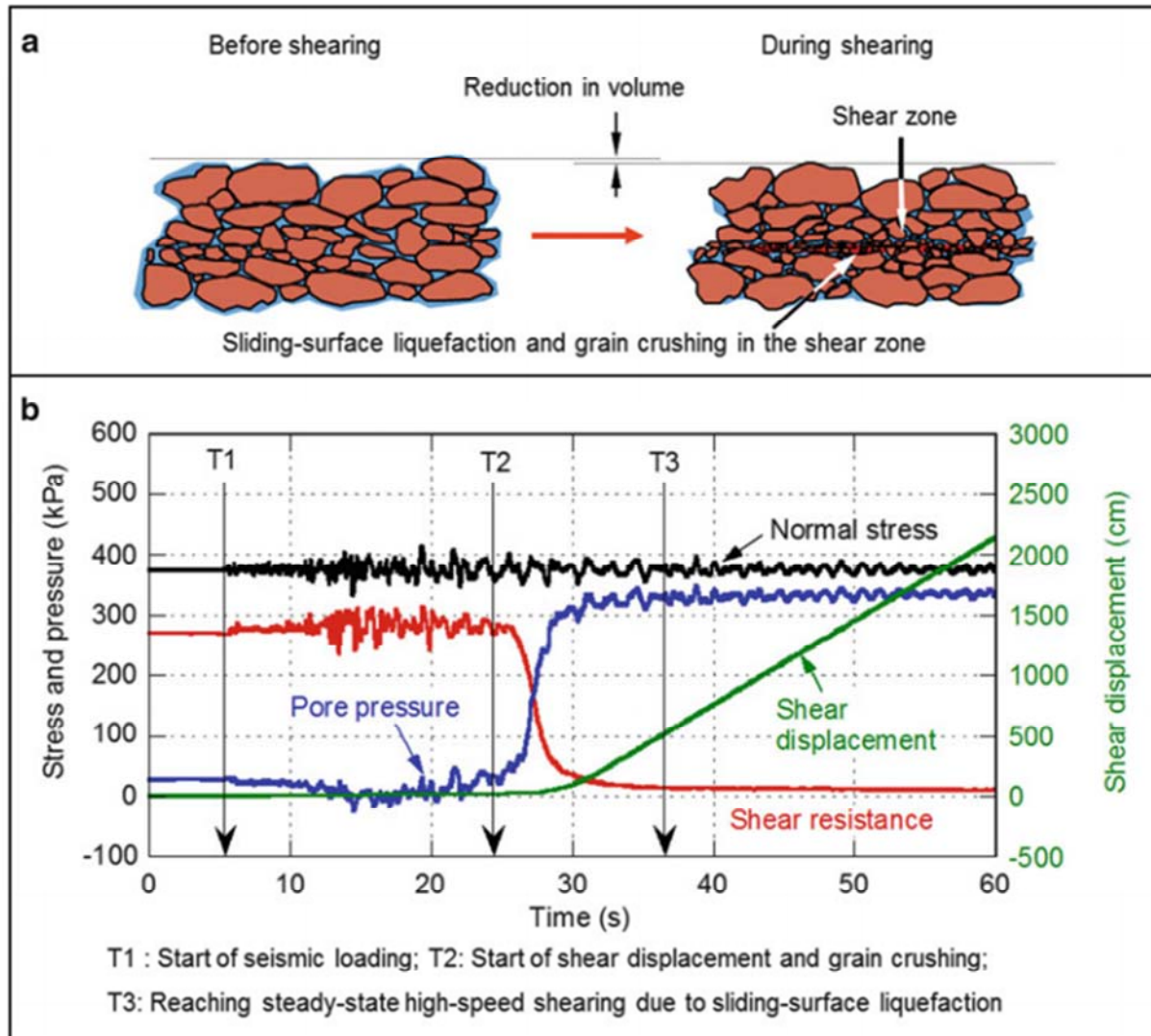


Fig. 18 The explanation of the sliding surface liquefaction using the test of Fig.17.(a) Illustration of the sliding-surface liquefaction, (b) Monitored pore pressure generation and mobilized shear resistance during the sliding surface-liquefaction in the undrained seismic-loading ring shear test on the sample taken from the 2006 Leyte landslide (Sassa et al.2010)

In the trial simulation, no landslide occurred when the pore-pressure ratios were $r_u = 0.10$ and 0.15 . However, the case of $r_u = 0.16$ caused a rapid landslide. Namely $r_u = 0.16$ (the ground-water depth was equal to about 30% of the depth of landslide mass) was the critical value to trigger a landslide without an earthquake. Then, various magnitudes of seismic shaking using the wave forms of EW, NS, and UD recorded at Maasin, Leyte were given in addition to a pore pressure ratio of 0.15 . The threshold to create a rapid landslide was between $K_{EW} = 0.11$ and 0.12 . We used $K_{EW} = 0.12$. Using the ratio of magnitudes of seismic records of EW, NS and UD, $K_{NS} = K_{UD} = 0.061$ were given. The seismic shaking of three directions of EW, NS and UD were

applied in this simulation. Unstable deposits three meters thick were assumed in the alluvial deposit area.

Blue dots shown in Fig. 19-A are the unstable soil deposits (initial landslide body) in the source area and also the unstable deposits in the alluvial flat area. A series of simulated positions of the landslide are presented in Fig. 19. Each step of A-E is explained as follows.

A: r_u rises to 0.15 and earthquake starts but no motion.

B: Continued earthquake loading (Max $K_{EW} = 0.12$, $K_{NS} = K_{UD} = 0.061$) triggers a small local failure as presented in red color mesh,

C: An entire landslide block is formed and moving,

D: The top of the landslide mass goes on to the alluvial deposits,
 E: Deposition at the end of landslide motion.

The travel distance and the major part of the landslide distribution were well reproduced (Sassa et al. 2007).

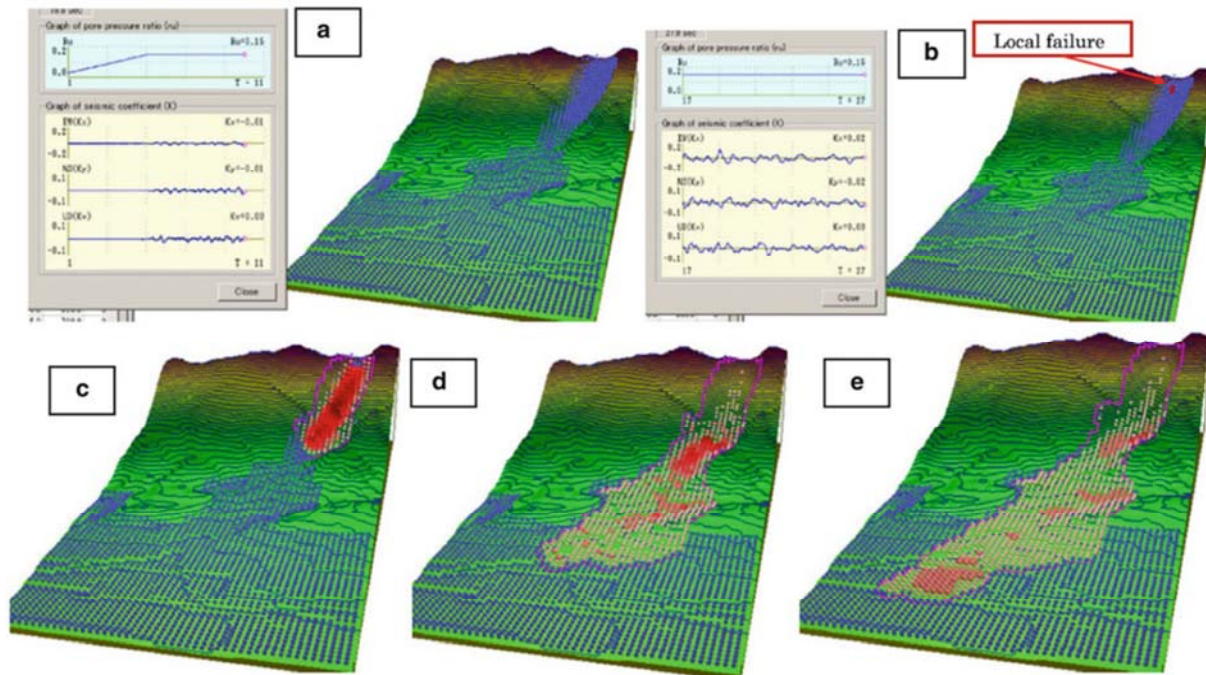


Fig. 19 Simulation result of the Leyte landslide. Pore pressure ratio due to ground water: $r_u=0.15$; Seismic coefficient by the earthquake: $KEW=0.12$, $KNS=KUD=0.061$; Mesh size is 40 m. Area is $1,960 \times 3,760$ m. Contour line is each 20 m. Three meter unstable deposits was assumed in the whole alluvial area. (a) Simulation result after 11 sec from loading the triggering factors. The upper-left figure shows pore pressure ratio, and the lower-left figure presents seismic loading. The right figure shows distribution of unstable soil mass without motion, (b) Simulation result after 27 sec, starting a local failure, (c-e) Simulation results showing the motion of landslide from the source area to the deposit

Latest progress of landslide dynamics

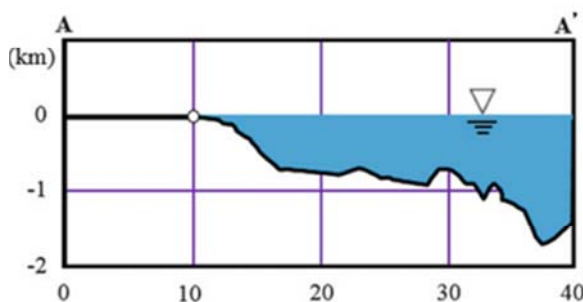
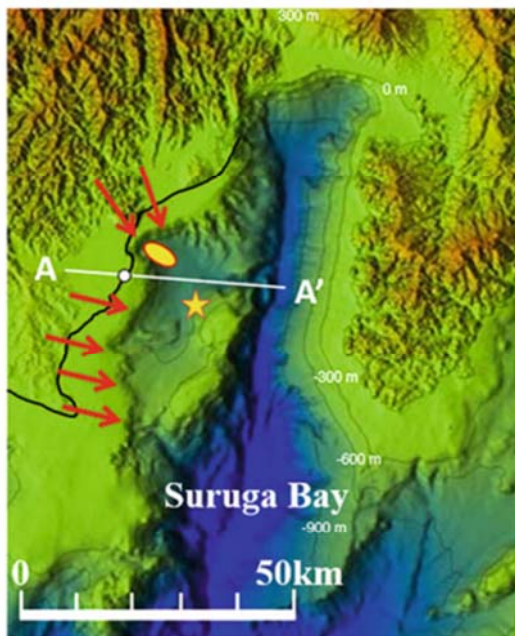
Study of dynamics of submarine megaslides

Fig. 20 presents the onland and submarine topography in Suruga Bay, Japan, where the Philippine Sea Plate subducts under SW Japan. A distinctive depression known as Senoumi (Sea of stone flower). Senoumi forms a step on the western side of the Suruga Bay with a gully. The section A-A' passing through this gully is shown in the lower figure of Fig. 20. The slopes in the steep parts of the head scarp and toe in the section A-A' are $8-12^\circ$. The shape of the Senoumi feature differs from those of most landslides as the exit to the Suruga Trough is very narrow relative to the width of the Senoumi depression. If Senoumi had formed by a blockslide, the mass could not move out through this narrow exit. However, it is possible to form such a shape if the landslide mass almost liquefies after failure and moves/flows downslope with very low shear resistance while the landslide enlarges retrogressively. The landslide is very large compared to terrestrial landslides. However, the sizes of submarine landslides are known to range very widely (Locat and Lee 2008, and others). Due to downward erosion rivers are well

developed on land, and therefore, the width of a single slope between rivers can not be so wide. However, the development of rivers is minimal beneath the sea. So a unit of slope can be very wide. It is one of the main reasons for the large size of submarine landslides. A detailed explanation on Senoumi is reported in Sassa et al (2012). We introduce the application of the undrained dynamic-loading ring-shear apparatus to Senoumi, to define a mechanism for a possible submarine landslide.

The application of the undrained dynamic-loading ring-shear apparatus to study the mechanism of submarine landslides attracted the Integrated Ocean Drilling Program (IODP) researchers. Sassa and colleagues applied to use a submarine sample recovered from the inferred base of a large paleo-landslide in the Nankai Trough cored at Site C0018 during Integrated Ocean Drilling (IODP) Expedition 333 in December 2010 (Strasser et al. 2012). The recovered section (0-315 m below sea bottom) records ~1 Ma of submarine landsliding history in this active tectonic setting. Six mass-transport deposits (MTDs) with thickness up to 60 m were identified in the drill cores. Fig. 21 summarizes location of MTDs, dominant lithology in the stratigraphic column and structural geological

observations (Strasser et al. 2012). A volcanic-ash layer inferred to be the base of the MTD 6 was used as the test sample in this study. A section photo of this part and also a microscope image are included in Fig. 21. This ash layer correlates to the “Pink” volcanic ash sourced from the Kyushu island, Japan and is dated to 0.99–1.05 Ma (Hayashida et al. 1996). Comparable volcanic-ash layers as cored at IODP Coo18 drill site are likely to have been deposited also in Suruga Bay, where no deep-drill hole is available as yet. We therefore tested a sample taken from this fine-grained volcanic ash layer at the base of the landslides (MTD) drilled at IODP Site Coo18 as an analog material for potential Suruga Bay sliding surfaces using Ring-shear apparatus ICL-1.



- Possible border of head scarp of landslide
- Epicenter of 2009 Suruga bay earthquake
- Submarine landslide induced by the earthquake which caused a small scale Tsunami
- Coast line

Fig. 20 A possible megaslide in the Suruga Bay in Japan

The effective unit weight of soils in the sea water is expressed by the difference between the unit weight of saturated soil and the unit weight of sea water. The total unit weight of soils in the

submarine layer was assumed to be 18.6 kN/m^3 from Coo18 drilling data (Expedition 333 Scientists 2012). The unit weight of sea water was 10.1 kN/m^3 from the average sea water density ($1,026 \text{ kg/m}^3$). The normal stress of $1,000 \text{ kPa}$ (the maximum capacity of ICL-1) corresponds to a burial depth of 117 m . The thickness of the largest landslide deposit from Site Coo18 (MTD 6) is 60 m , but the sample depth is 189 m below sea bottom (Fig. 21). A depth of landslide in Senoumi Bay was estimated to be $200\text{--}600 \text{ m}$ from current sea bottom. We selected $1,000 \text{ kPa}$ for the loaded normal stress since it is the upper limit of ICL-1. The angle of the slope is given by \tan^{-1} (initial stress/initial normal stress due to gravity). The angle of the steeper slopes in section A-A' of Fig. 20 is $8\text{--}12^\circ$. Thus, 160 kPa was assumed as the initial shear stress, which corresponds to a slope of $\tan^{-1}(160/1,000) = 9.09^\circ$.

The procedure of the test was as follows: (1) a necessary amount of sample was saturated with de-aired water and left in a vacuum cell for one night to remove air bubbles; (2) the sample box was filled with de-aired water; (3) the fully saturated sample was placed in the de-aired water in the shear box; (4) de-aired water was circulated for a while; (5) the B_D value ($\Delta u/\Delta \sigma$) was measured and confirmed to be greater than 0.95 ; (6) the normal stress was increased to $1,000 \text{ kPa}$ and the shear stress was increased to 160 kPa , both under drained conditions to create the initial stress state of the soil under gravitational loading; (7) a dynamic shear stress was applied using the predetermined program (either cyclic stress or seismic stress using the 2011 Tohoku Earthquake wave form).

The Tohoku earthquake is an example of the wave form of a megaquake which has two main shocks, and a long duration of shaking. We examined whether this Tohoku earthquake waveform could produce a rapid landslide motion in a gently dipping sea floor where a shear surface is formed either in volcanic ash or in Neogene silty sand. Various factors of testing conditions such as earthquake wave, loading stress, loading time were examined prior to beginning the undrained ring-shear test.

Examination of testing conditions

On 11 March 2011, a great earthquake occurred offshore of the Tohoku Region of Japan. Seismic acceleration from some hundreds to a few thousands gal were recorded at monitoring stations in the Tohoku Region. The largest measured earthquake acceleration ($2,933 \text{ gal}$ as the resultant acceleration of EW, NS, and UD components and $2,699 \text{ gal}$ as a single component) was recorded at station MYG004 at Tsukidate in Miyagi Prefecture, 176 km west of the epicenter.

Since mega earthquakes similar to the 2011 Tohoku earthquake have occurred in the past, and likely will occur in the future, the Cabinet Office of the Government of Japan is examining the risk of such a mega earthquake in the Suruga

trough (Cabinet Office 2011, 2012). The seismic record of the NS component of MYG004 was used for the ring-shear test as an example of mega-earthquake loading.

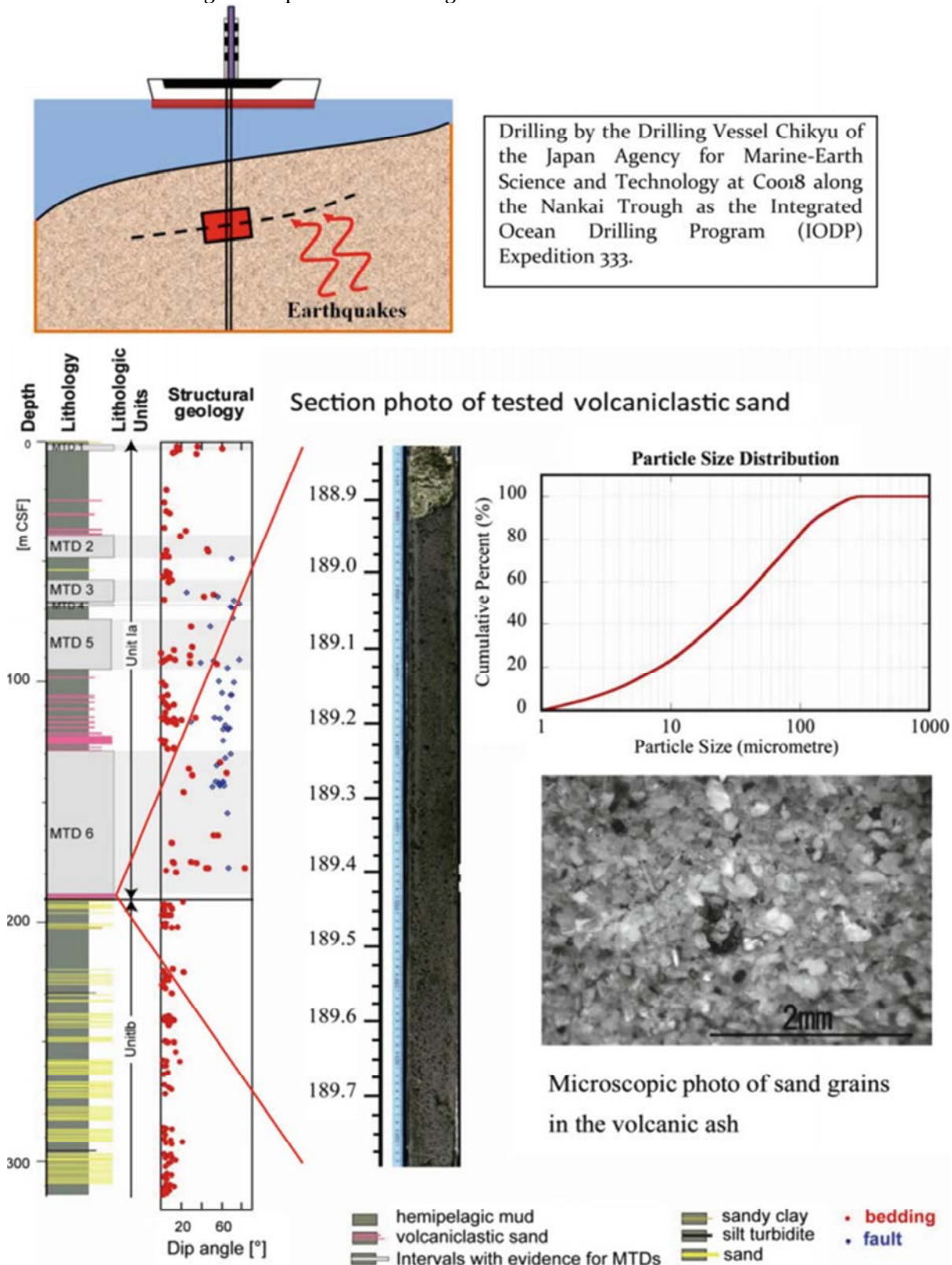


Fig. 21 Sampling of soils of submarine landslides and drilled core

Examination of loading shear stress

We examined the testing plan of seismic loading ring shear test based on the results of a cyclic loading test (Sassa et al 2012). Initial normal stress and shear stress was decided to be the same as used in the cyclic loading test, namely 1,000 and 160 kPa, which corresponds to the normal stress and shear stress due to gravity on a slope of 9.09°. According to the cyclic loading test, an additional 400 kPa of shear stress may fail the sample. So we used 0.3 times the MYG004 NS acceleration record as the maximum acceleration (810 gal) in this ring-shear test. The same value was recorded in FKSo09 in Ono of Fukushima Prefecture (217 km from the epicenter).

Examination of loading duration

The cyclic loading tests of 0.1 Hz were successful for this sample in ICL-1. The servo-shear stress control motor (400 W) cannot reproduce the high-frequency loading using the recorded data of the 2011 Tohoku earthquake. Preliminary tests were conducted to investigate the time required to reproduce the seismic wave form of MYG004 by increasing the shaking time by factors of 10, 20, and 30. We found that a 30-fold increase in time scale could reproduce shear stress changes similar to the recorded wave form. The ring-shear test is conducted under undrained conditions, and so pore pressure is unaffected by time because no pore-pressure dissipation occurs. The same stress path can be obtained in a 30-times longer test as would be obtained in a real-time test. The comparison of the monotonic (corresponding to 0.0 Hz) undrained shear stress loading test and 0.2, 0.4, and 1.0 Hz cyclic undrained shear stress loading test presented almost the same relationship between stress and shear displacement and also almost the same stress path between the curve of monotonic loading test and the curve connecting peak values of the cyclic loading test (Trandafir and Sassa 2005). Then, the test was conducted in the 30-times longer time period.

Fig. 22 presents the ring-shear simulation test for the behavior of a submarine slope including a volcanic ash layer subjected to the 0.3 times the largest acceleration history of the Tohoku earthquake. When the first shock of the seismic loading started, a high pore pressure was soon generated. The mobilized shear stress is smaller than the control signal (loaded shear stress). It means the failure occurred. However, the shear displacement was closely below DU (initiation of steady state), then, a rapid motion did not occur. When the second shock arrived, the sample failed before the peak of the second shock and shear strength reduction and rapid landslide motion started, probably the shear

displacement exceeded DU. In the lower figure, a negative shear stress failed the soil at the point A, and a large shear displacement started from the point B.

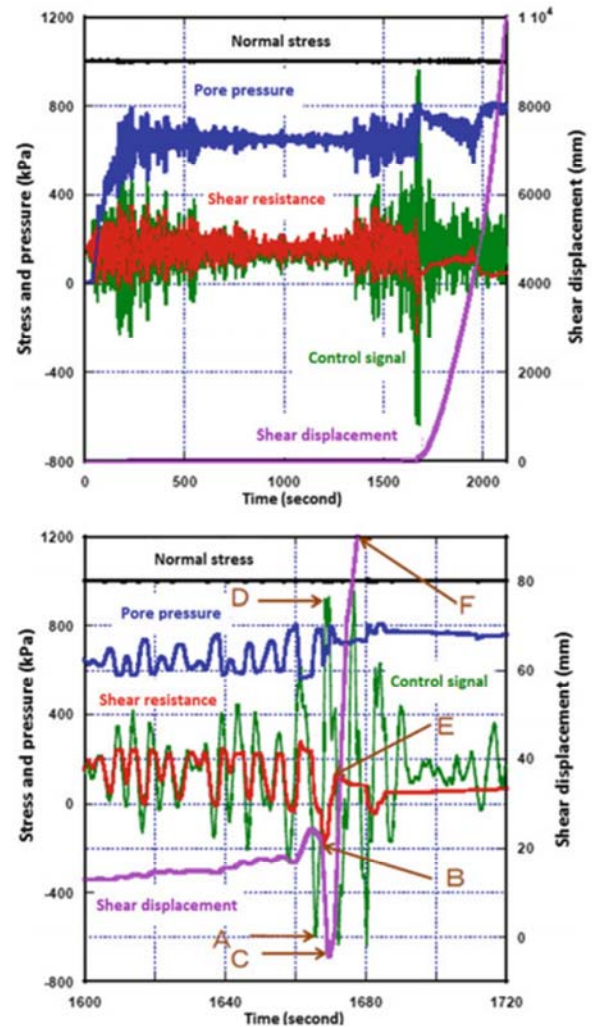


Fig. 22 Test result of seismic loading test on drilled core using the 2011 Tohoku earthquake wave form. The upper figure is the time-series data during the seismic loading test. The lower figure is the enlarged part of the failure and the start of rapid landslide motion. Black line is normal stress, red line is the monitored shear resistance during loading, blue line is the monitored generated pore pressure during loading, green line is control signal for shear stress which is the wave form of the 2011 Tohoku earthquake, but 0.3 times lower acceleration

When the peak acceleration D arrived, very rapid shear displacement occurred from C to F under a reduced shear resistance of E and later steady state shear resistance. Here, negative shear displacement means the landslide mass above the sliding surface moved upslope (namely the bed rock below the sliding surface moved downward). This can occur in seismic loading. This ring-shear test simulated experimentally the submarine slope including the volcanic ash layer and showed that it could fail even on a very gentle slope if a very large earthquake were to strike the area.

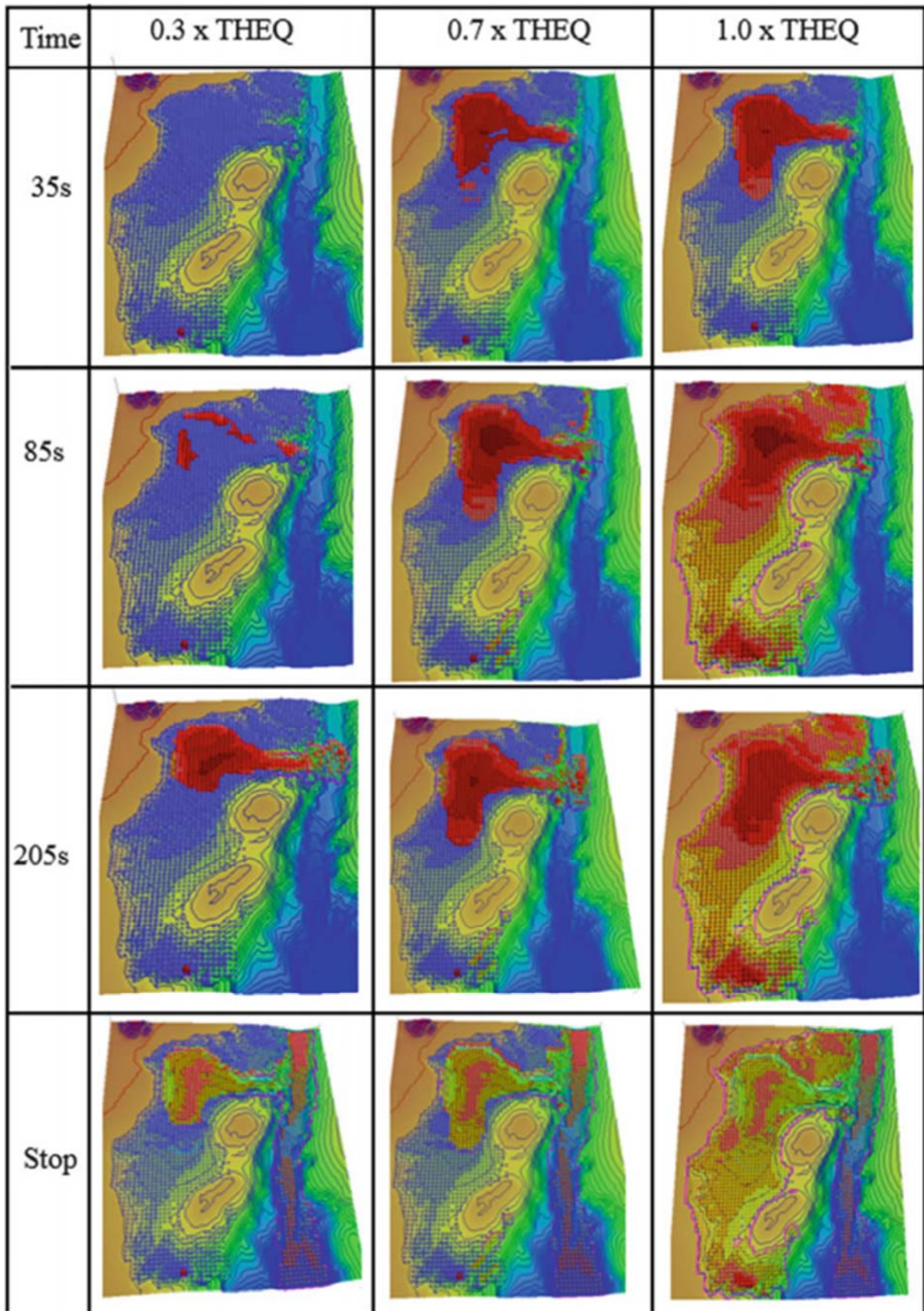


Fig. 23 Simulation result (LA-RAPID) of the Suruga Bay landslide

In order to examine the hypothesis that the Senoumi depression was formed by a submarine megaslide, we applied the new integrated computer simulation model (LS-RAPID) to this case. We input all of the soil properties including

key parameters of steady-state shear strength, the critical shear displacements of DU and DL, friction angles at the peak and during motion and others (Sassa et al 2012). We input all of three components of the MYG004 2011 Tohoku

Earthquake acceleration wave form as an example of a very strong earthquake in Japan. The record at MYG004 was the greatest in this earthquake. Recorded accelerations differ between recording stations even at almost the same distance from an epicenter such as 2,933 gal for 176 km at MYG004, 810 gal for 217 km at FKS009. We input the wave form of MYG004, but amplitudes of acceleration multiplied by 1.0, 0.7, 0.4, and 0.3 times, and the excess pore pressure ratio $r_u = 0.3$ in the central and deep area along the A-A' line of the Senoumi depression (Fig. 20) as another triggering factor into the computer simulation LS-RAPID.

The simulation results for IODP volcanic ash using 0.3 times, 0.7 times and 1.0 times MYG004 seismic record is shown in Fig. 4.1.4. Blue balls represent soil columns stable or less than 0.5 m/s moving velocity. Red balls show columns with values greater than 0.5 m/s velocity.

In Fig. 23, Time=35 second presents the situation soon after the first shock. A very small local failure was caused in the bottom of the figure by the first shock of 0.3 x THEQ (2011 Tohoku Earthquake acceleration). The deep central part subjected to $r_u = 0.3$ failed by 1.0 x THEQ. 0.7 x THEQ case is in between.

Time=85 second presents the situation after the second shock. The whole Senoumi area was failed by 1.0 x THEQ. But local failures around the central depression zone only occurred in 0.3 x THEQ.

Time=205 second presents the further movement of the initiated landslide mass into the Suruga trough.

The final figure (STOP) presents the deposition after the movement of all meshes was terminated.

This result presents that the whole Senoumi area could be formed by a single strong earthquake. An alternative interpretation is that a strong earthquake moved a central part of the Senoumi depression eastwards. Then, a series of subsequent backward development of landslides together with shallow landslides and submarine erosion could create the current whole Senoumi depression.

The ring-shear-simulation tests reproduced the situation of the central part along A-A' line by 0.3 x THEQ. This part failed in 0.3 x THEQ also in this simulation. Both results agree. The ring-shear test and the computer simulation result gave a reasonable interpretation of the formation of the central part of the Senoumi depression feature.

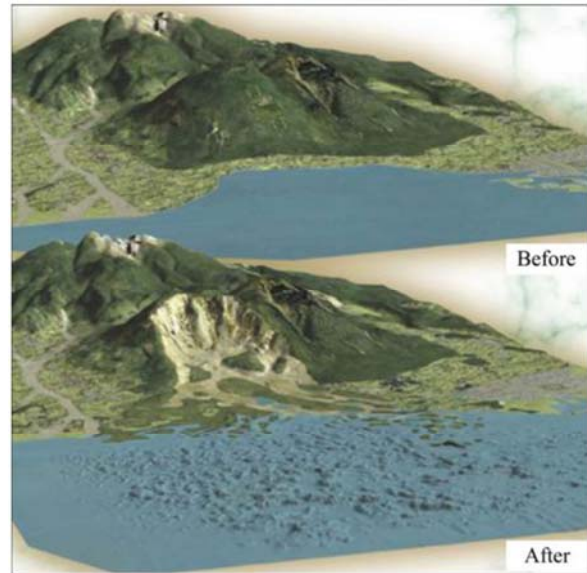


Fig. 24 The 1972 Mayuyama landslide before and after the event (Estimated by the Unzen Restoration Office 2003)

Application of ICL-2 and LS-RAPID to the 1792 Unzen Mayuyama landslides

The 1792 Unzen Mayuyama megaslide is the largest landslide disaster and also the largest historical volcanic disaster in Japan. This landslide killed a total of 15,153 people, 10,139 people in the Shimabara area, many other people were killed on the opposite banks by the landslide-induced Tsunami wave; 4,653 people in the Kumamoto Prefecture, 343 people in Amakusa Island and 18 people in other areas (Usami 1996). Fig. 24 presents a 3D view of the Unzen Mayuyama landslide area before and after the event. It is taken from the cover of Japanese leaflet published by the Unzen Restoration Office of the Ministry of Land, Infrastructure and Transport of Japan (2003) based on a topographic survey and analysis of available sources. The ground surface before the landslide was estimated from paintings of Unzen-Mayuyama from the top of Shimabara castle and others by the Unzen Restoration Office of Japan (2002) referring to Inoue K (1999, 2000). The bed-rock surface in the source area in the upper slope was drawn from the current topography and the location of the bed-rock surface of the lower area was estimated from drilled bore holes.

Fig. 25 presents the current images of the Unzen Mayuyama landslide (from Google Earth) and the location of sampling points S₁ for the landslide source area. S₂ location was selected outside of the landslide moving area to eliminate the effect of the displaced landslide mass. S₂ sample was tested to represent the soils in the deposition area before the event.

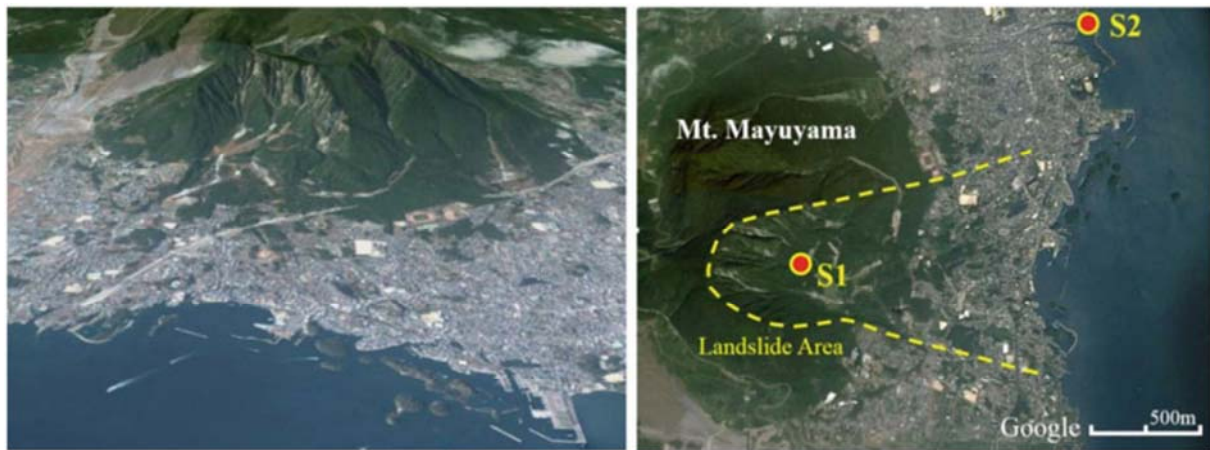


Fig. 25 The present 1972 Mayuyama landslide and the sampling point

We conducted many tests on sample S1. We introduce one of the basic tests (Fig. 26) which was to trigger the landslide only by increasing pore-water pressure. Firstly the sample was saturated (B_D value was 0.98). Then, it was consolidated to 3.0 MPa normal stress and 1.5 MPa shear stress in the drained condition. This initial stress corresponds to a slope of $\arctan(1.5/3.0)=26.5^\circ$ which was the initial average slope. Then, pore-water pressure was gradually increased at a rate of $\Delta u = 1$ kPa/sec. Failure occurred at pore-water pressure of 1.2 MPa, that is, a pore-water pressure ratio $r_u=1.2/3.0=0.4$. The friction angle at failure was 39.4° .

Fig. 26 presents the results of this pore-pressure control test on Sample 1. The value of pore pressure is automatically controlled by the servo-control system using the feedback signal from pore pressure sensor shown in Fig. 2.2.3 (D). The stress path moved to left direction as pore pressure increased until it reached the failure line. Then, the line dropped until the steady-state shear resistance was reached ($\tau_{ss} = 113$ kPa). The real effective stress acting on the sliding surface should be on the failure line after failure. So the pore pressure acting on the sliding surface and the pore pressure monitored by the pore-pressure sensor are different in the pore pressure control test. The time-series data of this test are shown in Fig. 26 (b). Pore pressure is steadily increased at a predetermined rate ($\Delta u = 1$ kPa/sec). At 1220 sec after the start of the test, shear displacement initiated, and simultaneously the shear resistance dropped and the pore pressure increased slightly. But the pore-pressure value was returned to the predetermined rate by the servo-control system. The tentative pore-pressure rise at the time of failure (Fig. 26 (b)(c)) suggested a volume reduction due to grain crushing. Thereafter, the shear resistance was maintained at a certain value shown in Fig. 26 (c). Pore pressure generated in the shear zone due to grain crushing in the shear zone should have dissipated. However, the shear

resistance exponentially decreased to the steady state from 1320 kPa to 113 kPa. During this period, the shear displacement increased from 1.5 m to 4.5 m. A pore-pressure controlled test is basically a drained test because pore water can move in or out of the shear box, as volume reduction due to grain crushing proceeds. A finite width of a less permeable silty layer formed by grain crushing can cause a difference between the pore-pressure value monitored by the pore-water pressure sensor and the pore pressure amongst the fine particles of the shear zone. That is, a high excess pore pressure builds up within the less permeable shear zone, while pore-water pressure outside maintains the value controlled by the pore-pressure servo-control system through the permeable sand sample beyond the shear zone. For comparison, the undrained monotonic shear-control test and the pore-pressure control test were conducted under the same normal stress (3 Mpa). Photos of shear zones in both tests are shown in Fig. 27.

This test result shows that this landslide mass could move rapidly even if it were triggered by a slow rate of pore-water rise during rain.

Another implemented test was a seismic loading ring-shear test to simulate initiation of the Mayuyama landslide by the combined effect of pore-water pressure and earthquake shaking. The Unzen Mayuyama landslide was triggered by a nearby earthquake; its magnitude has been estimated to be $M=6.4\pm 0.2$ (Usami 1996). Usami notes that the seismic intensity of this earthquake at Shimabara was around "V-VI?" The Unzen Restoration Office estimated that the seismic intensity which triggered the Mayuyama landslide was VII because more than 30 % houses were destroyed in the Shimabara area. The exact seismic acceleration is not known, but it may have been around 400 cm/sec^2 or greater.

The Japanese seismic intensities (Usami 1996) are:

V: $80\text{-}250 \text{ cm/sec}^2$ (where walls and fences are cracked and Japanese gravestones fall down)

- VI: 250-400 cm/sec² (where less than 30% of Japanese wooden houses are destroyed)
- VII: More than 400 cm/sec² (where more than 30 % houses are destroyed, landslides are triggered and faults rupture the ground surface).

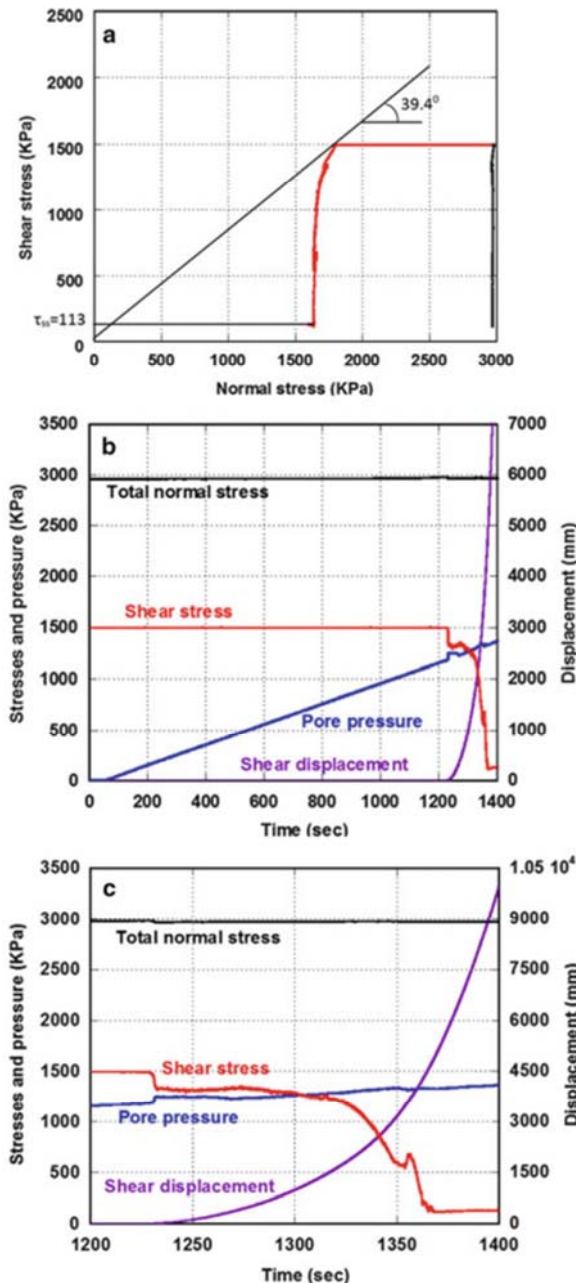


Fig. 26 Ring shear test result simulating the failure due to pore pressure increase (BD:0.98) (a) Stress path, (b) Time-series data of monitored stresses, (c) Time-series data around the failure

This earthquake was not recorded on a seismograph. We investigated recent landslide cases in Japan to find a similar earthquake record that could be used in landslide simulation. The 2008 Iwate-Miyagi Nairiku Earthquake ($M=7.2$) triggered the Aratozawa landslide (67 million cubic meters) in Miyagi Prefecture. The maximum recorded acceleration was 739.9 cm/sec² at MYG004 (National Research Institute for Earth

Science and Disaster, Prevention (NIED)). It would be similar to the earthquake which triggered the 1792 Unzen Mayuyama landslide and both earthquakes triggered megaslides. We used the Iwate-Miyagi earthquake wave form recorded in Miyagi Prefecture (MYG004) in the ring-shear test and the numerical simulation.

The adopted procedure of the ring shear test for this landslide was as follows.

Initially, the sample (S_1) was saturated ($B_D=0.94$) and consolidated to 3 MPa normal stress and 1.5 MPa shear stress. That is, the corresponding slope angle was $\arctan(1.5/3.0) = 26.6^\circ$. Then, pore-water pressure was increased up to 800 KPa (pore-water pressure ratio $r_u=800/3000=0.27$) as the initial slope condition (although the exact value was not known, but it must be smaller than 0.4). A preparatory test in Fig. 26 showed that $r_u=1.2/3.0=0.4$ was the critical pore water pressure which caused a landslide without an earthquake. As stated above, the earthquake which triggered the 1792 Unzen-Mayuyama landslide was estimated to be $M=6.4\pm 0.2$ with a Japanese Seismic intensity between VI (25-400 cm/sec²) and VII (more than 400 cm/sec²) during the earthquake. The maximum shaking was probably more than 400 cm/sec².

The maximum recorded seismic acceleration record of the 2008 Iwate-Miyagi earthquake was 739.9 cm/sec² which caused the Aratozawa landslide. We loaded the NS component 2008 Iwate-Miyagi earthquake record (maximum acceleration 739.9 cm/sec²) at MYG004 as the additional shear stress. For precise pore-pressure monitoring as well as servo-stress control, a 5-times slower speed of seismic acceleration record was applied. The test result is shown in Fig. 28 (a, b). Fig. 28 (a) presents the stress path and Fig. 28 (b) presents the time series data. The green line in the time-series data is the control signal. The maximum value is 2,469 KPa (1500+969 KPa) and the minimum value is 369 KPa (1500-1131). The loaded acceleration is calculated from the ratio of acceleration (a) and gravity (g): $a/g = 969/1500$ for positive acceleration or $a/g = -1131/1500$ for negative acceleration. The acceleration corresponds to $(969/1500) \times 980 = +633$ cm/sec² and $(-1131/1500) \times 980 = -739$ cm/sec². The control signal for shear stress given to the ring shear apparatus exactly corresponded to the monitored acceleration record.

As the figure shows, failure occurred around 1,825 KPa, at $a/g = (1825-1500)/1500=0.22$, the necessary acceleration at failure was 216 cm/sec². This test result suggested that around 1/3 smaller earthquake shaking (around $216/633 = 0.34$) than the Iwate-Miyagi earthquake could cause failure or the landslide could be triggered under a slope

condition with a pore pressure ratio of 0.27. The steady-state shear strength was 157 KPa. The

friction angle was 41.0° , slightly higher than that of the pore-pressure control test in Fig. 26 (39.4°).

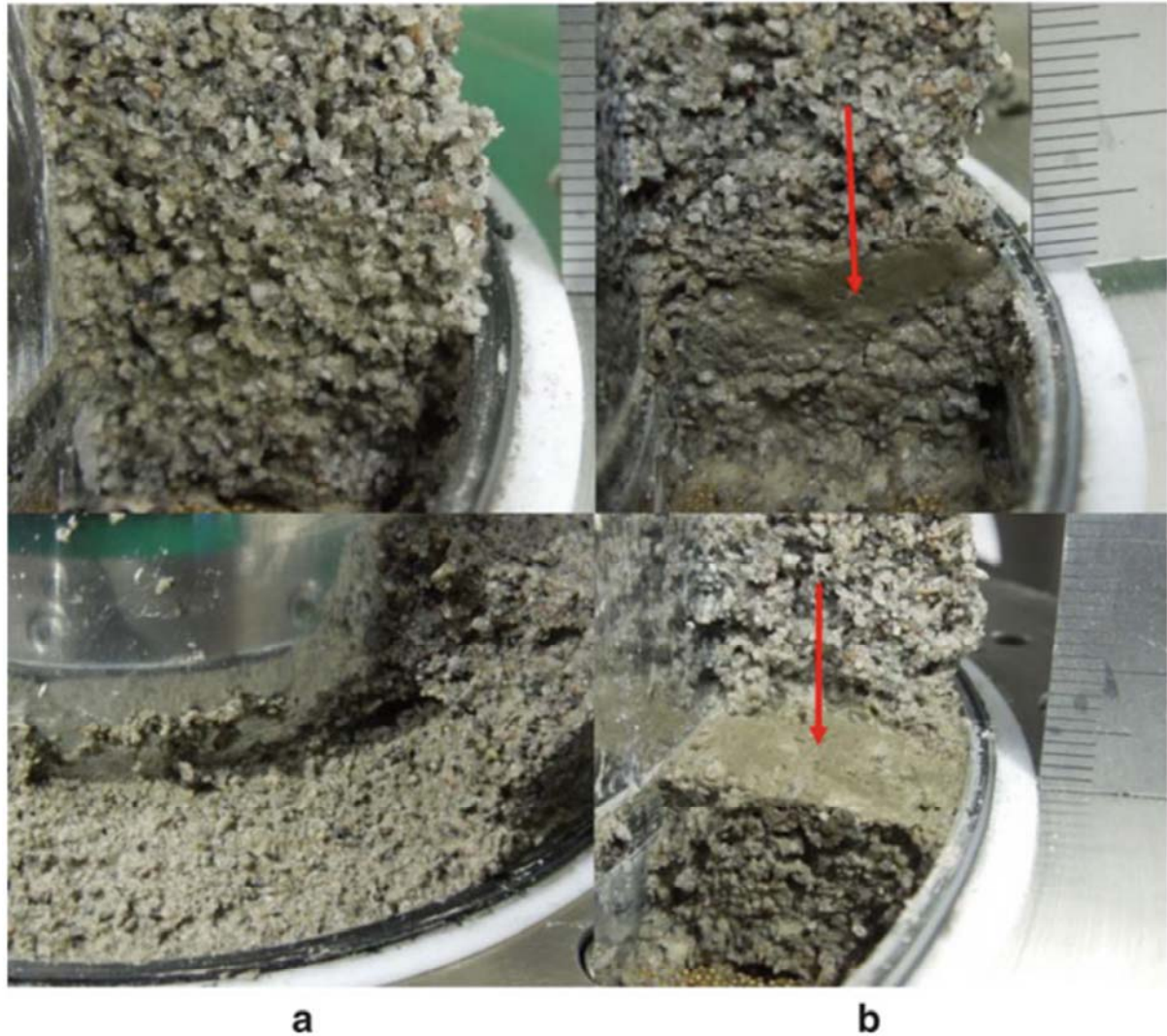


Fig. 27 Observation of shear zones in an undrained test and in a pore pressure control (drained) test Total normal stress: 3 MPa. (a) Photo of sample after the undrained monotonic shear stress control test. Any clear graincrushing shear zone was not observed (BD: 0.95). (b) Photo of the sample after the pore-pressure control test (BD: 0.99). A graincrushing silty shear zone was clearly observed (red arrow)

LS-RAPID was applied to the 1792 Unzen Mayuyama landslide. The simulation used the geotechnical parameters obtained in the ring-shear test on S₁ and S₂ and the earthquake record of the 2008 Iwate-Miyagi earthquake at MYG004. The parameters used were the following:

- 1) Steady-state shear resistance: 120 KPa in the landslide source area (deep soil layer), while 40-80 KPa in the landslide moving area (shallower soil layer) from the test results of normal stresses of 370 kPa, 1020 kPa, 1980 kPa (Sassa et al. 2014).
- 2) Friction angle during motion: 40° .
- 3) Peak friction angle: 42.0° . The maximum angle was 41.2° in this series of tests. However, the angle under field conditions can be greater.
- 4) Critical shear displacement for start of strength reduction (DL) and the start of steady state (DU)

were 6 mm and 90 mm from cyclic, monotonic and dynamic tests (Sassa et al. 2014).

5) Pore-pressure generation rate B_{ss} is 0.7-0.9 in the source area, and 0.99 under the sea (completely saturated). Outside of the landslide it was 0.2 as the ground was assumed to be unsaturated.

6) Lateral pressure ratio $k = 0.7-0.9$. We assumed 0.9 in the coastal area and under water. Outside of landslide was 0.4 assuming the ground was not saturated.

7) Unit weight of soils: 19.5 KN/m^3 .

The unit weight of soils at Unzen was not measured. To estimate it, we consolidated the sample (S₁) in the ring-shear apparatus in a saturated condition. The consolidation stress, sample height, dry unit weight and saturated unit

weight were measured (Sassa et al. 2014). The saturated unit weight can reach 21 KN/m³ at 3 MPa, but the dry unit weight was 19 KN/m³ at 3 MPa. Smaller values can exist in shallower area. We used one value for the whole area. We assumed this value to be 19.5 KN/m³.

The simulation results are presented in Fig. 29. At 11 sec, the pore water pressure reached 0.21 and the earthquake started, but no motion appeared. At 17 sec, the main shock of earthquake attached the area and the failure occurred within the slope. Failure started from the middle of slope. At 26 sec, the earthquake has almost terminated. The whole landslide mass was formed during the earthquake shaking. At 64 sec, the landslide mass continued to move after the earthquake and entered into the sea. At 226 sec, the landslide mass stopped to move and deposited.

The deposition area was compared with the figure made by topographic survey including the submarine state by the Unzen Restoration office (2002) (bottom-right of Fig. 29). Both landslide hazard areas are very similar. The section of line A in the right-bottom figure and the EW section (almost same with line A) of computer simulation were compared. Both travel distances from the headscarp of the initial landslide to the toe of the displaced landslide mass were also very close (about 6.0–6.5 km).

Significance and difficulties in Social implementation of the landslide dynamics

The World Landslide Forum (WLF) is a platform for scientists, engineers, practitioners and policy makers who are involved in landslide disaster risk reduction. It is not only a scientific and technical symposium. Please allow us to add the significance in the social implementation of the landslide dynamics and the difficulties to be solved as the background of this study.

The subtitle of WLF2 was “Putting Science into Practice”, the subtitle of WLF3 is “Landslide Risk Mitigation toward a Safer Geoenvironment”. Putting Science into Practice toward a Safer Geoenvironment is one of major objectives of WLF. The social implementation of the landslide dynamics is very important for this target. Sassa and his colleagues have focused on the development of landslide dynamics for its social implementation for landslide risk reduction as well as the basic science. The mechanism and dynamics of sliding-surface formation within a slope and its post-failure motion are not easy to explain and understand. Even strain is not defined in the shear zone. The material in the shear zone changes before the motion and during the motion

in terms of grain-size distribution (components of sands, silts, clays) and grain shape (angular, round). In addition, pore-pressure generation in the shear zone increases the difficulty of application of any universal theoretical analysis.

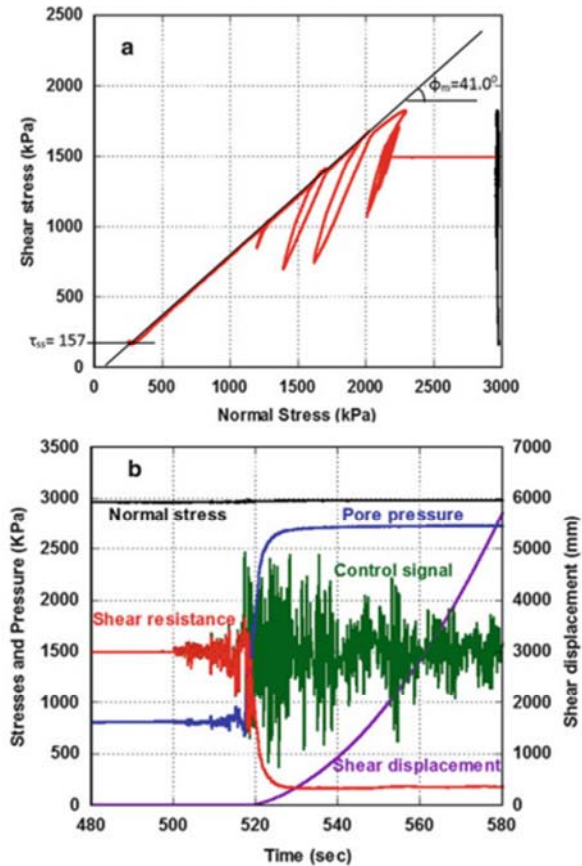


Fig. 28 Undrained ring shear test result simulating the failure due to pore pressure plus seismic loading using the 2008 Iwate Miyagi earthquake (BD: 0.94). (a) Stress path, (b) Time series data of monitored stresses, pore pressure and shear displacement as well as control signal

The most simple and practical method used for landslide risk assessment is to physically simulate the initiation and the motion of landslide by reproducing all of the stresses (gravity, pore-water pressure, seismic stress) on a sample taken from the field under a stress level the same as or similar to the field rather than a theoretical approach based on material science.

Among many soil mechanical tests, the ring-shear apparatus is one able to produce a sliding surface within a soil mass. Most ring-shear apparatus (Bishop et al 1971, Bromhead 1979, Sadrekrimi and Olson 2009) can shear samples at a certain speed. However, natural phenomena are controlled by the applied stress and stress-control apparatus are necessary to physical simulate natural sliding phenomenon. Then, efforts have been made to reproduce seismic stress loading by earthquakes, pore-pressure increase during rainwater infiltration, and dynamic loading on torrent deposits.

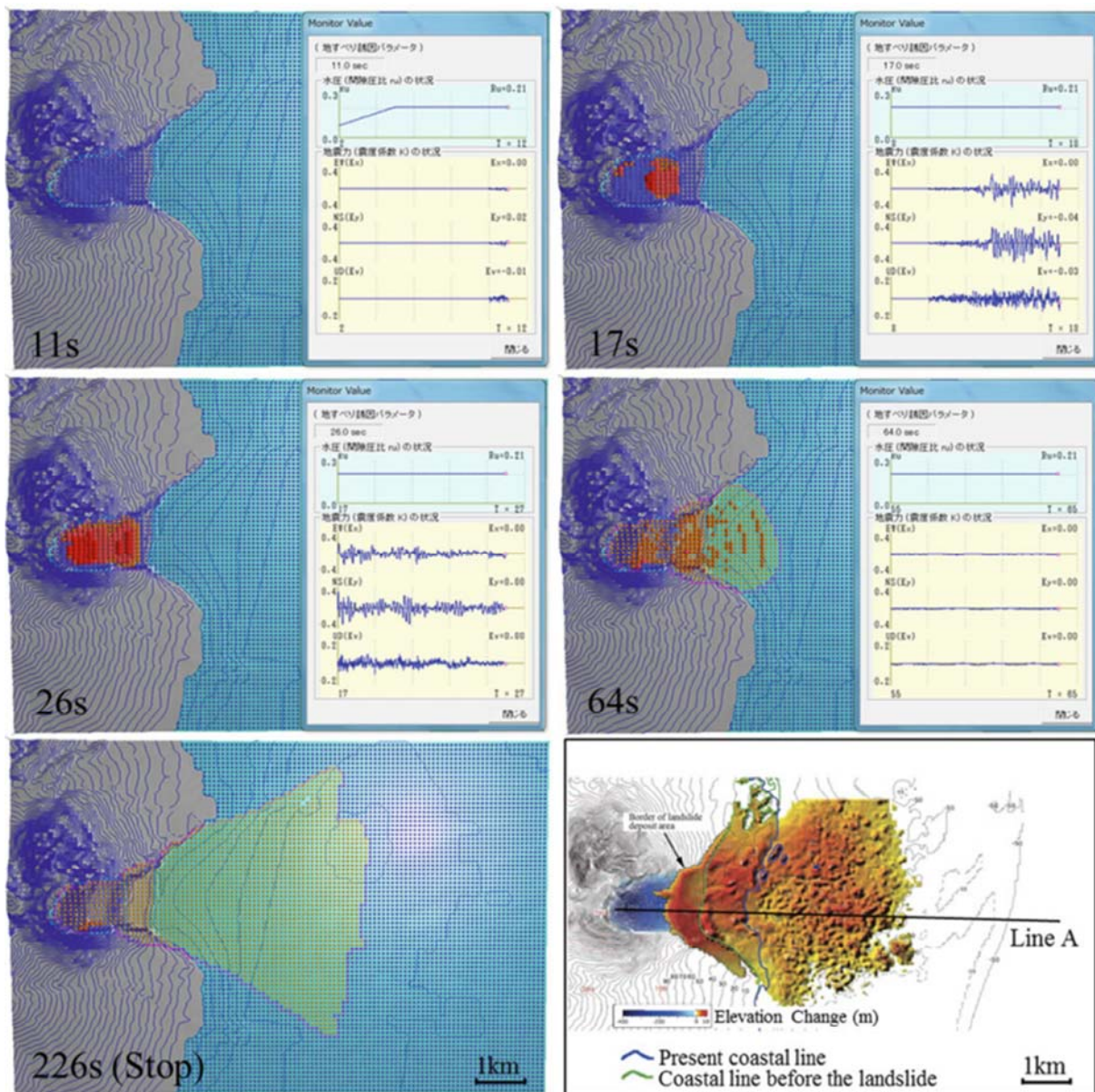


Fig. 29 Simulation result and topographic survey in the plan. Red color balls represent moving mass, while blue balls represent stable mass

Another important factor necessary for understanding landslide triggering and landslide dynamics is to measure pore-water pressure generated in the shear zone and the shear resistance mobilized on the shear surface during motion. Ring shear apparatus have a gap between the lower shear box and the upper shear box (Bishop et al 1971, Sassa et al. 2004 and others). Undrained conditions must be kept to measure pore-water pressure in the shear zone during motion (Maximum 5.4 cm/sec (ICL-1) to 300 cm/sec (DPRI-7) at the center of the sample) by preventing any leakage of water from the moving gap. Pore water pressure is desirable to be measured within or near the shear zone for understanding the mobilized shear resistance. Great effort has gone into solving these two tasks (Table 3 and the servo gap control system in Fig.6).

We believe that the current undrained dynamic loading ring-shear apparatus (landslide ring-shear apparatus) has been developed from a scientific tool to a practical tool for landslide risk assessment. However, further effort was needed to shift it from being a practical tool within Japan to being an internationally practical tool. Maintenance of the apparatus must be convenient, practical and inexpensive. A new programme known as the Science and Technology Research Partnership for Sustainable Development Program (SATREPS) of Japan has started since 2009 in cooperation with the Ministry of Education, Culture, Sports, Science and Technology (MEXT) and the Ministry of Foreign Affairs (MOFA) of Japan. The aim of this programme is to promote the application of Japanese science and technology to sustainable development in developing countries. ICL has obtained funding for two projects (for Croatia and

for Vietnam). During these projects, ICL has developed two types of undrained dynamic-loading ring-shear apparatus (ICL-1 for Croatia and ICL-2 for Vietnam). Those two apparatus were developed for use abroad by minimizing maintenance costs. ICL-1 was donated to Croatia in 2012 and it is well used at the University of Rijeka. The landslide ring-shear simulator is now an international practical tool as well as a scientific tool for landslide science.

The computer simulation for the initiation and the motion (LS-RAPID) has been developed from a scientific research code (initially Sassa 1988) to a user-friendly software used abroad (Sassa et al 2010) and further improvement through a SATREPS project. The English manuals for the undrained ring-shear apparatus (Ostic et al. 2013a, 2013b) and the computer simulation (LS-RAPID) (Sassa et al. 2013) were made as part of ICL Landslide Teaching Tools (He et al 2013, 2014). These manuals are available from <http://icl.iplhq.org/>.

Conclusion

- 1) A reliable and practical technology is needed to reduce landslide-disaster risk by assessing landslide initiation and motion including landslide velocity, moving area and area at landslide risk, and depth of soils.
- 2) Analyses of initiation and motion of landslide phenomena are complicated because of pore-pressure generation and changes of grain size, grain shape and water content of the involved soils in the shear zone due to grain crushing and mobilization.
- 3) Sassa and others together with the Disaster Prevention Research Institute, Kyoto University, and the International Consortium on Landslides have developed a series of ring-shear apparatus models from DPRI-1 to DPRI-7, ICL-1 and ICL-2.
- 4) The later series of apparatus developed after the 1995 Hyogoken Nambu earthquake can reproduce the sliding-surface formation and post-failure motion by cyclic loading/seismic loading and pore pressure increase within the apparatus.
- 5) The latest apparatus (ICL-1 and ICL-2 developed by SATREPS projects) increased undrained capacity from 500–630 kPa to 1 MPa (ICL-1) and 3 MPa (ICL-2) by changing the loading structure.
- 6) The purpose of SATREPS projects is that scientific research and technology developed in Japan can be applied for social implementation in developing countries, namely “Putting Science into Practice”
- 7) ICL-1 and ICL-2 were much improved from the previous DPRI series in manufacturing cost and maintenance in foreign countries. Improvements include the undrained sealing in the gap between the upper stable shear box and the lower rotatable shear box.
- 8) Key parameters in landslide dynamics including the steady-state shear resistance (τ_{ss}) and the critical shear displacement (D_L , D_U) and triggering factors of pore-water pressure and seismic records/waves are input to the integrated computer simulation model (LS-RAPID) simulating the initiation and the motion of the landslide. The simulation result can present the initiation from a local failure to formation of a landslide mass through progressive failure; and then present the initial motion of the landslide mass, entrainment of substrate deposits on the lower slopes and deposition with the cessation of motion.
- 9) Landslide dynamics is a scientific tool, but it is developing into a practical tool for landslide-disaster reduction in developed and developing countries alike with support from relevant institutions and colleagues.

Acknowledgments

The series of undrained dynamic-loading ring-shear apparatus have been supported by various funds from the Ministry of Education, Culture, Sports, Science and Technology of Japan (MEXT). The latest development of ring-shear apparatus models ICL-1 and ICL-2 and accompanied research have been financially supported by the Science and Technology Research Partnership for Sustainable Development Program (SATREPS) of Japan which are financed by the Japan Science and Technology Agency (JST) and the Japan International Cooperation Agency (JICA). Both are projects of the International Programme on Landslides (IPL): IPL-161 Risk identification and land-use planning for disaster mitigation of landslides and floods in Croatia and IPL-175: Development of landslide-risk assessment technology and education in Vietnam and other areas in the Greater Mekong Sub-region. We have obtained much support from ICL and ICL supporting organizations through these two projects. Development of LS-RAPID and currently developing “ICL Landslide Teaching Tools” which is an international joint activity are very important elements for the development of Landslide Dynamics as practical tools. Prof. Zeljiko Arabanas of Lijeka University, Croatian leader of the landslide group in IPL-161 and the user of ICL-1 donated to Croatia, is appreciated for his discussion on this paper. The promotion of these IPL projects by colleagues from ICL and ICL supporting members is very much appreciated.

References

- Bishop AW, Green GE, Garga VK, Andersen A, Brown JD (1971) A new ring-shear apparatus and its application to the measurement of residual strength. *Géotechnique* 21(1):273–328
- Bromhead EN (1979) A simple ring-shear apparatus. *Ground Eng* 12(5):40–44
- Cabinet Office of the Government of Japan (Committee on megaquake model in Nankai Trough) (2011) Intermediate report of the study team for the Megaquake model in Nankai trough. http://www.bousai.go.jp/jishin/chubou/nankai_trough/chukan_matome.pdf
- Cabinet office of the Government of Japan (Committee on Megaquake Model in Nankai Trough) (2012) The tsunami-fault model in the 2011 off the Pacific Coast of 2011 Tohoku Earthquake, Reference No. 1 of the 12th Meeting of Megaquake Model in Nankai Trough. http://www.bousai.go.jp/jishin/chubou/nankai_trough/12/sub_1.pdf
- Catane SG, Cabria HB, Tomarong CP, Saturay RM, Zarco MA, Pioquinto WC (2007) Catastrophic rockslide-debris avalanche at St. Bernard, Southern Leyte, Philippines. *Landslides* 4(1):85–90
- Expedition 333 Scientists (2012) Site C0018. In: Henry P, Kanamatsu T, Moe K, and the Expedition 333 Scientists, Proc. IODP, 333: Tokyo (Integrated Ocean Drilling Program Management International, Inc.). DOI:10.2204/iodp.proc.333.103.2012
- Hayashida A, Kamata H, Danhara T (1996) Correlation of widespread tephra deposits based on paleomagnetic directions: link between a volcanic field and sedimentary sequences in Japan. *Quat Int* 34–36:89–98
- He B, Sassa K, Ostric M, Takara K, Yamashiki Y. (2013). Effects of Parameters in Landslide Simulation Model LS-RAPID on the Dynamic Behaviour of Earthquake-Induced Rapid Landslides. In *Landslide Science and Practice* (pp. 119-125). Springer Berlin Heidelberg.
- He B, Sassa K, McSaveney M, Nagai O. (2014) Development of ICL Landslide Teaching Tools. *Landslides*. (Accepted, in press).
- Inoue K (1999) Shimabara-Shigatusaku Earthquake and topographic changes by Shimabara catastrophe. *Journal of Japan Society of Erosion Control Engineering* 52(4):45-54.
- Inoue K (2000) Shimabara-Shigatusaku earthquake and topographic change by Shimabara Catastrophe in 1792. *Geographical Reports of Tokyo Metropolitan University*, No. 35:59-69.
- Locat J, Lee H (2008) Submarine mass movement and their consequences: an over view. In: Sassa K, Canuti P (eds) *Landslides—disaster risk reduction*. Springer, New York: 115–142
- Okada Y, Sassa K, Fukuoka H (2000) Liquefaction and the steady state of weathered granite sands obtained by undrained ring shear tests: a fundamental study on the mechanism of liquidized landslides. *J Nat Disaster Sci* 22(2):75–85
- Ostric M, Sassa K, Ljutic K, Vivoda M, He B, Takara K (2013a) PDF-tool 3.081-1.1 Manual for ICL-1 – a Transportable Ring Shear Apparatus. ICL Landslide Teaching tools, p.362 and pdf (46 pages) in the attached CD.
- Ostric M, Sassa K, He B, Takara K, Yamashiki Y. (2013b). Portable Ring Shear Apparatus and Its Application. In *Landslide Science and Practice* (pp. 365-369). Springer Berlin Heidelberg.
- Sadrekarami, A., and Olson, S. M., 2009, “A new ring shear device to measure the large displacement shearing behavior of sands.” *Geotech. Test. J*, Vol 32, No 3: 197–208
- Sassa K (1984) The mechanism starting liquefied landslides and debris flows. *Proc. 4th International Symposium on Landslides*, Vol 2: 349-354
- Sassa K (1988) Geotechnical model for the motion of landslides. Special Lecture of 5th International Symposium on Landslides, “Landslides”, Balkema, Vol 1: 37–55
- Sassa K (1992) Access to the dynamics of landslides during earthquakes by a new cyclic loading high-speed ring-shear apparatus. 6th International Symposium on Landslides, “Landslides”, Balkema, Vol 3:1919-1937
- Sassa K (1996) Prediction of earthquake induced landslides. *Proceedings of 7th International Symposium on Landslides*. A.A. Balkema. Trondheim, 17–21 June, vol 1, pp 115–132
- Sassa K (2000) Mechanism of flows in granular soils. *Proceedings of GeoEng2000*, Melbourne. vol 1, pp 1671–1702
- Sassa K, Fukuoka H, Scarascia-Mugnozza G, Evans S (1996) Earthquake-induced landslides: distribution, motion and mechanisms. *Soils & Foundations*, Special Issue for the Great Hanshin Earthquake Disaster, pp 53–64
- Sassa K, Fukuoka H, Wang FW (1997) Mechanism and risk assessment of landslide- triggered-debris flows: lesson from the 1996.12.6 Otari debris flow disaster, Nagano, Japan. In: Cruden DM, Fell R (eds) *Landslide Risk Assessment*, *Proceedings of the international workshop on landslide risk assessment*. Honolulu, 19–21 February, pp 347–356
- Sassa K, Fukuoka H, Wang G, Ishikawa N (2004) Undrained dynamic-loading ring-shear apparatus and its application to landslide dynamics. *Landslides* 1(1):7–19
- Sassa K, Fukuoka H, Wang FW, Wang GH (2005) Dynamic properties of earthquake-induced large-scale rapid landslides within past landslide mass. *Landslides* 2 (2): 125-134.
- Sassa K, Fukuoka H, Wang FW, Wang GH (2007) Landslides induced by a combined effects of earthquake and rainfall. *Progress in Landslide Science* (Editors: Sassa , Fukuoka, Wang, Wang), Springer, Berlin. pp 311–325
- Sassa K , He B, Miyagi T, Strasser M, Konagai K, Ostric M, Setiawan H, Takara K, Nagai O, Yamashiki Y and Tutumi S (2012) A hypothesis of the Senoumi submarine megaslide in Suruga Bay in Japan—based on the undrained dynamic-loading ring-shear tests and computer simulation. *Landslides* 9 (4):439-455.
- Sassa K, He B, Dang K, Nagai O, Takara K (2014) Plenary: Progress in Landslide Dynamics. *Landslide Science for a Safer Geoenvironment*, *Proceedings of the Third World Landslide Forum*, Springer, Vol.1, pp.37-67.
- Sassa K, Nagai O, Solidum R, Yamazaki Y, Ohta H (2010) An integrated model simulating the initiation and motion of earthquake and rain induced rapid landslides and its application to the 2006 Leyte landslide. *Landslides* 7 (3):219–236
- Sassa K, Nagai O, He B, Gradiski K (2013) PDF-tool 3.081-1.2 Manual for the LS-RAPID software. ICL Landslide Teaching tools, p. 363, 43 pages (pdf) in the attached CD.

- Sassa K, Dang K.Q., He B, Takara K, Inoue K, Nagai O (2014). Development of a new high-stress undrained ring shear apparatus and its application to the 1792 Unzen-Mayuyama megaslide in Japan. (contributed to landslides in 2013)
- Strasser M, Henry P, Kanamatsu T, Thu M, Moore G, IODP Expedition Scientists (2012) Scientific drilling of mass-transport deposits in the Nankai accretionary wedge: first result of from IODP Expedition 333. Submarine mass movements and their consequences, *Advances in Natural and Technological Hazards Research* 31 (eds. Yamada et al.). New York: Springer, 671–681
- Trandafir A, Sassa K (2005) Seismic triggering of catastrophic failures on shear surfaces in saturated cohesionless soils. *Can Geotech J* 42:229–251
- Unzen Restoration Office of the Ministry of Land, Infrastructure and Transport of Japan (2002). The Catastrophe in Shimabara -1791-92 eruption of Unzen-Fugendake and the sector collapse of Mayu-Yama. An English leaflet (23 pages).
- Unzen Restoration Office of the Ministry of Land, Infrastructure and Transport of Japan (2003). The Catastrophe in Shimabara -1791-92 eruption of Unzen-Fugendake and the sector collapse of Mayu-Yama. A Japanese leaflet (44 pages).
- Usami T (1996) Materials for comprehensive list of destructive earthquakes in Japan. University of Tokyo Press



Proceedings of the SATREPS Workshop on Landslides in Vietnam, 2014

Recent Development of the New High Stress Undrained Ring Shear Apparatus (ICL-2) and its Application

Lam Huu Quang⁽¹⁾, Dang Quang Khang⁽²⁾, Pham Van Tien⁽¹⁾, Doan Huy Loi⁽¹⁾, Nguyen Kim Thanh⁽¹⁾

1) Institute of Transport Science and Technology, Hanoi, Vietnam, e-mail: lhqlinh@yahoo.com

2) Kyoto University, Kyoto, Japan, e-mail: khangdq@gmail.com

Abstract The design and construction of a new high stress undrained ring shear apparatus (ICL-2), which has been newly developed at Kyoto University and will be donated by Japanese government for analyses of landslides in Vietnam, are presented in detail. This apparatus is suited for undrained shear tests under all types of loading, and enables observing the undrained shear behaviour of soils in high stress undrained capability up to 3 MPa (100-300 m deep landslides can be simulated); at high speed motion (maximum shear speed 50 m/s) to an unlimited shear displacement. The ring shear apparatus has provided a new practical tool for landslide hazard assessment not only in Vietnam but also in over the world.

Keywords Speed control test, cyclic stress control test, ring shear apparatus, landslide

Introduction

Based on the agreed minutes of meetings on the Detailed Planning Survey on the project for Development of Landslide Risk Assessment Technology along Transport Arteries in Viet Nam signed on July 27, 2011 between Institute of Transport Science and Technology (hereinafter referred to as "ITST") of Ministry of Transport of the Socialist Republic of Viet Nam (hereinafter referred to as "MOT") and the Japan International Cooperation Agency (hereinafter referred to as "JICA"), JICA held a series of discussions with MOT and relevant organizations to develop a detailed plan of the Project. Both parties agreed the detail plan of the Project and the main points discussed. Both parties also agreed that MOT, the counterpart to JICA, will be responsible for the implementation of the Project in cooperation with JICA, coordinate with other relevant organizations and ensure that the self-reliant

operation of the Project is sustained during and after the implementation period in order to contribute toward social and economic development of Viet Nam. This project is to contribute to geo-disaster reduction along main transport arteries and on residential areas through development of new landslide risk assessment technology and its application to forecast, monitoring and disaster preparedness of landslides in Viet Nam in close cooperation between Japanese and Vietnamese organizations concerned. The project's activities are divided into 4 groups: (WG1) Preparation of integrated guidelines for the application of developed landslide risk assessment technology; (WG2) Wide-area landslide mapping and identification of landslide risk area; (WG3) Development of landslide risk assessment technology based on soil testing and computer simulation; (WG4) Risk evaluation and development of early warning system based on landslide monitoring.

Activity of WG3 outputs include: (1) Development of undrained dynamic-loading ring shear apparatus; (2) Elucidation of the initiation mechanism and the dynamics of post-failure motion of the targeted landslides; (3) Development of hazard assessment technology of the precursor stage of landslides. The system of laboratory equipment consist a new high stress undrained ring shear apparatus, funded by the Japanese government to serve the research landslides in Vietnam. Research areas are (1) Ho Chi Minh Road (between ALuoi town and Lo Xo Pass); (2) National Highway 1A (between Hue and Da Nang); (3) National railway (between Hue and Da Nang). For Hai Van Pass station on National railway, the project will install monitoring equipment and drill the soil sample for laboratory test on ring shear apparatus. The drilling depth is about 120m.

To research the deep landslide, a new high stress undrained ring shear apparatus has been newly developed by the International Consortium on Landslides from 2012-2014. This paper introduces the outline of the apparatus and its application to the 1792 Unzen-Mayuyama landslide from Sassa et al. (2014). In 2015, this ring shear apparatus will be donated by Japanese government for analyses of landslides in Vietnam (Fig. 1). This apparatus is suited for undrained shear tests under all types of loading, and enables observing the undrained shear behaviour of soils in high stress undrained capability up to 3 MPa (100-300 m deep landslides can be simulated); at high speed motion (maximum shear speed 50 m/s) to an unlimited shear displacement.



Figure 1 General View of ICL-2

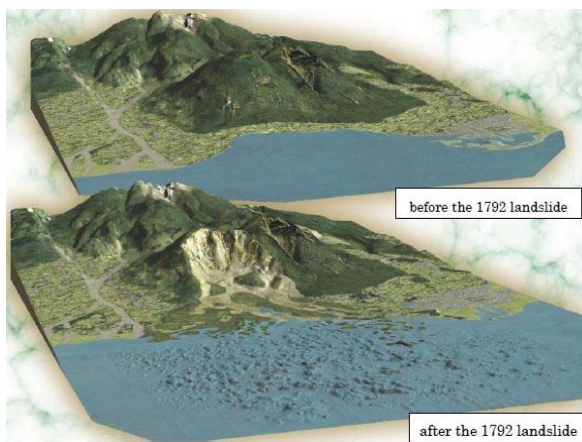


Figure 2 Unzen-Mayuyama landslide

To check the capability of the equipment to simulate the behaviour of deep landslides, the samples, taken from the sliding surface of the 1792 Unzen earthquakes of Japan, are tested. The 1792 Unzen earthquake and tsunami resulted from the volcanic activities of Mount Unzen (in the Shimabara Peninsula of Nagasaki Prefecture, Japan) on 21 May. This caused the collapse of the southern flank of the Mayuyama dome in front of Mount Unzen, resulting in a tremendous tsunami, killing 15,000 people altogether (Figure 2). This paper will present the concept, design testing procedure and test results of ring shear apparatus, ICL-2. Based on the capacity of the ring shear apparatus, ICL-2 continuously is used for research

landslide of Hai Van Pass station and landslide areas along transport arteries in Viet Nam.

Test Program

Ring Shear Apparatus

Ring shear apparatus has been widely used in the slope stability analysis, because the device can simulate landslide with unlimited shear displacement cutting unlimited transfer (Bishop, 1971, Sassa, 2004). Sassa and colleagues have developed a series of ring shear apparatus since 1984. Most recently, a new high stress undrained ring shear apparatus, ICL-2, designed by Sassa professor at Kyoto University. Although the dimension of ICL is smaller than previous generation (DPRI1-7), ICL-2 has high performance (Table 1). The volume of shear box is 300 cm³. The shear box is smaller than the previous DPRI versions. Therefore, ICL-2 is also suitable for testing in laboratory when the drilling samples are limited. Table 1 introduces the main parameters of ICL-2, compare with the previous version of the apparatus that were developed by Professor Sassa and colleagues at DPRI, Kyoto University.

In order to easily transport with long distance, ICL-2 is more compact than the previous version (DPRI 1-7). ICL-1 can maintain undrained condition up to 3000 kPa of pore water pressure. While the undrained condition was possible up to 400-600 kPa of pore water pressure in DPRI (Table 1). This special design allows simulating the large scale and deep landslide phenomenon.

The most important part of undrained ring shear apparatus is the shear box. The design of the shear box was introduced in Fig. 3. With an enlarged diagram of the left half of the cross section of the undrained shear box and its surroundings, including the water pressure measurement system.

The most difficult part of shear box is prevention of leakage of water through the gap between the upper shear box and the lower shear box during high-speed shearing (50 cm/s). This was perfected for ICL-2. A material with strong abrasion resistance, low friction characteristics and good performance as a sealant had to be found. Sassa tried various types and shapes of rubber edges, Teflon plates, and combined layers of Teflon plate underlain by rubber plate. The final selection was a stair-shaped rubber ring as shown in Fig. 3. Before each test, the rubber edges were covered with a friction coat of Teflon, and shear box surfaces were daubed with vacuum silicon grease. During the test, a certain amount of compression is applied between the upper pair of rings and the rubber edges by lowering the gap control oil piston to a specific value (hereinafter

termed as Gap Value). The lower half of shear box rotates while the shear box is retained by two load cell that measure the shear resistance. To maintain the undrained condition, contact pressure between the rubber edges and the upper pair of rings should be kept greater than the generated pore pressure in the sample. Then, during the test, an effort is made to keep this compression force constant by maintaining the Gap Value as constant as possible by an oil piston, using the feed-back signal obtained from a gap sensor with a precision of 1/1,000 mm.

Pore pressure generated in the shear zone is monitored by the pore pressure transducers P (Fig. 3). The pore pressure transducers are connected to a gutter extending around the whole circumference of the inner wall of the outer and upper ring. The gutter is covered by two metal filters and a felt cloth filter and located 3mm above the shear surface. This system is quite durable in regard to shearing and is sensitive to pore pressure monitoring, although the monitoring point is not at the center of the shear zone.

Table 1 Features of new Ring Shear Apparatus, ICL-2, compared with the previous versions

Author	Sassa (1992) DPRI-3	Sassa -1996 DPRI-4	Sassa -1997 DPRI-5	Sassa -1997 DPRI-6	Sassa -2004 DPRI-7	Sassa -2011 ICL-1	Sassa -2014 ICL-2
Inner diameter (cm)	21	21	12	25	27	10	10
Outer diameter (cm)	31	29	18	35	35	14	14.2
Max. height of sample (cm)	9	9.5	11.5	15	11.5	5.2	5.2
Shear area (cm ²)	408.41	314.16	141.37	471.24	389.56	75.36	79.79
Max. shear speed (cm/sec)	30	18	10	224	300	5.4	50
Max. normal stress (kPa)	500	3,000	2,000	3,000	500	1000	3000
Max. pore water pressure (kPa)	-	490	400-600	400-600	400-600	1000	3000

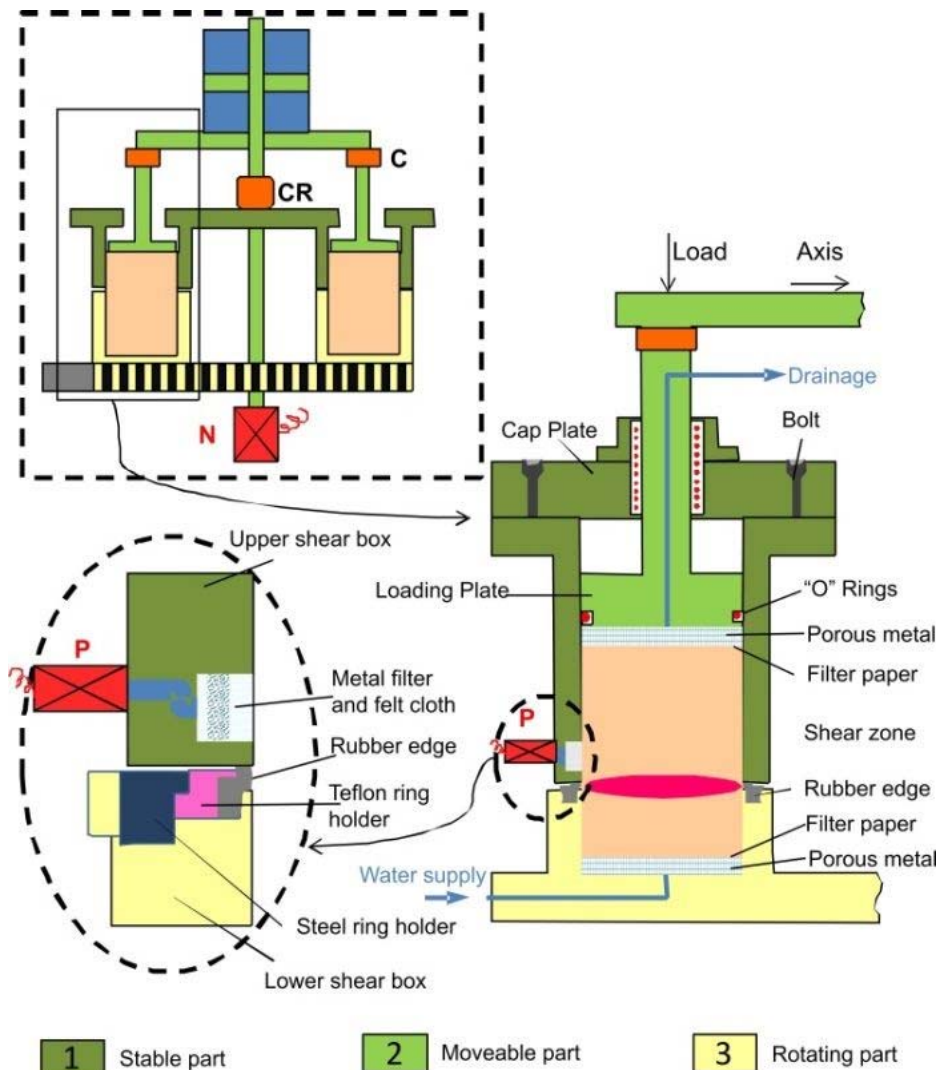


Figure 3 A half section of the shear box and the close-up diagram of the edges

Testing procedure

The testing procedure consists of the following: gap adjustment, sample saturation, sample consolidation and loading (by shear speed control; stress control – either cyclic or seismic loading).

First, the gap value should be adjusted to avoid leakage of water and sample, by applying vertical load of 1.5 kN. Then, during the test, it is kept constant during the test by an oil piston. Shear box without sample is filled with CO₂ and de-aired water. Then, sample that was saturated by de- aired water during night could be slowly placed in shear box. After that, the water circulation could start to enable full water saturation of the sample. De-aired water was slowly supplied through the lower drainage line, and discharged from the upper drainage line until all air bubbles were expelled.

The degree of saturation was checked by using B_D . B_D is a pore pressure parameter, related to the degree of saturation in the direct-shear state, that was proposed by Sassa (1988), and is formulated as:

The saturation of sample was then checked by measuring B_D value that for fully saturated samples should be greater than 0.95. B_D is a pore pressure parameter in direct shear state, related to the degree of saturation that was proposed by Sassa (1988), and is formulated as:

$$B_D = \Delta u / \Delta \sigma \quad (1)$$

Where Δu and $\Delta \sigma$ are increments of pore pressure and normal stress, respectively.

For Unzen samples, we already prepared with $B_D = 0.95-0.97$. It means that the samples were fully saturated.

After sample was fully saturated, the initial stress state of soils only due to gravity should be created. So, the sample was normally consolidated under normal and shear stress, depending on the sample depth and slope angle. After the consolidation, shearing is applied by stress control mode (cyclic test) or speed control test.

Change of mobilized shear resistance is measured by two load cells. Pore pressure, resulting shear displacement, and shear speed are also monitored. The shear resistance mobilized during shearing is obtained by subtracting the rubber-edge friction from the monitored shear resistance. This friction is not constant. However, the difference is the order of 1 kPa; thus, for practical purposes, friction can be regarded as constant throughout the test. The smaller rubber-edge friction is preferable. Therefore, in each test, a minimum gap pressure at which water leakage proof is ensured is checked and used.

Test Program

This paper presents experimental results of: Drained shear speed control test, undrained shear stress control, pore water pressure control test, cyclic stress control test, undrained pore water pressure and seismic loading test. The samples were taken from the landslide surface of the 1792 Unzen earthquakes in Japan.

Drained shear speed control test

The drained shear is best method to determine the friction angle under and test the ability of the device when not consider the influence of pore water pressure. Drained shear speed control is basic. The experiment was performed with the saturation of sample $B_D = 0.97$. When normal stress close to 3MPa, the sample was shear at 0.2cm/sec in drained conditions. After the shear stress was reached to the maximum shear resistance, the drained normal stress was reduced to zero at a rate of $\Delta \sigma = 5$ kPa/sec to obtain drained stress path and friction angle of the sample (Fig. 4). The maximum friction angle was 39.1°, and the friction angle during motion was 35.9°. The stress path and the friction angles were reasonable for the nature of the sample. The result of drained speed-controlled test indicated that the ICL-2 could successfully test even under the very high normal stress of 3 MPa.

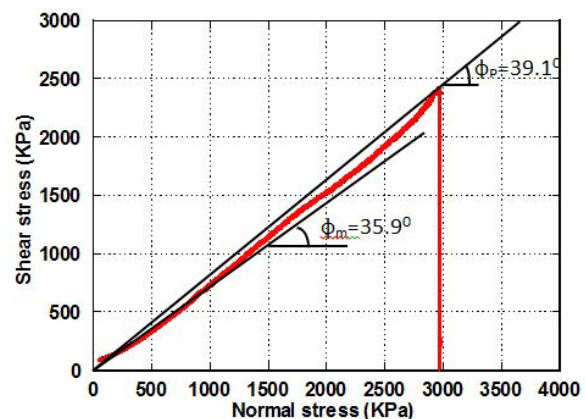


Figure 4 Drained shear speed control test

Undrained shear stress control test

After consolidation of the sample (by applying normal stress of 3,000 kPa), the shear box was changed to the undrained condition, and shear stress was loaded gradually at a rate of $\Delta \tau = 5$ kPa/sec. Samples were sheared until steady state obtained. In undrained conditions, the pore water pressure will increase during testing and the effective stress path closed to failure line. When the effective stress path reached the failure line, it began to decrease due to pore-pressure

generation along the failure line until the steady-state shear resistance reached. In Fig. 5, the red line was an effective path, the black line was the total stress path. From the graph we can determine the value of the friction angle was 40.3° and the steady-state shear resistance was 120kPa.

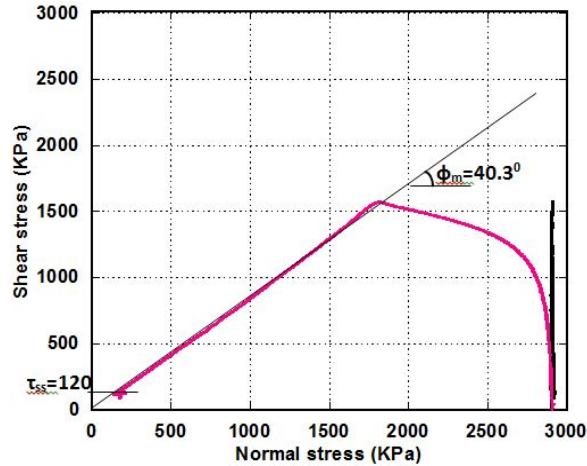


Figure 5 Undrained shear stress control test

Pore water pressure control test

Pore water pressure control test is most appropriate experiments to simulate the effects of rain to phenomenon. First, the sample was saturated (BD = 0.98) and consolidated close to 3 MPa and then sheared with 1.5MPa in undrained condition. Initial stress state corresponded to the slope of tangent ($\sigma_1/\sigma_3/30$) = 26.5° .

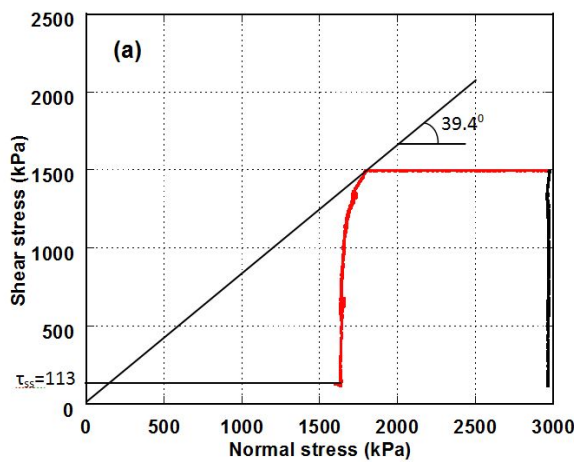


Figure 6 Pore water pressure control test

This is approximate the actual slope of landslide blocks (about 28°). To simulate the effects of pore waterpressure caused landslides phenomena, the pore water pressure increased with speed 5kPa/sec, In Figure 6, friction angle was 39.4° . Failure occurred when the pore water pressure increased up to 1.2MPa

Undrained pore water pressure and seismic loading test

Undrained pore water pressure and seismic loading test is the most important experiment. This experiment considering the impact of rain at the same time when earthquake occurred to landslide phenomenon. The saturated sample was consolidated close to 3 MPa and then sheared with 1.5MPa in undrained condition. To simulate the effects of rain water, pore water pressure was increased up to 800kPa kPa (a pore water pressure ratio $r_u=800/3000=0.27$). The earthquake which triggered the 1792 Unzen-Mayuyama landslide was estimated to be Magnitude $M=6.4\pm 0.2$, with a seismic intensity of VII during the earthquake; in the Japanese standard. Fig. 7 shows that the failure occurred around 1,825 kPa. This test result suggested that this earthquake shaking could have caused failure under a slope condition with a pore-pressure ratio of 0.27. The steady-state shear strength was 157 kPa

Summary and Conclusions

To research the deep landslide, a new high stress undrained ring shear apparatus has been newly developed at Kyoto University from 2012-2014. In 2015, this ring shear apparatus will be donated by Japanese government for analyses of landslides in Vietnam. This paper has presented the design testing procedure and test results of ring shear apparatus, ICL-2. This apparatus is suited for undrained shear tests under all types of loading, and enables observing the undrained shear behaviour of soils in high stress undrained capability up to 3 MPa (100-300 m deep landslides can be simulated); at high speed motion (maximum shear speed 50 m/s) to an unlimited shear displacement.

To check the capability of the equipment to simulate the behaviour of deep landslides, the samples, taken from the sliding surface of the 1792 Unzen earthquakes of Japan, are tested. This paper presents experimental results of: Drained shear speed control test, undrained shear stress control, pore water pressure control test, cyclic stress control test, undrained pore water pressure and seismic loading test. Typical test results are presented to show the efficiency of this ring shear apparatus. The result of these test indicated that the ICL-2 could successfully test even under the very high normal stress of 3 MPa. The ring shear apparatus has provided a new practical tool for landslide hazard assessment not only in Vietnam but also in over the world. ICL-2 continuously is used for research landslide of Hai Van Pass station and landslide areas along transport arteries in Viet Nam.

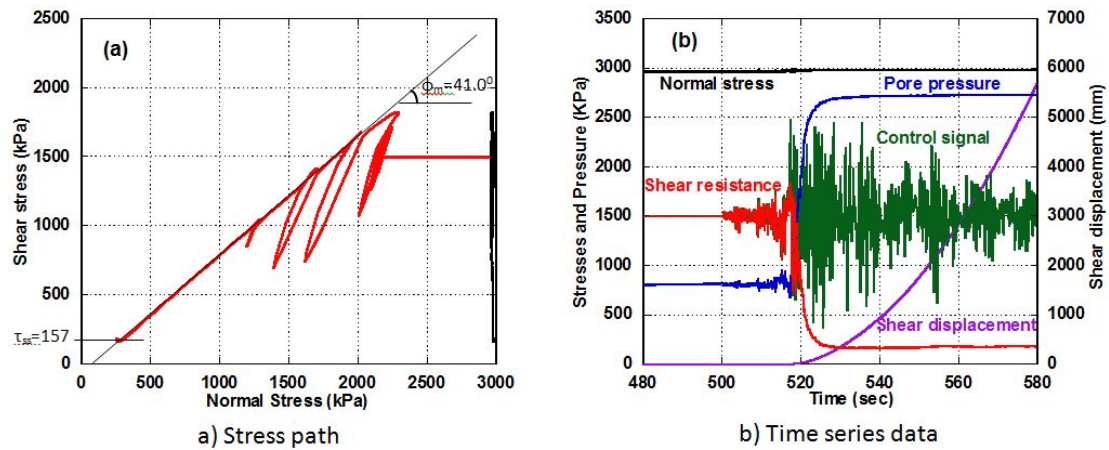


Figure 7 Undrained pore water pressure and seismic loading test

Acknowledgments

The design and construction of the ring shear apparatus ICL-2, was conducted under the support of SATREPS (Science and Technology Research Partnership for Sustainable Development) programme of the Government of Japan. This research is a part of the project for Development of Landslide Risk Assessment Technology along Transport Arteries in Viet Nam signed on July 27, 2011 between ITST of MOT Vietnam and JICA.

References

Bishop AW, Green GE, Garge VK, Andersen A, Brown JD (1971) A new ring shear apparatus and its application to the measurement of residual strength. *Geotechnique* 21:273–328

Sassa K (1996) Prediction of earthquake induced landslides. In: *Proceedings of 7th international symposium on landslides*, A.A. Balkema, Rotterdam, vol 1, pp 115–132

Sassa K, Fukuoka H, Wang G, Ishikawa N (2004a) Undrained dynamic-loading ring-shear apparatus and its application to landslidedynamics. *Landslides* 1(1):7–19

Sassa K, Wang G, Fukuoka H, Wang FW, Ochiai T, Sugiyama M, Sekiguchi T (2004b) Landslide risk evaluation and hazard mapping for rapid and long-travel landslides in urban development areas. *Landslides* 1(3):221–235

Sassa K, Fukuoka H, Wang FW, Wang GH (2007) Landslides induced by a combined effects of earthquake and rainfall. In: Sassa K, Fukuoka H, Wang FW, Wang GH (eds) *Progress in landslide science*. Springer, Berlin, pp 311–325

Kyoji Sassa, Khang Dang, Bin He, Kaoru Takara, Kimio Inoue, Osamu Nagai (2014) A new high-stress undrained ring-shear apparatus and its application to the 1792 Unzen–Mayuyama megaslide in Japan. *Landslides*, published online (DOI 10.1007/s10346-014-0501-1)

Tika THE, Hutchinson JN (1999) Ring shear tests on soil from the Vaiont landslide slip surface. *Geotechnique* 49:59–74



Proceedings of the SATREPS Workshop on Landslides in Vietnam, 2014

Simulation of a rapid and long-travelling landslide using 2D-RAPID and LS-RAPID 3D Models

Bin He⁽¹⁾, Kyoji Sassa⁽²⁾, Osamu Nagai⁽²⁾, Takara Kaoru⁽³⁾

1) Key Laboratory of Watershed Geographic Sciences, Nanjing Institute of Geography and Limnology, Chinese Academy of Sciences, China; e-mail: hebin@niglas.ac.cn

2) International Consortium on Landslides, Kyoto, Japan; e-mail: sassa@iclhq.org

3) Disaster Prevention Research Institute, Kyoto University, Japan; e-mail: takara.kaoru.7v@kyoto-u.ac.jp

Abstract In this study, two process-based computer numerical models for simulating the generation and propagation of landslide are developed by integrating the initiation process triggered by rainfalls and/or earthquakes and the development process to a rapid motion due to strength reduction and the entrainment of deposits in the runout path. Among them, the 2D-RAPID model is a two dimensional model and LS-RAPID 3D Model is a three dimensional model. Both of them were developed from the geotechnical model for the motion of landslides and its improved simulation model and new knowledge obtained from a new dynamic loading ring shear apparatus. The aim of this study is to validate and compare these two models. For this purpose, the two models were applied in a rapid and long-traveling landslide, which occurred on 17 February 2006 in the southern part of Leyte Island, Philippines and caused 154 confirmed fatalities, and with an additional 990 people missing in the debris. For comparison, all the parameters used in the 2D landslide model are using the same values used in the 3D landslide model. As simulation results, the application of these two simulation models could reproduce well the initiation and the rapid long runout motion of the Leyte landslide. However, for the deposition area, the 2D landslide model resulted in a higher and narrower mass volume than the 3D landslide model. Moreover, the 2D-RAPID shows a simple process to handle the input and output database, which is easily understood and can be used in engineering application. In addition, the LS-RAPID 3D Model shows an excellent interface for rainfall or/and earthquake induced landslide with spatially distributed complex topographic data. The distributional information of soil parameter can be set and the 3D view of the calculated landslide initiation and runout can be successfully achieved in LS-RAPID 3D Model. Thus, each of

these different dimensional landslide models has its respective advantages and disadvantages depending on the target study area and the type of the area.

Keywords Landslide, simulation, LS-RAPID model, 2D-RAPID model, rainfall, earthquake, Leyte

Introduction

Landslide is one of the most costly and damaging natural hazards of the world. In the recent decades, it has been increased rapidly all over the world due to severe rainfall by the global climate change. Thus, it is important to understand the process and mechanisms driving the instability, especially, the rapid and long-travelling landslide (Claessens et al., 2007; Sassa et al., 2004). So far, the landslides have been studied by many methods such as statistical analysis, geophysical mapping, and numerical modelling. The characteristics of landslide disasters present the necessity of a new and advanced modelling technology for disaster risk preparedness which simulates its initiation and motion.

Many numerical landslide models are available, with each of these methods having its respective advantages and disadvantages depending on the target study area and the type of the area (Jia et al., 2012; Liu and Wu, 2008). From the viewpoint of dimension, a vast range of slope stability analysis tools exist for both 2D and 3D landslide models. The conventional 2D numerical landslide models are simple, fast, inexpensive, and relatively accurate. Due to the rapid development of computing efficiency, several numerical 3D methods are gaining increasing popularity in slope stability engineering. The ability to manage and process fully three-dimensional information has only

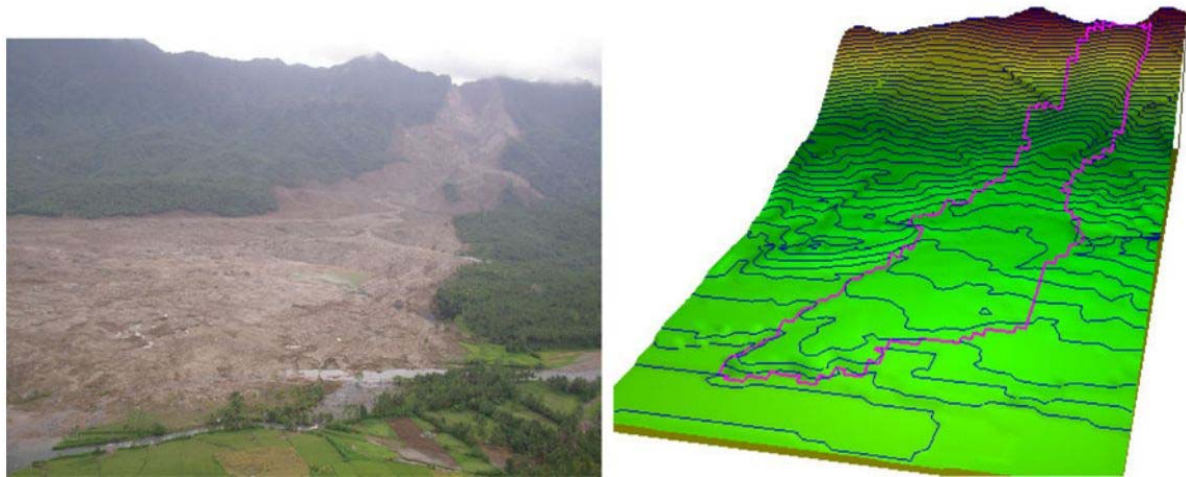


Fig. 1 Air photo and the result of computer simulation of the Leyte landslide. Air photo taken from the chartered helicopter by a member of Japan-Philippines investigation team (K. Araiba). The travel distance and the major part of landslide distribution were well reproduced. The secondary debris flow and muddy water spreads to the leftward in the photo and field observation.

recently been made available for a few Geographical Information Systems (GIS). An increasing number of investigators are now using 3D numerical calculations for estimating slope stability (Dawson & Roth 1999, Zettler et al. 1999, Hürlimann et al. 2002, Konietzky et al. 2004 & Yu et al. 2005). Thus, knowledge of these different methods is essential in view of the potential variation in the input parameters required and in the subsequent interpretation of the generated results. In complex cases, the required analysis methodology may not involve the use of a single technique, but may require the integrated use of several conventional and numerical methods (Eberhardt et al., 2002).

This paper presents the considerable differences between 2D and 3D models, giving 2D-RAPID and LS- RAPID 3D Models as examples. The results of this research can provide scientific information for the researchers on simulation of a rapid and long-travelling landslide using 2D and 3D Models.

Study site

In this study, the Leyte Landslide was used as a working example. A rapid and long-traveling landslide occurred on 17 February 2006 in the southern part of Leyte Island, Philippines (Fig.1). The landslide caused 154 confirmed fatalities and 990 people missing in the debris. The International Consortium on Landslides (ICL) and the Philippine Institute of Volcanology and Seismology (PHIVOLCS) organized a joint Japanese and Philippine team of 22 scientists and engineers. The team investigated the landslide from the ground and from a chartered helicopter. The investigation was reported at the

International Conference Workshop “Guinsaugon 2008-Living with landslides” (Sassa et al. 2008). The results were presented as a part of the paper on the combined effect of earthquake and rainfalls (Sassa et al. 2007). The estimated landslide volume was 20 million m³ (Catane et al. 2007) and 16–30 million m³ (Araiba et al. 2008). The geospatial data includes digital elevation data, soil types, land use, field survey data, etc.

Methodology

This study has developed the simulation framework for the rapid and long-travelling landslide modelling system characterized by rapidly moving flows of mixed soil and rock. These landslides are often occurred on saturated hill slopes due to extreme rainfall or earthquakes. The framework of the modelling system is to identify “from where” the landslides have been initiated, and “until where” landslides may occur in the large scale region.

In this study, the 3D and 2D landslide models were used to emphasize on how the advantages of the different modelling tools can be maximized to provide optimal results with respect to visualization and comprehension of the processes and mechanisms contributing to instability. The current work is basically an extension to the model developed by Sassa et al. (2010). The repeatability of experiments is first investigated by using 3D LS-RAPID model. Then the same parameters are applied in 2D-RAPID model.

Results and Discussion

The 3D simulation of landslide was firstly run by the LS-RAPID model and the results were

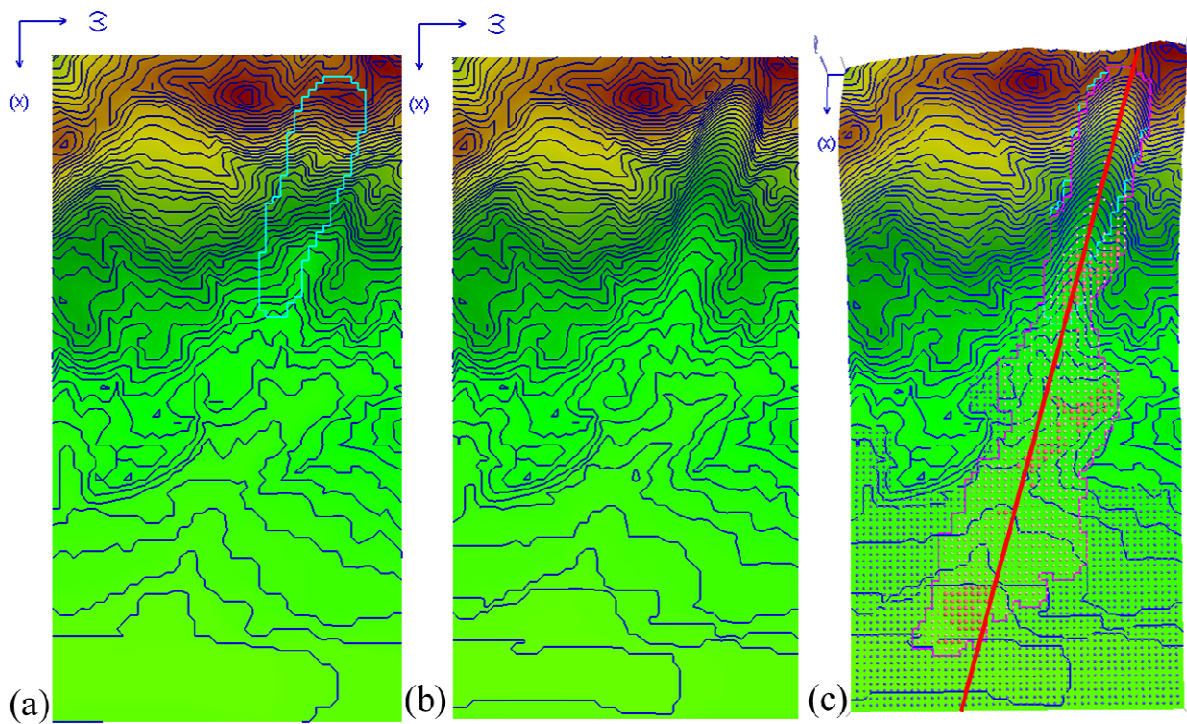


Fig. 2 Simulation area in the 3D landslide model. (a) shows the outline of the unstable mass. (b) shows the sliding surface created by ellipsoid method. The red line in (c) shows the location of cross section for 2D model.

published in Sassa et al. (2010). It shows that the 3D landslide model can represent well the slope failures at each grid element from initiation to long way runoff. The computer simulation reproduced a rapid landslide with a similar travel distance and distribution area which was triggered by a pore water pressure ratio of 0.15 and a small seismic shaking of $KEW=0.12$ and KNS and $KUD=0.061$ using the seismic wave forms recorded at the Maasin observatory. The simulation result almost corresponded that the rapid landslide triggered by a small nearby earthquake of $M_s = 2.6$ in 5 days after the consecutive heavy rains for 3 days intensity of over 100 mm/day.

To compare the results obtained by the 2D and 3D models, the red line in Fig.2 showing the location of the cross section has been selected for 2D landslide model. All the parameters used in 2D landslide model are using the same values which were used in 3D landslide model. While the 3D landslide model needs a lot of parameters, the 2D landslide model only needs several parameters such as soil unit weight, peak friction coefficient at sliding surface, peak cohesion at sliding surface, friction coefficient during motion at sliding surface, friction coefficient inside landslide mass, lateral pressure ratio, steady state shear resistance at sliding surface.

Figure 3 shows the cross-section of the ground surface before and after failure using 2D and 3D landslide models, respectively. From the Fig.3 (a) and (b), it can be clearly found that the

sliding surface calculated by LS-RAPID 3D model is more close to the ground surface and the assumed sliding surface. As for the initiation area, the results are almost same for 2D and 3D models. However, for the deposition area, the 2D landslide model has higher and narrow mass volume than the 3D landslide model. This is because the soil mass can move in both X and Y direction when using 3D landslide model. However, the soil mass can only move along X direction when using 2D landslide model.

Three-dimensional analyses of slope stability are not often used in practical applications as they are more elaborate than plane-strain analyses, and no convenient methods have been developed for performing such analyses. A two-dimensional (2D) plane strain analysis also can be regarded as conservative in cases where 3D failure should be expected, and it is often preferred in design (Cornforth, 2005). In spite of the fact that most landslides display not cylindrical but spatial slip surfaces, 2D slope stability analysis are widely used. Application of 2D modeling sometimes forces the user to consider the simplification of the real problem. The complexity of the slide geometry presents significant limitations with respect to the applicability of 2D solutions and uncertainty with regards to the underlying failure mechanism requires consideration of both continuum and discontinuum techniques (Cala et al., 2006; Konietzky et al., 2004).

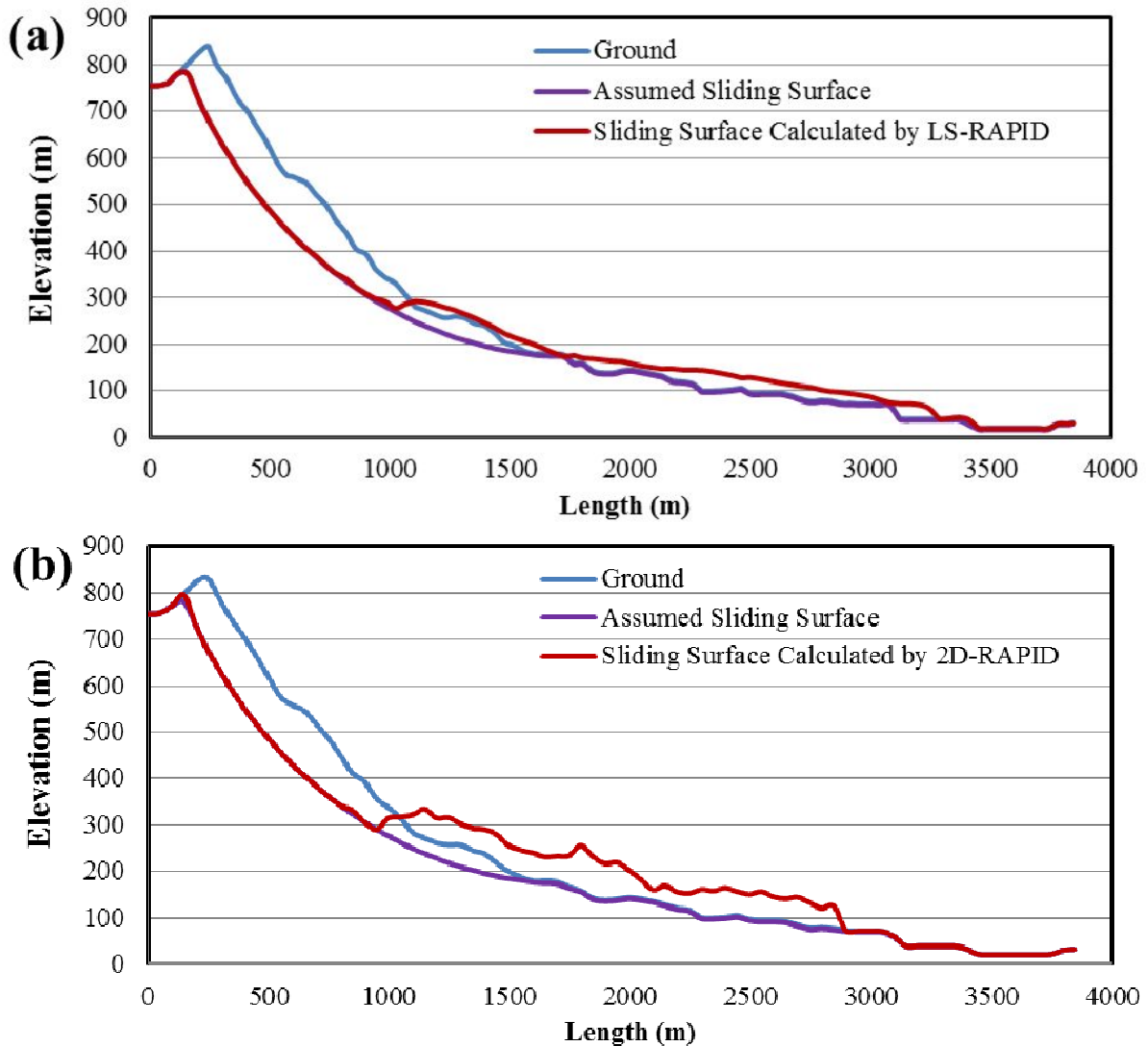


Fig. 3 Cross-section showing the ground surface before and after failure using 2D and 3D landslide models. The assumed sliding surface was decided by using the field survey data.

However, in some cases 3D calculations are necessary in order to take the complexity of geology under consideration. As shown in this study, the 3D simulation of Leyte Landslide can give a 3D view of the landslide initiation and deposition area. In addition, the application of 2D models, for certain cases, may lead to a very conservative approach. In case of the limited width of soft subsoil layer, Factor of Safety (FS) obtained from 2D calculations may be seriously underestimated. The results from the 2D-Rapid model shows the deposition area is smaller than that obtained from the 3D LS-RAPID model. It seems that there is a widespread opinion that considering problem in 2D is always conservative and that engineering design doesn't need the third dimension (Cala et al., 2006).

Conclusion

In this study, we can conclude with the following:

- 1) The framework for numerical assessment of a rapid and long run-out landslide using the distributed 2D and 3D landslide model has been developed.
- 2) The cross section simulated from the 2D and 3D landslide model shows the good relationship with the observed landslides cross section.
- 3) The 2D and 3D numerical modelling slope analysis techniques have their own advantages and disadvantages inherent in their respective methodologies.
- 4) The limitations of existing 2D and 3D landslide models should be recognized by the engineers. In complex cases, the required analysis methodology may not involve the use of a single technique, but may require the integrated use of several conventional and numerical methods. The

model and analysis will depend on the site conditions and the potential mode of failure identified through the field survey.

5) The availability of such program developed in this study is very useful in evaluating the safety and for remediation of rainfall/earthquake triggered landslides in different areas, including cut slopes and earth fill embankments in urban areas and along major highways. Moreover, they will be very useful for land use planning.

Acknowledgments

This work is funded by “One Hundred Talents Program” of Chinese Academy of Sciences. The authors also thank the support by the JSPS Grant-in-Aid.

References (in the alphabetical order)

- Araiba K, Nagura H, Jeong B, Koarai M, Sato H, Osanai N, Itoh H, Sassa K (2008) Topography of failed and deposited areas of the large collapse in Southern Leyte, Philippines occurred on 17 February 2006. In: Proc. International Conference on Management of Landslide Hazard in the Asia-Pacific Region (Satellite Symposium on the First World Landslide Forum). pp 434–443
- Catane SG, Cabria HB, Tomarong CP, Saturay RM, Zarco MA, Pioquinto WC (2007) Catastrophic rockslide-debris avalanche at St. Bernard, Southern Leyte, Philippines. *Landslides* 4(1):85–90
- Cala M, Flisiak J, Tajdus A (2006) Slope stability analysis with FLAC in 2D and 3D. In Proceedings of the Fourth International FLAC Symposium on Numerical Modeling in the Geomechanics, Madrid, Paper (01-02).
- Claessens L, Schoorl J, Veldkamp A (2007) Modeling the location of shallow landslides & their effects on landscape dynamics in large watersheds: Application for Northern New Zealand. *Geomorphology* 87(1–2), 16–27.
- Cornforth D (2005) Landslides in practice: Investigation, analysis, and remedial/preventative options in soils, Wiley, Hoboken, N.J.
- Dawson E, Roth W (1999) Slope stability analysis with FLAC. In Detournay & Hart (eds.) *FLAC and Numerical Modeling in Geomechanics*, Proceedings of the International Symposium, Minneapolis, MN, USA, 1-3 September. pp. 3-9. Rotterdam: Balkema.
- Eberhardt E, Stead D, Coggan J, Willenberg H (2002) An integrated numerical analysis approach applied to the Randa rockslide. Proceedings of 1st European Conference on Landslides, 24-26 June 2002, Prague, Czech Republic, pp. 355-362.
- Hürlimann M, Ledesma A, Marti J (2002) Geotechnical analysis of large volcanic landslides. The La Orotava events on Tenerife, Canary Islands. In Rybar, Stemberek & Wagner (eds) *Landslides*. pp. 571-577. Lisse: Swets & Zeitlinger.
- Jia N, Mitani Y, Xie M, Djameluddin I (2012) Shallow landslide hazard assessment using a three-dimensional deterministic model in a mountainous area. *Computers and Geotechnics* 45(0), 1-10.
- Konietzky H, Lorenz K, Witter W (2004) Complex 3D landslide simulation. In Lacerda, Ehrlich, Fontoura & Sayao (eds.) *Landslides: Evaluation and Stabilization*. pp. 1053-1059. London: Taylor & Francis.
- Liu CN, Wu CC (2008) Integrating GIS and stress transfer mechanism in mapping rainfall-triggered landslide susceptibility. *Engineering Geology* 101(1–2), 60-74.
- Sassa K, Fukuoka H, Wang FW, Wang GH (2007) Landslides induced by a combined effects of earthquake and rainfall. *Progress in Landslide Science* (Editors: Sassa, Fukuoka, Wang, Wang), Springer, Berlin. pp 311–325
- Sassa K, Fukuoka H, Solidum R, Wang G, Marui H, Furumura T, Wang F (2008) Mechanism of the initiation and motion of the 2006 Leyte landslide, Philippines. In: Proc International Conference-Workshop “Guinsaugon 2008 -Living with Landslides (in CD)
- Sassa K, Nagai O, Solidum R, Yamazaki Y, Ohta H (2010) An integrated model simulating initiation&motion of earthquake-rain induced rapid landslides&its application to 2006 Leyte landslide. *Landslides* 7-3:219–236.
- Yu Y, Xie L, Zhang B (2005) Stability of earth-rockfill dams: Influence of geometry on the three-dimensional effect. *Computer and Geotechnics* (32): 326-339.
- Zettler AH, Poisel R, Roth W, Preh A (1999) Slope stability based on the shear reduction technique in 3D. In Detournay & Hart (eds.) *Proceedings of FLAC and Numerical Modeling in Geomechanics Symposium*, Minneapolis, MN, USA, 1-3 September. pp. 11-16.



Proceedings of the SATREPS Workshop on Landslides in Vietnam, 2014

Landslide experiments on natural slopes and indoor landslide flume tests by artificial rainfall

Hiroataka Ochiai⁽¹⁾, Yasuhiko Okada⁽¹⁾, Mark E. Reid⁽²⁾, Kyoji Sassa⁽³⁾

1) Forestry and Forest Products Research Institute, Tsukuba, Japan, e-mail:ochi@ffpri.affrc.go.jp/okada10@ffpri.affrc.go.jp

2) US Geological Survey, CA, USA, e-mail: reid@usgs.gov

3) International Consortium on Landslides, Kyoto, Japan, e-mail:sassa@iclhq.org

Abstract An experiment to induce a fluidized landslide by artificial rainfall was conducted on a natural slope at Mt. Kaba-san in Yamato village, Ibaraki Prefecture, Japan. The experimental slope was 30 m long, 5 m wide, and the average slope gradient was 33 degrees. A landslide initiated 24,627.5 sec (410m27.5s) after the start of sprinkling at a rainfall intensity of 78 mm/h. The landslide mass was 14 m long and 1.2 m deep (at maximum). It first slid, then fluidized, and changed into a debris flow. The travel distance was up to 50 m in 17 seconds. The apparent friction angle of the fluidized landslide was 16.7 degrees.

Keywords landslide, experiment, natural slope, flume

Introduction

Rainfall-induced landslides often cause catastrophic disasters. For this reason, a project called APERIF (Areal Prediction of Earthquake and Rainfall Induced Rapid and Long-traveling Flow Phenomena) was launched by the Special Coordinating Fund for Science and Technology of the Ministry of Education, Cultures, Sports, Science and Technology (MEXT) of Japan. In 2002, this project was approved as part of the International Programme on Landslides (IPL M101-APERITIF Project to the International Consortium on Landslides). This paper reports some results from this project.

Fluidized landslides, which travel long distances at high speed, are one of the most dangerous types of landslides (Sassa 2000). Fluidized slope movement takes place both in artificial cut slopes and natural slopes and often results in extensive property damage and significant loss of life (Sassa 1984, 1998). Many

fluidized landslides have been observed in Japan, some of them have caused great disasters. Examples are: the 1984 Ontake debris avalanche, Nagano Prefecture; the 1995 Nikawa landslide, Hyogo Prefecture; the 1996 Otari-mura debris flow, Nagano Prefecture; the 1997 Sumikawa landslide, Akita Prefecture; the 1997 Harihara landslide-debris flow, Kagoshima Prefecture; the 1998 Taiyo-no-kuni and Hiegaeshi landslides, Fukushima Prefecture; the 1999 Kameyama debris flow, Hiroshima Prefecture; and the 2003 Minamata debris flow, Kumamoto Prefecture.

Liquefaction is an important mechanism in causing the fluidized motion of some landslides, where fluidization occurs along the sliding surface, or within the sliding zone during a rise in pore-water pressure which reduces shear resistance by decreasing the effective normal stress. Bishop (1973) noted that fluidization can be distinguished from general sliding, which usually has an intact soil mass above the sliding surface. Hutchinson (1969) noted that flow-like motion subsequent to fluidization is a neglected and little-understood group of movements with confusing terminology. Liquefaction phenomena as a result of cyclic loading have received much attention from many researchers since the drastic effects of liquefaction were noted after the 1964 Niigata earthquake Japan. Seed and Lee (1966), Yoshimi et al. (1977), Seed (1979), Ishihara et al. (1990) and (1993) discuss extensive laboratory soil tests attempting to reveal the liquefaction mechanism. Effects such as rainfall, as well as motion effects, can trigger fluidized landslides (Eckersley, 1985, 1990, and Sassa et al. 2004).

In order to reproduce a fluidized landslide at almost field scale, and to investigate its fluidization mechanisms, the National Research Center for Disaster Prevention (Independent Administrative Institution National Research Institute for Earth Science and Disaster

Prevention from April 2001), Tsukuba Japan, constructed an indoor rainfall simulator and large-scale flume model 10 m long, 4 m wide, and 1.2 m deep. By using such facilities, Fukuzono (1985) proposed that the initiation time of rainfall-induced slope failure was a function of inverse of shear velocity. Iverson and LaHusen (1989) pointed out that pore-water pressures

within the soil packed in the slope model were dynamically fluctuating during the rapid shearing at failure. These findings were obtained from indoor flume tests in which the soil sample was quasi-uniformly packed. Landslide experiments on natural slopes by sprinkling or water supplying from trenches have been reported four times in Japan and the United States.

Table 1 Examples of landslide experiments in natural slopes

References	Location	Volume W × L	Excavation etc.	Water supply	Sensors	Fluidization
Oka 1972	Ikuta, Kawasaki, Japan	500 m ³		Sprayed from fire hose		Yes
Yagi, Yatabe, & Enoki, 1985	Matsuyama, Japan	10 × 25 m	Trench cut at upper and both sides	Rainfall simulator (Sprayed on upper half slope)	Extensometer Piezometer Strain meter	Yes
Yamaguchi, Nishio, Kawabe, Shibano, & Iida, 1989	Yui, Shizuoka, Japan	10 × 30 m	Upper trench cut Lower open cut	Supplied from upper trench	Extensometer Piezometer Inclinometer	No
Harp, Wells & Samiento, 1990	Utah, USA	1.6 × 1.3 m 2.0 × 2.2 m 3.2 × 4.0 m	Upper trench cut Lower open cut	Supplied from upper trench	Extensometer Piezometer	No

We conducted a rainfall-induced landslide experiment on a natural slope which had more complex and heterogeneous characteristics than the indoor models, in an attempt to investigate the dynamic movements of the soil surface, the formation of the sliding surface, and hydrological characteristics, based on the results of the indoor flume testing. The experimental slope was 30 m long and 5 m wide, and mainly covered by weathered disintegrated granite sand. Ochiai et al. (2004) were monitored soil-surface movements by using stereo photogrammetry (5 stereo pairs of CCD video cameras) and wire extensometers. Hence white targets were placed on the experimental slopes and the movements of these targets were traced by image analysis. To detect the formation of the sliding surface, soil-strain probes were inserted into the soil to 2 m depth at deepest. Tensiometers were used to measure changes in pore-water pressures within the soil.

Experiment site and testing procedure

The purpose of our experiment is to produce hopefully a fluidized landslide on a natural slope by artificial rain fall. The test site was selected by two conditions; 1) to secure complete safety during the experiment, 2) to have a possibility producing a fluidized landslide. Then, a natural slope in the Koido National Forest at Mt. Kaba-san, Yamato village, 25 km north of Tsukuba-city, Ibaraki Prefecture, was selected for the controlled experiment on landslide and possible fluidization in cooperation with the Forestry Agency of Japan.

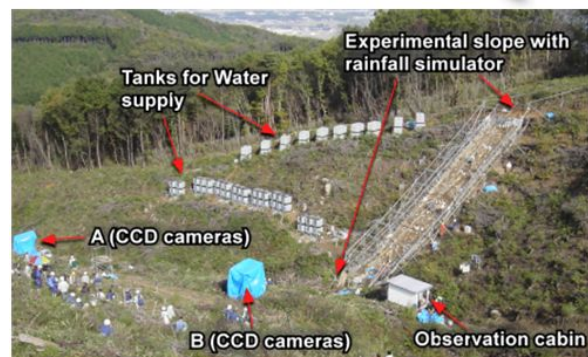
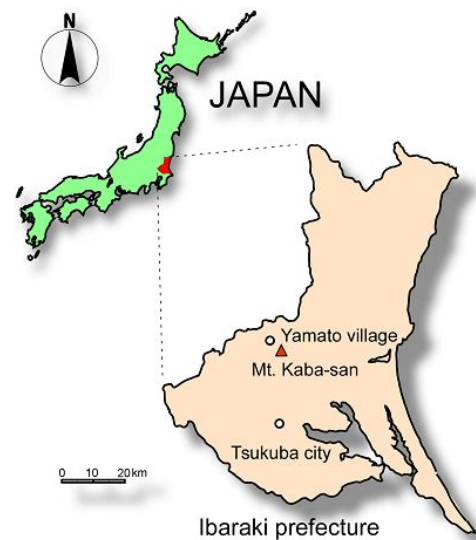


Figure 1 View of the experiment site at Mt. Kaba-san

The selected portion of hillslope (Fig. 1) was 30 metres long, with an average gradient of 33 degrees (maximum 35 degrees). The soil was 1 to 3 metres deep. A 5 m wide experimental slope was isolated from its surroundings by driving thin steel plates about 1 m deep into the soil. These

plates prevented lateral diffusion of infiltrated rain water and cut the lateral tree root network that imparts resistance within the soil layer. The surface of the slope was covered by straw matting to prevent surface erosion and promote rainfall infiltration. Surface material on the slope consisted of fine weathered surface erosion and promote rainfall infiltration. Surface material on the slope consisted of fine weathered disintegrated granite sand, called “Masa” in Japan.

Loamy soil blanketed the upper portion of the regolith to a depth of about 1 m; this soil mainly originated from tephra of Mt. Fuji, Mt. Akagi, and other volcanoes located west of Mt. Kaba-san.

Artificial rain at the rate of 78 mm/h was applied to the slope segment during the experiment by way of a rainfall simulator. The simulator consisted of a framework of steel pipes with 24 sprinkling nozzles arranged 2 m above the soil surface. Water for sprinkling was pumped from a dam constructed in a small creek at the base of the slope into 80 water storage tanks (1 m³ for each) on the neighboring hillslope prior to the experiment.

Soil-surface movement was measured by wire extensometers attached on the frame of water sprinkling system, connecting to the steel pipes on the slope surface, as shown in Fig. 3. Note that in Fig. 3, lines are drawn at the depths where values of $N_{c10} = 10$ and 50 were obtained by light weight cone-penetrometer testing (Noguchi et al. 1997). The N_{c10} values are the number of times it took to drop a weight (5 kg) from height of 50 cm to drive the cone 10 cm into the soil. These values defined the surface soil layer (5 N_{c10} o) and total soil depth (50 N_{c10} o), respectively.

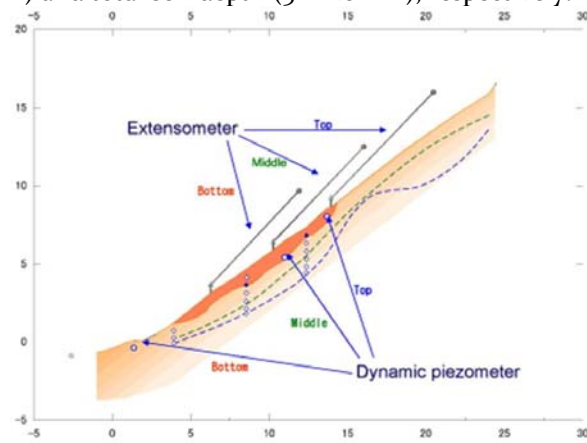


Figure 2 Location of extensometers and piezometers

To measure saturation conditions within the soil, tensiometers with porous ceramic cups were set into the slope. Tensiometer can measure negative pore water pressure in unsaturated soils and positive pore water pressure in saturated conditions.



Figure 3 Views of the landslide initiation between one second and four seconds after failure



Figure 4 Views of the debris flow resulting from the landslide fluidization between 5s and 7s after failure

The data from respective sensors were transmitted through cables to the observation cabin, where they were monitored and recorded. The data acquisition interval for tensiometers was one minute

Several digital video cameras were placed in positions of safety on a hillslope facing the experimental slope to film the entire scene of the fluidized landslide.

General landslide movement

On the 12 November 2003, artificial rainfall was given to the slope at a rainfall intensity of 78 mm/h for four hours and a half until sunset. No slope movement was observed. The second experiment was conducted on 14 November 2003. Artificial rainfall was started from 9:13 at a rainfall intensity of 78 mm/h, the slope deformation was detected from around 15:00, then a clear movement was observed to start at 16:03. The initiated landslide was a type of an expected fluidized landslide, the landslide mass rapidly moved and travelled long.

The cover of the tensiometer started to incline downslope at 24,627.5 sec (410m27.5s) after sprinkling commenced. We interpret this as indicating that slope failure initiated at 24,627.5 sec. Some images from the digital video camera are presented in Fig. 3a, b, c, and d. Fig. 3a is at

24,628.5 sec (one second after failure initiation), Fig 3b at 24,629.5 sec (two seconds), Fig 3c at 24,630.5 sec (three seconds), and Fig 3d at 24,631.5 sec (four seconds). As soil surface movement increased, a tension crack became visible at the head (Fig. 3a), and a compressive bulge resulting from downslope movement was observed 5 m above the base of the slope (Fig. 3b). The bulge enlarged (Fig. 3c) before the main landslide mass began to undulate and rapidly enter the stream (Fig. 3d). The compressive bulge was observed only in the left part of the landslide.

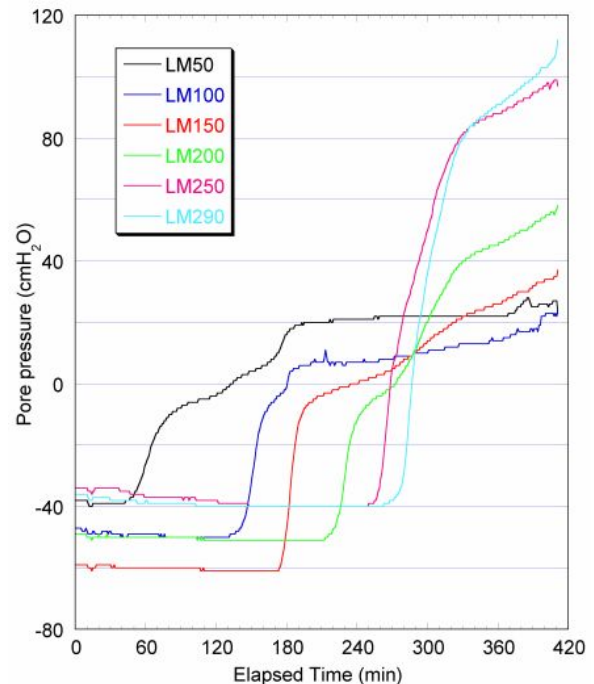


Figure 5 Changes in soil-water pressure in tensiometers at surface soil during the experiment.

Images at 24,632.5 sec (five seconds after failure) and 24,634.5 sec (seven seconds) are shown in Fig. 4a and b. Fig.4 presents the movement of liquefied landslide

mass. The failed landslide mass had entered the stream and was about to collide with the confronting slope (Fig. 4a). After collision, the fluidized landslide turned to the right (Fig. 4b), changed into a debris flow, and travelled downstream for 10 seconds on a ~10 degree gradient, as much as 30 m. It took 17 seconds from the initiation of the landslide to the end of deposition.

Changes of soil-water pressure in tensiometers at surface soil during the experiment

Changes in pore water pressure including suction monitored by the tensiometers. The tensiometers were placed at depths of 50, 100, 150, 200, 250, and 290 cm. All tensiometers showed negative pore pressures at the start of sprinkling, indicating that the soils at all depths were

unsaturated or partly saturated. When the wetting front passed, the tensiometers showed increases in pore pressure in sequence of the depths. At 410 min, when the failure took place, all of the tensiometers showed positive pore pressures. The pore pressure of the deepest tensiometer (290 cm) rapidly increased its values from about 290 min. This almost coincided with the time when the strain gauge at 110 cm depth (Fig. 5). Hence, it can be deduced that general slope instability increased from 290 min, before final failure at 410 min.

Dynamic changes of displacement and soil-water pressure at surface soil at the failure onset

Dynamic changes in surface displacements and pore water pressure including suction monitored by the extensometers and piezometers. The tensiometers were placed shown in Fig. 2. at depths of 50, 100, 150, 200, 250, and 290 cm. Two piezometers at the top and middle showed negative pore pressures just before the failure onset, indicating that the soils at all depths were fully saturated. After failure started, the piezometers showed fluctuations and indicated the maximum pore pressure 250 cmH₂O, which was enough value for the landslide fluidization at the depth.

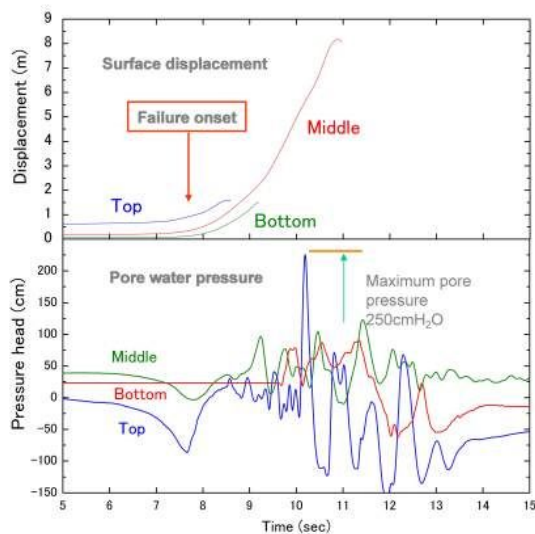


Figure 6 Dynamic changes of displacement and soil-water pressure at surface soil at the failure onset

Landslide experiment in Vietnam

To develop integrated automatic measuring system of rainfall, groundwater and slope movement, suitable to the tropical monsoon area by indoor landslide experiment with artificial rainfall for SATREPS project, landslide experimental facilities of ITST (shown in Fig. 6) was planned in Hanoi. Landslide flume was designed and will be made in the building based on the soil properties of the Granitic sand taken from Hai Van area in 2014.

Acknowledgments

We acknowledge the support of the APERIF (Areal Prediction of Earthquake and Rainfall Induced Rapid and Long-traveling Flow Phenomena) project which was launched by the Special Coordinating Fund for Science and Technology of the Ministry of Education, Cultures, Sports, Science and Technology (MEXT) of Japan. In 2002, this project was approved as part of the International Programme on Landslides (IPL M101-APERITIF Project to the International Consortium on Landslides). This paper reports some results from this project. Also, we are indebted to Ibaraki Prefectural Government and Kanto Regional Forest Office for the permission to conduct the experiment in the Suigo-Tsukuba Quasi-National Park and Koido National Forest.



Figure 7 Landslide experimental building in ITST and flume in FFPRI

References

- Bishop AW (1973) The stability of tips and spoil heaps. *Quarterly Journal of Engineering Geology*, 6: 335-376.
- Bromhead EN (1979) A simple ring shear apparatus. *Ground Engineering*, 12(5): 40-44.
- Eckersley JD (1985) Flowslides in stockpiled coal. *Engineering Geology*, 22: 13-22.
- Eckersley JD (1990) Instrumented laboratory flowslides. *Géotechnique*, 40(3): 489-502.
- Fukuzono T (1985) A new method for predicting the failure time of a slope. *Proceedings of IVth International Conference and Field Workshop on Landslides*, Tokyo, 23 - 31 August, 1, 145 - 150.

- Harp EL, Wells WG, Sarmiento JG (1990) Pore pressure response during failure in soils. *Geological Society of America Bulletin*, 102, 428-438.
- Hutchinson JN (1986) A sliding-consolidation model for flow slides. *Canadian Geotechnical Journal*, 23: 115-126.
- Ishihara K, Okusa S, Oyagi N, Ischuk A (1990) Liquefaction-induced flowslide in the collapsible loess deposit in Soviet Tajik. *Soils and Foundations*, 30(4): 73-89.
- Ishihara K (1993) Liquefaction and flow failure during earthquakes. *Géotechnique*, 43(3): 39-46.
- Iverson RM, LaHusen RG (1989) Dynamic pore-pressure fluctuations in rapidly shearing granular materials. *Science*, 246: 769-799.
- Noguchi S, Abdul Rahim N, Zulkifli Y, Tani M, Sammori T (1997) Soil physical properties and preferential flow pathways in tropical rain forest, Bukit Tarek, Peninsular Malaysia. *Journal of Forest Research*, 2: 125-132.
- Ochiai H, Okada Y, Furuya G, Okura Y, Matsui T, Samori T, Terajima T, Sassa K (2004) A fluidized landslide on a natural slope by artificial rainfall. *Landslides*, 3:211-219.
- Oka H (1972) Impacts by the "artificial landslide":re-examine the rage of nature. *Kagaku Asahi*, January issue:152-153. (in Japanese)
- Sassa K (1984) The mechanism starting liquefied landslides and debris flows. In *Proceedings of the 4th International Symposium on Landslides*, Toronto, 16-21 September, 2, 349-354.
- Sassa K (1988) Motion of landslides and debris flows - prediction of hazard area-, Report for Grant-in-Aid for Scientific Research by Japanese Ministry on Education, Science and Culture (Project No. 61480062), 4-52.
- Sassa K (1998) Mechanisms of landslide triggered debris flows. *Environmental Forest Science*, In *Proceedings of IUFRO Division 8 Conference*, Kyoto, 19-23 October, 499-518.
- Sassa K (2000) Mechanism of flows in granular soils. *Proceedings of GeoEng2000*, Melbourne. 1, 1671-1702.
- Sassa K, Fukuoka H, Wang G, Ishikawa N (2004) Undrained dynamic-loading ring-shear apparatus and its application to landslide dynamics. *Landslides*, 1, 7-19.
- Seed HB, Lee, KL (1966) Liquefaction of saturated sand during cyclic loading. *Journal of the Geotechnical Engineering Division, ASCE*, 92(CM6): 105-134.
- Seed HB (1979) Soil liquefaction and cyclic mobility evaluation for level ground during earthquakes. *Journal of the Geotechnical Engineering Division, ASCE*, 105: 201-255.
- Yagi N, Yatabe R, Enoki A (1985) Laboratory and field experiments on prediction method of occurring time of slope failure due to rainfall. *Landslide (Journal of Japan Landslide Society)*, 22(2), 1-7. (in Japanese)
- Yamaguchi I, Nishio K, Kawabe H, Shibano H, Iida C (1989) Initiation and fluidization of an artificial landslide. -Field experiment in Yui, Shizuoka Prefecture, Japan-, *Shinrin Kosoku(Areal Survey)* 158, 3-9. (in Japanese)
- Yoshimi Y, Richart FE, Prakash S, Balkan DD, Ilyichev, VA (1977) Soil dynamics and its application to foundation engineering. In *Proceedings of the 9th International Conference on Soil Mechanics and Foundation Engineering*, Tokyo, July, 2, 605-650.



Proceedings of the SATREPS Workshop on Landslides in Vietnam, 2014

Landslides on the road in Vietnam - Monitoring and solutions for landslide risk reduction

Huynh Dang Vinh⁽¹⁾, Huynh Thanh Binh⁽¹⁾, Do Ngoc Ha^(1,2)

1) Institute of Transport Science and Technology, Hanoi, Vietnam, e-mail: huynhdangvinh@gmail.com (WG4)

2) Shimane University, Project Center on Natural Disaster Reduction, Shimane, Japan (WG4)

Abstract Landslide is one of the disasters caused by natural and human activities. To assess the cause of the landslide, we need to conduct the survey and monitoring which can suggest the appropriate solutions.

Keywords landslide, monitoring, Ho Chi Minh route

Introduction

In Vietnam, the landslide is one of the most popular natural disaster occurring on the road systems. Every year, Landslide usually occurs in the rainy season with more than one million m³ of volume and damage property about hundreds of billions VND. In the early on October 2007, 60 dead and 13 missing in the storm number 5. The storm also causes long -term traffic congestion in some nation roads.



Figure 1 Landslide in Nghe An province, 2007

According to statistics of Directorate For Road of Vietnam in 2007, the road network has about 223.059 Km length. In particular, up to 3/4 of the total length roads cut through hilly terrain, that has many slopes with 60-70m high, especially some slopes are more than 100m high. According to the general report of Institute of Transport Science and Technology, the region usually occurs

landslides in Vietnam, mainly in the roads, mountainous northwest and the route along or cross Truong Son range from Quang Binh to Kontum, Gia Lai such as Nation road No.6, No.70, No.279, No.7, No.14 and Ho Chi Minh route. In summary, Vietnam has a tropical monsoon climate with average rainfall about 2000 mm, a local individual to reach 4000 mm/year (Northwest and Central of Vietnam). Therefore, due to high rainfall, high terrain and complex geological structures, landslide phenomena usually happen and impact on the stability of roads and life of people along the roads.

The classification of landslide in transportation

There are many landslide classifications in the world. It depends on characteristic of climate, geology and hydro geological. In order to identify the reason of landslide phenomena and proposal approximate solutions to reduce the impact of landslides, Institute of Transport Science and Technology has proposed division landslide in 04 typical forms that describe as follows:

Type 1: Landslide

Landslide that the material slid along the surface is curved upward (in the soil embankment or in the homogeneous structure slopes) or break into several sections of the surface depended on bedrock.

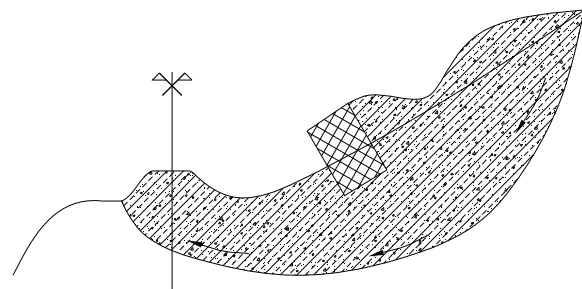


Figure 2 The schematic of landslide

When landslides occur almost materials inside the sliding mass will move simultaneously. On the surface, trees and infrastructures are tilted. Its bent toward the vertical. We will easily see the scrap and cracks in the top of sliding mass.



Figure 3 Landslide on Ho Chi Minh route

Type 2: Erosion

Erosion is the process by which soils are removed from the Earth's surface by exogenitic processes such as water flow and the effect of ground water.

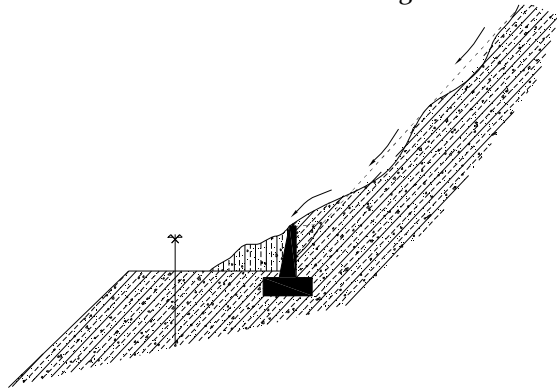


Figure 4 The schematic of erosion on talus.

The final result of this phenomenon is gullies or caves. A other form of erosion is debris flow stream from a cliff or from the watershed to the road.



Figure 5 Erosion in Ho Chi Minh route

Debris flow occurred in January 2000 on national road No.27 has caused serious consequences for

agricultural production, damaging dozens of kilometres of roads and cause damage to tens of billions VND.

Type 3: Topple

A topple is the final period of erosion phenomena. In the field investigation, it is difficult to identify scarp and sliding surface. The material in sliding mass is disturbance and tree collapse. Topples usually occur quickly and makes the soil around warped, cracked and affect the stability of the soil next to it.

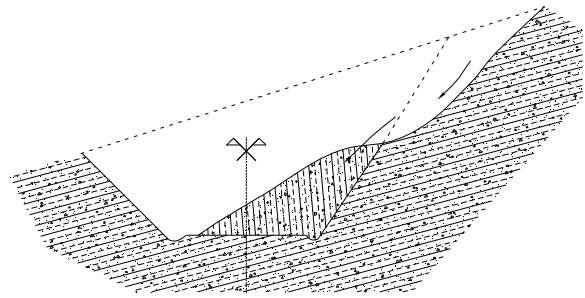


Figure 6 The schematic of topple



Figure 7 The topple in national road No.6

Type 4: Rock fall

Rock falls are abrupt, downward movements of rock or earth, or both, that detach from steep slopes or cliffs. Rock fall can occur in the rainy season or sunny day. The material volume is not so high, but it is dangerous for people and affect on the transportation system.

In summary, landslides phenomenon usually occurs roads network, especially during rainy seasons. Landslides damage roads, threatening the lives of the residential areas along the route, causing damage to life and property every year hundreds of billions VND. We have a national standard TCVN 9861:2013 about the investigation and design for landslide mitigation on the road. However, the landslide study in Vietnam is limited and has some problems. So, to assess the cause of landslide we need investigation experience and using the monitoring methods.

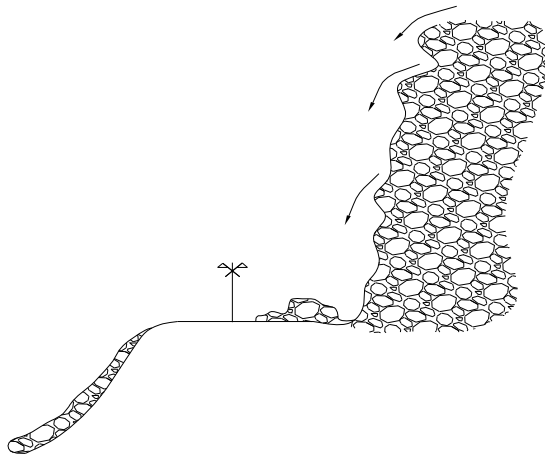


Figure 8 The schematic of rock fall



Figure 9 Rock fall on national road No.37

Some monitoring instrumentations for landslide

In recent year, we installed some monitoring instrumentations to observe and forecast landslides. In this part, we will introduce some instrumentations that have been used in Vietnam as follows:

Rain gauge



Figure 10 Rain gauge installed in Hai Van station

Landslides are related to rainy season (rainfall and rainy time). So, rain gauge usually uses for landslide monitoring and early warning. The rain gauge can connect to the siren system to warn the community if the precipitation reaches a certain value.

Inclinometer

Inclinometers are used for monitoring deformation normal to the axis of a pipe by means of a probe passing along the pipe. Inclinometers are installed to exceed the expected depth of sliding surface. So, the inclinometer provides data for defining sliding surface. At present, Institute of Transport Science and Technology is building the national standard for inclinometer.



Figure 11 Inclinometer system

Monitoring instrumentations for surface movement

One of the methods of landslide monitoring is to install posts that can be sequentially measured for landslide movement. However, these surface posts can be damaged by animals or people. Wooden, concrete or metal posts in the ground can be directly installed into a landslide. In addition, some stable reference points beyond the boundary of the moving landslide are needed.



Figure 12 Concrete post for landslide monitoring



Figure 13 Geodetic measurement for landslide movement



Figure 14 Checking the data of extensometer

Installation of extensometers is similar to establishing movement posts except for the wire connection between the landslide and the stable location adjacent to the landslide. For slow-moving landslides, it may be difficult to determine the location for installing a stable base for the extensometer. Additionally, if the ground is generally creeping outside of the landslide, then the measurement of landslide movement will not be accurate.

Piezometers

Piezometers are instruments that are installed within the ground to measure the groundwater pressure at specific depths.

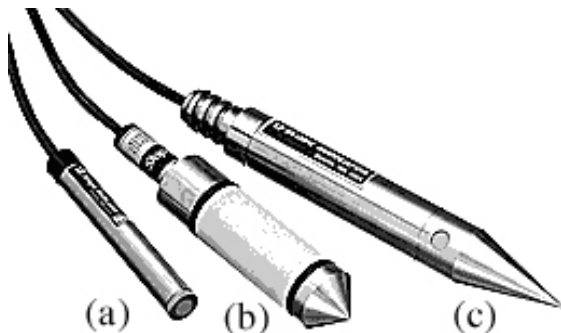


Figure 15 Probe piezometers

a- for bore hole, b- for embankment, c- for pressing into the soil

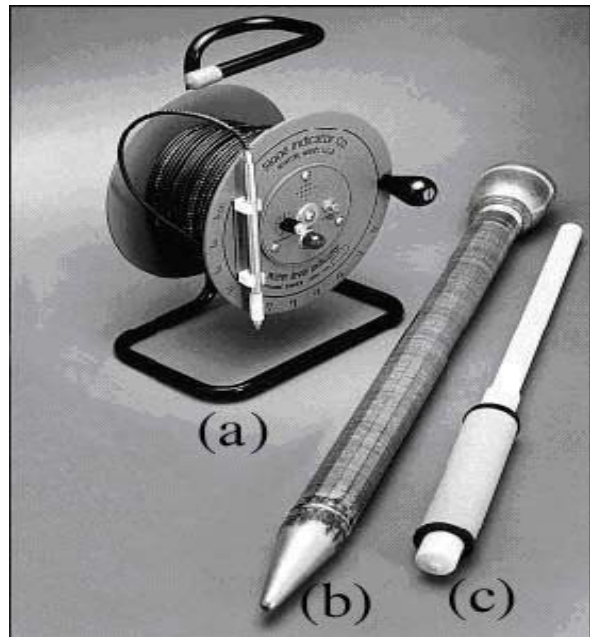


Figure 16 Groundwater measurement device

In addition, we need to measure the ground water level. Those information are useful for detailed long term monitoring of ground water level fluctuation and landslide movement.

Some Solutions for landslide mitigation

The group of structural solutions

In the structural solutions, we need to flexibly apply solutions to enhance the stability of the slope as:

Geometry modification measures, in which the geometry of the hillside is changed (in general the slope). This method easily to construct and is low cost but it need wide space.

Drainage measures aim to made lower ground water level or to reduce the water content of material. Drainage can be either surface or subsurface. Surface drainage measures require minimal design and costs and have substantial stability benefits. We applied the various methods of drainage such as: site levelling, ditches drains and drain pipes, deep drainage trenches.

Reinforcement measures aim to increase landslide resisting forces. It is a expensive measure and consists of two different approaches: insertion of reinforcement elements in the ground (anchor, nailing, geogrids, retaining walls, micro piles) and the improvement of the mechanical characteristics of the ground (chemical, thermal or mechanical treatment).

The group of non-structural solutions

Propagate widely to people to realize the importance of threats from natural hazards and

specially landslides hazards caused in particular for preventive measures.

Conclusions

Vietnam is located in tropical monsoon climate and topography and geology condition are complicated. So, landslides usually occur especially during rainy seasons. Therefore, we need the promotion of research and apply measures to prevent landslides efficiently on transport routes and in residential areas in the local mountains. In Vietnam, we study the reason of landslide and design the solution after the landslide happens but some landslides still occur. The monitoring system only install after we construct some structural solutions. It is problem in Vietnam. In the future, we will study some new technology for landside monitoring such as Hai

Van station case to observe the slope movement and develop the early warning system in Vietnam.

Reference

- Doan Minh Tam (2013) Research ground prestressed anchors technology on the road, Research project
- ITST (2005-2010) Investigation and design for landslides on Ho Chi Minh road, Results project
- ITST (2008) Research technology choices and conditions apply new technologies to combat soil loss on the road, Research project
- ITST (2006) Research technology anchors for landslide on the road, Research project
- Lomtadze V.D.(1982) Geological Engineering (in Vietnamese language - translation from Russian). Publisher College and Technical secondary schools in Hanoi
- Vietnam National Standard TCVN 8869 (2011) Method for measurements of pore pressures in soil



Proceedings of the SATREPS Workshop on Landslides in Vietnam, 2014

Development of landslide monitoring and data transfer system in the Hai van station landslide and the initial extensometer monitoring result behind the station

Shiho Asano⁽¹⁾, Shinro Abe⁽²⁾, Osamu Nagai⁽³⁾

1) Forestry and Forest Products Research Institute, Department of soil and water conservation, Tsukuba, Japan, e-mail: shiho03@ffpri.affrc.go.jp

2) Okuyama Boring Co., Akita, Japan, e-mail: abe@okuyama.co.jp

3) International Consortium on Landslide, Kyoto, Japan, e-mail: nagai@iclhq.org

Abstract Landslide monitoring system is important for early warning and alarming for landslide prevention. The system is needed to optimize by adjusting in each environment in order to obtain the appropriate data. In this study, the plan of the landslide monitoring system for early warning and alarm in the study area in Vietnam was shown. Before the system is installed, the preliminary observation of rain and displacement of gabion nearby railway was conducted. As a result, the relationship between rain and displacement was shown.

Keywords Landslide monitoring, Hai Van station landslide, displacement, rainfall

Introduction

Landslide monitoring system is important tool for landslide risk management. Landslide activity is often affected by their circumstance, therefore landslide monitoring system need to adapt to natural and social condition each other. A precedent of a monitoring system hasn't been in Vietnam yet. Therefore the prototype model which is adapted for natural and social condition in Vietnam has been needed to develop.

In this project, the prototype model of landslide monitoring system for early warning will be developed. It will tune up for actual landslide (Hai van station landslide) in Vietnam. And rainfall and displacement near railway was observed as previous study. In this study, we introduce the monitoring system plan and result of antecedent observation.

Study site

This study was conducted in Hai Van station landslide area. This area located near Danang city

in the centre part of Vietnam. Because the national railway of Hai van station is one of the most important lifelines, the safety management of landslide disaster is important. Hai van station landslide occurred in granite mountainous slope. Concrete wall, gabion and channel work had already been constructed as previous landslide countermeasure. Because some deformation of these is able to found, this landslide is probably still active (photo 1).



Photo 1 Topology of Hai van station landslide area

Development of monitoring system

Purpose of the monitoring system

The purpose of the landslide monitoring system is the prevention and safety management of railway against the landslide disaster. The details are as follows;

- 1) It gives the alarm just before landslide causes damage to railway.
- 2) The early warning of landslide activity is taken based on a minor change of data.

3) The landslide mechanism is clarified in order to do early warning and prevention work.

Alarm for landslide activity

Gabion was installed at the slope nearby track and it has been deformed. This shows that the soil movement gradually progresses now. The slope nearby railway track is relatively steep and it may be high-risk area of slope failure for railway. This zone nearby track should be set the monitoring sensor of soil movement for alarm. It is necessary to observe the displacement of the steep slope beside railway track for alarm (Figure 1). The displacement is observed using standard extensometer because of the stability, high resolution and reliability. Rainfall data is important for alarm of landslide. Therefore, the displacement gauge on the slope nearby railway track and rainfall gauge will install for alarm.

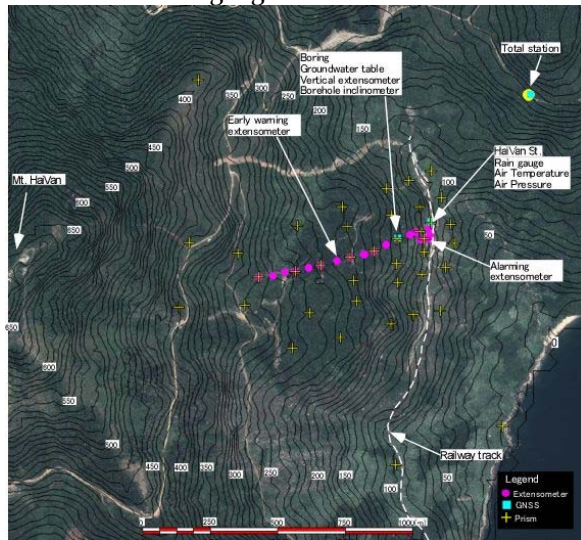


Figure 1 Location map of the monitoring sensors

Early warning and mechanism of landslide

Elucidation of characteristics and mechanism of the landslide is necessary in order to conduct the early warning. Characteristics of active area, transferring of soil and trigger of landslide is needed to clarify for mechanism. So the displacement of whole area and underground, rainfall and variation of groundwater are observed. Extensometer for the high resolution displacement gauge and groundwater level gauge are installed along the longitudinal direction of centre of the slope.

And prisms for total station for displacement survey are installed whole landslide area. All monitoring data will be transmitted to office and calculated. Result of monitoring will be reported to the relevant organizations (Figure 2).

Sensors

This monitoring system is consisted by some kinds of sensors and these are installed at the whole landslide area. The five extensometers are used for alarm and they are installed nearby railway track. Others are used for clarification of mechanism of landslide for early warning. The position of each sensor is decided in consideration of the characteristics. Characteristics of each sensor are shown as bellow.

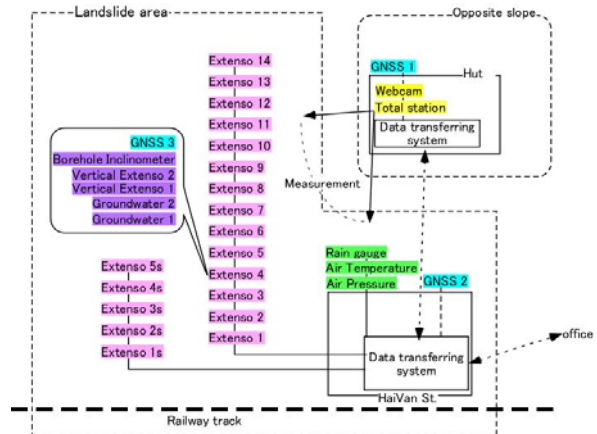


Figure 2 Schematic flow chart of the monitoring system

Robotic total station

Since mass movement is three-dimensional, the three-dimensional transfer direction and the field of activity are survey using the robotic total station. The robotic total station can measure the position of target automatically from a distant place by contactless (Photo 2). The exclusive prism on stand pole is used for the target.



Photo 2 Robotic total station

The targets are arranged equally in the whole landslide. Robotic total station can collimate and measure the target automatically by motor. It is possible to observe the movement of targets by automatically and repeatedly surveying. The distribution of the three-dimensional landslide displacement is automatically measured by the

installation of the total station in opposite slope of the landslide slope.

This total station (Leica Nova TM50, Leica Geosystem AG) has high accuracy and long range. In this study, totally 40 prisms will be installed as targets. Three prisms are installed out of landslide area and others are arranged equally inside of landslide area. Over 30 minutes are scheduled in the measurement interval time per site. Temperature and atmospheric pressure are also measured for the correction of the range meter in the station. It is advantageous to measure the soil movement from the stable position, but it is disadvantageous that it cannot measure, when the target is hidden for large displacement in the short time.

Global Navigation Satellite System (GNSS)

GNSS measures the position using the signal from the satellite. It needs enough canopy openness in the woods, but it has an advantage of freedom of selection of location without a bad effect of hiding. Each measurement location can be compare in global area because the position of world coordinate is measured. The position by GNSS is measured by the record of the signal of the satellite in which it changes every moment.

The dispersion of the position calculated using momentary signal is big. It is necessary to analyse using the data in which are got during the adequate period in order to increase the accuracy of the position. Therefore, it may be disadvantageous in order to use for the alarm. In this study, three GNSS are installed at the Hai Van station, total station installation site, boring site.



Photo 3 Antenna of GNSS

Extensometer

The extensometer is a method for measuring the change of the distance between 2 positions. The meaning of measurement data changes by the installation position, because it measures only distance data between 2 sites. The selection of the installation site is important.

The extensometer (LG501E OSASI Co.) used in this study connects 2 points by super invar wire, and it measures the change of the distance by unwinding amount of wire using the potentiometer. The measurement accuracy is 0.1mm, and it is advantageous to measure continuously from 0.1mm until about 1.0m, because the super invar wire does not expand with heat. The wire is easy to be affected by noise such as the contact. The extensometer is suitable for the continuous displacement measurement at many sites in the landslide area because the installation is easy and it is cheaper than the laser distance meter.

The maximum length of the wire is 20m on the normal model. In this study, it is called as “short span extensometer”. It is possible that the short span extensometer carries out the stable observation with the high reliability, but measurement distance is short. Therefore, it is used for the alarm by the installation to the steep gradient of the line side (Photo 4).



Photo 4 Extensometer of short span type in Hai van

It is necessary to measure the displacement of the whole landslide in order to clarify the mechanism of the landslide. Therefore, the long span extensometer is improved based on previous study in Croatia in order to observe at intervals of 50m (photo 5). 14 long span extensometers are arranged in centre longitudinal direction in whole landslide slope.



Photo 5 Extensometer of long span type in Croatia

Rainfall and groundwater observation

Rainfall and groundwater is important for cause of landslide occurrence. The tipping-bucket rain gauge (RS-1 and NetLG-201, OSASI Co.) of a tipping over 0.5mm is installed at Hai Van station. The groundwater table observation is carried out on the borehole of geological survey using water pressure gauge (NetLG-001 OSASI Co.).

Slip surface displacement in borehole

The displacement of the slip surface is also the necessary in order to clarify the mechanism of the

landslide. The displacement of the slip surface is observed used borehole inclinometer and vertical extensometer in borehole (Figure 3). Borehole inclinometer can measure the minute displacement in early landslide activity by the deformation of borehole. The vertical extensometer in borehole measure the shear displacement of slip surface by length of unwinding wire which is connected between sensor on the ground and anchor under depth of slip surface in borehole.

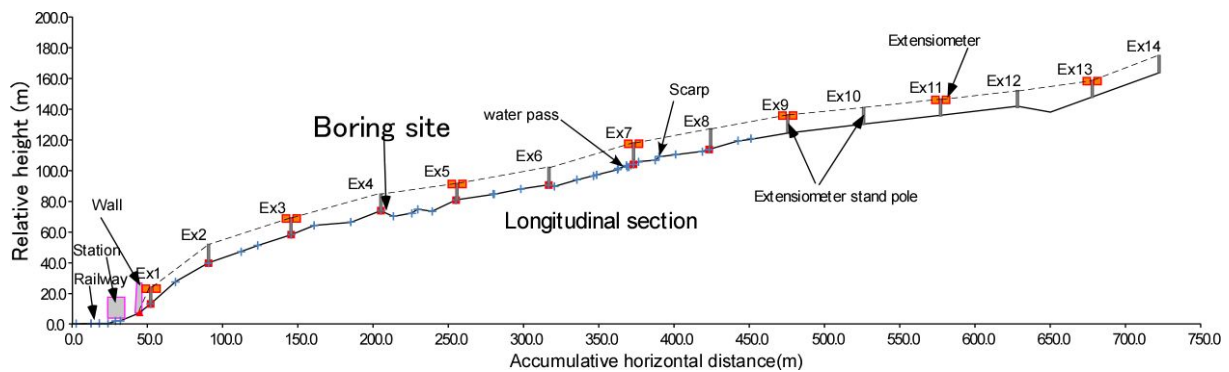


Figure 3 Longitudinal section profile along extensometer and location of boring.

Other monitoring sensor

CCD camera is installed near the landslide to check the situation from office when alarm or early warning situation start.

Data transferring system

All observation sensors are networked by cable or wireless LAN connection. And all data is transferred to computers in ITST office automatically. Each of extensometer, rain gauge and groundwater gauge has own data logger. Each data logger can send data to the computer using the network and issue the alarm by itself. Total station and GNSS can measure by command from

the computer and return the data to the computer.

Preliminary observation of displacement of gabion

Location and measurement item of preliminary observation

Rainfall and displacement of gabion on steep slope nearby railway track were observed as a preliminary observation for test. Rainfall observed using the rain gauge (RG3-M, Onset Co.) which is portable near the station. The displacement observation was carried out by the installation on the slope nearby railway using the short span extensometer (Photo 4).

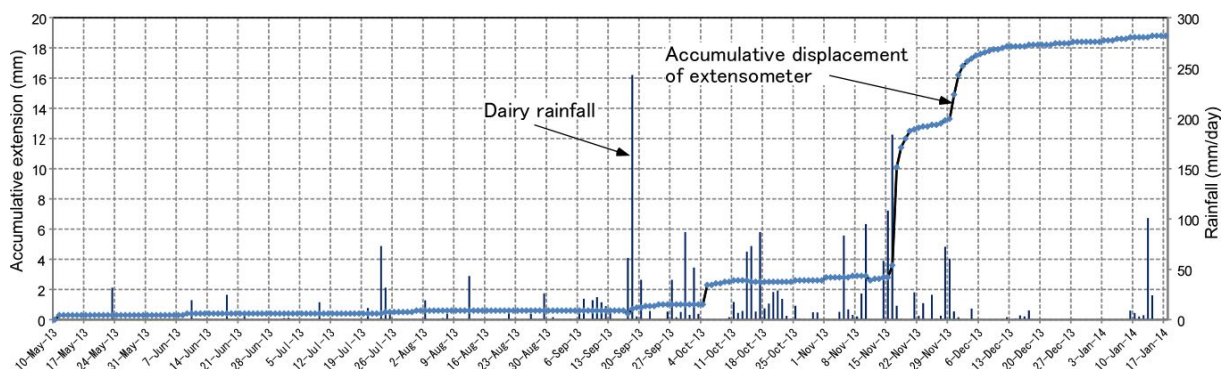


Figure 4 Result of rainfall and displacement of gabion nearby railway as preliminary observation.

The extensometer was set on the bottom of slope and wire was fixed to net of lower face of gabion. Measurement data was the deformation of gabion on the slope and not landslide. This data of preliminary observation was collected in order to confirm the observation method. Interval time of measurement was one hour.

Result and discussion

The dairy variation of rainfall and displacement since May 10, 2013 until January 17, 2014 was shown. Total amount of rainfall was 2425.2mm and maximum dairy rainfall was 243.2 in September 8, 2013. The rainy season was since September until November in this period.

Large observed displacement in this period was 9.8mm since November 16th until 20th and 3.5mm since November 28th until December 2nd. Each displacement was measured just after the heavy rain, rainfall intensity in November 16th was 183mm and it in November 28th was 72.4mm per day. But the displacement didn't appear in heavy rain before November 16th. Therefore, the working rainfall was compared with displacement occurrence.

The daily working rainfall is considered with effect of antecedent rainfall. The daily working rainfall (E_0) can be calculated as follows;

$$E_0 = \alpha \cdot R_0 + \alpha \cdot E_{-1} \quad [1]$$

$$\alpha = (0.5)^{1/M}$$

α : Decrease coefficient, M : half-life, R_0 : rainfall of target date, E_{-1} : working rain in the previous date.

It was compared in case of 7 days and 14 days of the half-life (M) (Figure 5). In $M=14$ case, the daily working rain when displacement was occurred was heavier than it when the displacement was not occurred. However in $M=7$ case, there were some cases that the displacement was not appeared in heavier of working rain. This result shows that the half-life of working rain may larger than 7 days in this case and the working rain may be one of the effective methods to early warning.

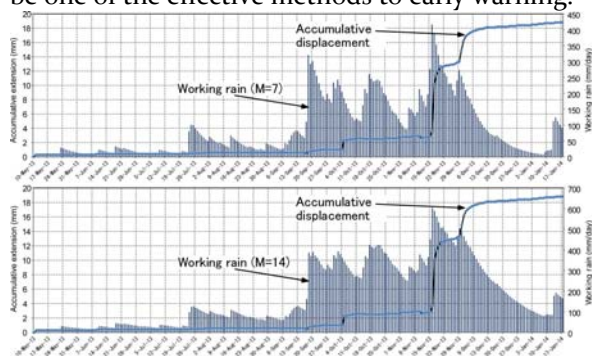


Figure 5 Comparison of effect of working rain

It is necessary to collect the more data in order to increase of the predictability of warning of gabion movement.

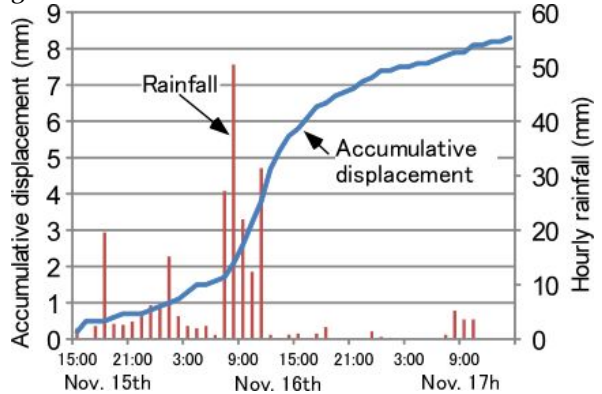


Figure 6 Variation of hourly rainfall and displacement

Hourly rainfall intensity and displacement of gabion were compared since 15:00 at November 15th until 14:00 on 16th (Figure 6). Displacement was continuously increased during rainy hours. There is the prediction method of slope failure time using the inverse number of speed of mass movement. It is regard the mass movement of landslide as like the creep deformation of rheology. Value of deformation accelerated in third creep of rheology. When the accelerated displacement data regarded as third creep are logged using monitoring system, the time prediction of landslide occurrence may be able to estimate.

Concluding remarks

In this study, the approach and design of practical observation system for alarming and early warning for landslide disaster was investigated. As a result, sensor of displacement and hydraulic condition were selected. And preliminary observation of rainfall and displacement of the gabion nearby railway track was conducted and observed data was compared for test. As a result, the analytic method of the working rain and displacement speed may be effective for alarming and early warning. When the all observed data will start collecting, the analysis for landslide mechanism for early warning and alarming will be carried out.



Proceedings of the SATREPS Workshop on Landslides in Vietnam, 2014

High-resolution rainfall simulations for disaster prevention using the Multi-Scale Simulator for the Geoenvironment (MSSG)

Ryo Onishi⁽¹⁾, Keiko Takahashi⁽²⁾, Wataru Sasaki⁽³⁾, Tooru Sugiyama⁽⁴⁾

1) Japan Agency for Marine-Earth Science and Technology (JAMSTEC), Center for Earth Information Science and Technology, Yokohama, Japan, e-mail: onishi.ryo@jamstec.go.jp

2) Japan Agency for Marine-Earth Science and Technology (JAMSTEC), Center for Earth Information Science and Technology, Yokohama, Japan, e-mail: takahasi@jamstec.go.jp

3) Japan Agency for Marine-Earth Science and Technology (JAMSTEC), Center for Earth Information Science and Technology, Yokohama, Japan, e-mail: wsasaki@jamstec.go.jp

4) Japan Agency for Marine-Earth Science and Technology (JAMSTEC), Center for Earth Information Science and Technology, Yokohama, Japan, e-mail: tsugi@jamstec.go.jp

Abstract MSSG (Multi-Scale Simulator for the Geoenvironment) is a global cloud-resolving model and is applicable to global, regional and local scales seamlessly. It has a wide applicability to weather and climate related phenomena. We introduce the MSSG and its wide applications.

Keywords heavy rain simulation, high-performance computing

Introduction

Climate and weather contain complex and multiscale phenomena by nature. High performance and high resolution simulations can expectedly capture those phenomena and thus lead to robust predictions of climate and weather.

The Center for Earth Information Science and Technology (CEIST), former Earth Simulator Center, in Japan Agency for Marine-Earth Science and Technology (JAMSTEC) has developed a high-performance coupled non-hydrostatic atmosphere-ocean general circulation model named the Multi-Scale Simulator for the Geoenvironment (MSSG). MSSG is designed to be applicable to seamless simulations from global to local scales (Takahashi et al. (2013) and Onishi & Takahashi (2012) and references therein). MSSG adopts the conventional latitude-longitude (lat-lon) grid system for regional simulations, and the Yin-Yang grid - consisting of two overlapping lat-lon grids (Kageyama and Sato, 2004; Baba et al., 2010)- for global simulations, thus avoiding the grid-convergence problem at the poles leading to a high computational performance.

Its high performance allows ultra-high resolution simulations leading to a wide range of

applications. This study introduces the MSSG and its wide applications focusing on rainfall simulations.

Multi-Scale Simulator for the Geoenvironment (MSSG)

The Multi-Scale Simulator for the Geoenvironment (MSSG) is an atmosphere-ocean coupled model aiming at seamless simulations for global, regional up to local scales (Takahashi et al. (2013) and Onishi & Takahashi (2012) and references therein). MSSG adopts the conventional latitude-longitude (lat-lon) grid system for regional simulations, and the Yin-Yang grid - consisting of two overlapping lat-lon grids (Kageyama and Sato, 2004; Baba et al., 2010)- for global simulations, thus avoiding the grid-convergence problem at the poles. MSSG has both the atmosphere component (MSSG-A) and the ocean component (MSSG-O) and is capable of atmosphere-ocean coupled simulations (see Fig. 1.).

The dynamical core of MSSG-A is based on the nonhydrostatic equations and predicts the three wind components, air density and pressure. The third-order Runge-Kutta scheme is used for time integrations, and the fast terms relating to acoustic and gravity waves are calculated separately with shorter time steps (Wicker and Skamarock, 2002). A fifth-order upwind scheme is usually chosen for advection, and for turbulent diffusion either the Mellor-Yamada-Nakanishi-Niino (Mellor and Yamada, 1982; Nakanishi and Niino, 2009) or static Smagorinsky model is used, depending on the resolution.

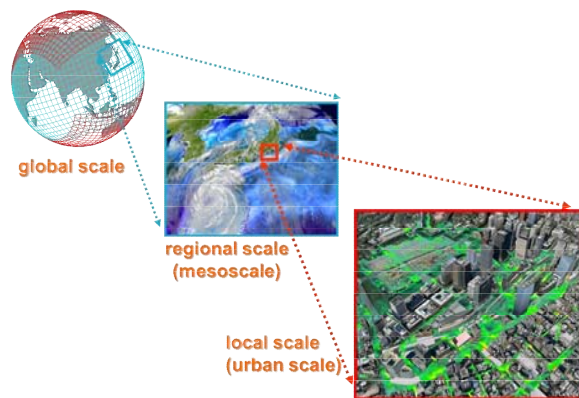


Figure 1 Multi-Scale Simulator for the Geoenvironment (MSSG). MSSG is designed to be seamlessly applicable to global, regional and local scales. MSSG has an ocean component (MSSG-O) as well as an atmospheric component (MSSG-A) and is capable of atmosphere-ocean coupled simulations.

MSSG has been used for a wide range of applications. Examples are as follows:

1. Operational typhoon forecast simulations for the JAMSTEC research vessel 'Chikyu'.
2. Heavy rain simulations (e.g., Sugunami heavy rain in September 2005, Zoshigaya heavy rain in August 2008 and Kyusyu heavy rain in July 2006)
3. Near future rain fall simulations in Tokyo urban area using the pseudo-global-warming method (Sato et al. 2007).
4. Research on the impact of local weather, focusing on Vietnam area, on the global circulation, focusing on the La-Nina in 1999.

Typhoon simulations

Atmosphere-ocean coupled simulation

Typhoon ETAU in 2003 hit Japan and caused a serious damage including nearly 20 casualties. We have performed the atmosphere-ocean coupled MSSG with a nesting technique. The global simulation was performed with approximately 10km horizontal resolution together with a nested Japan simulation with approximately 2.8km resolution.

The MSSG has successfully reproduced the intense activity of the typhoon and its impact on the ocean (see Figure 2). The result has confirmed that the sea surface temperature (SST) drops due to the strong mixing by the typhoon. This SST drop would in turn influence the typhoon activity suggesting a necessity of the coupled simulation for a robust prediction.

Operational typhoon simulation for 'Chikyu'

The Japan Agency for Marine-Earth Science and Technology (JAMSTEC) owns the research vessel named 'Chikyu', which aims to drill the Earth towards the mantle. Due to its drilling tower, Chikyu is weak against strong winds and has to

evacuate from typhoons. The MSSG-A had operationally provided the typhoon predictions to the vessel for an intra-institute use.

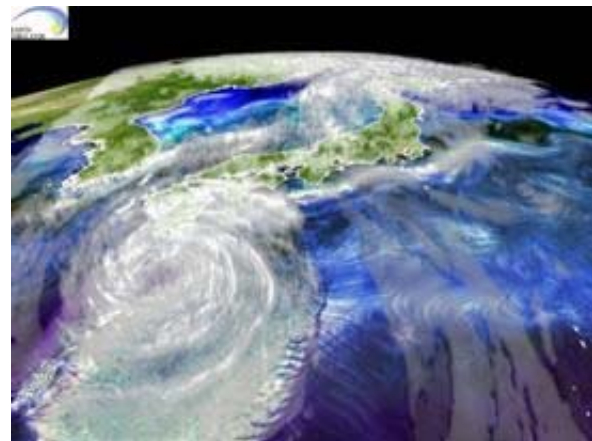


Figure 2 Atmosphere-ocean coupled simulation using the MSSG for Typhoon ETAU in 2003.

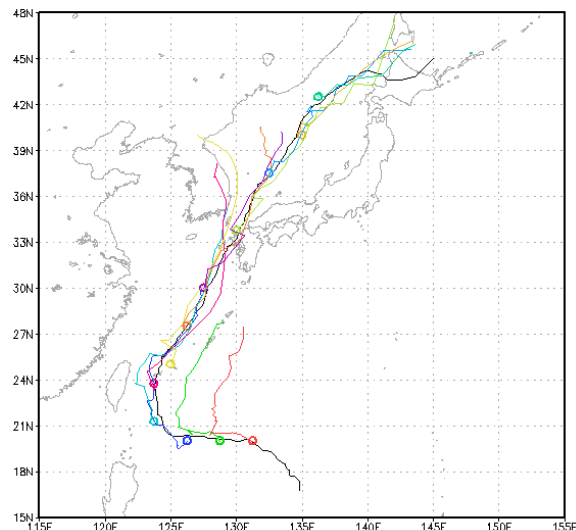


Figure 3 Simulated tracks of a typhoon in September 2006. The black solid line shows the observation and the colored ones the MSSG predictions. Circles indicate the initial locations of the typhoon in each MSSG simulation.

Figure 3 shows the simulated tracks of a typhoon in September 2006. The black solid line shows the observation and the colored ones the MSSG predictions. Circles indicate the initial locations of the typhoon in each simulation.

Heavy rain simulations

Suginami heavy rain in September 2005

A sudden local heavy rain, with which the Tokyo modern urban sewage system could not deal, caused floods in several districts in Tokyo on 4 September, 2005. Many observatory points recorded heavy precipitations with over 100 mm/hour.

We have performed a regional simulation using the MSSG-A with horizontal resolutions of

1km. The MSSG-A has successfully reproduced the localized heavy precipitations as in Figure 4.

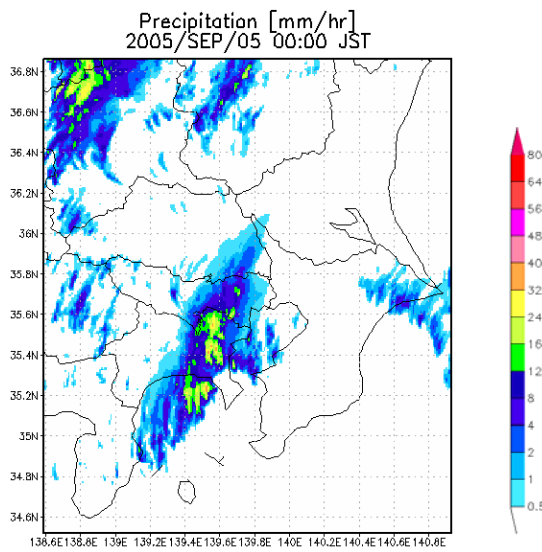


Figure 4 The surface precipitation at 00UTC on 4 September, 2005.

Kyusyu heavy rain in July 2006

Kyusyu had a record heavy rain during 19 to 23 July, 2006. The rain was reportedly caused by the baiu front stimulated by a typhoon. The accumulated rain fall exceeded 1,000 mm in 4 observatory points in Kyusyu. Floods and landslides caused a serious damage including 5 casualties.

We have performed a global simulation using the MSSG-A with approximately 20km horizontal resolution. In spite that its horizontal resolution was not so high for a regional weather, MSSG-A has succeeded in reproducing the persistent heavy rain as in Figure 5.

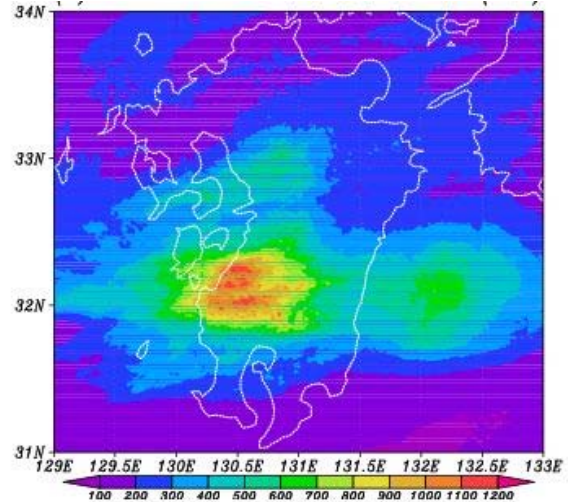
Downscale simulations

Pseudo-global warming experiment

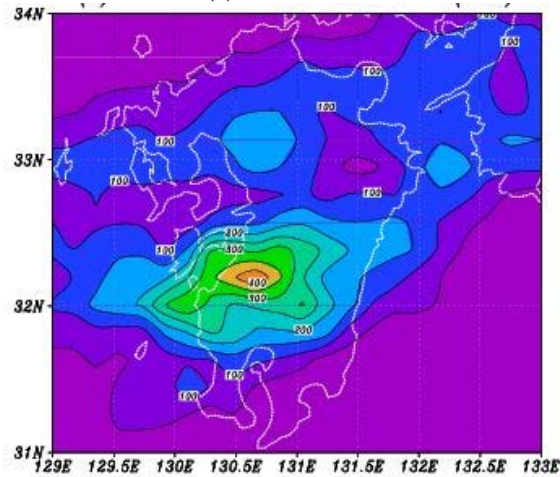
The pseudo-global warming method (e.g., Sato et al., 2007) is a downscale method that aims to project the regional climate change using the future boundary condition created from a projection by a global climate model.

We used the projection by Miroc3.2 hires for a near future run. We defined the projection for the 30 years starting from 2001 as a 'present climate' and that for the another 30 years starting from 2031 as a 'near future climate'. The difference between the two can be considered as the change due to the global warming. The computational domain was approximately 330km×250km in horizontal, covering the Kanto district, with 1km resolution and the 19km×8km area, which corresponds to the main watershed of the Kanda river, was selected for analysis (the yellow rectangular in Figure 6). For the present climate

run, we used the MSM data of the Japan Meteorological Agency. The change due to global warming was simply added to the MSM data for the near future climate run.



(a)observation



(b)MSSG

Figure 5 The accumulated rain fall in Kyusyu area during 19 to 23 July, 2006. (a)Radar-AMeDAS observation and (b)MSSG.

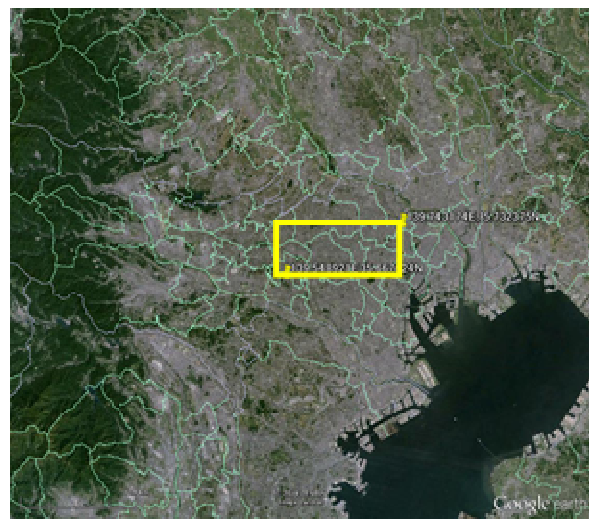


Figure 6 Analysis area with approximately 19km×8km which covers the major watershed area of the Kanda river.

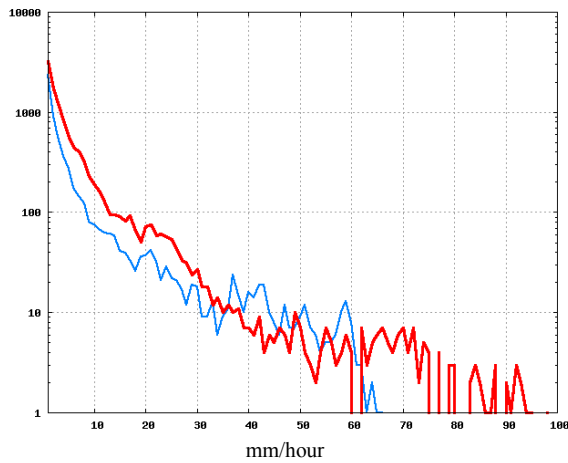


Figure 7 The frequent distribution of the surface precipitation averaged over the watershed area of the Kanda river. Blue line is obtained from the present climate run and the red from the near future (representing 30 years later) run.

Figure 7 shows the frequent distribution of the surface precipitation averaged over the watershed of the Kanda river, i.e., the yellow rectangular in Figure 6. Comparison between the present (blue) and future (red) shows that we would have more chance of severe heavy rains with over 70 mm/hour in the near future with warmer climate.

Vietnam rain fall simulation

Year 1999 was a strong La-Nina year. For Vietnamese people, it was rather a heavy rain year. In the early November 1999, Vietnam had a record heavy rainfall, which resulted in severe floods in Quang Nam, Thua Thien-Hue and Binh Dinh districts. The flood stayed for 2 weeks, causing about 600 casualties and serious infections for more than 10,000 people.

There would be a correlation between the strong La-Nina event, which is a global scale atmosphere-ocean coupled phenomenon, and the heavy rain event in Vietnam. The downscaling technique is promising for investigating such a global-local correlation. Therefore, we have performed the atmosphere-ocean coupled downscale simulation using the MSSG.

Figure 8(a) shows the global domain of the MSSG. The color shade shows the sea surface temperature (SST). The horizontal resolution for the globe was approximately 128km. The nested domain, shown in Figure 8(b), covered the South-East Asia and the horizontal resolution for it was approximately 7km.

Figure 9 shows the average surface precipitation [mm/day] for November 1999. The MSSG with 128km resolution cannot reproduce the heavy rain since the steep orography is not resolved by such a low resolution and the orographic precipitation could not be properly

described as a result. In contrast, the MSSG with 7km has succeeded in reproducing the heavy rain. This clearly shows the benefit of the downscale simulation.

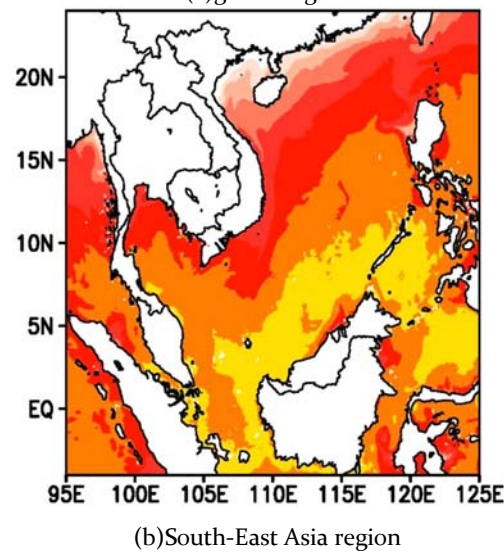
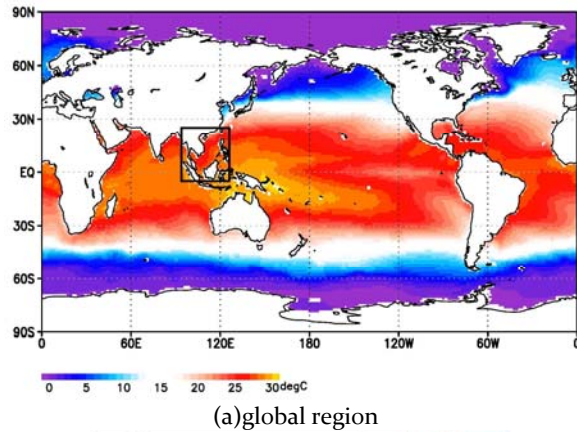


Figure 8 Computational domain of the atmosphere-ocean coupled downscale simulation using MSSG. (a) global region and (b) the nested region. Shaded color shows the sea surface temperature (SST).

Concluding remarks

The Center for Earth Information Science and Technology (CEIST), former Earth Simulator Center, in Japan Agency for Marine-Earth Science and Technology (JAMSTEC) has developed the Multi-Scale Simulator for the Geoenvironment (MSSG), which is an atmosphere-ocean coupled global cloud-resolving model and is applicable to global, regional and local scales seamlessly. It has a wide applicability to weather and climate related phenomena. We have introduced the MSSG and its applications for heavy rain events in this manuscript. The application experience would be very much helpful when we apply the MSSG to a possible future Vietnam landslide project.

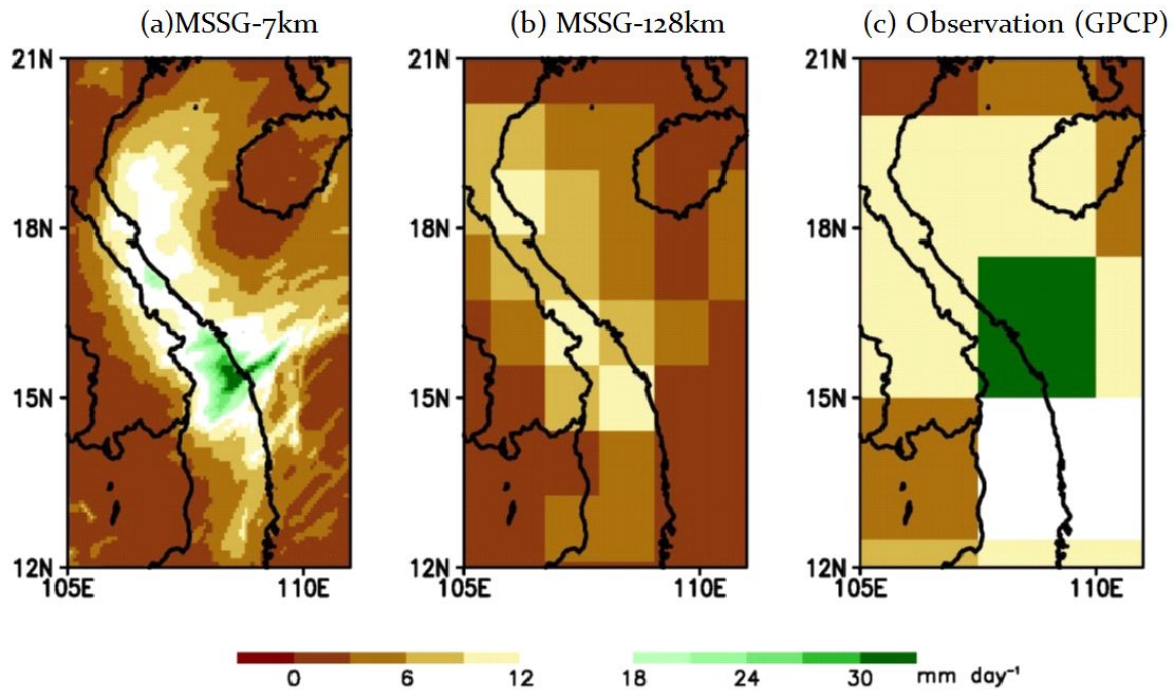


Figure 9 Average surface precipitation in November 1999. Vietnam had a record flood in this period. (a)MSSG with 7km horizontal resolution, (b)MSSG with 128km resolution and (c) observation (GPCP).

Possible applications will be, for example,

1. operational 72 hours rainfall simulations for land slide risks, and
2. assessment of the land slide risks in the near future with warmer climate.

Acknowledgments

The simulations were performed on the Earth Simulator 2 at the Japan Agency for Marine-Earth Science and Technology.

References (in the alphabetical order)

Baba, Y. and Takahashi, K. and Sugimura, T. (2010) Dynamical Core of an Atmospheric General Circulation Model on a Yin-Yang Grid, *Monthly Weather Review*, 138: 3988-4005.

Kageyama, A. and Sato, T. (2004) The "Yin-Yang grid": An overset grid in spherical geometry", *Geochem. Geophys. Geosyst.*, 5: Q09005.

Mellor, G. L. and Yamada, T. (1982) Development of a Turbulence Closure Model for Geophysical Fluid Problems, *Rev. Geophys. Space Phys.* 20: 851-875.

Nakanishi, M. and Niino, H. (2009) Development of an improved turbulent closure model for the atmospheric boundary layer, *J. Meteor. Soc. Japan*, 87: 895-912.

Onishi, R. and Takahashi, K. (2012) A Warm-Bin-Cold-Bulk Hybrid Cloud Microphysical Model, *Journal of the Atmospheric Sciences*, 69: 1474-1497.

Sato, T., Kimura, F., and Kitoh, A. (2007) Projection of global warming onto regional precipitation over Mongolia using a regional climate model. *Journal of Hydrology*, 333: 144 – 154.

Takahashi, K., Onishi, R. Baba, Y., Kida, S., Matsuda, K., Goto, K. and Fuchigami, H. (2013) Challenge toward the prediction of typhoon behavior and down pour, *Journal of Physics: Conference Series*, 454: 012072.

Wicker, L.J. and Skamarock, W.C. (2002) Time-splitting methods for elastic models using forward time schemes, *Monthly Weather Review*, 130: 2088-2097.



Proceedings of the SATREPS Workshop on Landslides in Vietnam, 2014

Identification, monitoring and simulation of landslides in the Rječina River Valley, Croatia

Željko Arbanas⁽¹⁾, Snježana Mihalić Arbanas⁽²⁾, Martina Vivoda⁽¹⁾, Josip Peranić⁽¹⁾, Sanja Dugonjić Jovančević⁽¹⁾, Vedran Jagodnik⁽¹⁾

1) University of Rijeka, Faculty of Civil Engineering, Rijeka, Radmile Matejčić 3, Croatia, e-mail: zeljko.arbanas@gradri.uniri.hr

2) University of Zagreb, Faculty of Mining, Geology and Petroleum Engineering, Zagreb, Pierottieva 6, Croatia, e-mail: snjezana.mihalic@rgn.hr

Abstract The Croatian-Japanese joint research SATREPS' project 'Risk Identification and Land-Use Planning for Disaster Mitigation of Landslides and Floods in Croatia' was performed from 2009 to 2014. Key objectives of the project were landslides and floods hazard analysis and the development of guidelines for use in urban planning. The aims of the working groups dealing with landslides were to establish a methodology of comprehensive real time monitoring at two most important landslides in Croatia based on the results of previous investigations and new in situ and laboratory testing and behaviour analysis; laboratory soil testing and numerical modelling of static and dynamic landslide behaviour; development of landslide inventories using direct sensing and remote sensing techniques followed by the development of methodologies of landslide hazard analysis and zonation in three pilot areas in Croatia. In this paper we will present the most important achievements of working groups related to landslide studies at the one of the Project pilot areas: the Rječina River Valley near the City of Rijeka. The identification and mapping of existing landslides in the Rječina River Valley so as establishment and results of the monitoring on the Grohovo Landslide, the most recent landslide in the pilot area will be described. It will be also pointed on activities whose would be performed to improve results of conducted investigations and analyses.

Keywords landslide, identification, monitoring, testing, simulation

Introduction

The Croatian-Japanese joint research project 'Risk Identification and Land-Use Planning for Disaster Mitigation of Landslides and Floods in Croatia'

was launched in 2008, when it was selected for the Science and Technology Research Partnership for Sustainable Development (SATREPS), and it was completed in March 2014. Key objectives of the project were landslides and floods hazard analysis and the development of guidelines for use in urban planning (Mihalić & Arbanas 2013). The project activities are organized into three working groups: Working Group on Landslides (WG₁), Working Group on Flash Floods and Debris Flows (WG₂) and Working Group on Landslide Mapping (WG₃). The aim of Working Group 1 on Landslides was to establish a methodology of comprehensive real time monitoring at two most important landslides in Croatia: the Grohovo Landslide in Primorsko-Goranska County and the Kostanjek Landslide in the City of Zagreb based on the results of previous investigations and new in situ and laboratory testing and behaviour analysis so as a laboratory soil testing and numerical modelling of static and dynamic landslide behaviour. The activities of Working Group 3 on Landslide Mapping (WG₃) were aimed at the development of landslide inventories using direct sensing and remote sensing techniques followed by the development of methodologies of landslide hazard analysis and zonation in three pilot areas in Croatia: two in Primorsko-Goranska County and one in the City of Zagreb. In this paper we will present the most important achievements of working groups related to landslide studies at the one of the Project pilot areas: the Rječina River Valley near the City of Rijeka.

The Rječina River is a typical karstic river originating from a strong karstic spring at the foot of the Gorski Kotar Mountains outside the City of Rijeka, the largest Croatian port on the north-eastern Adriatic coast. The Rječina River flows through a deep valley with slopes formed in flysch

deposit prone to sliding. There are more evidences of landslides occurrences near the Grohovo Village in the past 250 years found in numerous historical descriptions, figures and maps describing landslides in the Croatian State Archive (2011) in Rijeka. The last major landslide occurrence was the complex retrogressive Grohovo Landslide, reactivated in December 1996, after long dormant period and about 1.0×10^6 m³ moved down the slope and buried the Rječina river-bed (Benac et al. 2005). The Grohovo Landslide was chosen as a pilot area for monitoring system development and a comprehensive monitoring system consisting of geodetical and geotechnical monitoring was designed and established (Arbanas et al. 2012a). During the investigation of wider area of the Grohovo Landslide and analysing of existing data of landslide occurrences in the Rječina River valley (Benac et al. 2011), the necessity of the landslide inventory development was identified and a landslide zonation of the valley using LiDAR imagery (Mihalić Arbanas & Arbanas 2014). To predict possible development of the existing landslide and hazards of new landslides on flysch slopes of the valley and to establish an early warning system detailed analyses of preliminary monitoring results and current stability state of flysch slopes were performed (Arbanas et al. 2012b, 2012c, Wang et al 2013). Detailed laboratory soil testing as a base for prediction of landslides behaviour have been performed in a undrained ring-shear apparatus designed and developed for testing under static and dynamic conditions for deep seated large landslides in Croatia (Oštrić et al. 2012, 2013). Methodology for landslide susceptibility assessment was developed based on landslide simulation using LS-Rapid software (Vivoda et al. 2014). In this paper the review of previously noted activities conducted in the frame of Croatian-Japanese joint research SATREPS' Project in the pilot area of the Rječina River Valley.

Landslides in the Rječina River Valley, history and present state

Geological settings of the Rječina River Valley

The Rječina River is 18.7 km long, and the mouth is located in the center of the City of Rijeka. The Rječina River is a typical karstic river originating from a strong karstic spring at the foot of the Gorski Kotar Mountains. The annual average profusion of the Rječina spring is $7.76 \text{ m}^3\text{s}^{-1}$ with maximum flow rates ranging from 0 to over $100 \text{ m}^3\text{s}^{-1}$ (Karleuša et al. 2003). Some of the water from the Rječina spring is used for water supply of Rijeka City, while some of the water from the

Valići Lake is used for electric power production in the Rijeka Hydropower Plant.

The area of the valley is part of a dominant morphostructural unit that strikes in the northwest-southeast direction along the Rječina Valley (Velić & Vlahović 2009). The kinematics of the structural elements in the central part of the Rječina Valley are based on the relationship between relatively rigid carbonate rocks and ductile siliciclastic rocks during simultaneous deformations. The Cretaceous and Paleogene limestones are situated at the top of the slopes, while the Paleogene siliciclastic rocks and flysch are situated on the lower slopes and the bottom of the valley, Fig. 1. The flysch complex is a block that has been squeezed between the limestone rock blocks on the northeastern and southwestern sides. The effects of the deformation are most distinctive at the contacts between the two rocky complexes, where the relatively rigid limestone is pushed into the more ductile siliciclastic rocks. In this way, the formerly straight tectonic contact deformed into its present toothed appearance (Blašković 1999, Benac et al. 2005).

The siliciclastic or flysch bedrock is lithologically heterogeneous, with common vertical and lateral alternations of different lithological sequences. Microscopic petrological analysis of the bedrock has shown the presence of silty marl, laminated silt to silty shale and fine-grained sandstones (Benac et al. 2005, 2011). Unlike the limestone, the flysch deposits are prone to weathering, which causes the formation of a clayey weathering zone on the flysch bedrock. Over time, coarse-grained fragments originating from rockfalls were mixed with clay from the weathered flysch zone, forming slope superficial deposits a few meters thick (Arbanas et al. 2012d).

Historical landslides in the Rječina River Valley

Numerous historical descriptions, figures, photographs and maps describing landslides were found in the Croatian State Archive (2011) in Rijeka which provides evidence of the occurrence of landslides in the Rječina Valley near the Grohovo Village. Sliding was first documented in 1767, when numerous landslides and rockfalls in the Rječina River Valley were caused by the 1750 earthquake ($I=9$ according Mercalli-Cancani-Sieberg Intensity Scale), which had an epicenter in the City of Rijeka. Large landslides triggered by rainfall and floods were noticed on both river banks near the Grohovo Village at the end of 19th century. A large landslide occurred on the southwestern slope in 1870, and after reactivation of the slide in 1885 part of the Grohovo Village was buried by a rock avalanche (Fig. 1).



Figure 1 Aerial view of the Rječina River Valley: landslide and rock avalanche from 1870 and 1885 on the left (SW) side buried the Grohovo Village, landslide from 1893 reactivated in 1996 on right (NE) side, the river channel is situated in the bottom.

A large landslide occurred in 1893 on the northeast-ern slope of the Rječina River Valley at the location of the recent landslide, and the Rječina River channel was shifted to the south by approximately 50 m. Because of these landslides and the resulting damage, the Ministry of Agriculture of the Hungarian Kingdom designed the Rječina Recovery Project in 1894, and restoration began in 1889. The designer of the Rječina Recovery Project, civil engineer Bela Pech, mapped all the landslides on the 1894 topographic map which can be nominated as the one of the oldest landslide inventories. Restoration of the Rječina River banks was finished in 1908, and during construction sliding had to be stabilized using drain trenches and dikes (Anon 2011, Mihalić & Arbanas, 2013).

Numerous landslides occurred during the first half of the 20th century but did not cause significant damage to structures on the river banks. New problems with landslides in the Rječina valley occurred during construction of the Valići Dam in 1960, when landslides appeared on the northeast slope near the dam. This landslide was stabilized during the dam's construction (Arbanas et al. 2012d).

The large landslide, so called the Grohovo Landslide, occurred in December 1996 at the location of the landslide from 19th century on the northeast slope (Fig. 1). Comparison with old topographic map from 1894 shows that the landslide mass had a significantly smaller volume than the older sliding (Mihalić & Arbanas 2013). The slide mass completely buried the Rječina River channel, and a landslide foot formed a dam and the lake behind. Immediately after sliding, this landslide mass was removed from the river channel, eliminating the risk of dam collapse and

the resulting water wave that could have caused serious damage to the City of Rijeka but complete remediation of the landslide was never conduct (Arbanas et al. 2012d).

The most recent landslide occurred in February 2014 at the south-western slope of the valley after long period of heavy rain. The approximate volume of the landslide is about $1.0 \times 10^6 \text{ m}^3$ and the foot of the landslide reached the reservoir behind the Valići Dam. After lowering of water datum in the reservoir and surface drainage works the landslide stopped to move.

Description of the Grohovo Landslide

The results of investigation works on the Grohovo Landslide after sliding occurrence in December 1996 have shown the formation of a complex landslide with thirteen sliding bodies including movements of the carbonate mega-blocks at the top of the slope (Benac et al. 2005), Fig. 2. Boundaries between these bodies are mostly clearly expressed. Sliding bodies represent different types of mass movements. The whole reactivated sliding mass has a volume of approximately $3.0 \times 10^6 \text{ m}^3$. On the basis of geological mapping and geophysical surveys results, thickness of the displaced sliding mass could be estimated and the position of sliding surfaces could be determined. Geometry of the total complex landslide, described according to WP/WLI Suggested Nomenclature for Landslides (IAEG 1990), Tab. 1.



Figure 2 Aerial view of the Grohovo Landslide from 1893 reactivated in 1996; the Rječina River Channel is situated in the bottom.

Slip surface was formed on the contact of slope deposits and the flysch bedrock. Initial landslide body was the most moved one, what is visible from the range of displaced material in the Rječina River Channel, and by the tilted trees. Due to the magnitude of displacement (up to 20

m) primary geological settings was completely disturbed.

Table 1 Dimension of the Grohovo Landslide occurred 1996 according WP/WLI Suggested Nomenclature for Landslides (IAEG 1990).

Landslide dimension	Symbol	Distance (m)
Total length	L	425
Length of the displaced mass	L_d	420
Length of the rupture surface	L_r	405
Width of the displaced mass	W_d	200
Width of the rupture surface	W_r	200
Depth of the displaced mass	D_d	6-20
Depth of the rupture surface	D_r	6-9 (20)
Total height	ΔH	165

According to accepted classifications, the investigated landslide is a complex composite landslide. It is a complex and retrogressive landslide (Skempton & Hutchinson 1969, Hungr et al. 2014). Movements of mixed rock and soil material in initial landslide body have characteristics of debris avalanches, according to velocity of movements (Varnes 1978, Cruden & Varnes 1996). Block sliding of a rock mass is a special phenomenon. Due to the fact that the position of the slip surface was predisposed by geological settings, the landslide can also be considered as a consequent translational, as well as the blocky slide type IIIb (Antoine & Giraud 1995). According to landslide activity it could be considered a reactivated land-slide on unstable slope, type Ib (Crozier 1984).

Landslide identification in the Rječina River Valley

Techniques of landslide identification

Analyses of the past and prediction of the future landslide behaviour are the most important steps in hazard zonation so as in a landslide early warning system consideration (Arbanas et al. 2012c). With the knowledge about numerous landslide occurrences in the Rječina River Valley in the history and without landslide inventory which would offer insight in real landslide distribution in the area, the first step for necessary analyses was identification of existing landslides in the research area and assessment of their features.

The objective of landslide identification is the determination of landslide boundaries at the ground surface, including the source area and displaced mass (Mihalić Arbanas & Arbanas 2014). All of the techniques can be grouped into two broad categories according to Guzzetti et al. (2012): conventional methods and new (innovative) techniques. Conventional methods

used to identify landslides include: (i) geomorphological field mapping and (ii) visual interpretation of stereoscopic aerial photographs. Guzzetti et al. (2012) grouped recent and new methods and technologies for identification and mapping of landslides over large areas as follows: (i) analysis of surface morphology with very-high-resolution digital elevation models (DEMs) and (ii) interpretation and analysis of satellite images, that is, panchromatic, multispectral, and synthetic aperture radar (SAR) images.

Identification of landslides in the field is a component of standard geomorphological mapping (Brunsden 1993) or engineering geological mapping (Keaton and DeGraff 1996). The key features of landslide phenomena at the ground surface are the main scarp, lateral flanks, internal morphology, vegetation, and landslide toe. However, because considerable topographic details are required to locate many critical landslide elements, a detailed ground survey generally must be included as a major component of landslide identification at the detailed scale, which is economically justified only in the case of site-specific landslide investigation. A disadvantage of field mapping is the limited ability to accurately determine a landslide boundary in the field due to the reduced visibility of the slope failure (a consequence of the local perspective), the size of landslide, and the fact that the landslide boundary is often indistinct or fuzzy (Santangelo et al. 2010). Unlike field mapping of individual landslides, field work aimed at mapping of landslides over large areas should be of rather limited use (Guzzetti et al. 2012).

Over the last few years, airborne laser scanning has been made available and has been used to identify and map landslide morphology in areas that are partially or completely covered by dense vegetation (Carter et al. 2001; Razak et al. 2011). A relatively new remote-sensing tool uses airborne mounted lasers to obtain digital representations of the topographic surface for areas ranging from a few hectares to thousands of square kilometers (Shan and Toth 2009). Airborne LiDAR (Light Detection and Ranging) is also known as airborne laser scanning (ALS) or airborne laser swath mapping (ALSM). In these methods, a laser sensor measures the distance from the instrument and multiple points on the topographic surface. Although laser scanning measures the altitudes of all objects scanned, post-processing is necessary for creation of bare earth DEM to remove the undesired returns from buildings and canopies via filtering of the original data (Reutebuch et al. 2003). Visual analysis and interpretation of the topographic surface remain the most common and most promising

application of a very-high-resolution (metric to decimetric) DEM captured by airborne LiDAR sensors for detection and mapping of landslides over large areas (Guzzetti et al. 2012). The required resolution of a bare-earth LiDAR DEM for identification of landslides primarily depends on the landslide size.

Landslide identification in the Rječina River Valley using very-high resolution LiDAR DEMs

As an appropriate technique for landslide identification in the Rječina River Valley the analyses of very-high resolution DEMs obtained by airborne laser scanning in combination with field mapping was chosen. The visual identification of landslides is based on the recognition of landslide features on the following types of topographic derivative maps: contour map, hillshade map, slope map, curvature map and topographic roughness map. Fig. 3 shows contour map, hillshade map and slope map of landslide and rock avalanche from 1870 reactivated 1885 on the south western slope of the Rječina River Valley derived from 1-m resolution DEM scanned by ALS in March 2012. From these

maps it was possible to contour the landslide area, determine main landslide dimensions and assess a landslide model. The main landslide features (main scarp, flanks etc.) are checked by field mapping.

The same procedure was repeated for identification of all known historical landslides in the valley on the basis of historical descriptions and all these landslides are located and determined. During very-high resolution DEMs analyses a notable number of unknown landslides was identified and most of them are completely hidden covered by vegetation. Time of their occurrence is also unknown but scars and expression of their features indicate on relatively young phenomena. Historical landslides in the Rječina River Valley are major instabilities and their volumes vary from 6.1 to 25 million m³, while younger landslides are significantly smaller with volumes from 10 thousand to 3 million m³, and mostly occurred as reactivated parts of the older landslides. When all these landslides are presented on same DEM it is clearly visible that the both slopes of the valley are intensively affected by sliding, Fig. 4.

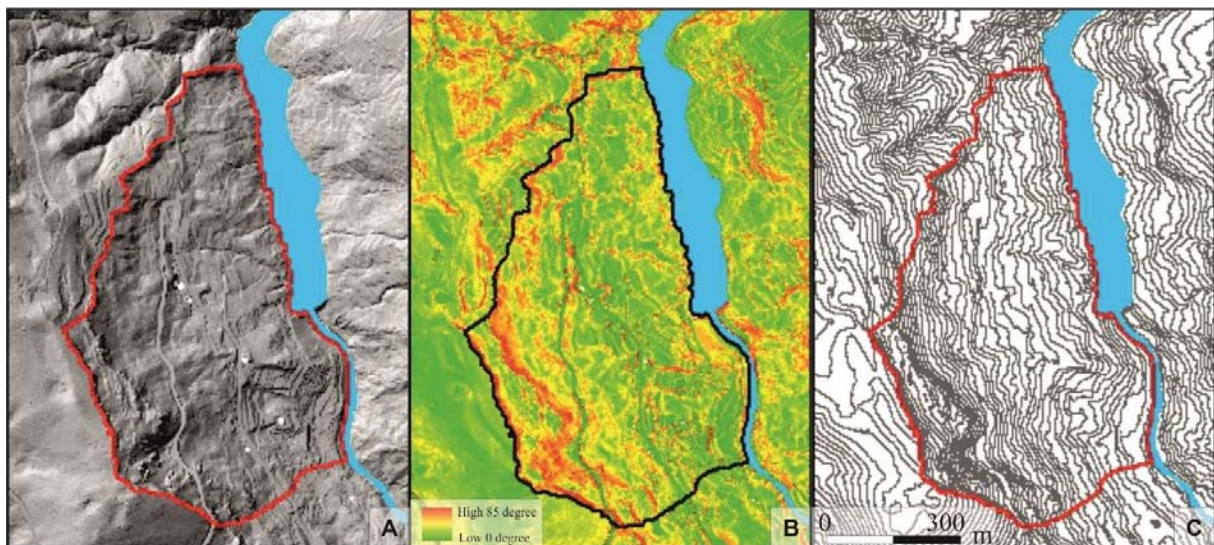


Figure 3 Composite displays of three different topographic derivative maps of the landslide and rock avalanche from 1870 reactivated 1885 on the south western slope of the Rječina River Valley. The estimated extent of the landslides has a red contour (A) Hillshade map draped over a bare earth DEM. (B) Slope map showing areas of high slope angle in warmer colors and areas of low slope angle in cooler colours. (C) Contour map generated with a 1-meter contour spacing.

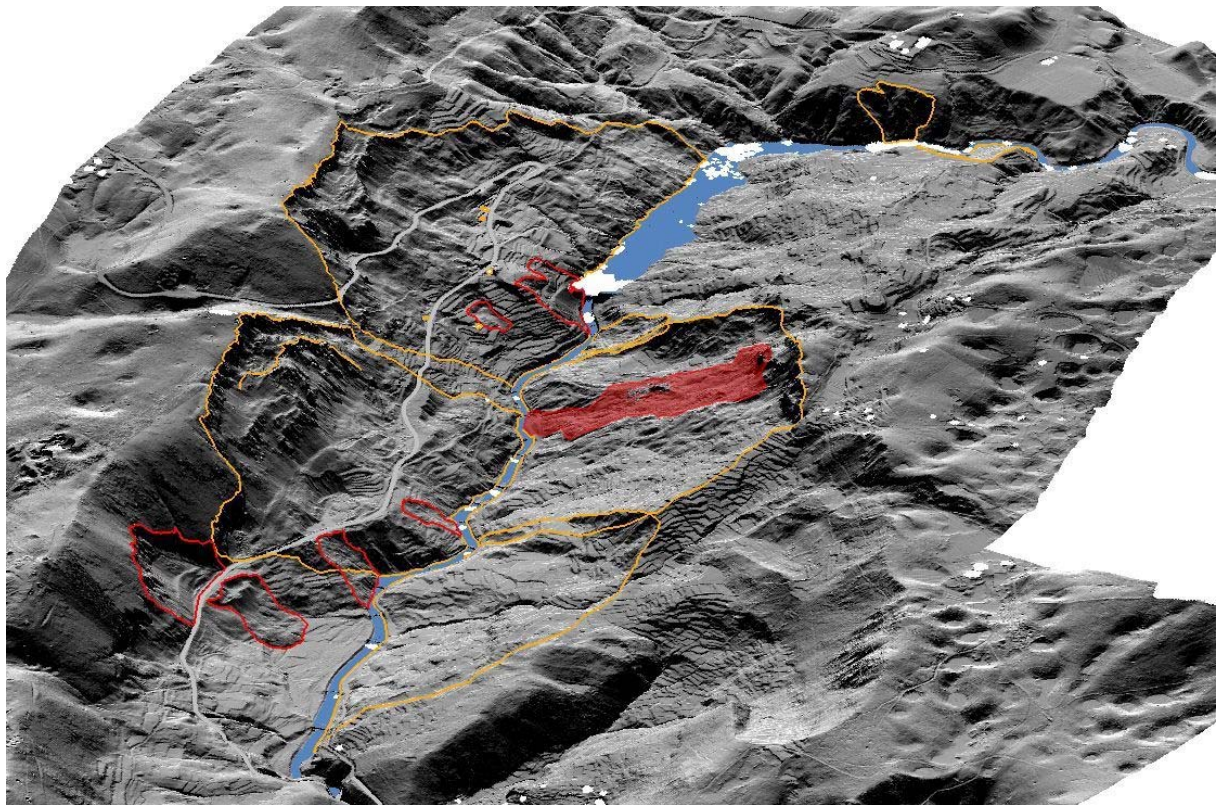


Figure 4 Oblique aerial view created from the LIDAR-derived bare-earth DEM of the Rječina River Valley. Landslide features of an unnamed landslide can be clearly identified. Yellow borders contour historical landslides from 1885 and 1750 on the left side and 1893 on the right side. Red coloured zone is area of reactivated landslide from 1996. Red borders contour younger landslides.

Monitoring of the Grohovo Landslide

Landslide monitoring techniques

By definition, landslides are characterized by movement. Knowledge of the movement magnitude and velocity distribution along the slope, are the most important data for all landslide analysis (Mihalić Arbanas & Arbanas 2014). Monitoring is required to observe the changing conditions that may lead to total failure of the slope where slope movement is occurring, where safety factors against sliding are low, or where high risk is present from a possible slope failure. Landslide movement monitoring expressed via ground surface displacements and deformation of structures (including the landslide body) related to landslides can be accomplished using different types of monitoring systems and techniques that are classified according to Savvaidis (2003) as follows: satellite and remote sensing techniques, photogrammetric techniques, geodetic or observational techniques, and geotechnical or instrumentation or physical techniques. The selection of measurement instrumentation and methods or the planning and design of a desirable monitoring system depends on the movement types and deformation as well as on the role and purpose of the monitoring campaign (Savvaidis 2003).

All satellite and remote sensing techniques (photography and imagery ranging from ground-based mobile units to airborne or satellite platforms using LiDAR, optical, and radar sensors) used for landslide mapping also can be used for landslide monitoring if multi-temporal images are available.

Photogrammetry is a three-dimensional measurement process that enables the determination of 3D motion vectors in long-term landslide monitoring (Brückl et al. 2006). Images can be acquired by satellites, aircraft, helicopters, or remote unmanned aerial vehicles (UAV) as well as from a ground-based observation points using such equipment as film cameras, digital cameras, scanners, among others. The main advantages of the photogrammetry technique are the reduced time of fieldwork, simultaneous three-dimensional coordinates, and in principle, unlimited number of points (targets) that can be monitored.

Conventional ground-based geodetic techniques have been used for surface displacement monitoring of landslides. Savvaidis (2003) differentiates between two basic methods for the design of a geodetic survey: (i) a horizontal or vertical control benchmark network established in the landslide area under monitoring with control points located in the landslide body and (ii) the total station instruments used to measure angles and distances

to target prisms located at the moving landslide mass.

The Global Positioning System (GPS) is often used as a surveying tool in landslide monitoring by positioning the 3D coordinate time series of displacements at discrete points on the landslide surface (Gili et al., 2000). The GPS positioning is based on measuring the transit time of radio signals emitted by stationary orbiting satellites and computing a receiver position, the unit must be in view of at least four satellites. The GPS is U.S. (military) system; other satellite-related positioning systems are the Russian GLONASS and the European Satellite System GALILEO complemented by the civil Global Navigation Satellite System (GNSS). Current GPS positioning techniques for landslide monitoring typically include the use of either episodic techniques or continuous monitoring and static, rapid-static, or real-time kinematic GPS surveying techniques (Savvaidis, 2003). Static or Relative GPS (RGPS) measurements are based on positioning of relative coordinates of the rover stations relative to the reference stations and precise determination of baseline distances between rover stations located on landslide surfaces and reference stations located outside the landslide body (e.g., Gili et al., 2000; Mora et al., 2003; Brückl et al., 2006). Real Time Kinematic GPS (RTK GPS) uses one or even a network of reference stations (Wang, 2011; Wang et al., 2014) set up as known points with fixed coordinates. The baseline distances between rover stations located on a landslide surface and fixed reference stations can be calculated quite accurately, but the absolute position of the rovers also can be found relative to the coordinates of the fixed reference stations.

Geotechnical sensors are used extensively in landslide monitoring to ensure efficient data for landslide behaviour prediction and landslide stability analysis. The main geotechnical sensors and instruments used for landslide monitoring include inclinometers, extensometers, crack meters, piezometers, deformaters, tiltmeters, clinometers, load and pressure cells, and geophones. Most of those geotechnical sensors store the measured data using internal loggers awaiting download or the measurements can be automatically logged to a connected computer unit (Savvaidis, 2003). An additional group of sensors necessary to complete the group of geotechnical monitoring sensors and enable analyses of measured data is the group of meteorological sensors that are usually integrated in a compact but efficient weather station.

Usually, different types of monitoring techniques and instrumentation are used in different combinations and connected in a unique comprehensive landslide monitoring system.

Because of the variability in landslide types and processes, targets of landslide investigation, field conditions, and ongoing technological development of monitoring sensors, no standardization can be adopted as a universal solution for landslide monitoring system setups. The use of multiple sensors for the same purpose (equipment fusion) and at the same position is recommended to guarantee redundancy of measurements and can prevent loss of data if one instrument fails (Arbanas et al. 2014, Mihalić Arbanas & Arbanas 2014). Using the same position for different types of monitoring sensors also enables spatial correlation of measurement data on the landslide surface and inside the landslide profile. Use of different geodetic and geotechnical sensors in combination with hydrological monitoring equipment, that is, to measure data on precipitation and pore pressures in the landslide profile, allows reconstruction of the relationships between rainfall, ground water level, and consequent landslide behavior as a base for establishing an early warning system. Comprehensive monitoring systems have been established on numerous landslides throughout the world and certain of them are described in detail in numerous papers in journals and conference proceedings.

The Grohovo Landslide comprehensive monitoring system

In the frame of Croatian-Japanese joint research SATREPS project "Risk identification and Land-Use Planning for Disaster Mitigation of Landslides and Floods in Croatia the Grohovo Landslide was chosen as a pilot area for comprehensive integrated real-time monitoring system development and an advanced comprehensive monitoring system was designed and installed. Installation of the monitoring equipment started in May 2011 and completed in October 2013, but further improvements of the system are still ongoing. The monitoring system was designed to consist of geodetic and geotechnical monitoring (Arbanas et al. 2012a).

Geodetic monitoring consists of a robotic total station (Leica TM30) measuring 25 geodetic benchmarks (prisms) and a Global Positioning System (GPS) master unit (Leica GMX901) with 9 GPS receivers (rovers). The robotic total station and the GPS master unit are located in a relatively stable area, on the top of the slope opposite to the landslide (Fig. 1), together with a meteorological sensor, and web cam. The robotic station measures 25 benchmarks (prisms) located on the landslide body, on the top of the main scarp and, as reference points, around the landslide, every 30 minutes. The GPS network is composed of the GPS master unit, which is a reference station for

four single frequency GPS rovers located in the landslide body, three single frequency GPS rovers located on top of the limestone scarp above the landslide (Fig. 5), a single frequency GPS rover

located on a dam near the landslide, and 1 reference single frequency GPS rover located on the roof of the Faculty building in University Campus, chosen as a stable reference rover. .

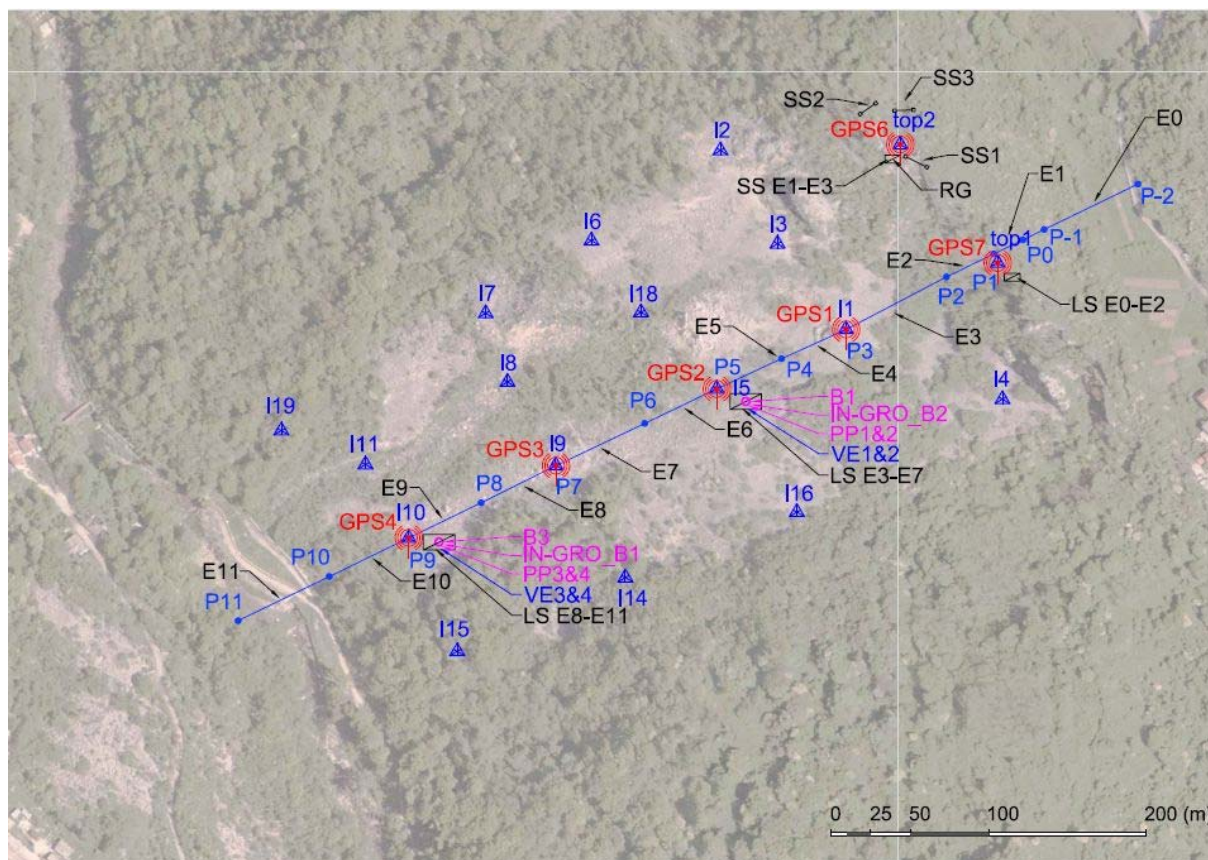


Figure 5 Installed sensors at the Grohovo Landslide: GPS - GPS rover; I - prism; E - long span extensometer wire, P - extensometer pole; SS -short span extensometer; B - position of borehole; IN - inclinometer casing in borehole; VE - vertical extensometer in borehole; PP -pore pressure gauge in borehole; LS -long span extensometer data logger; RG - rain gauge.

Data are transmitted by a Wi-Fi system from each rover to the GPS master unit connected to the field master unit PC, in which the GNSS Spider software creates measurement data files. The master unit PC can be reached remotely by an UMTS module from the main working station at the Faculty of Civil Engineering. The robotic total station, master GPS rover and field PC are powered from a windmill and solar panel mini power plant, while other GPS rovers in the landslide site use their own solar panel installations (Arbanas et al. 2014).

The geotechnical monitoring system includes two vertical inclinometers, and four wire extensometers; 13 long- and three short-span extensometers, four pore-pressure gauges, a weather station and a rain gauge. Pore-pressure gauges, inclinometers and vertical extensometers are installed at two locations inside the central part of the landslide body at the same locations as the GPS rovers and prisms (Fig. 5). Long-span extensometers (NetLG 501E Osasi, 13 pcs) are installed in a continuous line from the Rječina

riverbed to the limestone mega-blocks at the top of the slope (Fig. 2), while short-span extensometers (NetLG 501E Osasi, 3 pcs) are installed over the open cracks at the top of the landslide (Arbanas et al. 2014). To obtain the measured data from the geotechnical monitoring equipment, it is necessary to download data directly from the installed sensors. The installed equipment is presented on Fig. 5. After installation in summer 2011, geodetic monitoring and data collection were started in September 2011.

All installed equipment (except the vertical inclinometers) would be connected in one monitoring system with continuous measured data transmitting to the central computer unit at the Faculty of Civil Engineering in Campus. This is a necessary requirement for establishing a comprehensive monitoring system and early warning system and landslide risk management.

Results of the Grohovo Landslide monitoring

From obtained measurement results, it was very clearly visible that the collected data are liable to numerous significant influences such as daily, monthly and yearly temperature and humidity variation and local disturbing effects caused by

deformations of poles on whose robotic total station and GPS master unit receiver are installed. In order to eliminate local disturbing effects, a bi-axis clinometer type Nivel 220 Leica and meteorological sensor were installed (Arbanas et al. 2012d, 2014).

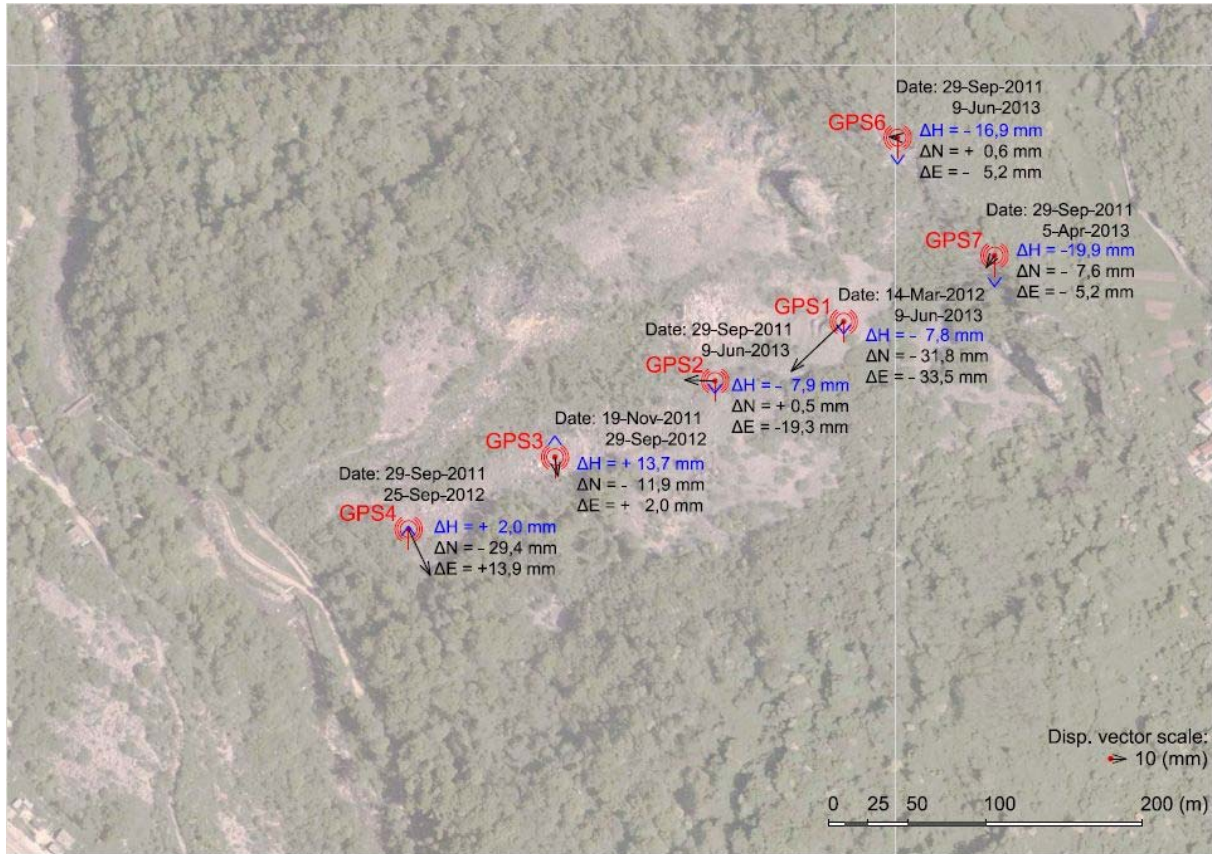


Figure 6 GPS rovers' displacement vectors for approximately two years monitoring period. Two vectors attached to each GPS rover indicate displacements in 2D and heaving (+) or lowering (-) of GPS rover. Monitoring period is noted near each GPS rover.

Results obtained from bi-axis clinometer about tilting of 4 m high concrete pillar could enable direct correction of measured results, but to appropriate reduction of weather condition influences, it should be necessary to have one year data collection and analysis (Arbanas et al. 2012d). It was also identified that the raw GPS measurement data are too rough and cannot indicate on real landslide behaviour. Post-processing of one hour and 12 hours enables more precise GPS rovers' movement control with accuracy less than 2 mm. Movements of GPS rovers in the landslide area presented on Fig. 6.

After reduction of weather condition influences on concrete pillar where the robotic total station is installed, TPS measurement shows very precise and accurate values of prisms' movements with accuracy less than 1 mm. Movements of prisms in the landslide area presented on Fig. 7 for monitoring period from 29 September 2011 to 9 June 2013 with maximum displacements in upper part of the landslide.

Both measurement's techniques (GS, TPS) show on higher landslide activity in the upper part of the slope while the compression of material and heaving of the GPS rovers and prisms are outlined in the lower part of the landslide body and in the landslide foot. These observations are confirmed by in-line installed long-span wire extensometers' measurements which show extension of in upper part of extensometers' line (E1-E4) and compression in lower part of extensometers' line (E7-E11).

A relationship between rainfall, ground water level, pore pressures and landslide movement is still very hard to establish because of numerous interruptions of in monitoring system working caused by low energy production of mini solar power plant that supply the main unit (robotic total station, main GPS unit, and site PC unit) during the winter period from end of October to early March when the landslide activity is the most expressed. The second reason

is very slow landslide activity that requires longer uninterrupted monitoring period.

From previous facts it is possible to conclude that the weakest link in the Grohovo Landslide monitoring system is power supply based on solar devices those cannot produce enough energy during a winter period. The consequences are

missing of TPS measurements and loss of GPS measured data because single frequency GPS units have no possibility to store measured data. It should be necessary to improve power supply and optimize energy consumption of main equipment (GPS, TPS, PC).

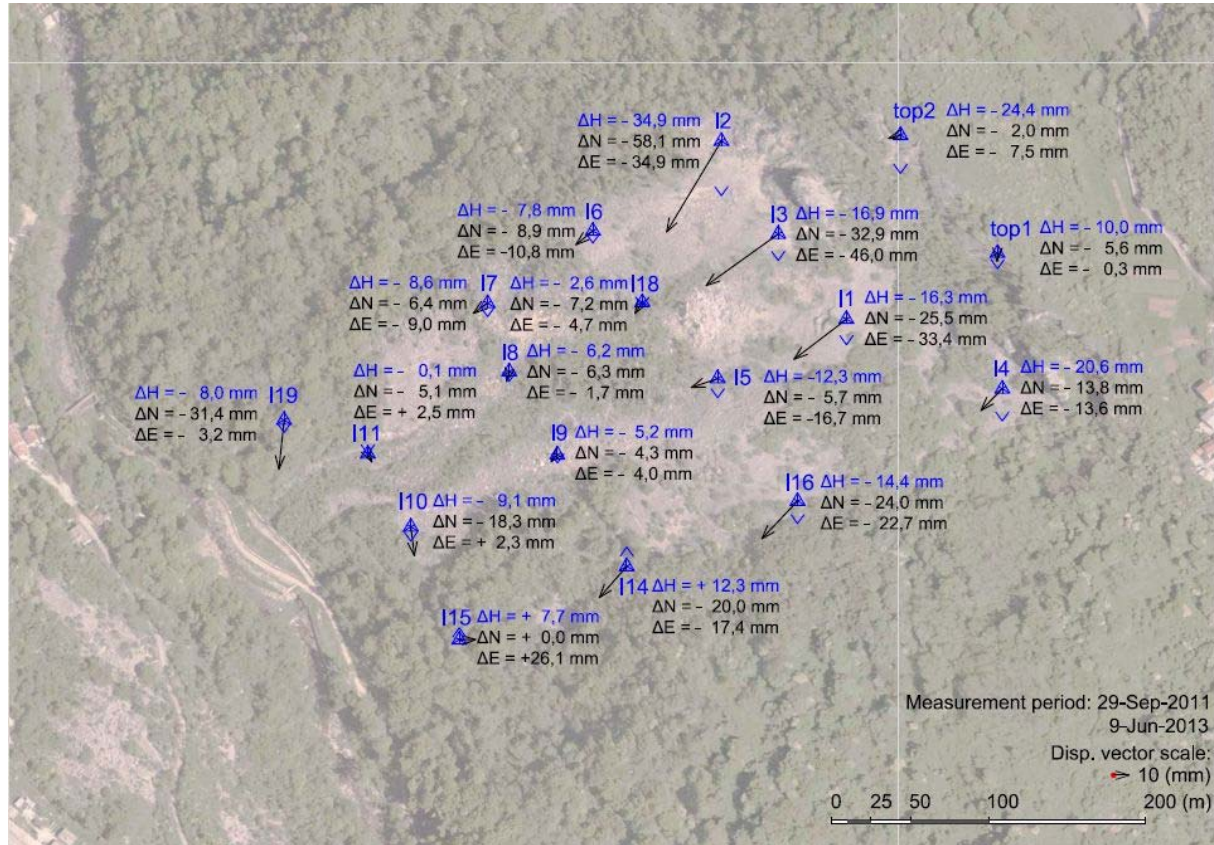


Figure 7 Prisms' displacement vectors for monitoring period from 29 September 2011 to 9 June 2013. Two vectors attached to each prism indicate displacements in 2D and heaving (+) or lowering (-) of prism.

The Grohovo Landslide early warning system establishment

The use of different geodetic and geotechnical sensor fusion in combination with hydrological monitoring equipment, which records data about precipitation and pore pressures in the landslide profile, enables reconstruction of relationships between rainfall, groundwater level and consequent landslide behavior as a base for establishing an early warning system. The analyses necessary for an early warning system should link sensor measurements data and possible failure mechanisms with consequences that would follow the sliding occurrence (landslide risk) (Arbanas et al. 2014). In designing the Grohovo Landslide early warning system it was necessary to: (i) Identify real hazards of further sliding and possible direct and indirect threats; (ii) Identify possible movements and landslide widening with high hazard; (iii) Select appropriate equipment relating to position in the field and measurement accuracy as a competent

equipment to initiate an alarm and (iv) Define critical limit values (criteria values) that indicating the onset of new sliding and trigger an alarm.

Analyses of the past and prediction of future landslide behavior are the most important steps to consider in development of an early warning system, while equipment selection should depend on measurement of appropriate values with required accuracy. In case of the Grohovo Landslide, the accuracy of the wire extensometer measurements (<0.1 mm) and real-time recording have an advantage over GPS and TPS measurements. Both measurements are still unreliable because of unstable power supply. The accuracy of TPS measurements is <1.0 mm but from the measurement results, it is very clear that the collected data are liable to numerous influences such as daily, monthly and yearly temperature and humidity variations and local disturbing effects caused by deformation of poles on which the robotic total station is installed

(Arbanas et al. 2012d). The accuracy of GPS measurement is <2.0 mm but this accuracy is obtained only after 6 hours of data post-processing. This fact eliminated GPS data as appropriate equipment to trigger the alarm in an early warning system.

The Grohovo Landslide early warning would be established after completion of the monitoring system and enabling of transmission of real-time extensometers data to the central computer unit with defined critical limit values that indicate the onset of new sliding and trigger the alarm (Arbanas et al. 2014).

Soil testing and landslide simulation

Soil testing

Detailed laboratory soil testing as a base for prediction of landslides behaviour are performed in a ring-shear apparatus that is designed for testing under static and dynamic conditions for deep seated large landslides in Croatia. The ring-shear apparatus was designed initially to investigate the residual shear resistance under the drained condition along the sliding surface at large shear displacements in landslides because it allows unlimited deformation of the specimen. Professor Sassa with his team has developed the undrained high speed ring shear apparatus to reproduce a rapid landslide motion after failure and to measure the generated pore pressure and the shear resistance mobilized on the sliding surface during motion (Sassa et al. 2003; Sassa et al. 2004; Okada et al. 2004; Fukuoka et al. 2006). The new developed apparatus is (Fig. 8), compared to previous ones, much smaller in dimensions and has higher performances. It can keep undrained condition up to 1 MPa of pore water pressure, up to 3 times more than in previous versions of apparatus and load normal stress up to 1 MPa. This makes it suitable for testing of soil samples in stress condition as on surfaces of rupture in deep seated landslides.



Figure 8 New developed portable ring-shear apparatus designed for testing under static and dynamic conditions for deep-seated large landslides in Croatia.

The soil samples from the Grohovo Landslide were taken from the flysch outcrop in the central part of the landslide body. Speed control test was conducted under constant shear speed of 0.002 cm/sec in undrained conditions. Sample was sheared until the shear displacement reached 1.0 m and the steady state conditions were obtained. As a results of this test, the basic parameters values (peak, mobilized and apparent friction angle, so as cohesion) as well as steady state normal and shear stress of soil sample were obtained. The straight line fitting the stress path gave values of the friction angle as $\phi_m=25.4^\circ$, cohesion as $c=15.2$ kPa and apparent friction angle $\phi_a=20.4^\circ$ (Oštrić et al. 2012, Vivoda et al. 2014).

The integrated model of landslide simulation

The LS-Rapid software is the first landslide simulation model possible to integrate the whole process of stable state, failure, post-failure strength reduction, motion and deposit of sliding mass (Sassa et al. 2010, 2014). In the simulation, the friction angle and cohesion will be reduced from their peak values to the normal motion time values within the source area in the determined distribution of the unstable mass. The strength reduction will be started in the moment when the travel length will become equal to shear displacement at the start of strength reduction (DL, mm). The strength reduction will be completed and the normal motion simulation will be started when the travel length will reach the value of shear displacement at the end of strength reduction (DU, mm).

The topography of the Rječina River Valley (Fig. 9) was determined using original DEM data. The limestone rock mass is situated at the top of the slopes, while the siliciclastic rocks and flysch are situated on the lower slopes and the bottom of the valley. Depth of the sliding mass varies from 3 to 10 m over the flysch bedrock and from 0.0 to 0.5 m over the limestone rock mass. This assumption is based on knowledge that the existing slip surface is positioned at the contact between superficial slope deposits and flysch bedrock (Benac et al. 2005). The long-term rainfalls and consequent ground water level rising were the main triggering factor for the existing landslide occurrences in the Rječina River Valley. This ground water level rising in the model was expressed by excess of the pore pressure ratio until the value of $r_u=0.60$, which is correspondent to the ground water level equal to terrain surface. The time period of ground water level rising in the model was set up as 60 seconds and one second in the model was correspondent to one day real time period (Vivoda et al. 2014). The most important simulation are the steady state shear resistance (τ_{ss}), the lateral pressure ratio ($k=s_h/s_v$)

and the critical shear displacements (DL, DU). The most of the soil parameters used in conducted computer simulation (Tab. 2) were determined from the undrained loading ring shear test and from older laboratory testing results (Benac et al. 2005).

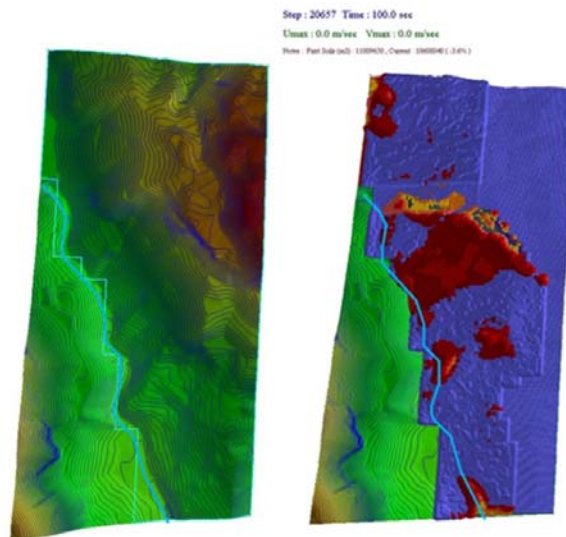


Figure 9 Numerical simulation of the Grohovo Landslide using LS-Rapid software (Vivoda et al. 2014). Digital elevation model on the left side and displaced mass on the right side.

Table 2 Soil parameters used in the LS-Rapid computer simulation (Vivoda et al. 2014).

Soil parameters	Value	Source
Total unit weight of the mass (γ_t)	20 kN/m ³	Benac et al., 2005
Steady state shear resistance in the source area (τ_{ss})	65 kPa	Test data Oštrić et al., 2012
Lateral Pressure ratio ($k=S_H/S_V$)	0.7	Estimation from the test data
Friction angle inside landslide mass (ϕ_l)	33°	Benac et al., 2005
Friction angle during motion (ϕ_m)	26°	Test data Oštrić et al., 2012
Peak friction angle at sliding surface (ϕ_p)	34°	Benac et al., 2005
Peak cohesion at slip surface (c_p)	7.5 kPa	Benac et al., 2005
Shear displacement at the start of strength reduction (DL)	30 mm	Test data Oštrić et al., 2012
Shear displacement at the end of strength reduction (DU)	1000 mm	Test data Oštrić et al., 2012
Pore pressure generation rate (B_{ss})	0.7	Estimation
Cohesion inside mass (c_l)	0.0 kPa	Benac et al., 2005
Cohesion at sliding surface during motion (c_m)	0.0 kPa	Benac et al., 2005
Excess pore pressure (r_u)	0.0 – 0.6	Assumption

The simulation results are shown on Fig. 9. The blue colored zones represent the stable areas or areas with movement velocity less than 0.1 m/s. The orange and red colored zones represent areas where the sliding occurred. The results of conducted simulation very clearly suggest that the new slides, caused by future unfavorable hydrogeological conditions, would be occurred in the area of the existing Grohovo Landslide and this fact confirm the correct selection of the Grohovo Landslide for monitoring and early warning system establishment.

Conclusion

The Croatian-Japanese joint research SATREPS' project 'Risk Identification and Land-Use Planning for Disaster Mitigation of Landslides and Floods in Croatia' was performed from 2009 to 2014. Key objectives of the project were landslides and floods hazard analysis and the development of guidelines for use in urban planning. The aims of the working groups dealing with landslides were to establish a methodology of comprehensive real time monitoring at two most important landslides in Croatia based on the results of previous investigations and new in situ and laboratory testing and behaviour analysis; laboratory soil testing and numerical modelling of static and dynamic landslide behaviour; development of landslide inventories using direct sensing and remote sensing techniques followed by the development of methodologies of landslide hazard analysis and zonation in three pilot areas in Croatia. As an appropriate technique for landslide identification in the Rječina River Valley the analyses of very-high resolution DEMs obtained by airborne laser scanning in combination with field mapping was chosen. The visual identification of landslides is based on the recognition of landslide features on the following types of topographic derivative maps: contour map, hillshade map, slope map, curvature map and topographic roughness map. A comprehensive integrated monitoring system established on the Grohovo Landslide, one of the landslide pilot areas, consists of a GPS survey network composed of a GPS master unit which is a reference station for 9 single frequency GPS rovers and a robotic total station which measures 25 benchmarks (prisms) every 30 minutes. The monitoring data collected may be influenced by local disturbing effects caused by deformation of the poles holding the robotic total station and GPS master unit. The geotechnical monitoring system includes 2 vertical inclinometers and 4 wire extensometers; 13 long- and 3 short-span extensometers, 4 pore pressure gauges, a weather station and rain gauge, installed on the same position as certain parts of the geodetic

monitoring equipment. Selection of the same position for different types of monitoring equipment enables spatial correlation of measurement data on the landslide. In combination with hydrological measurements it will be possible to construct relationships between rainfall, groundwater level and appropriate landslide behavior, to establish an early warning system. Definition of alarm thresholds will be based on existing knowledge of the Grohovo landslide behavior and on the collected consequent comprehensive monitoring data as well. Landslide simulation was based on detailed laboratory soil testing in a ring-shear apparatus designed for testing under static and dynamic conditions for deep seated large landslides in Croatia. The ring-shear apparatus was designed initially to investigate the residual shear resistance under the drained condition along the sliding surface at large shear displacements in landslides because it allows unlimited deformation of the specimen. The new developed apparatus is, compared to previous ones, much smaller in dimensions and has higher performances. It can keep undrained condition up to 1 MPa of pore water pressure, up to 3 times more than in previous versions of apparatus and load normal stress up to 1 MPa. The landslide simulation on the slopes of the Rječina River Valley was conducted using the LS-Rapid software; is the first landslide simulation model possible to integrate the whole process of stable state, failure, post-failure strength reduction, motion and deposit of sliding mass possible to integrate the whole process of stable state, failure, post-failure strength reduction, motion and deposit of sliding mass. The results of conducted simulation of landslide occurrence in the Rječina River Valley very clearly suggest that the new slides, caused by future unfavourable hydrogeological conditions, would be occurred in the area of the existing Grohovo Landslide and this fact confirm the correct selection of the Grohovo Landslide for monitoring and early warning system establishment.

References

- Anon. (2011). City of Rijeka. Technical department (1840-1918). State archive in Rijeka (unpublished documents).
- Antoine P, Giraud A (1995) Typologie des Mouvements de Versants dans un Contexte. Bulletin IAEG 51: 57-62.
- Arbanas Ž, Jagodnik V, Ljutić K, Dugonjić S, Vivoda M, (2012a) Establishment of the Grohovo Landslide monitoring system. In Proceedings of the 2nd Workshop of the Project Risk identification and Land-Use Planning for Disaster Mitigation of Landslides and Floods in Croatia, 15-17 December 2011. Rijeka, Croatia, pp. 29-32.
- Arbanas Ž, Dugonjić S, Ljutić K, Vivoda M, Jagodnik V, (2012b) Initial results of the Grohovo Landslide monitoring. In Proceeding of the 2nd Workshop of the Project Risk identification and Land-Use Planning for Disaster Mitigation of Landslides and Floods in Croatia, 15-17 December 2011. Rijeka, Croatia, pp. 33-36.
- Arbanas Ž, Vivoda M, Jagodnik V, Dugonjić S, Ljutić K, (2012c) Consideration of early warning system on the Grohovo Landslide. In Proceedings of the 2nd Workshop of the Project Risk identification and Land-Use Planning for Disaster Mitigation of Landslides and Floods in Croatia, 15-17 December 2011. Rijeka, Croatia, pp. 51-54.
- Arbanas Ž, Sassa K, Marui H, Mihalić S (2012d) Comprehensive monitoring system on the Grohovo Landslide, Croatia. In Proceedings of the 11th International and 2nd North American Symposium on Landslides: Landslides and Engineered Slopes: Protecting Society through Improved Understanding, June 2-8, 2012. Banff, Canada, pp. 1441-1447.
- Arbanas Ž, Sassa K, Nagai O, Jagodnik V, Vivoda M, Dugonjić Jovančević S, Peranić J, Ljutić K (2014) A landslide monitoring and early warning system using integration of GPS, TPS and conventional geotechnical monitoring methods. In Proceeding of In Proceeding of World Landslide Forum 3, Landslide Science for a Safer Geoenvironment, Volume: 2, Methods of Landslide Studies, 13-16 June 2014. Beijing, China, pp. 631-636.
- Benac Č, Arbanas Ž, Jurak V, Oštrić M, Ožanić N (2005) Complex landslide in the Rječina River valley (Croatia): origin and sliding mechanism. Bulletin of Engineering Geology and the Environment. 64(4): 361-371.
- Benac Č, Dugonjić S, Vivoda M, Oštrić M, Arbanas Ž, (2011) A complex landslide in the Rječina Valley: results of monitoring 1998-2010. Geologia Croatica. 64(3): 239-249.
- Blašković I (1999) Tectonics of part of the Vinodol Valley within the model of the continental crust subduction. Geologia Croatica 52(2):153-189.
- Brunsdon D (1993) Mass movements; the research frontier and beyond: a geomorphological approach. Geomorphology 7: 85-128.
- Brückl E, Brunner FK, Kraus K (2006) Kinematics of a deep-seated landslide derived from photogrammetric, GPS and geophysical data. Engineering Geology 88: 149-159.
- Carter W, Shrestha R, Tuell G, Bloomquist D, Sartori M (2001) Airborne Laser Swath Mapping shines new light on earth's topography. EOS, Transactions, American Geophysical Union 82(46): 549-555.
- Crozier MJ (1984) Field assessment of slope instability. In: Slope Instability. D. Brunsen & D.B. Prior (eds). John Wiley & Sons, New York, 103-142.
- Cruden DM, Varnes DJ (1996) Landslide type and processes. In: Landslides: Investigation and Mitigation. Special report 247. A.K. Turner & R.L. Schuster (eds), National Academy Press, Washington D.C., pp. 36-75.
- Fukuoka H, Sassa K, Wang G, Sasaki R, (2006) Observation of shear zone development in ring-shear apparatus with a transparent shear box. Landslides 3:239-251.
- Gili JA, Corominas J, Rius J (2000) Using Global Positioning System techniques in landslide monitoring. Engineering Geology 55: 167-192.
- Guzzetti F, Mondini AC, Cardinali M, Fiorucci F, Santangelo M, Chang K-T (2012) Landslide inventory maps: New

- tools for an old problem. *Earth-Science Reviews* 112: 42-66.
- Hungr O, Leroueil S, Picarelli L (2014) The Varnes classification of landslide types, an update. *Landslides* 11(2): 167-194.
- IAEG (1990) Suggested Nomenclature for Landslides. *Bulletin IAEG* 41: 13-16.
- Karleuša B, Oštrić M, Rubinić J (2003) Water Management Elements in Regional Planning in Karst, Rječina Catchment Area – Case Study. In *Proceedings of the Int. Conference on Water in karst area of watersheds Cetina, Neretva and Trebišnjica, Mostar, 25-27 September. Mostar, Bosnia and Herzegovina*, pp. 85-94 (in Croatian).
- Keaton JR, DeGraff JV (1996) Surface observation and geologic mapping. In: *Landslides: Investigation and Mitigation. Special report 247*. A.K. Turner & R.L. Schuster (eds), National Academy Press, Washington D.C., pp. 178-230.
- Mihalić S, Arbanas Ž (2013) The Croatian–Japanese Joint Research Project on Landslides: Activities and Public Benefits. In: Sassa K, Rouhban B, Briceno S, He B (eds) *Landslides: Global Risk Preparedness*. Springer Verlag, pp 345-361.
- Mihalić Arbanas S, Arbanas Ž (2014) Landslide mapping and monitoring: Review of conventional and advanced techniques. *Proceedings of the 4th Symposium of Macedonian Association for Geotechnics, 25-28 June 2014. Struga, Macedonia*, pp. 57-72.
- Mora P, Baldi P, Casula G, Fabris M, Ghirotti M, Mazzini E, Pesci A (2003) Global Positioning Systems and digital photogrammetry for the monitoring of mass movements: application to the Ca' di Malta landslide (northern Apennines, Italy). *Engineering Geology* 68: 103–121.
- Okada Y, Sassa K, Fukuoka H, (2004) Excess pore pressure and grain crushing of sands by means of undrained and naturally drained ring-shear tests. *Engineering Geology* 75: 325–343.
- Oštrić M, Ljutić K, Krkač M, Setiawan H, He B, Sassa K (2012) Undrained ring shear tests performed on samples from Kostanjek and Grohovo landslide. In *Proceedings of the 10th ICL Anniversary, 20 January 2012. Kyoto, Japan*, pp. 365-369.
- Oštrić M, Sassa K, He B, Takara K, Yamashiki Y (2013) Portable Ring Shear Apparatus and its application. In *Proceedings of the 2nd World Landslide Forum 'Landslide Science and Practice', Vol. 3, 3-9 October 2011. Rome, Italy*, pp. 365-369.
- Razak KA, Straatsma MW, van Westen CJ, Malet J-P, de Jong SM (2011) Airborne laser scanning of forested landslides characterization: Terrain model quality and visualization. *Geomorphology* 126: 186–200.
- Reutebuch SE, McGaughey RJ, Anderson HE, Carson WW (2003) Accuracy of a high-resolution LiDAR terrain model under a conifer forest canopy. *Canadian Journal of Remote Sensing* 29: 527–535.
- Santangelo M, Cardinali M, Rossi M, Mondini AC, Guzzetti F (2010) Remote landslide mapping using a laser rangefinder binocular and GPS. *Natural Hazards and Earth System Sciences* 10: 2539–2546.
- Sassa K, Wang G, Fukoka H, (2003) Performing undrained shear tests on saturated sands in a new intelligent type of ring shear apparatus. *ASTM Geotech Test J* 26(3): 257–265.
- Sassa K, Fukuoka H, Wang G, Ishikawa N, (2004). Undrained dynamic-loading ring-shear apparatus and its application to landslide dynamics. *Landslides*, 1: 7–19.
- Sassa K, Nagai O, Solidum R, Yamazaki Y, Ohta H (2010) An integrated model simulating the initiation and motion of earthquake and rain induced rapid landslides and its application to the 2006 Leyte landslide. *Landslides* 7(3): 219-236.
- Sassa K, He B, Dang K, Nagai O, Takara K (2014) Progress in Landslide Dynamics. In *Proceeding of In Proceeding of World Landslide Forum 3, Landslide Science for a Safer Geoenvironment, Volume: 1, Methods of Landslide Studies, 13-16 June 2014. Beijing, China*, pp. 37-67.
- Savvaidis PD (2003) Existing landslide monitoring systems and techniques. In *Proceedings of the Conference from Stars to Earth and Culture, in honor of the memory of Professor Alexandros Tsoumis. Thessaloniki, Greece*, pp. 242-258.
- Shan J, Toth CK (Eds.) (2009) *Topographic laser ranging and scanning: Principles and processing*. CRC Press, Taylor and Francis Group, Boca Raton, Florida.
- Skempton AW, Hutchinson JN (1969) Stability of natural slopes and embankment foundations, State of the Art Report. In: *Proceedings of 7th Int. Conf. Soil Mechanics and Foundation Engineering. Mexico City, Mexico*, pp 291-340.
- Varnes DJ (1978) Slope Movements, Types and Processes. In: *Landslides: Investigation and Mitigation. Special report 247*. A.K. Turner & R.L. Schuster (eds), National Academy Press, Washington D.C., pp. 11-33.
- Velić I, Vlahović I (2009) Geological map of the Republic of Croatia 1:300.000. Croatian Geological Survey, Zagreb (in Croatian).
- Vivoda M, Dugonjić Jovančević S, Arbanas Ž (2014). Landslide occurrence prediction in the Rječina River Valley as a base for an early warning system. In *Proceedings of the 3rd Croatian-Japanese Project Workshop and 1st Regional Symposium on Landslides in the Adriatic-Balkan Region 'Landslide and Flood Hazard Assessment', 6-9 March 2013. Zagreb, Croatia*, in press.
- Wang C, Arbanas Ž, Mihalić S, Marui H (2013) Three dimensional stability analysis of the Grohovo landslide in Croatia. In *Proceedings of the 2nd World Landslide Forum 'Landslide Science and Practice', Vol. 3, 3-9 October 2011. Rome, Italy*, pp. 47-52.
- Wang G (2011) GPS landslide monitoring: Single base vs. network solutions – A case study based on the Puerto Rico and Virgin Islands permanent GPS network. *Journal of Geodetic Science* 1(3): 191-203.
- Wang G, Kearns TJ, Yu J, Saenz G (2014) A stable reference frame for landslide monitoring using GPS in the Puerto Rico and Virgin Islands region. *Landslides* 11(1): 119-129.



Proceedings of the SATREPS Workshop on Landslides in Vietnam, 2014

Landslide mapping and monitoring in the City of Zagreb (Croatia, Europe)

Snježana Mihalić Arbanas⁽¹⁾, Martin Krkač⁽¹⁾, Sanja Bernat⁽¹⁾, Željko Arbanas⁽²⁾

1) University of Zagreb, Faculty of Mining, Geology and Petroleum Engineering, Zagreb, Croatia, e-mail: smihalic@rgn.hr, mkrkac@rgn.hr, sanja.bernat@rgn.hr,

2) University of Rijeka, Faculty of Civil Engineering, Rijeka, Croatia, e-mail: zeljko.arbanas@gradri.uniri.hr

Abstract This paper describes application of innovative technologies for landslide detection, mapping and monitoring in the City of Zagreb in the framework of the scientific Japanese-Croatian SATREPS FY2008 project (2009-2014). Summarized overview of study areas and research activities aimed at landslide inventory mapping and landslide monitoring are briefly introduced. The purpose of the overview is to provide the most important project results which illustrate usefulness of applied technologies: airborne LiDAR (Light Detection and Ranging) scanning of the whole hilly area of Medvednica Mt. in very-high-resolution and monitoring of the Kostanjek landslide by large number of sensors installed at the landslide area of 1 km². Information about project results will also serve as a basis for planning of further research activities important for characterization of landslides at the pilot area, including the Kostanjek landslide. The final aim of landslide mapping and monitoring is to provide necessary data and solutions for hazard and risk reduction to local authorities working in the system of land-use planning and civil protection.

Keywords landslide mapping, landslide monitoring, Kostanjek landslide, City of Zagreb

Introduction

Application of advanced technologies for landslide mapping and monitoring at the area of the City of Zagreb in Croatia has started in 2010 in the framework of the bilateral scientific Japanese-Croatian SATREPS FY2008 project described in Mihalić and Arbanas (2012). Implementation of project activities encompassed: (i) identification and mapping of landslides at the area of southern and south-eastern hills of Medvednica Mt. which belongs to the City of Zagreb County; and (ii) monitoring of the Kostanjek landslide, located in western part of the hilly area, in an urban part

of the City of Zagreb. Fig. 1 shows pilot area of the Japanese-Croatian project (total size is 180 km²) for the inventory mapping and location of the Kostanjek landslide where integrated monitoring system was installed.

Owing to its geomorphological and geostructural position, the area of the City of Zagreb is located in the mega-geomorphological region of the European Pannonian Basin, in its western part in NW Croatia. The city covers an area of 640 km² and includes the urban area (Zagreb City) and 69 settlements with 792,875 residents (approximately 18% of the total Croatian population). The urbanized area (220 km²) is located below the forest region of Medvednica Mt. to the north and extends to the flood plain of the Sava River on the south (Fig. 1). Climate is continental under a mild maritime influence with a mean annual precipitation (MAP) of 883.6 mm.

Hills in the northern part of the County were chosen as a pilot area because 32% of the Zagreb city belongs to this area. The pilot area is very attractive as a residential zone with continuous increase of population density. Kostanjek landslide is one of numerous landslides placed inside borders of pilot area, but it is specific according to its size (landslide volume is 32.6×10^6 m³) and depth (90 m) of the landslide. The landslide activity over the last 50 years has completely stopped urban planning and development at the area of the Kostanjek landslide, which size is approximately 1 km². Construction of new apartment buildings in this residential area is forbidden, and existing houses require repeating repairing and consolidation works. The local authorities from the City of Zagreb need to find cost-effective solution for this human and environmental threat. Potential hazard in the form of large displacement of reactivated landslide can become disastrous because of approximately 290 endangered buildings placed at the surface of landslide.

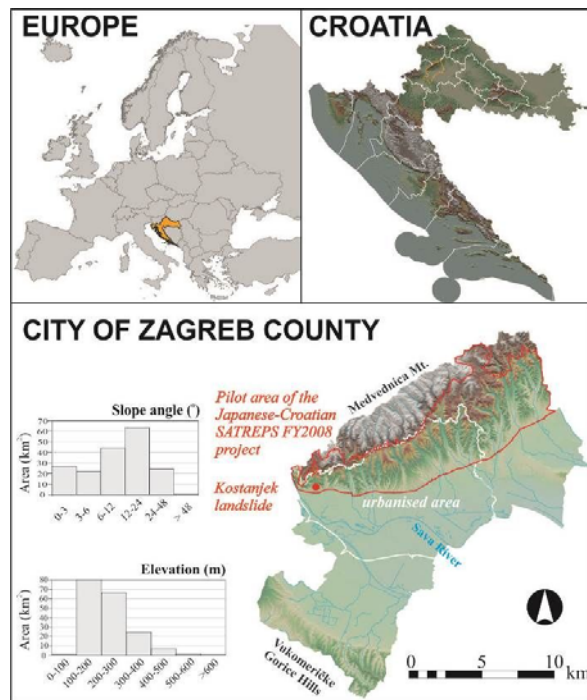


Figure 1 Relief map of the City of Zagreb County with urbanized areas (white line), the border of the Croatian-Japanese SATREPS FY2008 project's pilot area (red line) and location of the Kostanjek landslide (red dot). Histograms showing the elevation and slope angle computed from DEM.

The objective of identification and mapping of landslides at the area of hills of Medvednica Mt. was landslide inventory mapping, based on remote sensing. One of the task was to find technology appropriate for determination of landslide boundaries at the ground surface of very small to moderately large landslides (primarily $1,000 \text{ m}^2$) mostly covered by deciduous vegetation and partially masked by urbanisation. Part of project activities was also identification and mapping of landslides using conventional visual interpretation of stereoscopic aerial photographs (Podolszki et al. 2012, Podolszki 2014). Innovative method applied at the same pilot area was analysis of surface morphology with very-high-resolution digital elevation models (DEMs) captured by airborne LiDAR (Light Detection and Ranging).

The establishment of integrated monitoring system at the Kostanjek landslide was initiated in 2009 as one of main activities of the joint Japanese-Croatian project. In the period 2011-2013 various types of sensors for measurement of displacement, hydrological and seismological conditions were installed. The objective of the monitoring system is to provide high resolution spatial and temporal data, necessary to define critical thresholds of triggering factors and to setup an early warning system (EWS).

The following sections briefly introduces summarized overview of study areas, research activities aimed at landslide inventory mapping and monitoring and main results. The purpose of the overview is to provide information which will serve as a basis for planning further research activities.

Landslide inventory mapping

Study area

The hilly area of the southern foothills of Medvednica Mt. was a project pilot area in the period 2009-2014 (Mihalić and Arbanas 2012). This area of 180 km^2 is mostly urbanized and densely populated. The elevations in this area range from 115 to 612 meters a.s.l., the prevailing slope angles (59%) range from 6° to 24° and 84% slopes have slope angles $>3^\circ$ which are potentially prone to sliding. The dominant types are small and shallow landslides that mostly endanger residential structures and roads (Fig. 2). The pilot area is composed of Upper Miocene and Quaternary sediments (Fig. 3). The Upper Miocene deposits are stratified sands, silts and marls, with moderately to slightly-inclined bedding (bedding slope angle in range of $10\text{-}20^\circ$). The top parts of Miocene deposits are fine-grained soils, mostly silts. The Quaternary deposits are heterogeneous mixtures of unfoliated, mostly impermeable clayey-silty soils. The geologic contact between the Miocene sandy-silty soils and the Miocene or Quaternary clayey-silty soils is highly susceptible to sliding. The most frequent triggering factors are rainfall and man-made activities.

Mihalić Arbanas et al. (2012) described all historical projects implemented at the area of the City of Zagreb with the aim of landslide mapping. Despite the long tradition of landslide mapping at the area of the City, the main problem with the current practice of landslide risk management in the City of Zagreb is the lack of a suitable landslide inventory and landslide hazard and risk maps. Analysis of spatial distribution of landslides, performed by Podolszki (2014), shows that two historical inventories from 1967 (Šikić 1967) and 2007 (Miklin et al. 2007) contains inconsistent and unreliable landslide data, because of underestimated number of landslides and overestimated landslide areas. According to historical landslide inventory from 1979 (Polak et al. 1979), which encompass 93 km^2 of the same hilly zone, landslide frequency is 8.7 landslides per square kilometer. The number of landslides is even higher, because groups of very small landslides are drawn by single landslide contours, as stated in accompanying report.



Figure 2 Examples of landslides endangering/damaging houses or public roads in the winter of 2013 in Zagreb (Bernat et al. 2014a).

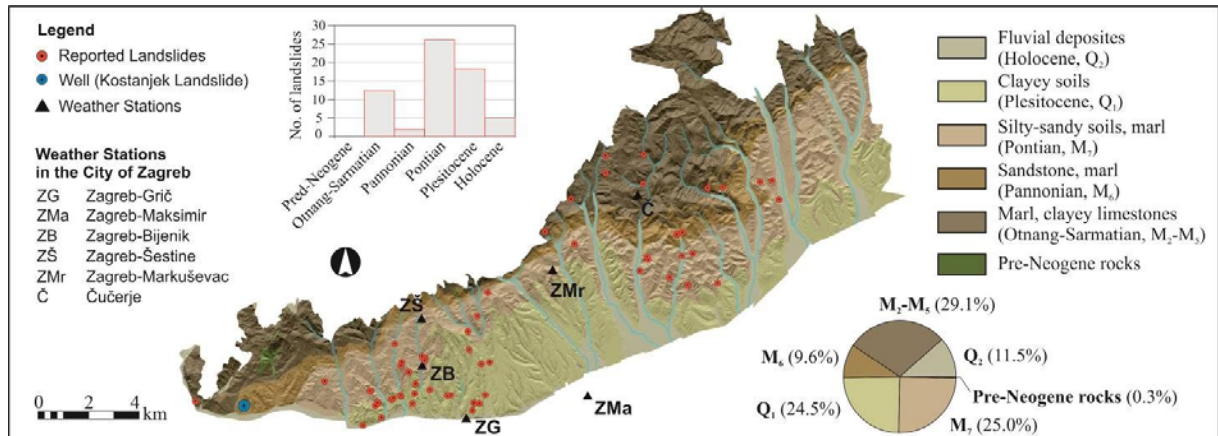


Figure 3 Precipitation triggered landslide inventory map for the period from 1st January to 7th April 2013 (Bernat et al. 2014a). Landslides are depicted by dots on generalized geological map together with weather stations and one well where continuous water level measurement is available (Krkač et al. 2014c). Pie chart shows the relative distribution of main stratigraphic units; histogram shows the number of (re)activated landslides per stratigraphic unit.

According to the same historical data, the most frequent landslides are in range of landslide areas from 1,200 m² to 7,200 m². Podolszki (2014) also performed conventional visual interpretation of stereoscopic aerial photographs from 1964 in a scale 1:8,000. The same author derived landslide inventory map at the area of 54.14 km² with 963 landslides, which gives average landslide density of 17.8 landslides per square kilometer, but reliable identification is estimated for only 50% of all mapped landslides. Stereoscopic analysis of historical aerial photographs from 1964 in large scale enabled identification of landslides in a range from 78 m² to 281,886 m². Landslide area of most of landslides (90.6%) is in a range 200-3,600 m². Ferić et al. (2012) performed preliminary visual analysis of surface morphology with 1-m resolution bare-earth airborne LiDAR DEM scanned in 2011 at the test area of the Japanese-Croatian project (total area is 24 km²). Result of analysis was inventory map with 176 landslides and average landslide density of 7.3 landslides per square kilometer. Most of mapped landslides are small in size, 60% of them are smaller than 1,000 m² (0.1 ha). The smallest identified landslide is unknown landslide with landslide area of only 48

m². The largest identified landslide is known historical landslide, Grmošćica landslide with the total length of 300 m and width of the rupture surface of 100 m.

Mihalić et al. (2012) analyzed data about 82 landslides from site investigation reports prepared in the period from 1968 to 2008. On the basis of available reports, the following information were extracted. Total areas of 47 investigated landslides are in a range of 4,000 – 180,000 m²; landslide depth for 15 landslides is in a range of 2-10 meters. Time of activation is known only for six landslides. Reactivated landslides are very often. Landslides causes are known only for 19 landslides (of 82 analyzed landslides) and all are anthropogenic in origin related to construction activities. From the same historical data it could be seen that the period of investigation of some landslides is extremely long. For example, the Bijenik landslide has been investigated few times in the period from 1968 to 2004, when it was finally successfully stabilized. One another example of long period of investigations and multiple stabilization works is the Česmički landslide with the period of geotechnical investigation and design from 1969 to 2004.

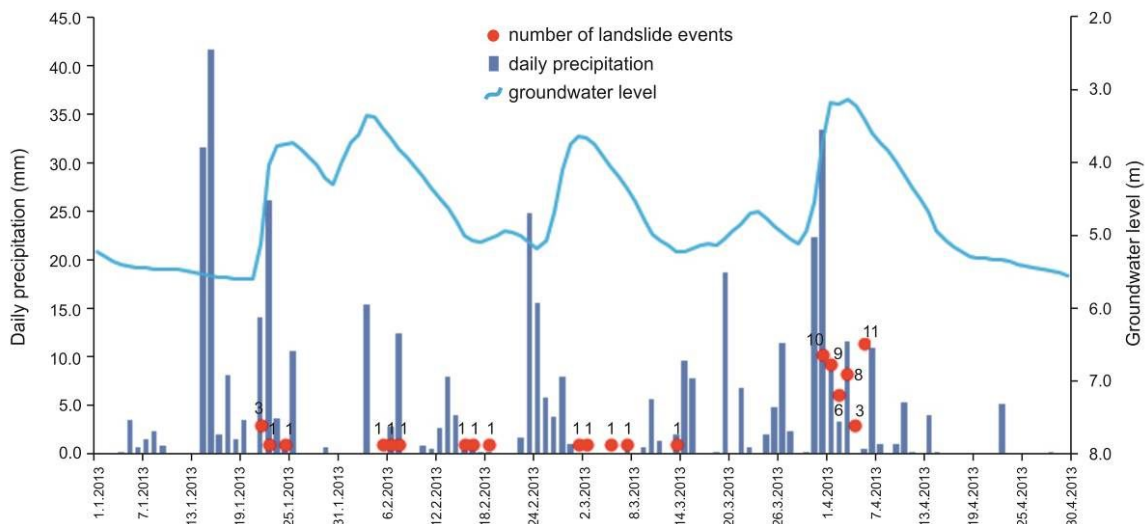


Figure 4 Daily precipitations recorded at the Zagreb-Grič meteorological station and the number of landslide events triggered in the City of Zagreb from January to April 2013. The continuous line depicts groundwater level changes registered by a water-level gauge at the Kostanjek landslide observatory established in the framework of the Japanese-Croatian (Mihalić Arbanas et al 2013).

Analysis of landslide contours, interpreted on the basis of engineering-geological field mapping during geotechnical investigations, also shows unreliable landslide contours, despite detailed scale of analysis (Gerber 2012). A disadvantage of field mapping was the limited ability to accurately determine a landslide boundary in the field due to the reduced visibility of the slope failure (a consequence of the local perspective), the size of landslide, and the fact that the landslide boundary is often indistinct or fuzzy (most often because of anthropogenic activities). One example of unsuccessful design of remedial measures due to wrong interpretation of landslide boundaries is Črešnjevec landslide, shortly described in Mihalić and Ferić (2010) and Mihalić et al. (2013). High uncertainty of identification of Črešnjevec landslide contours in 2001 was consequence of indistinct landslide boundaries which are interpreted by field mapping approximately 20 years after landslide initiation and in an environment with significantly modified natural morphology, as a result of urbanization in the period 1982-2001. Gerber (2012) showed that historical landslide boundaries of other landslides in Zagreb also vary significantly in size and shape, not only due to subjectivity of investigators, but mainly due to methodology of landslide mapping.

Fig. 3 presents a precipitation-triggered landslide inventory with 63 landslides, compiled on the basis of information collected from City administration, online media and field checking by a professional engineering geologist in November 2013 (Bernat et al. 2014a). From January 1st to April 7th, the City of Zagreb experienced a period of intense rainfall and snowfall with cumulative values over the 97-day period exceeding 400 mm, which presents 46% of the

MAP. Monthly precipitation in the same period of 2013 was two to three times higher than the average monthly values of the same period from 1862 to 2012 recorded at the Zagreb-Grič weather station. Analysis of the 3-month period from January to March showed that cumulative precipitation for the analyzed period in 2013 has the highest value (378.7 mm) measured in the last 150 years. Fig. 4 depicts daily precipitation data (amount of rainfall and snow depth) from January to April 2013 together with the number of landslide events per day and it shows that landslides occurred after significant rainfall and snow melting. The largest number of landslides (a total of 41 landslide events) occurred during the period from 30th March until 3rd April. On the basis of analysis of estimated landslide dimension it can be seen that 51% of all landslides were superficial landslides (depth <1 m), which occurred in colluvial deposits overlaying engineering soil and soft rocks (Bernat et al. 2014b). There were 28 shallow landslides, whose estimated depth ranges 3-12 m and the landslide area varies from approximately 220 m² to 14,000 m².

Airborne laser scanning

Over the last few years, airborne laser scanning has been made available and has been used to identify and map landslide morphology in areas that are partially or completely covered by dense vegetation (Carter et al. 2001; Razak et al. 2011). A relatively new remote-sensing tool uses airborne mounted lasers to obtain digital representations of the topographic surface for areas ranging from a few hectares to thousands of square kilometers (Shan and Toth 2009). Airborne LiDAR is also known as airborne laser scanning (ALS) or airborne laser swath mapping

(ALSM). In these methods, a laser sensor measures the distance from the instrument and multiple points on the topographic surface. Although laser scanning measures the altitudes of all objects scanned, post-processing is necessary for creation of bare earth DEM to remove the undesired returns from buildings and canopies via filtering of the original data (Reutebuch et al. 2003). Visual analysis and interpretation of the topographic surface remain the most common and most promising application of a very-high-resolution (metric to decimetric) DEM captured by airborne LiDAR sensors for detection and mapping of landslides over large areas (Guzzetti et al. 2012). The required resolution of a bare-earth LiDAR DEM for identification of landslides primarily depends on the landslide size. Recognition of small cracks and detailed geomorphological features might be the best surface landslide characteristics that can be interpreted from these images, which provides additional information compared with the interpretation of optical images, that is, aerial photos or satellite images.

For the LiDAR data used in this study, test flight (which covers 24 km²) took place in April 2011 and flight over the whole pilot area (180 km²) took place in December 2013, which corresponds to the leaf-off periods in Croatia. Airborne laser scanning system used for this research has measurement rate 266,000 Hz, effectively at 60° angle, with surface point horizontal accuracy of 8 cm and vertical accuracy of 4 cm. LiDAR ground-surface measurements were acquired at an average density of 5 points per square meter. Raw data were post-processed and 1-m resolution bare earth DEM was interpolated. Slope maps, contour line maps and hillshade maps were created from the DEM using standard tools in the ArcGIS. Contour line map was created with 1 meter interval and for the hillshade map an altitude angle of the light source above the horizon of 45° and azimuth angle of the illumination source of 315° was chosen. Landslide identification was performed by visual analysis and interpretation of the representation of topographic surface on all abovementioned DEM derivative maps.

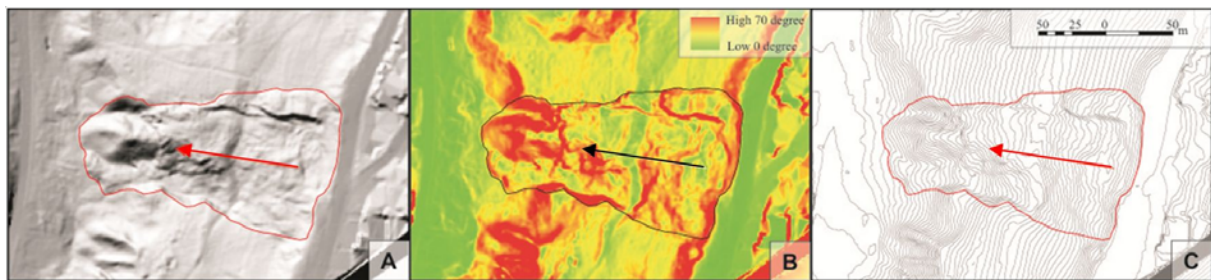


Figure 5 Composite displays of three different topographic derivative maps of the Vrhovec landslide. The estimated extent of displaced mass has a red and black contours (Ferić et al. 2012): (A) Hillshade map generated with an azimuth of 315° and a sun angle of 45° draped over a bare earth DEM. (B) Slope map showing areas of high slope angle in warmer colors (red, orange, yellow) and areas of low slope angle in cooler colors (green). (C) Contour map generated with a 1 meter contour spacing.

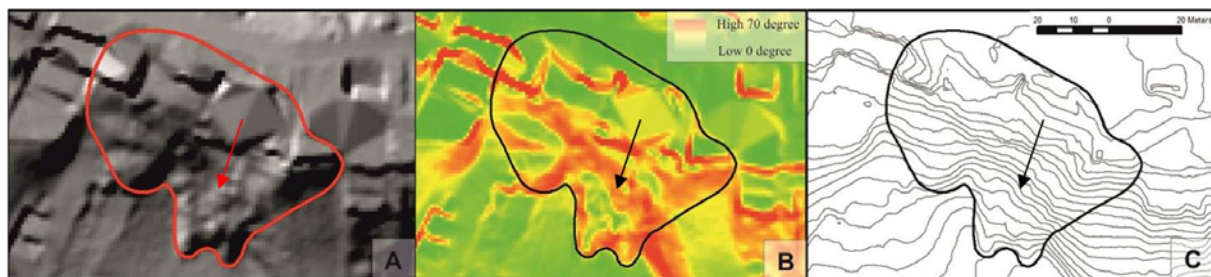


Figure 6 Composite displays of three different topographic derivative maps of the Črešnjevce landslide. The estimated extent of displaced mass has a red and black contours (Ferić et al. 2012): (A) Hillshade map generated with an azimuth of 315° and a sun angle of 45° draped over a bare earth DEM. (B) Slope map showing areas of high slope angle in warmer colors (red, orange, yellow) and areas of low slope angle in cooler colors (green). (C) Contour map generated with a 1 meter contour spacing.

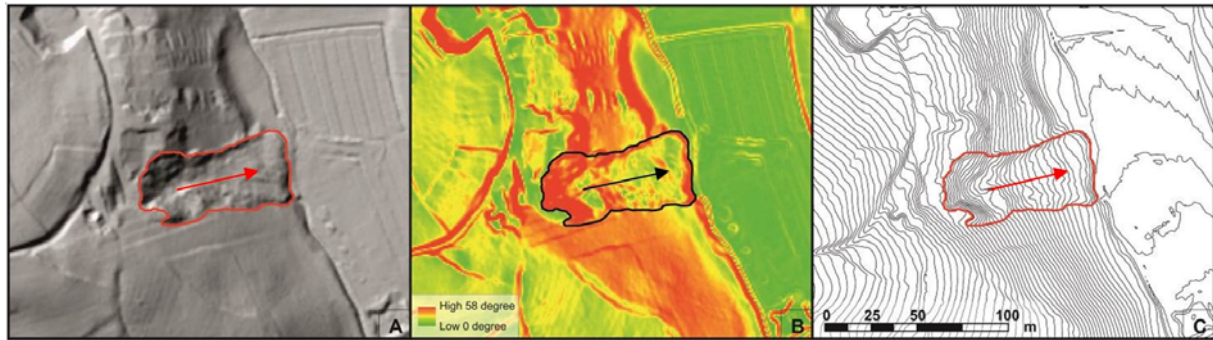


Figure 7 Composite displays of three different topographic derivative maps of the Lazina landslide, activated in 2013. The estimated extent of displaced mass has a red and black contours: (A) Hillshade map generated with an azimuth of 315° and a sun angle of 45° draped over a bare earth DEM. (B) Slope map showing areas of high slope angle in warmer colors (red, orange, yellow) and areas of low slope angle in cooler colors (green). (C) Contour map generated with a 1 meter contour spacing.

Results

The visual identification of landslides was based on the recognition of landslide features on three topographic derivative maps: contour map with 1 m contour span, hillshade map and slope map. Mapped landslides are characterized by visible main landslide features such as main scarp, landslide borders and toe part, as well as zone of depletion and zone of accumulation. The Vrhovec landslide is readily visible on the hillshade, slope and contour maps (Fig. 5) although it is approximately 8 years old landslide and today is completely covered by dense vegetation. The steepness of the main scarp is considerably higher than the slope itself. In the slope map these appear as the warmer colors (yellow, orange, red) while in the contour map the scarp is identified by a clustering of elevation contours. Hummocky topography, the flanks and the toe of the landslide are also clearly visible. Vrhovec landslide is typical landslide at the investigated area, formed along geological contact between Pleistocene (Q_1) fine-grained soils and Pontian (M_7) sandy-silty soils, initiated by human activities of uncontrolled disposal in upper part of the slope.

Fig. 6 presents result of identification of previously known Črešnjevce landslide, characterized by continuous reactivated movement of upper part of slope after unsuccessfully designed remedial measures, constructed in 2004. Red and black lines in Fig. 6 depict contours of active slow-moving retrogressive landslide (approximate area is 720 m^2). Combining hillshade, slope and contour map derived from airborne LiDAR data, it is possible to distinguish easily only lower part of displaced mass while main scarp with vertical displacement of approximately 10-30 cm is not clearly expressed. The bare earth DEM in upper part of

landslide is masked by artefacts remaining from buildings after post-processing of LiDAR data. On the basis of an experience with interpretation of the Črešnjevce landslide, it is possible to conclude that interpretation of landslides in built-up areas using airborne LiDAR data should be followed by field checking and mapping in order to achieve the best result.

Fig. 7 shows clearly visible contour of Lazina landslide initiated by extreme precipitation in spring period in 2013, on 3 March 2013. Landslide is also activated in landfilled material. Vegetation cover was completely removed by landsliding.

Landslide monitoring

Kostanjek landslide

Kostanjek landslide is a reactivated deep-seated large translational landslide formed in soft rock-hard soil, i.e. Pannonian and Sarmatian marls. Landslide velocities have been changing over the last 50 years, from landslide activation until today, in a range from extremely slow to very slow. The initial landslide was developed as a consequence of loss of global stability of gentle to steep slopes above an open pit mine of marl and a cement factory 'Sloboda' (Fig. 8). Slope movements were caused by mining activities, i.e., undercutting of the slope toe and uncontrolled massive blasting. Following the initial slow movements that caused settlement and fractures of industrial cement factory objects in 1963, and damaging numerous private houses within an area of approximately 1 km^2 in a very short period, attention shifted to the unstable slopes above the cement factory known as Kostanjek landslide. According to the photo interpretation of aerial stereo pairs from 1963 to 1988, horizontal displacements of the ground surface in the period 1963-1988 were detected in a range 3-6 meters (average 12-24 cm per year), as is depicted in Fig

8. Monitoring results of recent movements from the period 2010-2012 at the 35 stable geodetic points shows very similar movement directions to historical data (Fig. 9).

Although numerous surface exploration and visual studies were undertaken between the 1966 and 2010 (shortly described in Mihalić Arbanas et al. 2013) the rudimentary nature of the monitoring undertaken did not provide conclusive evidence regarding the rate and extent of the movement of the Kostanjek landslide. A geotechnical report prepared by Croatian Civil Engineering Institute (IGH) in 2008 provides a comprehensive review of all historical investigations at the area of the Kostanjek landslide, with the presentation of the historical landslide model, its geometry, mechanism and contributing factors interpreted by Ortolan (1996). With respect to an interpreted historical movement of the Kostanjek landslide, as the specific mechanism of recent movement is not known, there is need to better define the subsurface conditions and contours of landslide bodies contributing to the movement (Krkač et al. 2013, Furuya 2012) landslide.



Figure 8 Horizontal displacements (white arrows) at the Kostanjek landslide area in the period 1963-1988 based on interpretation of stereo pairs of aerial photographs from 1963, 1979, 1981, 1985 and 1988 (Ortolan and Pleško 1992). Red line depicts the outline of the Kostanjek landslide according to interpretation by Ortolan (1996). In the background is orthophoto image from March 2012. Devastated slopes of the abandoned open pit mine are clearly expressed by rough relief forms in the middle of the Kostanjek landslide. The former cement factory 'Sloboda' was placed in the plain area in the bottom middle part of the landslide.

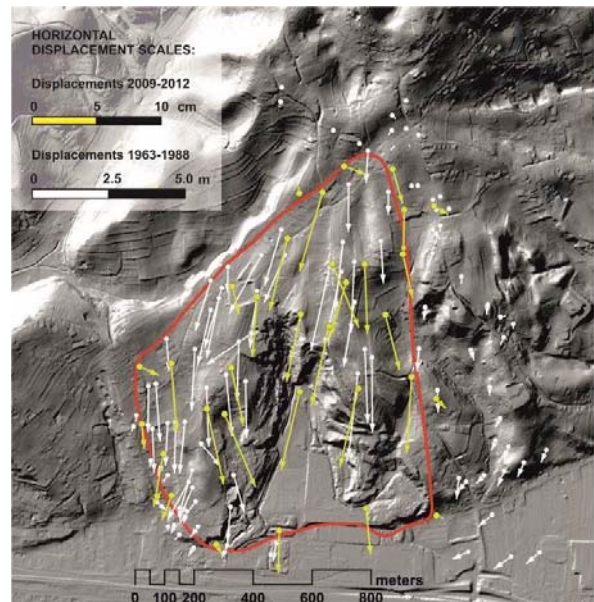


Figure 9 Recent horizontal displacements (yellow arrows) at the Kostanjek landslide area in the period 2010-2012 (Županović et al. 2012) compared with historical horizontal displacement (white arrows) for the period 1963-1988 (Ortolan and Pleško 1992). Red line depicts Kostanjek landslide outline according to Ortolan (1996).

The main objective of the joint research within the framework of the Japanese-Croatian project was to establish a landslide monitoring system for the purpose of an early warning system (EWS). Landslide monitoring project activities were initiated in 2011. Prior to the completion of the Kostanjek landslide monitoring system, in January 2011, the Government of the City of Zagreb determined that the continuous long-term monitoring of the Kostanjek landslide is important for the public safety of the residents. The secondary priority of the monitoring system is to provide an opportunity for the research community to test and develop instrumentation and monitoring technologies, as well as to better understand the mechanics of slow moving masses.

Monitoring system

The sensor network installed at the Kostanjek landslide area encompasses around 40 sensors for the monitoring of landslide movement and landslide causal factors. Figure 10 provides the layout of the sensor network which is currently installed at the Kostanjek landslide. The monitoring system consists of various sensors for the measurement of: (1) external triggers (1 rain gauge and 7 accelerometers); (2) displacement/deformation/activity (15 GNSS sensors, 7 extensometers, 4 borehole extensometers and 1 inclinometer); (3) hydrological properties (3 pore pressure gauges and 3 water level sensors in boreholes and domestic wells, 2 water level sensors at outflow

weirs). The general design of the monitoring system is described in Mihalić Arbanas et al. (2013) and Krkač et al. (2014c).

Rainfall and earthquakes are monitored by sensors for continuous measurement installed at the Kostanjek landslide. External trigger monitoring is of crucial importance because of their influence on reactivation of the landslide and establishment of a EWS.

A disadvantage of the installed rain gauge is that it does not provide accurate precipitation data during snowy periods. Moreover, the Kostanjek landslide reactivation in the winter and spring of 2013 was triggered by precipitation (rainfall and thick snow cover). Because of this reason it is necessary to install an additional meteorological station in the area of the Kostanjek landslide which will monitor precipitation and other meteorological factors.

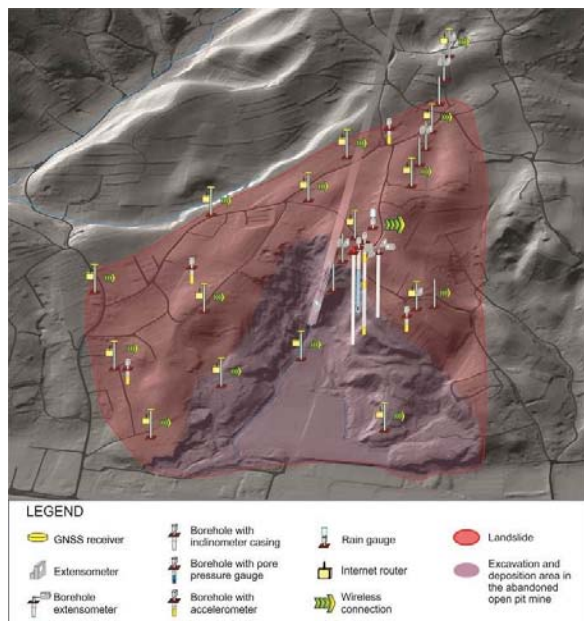


Figure 10 Sensor network at the Kostanjek landslide area established in the framework of Japanese-Croatian SATREPS FY2008 scientific joint research project (Krkač et al. 2014c).

Seven accelerometers with continuous monitoring, installed at five locations at the landslide surface and at different depths, provide good spatial and temporal data which can record changes according to local ground conditions inside the landslide body and in the rock mass below the sliding surface. These accelerometers are installed to record ground shaking (accelerations) in response to earthquakes (trigger) and response to landslide movements (activity).

Slope movement measurements provide data about the actual state of slope activity, i.e. they define the mass movement parameters, enable recognition and quantification of the reactivation phase, enable definition of threshold values

approaching critical acceleration and in the ideal case enable forecasting of the catastrophic phase (Baroň et al. 2012). Subsurface movement at the Kostanjek landslide, measured by inclinometer, provided reliable data about sliding surface depth, mechanical behavior and displacement rate until February 2013. After this period the inclinometer casing became impassable due to large displacement at the sliding surface. Although the inclinometer data are of good quality, the temporal resolution (just a few measurements in one year) and spatial resolution (only one borehole with inclinometer casing in the central part of the landslide) are very poor. A higher spatial resolution of inclinometer measurement is necessary to confirm the existing prognostic landslide model.

Improvement of the subsurface movement monitoring at the central location of a landslide was introduced by installation of four vertical wire extensometers of different depths, installed in the borehole near the existing inclinometer casing. They will provide continuous displacement monitoring data even in the case of larger displacements. However, additional inclinometers in different part of the landslide are necessary to provide reliable data about geometry of sliding surface.

High resolution temporal and spatial data at Kostanjek are obtained from surface movement monitoring by GNSS sensor network and a large number of wire extensometers. Fifteen densely distributed GNSS sensors can provide high accuracy data depending on post-processing time, while the temporal resolution of the data can be every second (in real time kinematic mode). These near-real and real time movement data satisfy the requirements for failure prediction, using for example the Fukuzono (1990) method. Seven extensometers provide data every one hour. Unreliability of extensometer data can be caused by significant influence of meteorological conditions to registered displacements, which is necessary to take into consideration during interpretation of movement, velocity and acceleration.

Properties that have the most significant influences on landslide behavior are hydrological properties. Equipment for monitoring of superficial movements measured landslide displacements of 4-20 cm in different parts of landslide, with periods of maximum velocities (≤ 4 mm/day) which correspond to the peaks of ground-water levels measured in the central part of the landslide (Fig. 4).

Pore water pressure/water level data at the Kostanjek landslide provide good temporal data (every one hour), but the sensors are installed at only few locations in different parts of the

landslide body. Three piezometers with pore pressure gauges are installed in the central part of the landslide body: one is in the zone of the sliding surface and two are in the landslide mass. Other water level gauges are installed in the upper part of the landslide body. Although water level sensors installed in the upper part of the landslide body do not actually measure water level in the sliding surface area, the data shows good correlation with landslide movements. However, additional piezometers are necessary, in different part of the landslide, to provide measurements of pore water pressure for better understanding of landslide behavior and correlation with causal factors.

Monitoring results

Monitoring sensors recorded landslide reactivation due to external triggers in the winter period of 2012/2013. During the period from September 2012 to March 2013 the total cumulative precipitation was 793.7 mm and horizontal displacements were in the range of 4 to 20 cm. The installed monitoring sensor network proved to provide reliable data for the establishment of relations between landslide causal factors and landslide displacement rates aimed at establishing threshold values for early warning system. Monitoring results from the winter period of 2012/2013 has been described in Krkač et al. (2014a) and Krkač et al. (2014b). Here are shortly presented only results of landslide movement monitoring from the same period.

An inclinometer tube was installed in March 2012 in a 100 meter deep borehole placed in the central part of the landslide. The inclinometric profile, obtained on the basis of three measurements, indicates that the failure occurs in a thin basal shear zone at the depth of 62.5 meters (Fig. 10). Deformation above 62.5 meters can be considered negligible related to landslide mechanisms. Deformation at the depth of 15 to 30 meters is most probably a consequence of borehole casing deformations due to improper inclinometer tube installation and voids between the inclinometer casing and the in-situ ground (Krkač et al. 2014a).

During the winter period of 2012/2013, all three installed extensometers (type NetLG-501E, Osasi Technos Inc), showed significant displacement, respectively the long-span extensometer crossing the main scarp, the short-span extensometer crossing the fracture in east part of the landslide and the short-span extensometer crossing the sliding surface in the abandoned tunnel (Fig. 11). All three extensometers displayed extension, but the amount of measured displacement varies from 40 mm on the fracture at the east side of the

landslide body to 72.5 mm on the main scarp and 97 mm in the central part where the sliding surface intersects the tunnel.

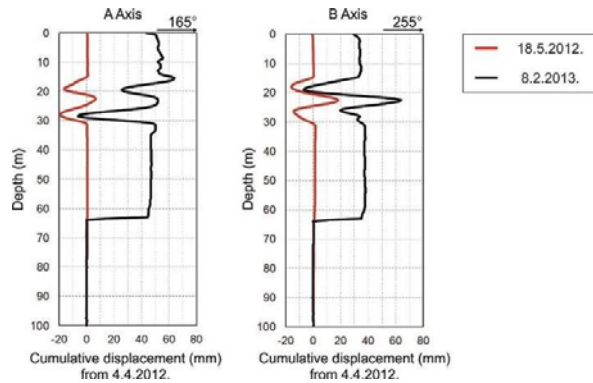


Figure 10 Cumulative inclinometer displacements for the A- and B-axes (Krkač et al. 2014b).

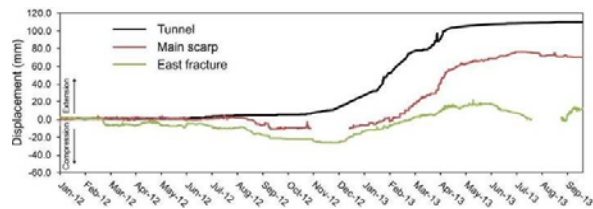


Figure 11 Extensometer measurements in the underground (installed across sliding surface in the abandoned tunnel) and at the surface (installed across main scarp and fracture in east part of the Kostanjek landslide) (Krkač et al. 2014b).

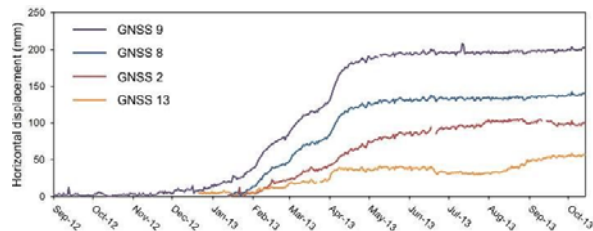


Figure 12 Cumulative horizontal displacements versus time for GNSS 2 and 13 (near the landslide boundary), GNSS 8 (central part of the landslide) and GNSS 9 (landslide foot) (Krkač et al. 2014b).

The first GNSS sensor (double-frequency NetR9 TI-2 GNSS reference station with Zephyr Geodetic 2 GNSS antenna, Trimble) for continuous surface displacement measurement, were installed in September 2012. During the monitoring period, almost all sensors measured horizontal displacement in a range from 4 to 20 cm.

Fig. 12 displays the evolution of 2D surface displacement registered by four GNSS sensors, within the period of major displacement from December 2012 to May 2013. The maximum rates of displacement, with velocities of 2 to 4 mm/day, occurred during the first week of April. On Fig. 12 it is evident that the amount of displacement in the central part of the landslide and in the foot part is approximately two to four

times higher than the displacement near the landslide borders. Cumulative horizontal displacements recorded by GNSS sensor network are shown in Fig. 13.

Preliminary application of monitoring results

This paper Gradiški et al. (2013) presents results of slope stability analyses of the Kostanjek landslide (Fig. 14) performed using the LS-RAPID software (Integrated Landslide Simulation Model) (Sassa and He 2013). Existing landslide model from Ortolan (1996) was modified on the basis of monitoring results by creation of ellipsoidal sliding surface with maximum depth of 65 m in the central part of the landslide body (according to maximal displacements). For more reliable interpretation of the sliding surface depths, additional subsurface investigations and monitoring are necessary. Parameters used for these analyses were determined from drained test of samples in ring shear apparatus in the framework of the Japanese-Croatian project.

According to the results of the analyses, the most unstable part of the landslide is the central part of the landslide body, i.e. the slopes of the abandoned open marl pit. In the analyses the movements started in the central part of the landslide body, and the failure area will expand around the initial failure zone. At the end of simulation the area of the whole landslide mass corresponds to the landslide contour from historical landslide model according to Ortolan (1996). This is also in accordance to the new surface deformations (cracks, bulging, and subsidence) developed by very recent landslide movement in 2013 (Fig. 14).

These analyses were performed for the assumed pore pressure on the sliding surface. For more precisely analyses it is necessary to define more precisely: sliding surface with more correct positions along particular landslide cross sections; water table surface derived on the basis of measured water levels; and performed undrained ring shear test to determined more appropriate soil parameters.

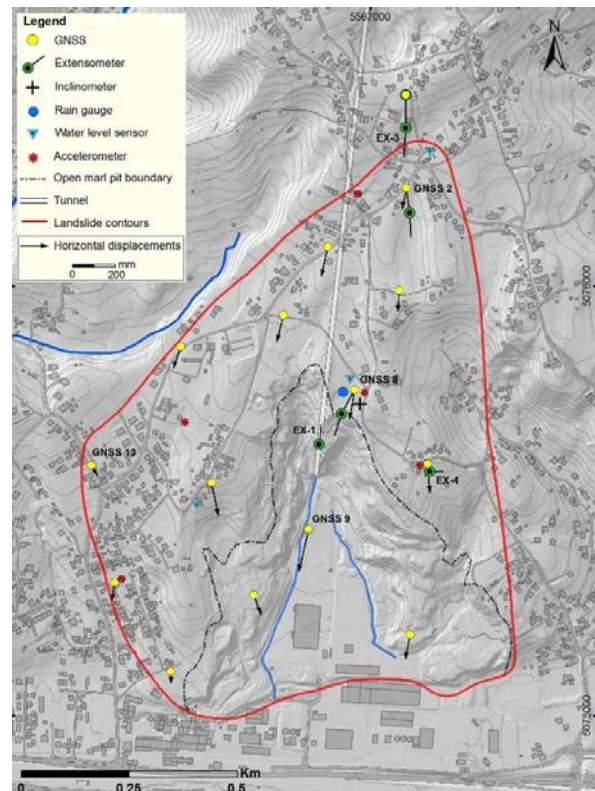


Figure 13 Locations of monitoring sensors at the Kostanjek landslide with cumulative horizontal displacements recorded by GNSS sensor network (Krkač et al. 2014a).

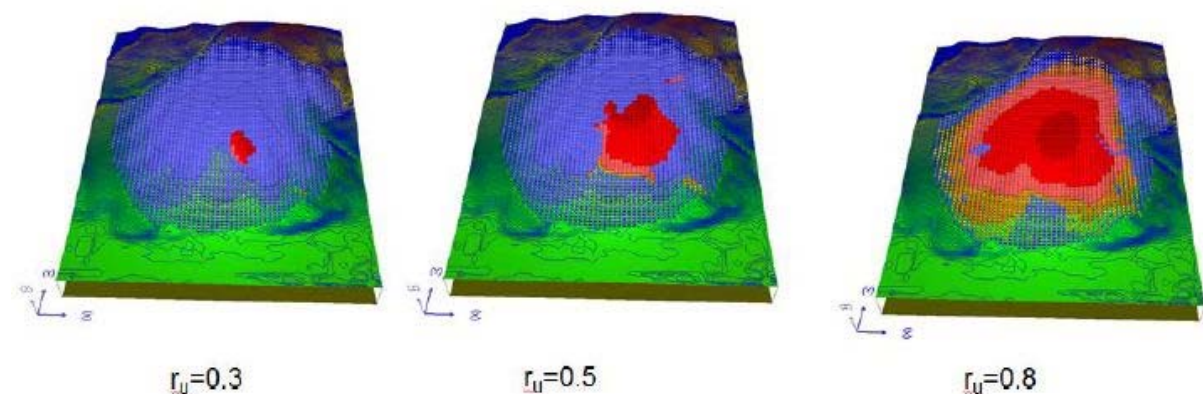


Figure 14 Slope stability analyses of the Kostanjek landslide for $r_u=0.3$, $r_u=0.5$, $r_u=0.8$ (Gradiški et al. 2013).

Discussion and conclusion

In the City of Zagreb landslides are the main geological hazard, as it was proved in 2013. The number of (re)activated landslides during extreme

hydro-meteorological conditions at the beginning of 2013 reached approximately 60 landslides which endangered residential houses and roads. Number of (re)activated landslides is even higher, but they are unknown because of its locations in

forested areas of the City and they were not reported to local government by citizens. Dense population and continuously increasing urbanization of hilly areas requires responsible management with the territory of the City and urban planning on the basis of inventory of existing landslides and prognostic maps with zones of potential landslides. According to the available data, average landslide density is higher than 8 landslides per square kilometer. This implies minimum number of 1,500 landslides at the hilly area of Medvednica Mt. in the City of Zagreb which was pilot area of the scientific Japanese-Croatian SATREPS FY2008 project for landslide inventory mapping.

In the framework of the Japanese-Croatian project it was verified visual analysis of airborne LiDAR DEMs of 1-m resolution with the purpose of landslide identification and mapping. Data captured at the end of 2013 will enable visual mapping of all landslides (re)activated during the extremely wet season in 2013, as well as old landslides, which size is greater than 50 m². Problematic are deformations of bare-earth DEM that remains after post-processing in built-up zones and in which is not possible to identify landslides without extensive field checking.

The Kostanjek landslide presents a hazard and risk for approximately 290 objects (mostly residential houses) in an area of 1 km² in the urban part of the city of Zagreb. The automated monitoring system with real-time or near real-time data, established in the framework of the Japanese-Croatian project, will also enable establishment of an EWS. Further development related to warning and response will be implemented in collaboration with City administration responsible for emergency management. Monitoring sensors at the Kostanjek landslide recorded landslide reactivation and external triggers in the winter period of 2012/2013 and spring period of 2013. Greater displacements in the central part of the landslide than the displacement at the landslide borders imply the necessity to identify zones within the landslide body with different hazard and risk levels. The installed monitoring sensor network proved to provide good quality data for the prediction of failure and the establishment of relations between landslide causal factors and landslide displacement rates aimed at establishing EWS threshold values.

Dealing with landslide detection, mapping, monitoring and hazard analysis in the City of Zagreb, it would be useful to define state of activity of numerous very small to moderately large landslides (primarily <1,000 m²) as well as of the large Kostanjek landslide. In particular, satellite SAR (Synthetic Aperture Radar)

interferometry (Tofani et al. 2013a) has proved a sound tool to assess changes on the Earth's surface for landslide mapping and monitoring purposes. Persistent Scatterer Interferometry (PSI) represents a powerful tool to measure landslide displacement, as it offers a synoptic view that can be repeated at different time intervals and at various scales.

Tofani et al. (2013b) integrated PSI data with in situ monitoring instrumentation, showing that the joint use of satellite and ground-based data facilitates the geological interpretation of a landslide and allows a better understanding of landslide geometry and kinematics. In the future work, PSI interferometry and conventional ground-based monitoring techniques can be used to characterize and to monitor the Kostanjek landslide. PSI analysis can contribute to a more in-depth investigation of this 50 years old phenomenon by better redefining of the landslide boundaries and the states of activity in different parts of the landslides, while the time series analysis can permit better understanding of the deformation pattern and its relation with the causes of the landslide itself. The integration of ground-based monitoring data and PSI data are promising to provide sound results for characterization of the slow moving Kostanjek landslide.

Acknowledgments

Results presented herein have been obtained with the financial support from JST/JICA's SATREP Program (Science and Technology Research Partnership for Sustainable Development). Ministry of Science, Education and Sports of the Republic of Croatia have been financing preparatory and installation works. City Office for Physical Planning, Construction of the City, Utility Services and Transport, City of Zagreb enabled and financed supply of the system with electricity from public network. These supports are gratefully acknowledged.

We would like to express our very great appreciation to the company Geomatika- Smolčak Ltd. for sponsoring the Kostanjek Landslide Observatory development with consultations during the planning and development of the system. Our special thanks is extended to our colleague Mr. Kristijan Špehar for his support in the site and cabinet work.

Authors want to thank the Emergency Management Office of the City of Zagreb for continuous collaboration. We are also thankful to the City Office for the Strategic Planning and Development of the City, City of Zagreb for enabling us use digital data, orthophoto maps and LiDAR DEM.

We wish to thank numerous citizens and the City of Zagreb for their contribution to this project, by enabling use of private and City's land for measurement stations establishment.

References

- Baroň I, Supper R, Ottowitz D (2012) Report on evaluation of mass movement indicators. Safeland deliverable D4.6. Geological Survey of Austria. Vienna, Austria. 382p.
- Bernat S, Mihalić Arbanas S, Krkač M (2014a) Inventory of precipitation triggered landslides in the winter of 2013 in Zagreb (Croatia, Europe). Proceedings of the 3rd World Landslide Forum, Vol. 2, 2-6 June 2014. Beijing, China. pp. 829-836.
- Bernat S, Mihalić Arbanas S, Krkač M (2014b) Landslides triggered in the continental part of Croatia by extreme precipitation in 2013. Proceedings of the XII IAEG Congress, 15-19 September 2014. Torino, Italy. in press.
- Carter W, Shrestha R, Tuell G, Bloomquist D, Sartori M (2001) Airborne Laser Swath Mapping shines new light on earth's topography. EOS, Transactions, American Geophysical Union. 82(46): 549-555.
- Ferić P, Mihalić S, Krkač M (2012) Visual mapping of landslides from LiDAR imagery, Zagreb, Croatia. Proceedings of the 2nd Workshop of the Croatian-Japanese SATREPS FY2008 Project, 15-17 December 2011. Rijeka, Croatia. pp. 130-133.
- Fukuzono T (1990) Recent studies on time prediction of slope failure. Landslide News. 4: 9-12.
- Furuya G, Miyagi T, Hamasaki E, Krkač M (2012) Geomorphological mapping and 3D modelling of the Kostanjek landslide, Zagreb. Proceedings of the 2nd Workshop of the Croatian-Japanese SATREPS FY2008 Project, 15-17 December 2011. Rijeka, Croatia. pp. 21-23.
- Gerber N (2012) Analysis of existing data on landslides and their initiators in hilly area of the Zagreb City. MS thesis, Faculty of Mining, Geology and Petroleum Engineering, University of Zagreb, Zagreb, Croatia. (In Croatian)
- Gradiški K, Krkač M, Mihalić Arbanas S, Bernat S (2013) Slope stability analyses of the Kostanjek Landslide for extreme rainfalls in the winter of 2013. Abstract Proceedings of 4th Workshop of the Croatian-Japanese SATREPS FY2008 Project, 12-14 December 2010. Split, Croatia. pp. 15-16.
- Gradiški K, Sassa, K, He B, Krkač M, Mihalić Arbanas S, Arbanas Ž, Oštrić M, Kvasnička P (2014) Application of integrated landslide simulation model using LS-Rapid software to the Kostanjek Landslide, Zagreb, Croatia. Proceedings of the 1st Regional Symposium on Landslides in the Adriatic-Balkan Region 'Landslide and Flood Hazard Assessment', 6-9 March 2013. Zagreb, Croatia. in press.
- Guzzetti F, Mondini A C, Cardinali M, Fiorucci F, Santangelo M, Chang K-T (2012) Landslide inventory maps: New tools for an old problem. Earth-Science Reviews. 112: 42-66.
- Krkač M, Mihalić S, Ferić P, Podolszki L, Toševski A, Arbanas Z (2013) Japanese-Croatian Project: preliminary investigations of the Kostanjek landslide. Proceedings of 2nd World Landslide Forum 'Landslide Science and Practice', Vol. 6, 3-9 October 2011. Rome, Italy. pp. 385-390.
- Krkač M, Mihalić Arbanas S, Arbanas Ž, Bernat S, Špehar K (2014a) The Kostanjek landslide in the City of Zagreb: Forecasting and protective monitoring. Proceedings of the XII IAEG Congress, 15-19 September 2014. Torino, Italy. in press.
- Krkač M., Mihalić Arbanas S, Arbanas Ž, Bernat S, Špehar K, Watanabe N, Osamu N, Sassa K, Marui H, Furuya G, Wang C, Rubinić J, Matsunami K (2014b) Review of monitoring parameters of the Kostanjek landslide (Zagreb, Croatia). Proceedings of the 3rd World Landslide Forum, Vol. 2, 2-6 June 2014. Beijing, China. pp. 637-645.
- Krkač M, Mihalić Arbanas S, Nagai O, Arbanas Ž (2014c) The Kostanjek landslide - Monitoring system development and sensor network. Proceedings of the 1st Regional Symposium on Landslides in the Adriatic-Balkan Region 'Landslide and Flood Hazard Assessment', 6-9 March 2013. Zagreb, Croatia. in press.
- Mihalić S, Ferić P (2010) Landslides In the area of Zagreb City. Abstract Proceedings of 1st Workshop of the Croatian-Japanese SATREPS FY2008 Project, 22-24 November 2010. Dubrovnik, Croatia. pp. 38-38.
- Mihalić S, Arbanas Ž (2012) The Croatian-Japanese joint research project on landslides: Activities and public benefits. In K Sassa, B Rouhban, S Briceño, M McSaveney, B He (Eds), Landslides: Global Risk Preparedness. Springer, Heidelberg, Germany. (ISBN 978-3-642-22086-9). pp. 333-349.
- Mihalić S, Bernat S, Hamasaki E, Gerber N (2012) Historical landslides in the City of Zagreb: landslide distribution analysis and 3D modeling of typical landslides in AdCALC3D. Proceedings of the 2nd Workshop of the Croatian-Japanese SATREPS FY2008 Project, 15-17 December 2011. Rijeka, Croatia. pp. 122-125.
- Mihalić S, Marui H, Nagai O, Yagi H, Miyagi T (2013) Landslide inventory in the area of Zagreb City: Effectiveness of using LiDAR DEM. Proceedings of 2nd World Landslide Forum 'Landslide Science and Practice', Vol. 1, 3-9 October 2011. Rome, Italy. pp. 155-162.
- Mihalić Arbanas S, Krkač M, Bernat S, Arbanas Ž (2012) Use of existing data in the City of Zagreb (Croatia, Europe) for the purpose of geo-planning. Proceedings 'Advances in Underground Space Development', 7-9 November 2012. Singapore, Singapore. pp. 465-477.
- Mihalić Arbanas S, Arbanas Ž, Krkač M (2013) Comprehensive landslide monitoring system: The Kostanjek Landslide case study, Croatia. In K Sassa, B He, M McSaveney, N Osamu (Eds), ICL Landslide Teaching Tools. International Consortium on Landslides, Kyoto, Japan. (ISBN 978-4-9903382-2-0). pp. 158-168.
- Miklin Ž, Mlinar Ž, Brkić Ž, Hećimović I, Dolić M (2007) Detailed engineering geological map of the Podsljeme urbanized zone in a scale of 1:5,000 (DIGK-Phase I). Croatian Geological Survey, Zagreb, Croatia. (In Croatian)
- Ortolan Ž (1996) Development of 3D engineering geological model of deep landslide with multiple sliding surfaces (Example of the Kostanjek Landslide). PhD thesis, Faculty of Mining, Geology and Petroleum Engineering, University of Zagreb, Zagreb, Croatia. (In Croatian)
- Ortolan Ž, Pleško J (1992) Repeated photogrammetric measurements at shaping geotechnical models of multi-layer landslides. Rudarsko-geološko-naftni zbornik. 4:51-58. (In Croatian)
- Podolszki L, Ferić P, Miyagi T, Yagi H, Hamasaki E, Mihalić S (2012) Aerial photo interpretation of landslides for the

- purpose of landslide inventory mapping in the area of the City of Zagreb. Proceedings of the 2nd Workshop of the Croatian-Japanese SATREPS FY2008 Project, 15-17 December 2011. Rijeka, Croatia. pp. 126-129.
- Podolszki L (2014) Stereoscopic analysis of landslides and landslide susceptibility on the southern slopes of Medvednica Mt. PhD thesis, Faculty of Mining, Geology and Petroleum Engineering, University of Zagreb, Zagreb, Croatia. (In Croatian)
- Polak K, Klemar M, Nejkova M, Radošević N, Stepan Z, Miroslav M, Križanić Z (1979) Lithological characterization and slope stability zonation of the hilly area of Medvenica Mt. at the area of the Zagreb city. Geotehnika-Geoexpert, Zagreb, Croatia. (In Croatian)
- Razak K A, Straatsma M W, van Westen C J, Malet J-P, de Jong S M (2011) Airborne laser scanning of forested landslides characterization: Terrain model quality and visualization. *Geomorphology*. 126: 186–200.
- Reutebuch S E, McGaughey R J, Anderson H E, Carson W W (2003) Accuracy of a high-resolution LiDAR terrain model under a conifer forest canopy. *Canadian Journal of Remote Sensing*. 29: 527–535.
- Sassa K, He B (2013) TXT-tool 3.081-1.2 Landslide dynamics. In K Sassa, B He, M McSaveney, N Osamu (Eds), *ICL Landslide Teaching Tools*. International Consortium on Landslides, Kyoto, Japan. (ISBN 978-4-9903382-2-0). pp. 215-237.
- Shan J, Toth C K (Eds) (2009) *Topographic laser ranging and scanning: Principles and processing*. CRC Press, Taylor and Francis Group, Boca Raton, Florida. (ISBN 978-1420051421). 590p.
- Šikić V (1967) *Engineering geology Zagreb – north and south*. Croatian Geological Survey, Zagreb, Croatia. (In Croatian)
- Tofani V, Segoni S, Agostini A, Catani F, Casagli N (2013a) Technical Note: Use of remote sensing for landslide studies in Europe. *Natural Hazards and Earth System Sciences*. 13: 299–309.
- Tofani V, Raspini F, Catani F, Casagli N (2013b) Persistent Scatterer Interferometry (PSI) Technique for Landslide Characterization and Monitoring. *Remote Sensing*. 5: 1045-1065.
- Županović Lj, Opatić K, Bernat S (2012) Monitoring of movements of the Kostanjek landslide using relative static method (GNSS technology). *Ekscentar*. 15: 46-53. (In Croatian)



Proceedings of the SATREPS Workshop on Landslides in Vietnam, 2014

Analysis of a Deep-seated Landslide in the Phan Me Coal Mining Dump Site, Thai Nguyen Province, Vietnam

Do Minh Duc⁽¹⁾, Nguyen Manh Hieu⁽¹⁾, Kyoji Sassa⁽²⁾, Eisaku Hamasaki⁽³⁾, Dang Quang Khang^(1,2), Toyohiko Miyagi⁽⁴⁾

1) VNU University of Science, Vietnam National University, Hanoi, Vietnam, e-mail: ducdm@vnu.edu.vn

2) International Consortium on Landslides, Kyoto, Japan

3) Advantech Co., Ltd, Japan

4) Tohoku Gakuin University, Miyagi, Japan

Abstract A large landslide occurred at the Pha Me coal mining dump site at 4:20 AM on 15 April 2012, buried a huge area, including tens of houses and 7 persons. There was no abnormal weather or seismic activity at the time of the landslide. A joint work between Vietnamese and Japanese experts was carried out to investigate characteristics and reasons of the landslide. The achieved results show that coal mining wastes are disposed of on low hill sites where granitic bedrock was intensively crushed due to tectonic activity. Weathering crusts include rich clays of over 15-20 m in thickness. The landslide has a volume of about 2.5 million m³, with a slip surface cut through weathering soils at a depth of about 10 m. The scarp of the landslide departs at an approximate elevation of 85-100 m. Travel distance is 300-350 m. Sliding materials are primarily mining wastes. However the sliding surface is defined to be situated at the depth of 12-15 m in the residual soils. There are two significant causes of the disaster. Firstly, the waste dump site plays a role as a water-storage layer which keeps residual soils permanently saturated. The second cause of the deep-seated landslide is over-loading of mining wastes. Prior evidences of the landslide such as cracks at the top, heave at the trough of the dump site were recognized a week before, however they were not seriously considered.

Keywords Deep-seated landslide, Coal waste dump site, Residual soils, Slope stability, Vietnam

Introduction

In recent years, landslides have occurred in dumps of municipal solid waste (Blightw and

Fourie 2005, Yilmaz and Atmaca 2006) and coal mine waste (Geertsema et al. 2006, Steiakakis et al. 2009), which are artificial mountains with heights of nearly a hundred meters. They are not only damaging the environment but are also dangerous to human life and property. For example, the Buffalo Creek disaster in the USA in 1972 that killed 118 people, made 4000 homeless and destroyed 50 million US dollars worth of property and facilities. The flow slide that occurred in the Umraniye-Hekimbasi refuse dump in Turkey in 1993 killed 39 people (Blightw and Fourie 2005).

Phan Me coal mine is situated in Thai Nguyen province, Northeast Vietnam (Fig. 1). Established in 1960, it had an initial designed capacity of 50,000 tons of coal per year. Recently, the mine had two sites of exploitation: North Lang Cam open pit mine with a reserve of 1,560,000 tons, designed capacity of 100,000 tons per year and South Lang Cam pit mine with usable reserves of 1,640,000 tons, designed capacity of 30,000 tons per year. The mine has 3 waste dump sites which are about 2-3 km away from the open pit.

A large landslide occurred at a dump site of Phan Me coal mining at 4:20 AM on 15 April 2012, buried a huge area, including tens of houses and 7 persons. There was no abnormal weather or seismic activity at the time of landslide. The achieved results show that coal mining wastes that were disposed of on low hill sites where bedrock is intensively crushed due to tectonic activities. This paper aims to define characteristics and causes of the landslide, including slope stability analysis of the Phan Me coal mining waste dump site using SLOPE/W software.

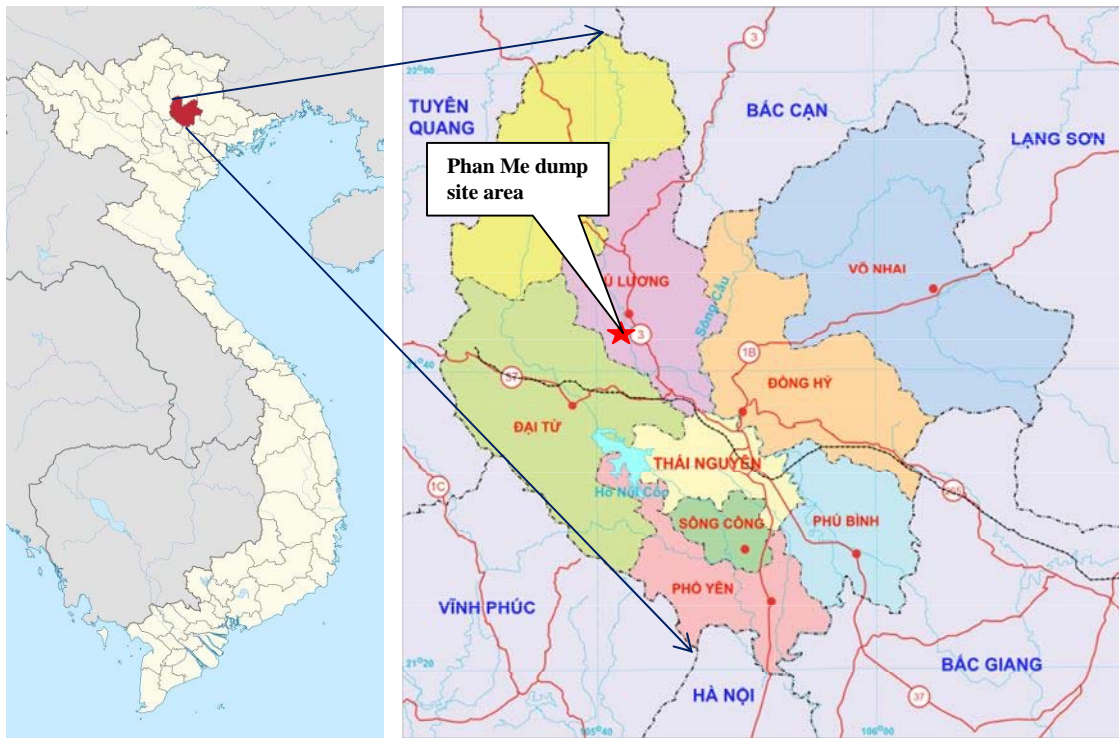


Fig. 1 Location of the study area

Study methods

Site investigation

After the landslide occurred, a research group investigated the boundary of the landslide by using a GPS Garmin 72 with an accuracy of $\pm 5\text{m}$. Boundary of the landslide was marked on the topography map, at a scale 1/10 000 and a Google Earth image. In-situ density of coal mining wastes and clay layers were also determined by digging holes and taking undisturbed samples, respectively (Fig. 2).



Fig. 2 Determine in-situ density of waste materials by digging hole

Waste materials mainly include sand, gravel and boulders. In order to determine the average internal friction angle of the waste materials, the internal friction angle of each kind of material was measured after landslide event. In-situ

samples included waste materials and weathered clay and were retrieved to determine physical and mechanical parameters that were used for stability analysis as density, effective cohesion, and effective internal friction angle.

Laboratory tests

Undisturbed samples and disturbed samples were taken from the site including weathered clayey soil and material from the dump site for laboratory tests. Tests were performed according to the specifications of ASTM (American Society for Testing and Materials 2001). Grain size analysis was conducted by the wet sieve method with sieve sizes of 20, 10, 5, 2.5, 1, 0.5, 0.25, 0.10, and 0.05 mm, respectively. Effective internal friction angle and cohesion of residual soils were determined by direct shear test (ASTM 2001 D3080). Density of soils was determined in both natural condition and saturated condition.

The other data used in the study includes topographic and geological maps at a scale of 1: 50,000 and data on the exploitation activities at the Phan Me coal mine.

Results and discussion

Topography and geological settings

The Phan Me community belongs to the Phu Luong district. It is located at tanhe elevation of 150 to 200 m. Slope angle of the terrain ranges between 5 deg and 20 deg. The dump site was located on hills with a natural slope angle of 15 to 20 degree.

A large area of the Phan Me community lies on the Nui Chua complex (vaT₃nnc) including pyroxene gabbro, biotite gabbro, gabbro diorite, pegmatite gabbro. The Coal mine is exploiting the Van Lang formation (T₃n-rvl) (Fig. 3). Coal mining waste was subsequently dumped on a hilly site which is a weathering crust of the Nui Dieng complex phase 2 (γT₂nd₂). Residual soils are rich clays of 15-20 m thickness. Composition of the Nui Dieng complex phase 2 includes dykes, veins and small bodies of aplite, and pegmatite. The area is characterized by a complex system of faults. Especially, the mine is in the area of interference between 3 faults.

Characteristics of the landslide

The dump site was 90 m high, including two steps in front of the landslide. The lower step was 35m in height and the upper part was 55m in height. Average slope angle was 34 degrees. Prior to the landslide, there were some cracks at the top

of the dumpsite. The trough heaved up to 0.5 m in some places (per communication with local people). However, these signs was not taken into account as early warnings of a landslide by both managers of the mine and local people.

The landslide occurred at 4:20 AM on 15 April 2012. There was no abnormal weather or seismic activity before or after the time of landslide. The scarp departed at an approximate elevation of 85-100 m. Landslide debris run out was up to 300-350 m (Fig. 4), buried 10 houses (2 houses were only 30 m away from the dump site). Rice fields were affected and 7 people were killed (Fig. 5 and 6). Rice fields at the outer side of landslide debris were pushed up several meters (Fig. 7) and displaced 20-30 m westwards. The landslide has a volume of about 2.5 million m³ with the slip surface cut through weathering soils at the depth of about 15 m.

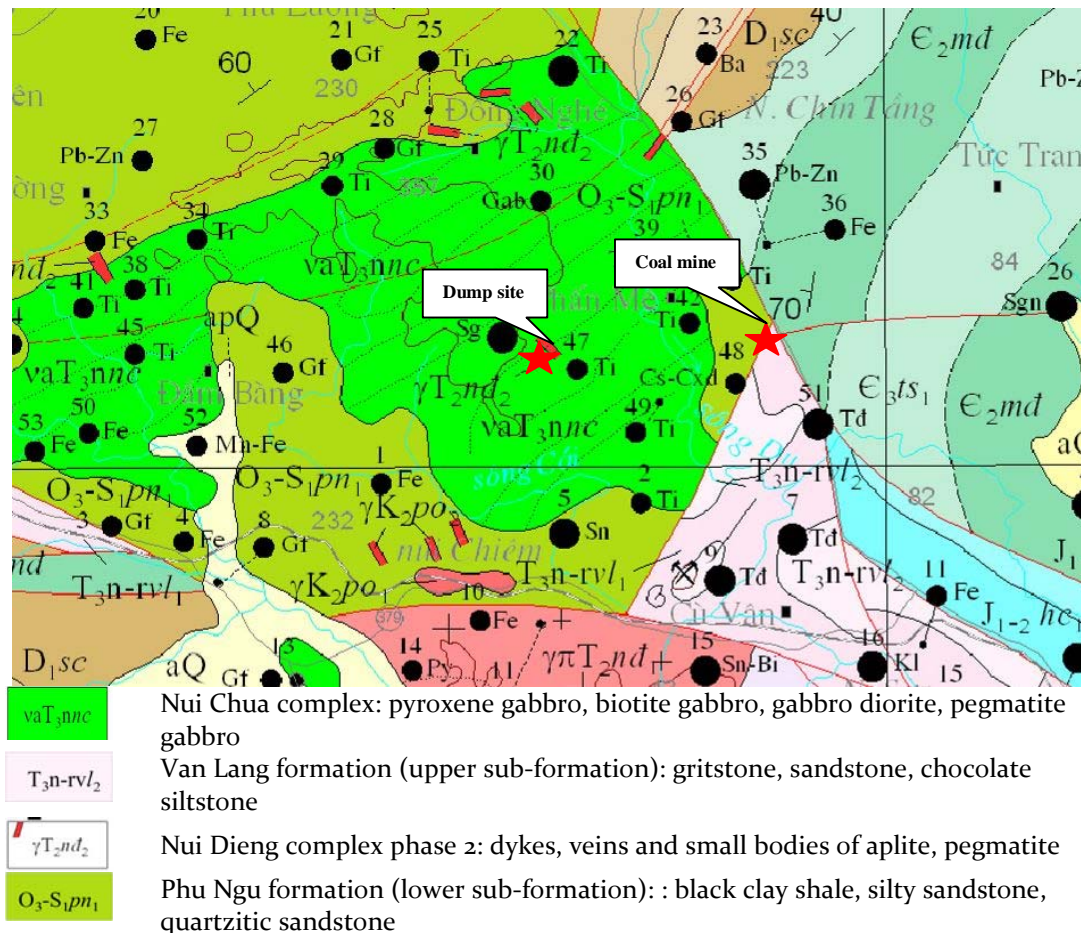


Fig. 3 Geological settings in Phan Me area



Fig. 4 Boundary of the landslide before and after event



Fig. 5 Dump site area after the landslide



Fig. 6 A house was completely destroyed

determined by field and laboratory tests. Factor of safety of the dump site was calculated by SLOPE/W software using the Bishop simplified method.



Fig. 7 Rice field was pushed up by the landslide debris

The deep-seated landslide in Phan Me coal mine occurred in the weathering crust. Residual soils are rich clays with a thickness of 15-20 m. Geotechnical properties of the soils and waste materials are shown in table 1. After the landslide, the slope angle of the sand and gravel material was 32 to 33 degrees; slope angle of the material containing boulders was 35 degree. An average value of 34 degree was used for stability analysis of the waste dump site. In terms of geometry, the dump site has two steps, the first step is 30 m high and the second step is 55 m high.

Results of slope stability analysis (Fig. 8) shows that the overburden load of mining wastes was above shear strength of the residual soils. Slip surface is about 35 m below the terrain and cut 14 m into the weathering crust.

Soil characteristics and slope stability analysis

Slope stability analysis have been carried out at several waste dump sites (Chaulya et al. 1999, Omraci et al. 2003, Nyssen and Vermeersch 2010, Wang et al. 2011, Pinto 2009). In order to analyze the stability of the Phan Me coal dump site, we used input data for the model as geometry measured on site, characteristics of soil layers

Table 1 Geotechnical properties of coal mining waste and residual soil

Soil	Grain size (mm) (%)						Bulk density (kN/m ³)	Effective cohesion (kPa)	Effective internal friction angle (degree)
	>20	10 -20	5 - 10	0.1 - 5	0.05 - 0.10	<0.05			
Coal mining waste	40.1	12.2	6.7	29.8	11.2	0	20.5	0	34
Residual soil	0	0	21.7	26.1	15.7	36.5	18.5	24	20

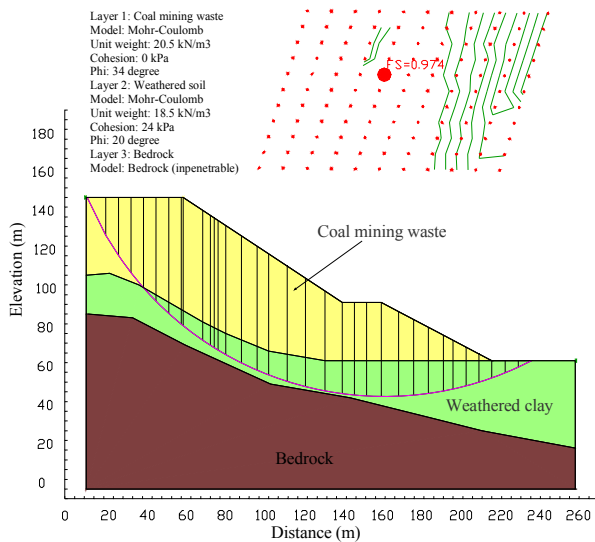


Fig. 8 Result of slope stability analysis using SLOPE/W

Conclusion

In spite of prior evidences of a large landslide at the Phan Me coal mine, waste materials were still disposed at the dump site. The deep-seated landslide occurred at 4:20 AM on 15 April 2012 without any abnormal weather or seismic activity. There are two main causes of the disaster. Firstly, the waste dump site plays a role as a water-storage layer which keeps residual soils permanently saturated. The second cause of the deep-seated landslide is over-loading of mining wastes. The landslide once again raises the awareness and serious warning of disaster risk management in mining areas in Vietnam and many other developing countries.

References

ASTM (2001) D3080 Test method for direct shear test of soils under consolidated drained conditions. ASTM Standards on Disc CD 1, Volume 04.08, Soil and Rock (I): D420 - D5779.

Blightw G E, Fourie A B (2005) Catastrophe revisited – disastrous flow failures of mine and municipal solid waste. *Geotechnical and Geological Engineering*, 219–248.

Chaulya S K, Singh R S, Chakraborty M K, Dhar B B (1999) Numerical modeling of biostabilisation for a coal mine overburden dump slope. *Ecological Modeling* 114 (1999) 275–286.

Geertsema M, Clague J J, Schwab J W, Evans S G (2006) An overview of recent large catastrophic landslides in northern British Columbia, Canada. *Engineering Geology* 83, 120– 143.

GEO-SLOPE International Ltd. (2004) *Stability Modeling with SLOPE/W – An Engineering Methodology*.

Nyssen J, Vermeersch D (2010) Slope aspect affects geomorphic dynamics of coal mining spoil heaps in Belgium. *Geomorphology* 123, 109–121.

Omraci K, Merrien-Soukatchoff V, Tisot J P, Piguat J P, Le Nickel SLN (2003) Stability analysis of lateritic waste deposits. *Engineering Geology* 68, 189–199.

Pinto PSS (2009) Static and seismic analysis of solid waste landfills. *Proc. of Int. Symp. on Geoenvironmental Engineering, ISGE2009, September 8-10, 2009, Hangzhou, China*.

Steiakakis E, Kavouridis K, Monopolis D (2009) Large scale failure of the external waste dump at the South Field lignite mine Northern Greece. *Engineering Geology* 104, 269–279.

Wang G, Kong X, Gu Y, Yang C (2011) Research on slope stability analysis of super-high dumping site based on cellular automaton. *Procedia Engineering* 12, 248–253.

Yilmaz and Atmaca E (2006) Environmental geological assessment of a solid waste disposal site: a case study in Sivas, Turkey. *Environmental Geology*, 50: 677–689, DOI 10.1007/s00254-006-0241-1.



Proceedings of the SATREPS Workshop on Landslides in Vietnam, 2014

Hybrid Socio-Technical Approach for Community-based Landslide Risk Reduction in Indonesia *)

Dwikorita Karnawati ⁽¹⁾, Teuku Faisal Fathani ⁽²⁾, Wahyu Wilopo ⁽¹⁾, Budi Andayani ⁽³⁾

1) Gadjah Mada University, Geological Engineering Department, Jl. Grafika No. 2, Yogyakarta, Indonesia

2) Gadjah Mada University, Civil and Environmental Engineering Department, Jl. Grafika No. 2, Yogyakarta, Indonesia

3) Gadjah Mada University, Faculty of Psychology, Bulaksumur, Yogyakarta, Indonesia

Abstract The importance of integrating social and technical approaches (which is so called a “hybrid socio-technical approach”) is promoted in this paper. Indeed, it is considered as one innovative and strategic program for community-based landslide disaster risk reduction. Such program mainly based on multi-disciplinary action-research to support the community empowerment program through public education. The technical approach was mainly conducted for geological and geotechnical investigation to analyse and predict susceptibility levels of the disaster prone area, as well as to develop an appropriate technology for hazard mapping and disaster early warning. Meanwhile, the social approach was necessary to be undertaken for analysing and mapping the psychosocial conditions of the disaster prone area, and accordingly an appropriate strategy and program to implement the produced technology can be formulated. Moreover, it is also important to establish a “community task force” as the driving power for landslide disaster risk reduction, which can sustain the program at the village level.

Keywords Hybrid socio-technical system, indigenous technology, life and environmental protection, community empowerment

Introduction

Situated in such a dynamic geological region, which is occupied by high density of population, Indonesia is frequently struck by various types of geological disasters, which leads to substantial death tolls, casualties and socio-economical loss.

*) This paper has been published in the *ASEAN Engineering Journal Part C Vol.2 No.1 June 2013 pp 22-49*, used here as a teaching material only

According to the Indonesian National Agency for Disaster Management, Indonesia has been struck by 6,632 events of natural disasters (mainly geological disasters), within the period of 1997 to 2009, with the total death tolls of 151,277 people. Therefore, it is very urgent to develop appropriate geo-disaster mitigation for life protection and environmental sustainability, through the improvement of society resilient in such disaster prone area.

Socio-technical challenges for landslide disaster risk reduction

Landslide is one of the most frequent disasters in Indonesia. Because of the geological conditions and the high rain precipitation, more than 50 % of Indonesian region is prone for this particular disaster. It is commonly found that the soil condition in this area is fertile with significant amount of water resources and the beautiful panorama to stay. That is why, most of the landslide prone areas have been developed as the villages or cities with high population density, such as in Java and Sumatera. As the results, the risk of landslide disasters seriously increases in response to the continuous growing of population and uncontrolled land use changing. Indeed, it has been thousands of people died, several thousands of houses damages and thousand hectares of land buried due to landslide disasters. Accordingly, the improvement of community resilience in landslide prone area has become critical challenges that should be tackled through the implementation of appropriate approach, technology and capacity development program as suggested by Karnawati et al (2009), Anderson et al (2010 and 2011), and also Holcombe et al (2012), in order to ensure the human survivability and environmental sustainability.

The development of hazard map and the application of an appropriate technology for early

warning system are considered as the crucial efforts to reduce the risk of landslide disasters. Unfortunately, the effectiveness in implementing hazard maps and an early warning system cannot be guaranteed due to less consideration on the social-cultural and socio-economical conditions at the disaster prone area. Accordingly, the needs to integrate social considerations into technical system should be addressed in order to assure the effectiveness in the implementation of such hazard map and early warning system for disaster risk reduction.

Hybrid Socio-technical Concept for Landslide Disaster Risk Reduction

To ensure the effectiveness in the implementation of any technology for disaster risk reduction, a combined (hybrid) system, which considers both social and technical conditions has been developed by Karnawati et al (2009 and 2011). Such approach mainly consists of the development of technical system for providing community landslide hazard/ risk map and early warning system, and also the social system for developing appropriate community empowerment program. The technical system is recommended to address the development of the existing indigenous or local knowledge and technology, by considering the simplicity of such system and technology. More over, the utilization of the local material is promoted, by encouraging the local knowledge (local experts and local operators) to drive the local participation program. Indeed, it is important that the hybrid system should be performed with a low cost and simple technology, approach and method, so that it can be easily understood, reproduced, operated and maintained by the local community, such as suggested by Karnawati et al (2008, 2009 and 2011). This empowerment program relies on the public education, encouraging community participation in developing and implementing action plan for disaster mitigation and risk reduction. Schematic concept of this approach is illustrated in Fig. 1.

All of this concept can be done only if the local community has been empowered. Therefore, process of technology development can be carried out during or as a part of the process of community empowerment.

Implementation of the Hybrid Socio-Technical System

A hybrid socio-technical system has been implemented in several pilot areas in West Sumatera (Nagari Tanikat at Padang Pariaman Regency and Tanjung Sani Regency at Agam Regency), West Java at

Cianjur Regency, Central Java (especially in Karanganyar Regency and Banjarnegara Regency) and also in East Java at Situbondo Regency, as illustrated in Fig. 2. All of those Regencies are situated at the slope of Volcanoes, in which about 30% - 60% of the region is highly risk for landslide. The high risk of landslides due to the high susceptibility conditions which is controlled by the geology and climate conditions, and also because of the high vulnerability of the socio-economical conditions in the landslide prone area (Karnawati et al 2009 and 2011).

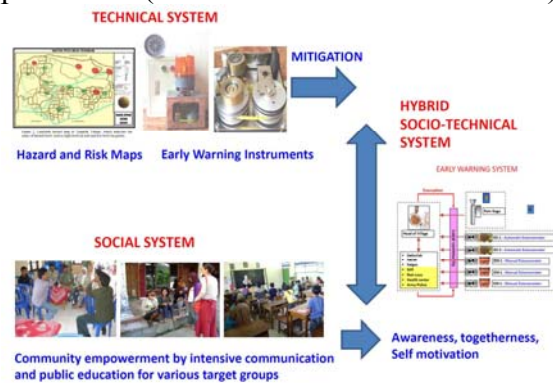


Figure 1 The concept and key component of a hybrid socio-technical system for landslide mitigation and early warning system (Karnawati et al 2009 and 2011).

It was considered to be more feasible to manage the social-conditions for reducing the socio-economical vulnerability in the landslide prone area, rather than changing the natural conditions, such as the geology and climate.



Figure 2 Location of the pilot areas of Hybrid Socio-Technical Approach in Landslide Disaster Risk Reduction in Indonesia.

Accordingly, landslide disaster risk reduction in those pilot study area was conducted by mitigating the social conditions through the adaptive management as suggested by Andayani et al (2008),

Karnawati et al (2009 and 2011), and also Halcombe et al (2012), which emphasized on the improvement of community resilience by implementing the hybrid socio-technical approach.

Development of Technical System

The technical system for landslide disaster risk reduction was developed by Karnawati et al (2009, 2011 and 2012), consisting of several technical components such as the instruments for landslide early warning system recommended by Fathani et al (2008) and also Fathani and Karnawati (2009), supported by the smart-grid for landslide hazard communication, monitoring and early warning developed by Karnawati et al (2012) as well as the community-based landslide hazard map suggested by Karnawati et al (2010).

Early warning instruments

The early warning instruments was designed by relying on the manual extensometers (5 sets) connected with the alarm generated by dry battery as illustrated in Fig. 3. Each of these instruments is facilitated with the automatically pull able wire installed across the progressive crack (Fig. 4), so that the progress of crack development due to the slope movement can be monitored. The instalment of extensometers was also supported by the rain-gauge (1 set) as illustrated in Fig. 3b and solar panel (1 set); so two different stage of warning levels can be defined. The first threshold of warning was set-up by setting the ON alarm in response to the rain precipitation of 70 mm/hour or the accumulative rain precipitation of 100 mm, whilst the second threshold was defined when the extension of pull able wire reached the distance of 5 cm. The function of first alarm was used for raising the community alert, and the second alarm was set-up for starting the evacuation process in the landslide prone zone.

Admittedly, the numbers of early warning instruments are limited which were not sufficient to cover the large area of prone zone. Therefore, a smart grid for landslide early warning has been developed by Karnawati et al (2012).

Smart grid for landslide hazard monitoring and early warning

Smart Grid is a participatory cyber-based communication and information system, developed as a system of handling networks of information nodes consisting of local experts, local surveyors, or selected members of local task force and the contact person in the local communities. The information is sent to the 'online' web or cyber system, with the specific

functions to facilitate the participatory data reporting via the online web, mobile phone (text message), or other various social media, and also to store and analyse those participatory input-reports (related to the geological/ geotechnical conditions and process, which considered as the symptoms or early indications of landslides), for defining the landslide hazard and risk level in any particular site or zone.



Figure 3a above, the manual extensometer (generation 1 on the left and generation 2 on the right), connected with alarm system in the middle, stem in the middle, and 3b below, the rain gauge with the alarm system (Fathani et al, 2008; Fathani and Karnawati, 2009).

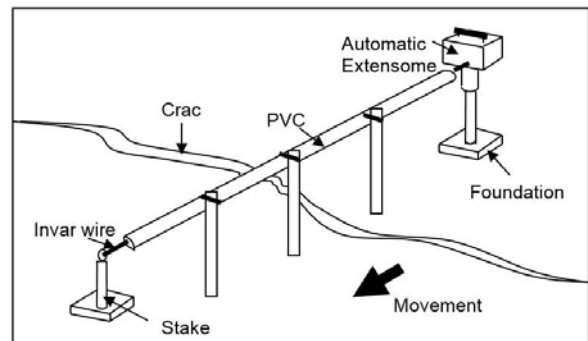


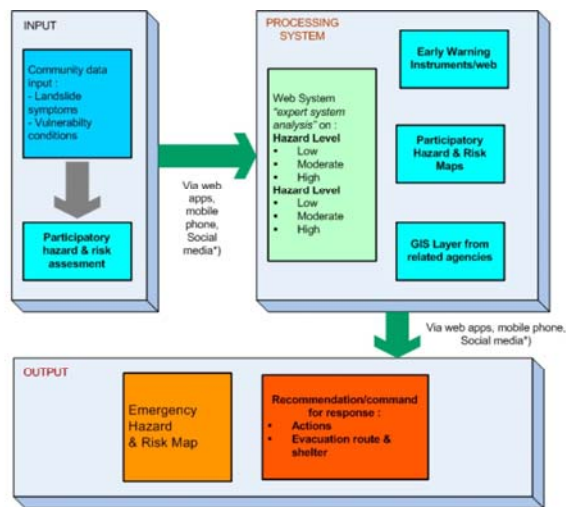
Figure 4 The automatically pull able wire, protected inside the PVC pipe and installed across the progressive crack (Fathani et al, 2008).

Results of the analyses are required to provide the emergency-decision supports, which relate to the information of the zone and level of landslide hazard/ risk, evacuation route and shelter, as well as the recommendation of method or approach for mitigation, preparedness and emergency actions. All of the information about hazard/risk and the guidance for response will be blasted/ transmitted back to the respective-reporting node as well as to the other relevant registered nodes. This participatory system can also be connected to various types of social media (mobile phone call/text, Twitter, Facebook, Google+, Yahoo, etc.).

It is also important that the multi-two way direction facilitates the communication flow in this participatory smart grid system. Such system

can also be linked to the existing community-based landslide early warning instruments developed in parallel with this smart grid system.

Concept of the smart grid design is illustrated in Fig. 5, whilst the example to the web performance of smart grid is displayed in Fig. 6.



*not available at first phase

Figure 5 Concept of expert system in the smart grid design developed by Karnawati et al 2012.

Community-based hazard map

The understanding and simplicity of the approach and method of mapping is the most critical part to guarantee the effectiveness of disaster risk reduction program.

Unfortunately, it is apparent that most of the technical landslide hazard map was not easy to be understood by the local community. That is why a simple participatory hazard mapping method was developed by Karnawati et al 2010, to facilitate the community landslide hazard mapping, which also addressing the Landslide Risk Assessment and Mitigation Strategy suggested by Lacasse and Nadim (2008). Therefore, the standard technical method for landslide hazard mapping was simplified to prepare a simple landslide hazard map which can be conducted by the local community on the existing village base-map (i.e. the village “situation” map), through the participatory mechanism. Such map was presented without any contour, but mainly showing the lay out of roads, rivers, houses and land farming areas which were very easy to be identified by the local community. Identification of the high susceptible zone (red zone) and low susceptible or safe zone (green zone) for landslides was carried out by the community task force through public participation, which is advised by the local expert. Fig. 7 shows the landslide hazard map which was develop by the local community in Tengklik Village, Tawangmangu District, Karanganyar Regency, Central Java. This map is also very important to

decide where the early warning instruments should be installed and how the evacuation route should be decided.

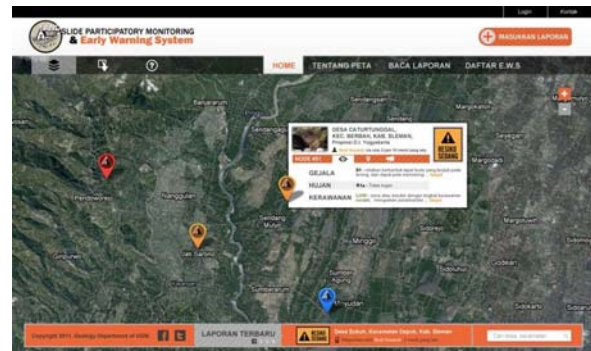


Figure 6 Web performance showing the geographical position of the reporting nodes.

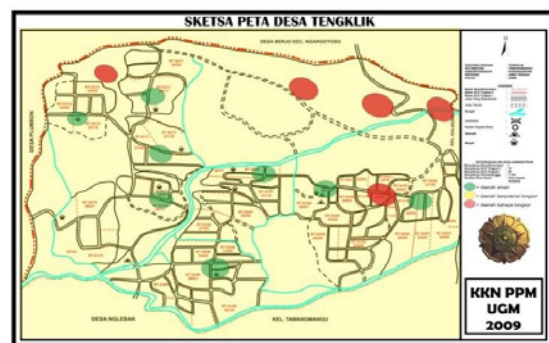


Figure 7 Community-based landslide hazard map of Tengklik Village, Karanganyar Regency, Central Java, indicating zones of hazard level (red is high level and green is low level), recommended by Karnawati et al 2010.

Development of Social

Development of the social component in the hybrid system was initiated by social survey, to identify the existing knowledge about the landslide hazard, which will affect the community’s perception about landslide risk and their expectation on the proposed developed-technology for landslide disaster risk reduction. Identification on all of those aspects significantly control their motivation or willingness for actively participating in any disaster risk reduction program. Results of this social survey will be crucial to formulate the appropriate and effective strategy for public education related to the effort for raising the community awareness and also for conducting community empowerment program.

Various target groups were defined, and those comprise the group of women (as the key person in the family), teachers, children as well as the young and senior leaders. The local government of Karanganyar Regency also continuously and actively supported this social development program.

Results of the social survey indicated that most of the community members had been quite aware with the potential occurrence of landslides at the rainy season, because the landslide disasters have quite frequently struck their living area, especially under the heavy or long continuous rainfall. Nevertheless, most of the community members preferred to remain living in their vulnerable region, instead of being relocated to the other safer areas. Obviously, the fertility of soil, the abundance of water resources, the beauty of mountainous panorama and the strong psychological engagement with their homeland or home-heritage, strongly prevented their willingness to leave their dangerous homeland. Unfortunately, they did not have enough knowledge, skill and capacity to decide about “what should” and “what should not do” for preventing the landslide as well as for protecting their life and environment from the landslide occurrences. Eventhough, they had not yet been capable to identify the sites (slopes), which were susceptible for landsliding, and to recognize the initial symptoms of landsliding. Therefore, the hybrid socio-technical approach for community-based landslide early warning was applied to develop their capacity for implementing the appropriate landslide disaster risk reduction program, which will support the improvement of the community resiliency in this landslide prone area.

A community task-force for disaster risk reduction at the village level was also established under the coordination with the Agency for Disaster Management at the Regency level (Fig. 8). This network is also linked to the local hospital (health centre), the local army and police, and also the Search and Rescue Team (SAR team) at the local Regency. Indeed, this task force played an important role as the driving power for the disaster risk reduction program, and also to effectively implement and sustain the technical system for landslide risk reduction.

Evaluation

It was apparent that the existence of a community task force for landslide disaster risk reduction at each village level was the most important factor to ensure the affectivity and sustainability of landslide mitigation and risk reduction program. This task force had an important role as the driving agent in the empowerment and mitigation program. In fact, since this proposed hybrid socio-technical approach implemented in several pilot areas in Karanganyar Regency, such as in Ledoksari Village in 2008, Tengklik Village in 2009, Matesih Village in 2010 and also Gempolan and Plosorejo Villages in 2011, the community resilience for landslide disasters has gradually increased, the socio-economical losses due to

landslides can be minimised and the numbers of landslide victims have been dropped to zero. It seems that this approach could effectively empowered to local community to mitigate the landslides. Eventhough, the key person who is also the member of the community task force and was in charged for the mitigation program, was also invited to share their experiences in facilitating the community empowerment actions to tackle the landslide problems in another landslide disaster area in Tanjungsani Village at Agam Regency, West Sumatera.

Therefore, the Hybrid Socio-Technical approach is also very applicable to be developed in several other disasters area in developing countries, although several adjustments may be required to address the social and environmental characteristics at the specific site. Moreover, the importance of commitment and leadership of the local Agency for Disaster Management at the Regency and District levels to support the effectiveness of the disaster management program at the village must be highlighted.

It was also obvious that the socio-cultural and socio-economical constrains during the mitigation program can be minimized by implementing the hybrid socio-technical approach. Indeed, the introduction and implementation of a new technology for early warning and disaster management system can be conducted more effectively through the public participation actions. That is why more enthusiastic response of the local community and local authority to actively participate in the landslide disaster risk reduction program can be performed as illustrated in Fig. 8.

Conclusion

One of the most critical considerations on disaster risk reduction in Indonesia is the assurance for the effectiveness and sustainability of the disaster management program. It is apparent that the proposed model, which is so called as the combined (hybrid) socio-technical approach has been quite effective and strategic to improve the community resilience at the landslide vulnerable village. It is also crucial that the system should be developed through community participation and the provision of simple and low cost technology for landslide hazard mapping and early warning. Indeed, the establishment of community task force at the village level is very important to ensure the effectiveness, continuity and sustainability of this proposed system. This approach may also be applicable to tackle similar problems for landslide risk reduction in other developing countries in Asia.



Figure 8 Activities to develop and empower the community task force at Tengklik Village which were facilitated by the student community service program conducted by Universitas Gadjah Mada.

Acknowledgments

Special thanks are directed to the Indonesian Agency of National Disaster Management, the British Council Delphe Program as well as the Directorate General of Higher Education – the Indonesian Ministry of National Education and the Fulbright Senior Research Program funded by US Department of State's Bureau of Education and Cultural Affairs for providing financial supports to carry out the pilot studies. The acknowledgments are also extended to Universitas Gadjah Mada for the provision of academic facilities, as well as to the research assistant at the Laboratory of Environmental Geology and the Computing Laboratory of Civil and Environmental Engineering at Faculty of Engineering, Universitas Gadjah Mada. This research can be successfully conducted was due to the continuous and intensive assistance of Mr. Sani Tanaka Ismawanto – the student of Magister Instrumentation at the Faculty of Engineering, Universitas Gadjah Mada.

References

Annoname, "Landslide disaster databased" Indonesian National Agency for Disaster Mitigation, 2009.

Andayani B, Karnawati D and Pramumijoyo S (2008) Institutional framework for community empowerment towards landslide mitigation and risk reduction in Indonesia. Proc. of the 1st World Landslide Forum, Tokyo, Global Promotion Committee of the Int. Program on Landslide (IPL) – ISDR, pp. 57-59.

Anderson MG, Halcombe E, Esquivel M, Toro J and Ghesquire F (2010) The Efficacy of a Program of Landslide Risk Reduction in Area of Unplanned Housing in the Eastern of Caribbean. *Environmental Management* (45): 807-821.

Anderson MG, Halcombe E, Blake JR, Ghesquire F, Holm-Nielsen N and Fisseha T (2011) Reducing Landslide Risk in Communities; Evidence for the Eastern Caribbean. *Applied Geography*. Elsevier (31): 590-599.

Fathani, T.F, Karnawati D, Sassa K, Fukuoka, H and Honda K (2008) Landslide Monitoring, Prediction and Early Warning in Banjarnegara, Indonesia. Proc. of 1st World Landslide Forum, Tokyo, pp. 195–198.

Fathani TF and Karnawati D (2009) Early warning of landslide for disaster risk reduction in Central Java Indonesia. Proc. of Int'l Workshop on Early Warning for Landslide Disaster Risk Reduction in the Eastern Asian Region: Kunming, China

Halcombe E, Smith S, Wright E and Anderson MG, (2012) Integrated Approach for Evaluating the Effectiveness of Landslide Risk Reduction in Unplanned Communities in the Caribbean. *Nat Hazards* (61): 351-385.

Karnawati, D., Maarif, S., Fathani, T.F., Wilopo, W. (2013). Development Of Socio-Technical Approach For Landslide Mitigation And Risk Reduction Program In Indonesia. *ASEAN Engineering Journal*, Part C. Vol. 2, No. 1, June 2013.

Karnawati D, Fathani, TF, Andayani B, Burton PW and Sudarno I. (2009) Strategic program for landslide disaster risk reduction; a lesson learned from Central Java, Indonesia Disaster Management and Human Health Risk; Reducing Risk, Improving Outcomes, WIT Transactions on the Built Environment Transaction, K. Duncan and C.A. Brebbia, Ed. Southampton: WIT Press. 115-126.

Karnawati D, Setianto A, Wilopo W, Andayani B and Suharto (2010) Development of Community Landslide Hazard Map for Landslide Risk Reduction. Proceeding of 11th Int. Assoc. of Engineering Geologist Congress, Auckland, 5-10 September, 2010. Auckland, New Zealand. pp. 1203 – 1208.

Karnawati D, Fathani TF, Andayani B, Legono D, and Burton PW (2011) Landslide hazard and Community-based Risk Reduction Effort in Karanganyar and the Surrounding Area Central Java, Indonesia. *Journal of Mountain Science*, 8(2): 149-153.

Karnawati D, Frost EG, Fathani TF and Subroto (2012) Smart Grid for Landslide Monitoring and Early Warning System in Indonesia. Proceedings of the 10th Anniversary of ICL – January 2012, Kyoto, In Press

Lacasse S and Nadim F (2008) Landslide Risk Assessment and Mitigation Strategy. In *Landslide Disaster Risk Reduction*. (eds). Sassa K and Canuti P, Springer Verlag Berlin Heidenberg. p. 31 – 61.



Proceedings of the SATREPS Workshop on Landslides in Vietnam, 2014

Distributed Hydrological Process through Vegetation & Surface Soil Layer using 30-minute Current Satellite-based Rainfall Intensity from NOAA-CPC

Apip⁽¹⁾⁽²⁾, Kyoji Sassa⁽³⁾

1) Research Centre for Limnology, Indonesian Institute of Sciences (LIPI), e-mail: apip@limnologi.lipi.go.id

2) Asia Pacific Centre for Ecohydrology (APCE), Indonesia

3) International Consortium on Landslides (ICL), Kyoto, Japan

Abstract Shallow landslides often occur during heavy rainfall events, especially in areas of mountainous terrain, in which soil's hydrological condition dominantly controls the shallow landslide mechanism. In areas subject to shallow landslides and operational landslide-hydrological monitoring as well as warning system is currently no in place, catchment scale hydrological modelling that uses recent advance in satellite-based rainfall information is one of new, low cost and innovative technologies for the establishment of an early shallow landslide-warning system. Therefore, this paper is primarily concerned with the potential capability analyses of a physically-based distributed hydrological model that uses 30-minute current satellite-based rainfall intensity, CMORPH, prepared by the National Oceanic and Atmospheric Administration (NOAA) for soil saturation dynamic and shallow landslide predictions at a large catchment area. A framework for predicting the dynamic soil saturation and its effect on landsliding initiation was developed using a grid-cell based distributed kinematic wave rainfall-runoff model and infinite slope instability approach. The potential applicability of the model for those purposes was tested and evaluated in the upland tropical basin, namely Upper Citarum River basin (2310 km²), Indonesia.

Keywords hydrological model, soil saturation dynamic, satellite-based CMORPH rainfall, shallow landslide

Introduction

Geographical location of the Monsoon Asian Countries causes most of the areas have experiencing with high rainfall, earthquake and numerous active volcanoes. Having those characteristics, Monsoon Asian Countries are

found to have high vulnerability to various natural disasters such as flood, various landslide types, droughts, earthquake, tsunami, and volcano eruption. Flood and landslides as the most widespread natural hazard cause casualties and millions of dollars in property damages almost annually. As the population increases and the social society become more complex, the economic and social cost of flood associated landslides will continue to rise unless there is a significant intervention and action. The government of monsoon asian countries has several policies and strategic plans for natural disasters preparedness and mitigation by promoting structural and non structural measures program.

The Upper Citarum River catchment, West Java, Indonesia is one of the persistently active landslides occurring in the Monsoon Asian Countries. The flood triggering landslides are hit almost in every year and caused extensive damages. Hydrologic characteristics have been changed by land degradation (Agus *et al.*, 2003), as a result, flood, debris flow and others landslide types are very frequent during the rainy season. The soils derived from volcanic tuff are easily erodible and prone to landslides. As suggested by field investigation, the type of landslide occurrence mainly is rapid shallow landslides (debris flow). According to the Geological Agency of Indonesia, since 1990 over 250 big landslides reported to have occurred there. Catchment erosion is also a serious problem in the upper river catchment where hillsides are steep. Shallow landsliding, as a form of mass movement, is one of the sources of hillslope erosion and catchment sediment yield. Therefore, there was an urgent need to devise countermeasure against frequent disasters. Herein, a new and innovative technology related disaster warning system as one of the most effective ways of nonstructural

measures to minimize the damages caused by water-induced disasters could be introduced. As there is no operational integrated flood-landslides forecasting and warning system in place in the Upper Citarum River catchment, this study focuses on development a hybrid physically-based distributed hydrological and slope stability models as well as to explore its application using near real-time satellite-derived rainfall products for hydrological estimation and shallow landslide simulation. The developed model considers the hydrological responses through vegetation and surface soil layers. This paper describes the preliminary results of this study on early warning system development.

In the following sections, the grid-based geo-hydrologic model used for surface soil saturation dynamic estimation is first described. Rainfall depth estimation using near real-time satellite-derived rainfall products is then explained briefly. The effect of rainfall depth and the canopy storage capacity of vegetation on net rainfall depth over land surface is then investigated using the developed model. Then, a set of model output evaluations at the basin scale is presented in the last section.

Physically-based Distributed Hydrological-Geotechnical Model

A recently developed physically-based hydrological-geotechnical model (Apip *et al.*, 2010a,b) was used in this study. The model consists of rainfall interception by vegetation, hillslope hydrology, soil erosion, slope instability, and sediment transport algorithm.

Effective Rainfall Sub-Model

The land use type and land cover condition affect the net of rainfall amount that can infiltrate to the surface soil layer. Effective rainfall is estimated from gross rainfall (R_g) received over the vegetation canopy. Herein, effective rainfall is defined as difference between gross rainfall and canopy interception. When the canopy of the particular vegetation intercept water, the rainfall is divided into two parts, as direct throughfall (DT) and intercepted rainfall (IC). The fraction of R_g contributes to DT is affected by the proportion of the land surface covered with the vegetation canopy (COV). The gross rainfall which is intercepted is stored on the leaves and branches of the vegetation as interception store (ICstore), it will become the source of evaporation. Interception store changes depends to the total gross rainfall for each time event and maximum capacity of the vegetation cover (ICmax). If the depth of IC is higher than ICstore, the remain of IC-ICstore will be not held in the ICstore, this is

termed as the temporarily intercepted throughfall (TIF). The source of stemflow (SF) and leaf drainage (LD) is comes from TIF. The depth of SF for each time is predicted as a function of landuse type and land cover as well as the average of acute angle (PA). The difference between TIF-SF for each time defined as LD.

The effective rainfall to the ground, which is available for runoff and shallow landslide modeling, is generated by the summation of the direct throughfall, stemflow, and leaf drainage. Conceptually all the processes explained above are simplified in Figure 1. For modeling interception process, this study used the same algorithm with KINEROS or EUROSEM model (Morgan *et al.*, 1998). The algorithm retains a strong physically-base, equations developed in laboratory experiment and validated by field observation as well as the algorithm is applicable for tropical region.

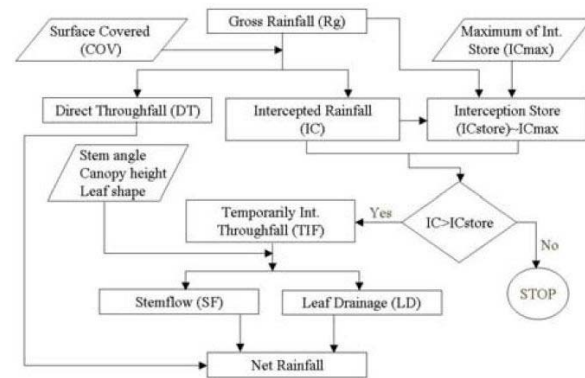


Figure 1. Schematic diagram of rainfall interception processes through a particular vegetation.

Hillslope Hydrology Sub-Model

The hydrologic model was based on a kinematic wave approach and simulates three lateral flow mechanisms including subsurface and surface flows (Tachikawa *et al.*, 2004). The model simulates: (1) subsurface flow through capillary pores; (2) subsurface flow through non-capillary pores; and (3) surface flow on the soil surface. These three flow processes are represented by the following single set of stage-discharge relationships (equation (1)):

$$q = \begin{cases} v_m d_m (h_w / d_m)^\beta, & 0 \leq h_w \leq d_m \\ v_m d_m + v_a (h_w - d_m), & d_m \leq h_w \leq d_a \\ v_m d_m + v_a (h_w - d_m) + \alpha (h_w - d_a)^m, & d_a \leq h_w \end{cases} \quad (1)$$

$$v_m = k_m i, \quad v_a = k_s i, \quad k_m = k_s / \beta, \quad \alpha = \sqrt{i} / n, \\ d_m = D\theta_m, \quad d_a = D\theta_a$$

where q is discharge per unit width; h_w is water level; i is the topographic gradient; k_m is the saturated hydraulic conductivity of the capillary

soil layer; k_s is the hydraulic conductivity of the non-capillary soil layer; d_m is the depth of the capillary soil layer; θ_m is the fraction of maximum volumetric water content in the capillary pore, d_a represents the depths of the capillary and non-capillary soil layers, θ_a is the fraction of maximum volumetric water content in the capillary and non-capillary pores; D is a soil depth; β is the exponent constant of unsaturated flow, v_m and v_a are the flow velocities of unsaturated and saturated subsurface flows, respectively, n is the Manning's roughness coefficient, which varies according to land use type, and m is a constant.

Infinite Slope Instability Sub-Model

The infinite slope method of slope stability analysis, a physically-based approach, was adopted for assessment of probable shallow landslide locations. The potential slope failure algorithm has two functions: failure prediction and downslope mass re-distribution of sediment released from slope failures. The infinite slope methods determines the slope stability factor, i.e. the slope factor of safety (FS), which expresses the ratio of stabilizing to destabilizing forces. The criterion to decide whether a slope is unstable or stable depends upon the value of FS being smaller or larger than 1. In this study, FS is calculated using a method adopted by Borga *et al.* (2002), as presented in equation (2).

$$FS = \frac{c^* + \cos \theta [1 - r_w] \tan \phi}{\sin \theta} \cdot \begin{cases} c^* = \frac{c_r + c_s}{d_a \rho_s g + W} \\ r_w = \frac{h_w \rho_w}{\left(1 + \frac{W}{gd_a \rho_s}\right) d_a \rho_s} \end{cases} \quad (2)$$

in which c^* is the total cohesion (c_r+c_s), c_r and c_s are the effective root and soil cohesion; ϕ is the effective internal angle of the soil; W is the vegetation surcharge; d_a is the effective soil depth; h_w is the saturated height calculated using a hydrological algorithm; θ is the slope angle; ρ_s is the density of soil at field capacity; ρ_w is the density of water. Most of these terms are spatially variable, but it is assumed that only m ($= h_w/d_a$) is time-varying, and therefore, the factor of FS is a function of m . Assuming that the value of every term in equation (2), except for m , is known or can be estimated for each local area/grid cell, a critical relative saturation level for a grid, m^c , can be determined, where $m^c = FS^{-1}$ as follows:

$$m^c = \left(\frac{\rho_s}{\rho_w} + \frac{W}{gd_a \rho_w} \right) \left(1 - \frac{\tan \theta}{\tan \phi} \right) + \frac{c_r + c_s}{d_a \rho_w g \cos \theta \tan \phi} \quad (3)$$

Based upon the concept of critical soil saturation, three slope stability classes can be defined:

1. Theoretically always stable which is expressed by

$$\tan \theta < \left(1 - \frac{1}{\frac{\rho_s}{\rho_w} \left(\frac{\rho_s}{\rho_w} + \frac{W}{gd_a \rho_w} \right)} \right) \tan \phi + \frac{c_r + c_s}{gd_a \rho_s \cos \theta \left(1 + \frac{W}{gd_a \rho_s} \right)} \quad (4)$$

2. Theoretically always unstable, which is expressed by

$$\tan \theta \geq \left(\frac{c_r + c_s}{gd_a \rho_s \cos \theta \left(1 + \frac{W}{gd_a \rho_s} \right)} \right) + \tan \phi \quad (5)$$

3. Potentially stable or unstable. Slope instability analysis is undertaken only for those grid cells with slope stability classified as potentially "stable/unstable" with FS predicted by equation (2).

Land surfaces theoretically always stable are those predicted to be stable even when saturated. Slope elements theoretically always unstable are those predicted to be unstable, even under dry conditions. There are five model parameters that have to be calibrated c_r , c_s , W , ϕ , and ρ_s .

Satellite-based CMORPH rainfall & HydroSHEDS Hydrotopographic Data

The National Oceanic and Atmospheric Administration (NOAA), USA, provided global precipitation data at very high spatial and temporal resolution. NOAA-QPC Morphing Technique (CMORPH) rainfall estimates are available within 30-minute of near real time and available on a grid with a spacing of 8 km. These data are then used in combination with the global coverage data sets of land surface characteristics (e.g., land use, digital elevation model (DEM)) from hydroSHEDS

(<http://hydrosheds.cr.usgs.gov/>).

In this study, the integrated application of the CMORPH-based satellite precipitation estimation and a hybrid hydrological-geotechnical modeling system is addressed.

Assessing Dynamic Map of Shallow Landslide Susceptibility Using Hydrological and Slope Stability Models

On shallow landslide occurrence, soil moisture plays an important control; increased soil water content increases the shear stress or decreases the shear strength of the soil mass. Therefore, an

accurate estimation of rainfall on slopes and calculation of the dynamic sub-surface water flows are the important factors in prediction of landslide susceptibility. The combined physically-based distributed hydrological model and slope stability model has been developed by authors. As mentioned above, the hydrological model considers three principal water flux pathways within a catchment: subsurface flow through unsaturated flow (capillary pore), subsurface flow through saturated flow (non-capillary pore), and surface overland flow. The soil water amount calculated with its model is then used for slope stability analysis. Herein, the factors of safety (see Equation 2), which represents the ratio of shear strength to shear stress of soil mass, are used to characterize slope stability. Slopes having safety factors smaller than one are considered unstable.

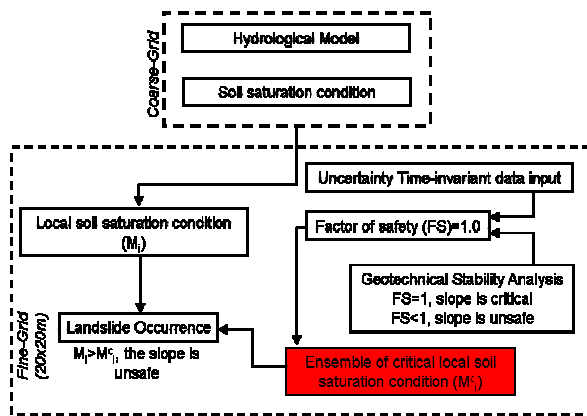


Figure 2. Methodology for spatiotemporal dynamics of landslide potential prediction.

A physically-based distributed hydrological was developed to determine the dynamic of soil moisture and runoff hydrograph. This model was used as tool to predict m^c at any locations inside study site (Figure 2). As further stage, the failure condition for each grid square can be written in terms of the time-varying relative saturated depth: for $m_i \leq m_i^c$, the slope is safe; and for $m_i > m_i^c$, the slope is unsafe.

Study Area, the Upper Citarum River catchment

The Citarum River catchment is the largest river on the West Java Island. Total area of the Upper Citarum Catchment is around 2,283 km².

The 269 kilometers Citarum River originates from Wayang Mountain with elevation of 2198 m above mean sea level south Bandung. In the first 25 km, the river follows a steep slope of 0.033 then flows onto the middle part of the basin with slope of 0.0033 starting at Bandung for another 169 km. In the lower parts, the river meanders across an alluvial plain for about 75 km before reaching the Java Sea. There are three cascading reservoirs in the Citarum river basin namely Saguling, Cirata and Jatiluhur. Those reservoirs are built not only for generating hydropower, water supply for irrigation, industrial and domestic but also uses to regulate and traps of sediment. Geomorphology of the catchment consists of volcanic cone, Tuff, Tuff Sand, Lapili, Breccia Aglomerat, Breccia and lahar, Breccia, Lava Andesit, Tuff Breccia lahar, and lava, Andesit and Dasit.

Based on the record of Meteorology and Geophysical Agency, the Citarum River catchment has an average monthly temperature of 22.8 to 26°C, average annual rainfall of 1500 – 4000 mm, average monthly wind speed about 2 to 9 knot and average monthly evaporation rate between 120 mm to 150 mm. The population in the Upper Citarum catchment is rapidly growing with the urban area expanding around Bandung, the capital of West Java. In the upper Citarum River catchment, there are 12 river sub catchments which have very steep slopes flow into upstream of Citarum River. Flood and associated landslides are frequent during the rainy season. Figure 3 shows the whole Upper Citarum catchment area, Saguling Dam as the river catchment outlet.

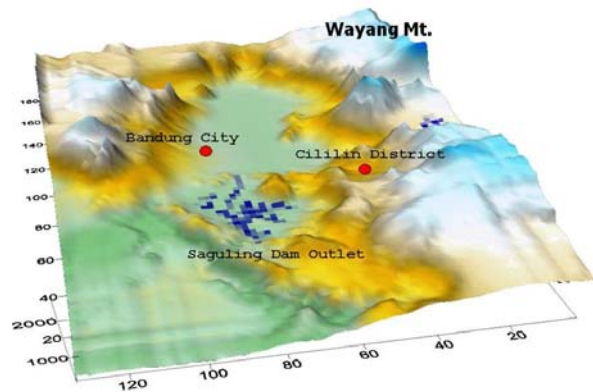


Figure 3. The topography view of the Upper Citarum River catchment.

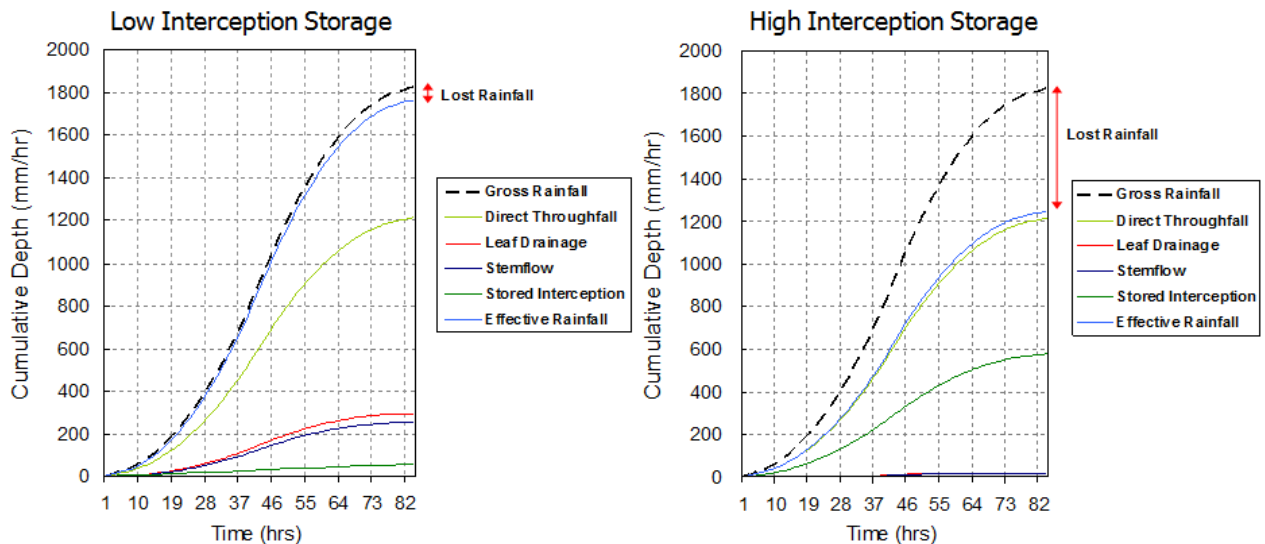


Figure 4. Comparison of the depth of simulated total intercepted rainfall (lost rainfall) and other components obtained by two types vegetation: low canopy storage capacity (left) and high canopy storage capacity (right). The model output shows how the vegetation controls the supply of net rainfall that can be passed to the surface soil layer.

Simulation Results

Impact of Vegetation Canopy to Effective Rainfall

As explained above, the distributed hydrological model uses effective rainfall data information as input forcing to predict runoff generation on each grid. Figure 4 illustrates the temporal dynamic change of the cumulative interception variables under two different types of vegetation: (a) canopy with low interception storage capacity, and (b) canopy with high interception storage capacity. The relative importance of leaf drainage and stemflow are seen to increase with low interception store, and otherwise.

Satellite-based Rainfall Estimates Performance

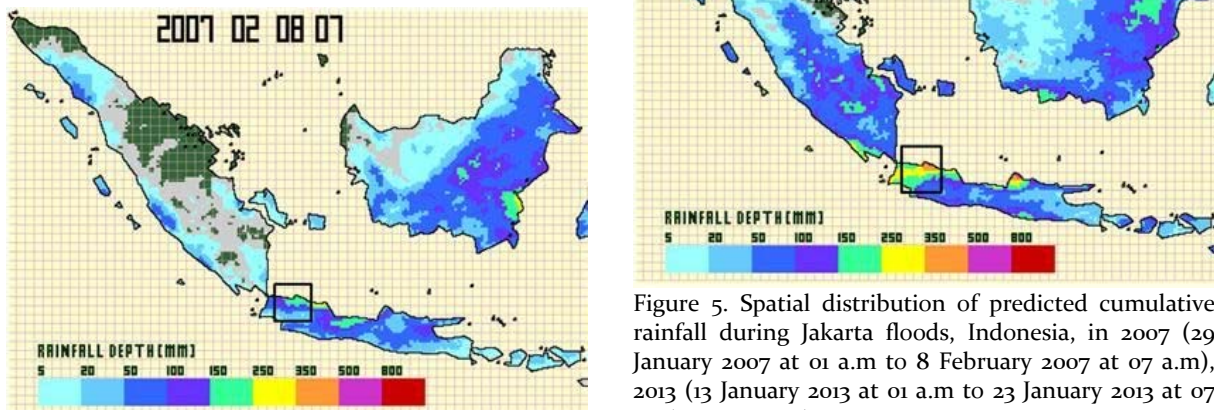


Figure 5. Spatial distribution of predicted cumulative rainfall during Jakarta floods, Indonesia, in 2007 (29 January 2007 at 01 a.m to 8 February 2007 at 07 a.m), 2013 (13 January 2013 at 01 a.m to 23 January 2013 at 07 a.m), and 2014 (11 January 2014 at 01 a.m to 21 January 2014 at 07 a.m) using near real-time 30-minute satellite-based rainfall products. Jakarta Metropolitan region and Citarum River catchment is located inside the area signed with a rectangle line.

The use of a rainfall product derived from satellite images is one of the alternatives for poorly gauged

areas such as the Upper Citarum River region. The main satellite data set such as CMORPH from NOAA, GSMaP (Global Satellite Mapping of Precipitation) product (http://sharaku.eorc.jaxa.jp/GSMaP_crest/) prepared by the JAXA Precipitation Measuring Mission (PMM) Science Team potentially can be utilized.

Further, the performance of near real-time 30-minute satellite-based rainfall estimates was evaluated during the Jakarta flooding in 2007, 2013 and 2014 (Jakarta is the capital of Indonesia, which is located at the down stream of Citarum River catchment). According to the rainfall duration and spatial distribution, the rainfall estimates well capture relatively higher cumulative rainfall depth over the Upper Citarum River and Jakarta Metropolitan Region region than other areas for each flooding case (see Figure 5). However, especially for high rainfall intensity, the rainfall estimates underestimate the magnitude of rainfall when compared with the observed data of specific stations, indicating a negative bias. In summary, these results indicate that the satellite-based rainfall product is reasonable ways by which to predict the spatial distribution of rainfall over this study region. The movement of satellite-based rainfall fields could be used to detect a particular extreme rainfall event and used it as the model input for flood-shallow landslide prediction and forecasting.

Hydrological Model's Output Evaluation

The application of the system for two past hydrological calendars (2004 as calibration period and 2005 as validation period) shows that the model successfully predict the effect of the rainfall movement and intensity on temporal dynamics of observed streamflow discharges at the inlet of Saguling Dam. The performance of the hydrological model shows good agreement in reproducing observed streamflow discharge at the catchment outlet (Figure 6). These results show that the potential exists for application of the system in improving the prediction of hydrological variables- triggered shallow landslides and its disaster warning.

Shallow Landslide Susceptibility & Uncertainty

To identify the area susceptible to shallow landslides and to take account of the stochastic nature of the system, the Generalized Likelihood Uncertainty Estimation (GLUE) concept was adopted and incorporated into the above deterministic hydrological and slope stability algorithms to generate 10 000 landslide susceptibility maps. The procedures include a number of steps:

1. Generate a probabilistic distribution and sample the parameter space of each model parameter 10 000 times using a Monte Carlo

- simulation technique
2. Measurement of model performance
3. Define the criteria for acceptance or rejection of model results.

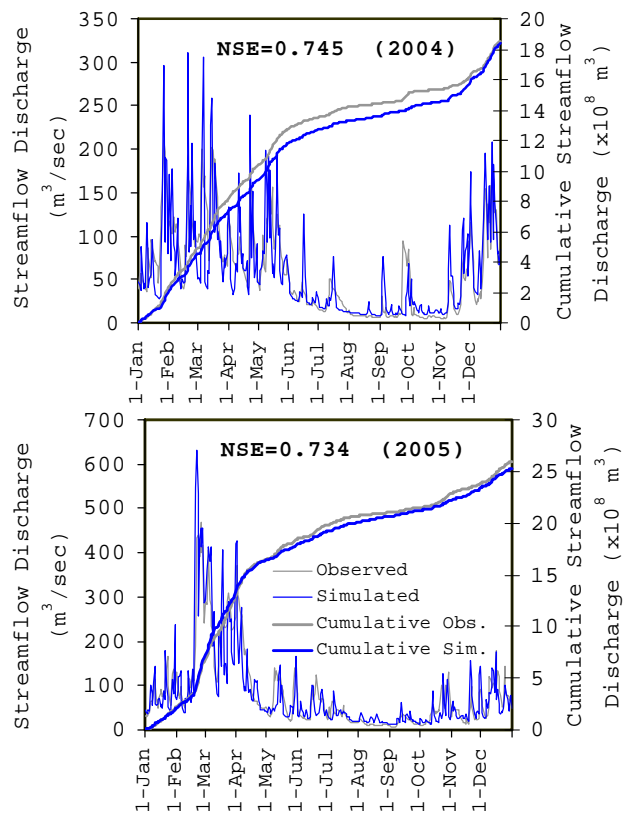


Figure 6. Streamflow model performance for the calibration period 2004 (upper figure) and the validation period 2005 (lower figure). Streamflow was evaluated at the upper basin outlet.

For each simulation, a grid cell with an *FS* value less than 1.0 is defined as a potential shallow landslide location, otherwise it is classified as stable. The long-term spatial pattern of recorded landslide locations (1985–2008) is overlaid on each susceptibility map. Two objective functions are used to measure the model performance for each susceptibility map, namely success rate in predicting unstable grid cells (OF₁) and success rate in predicting unstable grid cells associated with success rate in predicting stable grid cells (OF₂) (Huang & Kao, 2006). Accordingly, the cumulative probability of predicted landslides and a mean *FS* for each grid cell could be extracted; and thus a relative risk measure for landslide potential can be obtained. As a last stage, the probability of landslide potential, based on the slope instability index, is qualitatively classified as extremely low ($P \leq 0.2$), low ($0.2 < P \leq 0.4$), moderate ($0.4 < P \leq 0.6$), high ($0.6 < P \leq 0.8$), and extremely high ($0.8 < P \leq 1.0$).

Initial estimates for feasible ranges of the slope stability model parameters were based on field and laboratory measurements and the

literature, as well as maps of soil types and soil thickness. Following GLUE, we set a reference value for model performance ($OF_2 \geq 0.50$) to define the behavioural simulations. 2067 susceptibility maps were produced by applicable simulations. Here we demonstrate the advantage of using two objective functions; OF_1 and OF_2 to measure model performance and the problems of retrieving optimal model outcome. The 2067 top values of model performance derived from OF_2 (y-axis) are plotted against the OF_1 (x-axis) (Figure 7). The figure represents the performance of the model in representing the dynamic area of slope instability in response to a set rainfall data input. A dome-shape distribution is shown between the two objective functions. OF_2 -derived performance increases along with OF_1 -derived performance at the beginning. However, when OF_2 -derived performance reaches a best prediction (0.64) and starts to decrease, OF_1 -derived efficiencies keep increasing until its best prediction (1.0) is reached. The result suggests that the OF_2 -derived performance helps to reduce over prediction. For further probability analysis, we overlay the maps and take the mean for FS values in each grid cell for the best 2067 predictions. The occurrence probability of $FS < 1.0$ for each grid cell is calculated for the 2067 runs to quantify predicted shallow landslide potential. Each grid cell has a mean FS value and an occurrence probability for shallow landsliding (Figure 8).

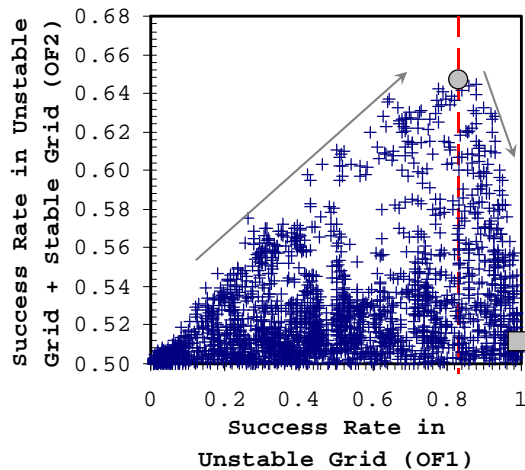


Figure 7. The scatter plots of Objective Function 1 (OF_1) against Objective Function (OF_2)-derived efficiencies for 2067 runs MCS.

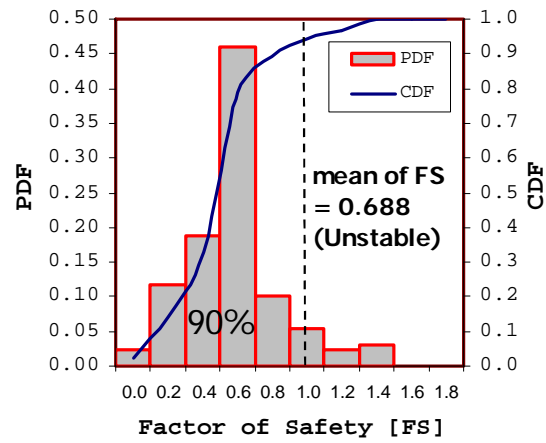


Figure 8. Probability functions and its cumulative probability of the Factor of Safety (FS) values in an example grid with mean $FS = 0.688$ (unstable).

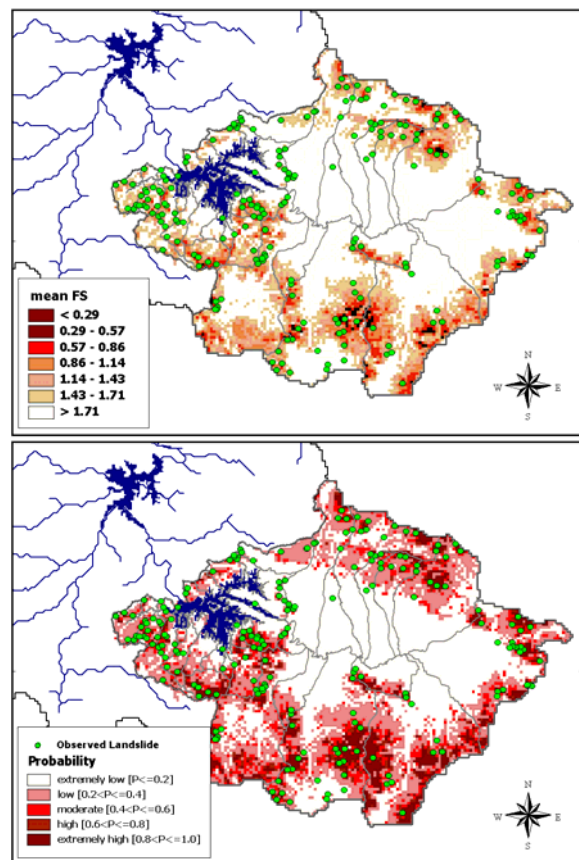


Figure 9. The mean FS (upper) and integrated landslide probability map (below) overlaid with the spatial distribution of observed landslide sites.

Figure 9 shows the integrated landslide probability map derived from the best 2067 simulations and the spatial distribution of mean FS . Figure 9 demonstrates the pattern of areas predicted to be susceptible to shallow landslides, as described above, along with the general pattern of observed landslide sources. The model reproduced several of the principle clusters in the observed pattern, notably the clusters along an escarpment in the western, southern, eastern, and northern sectors of the basin. The percentage of

catchment area used to simulate the dynamic of susceptible areas to shallow landsliding in response to a rainfall event amounted to 32.1% (636 318 grid cells). Two types of error appeared in the predicted shallow landslide susceptibility map (1) some grid cells were predicted as theoretically always stable, but past landslides were mapped in those grid cells, especially in the northern part of the study region; (2) some grid cells were characterized as zones of slope instability slope, but no scars were observed there. Such errors are typically caused by inaccuracies in the representation of topography. In steep terrain, the 90-m grid DEMs provided by HydroSHEDS for particular internal locations still do not capture the local slope steepness that controls shallow landsliding. Consequently, the model did not represent local topographic controls on potential shallow landsliding.

Summary

This study concerned with the potential capability analyses of a physically-based distributed kinematic wave hydrological model that uses 30-minute current satellite-based rainfall intensity for soil saturation dynamic and shallow landslide predictions at a large catchment area. The model has high capability to simulate the hydrological responses simultaneously with slope instability as a base information for shallow landslide prediction at river catchments such as in the Upper Citarum River catchment. The estimated satellite-based rainfall product was evaluated during the Jakarta floods on January-February 2007 and January 2013, 2014. The developed modeling system captured the temporal patterns and multiple peaks of the observed hydrographs and landslide inventory at specific locations of internal selected study area. Exploration and evaluation on the potential capability of the system for real-time flood-shallow landslide forecasting and associated water-related problems prediction as well as climate change impact assessment on flood, landslide risks should be directed as interesting points for further advancement of the model application. Additionally, utilizing radar information

technology and near real-time satellite-derived rainfall products such as CMORPH NOAA-CPC with deterministic or stochastic rainfall prediction, the capability of the model can be examined for short-term real-time flood-landslide forecasting and warning at the regional scale.

Acknowledgments

The financial and administrative supports received from the International Consortium on Landslides (ICL), the Disaster Prevention Research Institute (DPRI)-Kyoto University, the Research Centre for Limnology-Indonesian Institute of Sciences (LIPI) are gratefully acknowledged.

References

- Agus, F. & Wahyunto (2003) Evaluation of flood mitigation function of several land use systems in selected areas of west java, Indonesia. In: *Japan/OECD Expert Meeting on Land Conservation Indicators* (13–15 May, 2003, Kyoto, Japan).
- Apip, Sayama, T., Tachikawa, Y. & Takara, K. (2010a) Spatial lumping of a distributed rainfall-sediment-runoff model and effective lumping scale. *Hydrological Processes* (accepted).
- Apip, Takara, K., Yamashiki, Y., Ibrahim, A. B., Sassa, K. & Fukuoka, H. (2010b) A distributed hydrological-geotechnical model using satellite-derived rainfall for shallow landslide warning in a large basin. *Landslides Journal* **7**(3), 237–258.
- Borga, M., Fontana, G. D., Gregoretti, C. & Marchi, L. (2002) Assessment of shallow landsliding by using a physically based of hillslope stability. *Hydrol. Processes* **16**, 2833–2851.
- Huang, J. C. & Kao, S. J (2006) Optimal estimator for assessing landslide model performance. *Hydrol. Earth System Sci.* **10**, pp. 957–965.
- Morgan, R.P.C., Quinton, J.N., Smith, R.E., Govers, G., Poesen, J.W.A., Chisci, G., & Torri, D. (1998) The European soil erosion model (EUROSEM): a dynamic approach for predicting sediment transport from fields and small catchments. *Earth Surface Process and Landforms* **23**, pp. 527-544.
- Tachikawa, Y., Nagatani, G. & Takara, K. (2004) Development of stage-discharge relationship equation incorporating saturated-unsaturated flow mechanism. *Ann. J. Hydraul. Engng (JSCE)* **48**, 7–12.

Kyoji Sassa and Khang Dang *Editors.*

This proceedings contains papers presented in the SATREPS Mid-Term Activity Report Meeting and the Landslide Technical Forum of the SATREPS Project "Development of Landslide Risk Assessment Technology along Transport Arteries in Vietnam: 2011-2016". It was organized at the Institute of Transport Science and Technology, Ministry of Transport, Vietnam on 29-30 July 2014.

Kyoji Sassa is the Project leader of the SATREPS-Landslide Vietnam Project and Executive Director of the International Consortium on Landslides (ICL)

Khang Dang is a graduate student in Kyoto University invited from VNU University of Science as a part of the SATREPS project and ICL researcher.



ISBN: 978-4-9903382-2-0

July 2014